911 91 B

Journal of Geophysical Research

LUME 65 DECEMBER 1960 NUMBER 12

THE SCIENTIFIC PUBLICATION

OF THE AMERICAN GEOPHYSICAL UNION

Journal of Geophysical Research

An International Scientific Publication

This Journal welcomes original scientific contributions on the physics of the earth and its environment.

Manuscripts should be transmitted to J. A. Peoples, Jr., Geology Department, University of Kansas, Lawrence, Kansas. Authors' institutions, if in the United States or Canada, are requested to pay a publication charge of $25 per page, which, if honored, entitles them to 100 free reprints.

Subscriptions to the *Journal of Geophysical Research* and *Transactions, AGU* are included in membership dues.

Non-member subscriptions, *Journal of Geophysical Research*..$30 for back Volume of 1959, $5 for this issue; $20 for the calendar year 1960.

Non-member subscriptions, *Transactions, AGU*..................$4 per calendar year, $1.25 per copy.

Subscriptions, renewals, and orders for back numbers should be addressed to American Geophysical Union, 1515 Massachusetts Ave., Northwest, Washington 5, D. C. Suggestions to authors are available on request.

Beginning with the January 1959 issue (Vol. 64, No. 1) the *Journal of Geophysical Research* is published monthly by the American Geophysical Union, the U. S. National Committee of the International Union of Geodesy and Geophysics organized under the National Academy of Sciences-National Research Council as the U. S. national adhering body. Publication of this journal is supported by the National Science Foundation and the Carnegie Institution of Washington. The new monthly combines the type of scientific material formerly published in the bi-monthly *Transactions, American Geophysical Union*, and the quarterly *Journal of Geophysical Research*. The *Transactions, American Geophysical Union* will continue as a quarterly publication for Union business and items of interest to members of the Union.

Published monthly by the American Geophysical Union from 1407 Sherwood Avenue, Richmond, Virginia. Second class postage paid at Richmond, Virginia.

R SYSTEM
PLICATION

Climate Survey

Wind Transmitters

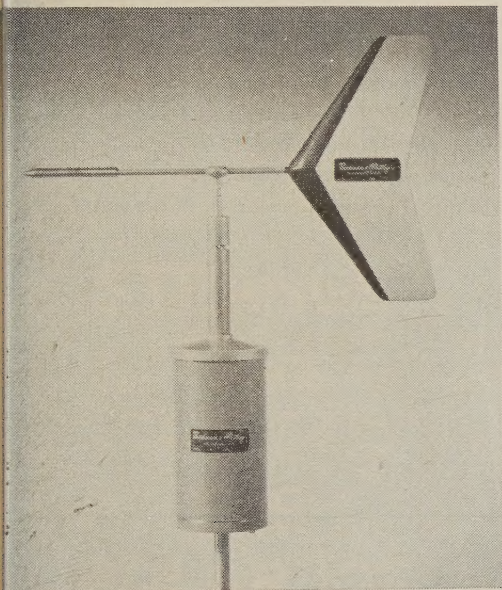

Highly adaptable, Beckman & Whitley Climate Survey Wind-Speed and -Direction Transmitters have wide applicability. They serve not only as elements in Beckman & Whitley Wind-Speed and -Direction Recorders, but also as basic standardized units for scientific weather measuring systems of special design and scope—involving telemetering, tape recording, other data-handling techniques.

←

WIND COMPONENT TRANSMITTERS with low threshold, providing sine and cosine vector resolution for wind-component determination. Also standard linear wind-direction transmitters in the same basic design.

→

VIND SPEED TRANSMITTERS based n dragfree light-beam chopper design, vailable in standard types providing ne, two, four, and 100 pulses per revo-ution. Complete series housed in identi-al environment-proved package with riple-labyrinth dust-seals, selected and pecially-processed low friction bear-ngs. Extremely rapid transient response —guaranteed threshold three-quarters nile per hour.

Send for details on these standard nits, or, if you have special problems, or recommendations on other instru-nents or special adaptations.

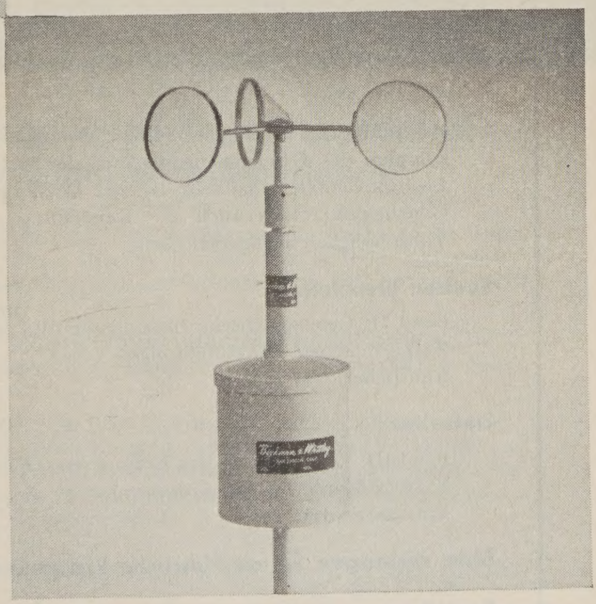

eckman & Whitley INC.

instruments for scientific meteorology

SAN CARLOS 15, CALIFORNIA

Journal of

GEOPHYSICAL RESEARCH

..UME 65 DECEMBER 1960 NO. 12

An Investigation of the Forbush Decreases in the Cosmic Radiation

JOHN A. LOCKWOOD[1]

University of New Hampshire
Durham, New Hampshire

Abstract. An analysis has been made of the large and rapid Forbush decreases in the cosmic radiation which occurred from 1954 to 1959. Data from the IGY network of cosmic-ray stations have been utilized to determine the changes in the primary rigidity spectrum, any significant differences in the onset times, and the existence of anisotropies during the decreases. To evaluate changes in the primary spectrum during a decrease it is necessary to know the spectrum before the event. It has been found that this long-term variation is adequately described by a modulation of the primary spectrum given by $1 - C(t)P^{-1}$, where $1 \leq C(t) \leq 2.5$ and $C(t)$ is a function of time in the solar activity cycle. For individual decreases the modulation is $1 - \{C(t_F)P^{-1} + k_F\}$, where $0 \leq k_F \leq 4$ per cent for nucleonic detectors at sea level and mountain elevations and $0.6 \leq C(t_F) \leq 2.2$. No systematic variations of the onset times were evident, except for the smaller decreases where the effect of any superimposed daily variation is important. The primary radiation remained isotropic during the large decreases. These events were preceded within 3 hours by a sudden commencement geomagnetic storm. These results are discussed in terms of possible solar-modulating mechanisms.

1. INTRODUCTION

..nce 1956 a number of large and sudden ..nmetrical decreases have occurred in the ..nic radiation at the earth; these are referred ..s Forbush decreases [*Forbush*, 1938]. Many ..hese decreases took place after the estab..ment of the IGY network of cosmic ray sta..s. Therefore, in principle it is possible to de..nine the changes in the primary rigidity ..trum of the cosmic rays, any large differ..s in the onset times, and the existence of ..otropies during these events. If data are ..cted from the world-wide distribution of nu..nic detectors, changes in the primary rigidity ..trum in the interval from ~2 BV to ~15 .. may be reliably evaluated. A very good esti..e may also be made of the changes for pri..y particles with rigidities $15 \leq P \leq 50$ BV ..comparing nucleonic and mesonic detectors located at the equator. The changes in the spectrum below ~2 BV have been evaluated by *McDonald and Webber* [1959] from recent measurements of the primary alphas and protons. From a study of such variations some conclusions may be drawn regarding the adequacy of various physical models proposed to explain these variations.

The purpose of this investigation of the Forbush decreases is to determine:

(1) the changes in the primary rigidity spectrum;
(2) any significant differences in onset times;
(3) the existence of any anisotropies during the main phase of the decrease and of any precursory increases.

Only those decreases were selected which had a magnitude of greater than 5 per cent and a decrease rate of greater than ~1 per cent hr^{-1} as measured by the nucleonic detector at Mt. Washington, N. H. [*Lockwood*, 1958]. For most

[1] On leave at the Department of Electronics, ..al Institute of Technology, Stockholm, Swe-

events this ensured that the decrease was much larger than the amplitude of the daily variation. By requiring that the rate of decrease be rapid, a more critical test of the adequacy of various physical models is possible. For the decreases selected, the data from nucleonic detectors located at sea level and at mountain elevations were analyzed separately. No attempt was made to use the data from mesonic detectors, except for the equatorial stations. For a mesonic detector the corrections for changes in atmospheric conditions are complicated and the magnitudes of the decreases much smaller because the effective primary spectrum has a maximum at ~ 15 BV. Data from some stations were not used because operational difficulties were encountered at the times selected, or because the stations had a long history of operational troubles.

Since it is known that the primary rigidity spectrum changes during the cycle of solar activity [*McDonald and Webber*, 1959; *Meyer and Simpson*, 1957; *A. G. Fenton, K. G. Fenton, and Rose*, 1958], the primary spectrum must be known just before the particular event to be studied. These long-term spectral changes may be evaluated from: (1) nucleonic detector records; (2) mesonic detector and ionization chamber records; (3) measurements of the primary spectrum; and (4) latitude surveys at sea level and airplane altitudes using nucleonic detectors. Data from all four of these methods were examined. It will be seen that the determination of the primary rigidity spectrum is critical to the correct evaluation of the changes which occur during Forbush decreases.

The Forbush decreases selected, referred to hereafter as F events, are listed in Table 1. In the discussion which follows we shall consider: first, the method for evaluating the long-term variation in the primary rigidity spectrum; second, the individual events; third, the general conclusions which can be drawn; and fourth, some comments on the various physical models which have been proposed.

2. Rigidity Dependence of the Long-Term Variation

In order to relate the variations in the secondary components of the cosmic radiation deep within the atmosphere to those in the primary spectrum, it is necessary to know the specific yield functions. The yield function relates the number of secondary particles produced at a depth as a function of the energy of the prim[ary] radiation. These functions can be obtained eit[her] by calculations or by an empirical method using simultaneous observations of the prim[ary] spectrum and of the secondary component. T[he] latter approach was first used by *Fonger* [19..] and more recently by *Webber and Quen[by]* [1959]. The derivation of the cosmic-ray s[pe]cific-yield functions by Webber and Quen[by] represent the best available data. They ha[ve] shown that the differential counting rate o[f a] nucleonic or an ionization detector located a[t] depth x, at the time t, with a vertical cut[off] rigidity P_c, due to particles arriving vertica[lly] in a very small solid angle at the top of [the] atmosphere, can be written

$$\frac{dN_v(P, x, t)}{dP} = \sum_z S_z(P, x) j_z(P, t)$$

where $jz(P, t)$ is the differential primary rigid[ity] spectrum in the vertical direction, and $S_z(P, ...$ is the specific yield function for the particu[lar] charge component. Then, as shown by Webb[er] and Quenby

$$N_v(P_c, x, t) = \sum_z \int_{P_c}^{\infty} S_z(P, x) j_z(P, t)\, dP$$

where $N_v(P_c, x, t)$ is the response of either t[he] nucleonic or ionizing component due to partic[les] arriving vertically at the top of the atmosphe[re]. Throughout this discussion we will use the mo[di]fied cutoff rigidities deduced by *Quenby a[nd] Webber* [1959], which take into considerati[on] both the dipole and nondipole portions of t[he] internal geomagnetic field.

The nucleonic detectors are omnidirection[al] and we can relate N_v to the measured respo[nse] N due to particles arriving from all directions [at] the top of the atmosphere by the Gross appro[xi]mation [*Janossy*, 1948]:

$$2\pi N_v = N\left(1 + \frac{x}{L}\right), \quad \text{where} \quad \frac{1}{L} = -\frac{1}{N} \ldots$$

In the discussion which follows we are interes[ted] only in variations of N. So if a variation occ[urs]

$$\frac{\delta N_v}{N_v} = \frac{\delta N}{N} - \frac{x}{L}\left[\frac{1}{1 + \frac{x}{L}}\right]\frac{\delta L}{L}$$

For depths greater than 500–600 g c[m...]

TABLE 1. Large Forbush Decreases in Nucleonic Intensity at Mt. Washington, 1954–1959

Event Number	Year	Month	Day	Onset UT	Magnitude of Decrease %	Duration of Decrease Phase, hr	Maximum Rate of Decrease %/hr	Onset Magnetic Storm, UT	Type III Polar Cap Absorption*: Onset	Type III Polar Cap Absorption*: Duration, day	Solar Flare*: Time	Solar Flare*: Imp.	Solar Flare*: Heliographic Position
I	1955	Nov.	19	1730	5.4	8.8	1.0	~1000†	...	...‡	...	...	...
II	1955	Dec.	6	0100	5.4	7.5	1.2	(12/5) 2200†	...	...‡	...	...	...
III	1956	Mar.	3	0100	6.9	10	1.5	~0000†	...	...‡	...	...	...
IV	1956	Sept.	2	0300	6.5	19	1.7	0230†	(8/31) 1500	2-1/2	(8/31) 1226	3	N16 E13
V	1956	Nov.	9	2100	8.3	11	2.2	(?)2030†	...	...	...	...	...
VI	1957	Jan.	21	1830 ± 10	17.0	14	2.5	1255	(1/20) 1500	2-1/2	(1/20) 1104	3	S29 W18
VII	1957	Aug.	29	2110^{+10}_{-05}	12.5	13	2.6	1910	(8/29) 1300	>1/2	(8/29) 1030	3	S24 E22
VIII	1957	Sept.	13	0330	6.1	3	3.0	0045	(9/12) ~1200	...	...	?	...
IX	1957	Oct.	22	0030 ± 10	8.2	8	1.5	(10/21) 2241	(10/21) 0630	2	(10/20) 1637	3+	S25 W45
X	1957	Nov.	26	0200	6.8	20	...	0155	...	...	...	...	...
XI	1957	Dec.	19	1700	9.2	13	2.2	0935§	...	...	...	...	...
XII	1958	Feb.	11	0245 ± 15	5.2	1	~7.0	0125	(2/10) 0800	1	(2/9) 2108	2+	S13 W14
XIII	1958	Mar.	25	1815 ± 05	11.1	18	1.4	1540	(3/25) 1300	4-1/2	(3/23) 0950	3+	S15 E80
XIV	1958	July	8	0915 ± 05	7.8	12	1.7	0750	(7/7) 0600	3	(7/7) 0039	3+	N24 W02
XV	1958	Aug.	17	0600^{+10}_{-05}	5.8	26	6.9	0622	(8/16) 0600	2-1/2	(8/16) 0432	3+	S14 W53
XVI	1958	Aug.	24	0230	9.1	8	3.2	0140	(8/22) 1700	3-1/2	(8/22) 1417	3	N21 W08
XVII	1959	Jan.	9	2000	5.0	2.5	2.5	1459	...	...	...	...	...
XVIII	1959	May	12	0000 ± 15	14.8	7	5.0	(5/11) 2318	(5/11) 0130	5-1/2	(5/10) 2055	3+	N23 E47
XIX*a*	1959	July	11	1715 ± 15	9.9	12	3.2	1625	(7/10) 1100	>4	(7/10) 0206	3+	N20 E60
b		July	15	0830 ± 15	14.5	10	6.1	0802	(7/14) 0800	>3	(7/14) 0319	3+	N17 E07
c		July	17	1930	13.5	7	4.5	1638	(7/17) 0300	5	(7/16) 2115	3+	N06 W30
XX	1959	Aug.	20	0415 ± 15	6.8	3	2.5	0412	...	...‡	...‡	...	...

* *Reid and Leinbach* [1959]. † Fredericksburg magnetograms. ‡ No data available. § Only 3 or 4 stations reported this storm.

$\delta L/L \rightarrow 0$ [*Simpson, and Fagot,* 1953]. Therefore

$$\frac{\delta N_v}{N_v} \cong \frac{\delta N}{N} \quad (4)$$

There is some evidence [*McCracken,* 1960] that L changes during the cycle of solar activity, but this is most probably less than 5 per cent. Therefore, (4) is a very good approximation. Consequently, we shall make no further distinction between N and N_v, except to note that the quantity always measured is N. From the differential response curves of Webber and Quenby, we can relate the time variations in secondary components to the primary radiation. We shall make the simplifying assumption that, in the latitude sensitive portion of the rigidity spectrum, the variations are the same in the proton and alpha components and neglect the contributions from nuclei with $Z > 2$. The recent results of *McDonald and Webber* [1959] on the primary proton and alpha spectra substantiate such an assumption.

Let us consider a variation in the primary rigidity spectrum in the vertical direction of the form [*McDonald and Webber,* 1959]:

$$\frac{\Delta j}{j_0} = -C(t)P^{-\gamma} \quad (5)$$

Hence,

$$j(P, t) = j_0(P, t_0)\{1 - C(t)P^{-\gamma}\} \quad (6)$$

is the primary rigidity spectrum at some time t. The fractional change in counting rate of a detector at depth x with vertical cutoff rigidity P_c is then

$$\frac{\Delta N}{N} = \frac{\int_{P_c}^{\infty} \frac{dN(P, x, t_0)}{dP} C(t)P^{-\gamma}\, dP}{N(P_c, x, t_0)} \quad (7)$$

The detailed methods for evaluating this quantity are given in Appendix A.

If we identify $j_0\ (P, t_0)$ with the undisturbed spectrum as measured in 1954 at the minimum of solar activity, then we can use (7) to determine the changes which have occurred during the last few years of enhanced solar activity. It has been definitely established that large changes in the spectrum take place during the solar cycle [*Fenton, Fenton, and Rose,* 1958; *Meyer and Simpson,* 1955; *Neher and Anderson,* 1958; *Lockwood,* 1958]. To determine these changes, we have available data from the balloon flig[hts] of *McDonald and Webber* [1959], the neut[ron] latitude surveys at airplane altitudes by *Me[yer] and Simpson* [1955; 1957], and the continu[ous] records of ionization and nucleonic detect[ors] operated at sea level and mountain elevatio[ns]. The spectrum $j(P, t)$ existing just before t[he] individual Forbush decrease may be evaluat[ed] by averaging data over several days before t[he] event. This spectrum $j(P, t)$ can then be u[sed] in (1) to find the new differential respon[se] dN/dP that we assumed to exist at the start [of] the F event.

The changes in the primary rigidity spectru[m] during the solar cycle, as defined by (5), a[re] given in Table 2. These were obtained by ave[r]aging the data over at least 10 days before t[he] F event. In many instances a monthly avera[ge] could be used if the fluctuations of the intensi[ty] were sufficiently small. Where data were ava[il]able from balloon flights or latitude surveys [at] airplane altitudes on a particular day, on[ly] daily averages could be used. These daily ave[r]ages were compared with the intensity for se[v]eral days before the decrease. The detailed eval[u]ation of these changes is given in Appendix [B]. It is apparent that better agreement with o[b]servations might be obtained by making small adjustments in the assumed values of γ, whi[ch] were 0.5, 0.75, 1.0, 1.5 and 2.0. We do not b[e]lieve that the data available justify this.

3. Analyses of Individual F Events

Having determined the long-term variatio[n] in the primary rigidity spectrum, we can no[w] evaluate the changes for individual Forbush d[e]creases. Let us again consider a variation of t[he] form given by equation 5:

$$\frac{\Delta j}{j} = -C(t_F)P^{-\gamma_F} \quad (\ldots)$$

Thus,

$$j_F(P, t_F) = j(P, t)\{1 - C(t_F)P^{-\gamma_F}\} \quad (\ldots)$$

where $j_F(P, t_F)$ is the differential primary rigid[ity] spectrum during the main phase of the Fo[r]bush decrease. (It is possible that γ_F is a fun[c]tion of P itself. In such a case this empiric[al] method can not be used.) We can write

$$\frac{\Delta N_F}{N} = \frac{\int_{P_c}^{\infty} \frac{dN(P, x, t)}{dP} C(t_F)P^{-\gamma_F}\, dP}{N(P_c, x, t)} \quad (10)$$

TABLE 2. Rigidity Dependence of the Long-Term Variation and the Forbush Decreases

Event Number	Date	Decrease at Mt. Washington %	Long-Term Change in Primary Rigidity Spectrum (Multiply by $1/P$ unless noted)	Rigidity Dependence of F Event* Sea level	Rigidity Dependence of F Event* 680 g cm^{-2}	σ† 680 g cm^{-2}	σ_s/σ 680 g cm^{-2}
IV	9/2/56	6.5	1 or $2/P^{1.5}$	...	$0.7/P$	...	...
V	11/9/56	8.3	1 or $2/P^{1.5}$	...	$0.75/P$	...	...
VI	1/21/57	17.0	1.2	...	$2.0/P$	...	...
VII	8/29/57	12.5	1.5	$1/P + 3.5$	$1/P + 3.5$	1.4	2.1
IX	10/22/57	8.2	1.5	$1/P + 4.0$	$1/P + 4.0$	0.8	3.1
X	11/26/57	6.8	2.0	$1/P + 1.0$	$1/P + 1.0$	1.2	1.4
XI	12/19/57	9.2	2.0	None		...	...
XII	2/11/58	5.2	2.5	$1/P$	$1/P$	1.7	1.1
XIII	3/25/58	11.1	2.5	$1/P + 3.0$	$1/P + 3.0$	1.1	2.0
XIV	7/8/58	7.8	2.0	$1.1/P$	$0.8/P$	1.1	1.9
XV	8/17/58	5.8	1.5	$0.5/P + 3.0$	$0.5/P + 3.0$	1.0	1.6
XVI	8/24/58	9.1	2.0	$1/P$	$1/P$	1.1	2.4
XVII	1/9/59	5.0	1.5–2.0	...	$0.6/P$	0.9	1.2
XVIII	5/12/59	14.8	1.5	...	$1.7/P$	1.4	2.5
XIX a	7/11/59	9.9	1.5	...	$1.0/P + 2.0$	0.7	4.0
b	7/15/59	14.5	2.5	...	$2.2/P$	1.3	3.1
c	7/17/59	13.5	2.5	...	$2/P + 1.0$ or $2.2/P$	1.7	2.1
XX	8/20/59	6.8	2.5	...	$0.9/P + 1.0$	0.4	4.0

* For some events rigidity dependence is of form $C_F/P + k_F$.

† Minimum σ based upon error assigned to magnitudes of the decreases, $\pm 0.5\%$.

where $dN(P, x, t)/dP$ is the differential counting rate of a nucleonic or mesonic detector at the time t just before the start of the F event. $N(P_c, x, t)$ is the integrated counting rate of the same detector. The quantity $\Delta N_F/N$ can be evaluated in the same way as for the long-term change. The details of these calculations are given in Appendix A.

For some events (5) should be changed by addition of a constant term:

$$\frac{\Delta j}{j} = -\{C(t_F)P^{-\gamma_F} + k_F\} \qquad (8a)$$

where k_F for the primary spectrum itself has not been evaluated for the F-events. Such an additional modulation represents a uniform attenuation of the primary spectrum. The effect of k_F can be estimated by considering an F event occurring when the long-term modulation constant $C(t) = 1.5$ and $C(t_F) = 1.0$. For nucleonic detectors at 680 g cm^{-2} we have the following calculated decreases:

P_c(BV)	$1/P$ modulation, %	Total, % $k_F = 1$	Total, % $k_F = 3$
15	2.5	3.5	5.5
5	6.9	7.9	9.9
1	9.4	10.4	12.4

Clearly the effect is greatest for stations with high cutoff rigidities.

In treating the individual Forbush decreases we have fitted the data from stations with different cutoff rigidities to the smooth curve calculated from (10), after determining the quantity $dN(P, x, t)/dP$ from (7) and (1). In this analysis we have selected data from as nearly world-wide a distribution of nucleonic detectors as possible. Data from nucleonic detectors have been used for two reasons: (1) simplicity and accuracy of corrections for changes in atmospheric conditions; and (2) the effective primary spectrum lies in the rigidity range most sensitive to changes in geomagnetic cutoff rigidities. Con-

siderable care has been taken to ensure that the data selected are reliable.

The stations have been separated into two groups: sea level and mountain elevations. Since not all the stations at mountain elevation are at the same atmospheric pressure, corrections have been applied to reduce the data to the same elevation. Only the quantity $\Delta N/N$ has been corrected for altitude. The details of these corrections are given in Appendix C. The elevation to which the data have been reduced is 3000 m above sea level or a 'standard atmosphere' pressure of about 700 g cm^{-2}. This pressure is very close to that used by *Webber and Quenby* [1959] for evaluating the differential response curve. The resulting corrections are in reasonable agreement with those deduced by *McCracken and Johns* [1959]. These corrections make an appreciable difference for the stations at Mt. Washington (1900 m) and Sulfur Mt. (2280 m). In the calculation of the altitude correction, the assumption was made that the energy spectrum j_0 measured in 1954 has been modulated as follows

$$j(P, t) = j_0(P, t_0)\left\{1 - \frac{1}{P}\right\}$$

The results are, however, insensitive to the form of the modulation (Appendix C).

The best form of the modulation given by (8) or (8*a*) was determined by minimizing the difference between the observed and calculated decreases for all stations. The value so determined should also agree with that from visual inspection of the data plots. The values of σ, the standard deviation of the observed from the calculated decreases, are given in Table 2. We do not believe that the magnitude of the decrease can be determined better than ± 0.5 per cent. This error is indicated on all curves of the intensity decrease versus cutoff rigidity. Thus the minimum value of σ to be expected is $\pm$ 0.5 per cent. σ was always compared with σ_s, the standard deviation from the mean of the observed decreases for all stations, which is equivalent to assuming the F event is rigidity independent. A summary of the rigidity dependence for the F events is presented in Table 2.

If (10) is used to determine the latitude dependence of the F event, some upper rigidity limit must be placed upon the modulating mechanism. We have assumed this limit to 1… $\gtrsim$ 100 BV. In fact, if the rigidity dependence … the modulation for an F event is $1/P$ and f… the long-term variation $2/P$, (10) yields valu… of 2.3 and 2.5 per cent for upper rigidity limi… of 50 and 100 BV respectively, considering a nu… cleonic detector at 680 g cm^{-2} elevation wit… vertical cutoff rigidity of 15 BV. Unless th… value of γ for the rigidity dependence is < … the fractional change of intensity for nucleon… detectors at the equator does not depend to… greatly upon the upper rigidity limit.

In this analysis of the individual F events w… have defined the magnitude and onset of th… decrease as follows. The magnitude, expressed a… a per cent is

$$\frac{\Delta N}{N} = \frac{N_0 - N}{N_0} 100$$

where N_0 is the average intensity for at least 1… hours before the onset of the decrease, N is th… lowest bihourly average during the main phas…

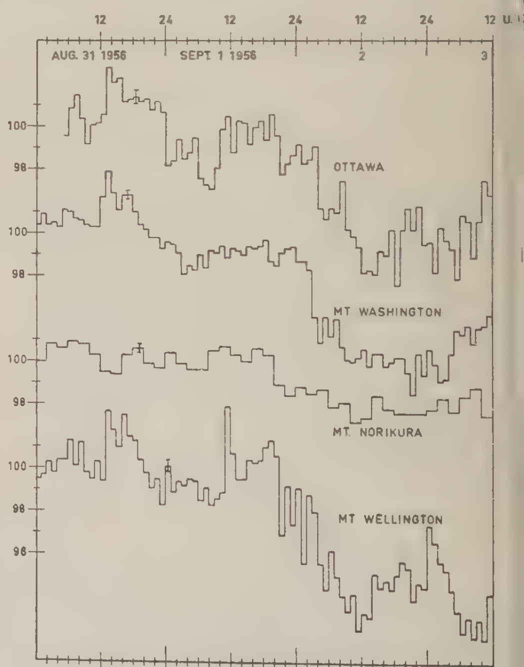

Fig. 1. Hourly average nucleonic intensity at Ottawa, Mt. Washington, Mt. Norikura, and Hobart during the Forbush decrease, September 2, 1956. The data are normalized to 100 per cent for the period 1300 on August 31, 1956, to 1200 on September 1. Twice the statistical error (2σ) for each station is indicated.

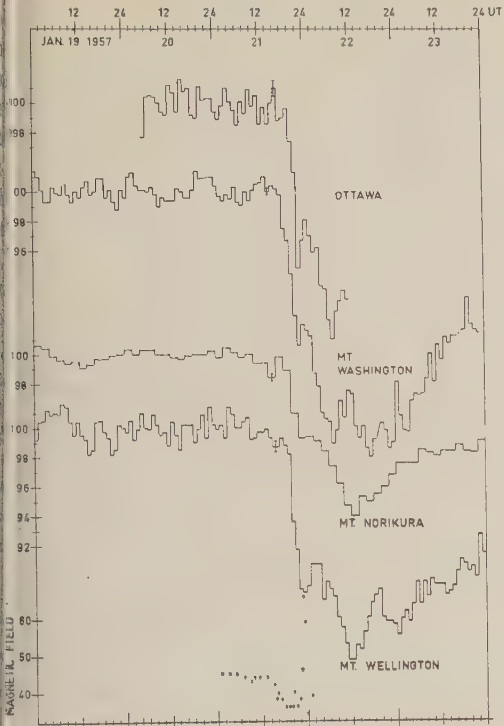

Fig. 2. Hourly average nucleonic intensity at Ottawa, Mt. Washington, Mt. Norikura, and Mt. Wellington on January 21, 1957. 100 per cent represents the average for the period from 0000 on January 20 to 1200 on January 21. 2σ is shown for each station. The horizontal intensity of the geomagnetic field at Fredericksburg, Maryland, is plotted for comparison. The scale for the magnetic field is 10 units = 175γ.

of the decrease. Any differences in the time of this minimum are noted in the consideration of the individual events. The onset of the decrease is the last hour before the main phase commences as indicated by a decrease in the counting rate of at least 2σ, where σ is the statistical standard deviation. This method is clear from an inspection of Figure 3.

1. *Events I–VI.* The *F* events of November 19 and December 6, 1955, commenced about 3 hours after magnetic storms. For both these events we have data available only from Mt. Washington and Mt. Norikura nucleonic detectors. The ratio of the decrease at Mt. Washington to that at Mt. Norikura is ~ 4, much greater than it was later in the solar cycle. If we assume that the full galactic cosmic-ray flux was present, then this indicates a steep rigidity dependence of $P^{-1.5}$.

The decrease of March 3 was also preceded by a magnetic storm, and the ratio of the decrease at Mt. Washington to Mt. Norikura was ~ 4, again indicating a fairly steep rigidity dependence.

The *F* event on September 2, 1956, for the stations at Ottawa (supplied by Dr. D. C. Rose), Mt. Washington, Mt. Norikura (supplied by Dr. Miyazaki), and Hobart (furnished by Dr. A. G. Fenton), is plotted in Figure 1. From these data we have estimated the rigidity dependence to be $0.7/P$. It is interesting to note that the increase presumably associated with the flare on August 31 is clearly evident at the high latitude stations [*McCracken*, 1959]. Another interesting feature of this decrease was the remarkable tracking of the horizontal component of the geomagnetic field and the cosmic-ray intensity changes. The magnetic storm started 30 minutes before the *F* event and the fluctuation of the field was completed when the cosmic-ray intensity reached a minimum. We do not know whether any significance can be attached to these rare events.

The *F* event on November 9, 1956 was unusual in that after this drop the low-energy portion of the primary radiation was reduced considerably. This has already been discussed [*Lockwood*, 1958]. The magnetic disturbances associated with this decrease were not unusual. A rather large anisotropy was present as indicated by the amplitude of the daily variation following the event.

On January 21 the first large and rapid decrease occurred. In Figure 2 representative neutron data are plotted. A difference in onset time of about 1½ hours is apparent for stations at practically the same location. The altitude dependence of the magnitude of this decrease is large, indicative of a primary spectrum which is not so hard as later in the solar cycle. From the magnetic data it can be seen that the change in the slope of the cosmic-ray intensity curve occurs at the time of a large magnetic pulse. Occasionally such tracking of the cosmic-ray variations with the geomagnetic field does occur. It should be noted that the precise onset time assigned to Mt. Washington was determined from 10-minute average counting rates, which are not shown.

2. *Event VII.* August 29, 1957. The nu-

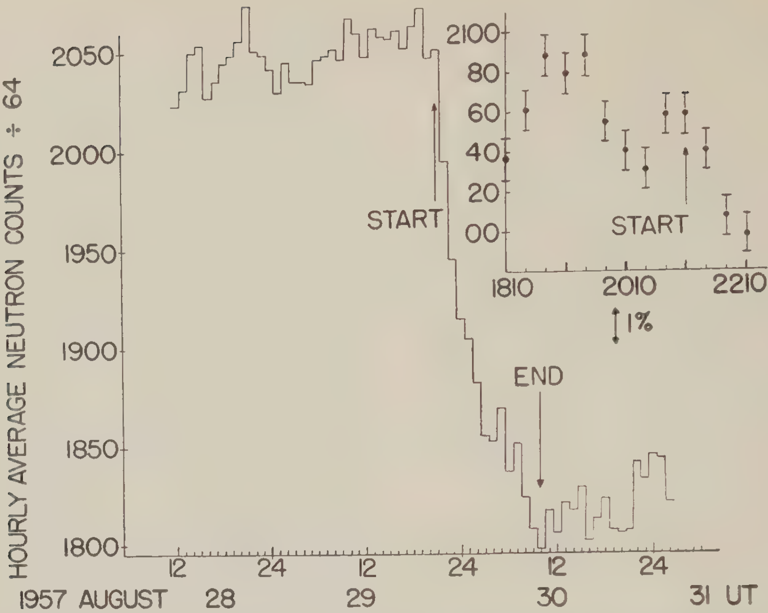

Fig. 3. The hourly average nucleonic intensity at Mt. Washington during the intensity drop of August 29, 1957. The 20-minute average counting rates near the onset are shown in the insert.

cleonic intensity at Mt. Washington during the decrease on August 29, 1957, is plotted in Figure 3. The dependence of the magnitude of the decrease upon the vertical cutoff rigidity is shown in Figure 4. Measurements of the change in the primary proton and alpha fluxes during the event were made by *Meyer* [1959]. He found that there was no significant rigidity dependence below ~ 4 BV, which is consistent with the curve shown in Figure 4. A comparison of the observed and calculated decreases based upon daily average intensities is shown in Table 3. The calculated decrease in the primary flux is, however, too large. If the modulation of the primary flux $\leq$ 2.5 BV is assumed to be rigidity independent, the decrease is 16 per cent (shown in parentheses, column 5, Table 3). The best agreement is given by a modulation of the form $1/P + k_F$, where k_F is 3.5 per cent for a mountain elevation nucleonic detector.

There does appear to be a slight difference in the magnitude of the decrease and the onset time with longitude. Those stations located so that local noon was also the time of the minimum intensity tended to exhibit the smallest decrease. At sea level this difference was ~ 1 per cent. Out of the total 28 stations considered, 20 had an onset time (using bihourly counting rates) at 2000 UT and 7 had an onset time of 2200 UT. These 7 stations all were located in the geomagnetic longitude interval 280°–05°E or 30°–70°W with respect to the earth-sun line. There were no differences greater than ±2 hr in the time of the minimum intensity. If a precursory increase occurred, it can not be separated from the expected maximum in the daily variation at ~ 1800 UT [*Lockwood,* 1958]. A difference in the shape of the decrease was evident at Weissenau and Zugspitze, indicative of local anomalies. The comparison of the variations in the nucleonic intensity at ground elevation with the high altitude primary radiation during this event [*Anderson,* 1958] has been previously reported [*Lockwood,* 1958].

3. *Event VIII.* September 13, 1957. This event has been previously reported [*Yoshida and Wada,* 1959; *Lockwood,* 1960]. This was a very unusual and unique *F* event, the duration of the decrease being $\gtrsim$ 2 hours. At some stations it was followed by a rapid rise to an intensity greater than before the decrease. There is no simple latitude or longitude dependency of the magnitude of the decrease. Indeed there is no apparent decrease for low-latitude stations.

TABLE 3. Comparison of the intensity decrease for nucleonic detectors at 680 g cm^{-2} based upon daily averages (100% on August 16, 1957) and for the primary proton flux [*Meyer*, 1959] with that calculated from a 1.5/*P* long-term modulation and 1.5/*P* or 1/*P* + 3.5% for the *F* event. P_c = vertical cutoff rigidity. The figure in parentheses is for rigidity independence below 2.5 BV.

Station	P_c, BV	Observed decrease %	Calculated decrease, % 1.5/*P*	Calculated decrease, % 1/*P* + 3.5%
Huancayo	15	5.7	3.8	6.0
Norikura	9.6	7.0	5.8	7.3
Sacramento Peak	4.7	7.9	10.5	10.5
Zugspitze	3.6	10.0	12.6	11.8
Climax	2.7	12.7	13.3	12.3
Sulfur Mt.	1.0	13.8	14.0	12.9
Mt. Washington	1.0	14.0	14.0	12.9
Primary proton flux	0.6	13.0	30	24 (16)

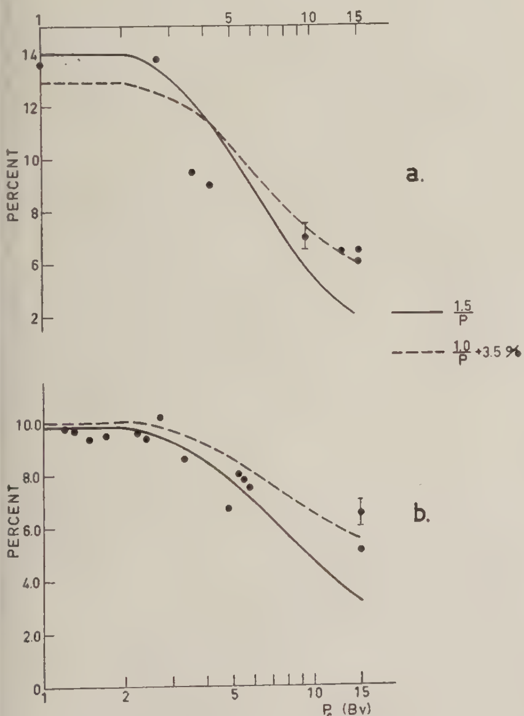

Fig. 4. Decrease in nucleonic intensity as a function of vertical cutoff rigidity during the Forbush decrease August 29, 1957, for stations at mountain elevations (*a*) and sea level (*b*). Long-term modulation is 1.5/*P*.

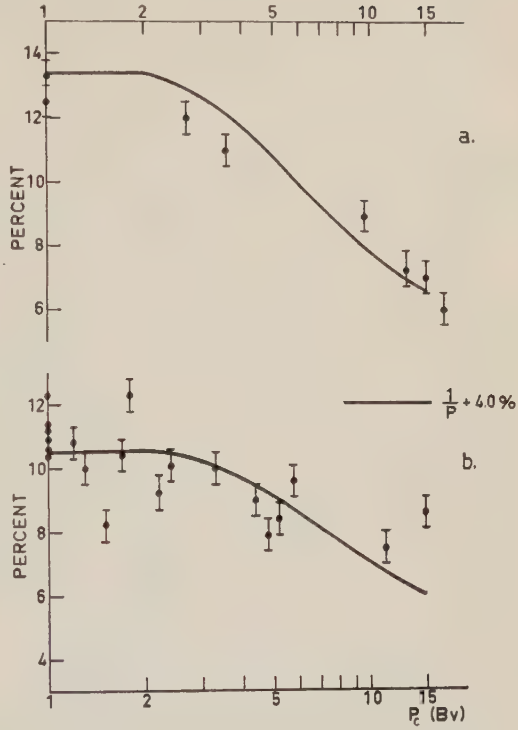

Fig. 5. Magnitude of the decrease in nucleonic intensity versus vertical cutoff rigidity during the decrease October 22, 1957, for stations at mountain elevations (*a*) and sea level (*b*). Long-term variation is 1.5/*P*.

Indications are that the decrease was confined to a region from 290°–90°E in longitude and 52°–90°N in latitude (geomagnetic). The onset of the sudden commencement magnetic storm preceded the *F* event by 1 hour, and the main phase of the magnetic storm was centered about the rapid and temporary recovery following the initial decrease. This decrease occurred while the intensity was rapidly recovering from the August 29 drop, and the amplitude of the daily variation was unusually large. In addition, there were five other heavy geomagnetic storms during September. These features complicate the analysis.

4. *Event IX*. October 21, 1957. The long-term variation just prior to this event was 2/*P* as given by (5), and the rigidity dependence of this event, shown in Figure 5, is of the form 1/*P* + k_F, where k_F is 4.0 per cent for nucleonic detectors at sea level and mountain elevations. The latitude dependence is observed to the rather flat.

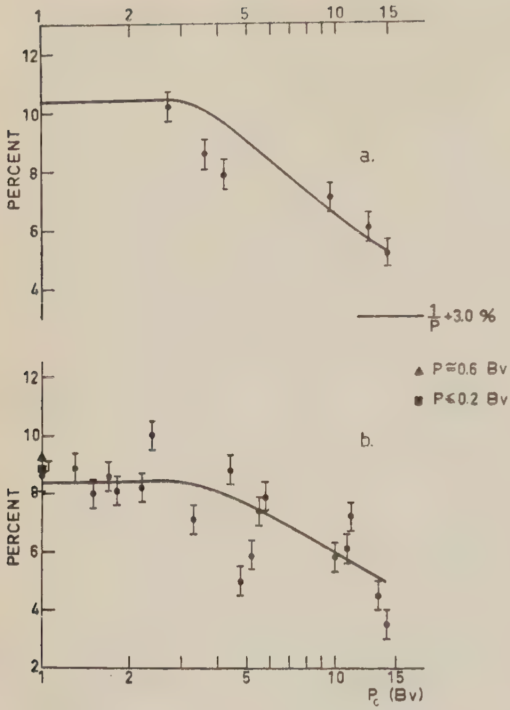

Fig. 6. Magnitude of the decrease in nucleonic intensity as a function of vertical cutoff rigidity during the drop of March 25, 1958, for stations at mountain elevations (a) and sea level (b). Long-term variation is $2.5/P$.

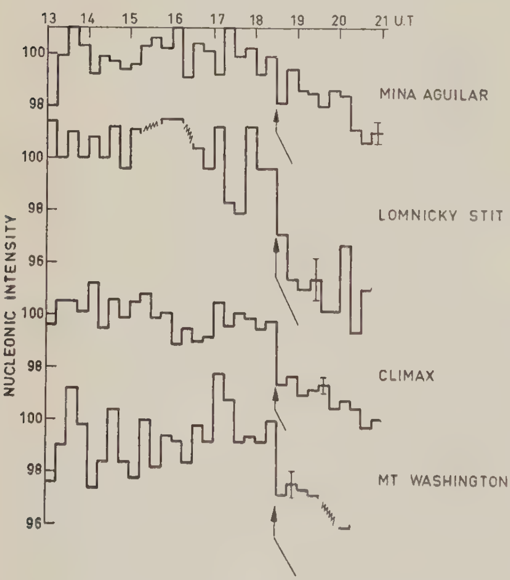

Fig. 7. 15-minute average counting rates near the onset of the decrease of March 25, 1958. Arrow indicates onset time. All data were normalized. 2σ is shown for each station.

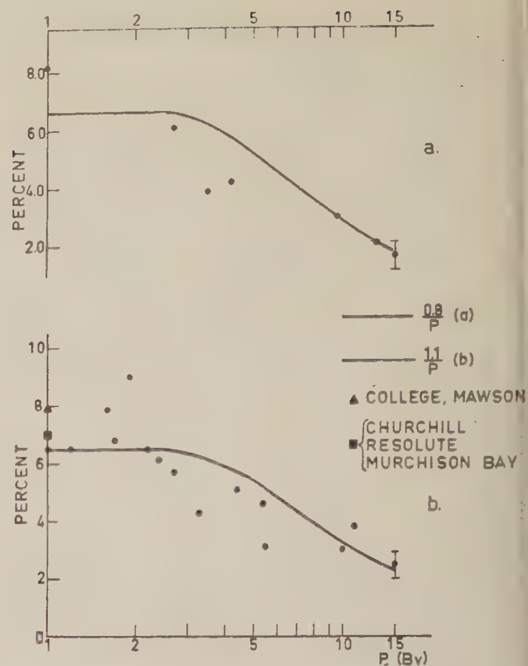

Fig. 8. Dependence of the magnitude of the decrease July 8, 1958, upon cutoff rigidity for neutron monitor stations at mountain elevations (a) and sea level (b). The long-term variation is $2/P$.

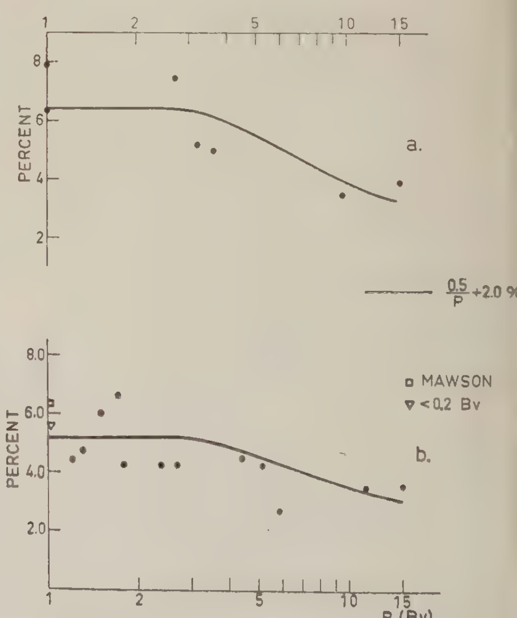

Fig. 9. Decrease in nucleonic intensity versus cutoff rigidity on August 17, 1958, for stations at mountain elevations (a) and sea level (b). The long-term variation is $1.5/P$.

Out of a total of 30 stations, 25 stations observed the decrease starting at 2300–2400 UT, 3 stations (Mt. Norikura, Hobart, and Yakutsk) at 1800–2000 UT, and 2 stations (Climax and Berkeley) at 0200–0400 UT, October 22. *Fenton, McCracken, Rose, and Wilson* [1959] have reported differences in onset times for this decrease. Those stations which did not exhibit the earlier onset times observed an intensity maximum of 1–2 per cent in the afternoon (local time) on October 21. The superposition of this maximum and the Forbush decrease (commencing at 2400 UT, October 21) could produce a significant dip in the intensity at about 1800 UT, which might lead to different interpretations of the onset.

5. *Event X*. November 26, 1957. This was a much smaller event, and the effects of the superimposed daily variations made the decrease look different at many stations. At most stations the initial drop at 0400 UT was followed within 8 hours by a temporary recovery and then a second decrease (see Fig. 10). A similar variation occurred on February 11, 1958 [*Lockwood*, 1960]. This temporary recovery was confined to a geomagnetic longitude interval 330°–105°E, quite independent of latitude. In the region 315°–330°E longitude a rather sharp transition in shape of the decrease takes place. The time (UT) of the maximum of this temporary recovery is independent of the geographic longitude of the station. We believe that this temporary recovery is associated with a spatial anisotropy and does not represent an enhanced daily variation. There also appeared to be some local differences, a feature which is not unusual for these smaller F events.

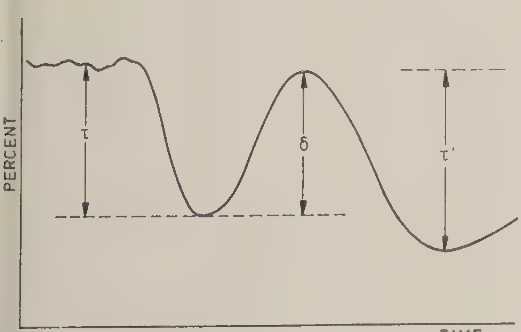

Fig. 10. Typical variation of the nucleonic intensity during the Forbush decrease August 17, 1958.

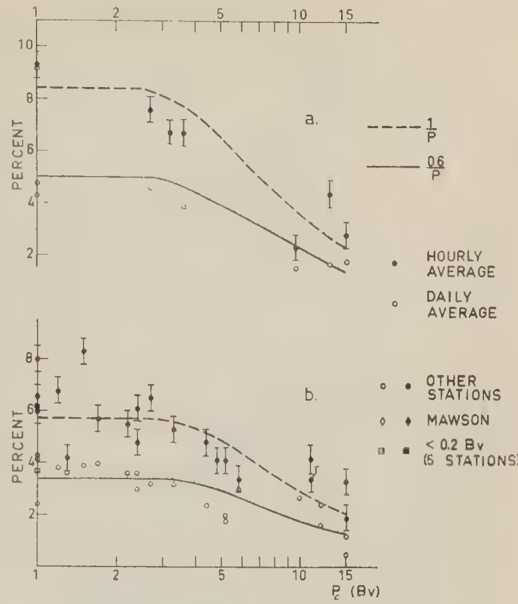

Fig. 11. Decrease in nucleonic intensity as a function of vertical cutoff rigidity August 24, 1958, at mountain elevations (*a*), and sea level (*b*), based upon daily and hourly average counting rates. Long-term variation is $2/P$.

6. *Event XI*. December 19, 1957. The magnitude of this decrease is rigidity independent in the region to which nucleonic detectors respond. There were no unusual magnetic disturbances prior to this event and no polar-cap absorption of cosmic radio noise. Large local differences in the magnitude and shape of the decrease were evident.

7. *Event XIII*. March 25, 1958. The latitude dependence of the magnitude of this decrease at sea level and mountain elevations is shown in Figure 6. The onset of this decrease was very sharp, as can be seen from the 15-min average neutron counting rates at Mina Aguilar, Lomnicky Stit, Climax and Mt. Washington plotted in Figure 7. The onset for these stations is 1830 +05, −15 UT. Only those stations in the geographic longitude range 150°–225°E showed an earlier onset of about 2 hours, but these are so located that the minimum in the daily variation occurred simultaneously with the onset of the F event. The rate of decrease at the beginning of the drop was greater than 1 per cent hr^{-1}. The minimum intensity was recorded within 18 hours after the start, although at some stations the decrease phase was completed in 8 hours and the

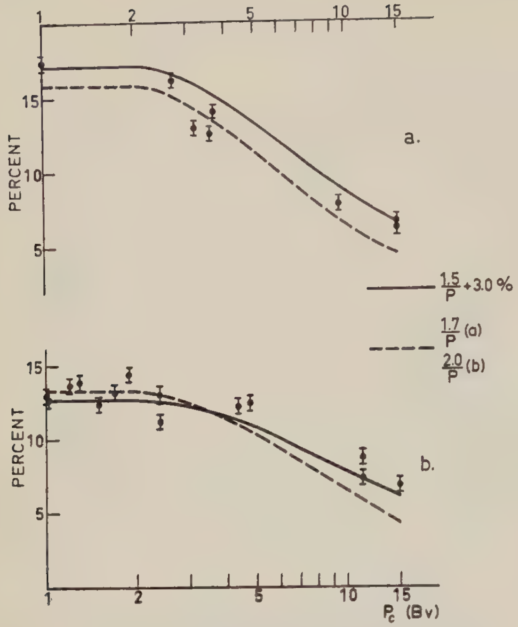

Fig. 12. Decrease in nucleonic intensity versus cutoff rigidity May 12, 1959, at mountain elevations (a) and sea level (b). Long-term variation is $1.5/P$.

intensity then remained depressed for an additional 12 hours. The phases of the onsets of the geomagnetic storm, polar-cap absorption, and the F event can be deduced from Table 1. The high altitude observations of *Freier, Ney, and Winckler* [1959] show that the primary flux was depressed 23 per cent on March 26 at about 1300 UT. If we assume the long-term modulation of the primary flux to be $2.5/P$ and during the F event to be $1.7/P$, the calculated change in the primary flux for $P_c \sim 1$ BV is 23 per cent. However, the latitude dependence observed at 680 g cm^{-2} and sea level indicates a flatter modulation of $1/P + k_F$, where k_F is 3.0 per cent. Such a modulation would reduce the primary radiation above $\sim$ 1 BV about 18 per cent, in reasonable agreement with observation.

8. *Event XIV*. July 8, 1958. The latitude dependence of the magnitude of this decrease is plotted in Figure 8. Most stations observed the onset of this variation at 0800–1000 UT, with the earliest onsets in the region of geomagnetic latitudes 20°–80°N and longitudes 240°–360°E and the latest in the region 50°–55°N and 70°–100°E. The shape of the decrease varied from station to station, which is usually the case for smaller decreases.

9. *Event XV*. August 17, 1958. From Figure 9 we can see that the magnitude of the decrease was essentially independent of rigidity. The onset of the decrease was at 0600 UT for 27 of the 32 stations considered. The other 5 stations did not show any regular dependence of onset times upon latitude or longitude. Many stations observed a decrease of the shape shown in Figure 10. At these stations (20 out of 32) the temporary recovery, indicated by T, occurred at the same universal time within 1 hour. If we define $R = \delta/\tau$, we observe that the magnitude of R has a regular dependence upon latitude and longitude, indicative of a spatial anisotropy. A similar feature was noted in the decrease on November 26, 1957. For February 11, 1958 it has been discussed previously [*Lockwood*, 1960].

10. *Event XVI*. August 24, 1958. The rigidity dependence of this decrease is shown in Figure 11. The same form of the rigidity dependence is obtained either from the bihourly or the daily average counting rates, but the magnitude of rigidity dependence is greater when the analysis is based upon bihourly averages. For rapid decreases a considerably smaller rigidity dependence is generally found if the analysis is based upon 24-hour average intensities. (This was not the case, however, for the F event on August 29, 1957, owing to the particular onset time and broad minimum in the intensity.) There was a spread of about 6 hours in the onset times. The data suggest that the earliest onset occurred for stations located near the Greenwich meridian with the onset increasing almost linearly with geographic longitude east of the station. A large daily variation was apparent after the main phase of the decrease. The analysis by *Parsons* [1960] of the daily variation of the nucleonic component indicates that this was a highly disturbed month. A daily variation was also detected at high altitudes [*Anderson, Arnoldy, Hoffman, Peterson, and Winckler*, 1959].

11. *Event XVII*. January 9, 1959. The rigidity dependence and onset times of this sudden drop were analyzed only for mountain elevation stations because of the small magnitudes. The long-term variation preceding the event could be described by a $1.5/P$ modulation, and the F event by an $0.5/P$ modulation. The standard deviation of the observed from the calculated

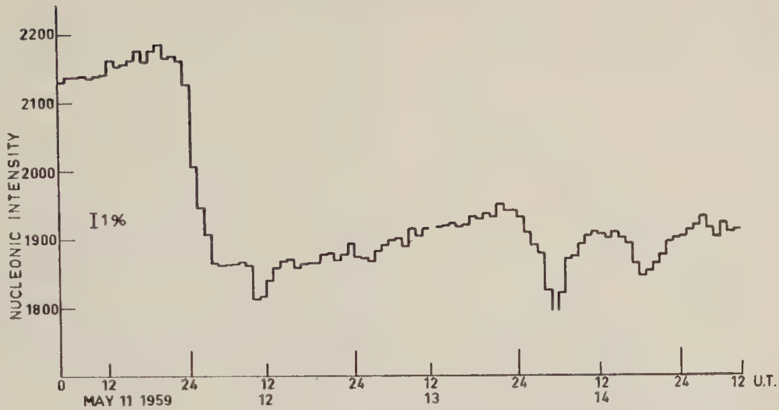

Fig. 13. The nucleonic intensity at Mt. Washington during May 1959. 2σ is $\sim$ 0.5 per cent.

percentage decreases in such a case is not significantly smaller than for no rigidity dependence. Some differences in onset times were observed. Those stations with an earlier onset ($\sim$ 4–6 hours) experienced a very gradual onset of the decrease. At those stations with low cut-off rigidities the rate of decrease was very rapid, e.g., at Mt. Washington $>$ 2.5 per cent hr^{-1}.

12. *Event XVIII.* May 12, 1959. The rigidity dependence for this event has been evaluated from the latitude dependence of the magnitude of the decrease as plotted in Figure 12. The magnitude of the decrease for stations with $P_c > 10$ BV is greater than calculated for a C_F/P modulation. Since the upper limit on the rigidity dependence is reasonable and the long-term variation is quite certain, it is impossible to account for the difference on this basis. We believe that this indicates the rigidity dependence should be given by $C_F/P + k_F$ where k_F is a constant.

The onset times ranged from 2200 to 0200 UT. The earliest onset times were recorded at those stations located on the opposite side of the earth from the sun and the distribution of onset times was roughly symmetrical with respect to the earth-sun direction.

From the plot of the nucleonic intensity at Mt. Washington shown in Figure 13, there is no enhancement of the daily variation until after a second sudden drop of intensity on May 14. The differences in the onset times for this second event followed the same pattern as for the first. The magnitude of the second decrease was dependent upon the cutoff rigidity of the station. The exact dependence upon P is uncertain because at high cutoff rigidities the magnitude was very small. This drop seemed much greater at stations with low cutoff rigidities [*Manzano, Roederer, and Santochi,* 1960.]

We have compared the nucleonic intensity data from Mawson and Resolute, two stations situated where the focusing effect of the geomagnetic field is considerable [*Astrom,* 1956]. The detectors at Mawson and Resolute track closely through the event, with the same onset time and magnitudes of 12.8 and 14.2 per cent respectively. This indicates that the modulation mechanism must operate over a large volume of space.

Since the magnitude of the decrease for neutron monitors at mountain elevations was so large, we can follow in detail the recovery from the main phase. The nucleonic intensity at Mt. Washington recovered linearly with time, provided that we start reckoning time from 2 days after the main decrease and note that a small Forbush decrease occurred on May 25. The relative recovery rate for nucleonic detectors at 680 g cm^{-2} as a function of cutoff rigidity is shown in Figure 14. The relative recovery rate is the per cent change per day divided by the magnitude of the main phase of the decrease. From Figure 14 it is evident that higher rigidity particles returned earlier. The time dependence of the primary modulation is given by Figure 15. Ten days after the initial decrease, the magnitude was so small at stations with large cutoff rigidities that the rigidity dependence became uncertain. From a study of the long-term variation we know that the rigidity dependence is about $1.5/P$ by June 1, so that for $t > 15$ in Figure 15 the curve must intersect the horizontal

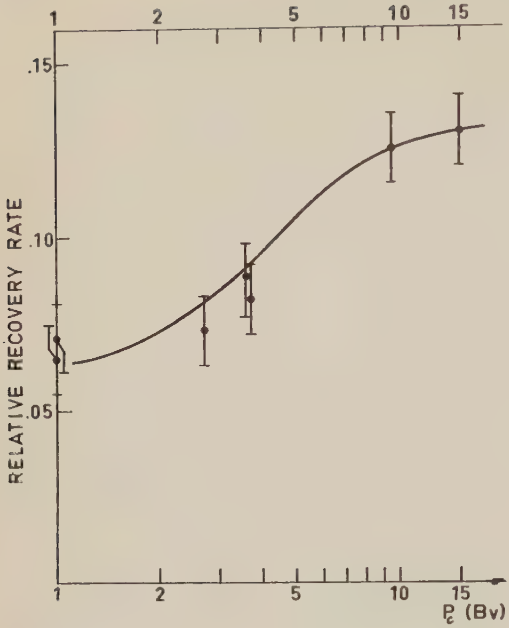

Fig. 14. The relative recovery rate for the nucleonic intensity at mountain elevations after the Forbush decrease May 12, 1959, as a function of cutoff rigidity.

axis. The ratio of σ_s/σ for all points plotted in Figure 15 is greater than 2.5, indicative of a high significance level for the form of the rigidity dependence.

In Table 4 we have compared the results obtained here with those of *McDonald and Webber* [1960] on the primary flux during this event. From the Mt. Washington nucleonic intensity we see that the proton flux on May 11 was probably the same as on June 2. The proton flux, calculated from the deduced rigidity dependence, is too small. The observed and calculated percentage decreases in the primary flux agree. Such agreement is not so good an indication of the correctness of the form of modulation as the absolute flux values. In the region below about 2.5 BV cutoff we cannot evaluate the rigidity dependence from nucleonic detectors, even at mountain elevations, since the effective primary spectrum decreases too rapidly in this rigidity interval. It appears that the rigidity dependence in the range 1.4 to about 3.0 BV should be $1/P$ for the long-term variation and about $1.5/P$ for the F event to give better agreement with primary flux measurements.

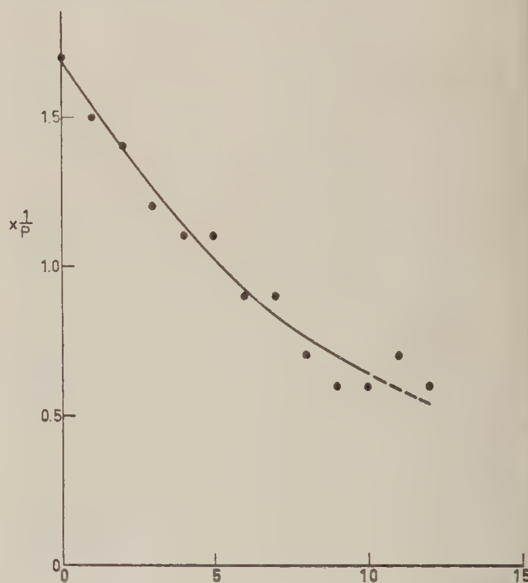

Fig. 15. The rigidity dependence of the primary modulation in the range $2 \leq P \leq 50$ Bv as a function of time after the main decrease May 12, 1959; $t = 0$ corresponds to May 14.

TABLE 4. Comparison of the Intensity Variations Recorded by Nucleonic Detectors at 680 g cm^{-2} and the Primary Proton Flux Measurements [*McDonald and Webber*, 1960] in May 1959

Date	Mt. Washington Nucleonic Intensity	Integrated Proton Flux $P > 1.4$ BV	Rigidity Dependence Deduced from Nucleonic Detectors		Calculated Proton Flux from Deduced Rigidity Dependence
			Long-term	F-event	
May 11, 1959	2104	...	$1.5/P$	...	900
May 16	1924 (−8.5%)	930 (−25%)	...	$1.4/P$	700 (−22%)
June 2	2101	1240	$1.5/P$	...	900

13. *Event XIX*. July 1959. The nucleonic intensity at Mt. Washington from July 11 to 18 is plotted in Figure 16. The nucleonic intensity remained constantly depressed for 3.5 days after the first decrease with no daily variation greater than 1 per cent. This was also observed at other stations. For a few hours on July 18 the intensity at Mt. Washington was about 60 per cent of the intensity in July-August 1954. The primary cosmic-ray beam at rigidities greater than 10 BV must have been considerably decelerated or attenuated, perhaps both, since 50 per cent of the counting rate of a nucleonic detector at 680 g cm^{-2} is derived from primaries above this rigidity.

The variations observed by nucleonic detectors at mountain elevations during these F events are shown in Table 5. We have made no attempt to analyze these events in detail since many observations have already been published [*Carmichael and Steljes*, 1959; *Wilson, Rose, and Pomerantz*, 1960; *Roederer, Santochi, Anderson, Cardozo, and Manzano*, 1960]. The rigidity dependence is the same as for the other F events when allowance is made for the 'long-term' variation occurring after the first Forbush decrease. Some uncertainty is attached to the magnitude of the third decrease owing to the rapid intensity fluctuations on July 17 (Fig. 16).

14. *Event XX*. August 20, 1959. The small but rapid drop on August 20 occurred while the cosmic radiation was recovering from the large decreases in July. From the nucleonic intensity measurements for 10 days prior to August 20 the long-term modulation of the primary spectrum is $2.5/P$, the same approximately as in March 1958. The rigidity dependence of the F event is shown in Table 6. The ratio σ_s/σ for a rigidity dependence of $0.9/P + k_F$ during the F event is > 5. The satellite measurements of *Fan, Meyer, and Simpson* [1960] at 6–7.5 earth radii during this decrease also fit the proposed form of modulation. The importance of these satellite measurements to the spatial extent of the modulating mechanism was noted by *Fan, Meyer, and Simpson* [1960]. A sudden commencement geomagnetic storm was reported by many stations [*Bartels*, 1960] at 0412 UT, the approximate onset time of the F event at Climax, Mt. Washington, and Sulfur Mt. The other stations (Huancayo, Mt. Norikura, and Zugspitze) experienced an early onset, partly explained by the existence of a large daily variation during this period.

4. Summary of Results

In summary we may state the following about the long-term variation and large Forbush decreases:

(1) The rigidity dependence of the long-term variation is adequately described by a modulation of the primary cosmic radiation given as $1–C(t)P^{-1}$, where $C(t)$ varies from 1 to 2.5. Very

TABLE 5. Nucleonic Intensity at Mountain Elevations during Forbush Decreases in July 1959

Station	P_c, BV	F-1 July 11: Onset UT	F-1: Decrease %	F-1: *Calculated Decrease, %	F-2 July 15: Onset UT	F-2: Decrease %	F-2: †Calculated Decrease, %	F-3 July 17: Onset UT	F-3: Decrease %	F-3: ‡Calculated Decrease, %
Huancayo	15	...	4.8	4.5	0800	6.3	5.1	1900	6.2	5.1
Mina Aguilar	13	1800	5.2	4.9	0900	7.4	5.8	1800	8.0	5.8
Mt. Norikura	9.6	1600	4.9	6.0	1200	6.2	8.1	1800	8.0	8.1
Zugspitze	3.6	1600	9.3	10.2	0800	13.8	15.6	1800	12.2	15.6
Climax	2.7	1600	9.8	10.9	0800	14.3	16.3	1800	15.1	16.3
Mt. Washington	1.0	1715±15	11.7	11.4	0815±15	17.2	16.3	1830	18.0	16.3
Sulfur Mt.	1.0	1600	11.0	11.4	0800	16.3	16.3	...	?	...

* Long-term modulation $1.5/P$ and for F-1 modulation $1/P + 2.0\%$.
† Long-term modulation $2.5/P$ and for F-2 modulation $2.2/P$.
‡ Long-term modulation $2.5/P$ and for F-3 modulation $2.2/P$.

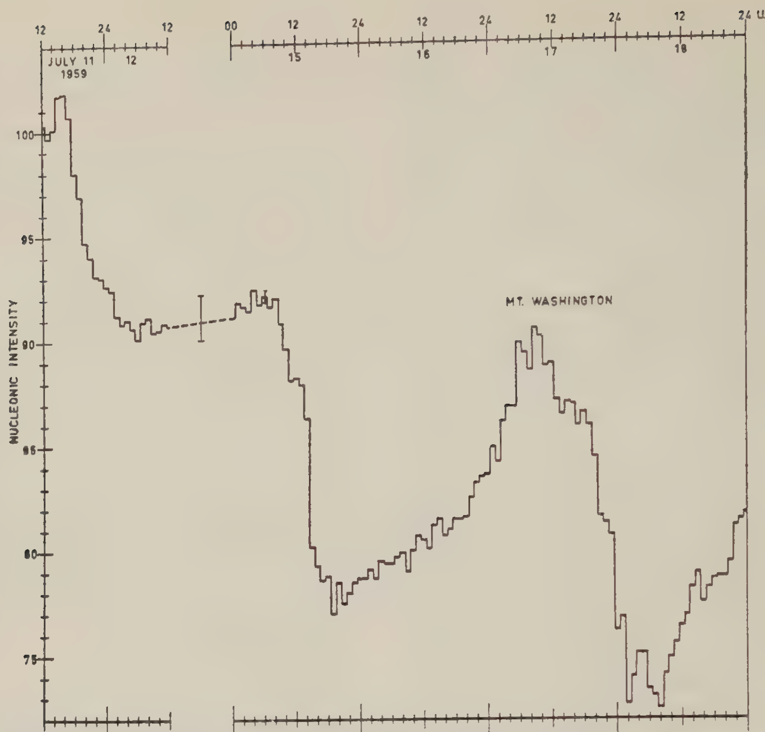

Fig. 16. The nucleonic intensity at Mt. Washington from July 11 to 18, 1959. The period from 1200 on July 12 to 0000 on July 15 was omitted and the variation of intensity, which is small is given by the extent of the vertical line. 2σ is indicated.

TABLE 6. Rigidity Dependence of the F Event August 19, 1959 (680 g cm^{-2} Pressure)

Cutoff Rigidity BV	Observed Decrease, %	Calculated Decrease $0.9/P + 1.0\%$
15	3.3	3.1
9.6	5.0	4.3
3.6	7.2	7.4
2.7	7.1	7.6
1.0	7.4	7.6
1.0	8.1	7.6
Primary Radiation*	15	14

* Observations of *Fan, Meyer, and Simpson,* 1960.

early in the solar activity cycle the modulation is steeper (Table 1).

(2) For F-events, the modulation of the primary radiation is given by $1-\{C(t_F)/P + k_F\}$, where k_F ranges from 0 to 4 per cent for nucleonic detectors at sea level and at mountain elevations and $0.6 \leq C(t_F) \leq 2.2$.

(3) In a few instances there was a systematic variation of the onset time with geographic longitude, but for the large, rapid decreases the onset times were the same to within 2 hours. When there is a systematic variation in onset times, it appears to be related to the existence of a large daily variation before the F event.

(4) From an inspection of the nucleonic intensity data at widely separated stations, it is evident that the primary radiation remains isotropic during the large F events.

(5) All the F events selected, representing the most asymmetrical and largest from 1954 to 1959, were preceded by a sudden commencement magnetic storm. For the larger events, except January 21, 1957, the cosmic-ray decreases followed the geomagnetic storm by $\leq$ 3 hours.

(6) Most of the decreases occurred 6–36 hours subsequent to a polar-cap absorption, Type III.

(7) We are unable to substantiate the existence of any precursory increase [*Lockwood,* 1958].

(8) For the Forbush decrease May 12, 1959, the relative recovery rate of nucleonic detectors

s much greater for stations with higher cutoff rigidities, indicating that the higher rigidity particles returned earlier. The rigidity dependence for the modulation during the recovery phase was $1-C(t)/P$, where $C(t)$ changed from 1.7 to 0.5 in 10 days after the main phase.

5. Concluding Remarks

Various physical models have been proposed to explain the long-term variation, Forbush decreases, and the smaller changes: the quasi-periodic 27-day variation and the solar daily variation. These models must also permit the propagation of protons along simple orbits to the earth during large solar flare events, such as on February 23, 1956, and in the more commonly observed low-energy solar proton events [*Anderson, Arnoldy, Hoffman, Peterson, and Winckler*, 1959]. We may compare the results obtained here, which are significant in a limited rigidity interval, with certain features of these models.

The rigidity dependence of the long-term variation does not agree with that calculated by *Parker* [1958] for the effect of a heliocentric shell of disordered magnetic fields in the presence of the solar wind. In particular, the observed variation is much greater than predicted at energies greater than 10 BV. The rigidity dependence of the F events (Table 2), changed to an energy dependence, is intermediate to the two cases of disordering considered by *Parker* [1958]. The rate of change with rigidity for the fractional reduction in the primary flux is also different. The calculations have not been extended, however, to rigidities $\geq$ 10 BV, an important region for these results. The observations of *Fan, Meyer, Simpson* [1960] that Forbush decreases are measured at 7.5 R_E tend to exclude such geocentric modulation mechanisms.

Hence, we must consider the effect upon cosmic rays of an ionized solar gas cloud or beam with dimensions comparable to the earth-sun distance. This type of beam was originally suggested by Alfvén. In considering the effects of such beams upon the cosmic radiation, the following features of the large decreases investigated here are important: (a) the primary radiation remained isotropic to a large extent; (b) a large fraction of the particles with rigidities up to 50 BV incident at the earth from all directions were decelerated by the 'beams,' with some attenuation due to scattering; (c) the rates of decrease were several per cent hr^{-1}; (d) nucleonic detectors at polar stations had similar decreases; (e) after some decreases there was no daily variation (e.g., July 11, 1959).

Calculations have been made on the expected variations in the cosmic-ray flux at the earth due to the decelerating action of the electric polarization field in the beam [*Alfvén*, 1954; *Brunberg and Dattner*, 1954], provided there is no turbulence. In this model we must assume a general although weak magnetic field between the sun and the earth, producing a general particle drift to prevent the acceleration of cosmic rays by the same electric field. Since we are concerned with deceleration by an electric field, the resulting spectral modulation is K/P, for $P >$ 2.5 BV, during an F event. The long-term modulation would similarly follow a $1/P$ rigidity dependence.

On the other hand, there probably is much turbulence within the gas cloud, and it is expanding as it travels from the sun to the earth. A model based upon such considerations, the 'diffusive deceleration' mechanism, was proposed by *Singer* [1958] to account for Forbush decreases. Essentially the cosmic rays are decelerated by a combined betatron action and inverse Fermi mechanism within the expanding and turbulent gas cloud ejected from the sun. Recent calculations [*Laster, Lenchek, and Singer*, 1960] show that the reduction of the cosmic radiation within the gas cloud as a function of time is

$$\frac{j(P, t)}{j_0(P)} = 1 - \frac{K_1(t)}{P} + \frac{K_2(t)}{P^2} - \cdots$$

where $j(P, t)$ and $j_0(P)$ are the primary differential rigidity spectra inside and outside the cloud. This agrees to the first order with the empirical form of modulation adopted in this study, a form originally suggested by *McDonald and Webber* [1959]. Two points should be considered. First, *Singer* [1958] proposed that the long-term variation might be due to the accumulative effect of such solar corpuscular emissions. If this is so, we would expect the rigidity dependence of the long-term and the transient variations to be the same. The 'long-term' modulating mechanism must operate, however, over a much bigger volume. Second, *Laster, Lenchek, and Singer* [1960] have pointed out that for larger magnetic fields in the cloud, the 'sweeping'

action of the cloud is important. We believe that this effect is the reason for the additional rigidity independent term necessary to account for the small rigidity dependence of some Forbush decreases.

From these results, we conclude that both the Forbush decreases and the long-term variation can be attributed to the effects of solar gas clouds or beams, containing either regular or turbulent magnetic fields. The isotropy observed during the Forbush decreases plus no necessity for making assumptions concerning the general solar magnetic field lead us to favor the 'diffusive deceleration' mechanism.

Acknowledgments. This investigation was made during a stay at the Royal Institute of Technology, Stockholm, Sweden. The author is very grateful to Prof. H. Alfvén and Dr. E. Brunberg for many stimulating discussions. Some suggestions made by Dr. W. R. Webber were of great assistance. The cosmic-ray data supplied by Dr. John Simpson, University of Chicago, Dr. Hugh Carmichael, Deep River, Dr. D. C. Rose, National Research Council, Ottawa, Dr. Yukio Miyazaki, Tokyo, and Dr. A. G. Fenton, Hobart, Tasmania, were invaluable to this study. The use of the data sent by many investigators to the World Data Center C, Stockholm, is gratefully acknowledged. Most of the data reductions and analyses were done by Messrs. C. Boghosian, L. Hubbard, and Miss M. Shea.

This research was supported by the National Science Foundation and the Geophysical Research Directorate, Air Force Cambridge Research Center.

Appendix A

Method for determination of the rigidity dependence of variations in the cosmic radiation. In section 2 the differential counting rate of a nucleonic or an ionization detector located at a depth x, at the time t, with a vertical cutoff rigidity P_c, due to particles arriving vertically in a very small solid angle at the top of the atmosphere is given by

$$\frac{dN_v(P, x, t)}{dP} = \sum_z S_z(P, x) j_z(P, t) \qquad \text{(A-1)}$$

where $j_z(P, t)$ is the differential primary rigidity spectrum in the vertical direction, and $S_z(P, x)$ is the specific yield function. If we assume the Gross approximation to be valid here (see section 2), then the counting rate of the nucleonic or ionization detector is

$$N(P_c, x, t) = \sum_z \int_{P_c}^{\infty} S_z(P, x) j_z(P, t)\, dP \cdot \left[2\pi\left(1 + \frac{x}{L}\right)^{-1}\right] \qquad \text{(A-2)}$$

From the available data on airplane and sea-level latitude surveys, *Webber and Quenby* [1959] have constructed the differential response curves for nucleonic detectors and ion chambers at various depths x in the atmosphere. In using these curves, it is convenient to replace equation A-2 by the following for any given depth x:

$$N(P_c, t) = \sum_{P_c}^{15} \frac{\Delta N(P, t)}{\Delta P} \Delta P + \int_{15}^{100} \frac{dN(P, t)}{dP}\, dP \qquad \text{(A-3)}$$

In this analysis ΔP is 1 BV and $dN(P, t)/dP$ can be approximated by a power law expression for nucleonic detectors. The second term in (A-3) represents the counting rate of a detector at the equator. An upper rigidity limit of 100 BV is a good approximation for nucleonic detectors.

If the variation in the primary rigidity spectrum is of the form [*McDonald and Webber*, 1959]

$$\frac{\Delta j}{j_0} = -C(t) P^{-\gamma} \qquad \text{(A-4)}$$

then the fractional change in the counting rate $N(P_c, t)$ is

$$\frac{\delta N(P_c, t)}{N} = \frac{-\sum_{P_c}^{15} C(t) P^{-\gamma}\left(\frac{\Delta N}{\Delta P}\right) \Delta P - \int_{15}^{100} C(t) P^{-\gamma}\left(\frac{dN}{dP}\right) dP}{\sum_{P_c}^{15}\left(\frac{\Delta N}{\Delta P}\right) + 100} \qquad \text{(A-5)}$$

The simplifying assumption is made that in the latitude sensitive portion of the rigidity spectrum, the variations are the same in the proton and alpha components and the contributions

from nuclei with $Z > 2$ are neglected [*McDonald and Webber*, 1959]. Therefore, we have

$$\frac{\delta N(P_c, t)}{N} = -C(t)\frac{\delta N'(P, t)}{N} - \frac{\beta}{\sum\left(\frac{\Delta N}{\Delta P}\right) + 100} \qquad \text{(A-6)}$$

The quantity $\delta N'(P_c, t)/N$ has no physical significance but is convenient for calculation. We may consider the two terms on the right hand side of the equation A-6 separately to evaluate the total change in counting rate of a detector located such that the vertical cutoff rigidity is P_c. This expression has been used to determine the long-term variation by finding the value of $C(t)P^{-\gamma}$ which best fitted the observed decreases.

To determine the rigidity dependence of the individual F events a variation of the form

$$\frac{\Delta j}{j} = -C(t_F)P^{-\gamma_F} \qquad \text{(A-7)}$$

is introduced (section 3). This modulation is superimposed upon the differential rigidity spectrum existing at the time t just prior to the onset of the F event. The primary rigidity spectrum during the main phase of the F event is then

$$j_F(P, t) = j(P, t)\{1 - C(t_F)P^{-\gamma_F}\} \qquad \text{(A-8)}$$

where $j(P, t)$ is given by (6), section 2. In the same manner as for the long-term variation, we may write

$$\frac{\delta N_F(P_c, t_F)}{N} = \frac{-\sum_{P_c}^{15} C(t_F)P^{-\gamma_F}\left(\frac{\Delta N'}{\Delta P}\right)\Delta P - \int_{15}^{100} C(t_F)P^{-\gamma_F}\left(\frac{dN'}{dP}\right)dP}{\sum_{P_c}^{15}\left(\frac{\Delta N'}{\Delta P}\right) + Q} \qquad \text{(A-9)}$$

$(\Delta N'/\Delta P)$ and (dN'/dP) are the differential response curves modulated by the long-term variation and Q is the total counting rate of a detector at the magnetic equator, which is now less than 100 owing to the long-term variation. We may write (A-9) in the form

$$\frac{\delta N_F(P_c, t_F)}{N} = -C(t_F)\frac{\delta N_F'(P, t_F)}{N'} - \frac{\beta_F}{\sum\left(\frac{\Delta N'}{\Delta P}\right) + Q} \qquad \text{(A-10)}$$

In the same manner as for the long-term variation, we determine the rigidity dependence of the F events by comparing the observed decreases with those calculated from (A-10) after the long-term variation has been properly evaluated.

Appendix B

Rigidity dependence of the long-term variation. To evaluate the rigidity dependence of the long-term variation, the results of which are shown in Table 2, section 2, we have used published data from airplane and balloon flights and the changes of intensity recorded by detectors located at ground elevations. Comparing these data, it is necessary to realize that the balloon flights and airplane latitude surveys provide '1 day' of data, generally not just preceding or during the main phase of an F event. Consequently, the general trend of the variations before and after the flights must be carefully examined. In this section we have collected the data which form the basis of the rigidity dependence shown in Table 2.

First, we have available the data from the Mt. Washington nucleonic detector for the period 1954–1959. In addition, data have been obtained from other cosmic-ray stations, principally those operated by Prof. J. A. Simpson, Dr. D. C. Rose, Dr. Miyazaki, Dr. S. E. Forbush, and Dr. A. G. Fenton. The data from these stations have enabled us to construct the curves shown in Figure B-1. (The data from the Zugspitze station have been supplied to the World Data Center at the Royal Institute of Technology, Stockholm, Sweden.) In determining the per cent decrease at Climax and at Huancayo, we assumed that the counting rate at Climax in July–August 1954 was 7000 and at Huancayo was 5400 [*Simpson*, 1958]. We normalized the data for Zugspitze in July 1957 to 81.5 per cent of 1954 counting rate. Second, a comparison of Mt. Norikura and Mt. Washington from 1954 to 1958 is shown in Figure B-2, along with the calculated variation for

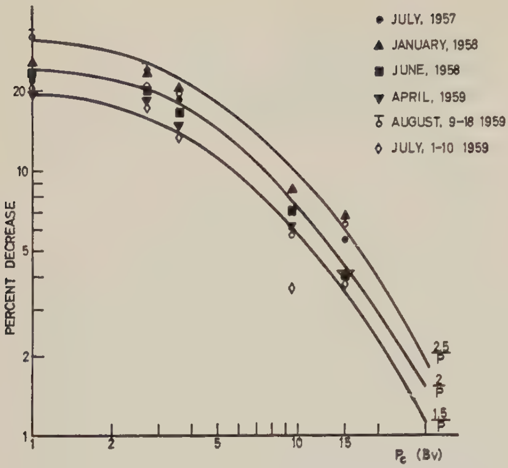

Fig. B-1. The long-term variation measured by nucleonic detectors at 680 g cm^{-2} versus cutoff rigidity. The curves represent the calculated decreases for different rigidity dependencies.

different forms of the modulating function $C(t)P^{-\gamma}$.

Third, the recently published results of *Meyer* [1959] have provided additional data on the long-term variation and the changes occurring during F events. These results are shown in Figure B-3. Here the change from August 16, 1957, to July 12, 1958, for mountain elevation stations

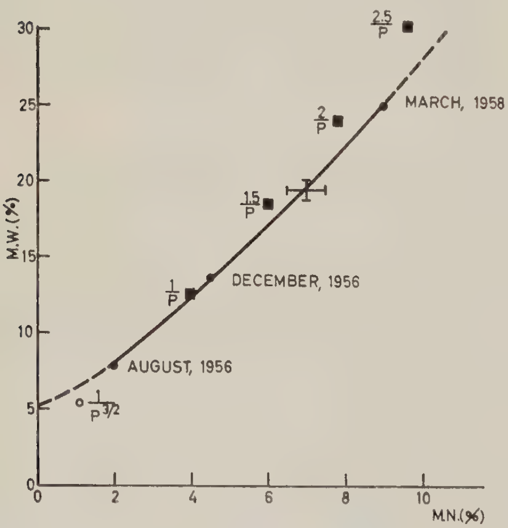

Fig. B-2. The percentage decrease of nucleonic intensity at Mt. Washington against that at Mt. Norikura from August 1956 to March 1958. A smooth curve has been drawn through the observed points. The calculated decreases for different modulations of the primary flux are plotted.

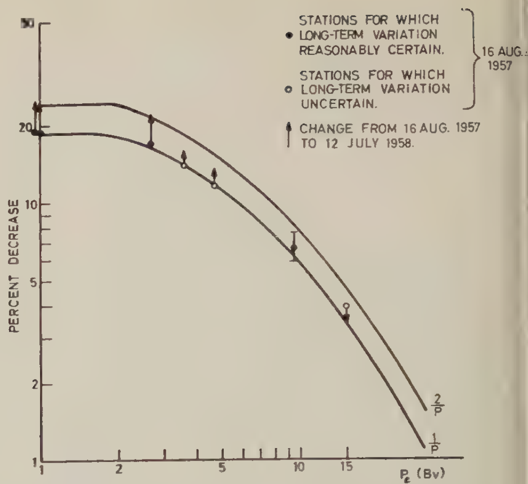

Fig. B-3. The long-term variation between August 16, 1957, and July 12, 1958, for nucleonic detectors at mountain elevations. The smooth curves represent the calculated per cent decrease, assuming a $1/P$ modulation on August 16, 1957, and $2/P$ on July 12, 1958.

only, is plotted. The decrease in the proton flux during this same period [*Meyer*, 1959] was (16 $\pm$ 2) per cent. If the primary flux on August 16, 1957 was given by

$$j(P) = j_0(P)\left\{1 - \frac{1.5}{P}\right\}$$

and on July 12, 1958, by

$$j(P) = j_0(P)\left\{1 - \frac{2.0}{P}\right\}$$

the decrease would be (20 $\pm$ 2) per cent. This is consistent with the observed decrease [*Meyer*, 1959].

Fourth, the latitude surveys at 312 g cm^{-2} made by *Meyer and Simpson* [1955, 1957] provide further data on the long-term variations. Comparison of flights made in 1954 and 1956 between latitudes corresponding to vertical cutoff rigidities of 4.7 and 1.0 BV (at 90°W geographic longitude) show that a modulation of the form $1/P$ would account for the change in latitude curve.

Fifth, *Storey* [1960] has published the results of a recent series of latitude surveys at an altitude corresponding to 475 g cm^{-2} along a geographic longitude of 147°E between latitudes of 10°S and 44°S made in July 1957 and July 1958. The results obtained are consistent with the assumption of a change in the modulation from $1.5/P$ to $2.0/P$.

TABLE B-1. Rigidity Dependence of the Long-Term Variation

Station	Detector	Pressure g cm^{-2}	Aug. 1–28, 1957 % Obs.	Aug. 1–28, 1957 % Calc. $1.5/P$	Jan. 1–31, 1958 % Obs.	Jan. 1–31, 1958 % Calc. $2.5/P$	Nov. 1–9, 1956 % Obs.	Nov. 1–9, 1956 % Calc. $2/P^{1.5}$	Jan. 1–20, 1957 % Obs.	Jan. 1–20, 1957 % Calc. $1.2/P$
Huancayo	IC	680	2.4	2.3	3.6	3.5	0.7	0.6	1.9	1.8
Huancayo	NM	680	5.5	3.9	6.7	6.1	...	...	...	...
Ottawa	MT	S.L.	5.0	3.8	5.0	5.8	1.8	1.5	3.2	2.9
Mt. Norikura	NM	680	6.0	6.0	8.5	9.6	2.0	2.3	5.0	4.8
Ottawa	NM	S.L.	19.5	13.0	22.0	20.0	9.5	6.5	14.0	9.5
Climax	NM	680	20.5	16.0	23.0	26.0	...	...	...	...
Mt. Washington	NM	820	19.0	18.5	26.0	30.0	8.8	10.8	16.9	14.8

Sixth, some representative data used to determine the long-term variation from ground elevation detectors are shown in Table B-1. The variations observed with ground level detectors have been compared with the measurements of the low-energy primary flux by *McDonald and Webber* [1959], and, generally, the observed variation in the low-energy primary spectrum is less than that deduced from ground-level detectors. This point is elaborated upon in section 4.

Appendix C

Altitude corrections for the observed variations in nucleonic intensity. Webber and Quenby [1959] have determined the differential response curves for nucleonic and ionization detectors at 1030 (sea level), 680 and 312 g cm^{-2}. According to the methods outlined in sections 2, 3, and Appendix A, we may calculate from these curves the expected variations in the counting rates of nucleonic detectors which result from changes in the primary rigidity spectrum. If we assume the primary rigidity variation to be given by $1/P$, the expected percentage decreases for nucleonic detectors as a function of atmospheric depth with different vertical cutoff rigidities are shown in Figure C-1.

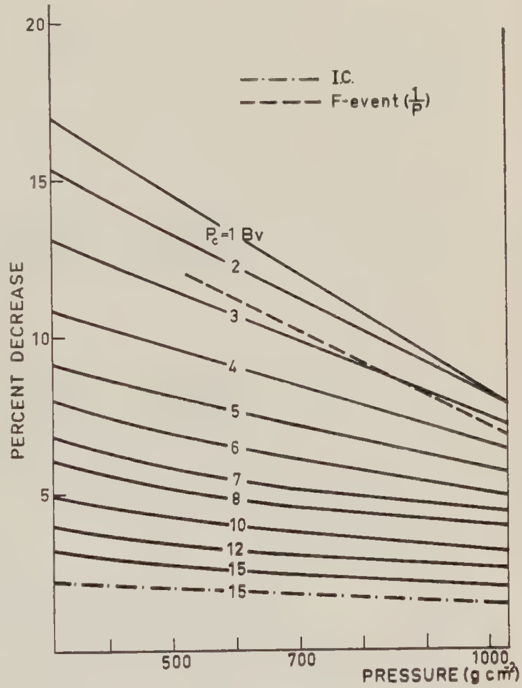

Fig. C-1. The percentage decrease for a nucleonic detector as a function of altitude with the vertical cutoff rigidity as a parameter. A $1/P$ modulation of the primary rigidity spectrum has been assumed. The altitude dependencies for an ion chamber with $P_c = 15$ BV and for a nucleonic detector with $P_c = 1$ BV during an F event are also shown.

TABLE C-1. Altitude Corrections for Nucleonic Detectors in the Range 600–800 g cm^{-2}, Expressed as a Per Cent/100 g cm^{-2}

P_c, BV	%/100 g cm^{-2}
1	9.7
2	8.8
3	8.2
4	7.6
5	7.0
6	7.2
7	6.6
8–15	6.3 (±0.3)

Since the atmospheric depths of the mountain stations vary from 600–800 g cm^{-2}, the corrections to be applied are listed in Table C-1. If we assume that during an F event a superimposed $1/P$ modulation of the primary spectrum occurs, the dotted curve in Figure C-1 indicates the altitude dependence of the magnitude of the decrease for a station with $P_c = 1$ BV. This correction is 9.6 per cent/100 g cm^{-2}, essentially

TABLE C-2. Corrections to be Applied to the Observed Variations at Mountain Stations to Reduce Them to a Standard Elevation of 3000 m or 700 g cm^{-2} (standard atmosphere)

Station	Altitude, km	Pressure, g cm^{-2}	% Correction
Zugspitze	2.96	720	—
Hobart	0.725	950	(−11)*
Mt. Norikura	2.84	730	—
Mina Aguilar	4.00	635	−4.7
Huancayo	3.40	680	—
Climax	3.40	680	—
Sulfur Mt.	2.28	790	+8.5
Mt. Washington	1.90	820	+12.5
Kodaikanal	2.44	470	+5.5
Pic du Midi	2.86	725	—
Alma Ata	0.81	940	(0)*
Makerere	1.20	920	+7.0(−5.0)*
Lomnicky Stit	2.63	735	+6.0

* The correction is too large for the station to be grouped with the other mountain stations and the percentage shown in parentheses represents the correction to reduce the data to sea level. Makerere is an exception.

the same as for the original $1/P$ modulation. Hence, the corrections given were used for both the long-term variation and the individual F events. Table C-2 presents the corrections for the particular stations used. No correction was applied if it was less than 0.5 per cent.

We have also determined from these differential response curves the approximate altitude correction for an ionization chamber located at the equator (P_c = 15 BV). An increase of ~ 20 per cent occurs between sea level (1030 g cm^{-2}) and Huancayo (680 g cm^{-2}).

McCracken [1959] has determined experimentally the corrections to be applied for both the long-term variation and transient decreases. The corrections given here are in agreement with his values for transient decreases.

References

Alfvén, H., *Tellus, 6,* 232, 1954.
Anderson, K. A., *Phys. Rev., 111,* 1397, 1958.
Anderson, K. A., R. Arnoldy, R. Hoffman, L. Peterson, and J. R. Winckler, *J. Geophys. Research, 64,* 1133–1147, 1959.
Astrom, E., *Tellus, 8,* 254, 1956.
Bartels, J., *J. Geophys. Research, 65,* 788–789, 1960.
Brunberg, E. A., and A. Dattner, *Tellus, 6,* 254, 1954.
Carmichael, H., and J. F. Steljes, *Phys. Rev. Letters, 3,* 392, 1959.
Dorman, L. I., *Cosmic-Ray Variations,* State Publishing House Technical and Theoretical Literature, Moscow, 1957. (Technical Document Liaison Office, Wright-Patterson Air Force Base.)
Fan, C. Y., P. Meyer, and J. A. Simpson, *Phys. Rev. Letters, 4,* 421, 1960.
Fenton, A. G., K. G. Fenton, and D. C. Rose, *Can. J. Phys., 36,* 824, 1958.
Fenton, A. G., K. G. McCracken, D. C. Rose, and B. G. Wilson, *Can. J. Phys., 37,* 970, 1959.
Fonger, W. H., *Phys. Rev., 91,* 351, 1953.
Forbush, S. E., *Phys. Rev., 54,* 975, 1938.
Freier, P. S., E. P. Ney, and J. R. Winckler, *J. Geophys. Research, 64,* 685–688, 1959.
Janossy, L., *Cosmic Rays,* Oxford University Press, p. 139, 1948.
Laster, H., A. M. Lenchek, and S. F. Singer, *Bull. Am. Phys. Soc.,* Ser. II, *5,* 259, 1960.
Lockwood, J. A., *Phys. Rev., 112,* 1750, 1958.
Lockwood, J. A., *J. Geophys. Research, 65,* 27–37, 1960.
McCracken, K. G., *Nuovo cimento, 13,* 1081, 1959.
McCracken, K. G., *Phys. Rev., 117,* 1570, 1960.
McCracken, K. G., and D. H. Johns, *Nuovo cimento, 13,* 96, 1959.
McDonald, F. B., and W. R. Webber, *Phys. Rev., 115,* 194, 1959.
McDonald, F. B., and W. R. Webber, *J. Geophys. Research, 65,* 767–770, 1960.
Manzano, J. R., J. G. Roederer, and O. R. Santochi, (to be published), 1960.
Meyer, P., *Phys. Rev., 115,* 1734, 1959.
Meyer, P., and J. A. Simpson, *Phys. Rev., 99,* 1517, 1955.
Meyer, P., and J. A. Simpson, *Phys. Rev., 106,* 568, 1957.
Neher, H. V., and H. Anderson, *Phys. Rev., 109,* 608, 1958.
Parker, E. N., *Phys. Rev., 110,* 1445, 1958.
Quenby, J. J. and W. R. Webber, *Phil. Mag., 37,* 90, 1959.
Parsons, N. R., (to be published), 1960.
Reid, G. C., and H. Leinbach, *J. Geophys. Research, 64,* 1801, 1959.
Roederer, J. G., O. R. Santochi, J. C. Anderson, J. M. Cardozo, and J. R. Manzano (to be published), 1960.
Simpson, J. A., *Bull. Intern. Geophys. Year, 15,* 11, 1958.
Simpson, J. A., and W. C. Fagot, *Phys. Rev., 90,* 1068, 1953.
Singer, S. F., *Nuovo cimento Suppl.,* Ser. X, *8,* 161, 1958.
Storey, J. R., *Phys. Rev., 117,* 573, 1960.
Webber, W. R., and J. J. Quenby, *Phil. Mag., 41,* 654, 1959.
Wilson, B. G., D. C. Rose, and M. A. Pomerantz,
Yoshida, S., and M. Wada, *Nature, 183,* 381, 1959.

(Manuscript received August 22, 1960; revised September 20, 1960.)

The Cosmic Ray Alpha-Particle Flux during Sharp Forbush Intensity Decreases

PETER MEYER

Enrico Fermi Institute for Nuclear Studies
and
Department of Physics
University of Chicago
Chicago 37, Illinois

Abstract. During three large Forbush-type intensity decreases which occurred on May 12, July 15, and July 18, 1959 the primary cosmic ray α-particle flux was measured at balloon altitudes. A comparison with the α-particle flux in an undisturbed period on September 28, 1959, and with the total cosmic-ray intensity as observed by neutron monitor stations shows a close correlation between the α-particle flux and the total cosmic-ray flux during Forbush decreases. This evidence clearly establishes the fact that the proton and α-particle components are modulated by a common mechanism during the sharp intensity decreases. The measurement of May 16, 1959, exhibits an increase in the α-particle flux by 30 per cent within approximately 9 hours which is not accompanied by a comparable variation in the proton flux. Similar, independent changes in the α-particle flux have been noted earlier to follow Forbush decreases. During quiet days the primary α-particle flux with energies exceeding 560 Mev/nucleon is about 20 per cent higher in 1959 than in 1958. This change in intensity is probably related to the beginning decline in average solar activity.

INTRODUCTION

A characteristic type of sharp cosmic-ray intensity decrease was discovered by *Forbush* [1938]. This phenomenon follows solar flares within 1 or 2 days and is frequently accompanied by a geomagnetic storm. During large events, up to 50 per cent of the total cosmic-ray flux with rigidities above 1 BV may be removed within a few hours, and it requires days or weeks for the particle flux to recover its initial value.

There is good reason to believe that highly ionized gas emitted by the sun and traveling with velocities of 1000 to 2000 km/s is responsible for the Forbush-type decrease and the associated geomagnetic effects. More recently it became possible to show experimentally that the mechanism affects a substantial portion of the solar system surrounding the sun-earth line [*Fan, Meyer, and Simpson*, 1960*a*, 1960*b*].

A method to obtain more information on the properties of the modulation mechanism responsible for the Forbush-decrease comes through a study of the behavior of the nonprotonic (e. g., $Z \geq 2$) components of the primary cosmic radiation. We, therefore, have in the past 3 years carried out a number of experiments which were designed to investigate the behavior of the primary cosmic-ray α-particle flux during this type of event [*Meyer*, 1959].

Several outstanding sharp cosmic-ray decreases occurred in 1959 which were suitable for additional study of the modulation of the α-particle component. These events took place on May 12, July 15, and July 18. The July events were most remarkable and the total cosmic-ray intensity as measured by the Climax neutron monitor temporarily reached the lowest value over observed. On May 12, as well as in the July period, the arrival of low-energy solar protons was reported at latitudes normally forbidden to those particles by the Stormer cutoff [*Ney, Winckler, and Freier*, 1959; K. B. Fenton and J. A. Simpson, to be published].

We carried out four balloon flights for α-particle flux measurements in 1959. Three of these flights were made during times when the cosmic-ray intensity was depressed after a sharp decrease, while the fourth flight took place on September 28, a period of quiet solar condition. The flux value observed on that day should be representative for the cosmic-ray α-particle intensity in the latter part of 1959. All the measurements of 1959 were carried out from Sioux

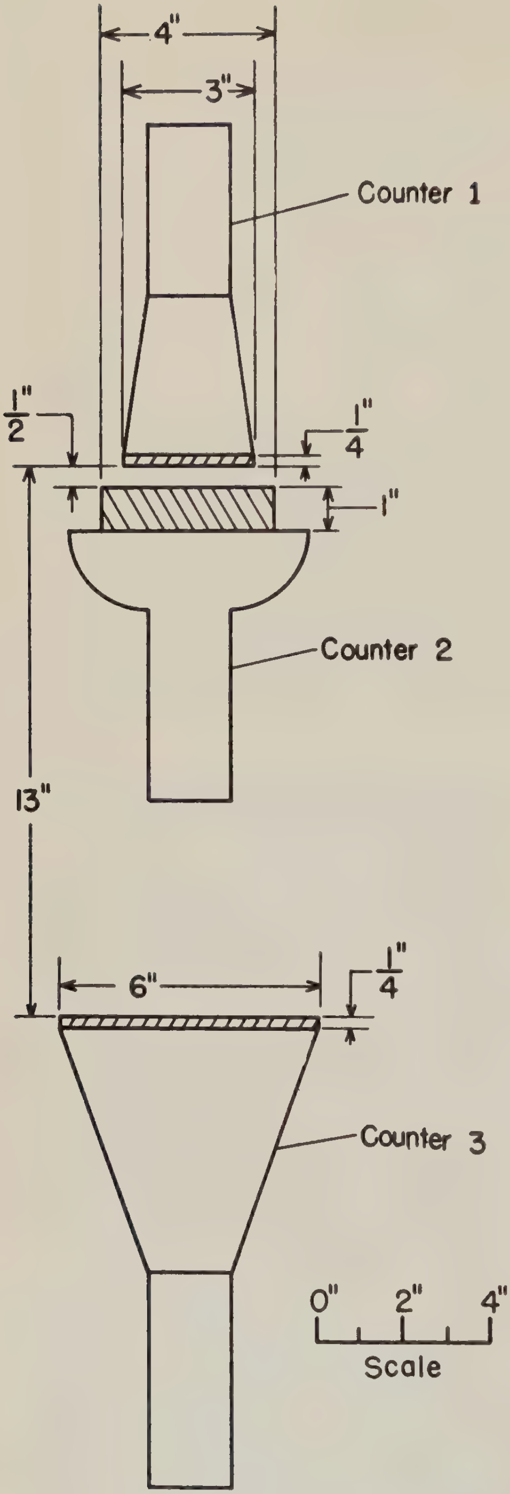

Fig. 1. Schematic diagram of the counter telescope. Counters 1 and 3 are plastic scintillators; counter 2 is a Cerenkov counter.

Falls, South Dakota, where we kept two sets of equipment ready to launch on short notice after the occurrence of a solar event.

Instrumentation and Measurements

The instrument used for the measurement of the α-particle flux consists of a combination of two scintillation counters and a Cerenkov counter, described in an earlier paper [*Meyer,* 1959] and shown schematically in Figure 1. A coincidence between counter 1 and counter 3 is required to trigger the apparatus. A simultaneous measurement of the energy loss of the particle in counter 1 and its velocity in the Cerenkov counter 2 is then made, which yields good discrimination between protons and α-particles down to 450 Mev/nucleon. We measured the total flux of α-particles exceeding 530 Mev/nucleon at about 13.5 g/cm^2 below the top of the atmosphere. This lower energy limit was determined by the Cerenkov counter pulse height, and corresponds to a primary energy at the top of the atmosphere of 560 Mev/nucleon or a rigidity of 2.3 BV, which is considerably higher than the geomagnetic cutoff at Sioux Falls (1.65 BV). The α-particle flux, therefore, did not require corrections for small latitude drifts of the balloon during the measurement. Continuous calibration of the apparatus was achieved using the relativistic α-particles.

Figures 2, 3, and 4 show the total cosmic-ray intensity as a function of time measured by the Climax nucleonic component monitor for the periods in which flights were carried out. The arrows indicate the days of the α-particle measurements. Table 1 lists the flux of α-particles with energies exceeding 560 Mev/nucleon at the top of the atmosphere which were obtained on the various days of measurements together with the average count rates of neutron monitor stations for the hours of balloon measurements. The following corrections were taken into account [see *Meyer,* 1959, for details].

(A) α-particle flux ($E > 530$ Mev/*nucleon*) normalized under 13.5 g/cm^2 of air.

1. Altitude changes of the balloon during each flight using an absorption mean free path of α-particles in air of 45 g/cm^2.
2. General background in α-particle pulse height region.

(B) α-particle flux ($E > 560$ Mev/nucleon) extrapolated to the top of the atmosphere.

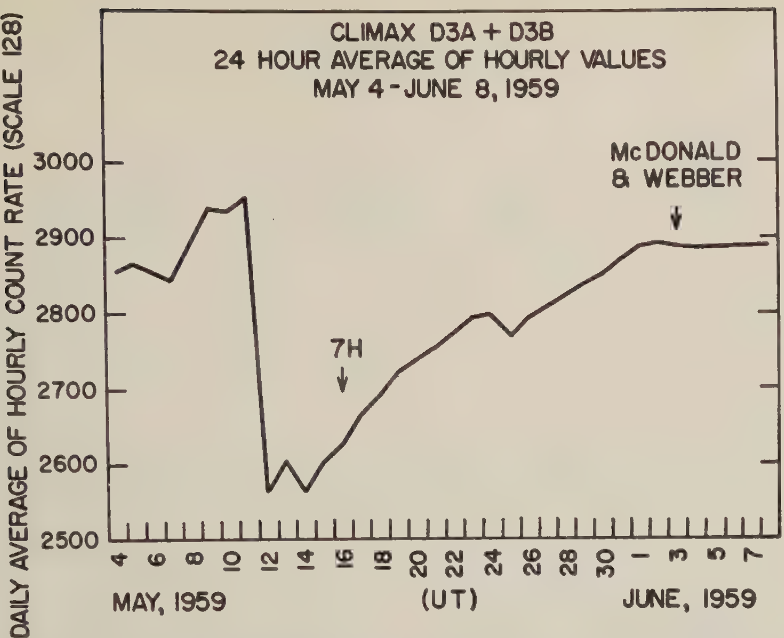

Fig. 2. The total cosmic-ray intensity as a function of time as measured by the Climax neutron monitor from May 4 to June 8, 1959.

Altitude changes of the balloon.
General background in α-particle pulse height region.
Contribution of α-particle fragments from heavier nuclei colliding above the apparatus.

RESULTS AND DISCUSSION

orbush decreases in the α-particle flux. The measurements that we carried out in 1959 were all made from the same location—Sioux Falls, S. D.—with a geomagnetic cutoff of 1.65 BV according to *Quenby and Webber* [1959]. This cutoff rigidity is appreciably higher than during our previous measurements which were made from Canadian launching sites. We still can directly compare the flux of primary α-particles above 530 Mev/nucleon—or 2.3 BV rigidity—

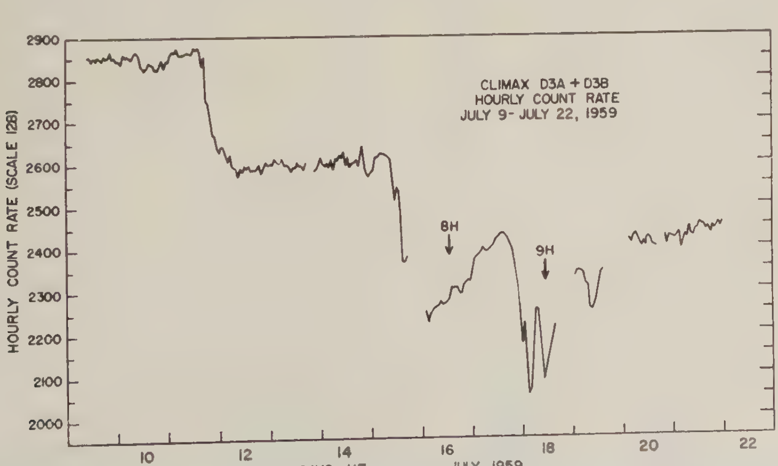

Fig. 3. The total cosmic-ray intensity as a function of time as measured by the Climax neutron monitor from July 9 to July 22, 1959.

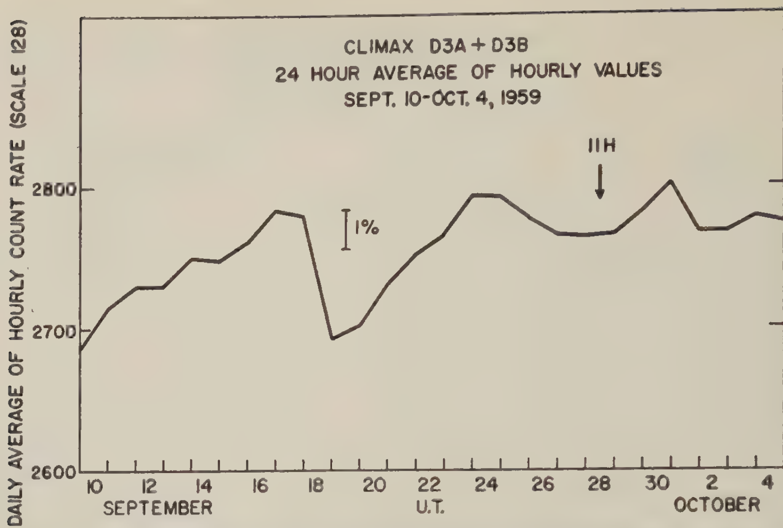

Fig. 4. The total cosmic-ray intensity as a function of time as measured by the Climax neutron monitor from September 10 to October 4, 1959.

in the different periods. This is not possible in the case of the proton flux because no attempt was made to divide the protons into different energy groups and their flux will therefore depend on the geomagnetic latitude at which the measurement is made. We, therefore, use neutron monitor station data as a measure of the cosmi ray proton intensity for a correlation with th α-particle flux over several years. A plot of th α-particle flux as a function of time togeth with the Climax neutron monitor data for th periods of α-particle measurements through th

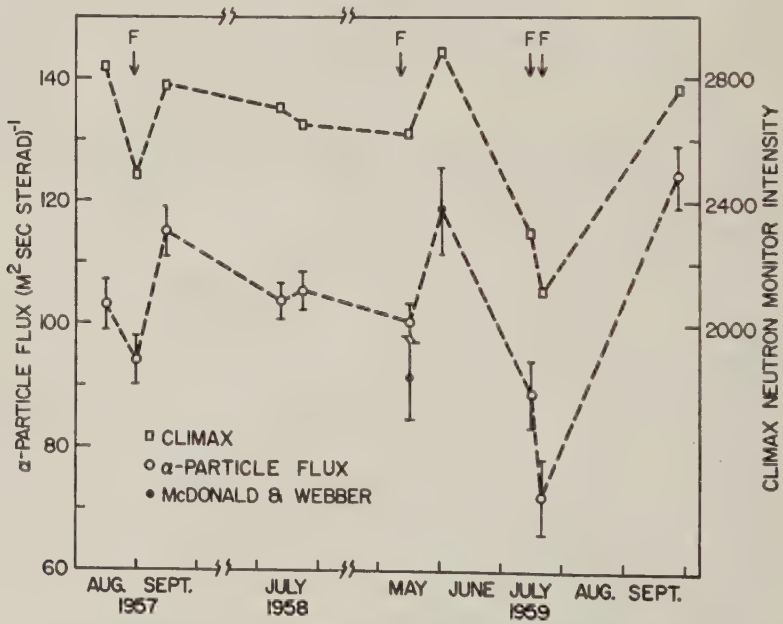

Fig. 5. The α-particle flux with energy ≥ 530 Mev/nucleon under 13.5 g/cm² of residual atmosphere and the nucleonic component intensity as measured by the Climax neutron monitor as a function of time. Measurements carried out during a Forbush-type decrease are indicated by an arrow.

TABLE 1. The α-Particle Flux and Neutron Monitor Intensity during Four Balloon Measurements in 1959

Date	Hours CST	Average Pressure during Flight, mm Hg	Climax Neutron Monitor Intensity, $R = 2.71$ BV	Sulphur Mountain Neutron Monitor Intensity, $R = 0.98$ BV	Total Number of α-Particles Counted in Flight ($E \geq 530$ Mev/nucleon)	α-Particle Flux Corrected for 13.5 g/cm² and Background ($E \geq 530$ Mev/nucleon), m^{-2} sec^{-1} $ster^{-1}$	α-Particle Flux at the Top of the Atmosphere ($E \geq 560$ Mev/nucleon), m^{-2} sec^{-1} $ster^{-1}$
/59	0158–1806	8.3	2621	1849	4822	100.5 ± 3%	132 ± 8%
/59	0737–0927	9.7	2294	1638	470	88.7 ± 6%	113 ± 10%
/59	0401–0506	6.3	2101	1480	248	77.2 ± 8%	94 ± 12%
–28/59	2326–1145	9.0	2760	1952	4413	124.3 ± 4%	163 ± 9%

rs 1957 to 1959 shows most clearly the close elation between the total cosmic-ray inten- and the intensity of the α-particle compon- during Forbush decreases. This is shown in ire 5 where arrows indicate those measure- its that were made during a Forbush de- se. We have included in this curve the values he α-particle flux measurements of May 16 June 2, 1959, published by *McDonald and bber* [1960]. The June 2 measurement of Donald and Webber helps to demonstrate the gnitude of the α-particle intensity decrease ing the July events. Their measurement on y 16 coincided with our own measurement

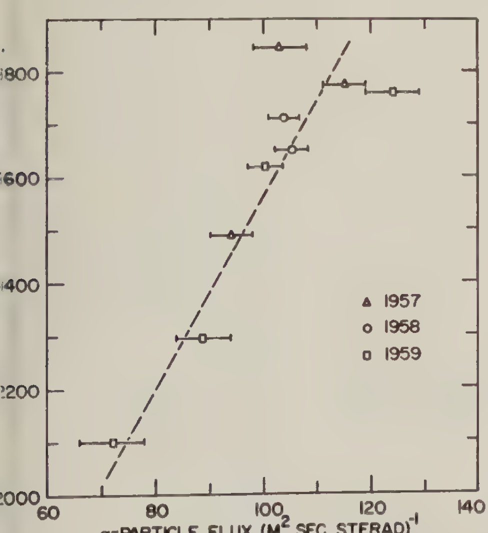

Fig. 6. The α-particle flux with energies > 30 Mev/nucleon vs. the Climax neutron onitor intensity for all measurements from 957 through 1959.

and, within the experimental errors, there is agreement between the two independent flux determinations. From Figure 5 it is seen that more than 40 per cent of the primary α-particle flux with an energy exceeding 560 Mev and which is normally present during the summer of 1959 was removed by the Forbush decrease mechanism on July 18. On this day the primary α-particle flux reached the lowest value ever observed. In Figure 6 we have plotted the α-particle flux versus the Climax neutron monitor (cut off at 2.7 BV) station intensity for all data obtained from 1957 through 1959. If the distribution is approximated by a straight line, we find that the ratio between relative intensity changes of the α-particles ($E > 560$ Mev/nucleon) and the neutron monitor is close to 1.3. It is expected that the relation between α-particle flux and Climax neutron monitor intensity changes with the variations in the primary energy spectrum that are observed throughout the solar cycle, due to the energy dependence of the yield function that relates the observed intensity at Climax to the flux at the top of the atmosphere.

The closely linear relation between the α-particle flux and the total intensity during Forbush decreases demonstrates the common modulation of primary protons and α-particles in this phenomenon.

Short-term variation of the α-particle flux. In an earlier paper we have reported increases in the α-particle flux within a few hours which were not accompanied by corresponding changes in the proton flux. The results indicated that such independent intensity variations of the α-particle component occur in the periods that

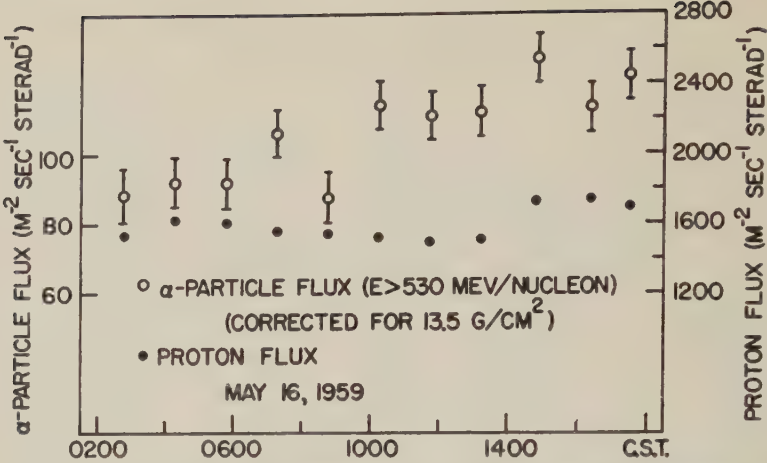

Fig. 7. The flux of α-particles and protons under 13.5 g/cm² residual atmosphere as a function of local time during the balloon flight of May 16, 1959. (These data are not corrected for background in the α-particle region.)

follow a sharp Forbush-type decrease of total cosmic-ray intensity. We were able further to investigate this point using the measurements of May 16 and September 28, 1959. For comparison we use the proton flux that was measured at balloon altitude. Although this flux is latitude dependent and cannot be directly compared with data obtained earlier at other latitudes, it may be used to establish the correlation between the α-particle and proton flux for the time of a single flight. In Figures 7 and 8 the α-particle and proton fluxes obtained on those days have been divided in approximately 90-minute intervals and are plotted as a function of time. Du

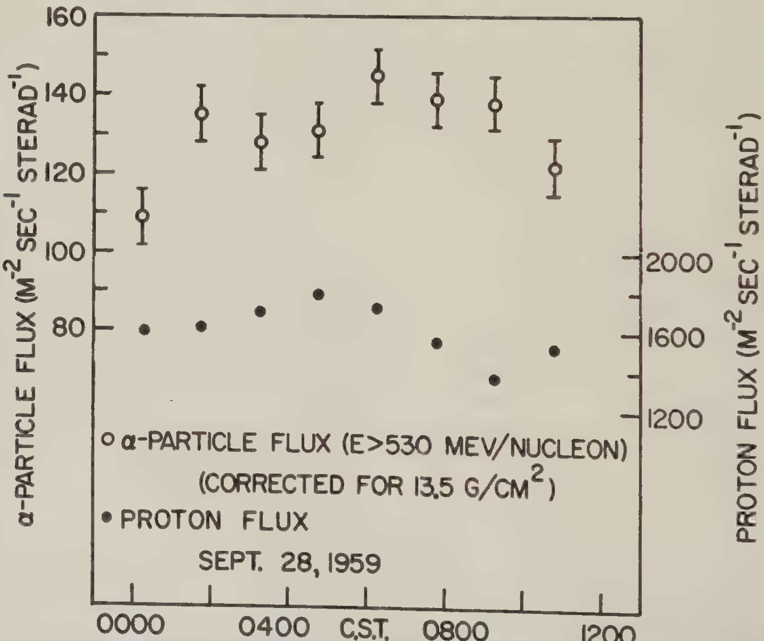

Fig. 8. The flux of α-particles and protons under 13.5 g/cm² residual atmosphere as a function of local time during the balloon flight of September 28, 1959. (These data are not corrected for background in the α-particle region.)

ne measurement of May 16 which followed ·bush-decrease by 4 days, we observe a rise particle flux by approximately 30 per cent een 0600 and 1500 local time, while the pro- ux showed an increase of less than 10 per and the Climax neutron intensity an in- e of 2 per cent. The flight of September 28, took place at a time when the total cosmic- ntensity had not undergone any substantial ge. As seen in Figure 8, the ratio of α-parti- proton flux did not vary within the experi- al errors on this day. During the measure- s of July 16 and 18, 1959, data could not llected for a sufficiently long period to on this point.

Summary and Conclusion

ree measurements of the primary cosmic α-particle flux were made during 1959 im- ately following a sharp Forbush-type de- e. A comparison with the α-particle flux g quiet periods and with the total cosmic- intensity as observed by nucleonic com- nt monitors at the surface of the earth s that during the large Forbush decreases ay 12, July 15, and July 18, 1959, the pro- component and the α-particle component rgo proportional intensity changes. This rms the conclusions reached in an earlier r [*Meyer*, 1959], that a common modu- g mechanism is operating on both com- nts during a Forbush decrease.

May 16 we were able to measure the vari- s of the α-particle flux and the proton flux bout 16 hours and noted an increase of 30 ent in the α-particle flux with no compara- change in the flux of protons during the s of the balloon flight. This adds to the nce, reported earlier, that a short-term tion in the α-particle component is pres- in the periods following a sharp Forbush ease.

The α-particle flux observed on quiet days in 1959 seems to be about 20 per cent higher than during 1958. We interpret this intensity increase as due to the decline in average solar activity during 1959.

Acknowledgments. We wish to thank Mr. Rochus Vogt and Mr. Thomas Burdick for their assistance in carrying out the balloon flights. We gratefully acknowledge the contributions of Mr. Gordon Lentz and the computing group to the reduction of the data; and of Mr. R. Tjonaman, who maintained the neutron monitor network. Dr. Rose, National Research Council, Ottawa, has kindly provided the Sulphur Mountain neutron intensity data.

This work was supported in part by the National Science Foundation, grant NSFG8729, and by the Air Force Office of Scientific Research, Air Research and Development Command under contract AF18(600)-666.

References

Fan, C. Y., P. Meyer, and J. A. Simpson, Cosmic radiation intensity decreases observed at the earth and in the nearby planetary medium, *Phys. Rev. Letters, 4,* 421, 1960*a*.

Fan, C. Y., P. Meyer, and J. A. Simpson, Rapid reduction of cosmic-radiation intensity, measured in interplanetary space, *Phys. Rev. Letters, 5,* 269, 1960*b*.

Forbush, S. E., On world-wide changes in cosmic ray intensity, *Phys. Rev., 54,* 975, 1938.

McDonald, F. B., and W. R. Webber, Changes in the low-rigidity primary cosmic radiation during the large Forbush decrease of May 12, 1959, *J. Geophys. Res., 65,* 767–770, 1960.

Meyer, Peter, Primary cosmic-ray proton and alpha-particle intensities and their variation with time, *Phys. Rev., 115,* 1734, 1959.

Ney, E. P., J. R. Winckler, and P. S. Freier, Protons from the sun on May 12, 1959, *Phys. Rev. Letters, 3,* 183, 1959.

Quenby, T. T., and W. R. Webber, Cosmic ray cut-off rigidities and the earth's magnetic field; *Phil. Mag., 4,* 90, 1959.

(Manuscript received August 18, 1960; revised September 27, 1960.)

The Solar Cosmic-Ray Outburst of May 4, 1960

J. C. Anderson, R. L. Chasson, M. P. Liwschitz, and T. Suda

Department of Physics
University of Nebraska
Lincoln, Nebraska

Abstract. Low-energy nucleonic cosmic-ray data from stations at Lincoln, Mt. Washington, ulfur Mountain, and Deep River were studied with regard to onset times, time and magnitude f maximum increase, and decay characteristics. The decay behavior underwent a definite ransition that is clearly related to the termination of the optical flare. The first part of the ecay is clearly exponential, with a time constant in the neighborhood of 17 minutes, whereas he latter part is not distinctly established either as exponential (with a possible time constant f 78 minutes) or as following a $t^{-1.5}$ law. Ordinary impact zones do not seem to fit the pattern f increases observed at various stations in the northern hemisphere.

roduction. Observations at appreciable s in the atmosphere of substantial increases smic-ray intensity coherently associated flare activity on the sun have been so in- ent (only six significant ones to date) that s not been possible to make any strong alizations concerning the space and time cteristics of the observed effects. Of these ents only the most recent two have been ed quantitatively by a wide network of ns using low-energy nucleonic component tors, and although the first four were ob- d in many places, only the last of these ember 19, 1949) was studied with a neu- monitor [*Adams,* 1950]. The remaining vations of these earlier events were with us types of meson detectors, including ter telescopes and ionization chambers, do not give information about particle sity in the lower range of the incident mo- um spectrum. It is reasonable to believe particles produced and accelerated in the processes will be found mainly in this range (< 20 bev/c).

e development of neutron monitors and subsequent general use (in addition to lard meson monitors) during and following have made it possible to study these rare -flare events in greater detail and with y improved statistics. For example, the lent coverage of the event of February 23, made possible an accurate calculation of hape of the particle spectrum and its time ndence. [*Meyer, Parker, and Simpson,* 1956; *Pfotzer,* 1958]. Also orbit calculations [*Firor,* 1954; *Lüst,* 1957; 1958] and model experiments [*Brunberg,* 1956] demonstrated an impact zone property for solar particles arriving at the earth; this property was evident in the data available for the first four flare increases and was confirmed for the onset period of the 1956 event. The time-dependence of the postflare intensity trace of the 1956 event was also unambiguously determined, and hypotheses were advanced to explain it and the essential world-wide isotropy that obtained for the postflare radiation.

The search for demonstrably characteristic quantitative features of these solar-flare cosmic-ray events continues, with new evidence being made available on the average of once every 5 years. It is reasonable to anticipate considerable variation of detail from event to event [*Dorman,* 1957] and to expect that predictable detailed quantitative behavior will not be revealed for many years. Initial conditions and subsequent space-time variations of the following factors all fold together to give the appearance of the cosmic-ray flare spike and its tail: the particle spectrum as produced at the sun, location and directional properties of the source, and pre-existing corpuscular and electromagnetic field conditions in the whole interplanetary space accessible to the particles.

We have recently obtained new evidence concerning the flare phenomenon; a solar injection of cosmic-ray particles occurred in association with a Class 3 limb flare observed optically be-

TABLE 1. Monitor Stations Supplying Data

Station	IGY Number	Geomagnetic Co-ordinates		Altitude
Deep River	B211	57.5°N	358°W	145 m
Lincoln	B285	50.8	326	350
Mt. Washington	B306	55.6	356	1917
Sulfur Mountain	B115	58.2	300	2283

tween 1015 and 1105h UT on May 4, 1960. [*Solar-Geophysical Data,* 1960]. Polar cap cosmic radio noise absorption took place, and an increase of corpuscular radiation was measured by detectors aboard the artificial satellite Explorer VII. During this period the cosmic rays were recovering from a moderate Forbush decrease following the solar activity of late April 1960.

It is our present purpose to make limited calculations of some of the characteristics of this latest event and to attempt to relate the results to those found previously. Our discussion will be based mainly upon the behavior of the low-energy nucleonic component as it has been observed at the locations given in Table 1.

Sizable increases of the nucleonic component were noted at these stations, and corresponding, but much smaller, pulses of increased meson intensity were also observed at several of them.

Observations. The nucleonic intensity crease observed at these several station plotted against time in Figure 1. It is seen the leading edge of the cosmic-ray impuls not very steep and that there is a mar precursor increase that immediately prec the main impulse. Two traces are presented Lincoln, one being that obtained from the minute digital recordings (the flare alarm not operative at the time, and thus digital re ings at shorter intervals were not provide the reconstructed Lincoln trace is derived fr an ink-chart recording produced by a precis differential counting rate meter having a l time constant [*Schmidt,* 1957].

This reconstructed intensity graph was p duced in the following way: a rough idea of event was deduced from the 15-minute d and the rate meter was disconnected from neutron monitor after the intensity had retur essentially to its preflare value (although general level remained high for several d after the flare); the rate meter was connec to a pulse generator, and the input pulse r was adjusted to give the preflare inked tr level. Following this initial adjustment, the put pulse rate was varied in such a man that it would give integrated counts that co sponded with the 15-minute digitally measu

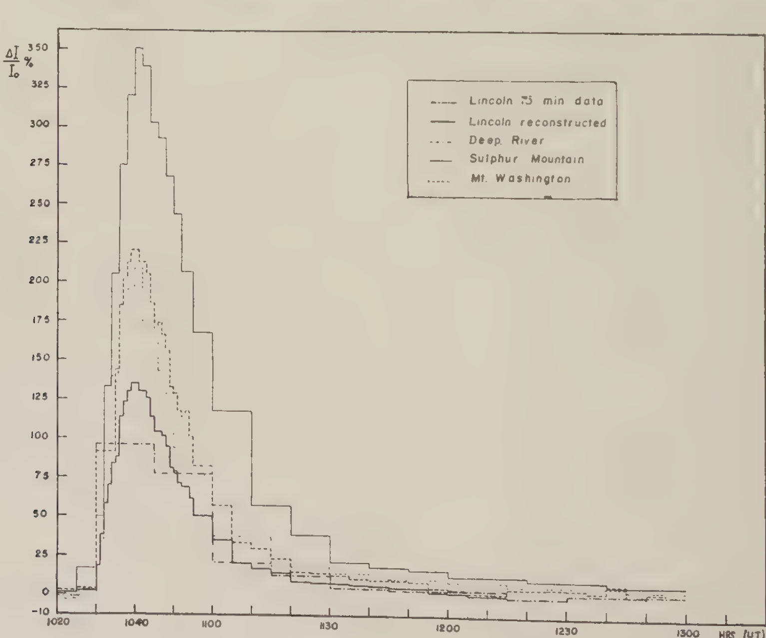

Fig. 1. Nucleonic intensities (relative to pre-flare value) vs. time.

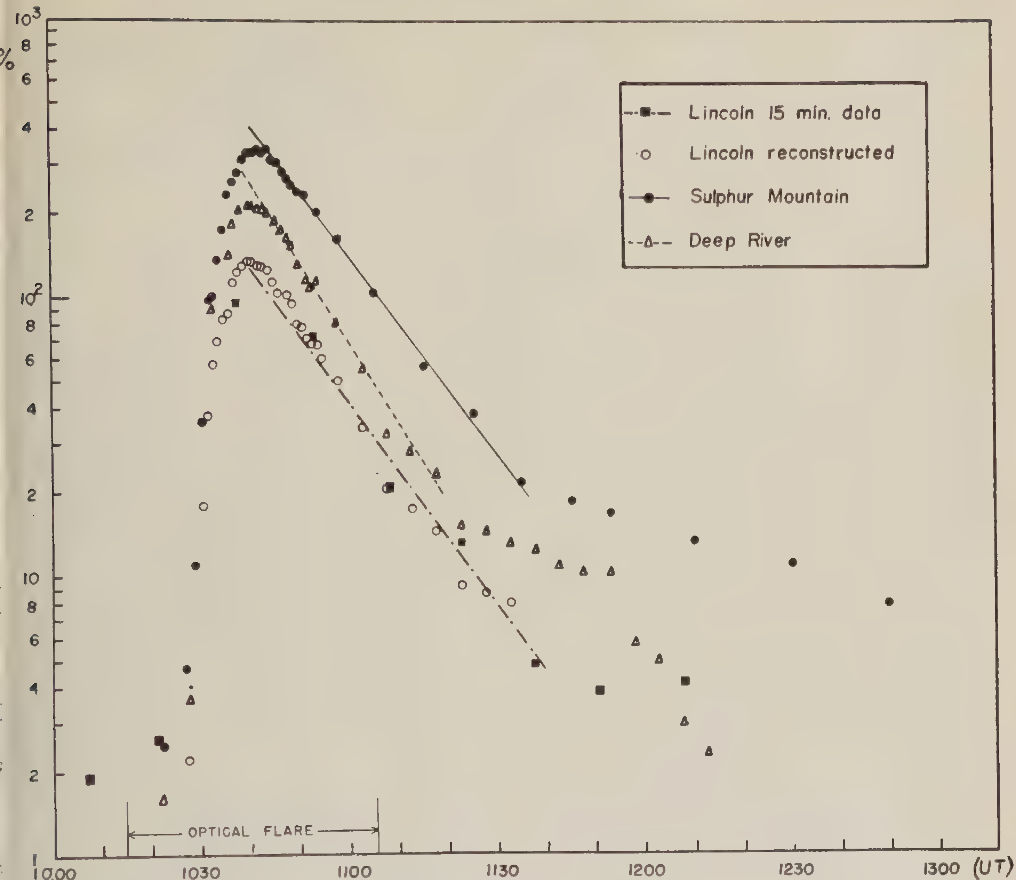

Fig. 2. Semi-log plot of nucleonic intensities (relative to pre-flare value) vs. time.

es and also followed the relative intensities n in the Deep River digital data. Thus the rved rate meter trace was duplicated very ely after a series of trials with the time-endent artificial pulse input.

rom the series of traces obtained in several ccessful reconstruction trials, it was found a deviation of 5 per cent from the proper intensity trend would yield an easily detectable departure of the reconstruction trace from the one obtained during the actual flare event. Integrals of this reproduced differential curve yielded the measured 15-minute results to within the statistical standard error of counting. We conclude, therefore, that the artificially produced time development of the flare spike gives

TABLE 2. **Results of Decay Law Calculations**

Station	Peak Relative Increase (%)	$e^{-t/\tau}$ Law		$t^{-\beta}$ Law	
		τ(min.)	Period of Fit (UT)	β(min.)	Period of Fit (UT)
coln (15 min.)	96	17.5 ± 5.3	1040–1145	...	...
coln (reconstructed)	135	...	...	...	...
p River	220	15.4 ± 0.5	1042–1105	1.51 ± 0.05	1110–1150
Washington	209	16.7 ± 0.3	1041–1120	1.27 ± 0.02	1053–1315

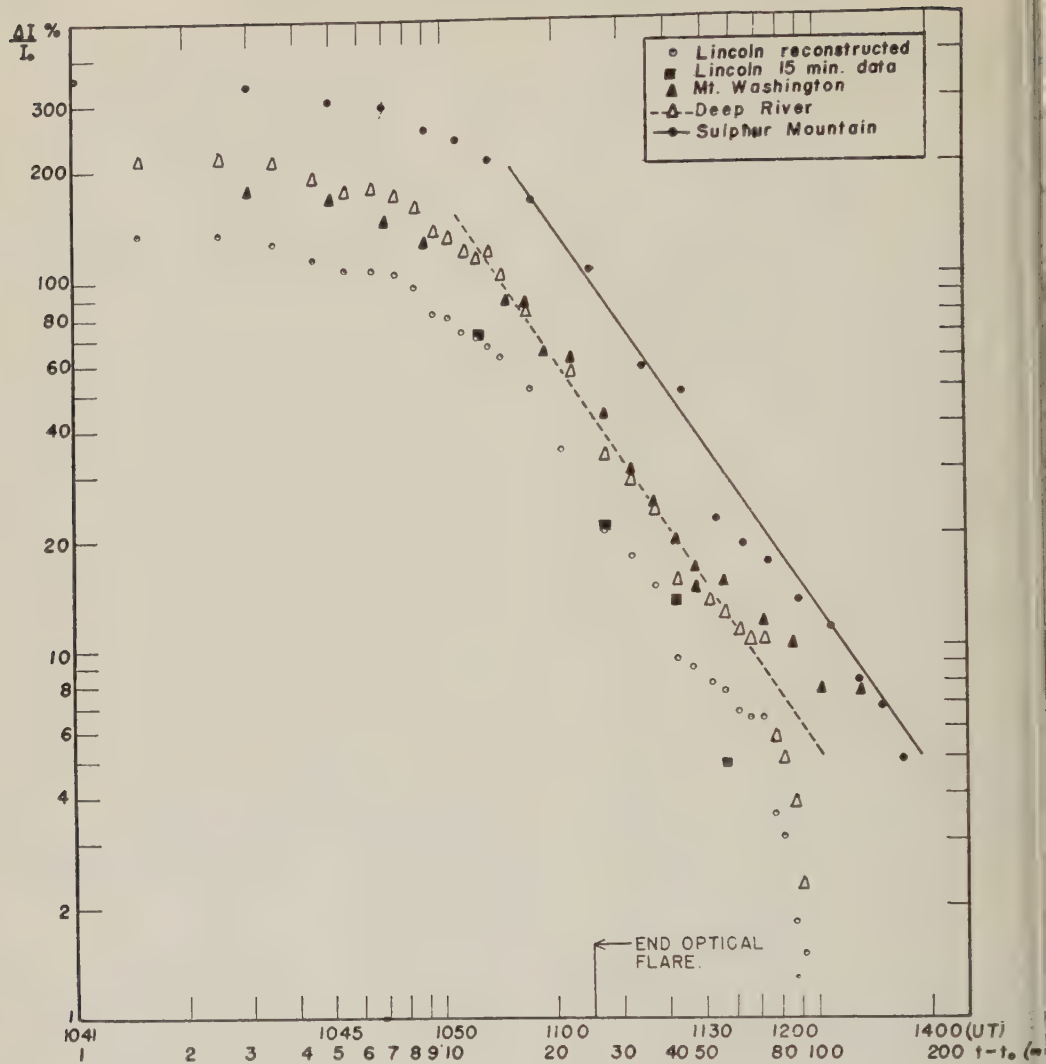

Fig. 3. Log-log plot of nucleonic intensities (relative to pre-flare value) vs. time.

a rather accurate image of the actual event, at least in its more important dynamic stages.

It is particularly easy to extract the Lincoln onset time and the time of maximum intensity from the rate meter trace. These times were at 1031 and 1041½ hours UT, respectively, with an uncertainty of ±½ minute in each case. The time of maximum is obtained from the point of inflection clearly seen on the leading edge of the rate meter curve.

Reduction of Observations and Discussion of Results. From the directly recorded 15-minute data, and more clearly from the reconstructed fine structure for Lincoln, it appears that the intensity increase decayed exponentially for so time after the peak was reached. This obser tion is strongly supported by data from other stations, as may be seen on the se logarithmic plot of intensity change vs. tim Figure 2. For the first part of the decay we sumed the following law to hold

$$\Delta I/I_0 = A \cdot \exp\left[-(t - t_0)/\tau\right]$$

$$\Delta I = I(t) - I_0$$

where I_0 is the preflare intensity and t_0 is time of intensity maximum. A series of le squares calculations was made to find the

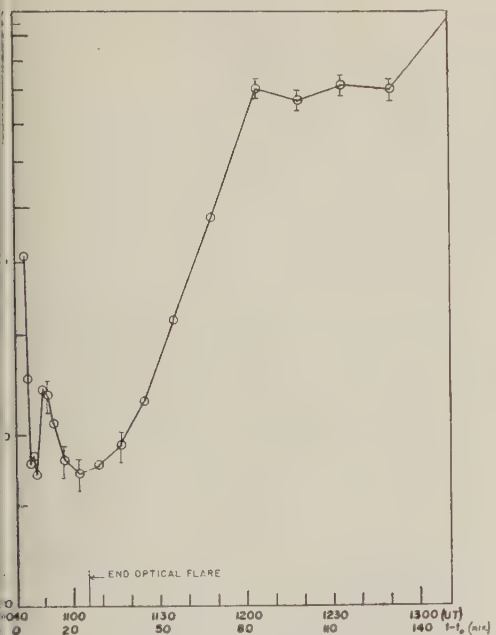

Fig. 4. Decay law exponent (for Sulfur Mountain nucleonic data) computed by method of moving averages.

istant τ for each of the stations; the values nd for his parameter, with corresponding ndard errors of fit, are found in Table 2 along h the applicable period of fit for each station. e general duration of exponential fit is from 40 to 1120–1150 hours UT. The simple mean lue of τ for the stations listed in Table 2 is minutes, which may be compared with a lue of 180 minutes observed at Manchester the flare of November 19, 1949 [*Adams*, 50].

There is an obvious change in the decay aracteristic starting at about 1115 hours; this ne actually varies from station to station, but e data recording intervals do not permit a ry exact determination of the transition times. logarithmic plot of intensity change vs. time shown in Figure 3, indicating a possible power v time-decay characteristic starting at 1110–15 hours. Table 2 also contains values of the wer-law exponent β obtained from least-uares fitting the data to a decay law of the rm

$$\Delta I/I_0 = B\cdot(t - t_0)^{-\beta} \qquad (2)$$

ble 2 also includes the time intervals pertint to these calculations.

A power-law description of the shape of the second part of the tail cannot be regarded as conclusive, however, since from the semilog plot (Fig. 2) it is seen to appear somewhat exponential. An attempt was made to decide between these two possibilities for a decay law that will describe the latter section of the tail; the calculation consisted of a least-squares analysis of moving averages of intensity, starting with the time of the peak value of the flare spike (about 1040 hours UT) and continuing to the end of the tail (about 1300 hours). An average of five measured values of intensity and time was made, including values from the two nearest datum periods preceding and following the nominal central period and the central period itself, and a time constant was calculated for each average value according to the exponential decay law given in equation 1. The results for Sulfur Mt. are shown in Figure 4, where it can be seen that the slope of the five-points time-constant plot decreases at first, when points surrounding the intensity peak are included. The time constant reaches a fairly stable value (of the order of 20 minutes) lasting from 1045 to about 1140 hours, and then it rises to a quite steady value (approximately 78 minutes) that persists from 1200 to 1250 hours.

We can say that at about 1115 hours the decay law changes either from $\exp(-t/17)$ to $\exp(-t/78)$ or from $\exp(-t/17)$ to $t^{-1.5}$. Limitations of statistics available do not permit a decision between these two possibilities for the transition of decay characteristics. It seems certain, however, that the transition is properly time-associated with the termination of the optical flare at 1105 hours.

Such a transition seems to have occurred also during the decay of the 1949 cosmic-ray increase, especially as it appeared in the neutron trace at Manchester, although the magnitudes of intensity change and decay times were much greater for that event than for the one of May 4, 1960.

An attempt has also been made to establish impact zones for the various stations. It became clear that even during the first few minutes of the increase the geographical distribution of particles did not follow the expected pattern. It was also apparent that at least two well-defined groups of particles arrived in the northern hemisphere, one over North America and the

other over the Atlantic Ocean, England, and Northern Europe. To explain the remarkable increase observed at Ft. Churchill as well as at Deep River, Sulfur Mt., Ottawa, Mt. Washington, and Lincoln, it would be necessary to shift the whole zone to the northeast (or the stations to the southwest) and also to give it a slight counterclockwise rotation. A zone shift would be caused, for example, if the solar particles had traversed a heliomagnetic field [*Dorman,* 1957] or if there were a magnetized cloud between sun and earth; in any event, the production of an effectively displaced source would result in an impact zone shift. A station shift would be necessary if there were an effective change of geomagnetic latitude or if the usual expression for geomagnetic time [*McNish,* 1936] were not applicable at the time of the event.

An investigation is being made of various models to explain the observed effects, and any tangible results will be the subject for future publication.

Acknowledgment. We are grateful to Drs. D. C. Rose, H. Carmichael, and J. Lockwood for use of their data relating to this event. Discussions with Prof. I. Escobar and Miss Margaret Shea were helpful to us also. General thanks are due those investigators who supplied their May 4, 1960 data to form a central collection at World Data Center A for Cosmic Rays under the direction of Professor Paul Kellogg.

Work on which this paper is based was performed under National Science Foundation Grant No. G8838 and under auspices of the U. S. National Committee for IGY and IGC-59 and its continuing agency.

References

Adams, N., A temporary increase in the neu[...] component of cosmic rays, *Phil. Mag., 41,* [...] 505, 1950.

Brunberg, E.-Å., Cosmic rays in the terrest[...] magnetic dipole field, *Tellus, 8,* 215–233, 1[...]

Dorman, L. I., Cosmic ray variations, *State P[...] lishing House for Scientific and Technical [...] erature, Moscow,* 1957 (English translation [...] U. S. Air Force Technical Documents Lia[...] Office).

Firor, J., Cosmic radiation intensity-time va[...] tions and their origin, IV. Increases associa[...] with solar flares, *Phys. Rev., 94,* 1017–1029, 1[...]

Lüst, R., Impact zones for solar cosmic-ray pa[...] cles, *Phys. Rev., 105,* 1827–1840, 1957.

Lüst, R., Impact zones for solar cosmic ray pa[...] cles, *Nuovo cimento, 8 (Suppl.),* 176–179, 1[...]

McNish, A. G., Geomagnetic coordinates for [...] entire earth, *Terrestrial Magnetism and Atm[...] pheric Elec., 41,* 37–43, 1936.

Meyer, P., E. N. Parker, and J. A. Simpson, So[...] cosmic rays of February, 1956, and their pro[...] gation through interplanetary space, *Phys. R[...] 104,* 768–784, 1956.

Pfotzer, G., On the separation of direct and [...] direct fractions of solar cosmic radiation on F[...] ruary 23, 1956 and on the difference in steepn[...] of the momentum spectrum of these two co[...] ponents, *Nuovo cimento, 8 (Suppl.),* 180–1[...] 1958.

Schmidt, J. J., A differential counting rate me[...] for low counting rates, *M.S. Thesis,* Univers[...] of Nebraska, June, 1957.

Solar-Geophysical Data, *Central Radio Propa[...] tion Laboratory Report CRPL-F190 (Part [...]* June 1960.

(Manuscript received August 11, 1960; revi[...] September 13, 1960.)

Cosmic Noise Absorption Measurements at Stanford, California, and Pullman, Washington

BRUCE LUSIGNAN

Radioscience Laboratory
Stanford University
Stanford, California

Abstract. Results of cosmic noise absorption measurements at 27.5 Mc made at Stanford, California, and Pullman, Washington, during 1958 are presented. A method introduced by Mitra and Shain of extracting F-layer absorption from total absorption and an extension of this method to remove D-layer absorption are described. Subtracting these two components from the total absorption leaves an extra component of absorption. The diurnal and annual variation of all these components is presented graphically and discussed. Errors in the cosmic noise curves are discovered and corrected for. The cause of these errors and its relation to assumptions of the cosmic noise absorption method is discussed.

Introduction. The IGY riometer [*Little,* 57; *Little and Leinback,* 1959] measures total iospheric absorption by continuously record- g cosmic noise power. The frequencies used high enough to allow the cosmic noise to netrate the ionosphere even during magnetic orms and yet low enough to show measurable sorption of the signal. Normally the receiving tenna is beamed vertically.

The input to a high-gain receiver is elec- onically switched between the antenna and ise diode 340 times a second. The resulting gnal, proportional to the difference in powers, used to adjust the noise diode power to equal e antenna power, thus keeping diode current oportional to cosmic noise power. This cur- nt is continuously recorded by a pen recorder. The receiver frequency is swept continuously rough a 100-kc range at 2.5 kc/s. The lowest wer level found in the 100-kc range is taken be the cosmic noise level on the assumption at this lowest level is free of terrestrial inter- rence.

Once a day the records are calibrated by con- ecting a second noise diode in place of the tenna. Four or five consecutive values of cur- nt are run through this diode, and these alues are marked on the resulting readings on e riometer. The long-term stability of the ometer thus depends on the stability of the librating diode.

To obtain a value for total ionospheric ab- orption from the riometer records it is necessary to derive a quiet-day curve—a plot of expected cosmic noise power in the absence of absorption versus sidereal time. The curve is found by studying riometer records for IGY quiet days throughout the year. The current for these days is transferred to the correct sidereal time, and all readings are compared. The highest 'reliable' readings are taken as points on the quiet-day curve. The absorption is then given by

$$\text{Absorption (db)} = 10 \log_{10} (I_r/I_q)$$

where I_r is the current on a particular day and time and I_q is the current from the quiet-day curve for the corresponding sidereal time.

Two methods are used in reducing the riometer data [*URSI-AGI Committee,* 1958]. Type I records the average absorption during the first minute of each hour of the day, every day of the year. These results are used in studying gross daily and seasonal variations of ionospheric absorption. Type II scaling records the maximum absorption during each hour and its time of occurrence. It is useful in studying sporadic events such as solar flares and noise bursts.

Scope of report. This study deals with Type I scalings of records from IGY riometers at Stanford, California (37°26′N, 122°10′W), and Pullman, Washington (46°43′N, 117°10′W), for the year 1958. Both stations operate on a frequency of 27.5 Mc/s. The data have been published in a data summary [*Stanford Electronics Laboratories,* 1958]. This summary also con-

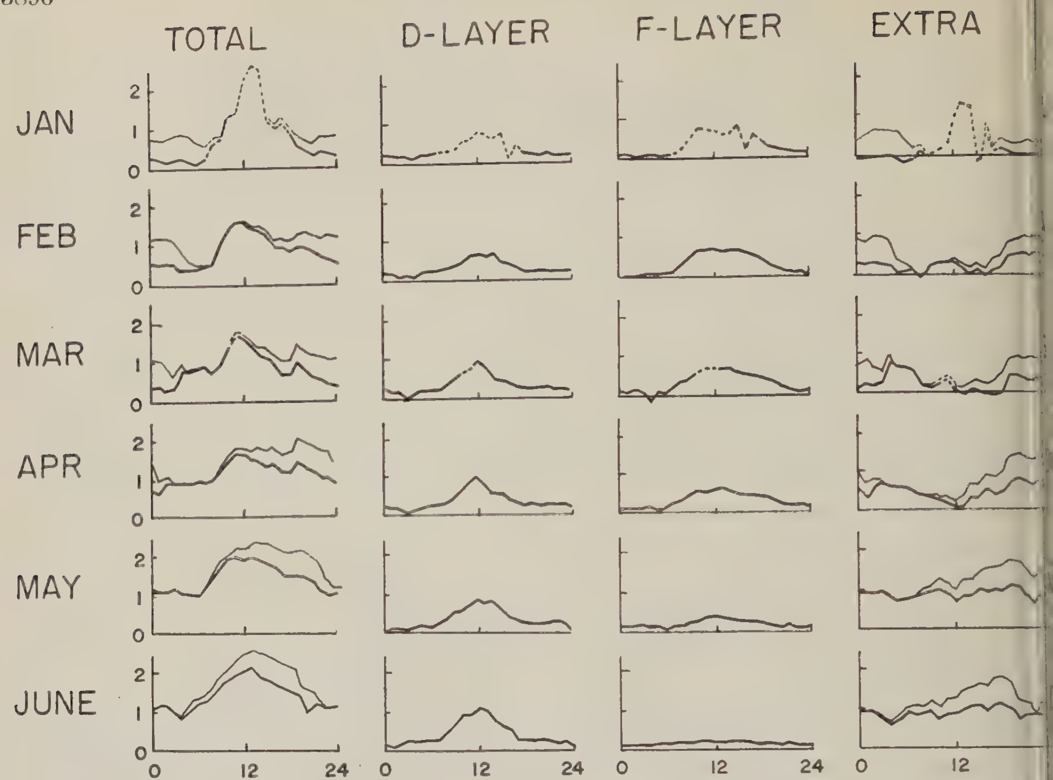

Fig. 1. Absorption components, Stanford.

tains a description of a nomographic device for reading riometer records directly in terms of db of absorption. The study also used scalings of San Francisco, California, ionosonde records provided by the IGY World Data Center, Boulder, Colorado [*National Bureau of Standards*, 1958].

The quality of records from the riometer stations is not perfect. During a few months terrestrial interference made over half the daytime records unreadable. Other months, however, were complete, and most nighttime readings were good. In all the data were sufficient to give reasonable results with the methods described below and to illustrate certain difficulties of the basic riometer theory.

Methods. Using the methods described in the introduction, the average absorption for each month for each hour of the month was computed. The results for the two stations are shown in Figures 1 through 4 under the left column marked 'Total.' For each month a plot of average absorption versus local time is recorded hour by hour. The upper (lighter) curv are the ones from this step. The ordinate sca is in decibels of absorption and the abscissa the hour of the day.

An unexpected feature is apparent in the curves. There is an increase in absorption in t middle of the night in the winter months. Sim lar results have been reported by *Ramanath and Bhonsle* [1959]. These authors used method proposed by *Mitra and Shain* [1953] separate D- and F-layer components of absor tion. An extension of this method, described b low, was applied to the Stanford and Pullm data to isolate the anomaly.

Mitra and Shain's procedure makes use hourly values of the critical frequency of t F layer, f_oF_2, obtained from ionosonde recor Mean values of absorption for given interva of f_oF_2 are plotted against the middle values f_oF_2 in the intervals. This is comparable to r ducing scatter plots of f_oF_2 versus absorption single points for each interval of f_oF_2. The r sulting points form a curve which shows increa

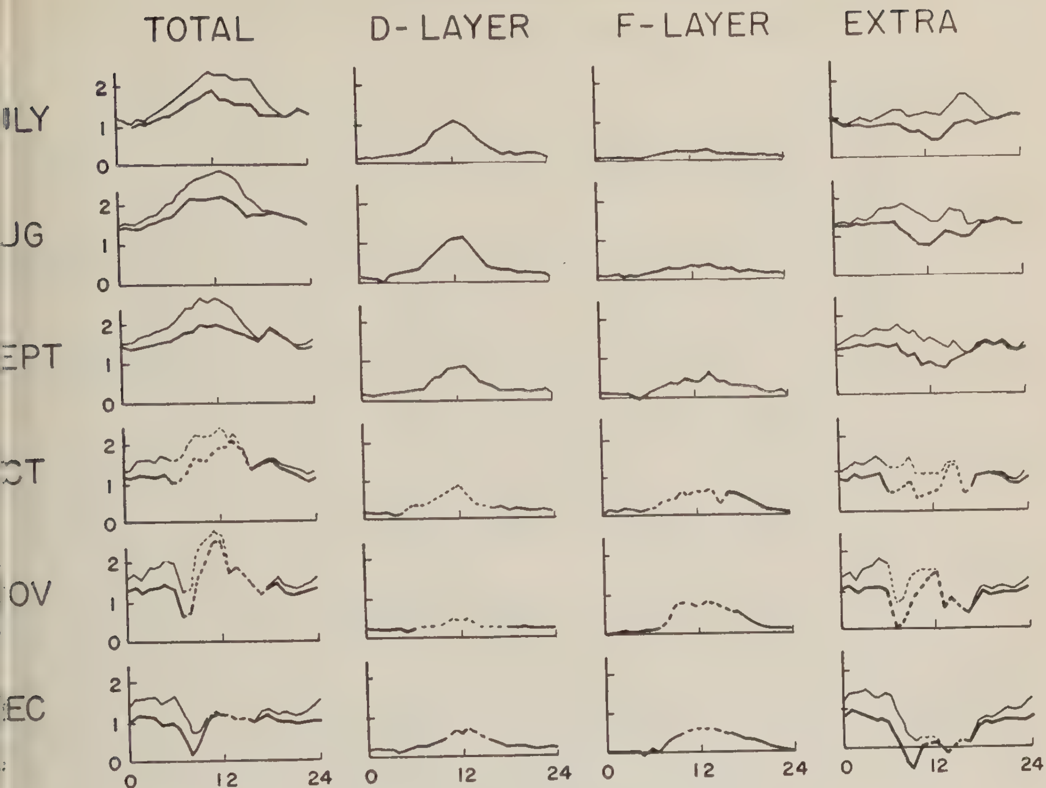

Fig. 2. Absorption components, Stanford.

ig absorption with increasing f_oF_2. The shapes f the curves are nearly independent of the time f day or year, but the curves do differ in placeient with respect to the absorption axis.

If there were only F-layer absorption, varying rith f_oF_2, the placement of the curves should ot vary. In fact, the curves should be placed so hat absorption does go to zero as f_oF_2 goes to ero. Any absorption independent of f_oF_2 will aise the whole curve by an amount equal to he mean of this additional absorption.

In Mitra's method the shape of the curve is irst determined. Then for a group of points (for example, all points at noon in January) the nean absorption versus f_oF_2 is plotted. The urve is then adjusted along the absorption axis o fit these points best. The value of absorption where the curve crosses $f_oF_2 = 0$ is the mean of all absorption independent of f_oF_2. Mitra assumes this to be D-layer absorption. The difference between this and the mean of total absorption is the mean F-layer absorption for that group of points.

An obvious difficulty in this method is that any absorption which is uncorrelated with f_oF_2 is assumed to be D-layer absorption. If there is a third component of absorption, neither due to D layer nor correlated with f_oF_2, it is assigned to the D layer. (From the results given by *Ramanathan and Bhonsle* [1959] it appears they have assumed nighttime D-layer absorption to be zero and thus assigned the extra component of absorption to the F layer.)

This difficulty can be overcome by extending the method. It has been shown previously that f_{min}, the lowest recorded ionosonde echo from the F layer, is a reasonable measurement of absorption below the F layer [*Piggot, Beynon, and Brown*, 1957], presumably most of which is in the D layer. The variation of absorption with f_{min} is hard to obtain analytically since it depends on equipment parameters as well as ionospheric considerations. This function can be found empirically in exactly the same way as was that of f_oF_2 versus absorption above. Once this curve is found, D-layer absorption can be

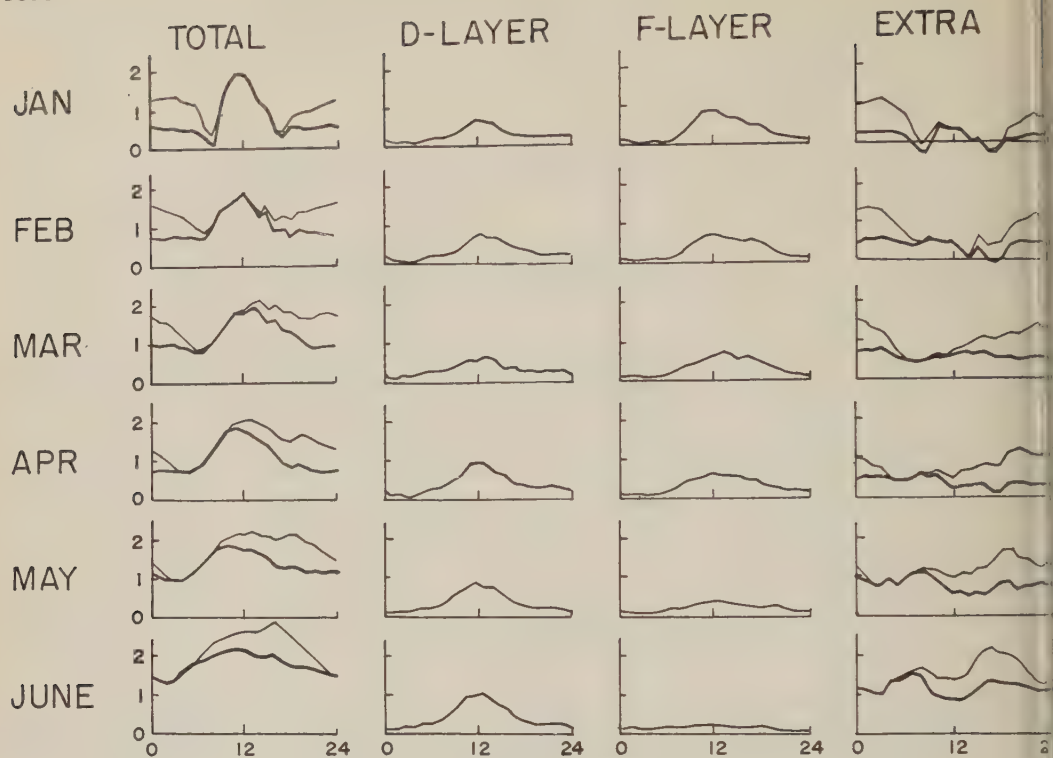

Fig. 3. Absorption components, Pullman.

separated from total absorption as F layer was by Mitra's original method.

By subtracting both F- and D-layer components as obtained above from total absorption a check is obtained. If these components account for all absorption, the result should be zero. A finite result would indicate either errors in instrumentation or data reduction or additional sources of absorption completely independent of f_oF_2 and f_{min}. Any error in the quiet-day curve would show in this component as an anomaly in absorption constant in amplitude and constant with respect to sidereal time, i.e., a bump or trough getting earlier at a rate of 2 hours per month throughout the year.

Results. The curves of absorption versus f_{min} and absorption versus f_oF_2 were determined as described above. They are the lower curves (passing through absorption = 0) in Figure 5(a) and (b). The broken parts of these curves, above $f_{min} = 2.9$ and $f_oF_2 = 15$, indicate where not enough readings were available to determine the curves to 0.1 db. Too few readings fell into these ranges, however, to affect any results appreciably. So far as could be determined, th[e] shapes of the curves did not vary by more tha[n] 0.1 db from day to night or season to seaso[n].

Also shown in Figure 5 is an example of ho[w] the D- and F-layer components are remove[d]. The readings for 1 hour through the mont[h] (thirty readings in all) are treated as describe[d] above. The values of f_{min} in this group fell int[o] three intervals and those of f_oF_2 into five inte[r]vals. Thus three and five points (x), respec[-]tively, appear on the graphs. The lines marke[d] 'Total' in Figure 5a and b, are the averages o[f] all the absorption in the group. This of cours[e] is the same in (a) and (b). The curves are ad[-]justed to fit the points best. The difference be[-]tween 'Total' and the zero crossings of th[e] curves are D, the extracted D-layer componen[t] and F, the extracted F-layer component. Sub[-]tracting D and F from *Total* leaves *Extra*, th[e] amount of apparent absorption not accounte[d] for, Figure 5(c).

This procedure is carried out for each hou[r] of each month. The only difference from th[e] graphical method described above is that th[e]

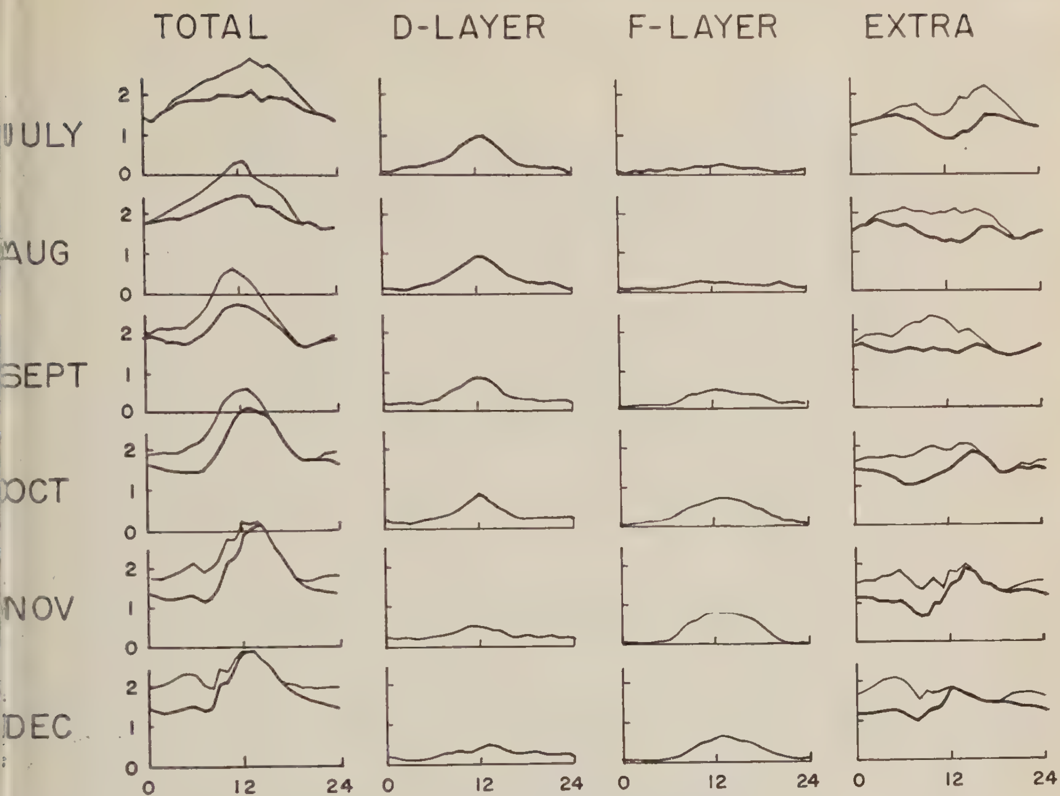

Fig. 4. Absorption components, Pullman.

curve adjustment is done on an IBM 650 electronic computer and the points are weighted in the adjustment in accordance with the number of readings contained in them.

The results of these steps are shown in Figures 1 through 4. The scales are the same in all the graphs. Where two lines appear, the upper (lighter) one is the result of this step. Dotted lines indicate that less than ten readings out of the month were scalable for those hours.

To check for errors in the quiet-day curves the *Extra* is plotted against sidereal time (for convenience the reference time was chosen as local time in January instead of the normal sidereal reference). All months are thus adjusted and plotted point by point. The results for the Stanford station are shown in Figure 6(a). From this it is quite apparent that there is an error in the shape of the quiet-day curve. From the points the amount of the error can be determined within at least 0.2 db. This correction is shown in Figure 6(b). The results for Pullman are similar.

Once the error in decibels of the quiet-day curve is known, the data can be easily corrected by subtracting this error from the curves for *Total* and *Extra* absorption with shifts for sidereal time being used. The *D-Layer* and *F-Layer* components are almost unaffected (actually there would be a very small effect caused by the sidereal shift through the month). These corrections have been made and are shown in Figures 1 through 4 as the lower (darker) lines for the *Total* and *Extra* components.

Discussion. This discussion is concerned with the corrected values of absorption components (the lower heavier lines in Figures 1 through 4). The cause of the error in the quiet-day curves and its relation to riometer methods will be discussed last.

Study of the method of extracting D- and F-layer components shows that the shapes of these curves are determined very strongly by variations in f_{min} and f_oF_2 and not by variation in total absorption. The magnitudes of the D- and F-layer curves are determined, however, by

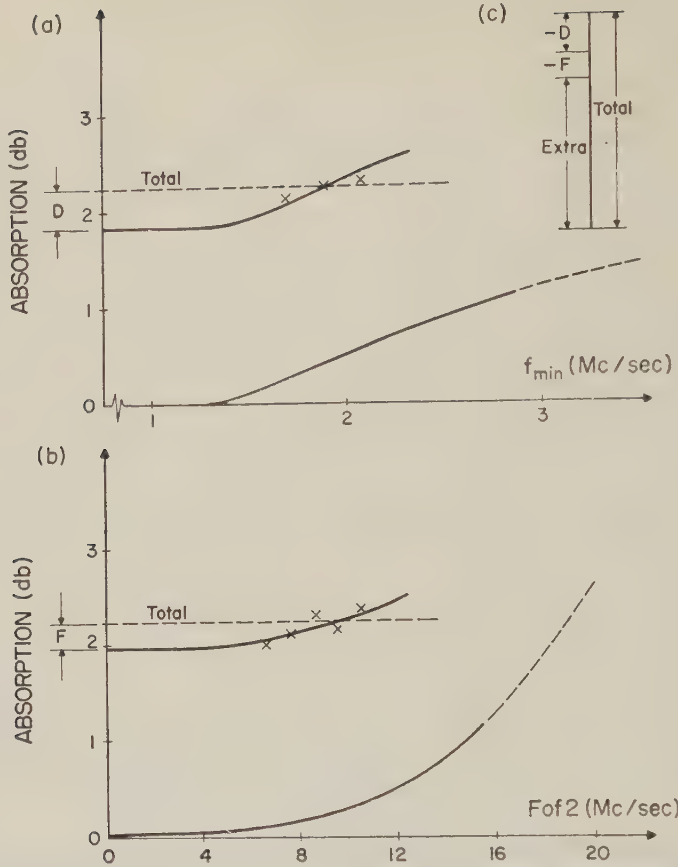

Fig. 5. Determination of components of absorption; (*a*) *D* layer; (*b*) *F* layer; (*c*) extra.

the shapes of the f_{min} versus absorption and f_oF_2 versus absorption curves. Thus observations on the shape of the *D*- and *F*-layer components could be derived from f_{min} and f_oF_2 studies alone, but magnitude of the absorption depends on these riometer studies.

The *D*-layer component of absorption obeys classical theory quite well, showing strong daily and seasonal dependence on solar zenith angle. The absorption starts rising shortly after dawn, reaches a peak within ½ to 1 hour after noon, and is falling as the sun sets. The midday peak reaches about 1.1 db in the summer and about 0.7 db in the winter.

As is usual with *F*-layer studies, classical considerations do not explain adequately the *F*-layer component of absorption. The daily variation does depend on zenith angle, rising after dawn and decreasing slowly through the night. The rise and fall of absorption are more gradual than in the *D*-layer component, and the peak of absorption generally is reached 1 to 2 hours after noon. This is due to slower recombination rates at *F*-layer altitudes. The seasonal variation does not depend on zenith angle, but is in fact 180° out of phase. Midday absorption reaches a maximum of about 0.8 db in winter and only 0.2 db in summer. This variation has been observed previously [*Rastogi*, 1960] and is connected with the 11-year solar activity cycle.

Whereas the accuracy in *Total, D-Layer,* and *F-Layer* components is about ± 0.1 db, the calculation of *Extra* from the three others reduces its accuracy to about ± 0.3 db. This shortcoming is quite apparent from the variations in the *Extra* component curves. Consequently only very general trends can be seen. There is definitely absorption present, the total amount of which is higher in the summer than in the winter. There does appear to be a diurnal variation with the maximum being reached at night, although this trend is not well defined.

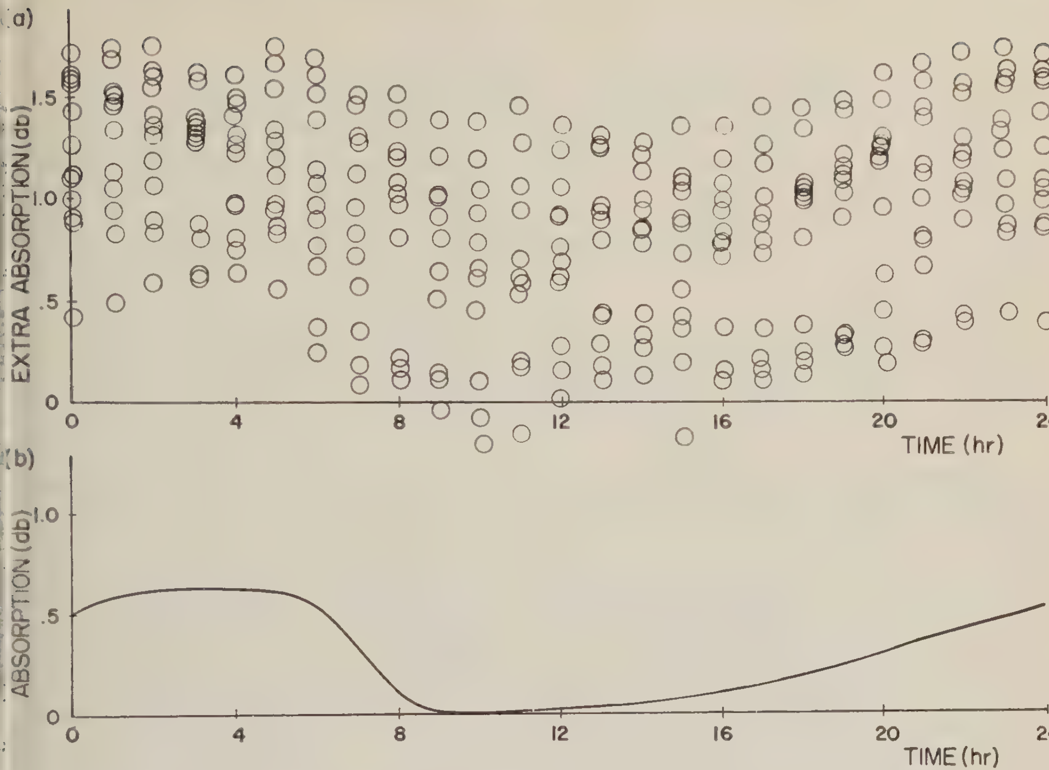

Fig. 6. (*a*) Extra component of absorption. (*b*) Correction to quiet-day curve.

The possibility that this *Extra* component is due only to equipment errors is quite remote. The long-term stability of the riometer is very good and certainly would not cause the daily variations observed. On the Pullman records there is, however, an indication of a yearly drift in some equipment parameter. The average absorption from July or August onward for Pullman is about 0.5 db higher than for Stanford. Comparison of *Total* absorption in the early months of 1958 with the same months of 1959 for the Pullman station also shows this drift. The readings for the same months are the same in shape, but 1959 readings are about 0.5 db higher than 1958 readings. This is not present in the Stanford readings.

Although no detailed attempt will be made in this paper to explain the *Extra* component of absorption, some requirements that any adequate explanation must satisfy will be outlined. It is obvious both from the method used and from other investigations of ionospheric absorption that the *Extra* is not in the *D* or *E* layers. The method used seems also to require that it not be in the *F*-layer. This is, however, not quite true. The method only requires that the *Extra* component not vary with f_oF_2. Thus it could be connected with spread *F*, as suggested by *Ramanathan and Bhonsle* [1959], or with the apparent nighttime thickening of the *F* layer. Thus any theory outlining the origin of this *Extra* component as being in the *F* layer but relatively independent of f_oF_2 or above the *F* layer meets the requirements.

The error found in the quiet-day curves for both stations is about the same. The curves and corrections are shown in Figure 7. The time reference again is local time January. The corrected curves are shown as solid lines, the original ones broken. The similarity of the corrections illustrates a basic weakness in the riometer method.

In determining the quiet-day curve for a station the highest readings (greatest noise power) are sought. These of course come from the early morning hours from about 4 to 7. The readings from these hours are shifted to the correct sidereal time and entered on the quiet-day curve.

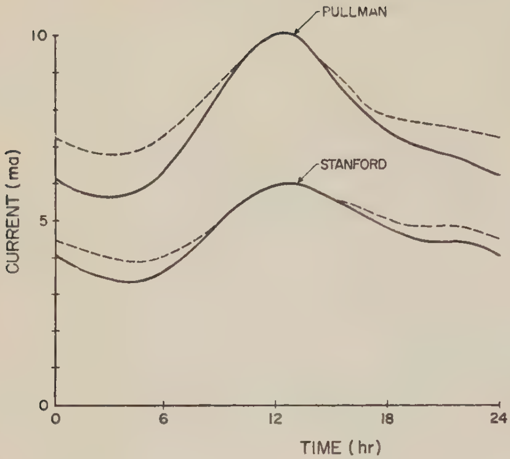

Fig. 7. Quiet-day curves for Stanford and Pullman. Dotted line: original curves. Solid line: corrected curves.

The early morning readings from different months will of course be transferred to different parts of the curve. If absorption is truly zero for these hours throughout the year, there is no problem. If early morning absorption is present, however, and its amplitude depends on the time of year, an error will be introduced into the curve.

As the graphs of total absorption show, there is early morning absorption of at least 0.5 db in the summer. As a result portions of the curve corresponding to these readings are too low. Portions of the curves corresponding to January and February (where absorption was very low) are higher, closer to the true values. For convenience in correcting the shape of the quiet-day curves, the truer readings have been lowered, rather than the too-low readings raised. Whereas theoretically this is backward, actually it is of little importance since the method cannot possibly establish the true base level of absorption, but only its shape. Thus the absorption should be raised 0.5 db or more. How much more is not known.

Conclusions. The results of this investigation reveal a component of absorption that is not accounted for by absorption below the F layer or by absorption in the F layer which depends on f_oF_2. Due to the large statistical fluctuations in this extra component, only very general properties of its diurnal and seasonal variations can be seen. It is hoped that studies of other investigators using similar methods will further define this component. It is for this purpose that the methods used have been described in detail.

A shortcoming in the basic riometer method has been found in the derivation of the quiet-day curves. A finite amount of absorption remains in the early morning hours when the riometer theory assumes it is zero. A seasonal variation in this absorption introduces errors into the quiet-day curve. A method for correcting this has been described. This method makes use of the *Extra* absorption results but could also be applied to total absorption results with possibly less accuracy.

The correction method only applies to variations in the quiet-day curve. Its absolute level cannot be found from the given data. To find this level noise charts of the sky or riometer records made at the time of sunspot minimum could possibly be used.

Acknowledgments. The above work was supported by National Science Foundation grants Y-1.44/183 and G-8835. During the preparation of the report the author was studying under a Bell Telephone Laboratories Fellowship.

References

Little, C. G., The measurement of ionospheric absorption using extraterrestrial radio waves, *Ann. IGY, 3* (II), 207–226, 1957.

Little, C. G., and H. Leinback, The riometer—a device for the continuous measurement of ionospheric absorption, *Proc. IRE, 47*, 315–320, 1959.

Mitra, A. P., and C. A. Shain, The measurements of ionospheric absorption using observations of 18.3 Mc/s cosmic radio noise, *J. Atmospheric and Terrest. Phys., 4*, 204–218, 1953.

National Bureau of Standards, *Data compilations,* Detailed values of ionospheric characteristics and F-plots, for San Francisco, Jan.-Feb., Mar.-Apr., . . . Nov.-Dec., 1958, CRPL, Boulder, Colorado, 1958.

Piggott, W. R., W. J. G. Beynon, and G. M. Brown, Ionospheric absorption and f-min, *Ann. IGY, 3* (II), 204–206, 1957.

Ramanathan, K. R., and R. V. Bhonsle, Cosmic radio noise absorption on 25 Mc/s and F scatter, *J. Geophys. Res., 64*, 1635–1637, 1959.

Rastogi, R. G., Asymmetry between the F_2 region of the ionosphere in the northern and southern hemispheres, *J. Geophys. Res., 65*, 857–868, 1960.

Stanford Electronics Laboratories, Riometer measurements, *Data Summary 1, January to December 1958*, Stanford University, 1958.

URSI-AGI Committee, Letter in *Questionnaire on ionospheric absorption measurements,* A2, Appendix A, September 15, 1958.

(Manuscript received September 9, 1960; revised September 30, 1960.)

Solar Radio Emission on Centimeter Waves and Ionization of the *E* Layer of the Ionosphere

M. R. Kundu

The Observatory, University of Michigan
Ann Arbor, Michigan

Abstract. It is shown that solar radio emission on any wavelength shorter than 30 cm is good as a solar index for ionospheric studies. The coefficient of correlation between E-layer ionization index and solar radiation decreases to a low value for wavelengths greater than about 30 cm, indicating that a major part of solar X radiation responsible for E-layer ionization originates in the solar atmosphere below the height of origin of 30-cm solar radio emission.

Introduction. It is known that the ionization of the E layer of the ionosphere is caused mainly by solar X radiation of wavelengths lying between 10 and 100 A. It is believed [*Elwert,* 1954; *Kazachevskaya and Ivanov-Kholodnyi,* 1960; *Friedman,* 1960] that this radiation, if of thermal origin, can be generated in discrete regions of the solar corona, having temperatures greater than about 10^{6}°K. On the other hand, we know that a part of the solar radio emission —the slowly varying component—originates in very hot regions in the solar corona. The radio emission from these regions has been explained in terms of thermal emission from high-density regions at coronal temperatures. Interferometric measurements [*Kundu,* 1959; *Tanaka and Kakinuma,* 1955; *Christiansen and Mathewson,* 1958] have shown that these hot regions have temperatures of the order of 10^{6}°K on wavelengths lying between 3 to 21 cm. These facts suggested a possible relationship between solar radio emission on decimeter waves and solar X radiation measured indirectly by the ionization of the E layer of the ionosphere.

Denisse and Kundu [1957] pointed out that a good correlation exists between the E layer ionization and solar radio emission on decimeter waves. Their study was based upon observations of solar radio emission made by Covington at Ottawa on 10.7-cm wavelength and measurements of E layer critical frequency (f_oE) made at Frieburg and Puerto Rico. Studies of correlation between 10.7-cm solar radio emission and E-layer ionization on both monthly and daily basis led them to suggest that the flux density of solar radiation on 10.7-cm wavelength can be used as a solar index for ionospheric studies; this index is as good as any other index (for example, Wolf sunspot number) on a time scale of the order of a month or larger, and it is better than the others on a shorter time scale [*Kundu and Denisse,* 1958]. Later on, *Minnis and Bazzard* [1958] found a similar correlation between solar radio emission on 10.7-cm wavelength and E-layer ionization at Slough.

In studying these relationships, the selection of 10.7-cm wavelength was made mainly for the reason that measurements of solar decimeter radio emission were available at this wavelength over a period of more than one solar cycle and were probably internally consistent with a relative accuracy of a few per cent [*Medd and Covington,* 1958]. From 1957, however, there exist daily measurements of solar radio emission over several wavelengths in the centimeter and decimeter regions. The relative accuracy of these measurements are comparable to those of Covington's 10.7-cm measurements within ±3 per cent [*Tanaka,* 1955]. With the availability of such measurements of solar radio emission on centimeter and decimeter wavelengths, it seemed interesting to study the relationship between E-layer ionization and solar radio emission over different wavelengths in the centimeter and decimeter regions.

Data. For this study, daily data of solar radio emission and of f_oE over the period from July 1957 to December 1959 have been used. The daily values of E-layer ionization index (J_E) over the period from July 1957 to December 1958 have been taken from the data published by *Minnis and Bazzard* [1959*b*]. The daily values of index J_E for 1959 were kindly supplied by Dr. Minnis of Radio Research Sta-

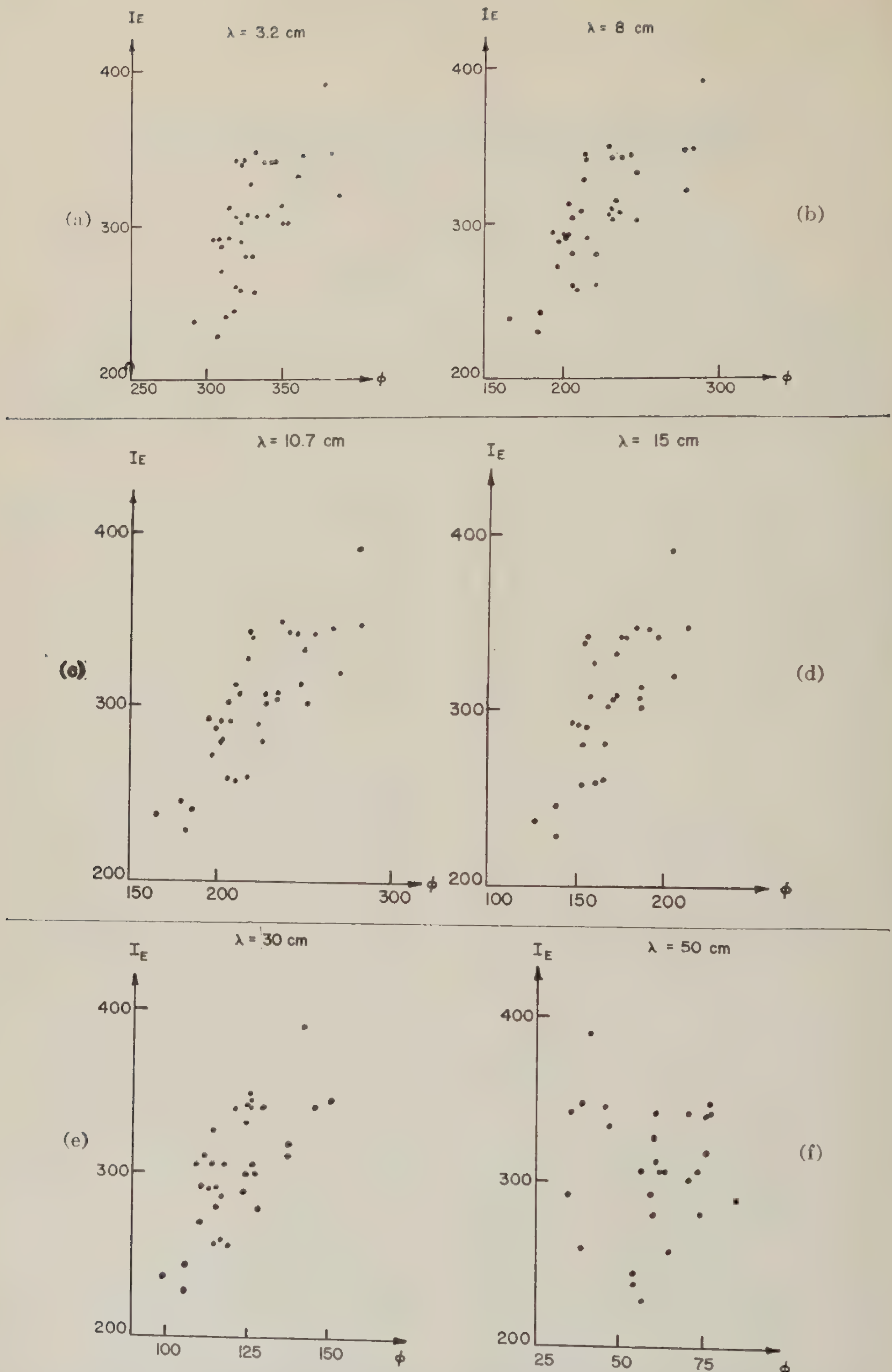

Fig. 1. Correlation diagrams of monthly mean ionospheric index I_E versus solar radiation on (*a*) 3.2 cm, (*b*) 8 cm, (*c*) 10.7 cm, (*d*) 15 cm, (*e*) 30 cm, and (*f*) 50 cm, expressed in units of $10^{-22} wm^{-2}(c/s)^{-1}$. The data cover the period July 1957–December 1959.

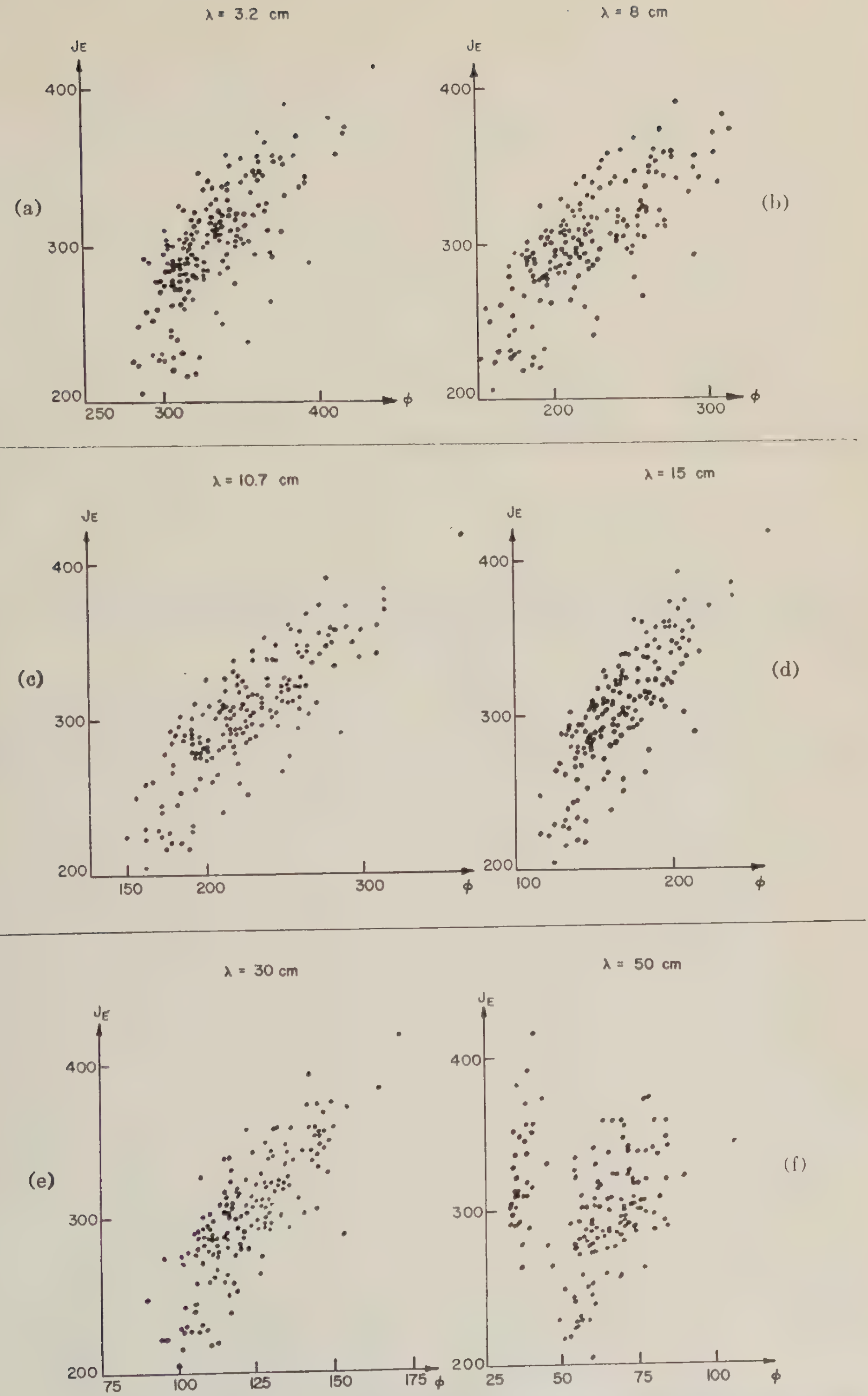

Fig. 2. Correlation diagrams of 5-day mean values of daily ionospheric index J_E versus solar radiation on (*a*) 3.2 cm, (*b*) 8 cm, (*c*) 10.7 cm, (*d*) 15 cm, (*e*) 30 cm, and (*f*) 50 cm, expressed in units of $10^{-22} wm^{-2}(c/s)^{-1}$. The data cover the period July 1957–December 1959.

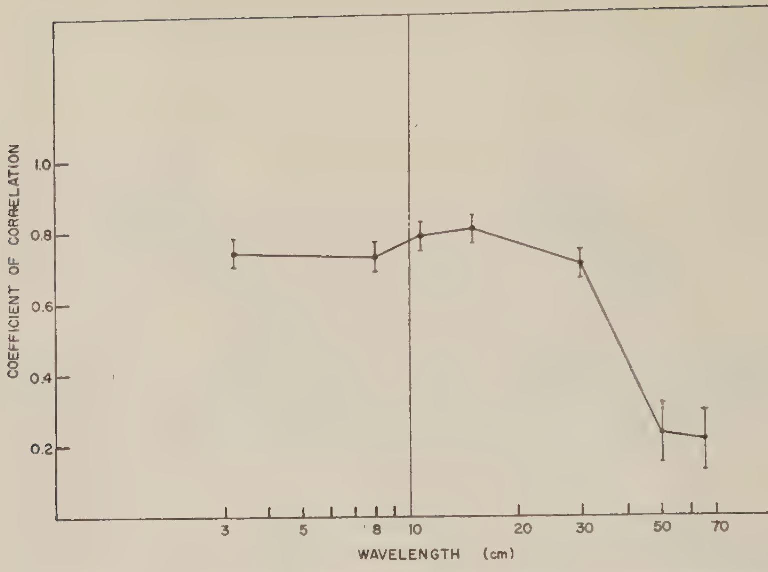

Fig. 3. Coefficient of correlation between 5-day mean values of J_E and solar radiation as a function of wavelength. The data for all wavelengths except 65 cm cover the period January 1958–December 1958. The data for 65 cm cover the period July 1957–June 1958. A short vertical line at each wavelength represents the probable error.

tion of Slough. We have also used the mean monthly index (I_E) published by *Minnis and Bazzard* [1959*a*]. The daily values of solar radio emission on 3.2-, 8-, 15-, and 30-cm wavelengths have been taken from the published data of the Nagoya University of Japan. The 10.7-cm daily values used are those of Ottawa. The 50-cm data have been obtained from the published bulletins of the Royal Observatory of Belgium. The Nagoya measurements of solar radio emission are done in the same way over all wavelengths and the relative accuracy of different sets of measurements are comparable to each other within a few per cent. The Ottawa measurements have a relative accuracy of 3–4 per cent [*Medd and Covington,* 1958] and it is claimed that the 50-cm measurements of Belgium are consistent among themselves within a few per cent during the period considered in this paper.

Discussion. Figures 1*a*, *b*, *c*, *d*, *e*, and *f* show the correlation diagrams of mean monthly index I_E versus solar radio emission on wavelengths of 3.2, 8, 10.7, 15, 30, and 50 cm, respectively, in units of $10^{-22} wm^{-2}(c/s)^{-1}$. It is seen that the correlation is good and more or less similar over any of the wavelengths between 3 and 30 cm. There is, however, a tendency for the correlation to be better on wavelengths between 10.7 and 30 cm than on the shorter wavelengths. The correlation on 50 cm is rather poor. To examine this correlation on a time scale shorter than a month, we have used the 5-day average values of index J_E and of solar radio emission on different wavelengths. Figures 2*a*, *b*, *c*, *d*, *e*, and *f* show the corresponding correlation diagrams. It appears from these diagrams that the correlation is reasonably good over the range of wavelengths 3 to 30 cm and is poor on 50 cm wavelength. It should also be noted that the use of solar radio emission on 65 cm (Boulder data) has shown a correlation as poor as on 50 cm wavelength. Such poor correlations have no statistical significance. One may notice that the correlation is slightly better on 10.7 and 15 cm than on the other wavelengths between 3 and 30 cm. This may mean either that the correlation is really better on wavelengths between 10.7 and 15 cm, or that the measurements of solar radio emission are more accurate on these than on other wavelengths. In Figure 3 is plotted the coefficient of correlation between 5-day average values during 1958 as a function of wavelength. We find that the coefficient of correlation is about 0.75 on 3.2 and 8 cm, reaches a maximum value of about 0.8 on 10.7- and 15-cm wavelengths, and

then decreases through 0.7 on 30 cm to about 0.2 on 50- and 65-cm wavelengths. The slight increase of the correlation coefficient on 10.7 cm and 15 cm as compared to that on other wavelengths between 3 and 30 cm has probably no statistical significance.

The present study shows that solar radio emission over any wavelength in the range 3 to 30 cm is good as a solar index for ionospheric studies on a time scale of the order of a month or larger. On the basis of present measurements, however, it appears that on a shorter time scale solar radio emission on wavelengths between 10.7 and 15 cm is probably the best index for ionospheric studies. The fact that the coefficient of correlation is quite high at wavelengths shorter than 30 cm and is low at longer wavelengths suggests that a major part of the solar radiation (soft X rays) responsible for *E*-layer ionization originates in the solar atmosphere below the height of origin of 30-cm solar radio emission.

Acknowledgment. I wish to thank Mr. J. R. Tanner for assistance in the necessary computations. This work was supported by the Office of Naval Research Contract Nonr 1224 (16).

References

Christiansen, W. N., and D. S. Mathewson, *Paris Symposium on Radio Astronomy,* edited by R. N. Bracewell, Stanford University Press, Stanford, California, p. 109, 1958.

Denisse, J. F., and M. R. Kundu, *Compt. rend., 244,* 45, 1957.

Elwert, G., *Z. Naturforsch., 9a,* 637, 1954.

Friedman, H., *Physics of the Upper Atmosphere,* edited by J. A. Ratcliffe, Academic Press, New York and London, p. 144, 1960.

Kazachevskaya, T. V., and G. S. Ivanov-Kholodnyi, *Soviet Astronomy, AJ, 3,* 937, 1960.

Kundu, M. R. *Ann. astrophys., 22,* 1, 1959.

Kundu, M. R., and J. F. Denisse, *J. Atmospheric and Terrest. Phys., 13,* 176, 1958.

Medd, W. J., and A. E. Covington, *Proc. IRE, 46,* 112, 1958.

Minnis, C. M., and G. H. Bazzard, *Nature, 181,* 1796, 1958.

Minnis, C. M., and G. H. Bazzard, *J. Atmospheric and Terrest. Phys., 14,* 213, 1959*a*.

Minnis, C. M., and G. H. Bazzard, *J. Atmospheric and Terrest. Phys., 17,* 57, 1959*b*.

Tanaka, H., *Proc. Res. Inst. Atmos., Nagoya Univ., 3,* 117, 1955.

Tanaka, H., and T. Kakinuma, *Proc. Res. Inst. Atmos., Nagoya Univ., 3,* 84, 1955.

(Manuscript received August 25, 1960.)

Doppler Shifts and Faraday Rotation of Radio Signals in a Time-Varying, Inhomogeneous Ionosphere Part I. Single Signal Case

JOHN M. KELSO

Space Technology Laboratories, Inc.
Los Angeles 45, California

Abstract. Equations are derived for the frequency shift of a radio signal transmitted to the ground from a space vehicle in or above the ionosphere. The principal restriction on the generality of the results is that the ionosphere is treated as quasi-isotropic; i.e., the ray paths are obtained by methods which would be exact in a slowly varying isotropic medium, but the refractive index is permitted to be a function of ray direction (implying an anisotropic ionosphere).

The following conditions prevail: (*a*) the (slowly varying) ionosphere may be a general function of three spatial coordinates and of time; (*b*) the vehicle may follow an arbitrary (nonrelativistic) trajectory; (*c*) the magnetic field, which characterizes the dependence of the refractive index on direction, may have arbitrary form.

Introduction. A radio signal passing through the ionosphere suffers a shift in frequency caused by the change in phase resulting from time variations in the ionosphere and motions of the source or receiver. This effect is of considerable importance for signals between the earth and a space vehicle (rocket, satellite, or space probe). On the one hand, the frequency shifts may be made useful in the study of the properties of the ionosphere; on the other hand, such frequency shifts are unfortunate because they disturb delicate guidance and tracking operations.

In the present paper (Part I) we consider a medium in which the refractive index is an arbitrary function of the three rectangular coordinates, x, y, z, the time t, and, in some cases, of the ray direction. We determine the rate of change of phase (or the instantaneous frequency) of a signal transmitted between a fixed point and a space vehicle moving along an arbitrary trajectory.

In a later paper (Part II) we compute the rate of change of the difference in phase path of two signals whose refractive indices differ slightly. The latter derivation is used to determine the quantity observed in the Seddon-Jackson two-frequency Doppler experiment for the measurement of electron density [*Seddon*, 1953; *Jackson and Seddon*, 1958] and it is also used to compute the rate of change of the Faraday rotation of the plane of polarization in a magneto-ionic medium [*Browne, Evans, Hargreaves, and Murray*, 1956].

The derivations result in expressions containing terms to be evaluated at the position of the vehicle plus integrals evaluated along the ray path. An application to a specific problem, therefore, requires a knowledge of the ray path from the ground to the vehicle at the instant for which the frequency shifts are to be evaluated. For an ionosphere of complicated form, the calculation of the ray path will require the use of a high-speed digital computer.

Since the entire problem can be handled on a digital computer by calculating the phase along a number of ray paths corresponding to successive vehicle positions and differentiating the phase numerically, it is reasonable to ask what advantages the present method offers beyond those obtained from purely numerical methods.

Clearly, for the purpose of obtaining a general understanding of the problems, relatively simple expressions of the present form have a great advantage over the digital method. The present procedure requires the calculation of only one ray path for each evaluation of the frequency shift. In general, the numerical evaluation of the present expressions along the one ray path would require less computing time than would the calculation of successive ray paths for the use of the digital methods. These comparisons will be treated in greater detail in a later publication

concerning the numerical application of these methods.

In the present derivations the problem studied has the following general properties: (1) the (slowly varying) refractive index is an arbitrary function of position and time; (2) the vehicle moves in an arbitrary trajectory; (3) the magnetic field may have an arbitrary form; (4) the effects caused by variations in the shape of the ray are included.

In most of the derivations given in the literature, one or more of these properties are restricted by special assumptions. For example, it is common to permit the refractive index to vary with height only. Or, in some derivations, the ray along which the signal propagates is assumed to be straight.

The restriction, used in the following derivations, to the case of one fixed endpoint for the ray path can easily be removed by repeating the derivations with obvious modifications.

A basic assumption used in the following work is the validity of Fermat's principle in the form,

$$\delta \int n\,ds = 0$$

where this expression means that the variation of the integral of the phase index of refraction along the ray path must vanish. From this principle, one may derive Euler's equations, stated below as (7).

Thus, the present work is subject to the usual restrictions of ray optics such as the necessity to avoid caustics and regions of rapid change in the refractive index; i.e., the medium is slowly varying. In addition, it should be noted that Fermat's principle in the present form is not rigorously correct in an anisotropic medium [see *Hasselgrove*, 1955]. In what follows, the ionosphere is treated as quasi-isotropic; i.e., theory appropriate to an isotropic medium is applied, but refractive indices appropriate for the (anisotropic) ionosphere in the presence of the geomagnetic field are used. It is also supposed that collisions between electrons and uncharged particles are infrequent; i.e., that the absorption is small. The error in this treatment is negligible for many frequencies used in present satellite work, but it could be quite important at lower frequencies.

Phase path variation and instantaneous frequency for a single signal. Consider a medium in which the refractive index μ is a function of the rectangular co-ordinates x, y, z, the ray slopes x' and y' defined in equations 3 and 4 below, and of the time t. We consider a signal transmitted between the origin ($x = y = z = 0$) and a moving vehicle, whose position at time t is denoted by ξ, η, ζ. Let the ray path at time t be Γ_1 and let $ds = (dx^2 + dy^2 + dz^2)^{1/2}$ be the element of arc along Γ_1.

As will be shown below, we can compute the instantaneous frequency if we know the time derivative of the phase path (or optical path) P, which, as is well known, may be written,

$$P = \int_{\Gamma_1} \mu(x, y, z, x', y', t)\, ds = \int_0^{\zeta} g(x, y, z, x', y', t)\, dz \qquad (1)$$

where

$$g(x, y, z, x', y', t) = \mu(x, y, z, x', y', t) \cdot \sqrt{1 + (x')^2 + (y')^2} \qquad (2)$$

$$x' = \frac{\partial x}{\partial z} \qquad (3)$$

$$y' = \frac{\partial y}{\partial z} \qquad (4)$$

We wish to find the time variation of P as the vehicle moves in its trajectory. We note that P is a function of x, y, ζ, x', y' (all of which are functions of t), and of t.

Then, differentiating (1), we find,

$$\frac{dP}{dt} = g_v \frac{d\zeta}{dt} + \int_0^{\zeta} \frac{\partial g}{\partial t}\, dz + \int_0^{\zeta} \left(\frac{\partial g}{\partial x}\frac{\partial x}{\partial t} + \frac{\partial g}{\partial x'}\frac{\partial x'}{\partial t}\right) dz + \int_0^{\zeta} \left(\frac{\partial g}{\partial y}\frac{\partial y}{\partial t} + \frac{\partial g}{\partial y'}\frac{\partial y'}{\partial t}\right) dz \qquad (5)$$

where g_v denotes the value of g taken at the vehicle. Now consider the integral

$$J = \int_0^{\zeta} \left(\frac{\partial g}{\partial x}\frac{\partial x}{\partial t} + \frac{\partial g}{\partial x'}\frac{\partial x'}{\partial t}\right) dz$$

By definition of x', we have

$$\frac{\partial x'}{\partial t} = \frac{\partial}{\partial t}\left(\frac{\partial x}{\partial z}\right)$$

ne operators $\partial/\partial t$ and $\partial/\partial z$ are commutative. ence,

$$\frac{\partial x'}{\partial t} = \frac{\partial}{\partial z}\left(\frac{\partial x}{\partial t}\right)$$

hen J may be written,

$$J = \int_0^{\zeta} \frac{\partial g}{\partial x}\frac{\partial x}{\partial t}\,dz + \int_0^{\zeta} \frac{\partial g}{\partial x'}\frac{\partial}{\partial z}\left(\frac{\partial x}{\partial t}\right) dz$$

ntegrating the second integral by parts, we btain

$$= \int_0^{\zeta}\left[\frac{\partial g}{\partial x} - \frac{\partial}{\partial z}\left(\frac{\partial g}{\partial x'}\right)\right]\frac{\partial x}{\partial t}\,dz + \left(\frac{\partial g}{\partial x'}\frac{\partial x}{\partial t}\right)_0^{\zeta} \qquad (6)$$

pplying Fermat's principle to the ray, we btain Euler's Equations,

$$\begin{aligned}\frac{\partial g}{\partial x} - \frac{\partial}{\partial z}\left(\frac{\partial g}{\partial x'}\right) &= 0\\ \frac{\partial g}{\partial y} - \frac{\partial}{\partial z}\left(\frac{\partial g}{\partial y'}\right) &= 0\end{aligned} \qquad (7)$$

ndependently of the value of t. Thus, the integral n equation 6 vanishes, and noting that $\partial x/\partial t = 0$ t $z = 0$, we find

$$J = \left(\frac{\partial g}{\partial x'}\frac{\partial x}{\partial t}\right)_{z=\zeta}$$

reating the integral in y in the same manner, quation 5 is reduced to

$$\frac{dP}{dt} = g_{\zeta}\frac{d\zeta}{dt} + \left(\frac{\partial g}{\partial x'}\frac{\partial x}{\partial t} + \frac{\partial g}{\partial y'}\frac{\partial y}{\partial t}\right)_{z=\zeta} + \int_0^{\zeta}\frac{\partial g}{\partial t}\,dz \qquad (8)$$

ntroducing equation 2, we have

$$\begin{aligned}\frac{dP}{dt} = {}&\left[\mu\sqrt{1+(x')^2+(y')^2}\,\frac{d\zeta}{dt}\right]_{z=\zeta}\\ &+\left[\frac{\mu x'}{\sqrt{1+(x')^2+(y')^2}}\frac{\partial x}{\partial t}\right.\\ &\left.+\frac{\mu y'}{\sqrt{1+(x')^2+(y')^2}}\frac{\partial y}{\partial t}\right]_{z=\zeta}\\ &+\int_{\Gamma}\frac{\partial \mu}{\partial t}\,ds + \left[\left(\frac{\partial \mu}{\partial x'}\frac{\partial x}{\partial t} + \frac{\partial \mu}{\partial y'}\frac{\partial y}{\partial t}\right)\right.\\ &\left.\cdot\sqrt{1+(x')^2+(y')^2}\right]_{z=\zeta}\end{aligned} \qquad (9)$$

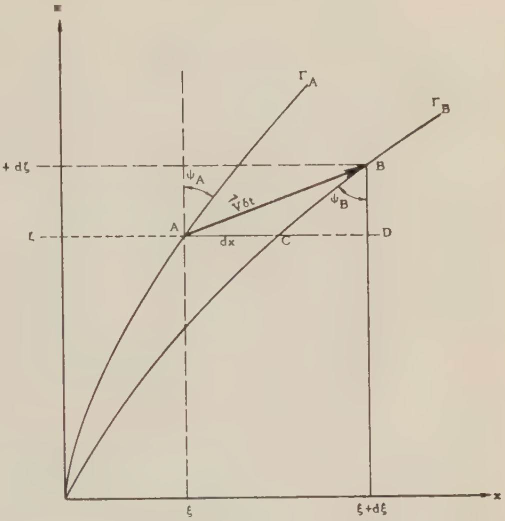

Fig. 1. Ray path geometry.

It is important to note that $\partial x/\partial t$ and $\partial y/\partial t$ do not represent the horizontal components of the vehicle velocity. Rather, these partial derivatives represent the rate of horizontal motions of a point on the ray at a fixed height $z = \zeta$. This distinction is illustrated in Figure 1 for an instance in which the ray and the vehicle are both confined to the xz plane. At time t, the vehicle is at the point A, which has coordinates $(\xi, 0, \zeta)$, and the ray from the origin is Γ_A. At time $t + dt$, the vehicle is at the point B, which has coordinates $(\xi + d\xi, 0, \zeta + d\zeta)$, and the ray from the origin is Γ_B. At the height $z = \zeta$, the x displacement from Γ_A to Γ_B is $\overline{AC} = dx$. The horizontal vehicle displacement is $\overline{AD} = d\zeta$. Thus:

$$dx = d\zeta - \overline{CD}$$

From Figure 1, we see that $\overline{CD} = d\zeta \tan\psi_B$. Now, the quantity $\tan\psi_B$ differs from $\tan\psi_A$ by a quantity of the second order in dt. Hence, in the limit as $dt \to 0$, we may write,

$$dx = d\xi - d\zeta \tan\psi_A$$

Since $\tan\psi_A$ is the local slope of the ray, we may write $\tan\psi_A = \partial x/\partial z = x'$, and thus,

$$\frac{\partial x}{\partial t} = \frac{d\xi}{dt} - \frac{d\zeta}{dt}x'$$

Clearly, we may also write for three dimensions,

$$\frac{\partial y}{\partial t} = \frac{d\eta}{dt} - \frac{d\zeta}{dt} y'$$

Substituting in equation 9 and invoking equations 3 and 4, we obtain

$$\frac{dP}{dt} = \mu_v \left[\frac{\frac{d\xi}{dt} dx + \frac{d\eta}{dt} dy + \frac{d\zeta}{dt} dz}{\sqrt{dx^2 + dy^2 + dz^2}} \right]_{z=\zeta} + \int_\Gamma \frac{\partial \mu}{\partial t} ds + \left[\left(\frac{\partial \mu}{\partial x'} \frac{\partial x}{\partial t} + \frac{\partial \mu}{\partial y'} \frac{\partial y}{\partial t} \right) \cdot \sqrt{1 + (x')^2 + (y')^2} \right]_{z=\zeta} \tag{10}$$

where μ_v is the value of μ evaluated at the vehicle.

Now the unit vector in the direction of the ray at A is:

$$\mathbf{m} = \frac{\mathbf{i}\, dx + \mathbf{j}\, dy + \mathbf{k}\, dz}{\sqrt{dx^2 + dy^2 + dz^2}},$$

The vehicle velocity is,

$$\mathbf{v} = \mathbf{i} \frac{d\xi}{dt} + \mathbf{j} \frac{d\eta}{dt} + \mathbf{k} \frac{d\zeta}{dt}$$

Hence, we may write (8) as

$$\frac{dP}{dt} = \mu_v V_{11} + \int_\Gamma \frac{\partial \mu}{\partial t} ds + \left[\left(\frac{\partial \mu}{\partial x'} \frac{\partial x}{\partial t} + \frac{\partial \mu}{\partial y'} \frac{\partial y}{\partial t} \right) \cdot \sqrt{1 + (x')^2 + (y')^2} \right]_{z=\zeta} \tag{11}$$

where

$$V_{11} = \mathbf{m} \cdot \mathbf{v}$$

is the component of vehicle velocity along the ray path.

The phase ϕ is equal to k_0 times P, where $k_0 = 2\pi f_0/c$, f_0 is the transmitted frequency, and c is the velocity of light in free space. The change, Δf, in the instantaneous frequency is given by

$$\Delta f = \frac{1}{2\pi} \frac{d\phi}{dt} = \frac{f_0}{c} \left\{ \mu_v V_{11} + \int_\Gamma \frac{\partial \mu}{\partial t} ds + \left[\left(\frac{\partial \mu}{\partial x'} \frac{\partial x}{\partial t} + \frac{\partial \mu}{\partial y'} \frac{\partial y}{\partial t} \right) \cdot \sqrt{1 + (x')^2 + (y')^2} \right]_{z=\zeta} \right\} \tag{12}$$

These relations are valid for any arbitrary three-dimensional refractive index distribution for which quasi-isotropic ray theory is applicable.

In an isotropic medium the refractive index μ is independent of the direction of the ray, and hence, is independent of x' and y'. In this case the last term of equations 11 and 12 vanishes and we obtain

$$\frac{dP}{dt} = \mu_v V_{11} + \int_\Gamma \frac{\partial \mu}{\partial t} ds \tag{13}$$

$$\Delta f = \frac{f_0}{c} \left(\mu_v V_{11} + \int_\Gamma \frac{\partial \mu}{\partial t} ds \right) \tag{14}$$

It is worthy of note that equations 11 and 12 are written independently of the coordinate system.

Alternative derivation. As an alternative to the preceding derivation, we can use a method which is a generalization of a procedure used by Altshuler (unpublished memorandum) in studying the Doppler shift in a time-invariant isotropic medium. This alternative derivation is presented because it helps to clarify the nature of the present problem, and because it serves as an introduction to the method applied to the more complex problems to be treated in Part II.

In this derivation, we begin with the ray path Γ_A between the ground and the vehicle at position A and at time t. Using Γ_A as a basis, we note that the quantity g at an arbitrary height z is specified by the variables x, y, z, x', y', t. The quantity g at a corresponding point (at a height z) on ray Γ_B is specified by the variables $x + \delta x, y + \delta y, z, x' + \delta x', y' + \delta y', t + \delta t$.

Then the phase path P_A along path Γ_A, and the phase path P_B along Γ_B may be written in the form of equation 1,

$$P_A = \int_0^\zeta g(x, y, z, x', y', t)\, dz \tag{15}$$

$$P_B = \int_0^{\zeta + d\zeta} g(x + \delta x, y + \delta y, z, x' + \delta x', y' + \delta y', t + \delta t)\, dz \tag{16}$$

Expanding the integrand of equation 16 in a Taylor series neglecting terms of order higher than the first,

$$P_B = \int_0^{\zeta + d\zeta} \left[g + \frac{\partial g}{\partial x} \delta x + \frac{\partial g}{\partial y} \delta y + \frac{\partial g}{\partial x'} \delta x' + \frac{\partial g}{\partial y'} \delta y' + \frac{\partial g}{\partial t} \delta t \right] dz \tag{17}$$

e change in phase path is

$$\delta P = P_B - P_A \tag{18}$$

Then, substracting (15) from (17), we have

$$= \int_0^{\zeta} \frac{\partial g}{\partial t}\, dz + \int_0^{\zeta} \left(\frac{\partial g}{\partial x}\, \delta x + \frac{\partial g}{\partial x'}\, \delta x'\right) dz$$

$$+ \int_0^{\zeta} \left(\frac{\partial g}{\partial y}\, \delta y + \frac{\partial g}{\partial y'}\, \delta y'\right) dz$$

$$+ \int_{\zeta}^{\zeta+d\zeta} g\, dz + \int_{\zeta}^{\zeta+d\zeta} \left(\frac{\partial g}{\partial x}\, \delta x + \frac{\partial g}{\partial x'}\, \delta x'\right.$$

$$\left. + \frac{\partial g}{\partial y}\, \delta y + \frac{\partial g}{\partial y'}\, \delta y' + \frac{\partial g}{\partial t}\, \delta t\right) dz \tag{19}$$

e now divide δP by δt take the limit as δt proaches zero. After division by δt, all the ms of the last integral can be shown to be of ler δt, and, hence, this last integral vanishes δt approaches zero. Thus, we can readily see at $\delta P/\delta t$ is given by equation 5 in the limit δt approaches zero. Therefore, this derivation ovides an alternative method for obtaining (5).

Discussion and examples. It is interesting to nsider the application of these results to an tropic and time-invariant medium in which e vehicle is moving parallel to the surfaces of atification in a spherically stratified medium. t us suppose that the ray is confined to the ϕ plane and let the vehicle coordinates at time be r and ϕ. We suppose the medium below me height r_o to have a refractive index $\mu_o = 1$, d that the ray makes an angle θ_o with the dial direction at the height r_o. Thus, θ_o is the gle of incidence. At the vehicle, the ray makes angle θ, and by the well-known Bouger's rule, e have

$$\mu r \sin \theta = \mu_0 r_0 \sin \theta_0 = r_0 \sin \theta_0 \tag{20}$$

y definition, V_{11} is the component of V along e ray path. Since the vehicle is moving in the ϕ rection, we have

$$V_{11} = V \cos (90^0 - \theta) = V \sin \theta \tag{21}$$

Then, from equation 13, and using (20) and 1), we find

$$= \mu_v V_{11} = \left(\frac{r_0 \sin \theta_0}{r \sin \theta}\right) V \sin \theta$$

$$= \left(\frac{r_0}{r}\right) V \sin \theta_0 \tag{22}$$

Therefore, if we are given r_o, r, and V, the rate of change of phase path or the instantaneous frequency may be considered to be a function of the angle of incidence θ_o only. This special case was previously established by *Weeks* [1958], using a different type of derivation.

In a previous paper [*Kelso*, 1960], an equation equivalent to equation 14 was derived by a procedure which was more intuitive than the methods used here. Following this earlier paper, we assume that the frequency is high enough to permit the use of the approximation

$$\mu = 1 - \frac{40N}{f_0^2} \tag{23}$$

where N is the number of electrons per cubic meter, and f_o is the transmitted frequency in cycles per second. Then equation 14 becomes, approximately,

$$\Delta f = \frac{f_0 V_{11}}{c}$$

$$- \frac{40 V_{11}}{c f_0} \left[N_v + \frac{1}{V_{11}} \int_\Gamma \frac{\partial N}{\partial t}\, ds \right] \tag{24}$$

The first term represents the Doppler shift in the absence of ionization. The first term in the brackets results from the electrons in the neighborhood of the vehicle, and the second term in brackets yields the contribution to the frequency shift caused by changes in electron density along the path.

In this earlier paper by the author, data obtained by *Evans* [1957] were used to show that for great vehicle attitudes the contribution due to the integral term can exceed that due to the presence of N_v. Evans's results indicate that in the morning or afternoon hours we may find along a vertical path the value

$$\int_\Gamma \frac{\partial N}{\partial t}\, ds = 1.4 \times 10^{13}$$

electrons meter^{-2} sec^{-1}

Then supposing that the vehicle moves vertically above the observation point with a velocity of $V_{11} = 1.1 \times 10^4$ meter sec^{-1}, the integral term in the brackets of equation 24 becomes,

$$\frac{1}{V_{11}} \int_\Gamma \frac{\partial N}{\partial t}\, ds = 1300 \text{ electrons cm}^{-3}$$

This value is greater than the N_v expected at heights of a few thousand kilometers. Some addi-

tional computations made in the earlier paper for the case of a horizontally stratified ionosphere require reconsideration because at the time that paper was written, the terms in the expression for the frequency shift were not defined with the precision available from the present results, and it was then believed that the term corresponding to the integral term of equation 24 should explicitly include effects due to the vehicle motion across the ray path. The present derivation proves that this apparently reasonable belief is not correct.

Conclusion. An expression for the frequency shift for a radio signal propagated through the ionosphere between a space vehicle and the ground has been derived by rigorous mathematical methods for physical conditions of wide applicability in ionospheric problems.

As indicated in the introduction, a second part of the paper to be published later will show the application of similar procedures to the problem of two signals transmitted simultaneously. The two signal results have special applicability to the study of electron densities by a two-frequency Doppler method, and to the problem of the Faraday rotations of the plane of polarization.

Acknowledgments. The author would like t[o] express his indebtedness to Drs. C. D. Grave[s], S. Altshuler, and A. R. Sims, all of Space Technol[o]gy Laboratories, Inc., and to Dr. O. K. Garriot[t] of Stanford University, for their advice and sug[g]estions in numerous discussions.

References

Browne, I. C., J. V. Evans, J. K. Hargreaves, an[d] W. A. S. Murray, *Proc. Phys. Soc., B., 69,* 901–920, 1956.

Daniels, Fred B., and Siegfried J. Bauer, *J. Franklin Inst., 267,* 187–200, 1959.

Evans, J. V., *J. Atmospheric and Terrest. Phys., 1[1],* 259–271, 1957.

Hasselgrove, J., *Proceedings of Cambridge Conference Ionospheric Research,* 355–364, The Physical Society, London, 1955.

Jackson, John E., and J. Carl Seddon, *J. Geophys. Res., 63,* 197–208, 1958.

Kelso, John M., *Electromagnetic Wave Propagation* (Edited by M. Desirant and J. L. Michiels), 291–298, Academic Press, London and New York, 1960.

Seddon, J. Carl, *J. Geophys. Res., 58,* 323–335, 1953.

Weeks, K., *J. Atmospheric and Terrest. Phys., 12,* 335–338, 1958.

(Manuscript received August 11, 1960.)

. of Geophysical Research Volume 65, No. 12 December 1960

Origin of the Sodium Airglow

Andrew E. Potter, Jr., and Betty S. Del Duca

Lewis Research Center
National Aeronautics and Space Administration
Cleveland, Ohio

Abstract. Comparison of observed and calculated altitude distributions for the sodium irglow indicates that airglow processes involving combined sodium cannot account for the bservations. It is suggested that the airglow results from collisions of neutral atomic sodium vith vibrationally excited oxygen. This process can account for the observed altitude distri- ution and, possibly, the total intensity of the sodium airglow.

Introduction

ice the discovery of the sodium D lines in airglow by *Bernard* [1938], a number of nations have been offered for their pres- . It is the purpose of this paper to discuss ally the most plausible of these explana- and to propose a new explanation based ipally on the rocket observations of *Hepp- ind Meredith* [1958], *Koomen, Scolnik, and ey* [1957], and *Bedinger, Manring, and sh* [1957, 1958]. None of the previously pro- d explanations of the sodium airglow can in the observed altitude distribution of the im airglow. It is concluded that only a proc- that does not involve chemically combined im can do so. Hence, a process involving sodium, probably neutral atomic sodium, he origin of the sodium airglow. The most y process is thought to be the excitation of im by collisions with vibrationally excited gen. This process appears to be capable of unting aproximately for both the intensity the altitude distribution of the sodium air- w.

Previously Proposed Mechanisms for Airglow

he various explanations that have been red for the sodium airglow are summarized Table 1, which lists the processes explaining airglow, the author who proposed each proc- , and the author who criticized it.

he only explanations to gain some degree of eptance are the following:

$$NaH + H \rightarrow Na(^2P) + H_2 \quad (1)$$

$$NaH + O \rightarrow Na(^2P) + OH \quad (2)$$

$$NaO + O \rightarrow Na(^2P) + O_2 \quad (3)$$

(followed by $Na(^2P) \rightarrow Na(^2S) + h\nu$). Recently, *McKinley and Polanyi* [1958] studied the reaction of sodium and atomic hydrogen, and concluded that reaction 1 does not occur. Consequently, we shall not discuss it any further. Although no experimental verification of reaction 2 exists, it must be admitted as a possibility, since it is exothermic. Concerning reaction 3, there is some evidence that it does not occur. According to estimated heats of formation, the reaction is endothermic. Since estimates are often incorrect, it is important to note experiments by *Ogawa* [1954], in which the admixture of oxygen atoms to a gas stream believed to contain NaO failed to show any evidence of sodium D line emission. This result supports the thermodynamic calculation and leads to the conclusion that the process probably does not occur. Even so, we shall discuss it further, chiefly because of its earlier widespread acceptance.

A primary requirement of any airglow process is that it be capable, at least in principle, of accounting for the observed intensity of the airglow. It is not immediately obvious whether or not the NaH + O reaction can do this. To find out, we will assume that NaH is produced by the reaction

$$NaO_2 + H \rightarrow NaH + O_2 \quad (4)$$

and destroyed by the luminescent reaction 2. (*Bates* [1957] suggested reaction 4, and no other is at all obvious.) Then, in the steady

TABLE 1. Processes Proposed to Explain Sodium Airglow

Process	Proposed by	Critic
Meteoric excitation	Cabannes, Dufay, and Gauzet, 1938	Chapman, 1939
Electron impact	Russell, 1939	Chapman, 1939
Reactions of molecular Sodium Na_2	Penndorf, 1950	Kahn, 1950; Ogawa,
Neutralization of Na^+	Saha, 1951; Mitra, 1952	Saha, 1951; Mitra, 19
Transmission of light from sunlit side of earth	Foderaro and Donahue, 1953	Hunten, 1955*a*
$NaO + O \rightarrow Na(^2P) + O_2$	Chapman, 1939; Bates and Nicolet, 1950	Ogawa, 1954; Bates,
High-energy incoming sodium	Bates and Nicolet, 1950	Bates and Nicolet, 19
$NaH + O \rightarrow Na(^2P) + OH$	Bates and Nicolet, 1950	
$NaH + H \rightarrow Na(^2P) + H_2$	Bates, 1954; private communication to M. Ogawa	

state, the rate of formation of NaH exactly equals the rate of destruction, and hence also the rate of light emission. Assuming reasonable values for the reactant concentrations and the rate constant, we find that reaction 4 can yield NaH at a sufficient rate to account for the airglow intensity by reaction 2.

In a similar fashion, by assuming reasonable values for reactant concentrations and the rate constant, the reaction of NaO and O can be shown to be capable of yielding the observed intensity.

No further progress can be made in the choice of a sodium airglow mechanism without the application of further tests. One test is provided by comparison of the observed and predicted altitude distribution of the sodium airglow. In order to make this comparison, both the sodium airglow distribution and the distribution of reactants with altitude must be known. The former is provided by the rocket measurements of *Heppner and Meredith* [1958] and *Koomen, Scolnik, and Tousey* [1957]. In order to find the latter, we shall calculate the altitude distribution of sodium and its oxides.

Distribution of Free and Combined Sodium in Upper Atmosphere

In order to calculate an approximate distribution of sodium among its free and combined forms as a function of altitude, all reactions of sodium and sodium oxides with oxygen atoms and molecules and ozone that are believed to have appreciable rates must be considered, in addition to photoionization, photodissociation, and ion recombination. These reactions are listed in Table 2, along with rate const estimated for some of them. Pre-expone factors for the rate constants of the bimolec reactions were estimated according to the th of absolute reaction rates [*Benson*, 1960]. activation energies for these reactions estimated using Hirschfelder's rule [*Hirschfe* 1941], according to which the activation en is 5.5 per cent of the energy of the bond bro in the reaction. The bond energies required calculated from the heats of formation of sodium oxides (assuming $(\Delta H_f)_{NaO} \approx -$ kcal/mole from theoretical estimates and *B and Evans* [1937]; $(\Delta H_f)_{NaO_2} \approx -40$ kcal/mole f *Bawn and Evans* [1937]). The rate constants all termolecular reactions were assumed eq to the value reported by *Haber and Sch* [1931] for the association of sodium and oxyg This assumption was made because of similarity of the chemical bond formed in e case.

The differential equations for the rates change of Na, Na^+, NaO, and NaO_2 are follows:

$$\frac{d[\mathrm{Na}]}{dt} = k_2[\mathrm{NaO}][\mathrm{O}] - k_3[\mathrm{Na}][\mathrm{O}][M] - k_4[\mathrm{Na}][\mathrm{O_2}][M] - k_6[\mathrm{Na}][\mathrm{O_3}] + k_8[\mathrm{NaO}] + k_9[\mathrm{NaO_2}] - k_i[\mathrm{Na}] + k_r[\mathrm{Na^+}][e] + k_r'[\mathrm{Na^+}][M^-]$$

$$\frac{d[\mathrm{Na^+}]}{dt} = k_i[\mathrm{Na}] - k_r[\mathrm{Na^+}][e] - k_r'[\mathrm{Na^+}][M^-]$$

TABLE 2. Important Reactions Involving Sodium and Oxygen above 70 Kilometers

Reaction	Rate Constant
$NaO + O + M \rightarrow NaO_2 + M$	$k_1 = 5 \times 10^{-30}$ cm^6/sec
$NaO + O \rightarrow Na + O_2$	$k_2 = 5 \times 10^{-11}\, e^{-4000/RT} = 6 \times 10^{-14}$ cm^3/sec
$Na + O + M \rightarrow NaO + M$	$k_3 = 5 \times 10^{-30}$ cm^6/sec
$Na + O_2 + M \rightarrow NaO_2 + M$	$k_4 = 5 \times 10^{-30}$ cm^6/sec
$NaO_2 + O \rightarrow NaO + O_2$	$k_5 = 5 \times 10^{-12}\, e^{-2000/RT} = 2 \times 10^{-13}$ cm^3/sec
$Na + O_3 \rightarrow NaO + O_2$	$k_6 = 5 \times 10^{-12}\, e^{-1500/RT} = 4 \times 10^{-13}$ cm^3/sec
$NaO_2 + h\nu \rightarrow NaO + O$	$k_7 = ?$
$NaO + h\nu \rightarrow Na + O$	$k_8 = ?$
$NaO_2 + h\nu \rightarrow Na + O_2$	$k_9 = ?$
$Na + h\nu \rightarrow Na^+ + e$	$k_i = 2 \times 10^{-5}$/sec
$Na^+ + e \rightarrow Na$	$k_r = ?$
$Na^+ + M^- \rightarrow Na + M$	$k_r' \approx 10^{-8}$ or 10^{-9} cm^3/sec

$$\frac{\ldots aO_2]}{\ldots t} = k_1[NaO][O][M] + k_4[Na][O_2][M]$$

$$\ldots_5[NaO_2][O] - k_7[NaO_2] - k_9[NaO_2] \quad (7)$$

$$\frac{\ldots aO]}{\ldots t} = -k_1[NaO][O][M] - k_2[NaO][O]$$

$$\ldots k_3[Na][O][M] + k_5[NaO_2][O]$$

$$\ldots k_6[Na][O_3] + k_7[NaO_2] - k_8[NaO] \quad (8)$$

…suming that the concentrations of Na, Na^+, …, and NaO_2 do not change with time, equa… 5 to 8 can be set equal to zero. Algebraic …ipulation then yields expressions for mole …ions of the total sodium present as Na, …, NaO, and NaO_2 in terms of the total …icle density M, the concentrations of O, …nd O_3, and the sodium atom-ion ratio.

…n order to evaluate the various fractions of … and combined sodium, the sodium atom-ion … $[Na]/[Na^+]$ must be known. This is very …ult to evaluate, because the negative ion …entration and charge transfer coefficients … not known with certainty. *Hunten* [1954] assumed that $[Na] \approx [M^-]$, that the charge …sfer coefficient is $10^{-8} - 10^{-9}$ cm^3/sec, and … the rate constant for sodium ionization is … 10^{-5}/sec. He then finds values of the ratio …ch range from 1 to 1/10 (most commonly 1) …ltitudes near 90 km. We shall assume the …o to be independent of altitude and equal …nity.

…othing is known about the photodissocia… of the sodium oxides. Examination of the …iled expressions for the mole fractions for … various forms of sodium shows that the rate constants must be quite large (order of 10^{-3}/sec) to be significant. Hence, it is thought that they can be neglected without serious effect, and this was done.

The concentrations of O, O_2, O_3, and M (the total particle density) needed for the calculation of the sodium distribution were taken from *Barth and Kaplan* [1957].

The distribution of free and combined sodium as a function of altitude calculated as indicated above is shown in Figure 1. The distribution has been normalized so that the maximum particle density for free sodium is unity. The distribution is almost wholly speculative in that nearly all the rate constants are calculated. It would be most surprising if these calculated rate constants were correct to within an order of magnitude. Thus, little reliance can be placed on the calculated concentrations at any particular altitude. The essential feature of the distribution, which is thought to be reliable, is the general relative positions of sodium and its oxides with altitude. This arrangement arises from the basic fact that all important oxidation reactions are termolecular, and all reduction reactions are bimolecular. The calculated distribution of atomic sodium agrees within a few kilometers with the mean distribution calculated from twilight glow measurements (maximum at 87.9 km, 14 km wide [*Blamont, Donahue, and Stull*, 1958; *Blamont, Donahue, and Weber*, 1958]). In a later part of the paper, sodium airglow distributions will be calculated using the distributions shown in Figure 1. Calculated distributions involving the sodium oxides must be regarded as speculative, except for their approximate altitudes relative

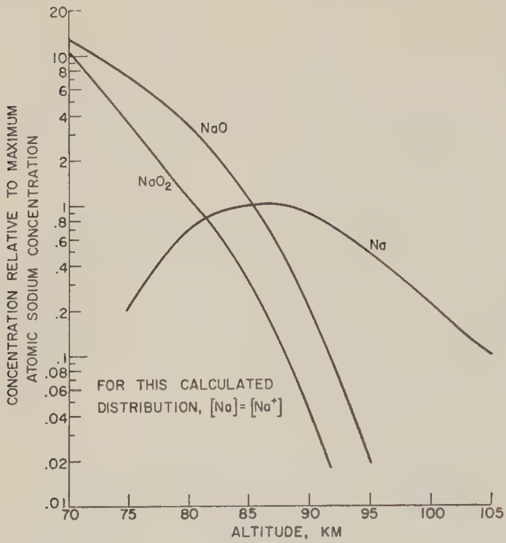

Fig. 1. Calculated distribution of sodium and its oxides with altitude.

to free sodium. Those involving free sodium may be considered more reliable, since the calculated and observed distributions of free sodium are in approximate agreement.

Sodium Airglow Intensity Distributions Predicted by Processes Involving Combined Sodium

As was noted previously, the rate of light production by the reaction of NaH and O is governed by the rate of NaH production from NaO_2 and H (equation 4). Hence, the predicted airglow intensity for this process is proportional to the product of the H and NaO_2 densities. The density of H at the altitudes of interest was taken from *Bates and Nicolet* [1950]. The relative density of NaO_2 was obtained from Figure 1. The product of the H and NaO_2 densities, which is proportional to the intensity predicted by the NaH reaction, was then calculated. The results are compared (curve *B*) with the observed intensity distributions given by *Heppner and Meredith* [1958] and *Kooman, Scolnik, and Tousey* [1957] in Figure 2*a*. All the data have been normalized to unity. No correlation between the distribution of observed and calculated airglow intensity can be observed. We conclude that the NaH process is probably not the origin of the sodium airglow. The predicted intensity distribution was also calculated for the Chapman process (reduction of NaO by O) an shown in Figure 2*a* (curve *A*). It also does correlate with the observed distribution. In f any luminescent process that involves combi sodium will not explain the altitude distribut of the sodium airglow, since the airglow ori nates at altitudes where the sodium is predo nantly free. This possibility has been previo noted by *Bates and Nicolet* [1950], who c cluded that chemical reactions involving co bined sodium could not explain the airglow the altitude of the airglow was greater than km. The more detailed analysis given in t paper enables us to conclude that, even at 80 85 km, mechanisms involving combined sodi probably cannot explain the airglow.

A New Mechanism to Explain Sodium Airglow

An obvious inference from the preceding c cussion is that the sodium airglow involves f sodium. If we rule out (see Table 1) reacti of ionic sodium [*Saha*, 1951; *Mitra*, 1952], citation by particle impact [*Norrish* and *Sm* 1940], and high-energy incoming sodium [*Ba and Nicolet*, 1950], the only remaining proc is a reaction involving neutral atomic sodiu Positive evidence that such a reaction occ near the altitude of the sodium airglow is giv by the work of *Bedinger, Manring, and Gh* [1957, 1958], who ejected atomic sodium at hi altitudes from rockets at night. These work observed the emission of sodium light at 65, 1 and 140 km. They were careful to confirm absence of molecular sodium (Na_2) and sodi oxides in the ejected sodium gas. As is sho in Figure 1, free sodium is stable at 100 km a does not react chemically with the atmosphere this altitude to any appreciable extent. Con quently, the emission observed at 100 and 1 km must be the result of processes involv neutral atomic sodium. Bedinger, Manring, a Ghosh recognized this fact, and suggested t the ejected sodium was excited by collisions w electronically excited atomic nitrogen. Althou this seems unlikely, because of the lack of s conservation in the reaction, their proposal important, since it suggests a new concept as how sodium might be excited in the airgl namely by collision with metastable exci atoms or molecules. It seems quite likely t the excitation process responsible for the em

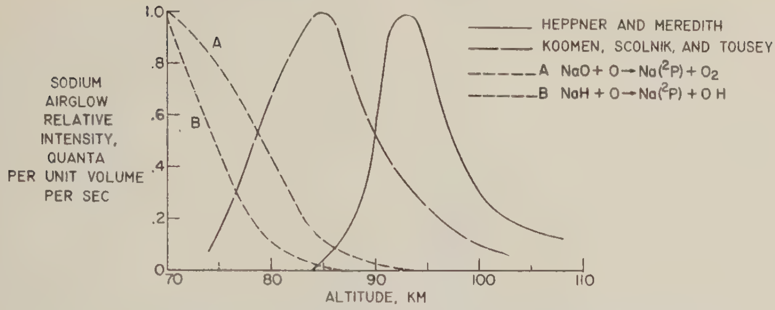

Fig. 2. Comparison of calculated and observed sodium airglow distributions. (*a*) Processes involving combined sodium.

observed at 100 km is the same as that ch produces the airglow.

hus, we shall consider as a possible mode of tation for the sodium airglow a collision of second kind, in which an excited atom or ecule transfers its excitation energy to the um atom, or

$$\mathrm{Na}(^2S) + M^* \rightarrow \mathrm{Na}(^2P) + M \qquad (9)$$

re are two basic requirements for the excited cies M^*. It should yield an energy of at least kcal/mole upon deactivation. Also, it must present at the required altitude in high enough centration to yield the observed intensity the airglow. If we assume a fast reaction h a rate constant of 10^{-9} to 10^{-10} cm³/sec, the uired concentration of the excited species can estimated as follows: The average sodium m concentration, assuming a layer thickness 10 km, ranges from 1×10^3 to 9×10^3/cm³ *unten,* 1955*b*]. The sodium airglow intensity ges from about 20 to 500 rayleighs [*Pettit,* *ch, St. Amand, and Williams,* 1954], which responds to 20 to 500 quanta/(cm³)(sec) in a 10-km layer. Then, according to reaction 9, the concentration of M^* should range between 10^7 and 10^8/cm³. This requirement apparently eliminates such species as $\mathrm{O}(^1S)$, and $\mathrm{O}_2(^3\Sigma^+_u)$, whose concentrations, estimated from the intensity of their emission lines in the airglow, are (certainly in the first case, probably in the second) much too small to be of account.

The only remaining possibility seems to be excitation by collisions with vibrationally excited oxygen or nitrogen. There is evidence that such a process can occur. For example, *M. Polanyi* [1932] observed excitation of sodium by collisions of the second kind with vibrationally excited NaCl [see also *Magee,* 1940]. *Clouston, Gaydon, and Glass* [1958] [see also *Gaydon* 1954] have observed in shock waves in nitrogen that the sodium emission follows the vibrational temperature of the shocked gas rather than the translational temperature. This indicates an extremely rapid rate of transfer of vibrational energy from the nitrogen to electronic energy of the sodium.

In addition, we may consider the rate of the

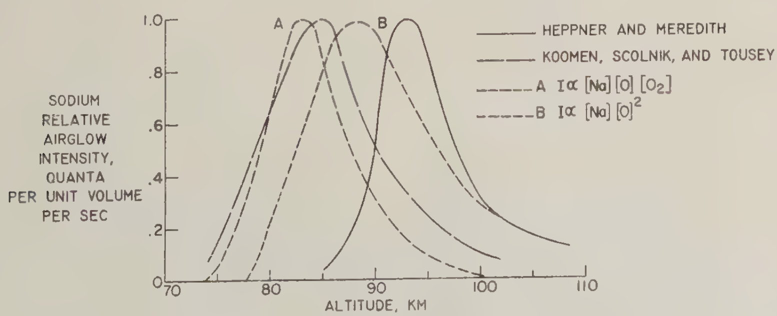

Fig. 2. *continued.* Comparison of calculated and observed sodium airglow distributions. (*b*) Excitation of free neutral sodium.

reverse process, deactivation of sodium, since, for collisions of the second kind at exact energy resonance and no multiplicity change, the equilibrium constant is unity, and forward and reverse rate constants are equal. A considerable amount of work has been done on the physical quenching of excited sodium. When the quenching molecule is a diatomic molecule, the theory developed by *Laidler* [1942] indicates that the energy of the excited sodium atom is tranfserred principally into vibrational energy of the quenching molecule. Thus, to a first approximation, we may equate the rate constants for sodium deactivation to those for the reverse process, excitation of the sodium by vibrationally excited molecules. The quenching results of *Norrish and Smith* [1940] yield a rate constant of 4×10^{-10} cm^3/sec for N_2, and those of *Terenin and Prileshajewa* [1932] yield a rate constant of 2×10^{-9} cm^3/sec for Br_2. No data exist for O_2, but we might expect the rate constant to be similar to that of Br_2, because of the strong chemical interaction between Na and O_2. Laidler's theory shows that the transfer of electronic to vibrational energy occurs with particular ease because of the existence of an ionic complex between the sodium and the quenching molecule. Normally, such complexes do not exist, and the transfer of electronic energy to vibrational energy, and vice versa, is a very slow process.

We conclude that electronic excitation of sodium by vibrationally excited oxygen or nitrogen can occur possibly with a rate constant of 10^{-9} to 10^{-10} cm^3/sec.

Concentration of vibrationally excited nitrogen. A possible source of excitation for atomic sodium is vibrationally excited nitrogen. The rate of deactivation of vibrationally excited nitrogen is slow, requiring about 10^7 collisions with N_2 and 10^5 collisions with O_2 to change the vibrational quantum number from 1 to 0 [*Schwartz, Slawsky, and Herzfeld,* 1952]. This means that a rather slow rate of production may suffice to maintain the concentration of excited nitrogen at a level sufficient to cause the excitation of sodium by collisions of the second kind. Several processes in the upper atmosphere yield vibrationally excited nitrogen N_2*. None of these seem capable of yielding sufficient N_2*, with the possible exception of collisions of the second kind with electronically excited oxygen formed by atom recombination. If this is a fast process, and the steady-state concentration of O'_2 is of the order of 10^4 to $10^5/cm^3$, the concentration of vibrationally excited nitrogen will be sufficient to excite the airglow. However, in the absence of strong chemical forces between N_2 and O_2, it is not likely that the process is very fast. Auroral activity apparently yields vibrationally excited nitrogen [*Clark and Belon,* 1959]. This may excite the sodium D lines observed in low-level auroras [*Hunten,* 1955*c*] but cannot account for the airglow because of its intermittent nature. Tentatively, we conclude that vibrationally excited nitrogen does not excite the airglow.

Concentration of vibrationally excited oxygen. Vibrationally excited oxygen with sufficient energy to excite sodium is formed in the upper atmosphere by direct and indirect recombination of oxygen atoms. The excited oxygen is deactivated by collisions with inert molecules. In the steady state, when the rates of formation and deactivation are equal, the concentration of vibrationally excited oxygen O_2* is

$$[O_2^*] = \frac{G}{k_d[M]} \tag{10}$$

where G is the rate of generation of excited oxygen, k_d is the rate constant for deactivation by collisions with molecules of concentration $[M]$. As noted by *Bates and Moiseiwitsch* [1956], the average rate of formation of vibrationally excited oxygen by atom recombination must equal the average rate of photodissociation, about $5 \times 10^{11}/(cm^2)(sec)$. Assuming that the recombination occurs in a 10-km layer, the mean rate of production G of vibrationally excited oxygen is $5 \times 10^5/(cm^3)(sec)$. This probably represents a maximum rate. Then, in order to obtain the required minimum concentration of excited oxygen of $10^7/cm^3$ near 90 km (where the airglow is brightest), the product $k_d[M]$ must not exceed 5×10^{-2}/sec. Near 90 km $[M]$ is about $10^{14}/cm^3$, so that the required value of k_d is 5×10^{-16} cm^3/sec. Assuming normal collision diameters, this implies that vibrationally excited oxygen must survive at least 5×10^{4} collisions before deactivation. This seems to be possible, as vibrationally excited oxygen in the sixth vibrational level has been observed to need more than 10^7 collisions with nitrogen for deactivation [*Lipscomb, Norrish, and Thrush,* 1956].

However, *Bates and Moiseiwitsch* [1956] have pointed out that oxygen atoms may be excep-

.lly efficient deactivation agents for vibra- .lly excited oxygen. They assume that com- deactivation occurs upon every collision. ld this be true, the concentration of vibra- .lly excited oxygen will not be high enough xplain the sodium airglow. Their suggestion sed on the existence of O_3, which indicates ong chemical interaction between O and O_2. ly collisions in which a strong chemical in- tion occurs can be expected to be excep- ally efficient for the removal of vibrational ita. Since the rate of reaction of O to O_2 orm O_3 is 20 times slower than the reaction xygen atoms to form O_2 [*Kretschmer*, 1959], opears that the number of collisions along a ding potential path is 20 times less for the raction of O + O_2 than for O + O. Not y collision of O + O occurs along a bonding ntial path, so that less than 1/20 of the sions of O + O_2 occur along a bonding po- ial path and are hence effective for the re- al of vibrational quanta. In addition, quanta normally removed one at a time. As noted w, O_2 formed by direct recombination of O ns is excited to a vibrational quantum num- v of about 50, so that about 40 quanta must removed before the molecule can no longer te sodium. These considerations make it ear possible that the efficiency of atomic gen for the deactivation of excited oxygen not be as high as Bates and Moiseiwitsch e assumed. Experimental studies would be y desirable.

n the absence of conclusive evidence to the trary, we shall assume that the rate of deac- tion of vibrationally excited oxygen is slow ugh to maintain the excited oxygen concen- tion high enough to yield the observed sodium low intensity.

Predicted altitude distribution of airglow. ording to the mechanism considered here, intensity of the airglow at any given altitude st be proportional to the product of the ium atom concentration and the excited oxy- concentration. The atomic sodium distribu- n is known approximately. We must now ulate the distribution of vibrationally excited gen. Only processes that produce oxygen h vibrational quantum numbers equal to greater than 12 need be considered, because gen excited to any lower state does not e enough energy to excite sodium.

Two processes produce sufficiently energetic oxygen. The first is the direct recombination of atomic oxygen:

$$O + O + M \rightarrow O_2^*(v \approx 50) + M \quad (11)$$

According to *J. C. Polanyi* [1959] the vibrationally excited molecule formed by atom recombination is in a highly vibrating state, with a vibrational energy only a few quanta less than the dissociation energy. This corresponds to a vibrational quantum number for ground-state oxygen of about 50.

The second is an indirect process involving ozone:

$$O + O_2 + M \rightarrow O_3 + M \quad (12)$$

$$O + O_3 \rightarrow O_2^*(v = 12 \text{ to } 16) + O_2 \quad (13)$$

The vibrationally excited oxygen formed in reaction 13 is mostly in the 13th vibrational level [*McGrath and Norrish*, 1957].

Both of these two processes form one molecule of excited oxygen from two oxygen atoms. Their relative importance may be gauged as follows: The rate of the indirect production of excited oxygen (from ozone) R_i relative to the rate of production by direct recombination R_d is

$$\frac{R_i}{R_d} = \frac{k_{13}[O_3]}{k_{11}[O][M]} \quad (14)$$

In the daytime, this ratio is very small, since ozone is photodecomposed rapidly at the altitudes considered here (80 to 100 km), and its concentration is negligible.

At night, photodecomposition does not occur, and reactions 12 and 13 control the ozone concentration. By integration of the rate expressions corresponding to these reactions, the ozone concentration as a function of time after sunset t can be found. Substituting the result in equation 14, we find

$$\frac{R_i}{R_d} = \frac{k_{12}[O_2]}{k_{11}[O]} \{1 - \exp(-k_{13}[O]t)\} \quad (15)$$

Using this equation, the minimum times after sunset required for the indirect process to become dominant (i.e., for $R_i/R_d \geq 1$) were calculated for various altitudes. For this calculation, the ratio k_{12}/k_{11} was taken as 20 [*Kretschmer*, 1959], k_{13} as 2×10^{-16} cm^3/sec [*Benson and Axworthy*, 1957], and O and O_2 concentrations as those from

Barth and Kaplan [1957]. It is found that an hour or so after sunset the indirect process predominates below 90 km. It is therefore an important mode of atom recombination. Above 95 km, the indirect recombination never becomes important, and the direct process predominates at all times.

Since the free-sodium layer extends from altitudes where the indirect process predominates up to altitudes where the direct process is dominant, it is probable that excited oxygen from both modes of recombination contributes to the airglow. At present we cannot estimate which is more important, because we do not know the relative lifetimes and sodium excitation efficiencies of the two types of excited oxygen ($v \approx 50$ and $v \approx 13$) formed by the two processes. Hence, we shall consider two extreme cases: First, the direct process is dominant. Then, it may be shown that the concentration of vibrationally excited oxygen in the steady state is

$$[O_2^*] \propto [O]^2 \qquad (16)$$

provided that the same inert molecules are effective in the termolecular recombination as in the vibrational deactivation. If the sodium airglow results from collisions of sodium atoms with vibrationally excited oxygen, the intensity is

$$I \propto [Na][O_2^*] \qquad (17)$$

so that, for the direct process,

$$I \propto [Na][O]^2 \qquad (18)$$

In the second extreme case, the indirect process is dominant. Then it can be shown that in the steady state the airglow intensity is

$$I \propto [Na][O][O_2] \qquad (19)$$

The relative intensity distributions for the two extreme cases, equations 18 (curve B) and 19 (curve A), are compared with the observed airglow distributions [*Heppner and Meredith*, 1958; *Kooman, Scolnik, and Tousey*, 1957] in Figure 2*b*. Atomic sodium densities were taken from Figure 1. The densities for O and O_2 were taken from *Barth and Kaplan* [1957]. Inspection of Figure 2*b* shows reasonably good agreement between the shape and altitude of the observed and calculated airglow distributions. The difference between the distributions predicted by the two extreme cases is not large enough to be significant. We conclude that the proposed mechanism can explain the observed sodium airglow distribution.

J. W. Chamberlain (in a private communication) has pointed out that, if excited oxygen from the direct process is the dominant excitation agent, the intensities of the sodium D lines and the oxygen green line might be expected to covary. This is not the case. However, if excited oxygen from the indirect process is the dominant excitation agent, one might expect the sodium D lines and the Meinel hydroxyl bands to covary, since both are dependent on the steady-state ozone concentration. A fairly definite covariation of sodium and hydroxyl emissions in the airglow has been observed [*Berthier*, 1954]. This seems to favor the indirect process, but the situation is too complex for certainty.

Returning finally to the sodium emissions at 100 and 140 km observed by *Bedinger, Manring, and Ghosh* [1957, 1958], we may suggest that the emission at 100 km arises from excitation of sodium by vibrationally excited oxygen produced by direct recombination of oxygen atoms. The emission at 140 km cannot reasonably be explained in this way but might result from vibrationally excited nitrogen produced in the course of auroral activity.

Conclusions

Comparison of observed and calculated sodium airglow distributions shows that airglow processes involving combined sodium (NaH, NaO) probably cannot explain the airglow. Consequently the airglow process involves free sodium. It is suggested that the sodium atoms are excited in the airglow by collisions with vibrationally excited oxygen. That this process can yield the observed airglow intensity appears possible. The altitude distribution of the airglow predicted by this mechanism agrees with observation.

References

Barth, C. A., and J. Kaplan, *The Threshold of Space*, Pergamon Press, pp. 3–13, 1957.

Bates, D. R., *Sci. of Light (Tokyo)*, *3*, 47, 1954.

Bates, D. R., *The Threshold of Space*, Pergamon Press, pp. 14–21, 1957.

Bates, D. R., and B. L. Moiseiwitsch, *J. Atmospheric and Terrest. Phys.*, *8*, 305, 1956.

Bates, D. R., and M. Nicolet, *J. Geophys. Research*, *55*, 235, 1950.

Bates, D. R., and M. Nicolet, *J. Geophys. Research*, *55*, 301, 1950.

n, C. E. H., and A. G. Evans, *Trans. Faraday* ɔ., *33,* 1571, 1580, 1937.
nger, J. F., E. R. Manring, and S. N. Ghosh, *e Threshold of Space,* Pergamon Press, pp. 5–231, 1957.
mger, J. F., E. R. Manring, and S. N. Ghosh, *Geophys. Research, 63,* 19–29, 1958.
on, S. W., *The Foundations of Chemical Kitics,* McGraw-Hill Book Company, New York, 280, 1960.
son, S. W., and A. E. Axworthy, Jr., *J. Chem. ys., 26,* 1718, 1957.
ard, R., *Z. Physik, 110,* 291–302, 1938.
hier, P., *Compt. rend., 238,* 263, 1954.
nont, J. E., T. M. Donahue, and V. R. Stull, *n. géophys., 14,* 253, 1958.
nont, J. E., T. M. Donahue, and W. Weber, *n. géophys., 14,* 282, 1958.
annes, J., J. Dufay, and J. Gauzet, *Compt. nd., 206,* 1525, 1938.
pman, S., *Astrophys. J., 90,* 309, 1939.
k, K. C., and A. E. Belon, *J. Atmospheric and errest. Phys., 16,* 205, 1959.
iston, J. G., A. G. Gaydon, and I. I. Glass, *roc. Roy. Soc. London, A, 248,* 429, 1958.
eraro, A., and T. M. Donahue, *Phys. Rev., 91,* 561, 1953.
don, A. G., Energy transfer in hot gases, *Natl. ur. Standards U. S., Circ. 523,* 1954.
ɔer, F., and H. Schasse, *Z. physik. Chem. Bonstein-Festband,* p. 831, 1931.
pner, J. P., and L. H. Meredith, *J. Geophys. esearch, 63,* 51–65, 1958.
schfelder, J., *J. Chem. Phys., 9,* 645, 1941.
nten, D. M., *J. Atmospheric and Terrest. Phys.,* , 44, 1954.
nten, D. M., *Phys. Rev., 97,* 1178, 1955*a*.
nten, D. M. *The Airglow and the Aurorae,* Peramon Press, pp. 114–121, 1955*b*.
Hunten, D. M., *J. Atmospheric and Terrest. Phys., 7,* 141, 1955*c*.
Kahn, F. D., *Phys. Rev., 78,* 167, 1950.
Koomen, M. J., R. Scolnik, and R. Tousey, *The Threshold of Space,* Pergamon Press, pp. 217–224, 1957.
Kretschmer, C. B., Investigation of atomic-oxygen recombination rates, Aerojet-General Corp., Azusa, Calif., Rept. 1611, May 1959, ASTIA Document 217-008, 1959.
Laidler, K. J., *J. Chem. Phys., 10,* 34, 1942.
Lipscomb, F. J., R. G. W. Norrish, and B. A. Thrush, *Proc. Roy. Soc. London, A, 233,* 455, 1956.
McGrath, W. D., and R. G. W. Norrish, *Proc. Roy. Soc. London, A, 242,* 265, 1957.
McKinley, J. D., Jr., and J. C. Polanyi, *Can. J. Chem., 36,* 107, 1958.
Magee, J. L., *J. Chem. Phys., 8,* 687, 1940.
Mitra, S. K., *The Upper Atmosphere,* 2d ed., Asiatic Society, Calcutta, 1952.
Norrish, R. G. W., and W. Mac F. Smith, *Proc. Roy. Soc. London, A, 176,* 295, 1940.
Ogawa, M., *Sci. Light, 3,* 47, 1954.
Penndorf, R., *Phys. Rev., 78,* 66, 1950.
Pettit, H. B., F. E. Roach, P. St. Amand, and D. R. Williams, *Ann. géophys., 10,* 326, 1954.
Polanyi, J. C., *J. Chem. Phys., 31,* 1338, 1959.
Polanyi, M., *Atomic Reactions,* Williams & Norgate, London, 1932.
Russell, H. N., *Sci. American, 160,* 88, 1939.
Saha, A. K., *Indian J. Phys., 25,* 375, 1951.
Schwartz, R. N., Z. I. Slawsky, and K. F. Herzfeld, *J. Chem. Phys., 20,* 1591. 1952.
Terenin, A., and N. Prileshajewa, *Z. physik. Chem., 13B,* 72, 1932.

(Manuscript received June 17, 1960; revised September 7, 1960.)

Spread F and Multiple Scattering in the Ionosphere

DIMITRI S. BUGNOLO

Bell Telephone Laboratories, Inc.
Holmdel, New Jersey

Abstract. The problem of spread F is examined statistically, and a resulting theoretical model is obtained to explain the usual spread-F ionogram. The results are applied in detail to a typical example of arctic spread F. The statistical model is based on the assumption of Gallet turbulence in the underside of the F layer under nighttime conditions.

1. INTRODUCTION

The statistical analysis of scattering by the lerside of the F layer under nighttime conions has led to a model for radio star scintilion [*Bugnolo,* 1960*c*]. In view of this, it is eresting to apply the present theory to the oblem of spread-F phenomena and in particu- to the problem of the spread-F *ionogram.*

The statistical parameters of interest in the dy of the irregular ionosphere are: (1) total oss section for scattering, Q_s; (2) probability at any ray of the incident field will be scattered least once, P_1.

The above will be discussed in detail under e assumption of a Gallet layer [*Gallet,* 1955] the underside of a typical model for the nightne F layer. It will be shown that:

1. Total cross section for scattering Q_s

$$Q_s \sim \frac{1}{f^2}\left\{1 - \frac{u}{2}\right\}^2 \tag{1.1}$$

here u is the distance from the bottom of the layer as measured in scale heights and f is the equency of observation.

2. A surface of constant probability P_1 corsponds to the general shape of a typical read-F ionogram.

2. A MODEL FOR THE TURBULENT F LAYER

It would appear that turbulence in the F yer is restricted to its underside at moderate titudes and occurs mainly at night [*Martyn,* 959]. During this time the underside of the gion assumes a *nearly* parabolic form [*Martyn,* 959]. The electron density, N per meter uared, is therefore given by:

$$N = N_M \frac{x}{H}\left\{1 - \frac{x}{4H}\right\} \tag{2.1}$$

where N_M is the maximum electron density and x is the distance as measured in meters from the bottom of the F layer. H is the appropriate scale height in meters [*Martyn,* 1959, p. 150]. (The 'scale height' H in a parabolic layer is just half the semithickness).

Gallet [1955] has shown that, when the turbulence in an ionized medium is caused by the vertical transport of electrons, the mean squared variations in the electron density are given by

$$\left\langle\left|\frac{\Delta N}{N}\right|^2\right\rangle \cong \frac{l_0^2}{3}\left|\frac{\nabla N}{N}\right|^2 \tag{2.2}$$

where l_0 is the mean scale size in the layer and ∇N is the gradient of the electron density.

Variations in the effective dielectric constant of the layer can then be found by means of the usual Appleton-Hartree formula. Under the assumption of a longitudinal mode of propagation, the dielectric constant ϵ is given by

$$\epsilon = \epsilon_0\left\{1 - \frac{\omega_{cr}^2}{\omega(\omega \pm \omega_H)}\right\} \tag{2.3}$$

where

$\omega_{cr}^2 = Ne^2/m\epsilon_0$, the critical frequency.
$\omega_H = (-e\mu_0/m)H_0$, the gyro frequency.
e = electron charge in coulombs.
m = electron mass in kilograms.
ϵ_0 = dielectric constant of free space.
H_0 = earth's magnetic field.

The rms magnitude of the fluctuations in the dielectric constant can be found by differentiating equation 2.3. This yields

$$\left\langle \left| \frac{\Delta\epsilon}{\epsilon} \right|^2 \right\rangle = \left\langle \left| \frac{\Delta N}{N} \right|^2 \right\rangle \left\{ \frac{\omega_{cr}^{\ 2}}{\omega(\omega \pm \omega_H) - \omega_{cr}^{\ 2}} \right\}^2 \qquad (2.4)$$

Substituting for the rms electron noise from (2.2) yields

$$\left\langle \left| \frac{\Delta\epsilon}{\epsilon} \right|^2 \right\rangle \cong \frac{l_0^{\ 2}}{3} \left\{ \frac{\omega_{cr}^{\ 2}}{\omega(\omega \pm \omega_H) - \omega_{cr}^{\ 2}} \right\}^2 \left| \frac{\nabla N}{N} \right|^2 \qquad (2.5)$$

Finally, using the parabolic model for the underside of the F layer (2.1) and taking

$$\omega > \sqrt{10}\omega_H$$

yields a rather simple result:

$$\left\langle \left| \frac{\Delta\epsilon}{\epsilon} \right|^2 \right\rangle \cong \frac{l_0^{\ 2}}{3} \left(\frac{\omega_{cr\,M}}{\omega} \right)^4 \cdot \frac{1}{H^2} \frac{[1 - (x/2H)]^2}{\left[1 - \left(\frac{f_{cr\,M}}{f} \right)^2 \frac{x}{2} \right]^4} \qquad (2.6)$$

where $\omega_{cr\,M}$ is the maximum critical frequency and where x is the distance of penetration in meters as measured from the bottom of the layer. As expected from the model, we note that the rms electron variations are a maximum at the bottom and a minimum at the top of the F layer. This is sketched in Figure 1 for $\omega \gg \omega_{cr\,M}$ together with the parabolic model. For ω close to $\omega_{cr\,M}$ it is evident that the normalized rms fluctuations will lie above the sketched result.

3. Statistical Parameters

As was mentioned in the introduction, the parameters of interest are the total cross section for scattering, Q_s, and the probability that any ray of the incident field is scattered at least once, P_1.

Consider the following definitions:

$\sigma(\gamma, K)$ = cross section for scattering per unit volume per unit solid angle

$Q_s(\gamma, K)$ = total cross section for scattering per unit volume at the wave number k

where γ is a function of position.

The total cross section is related to $\sigma(K)$ in the usual manner [*Morse and Feshbach*, 1953] by

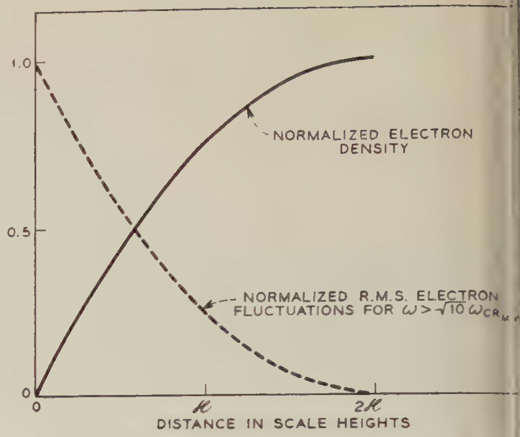

Fig. 1. Electron-density profile and normalized rms electron fluctuation for the underside of a parabolic F layer.

$$Q_s(k) = \int \sigma(K)\, d\Omega \qquad (3.1)$$

This is simply a measure of the total power scattered by the rms dielectric fluctuations, per unit volume.

Let a bundle of photons move through a region of space characterized by (3.1). A certain percentage of the photons will be scattered as they traverse each unit distance in the medium. It therefore follows that the probability that any photon has been scattered at least once in the distance X is given by (see *Bugnolo* [1961])

$$P_1(X, k) = 1 - \epsilon \exp\left\{ -\int_0^X Q_s(\gamma, k)\, d\gamma \right\} \qquad (3.2)$$

This is a function of both position and frequency.

Relationship of the cross section to the dielectric fluctuations. Before discussing the spread-F ionogram it is necessary to relate the cross section Q_s to the rms dielectric fluctuations discussed in section 2. This can be done by first relating the dielectric fluctuations to $\sigma(K)$, the cross section per unit volume per unit solid angle. The result is at best approximate since it depends on the choice of a model for the random character of the dielectric constant. The standard derivations also assume a first Born approxi-

on for the scattered field in determining). (For example, see *Wheelon* [1959], p. and *Bugnolo* [1960*b*].) Such an approxima- is not unusual in multiple scatter problems *vis,* 1950]. The choice of a particular model the random dielectric fluctuation may ap- rather obtrusive; it will be shown, how- that the resulting total cross section is ost independent of the initial choice.

et us assume that the spacewise correlation tion for the dielectric fluctuations is given ny one of the following:

$$= \frac{2^{1-\mu}}{\Gamma(\mu)} \left(\frac{r}{l_0}\right)^{\mu} K_{\mu}\left(\frac{r}{l_0}\right)\left\langle\left|\frac{\Delta\epsilon}{\epsilon}\right|^2\right\rangle; \quad \mu = \tfrac{1}{2}, 1, \tfrac{3}{2}, \text{etc.} \tag{3.3}$$

re $\Gamma(\mu)$ is the usual gamma function. This s of models was first proposed by *Norton* 60] in applications to the troposphere. As noted by *Bugnolo* [1960*a*], this results in a l cross section of

$$\gamma) \cong \frac{2\pi^{3/2}}{\lambda} \frac{\Gamma(\mu + \frac{3}{2})}{\Gamma(\mu)} \frac{2\pi l_0}{\lambda} \cdot \frac{1}{2\mu + 1} \left\langle\left|\frac{\Delta\epsilon(\gamma)}{\epsilon}\right|^2\right\rangle \tag{3.4}$$

s evident that the variation of Q_s with fre- ncy is independent of the parameter μ. As a ilt of this, the shape of the spread-F iono- m will be independent of the choice of μ. nsequently, the results to follow are not criti- y dependent on the choice of $R(r)$ within above class.

The probability function P_1. Substituting ations 2.6 and 3.4 into 3.2 yields

$$X, f) = 1 - \exp - \left\{\frac{1}{2\mu + 1} \frac{\Gamma(\mu + \frac{3}{2})}{6\Gamma(\mu)} \frac{(2\pi l_0)^3}{\sqrt{\pi}} \frac{1}{C^2} \frac{f_{crM}^4}{f^2} \frac{1}{H^2} \int_0^{X/H} \frac{(1 - u/2)^2\, du}{\left[1 - \left(\frac{f_{crM}}{f}\right)^2 \frac{u}{2}\right]^4}\right\} \tag{3.5}$$

ere u is the normalized distance from the tom of the F layer as measured in scale ghts. This, then, is the probability that a ray the incident field will be scattered at least ce.

4. A Model for the Spread-F Ionogram

The theoretical model to follow is based on the assumption that spread F is a *multiple backscatter* phenomenon. This not unreasonable assumption serves to explain the spread in range as observed on the usual A-type presentation at a single frequency.

In the usual type of spread-F experiment a transmitter located on the ground is swept through a frequency range of about 1 to 10 Mc/s at a rather slow rate. A receiver located in the same general area is used to monitor the signal as returned by the F layer. The received signal is displayed in a range-frequency fashion. A typical spread-F ionogram is illustrated by Figure 2. The reader is referred to a recent paper by *Reber* [1956] for other examples.

Consider a bundle of photons from the source at some frequency f. For simplicity, let us restrict the analysis to photons incident normally or nearly normally on the ionosphere. Photons incident at an angle will be delayed relative to the normally incident and will be discussed later. The normally incident photons will constitute the usual longitudinal mode of propagation in the northern part of the United States or in the arctic region. After some time delay τ, the receiver will begin to detect a backscattered signal from the turbulent F layer. The time of first arrival will depend on the scattering parameters of the F layer and the sensitivity of the receiving equipment.

As the original bundle of photons penetrates the turbulent F layer, a certain percentage of them will be scattered per unit distance. This is obviously given by the probability that any ray will be scattered at least once: P_1, of equation 3.5. A certain percentage of these photons will be backscattered to the receiver. If the sensitivity of the receiver is constant across the frequency band of interest, the lower band of the spread-F ionogram is simply a contour of constant probability, P_1. It is also evident that any photon incident at some angle other than the normal will be delayed relative to this contour. These rays and higher-order scattering from the normally incident bundle will result in a 'filling in' of the ionogram, as observed in Figure 2, or a spread in range.

The above discussion can be applied in detail to the example illustrated by Figure 2.

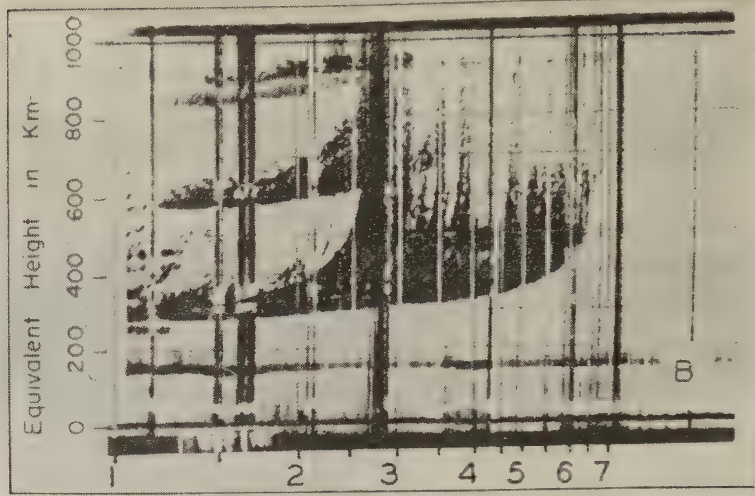

Fig. 2. An example of arctic spread F [*Reber,* 1956]. Courtesy of Professor H. G. Booker.

Consider the received signal as a function of range for any given frequency f. This time function is a member of an ensemble of all possible A-type presentations at the particular frequency. Let this be denoted by $v(x, f)$, where x is the range and f the frequency. The expectation of all possible members of the ensemble at a particular frequency, f_0, is denoted by

$$\langle v(x, f_0)\rangle$$

From the notion of total cross section (3.1) and the definition of $P_1(x, f)$ as given by (3.2), it follows that $\langle v\rangle$ must be directly proportional to P_1. Hence

$$\langle v(x, f_0)\rangle \sim P_1(x, f_0) \tag{4.1}$$

Since the ionospheric station is assumed to be frequency independent, it follows immediately that the lower bound of the ionogram is simply a trace of the function

$$P_1(x, f_0) = \text{constant} \tag{4.2}$$

It should be stressed that this result is exact if the ionogram is indeed an average of many traces in range at each particular frequency band $(f_0 - \Delta f, f_0 + \Delta f)$.

The particular magnitude of the constant cannot be predicted without a detailed analysis of the ionospheric scattering cross section and the electromagnetic parameters of the sounding station. However, in the opinion of this author, it is sufficient to note the following:

Theorem I. There exists class $P_1(x, f_0) = C_i$ where C_i is a constant, such that, given the ensemble average of all possible A-type presentation at the frequency f_0, $\langle v(x, f_0)\rangle$, its lower bound in x, $\langle v(x_i, f_0)\rangle$, corresponds to a member of the class C_i.

Corollary 1. There exists a class $P_1(x_i, f)$ satisfying theorem I such that the contour

$$P_1(x_i\ , f) = C_i$$

corresponds to the lower bound of the *ensemble* average of all possible spread-F ionograms at one particular location, given a statistically stationary process.

Corollary 2. There exists a class $P_1(x_i, f)$ satisfying theorem I such that the contour

$$P_1(x_i\ , f) = C_i$$

corresponds to the lower bound of the *time average* of a finite but large number of possible spread-F ionograms provided that length of the sample T is large as compared with the time rate of change of the statistical parameters of the ionosphere but small as compared with any nonstationary effect.

In keeping with the above, equation 3.5 can be used to determine the contour of interest. It is evident that $P_1(x, f)$ = constant provided that

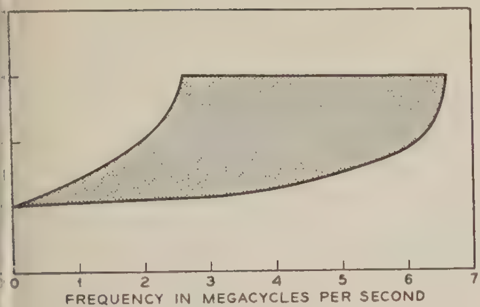

g. 3. A sketch of the Function $P_1(x, f) = c$.

$$\left.{}_{M}\right)^2 \int_0^{X/H} \frac{(1 - u/2)^2}{\left[1 - \left(\frac{f_{crM}}{f}\right)^2 \frac{u}{2}\right]^4} du$$

$$= \text{constant} \qquad (4.3)$$

ce the parameters of the ionospheric station unknown, the particular constant must be usted at some particular frequency, given experimental result of Figure 2. By so ad-ting C_t it is possible to solve equation 4.3 and tch the results as a function of altitude and quency. This has been done, and the results e been plotted as Figure 3. The upper bound plot of the function

$$1 - \left(\frac{f_{crM}}{f}\right)^2 \frac{u}{2} = 0 \qquad (4.4)$$

e shading is a result of multiple backscatter- from normally incident photons or scatter- of photons incident at an angle. The shading restricted to altitudes below that of maximum ctron density (on the average) since the tur-lence is so restricted. Note that Figure 3 is otted as a function of scale heights whereas gure 2 uses group height as its vertical scale. uation 4.3 could be modified to include this fect, but such a change would not modify the sulting sketch by any appreciable magnitude. his is evident from an inspection of equation 3, and noting that consideration of group de-y would only change the power of the de-minator by a factor of one-half.

It is of importance to note that the *shape* of y one surface $P_1(x, f) = C_t$ is independent of e statistical parameters of the ionosphere, l_0 and μ of equation 3.3, provided that the assumption of Gallet turbulence is valid.

The statistical nature of this model should be emphasized. The model is incapable of predicting any *one* trace on the A-type presentation.

5. Conclusion

A statistical model has been developed to explain the usual spread-F ionogram. It is relatively insensitive to the parameters of the dielectric noise if the assumption of Gallet turbulence is justified.

A particular example of arctic spread F was examined in detail with good agreement as far as the general over-all shape is concerned. This particular example could not be explained in terms of the E-layer screen postulated by *Renau* [1959].

References

Bugnolo, D. S., On the question of multiple scattering in the troposphere, *J. Geophys. Research*, *65*, 879–884, 1960*a*.

Bugnolo, D. S., Transport equation for the spectral density of a multiple-scattered electromagnetic field, *J. Appl. Phys.*, *31*, 1176, 1960*b*.

Bugnolo, D. S., Radio star scintillation and multiple scattering in the ionosphere, presented in part at the Spring URSI-IRE Meeting in Washington, D. C., May 1960, *Trans. PGAP, IRE.* To be published 1961.

Gallet, R. M., Electron density fluctuations in turbulent ionized layers, *Proc. IRE*, *43*, 1240, 1955.

Lewis, H. W., Multiple scattering in an infinite medium, *Phys. Rev.*, *78*, 526, 1950.

Martyn, D. F., The normal F region of the ionosphere, *Proc. IRE*, *47*, 147, 1959.

Morse, Philip M., and H. Feshbach, *Methods of Theoretical Physics*, McGraw-Hill Book Company, 1953.

Norton, K. A., Carrier frequency dependence of the basic transmission loss in tropospheric forward scatter propagation, *Mem. Rept. PM-83-21*, National Bureau of Standards, 1960.

Reber, G., World-wide spread F, *J. Geophys. Research*, *61*, 157, 1956.

Renau, J., A theory of spread F based on a scattering-screen model, *J. Geophys. Research*, *64*, 971–977, 1959.

Wheelon, A. D., Radio-wave scattering by tropospheric irregularities, *J. Research NBS*, *D*, *63* (9, 10), 205, 1959.

(Manuscript received August 11, 1960; revised September 16, 1960.)

On the Generalization of the Appleton-Hartree Magnetoionic Formulas

H. K. SEN AND A. A. WYLLER

Geophysics Research Directorate
Air Force Research Division
Bedford, Massachusetts

Abstract. The complex refractive index and the state of polarization in a weakly ionized gas with an alternating electric field and a steady magnetic field are given by the ordinary Appleton-Hartree formulas. In the original derivation a 'frictional' term is utilized which is assumed to be independent of the electron velocity, v, and the electron velocity distribution. It represents a first approximation to an effective collision frequency, ν_{AH}, for the collisions between electrons and neutral molecules.

The present work is an extension of Jancel and Kahan's magnetoionic theory, which is based upon solutions of the Boltzmann equation, when $\nu = \nu_m f(v)$. The expression for the complex refractive index and the state of polarization are rederived, utilizing a generalized conductivity tensor for the Lorentz gas. The resulting solutions are shown to be identical with the ordinary Appleton-Hartree formulas when ν = constant. In the general case, $\nu = \nu_m f(v)$, a new angular dependent term appears, the coefficient of which vanishes, when ν = constant.

The elements of the generalized conductivity tensor are integrals involving the electron velocity distribution function. The general non-Maxwellian distribution function for the electrons is derived as a function of the alternating electric field and a steady magnetic field, when the two field vectors have an *arbitrary* inclination to each other. In the ionospheric wave propagation, the electrons are assumed to have a Maxwellian velocity distribution, as the electric and magnetic field effects will be negligible. The elements of the generalized conductivity tensor are then expressible in terms of previously tabulated integrals, when use is made of Phelps and Pack's laboratory results, viz., $\nu \propto v^2$ in air. This greatly eases the computational use of the generalized formulas.

Calculations have been carried out for longitudinal and transverse propagation in the cases, $\nu_{AH} = \nu_m = \frac{1}{10}\omega$, $\nu_{AH} = \nu_m = \omega/2$, and $\nu_{AH} = \nu_m = 2\omega$, and with s (electron gyrofrequency) the same order of magnitude as ω.

Generally the birefringent properties of the medium are *decreased*, when the velocity dependence of the collision frequency is taken into account through the general theory. In all cases the absorption factors based on the generalized theory differ from those based on the ordinary Appleton-Hartree formulas by amounts from 30 to 100 per cent.

Improved agreement is obtained when ν_{AH} in the Appleton-Hartree formula is associated with the mean energy instead of the most probable energy as in the generalized theory; i.e. when $\nu_{AH} = \frac{3}{2}\nu_m$ instead of $\nu_{AH} = \nu_m$. In the asymptotic limit, $\nu \ll \omega \pm s$, the ordinary Appleton- Hartree formula can be retained, provided that $\nu_{AH} = \frac{5}{3}\times\frac{3}{2}\nu_m = \frac{5}{2}\nu_m$. In the other asymptotic limit, $\nu \gg \omega \pm s$, these same formulas can also be retained when $\nu_{AH} = \frac{3}{2}\nu_m$. For the intermediate case, $\nu \sim \omega \sim s$, differences in the absorption factors between the two theories persist with amounts up to 100 per cent, even though $\nu_{AH} = \frac{3}{2}\nu_m$. It is concluded that the generalized theory should be utilized in this case for all precise experimental work.

1. INTRODUCTION

Appleton [1927] generalized Lorentz's theory [of] the propagation of an electromagnetic wave [th]rough a slightly ionized medium with an arbi[tra]ry inclination of the external magnetic field [to] the direction of propagation. *Lorentz* [1909] [ha]d earlier treated the special cases of propa[ga]tion along the magnetic field and perpendicular [to] it. *Goldstein* [1928] and *Hartree* [1929] shortly [af]terward independently derived the same for[m]ula as Appleton but by different methods.

In the above derivation of the magnetoionic dispersion and polarization of the electromagnetic wave, the effect of collisions between the various constituents of the ionized medium was taken into account under certain simplifying assumptions. Owing to the low degree of ionization in the ionosphere the most significant collisions are those between the electrons and the neutral molecules. The electron-electron and electron-ion encounters are usually neglected, an assumption particularly valid in the lower ionosphere, such as the D layer.

The effect of collisions between electrons and

neutral molecules was in the original work expressed by a 'friction term' in the equation of propagation [*Appleton and Chapman*, 1932]. This term, which can be formally identified with the collision frequency, ν, is assumed to be independent of the electron velocity. Thus is singled out a very special case of possible velocity dependences for the collision frequency, viz, $\nu =$ constant.

In recent years evidence has accumulated, particularly through research on microwave propagation in various gases, that this velocity dependence varies from gas to gas [*Molmud*, 1959]. For the major constituent of the ionosphere, nitrogen gas, *Phelps and Pack* [1959] have shown that the collision frequency is proportional to the individual electron energy. According to *Huxley* [1959] the effects of oxygen are not significantly different, as evidenced from observations of collision cross sections in air.

Previously several workers [*Huxley*, 1937; *Jancel and Kahan*, 1954; *Pfister*, 1954; *Westfold*, 1953; *Alpert, Ginzburg*, and *Feinberg*, 1953] have tried to generalize the classical Appleton-Hartree formulas suitably, taking into account the effects of the velocity distribution function for the electrons. Probably the most lucid treatment closely related to the form of the Appleton-Hartree expressions is the work of Jancel and Kahan. Their method is based upon Chapman-Enskog's expansion of the velocity distribution function and a subsequent solution of the Boltzmann equation in kinetic theory. However, at the time of their study (incidentally this holds also for the other works cited), the laboratory results on the velocity dependence of the collision frequency in nitrogen were not known. Consequently the theory was not pushed to a practical limit in its applications.

In the present paper we propose to rederive the generalized expression for the complex refractive index and the state of polarization of a slightly ionized Lorentz gas in an external magnetic field and oscillating electric field. We will follow Chapman-Enskog's method, as applied by Jancel and Kahan, but with a physically somewhat more significant ordering of terms and simplified algebraic expressions for the conductivity tensor elements. The effects of the velocity dependence of the collision frequency will be evaluated in closed analytic forms. Numerical applications will be made, with a subsequent discussion of the realms of applicability for the generalized and classical Appleton-Hartree expressions.

2. Theory

The dispersion and polarization of an electromagnetic wave propagating through a slightly ionized medium are conditioned by the properties of the conductivity tensor, σ, and the dielectric tensor, ϵ, of the medium. Any effects of the velocity dependence for the collision frequency will reside in these quantities and will not alter the form of the actual wave equation, which is derived from Maxwell's equations in conventional manner. The wave equation for an electromagnetic wave with alternating amplitude, $\mathbf{E}\cos\omega t$, and in the presence of a steady external magnetic field, $\mathbf{H}_0$, is

$$\frac{c^2}{u^2}\mathbf{E} - \mathbf{D} - \frac{c^2}{u^2}(\mathbf{E}\cdot\mathbf{N})\mathbf{N} = 0 \tag{1a}$$

$$\mathbf{D} = \mathbf{E} + 4\pi\mathbf{P} = ||\epsilon||\,\mathbf{E}$$

$$\left(\frac{c^2}{u^2} - 1\right)\mathbf{H}_0 = 4\pi\frac{c}{u}\,\mathbf{N}\times\mathbf{P} \tag{1b}$$

$$\mathbf{I} = \frac{\partial\mathbf{P}}{\partial t} = ||\sigma||\,\mathbf{E}$$

Here u is the phase velocity of the wave, $\mathbf{N}$ is the wave normal, $\mathbf{P}$ is the polarization vector, $\mathbf{D}$ is the displacement vector and $\mathbf{I}$ is the current vector.

The problem is then reduced to consider the generalization of the conductivity and dielectric tensors of the medium for the case $\nu = \nu_m f(v)$. The generalized expressions for the complex refractive index, c^2/u^2, and the polarization can then be contrasted with the Appleton-Hartree formulas (case $\nu =$ constant).

We consider a slightly ionized Lorentz gas with a number density of electrons, n_2, and neutral molecules, n_1. In a Lorentz gas the mass of one constituent is assumed to be much larger than that of the second constituent, or $m_1 \gg m_2$. In what follows all quantities with subscript 2 refer to electrons, those with subscript 1 refer to neutral molecules. For purposes of comparison we shall in the main adopt the notations of Jancel and Kahan. In a Lorentz gas the effects of mutual collisions among particles of the lighter constituent are negligible as compared with the influence of the collisions between the heavy and the light components of the gas, or $n_1 \gg n_2$. As a further consequence

heavy constituent maintains a Maxwellian ·city distribution, f_1, even when the lighter exhibits a non-Maxwellian distribution ·ction, f_2. It thus suffices to study the Boltz- ·nn equation governing the velocity distri- ·ion function of the electrons under the ·uence of an external alternating electric ·l, $\mathbf{E}\cos\omega t$, and a steady external magnetic ·l, $\mathbf{H}_0$. We consider only elastic collisions · propagation in a uniform plasma.

·he Boltzmann equation for the electrons ·hen of the form:

$$+\left[\mathbf{\Gamma}_2\cos wt+\frac{e_2}{m_2}(\mathbf{v}_2\times\mathbf{H}_0)\right]\mathrm{grad}_{\mathbf{v}_2}f_2$$

$$=\iiint(f_1'f_2'-f_1f_2)gb\,db\,d\epsilon\,d\mathbf{v}_1 \qquad (2)$$

·ere $\mathbf{\Gamma}_2=(e_2/m_2)\,\mathbf{E}$, b, and ϵ are impact ·ameters as defined by *Chapman and Cowling* ·58, p. 61], g is the relative velocity, $|\mathbf{v}_2-\mathbf{v}_1|=$ · $-\mathbf{v}_1'|$, equal before (unprimed) and after ·imed) the collisions.

·The neutral molecules will preserve their ·tial Maxwellian velocity distribution, which is

$$f(v_1)=n_1\left(\frac{m_1}{2\pi kT}\right)^{3/2}e^{-m_1v_1^2/2kT} \qquad (3)$$

However, the velocity distribution function · the electrons is in general not Maxwellian, ·d the departures will be functions of $\mathbf{E}$ and $\mathbf{H}_0$. ·In order to obtain solutions for f_2 from the ·ltzman equation (2) we expand f_2 in a double ·wer series in $\mathbf{\Gamma}_2$ and spherical harmonics ·hapman-Enskog method).

$$\begin{aligned}= f_2^{(0)} &+ (\mathbf{\Gamma}_2\times\mathbf{v}_2)(\alpha_2\cos\omega t+\beta_2\sin\omega t)\\ &+(\mathbf{H}_0\times\mathbf{\Gamma}_2)\cdot\mathbf{v}_2(\xi_2\cos\omega t+\eta_2\sin\omega t)\\ &+[\mathbf{H}_0\times(\mathbf{H}_0\times\mathbf{\Gamma}_2)]\\ &\cdot\mathbf{v}_2(\gamma_2\cos\omega t+\delta_2\sin\omega t) \qquad (4)\end{aligned}$$

Here the isotropic part, $f_2^{(0)}$, and the coefficients α_2, β_2, ξ_2, η_2, γ_2, and δ_2 are only functions of $v_2=|\mathbf{v}_2|$.

For the collision integral on the right-hand side of the Boltzmann equation (2) we adopt the expression given by *Chapman and Cowling* [1958, p. 350] valid for a Lorentz gas,

$$\iiiint(f_1'f_2'-f_1f_2)gb\,db\,d\epsilon\,d\mathbf{v}_1\,d\mathbf{v}_2$$

$$=\frac{kT}{m_1\lambda}v_2^{\,3}\frac{\partial f_2^{(0)}}{\partial v_2}+\frac{m_2v_2^{\,4}}{m_1\lambda}f_2^{(0)} \qquad (4a)$$

where $\lambda=v_2/\nu$.

We introduce expression 4 into equation 2 and evaluate $f_2^{(0)}$, α_2, β_2, ξ_2, η_2, γ_2, and δ_2 by equating on both sides of the equation coefficients pertaining to the same terms in the scalars $\mathbf{\Gamma}_2^2$, $\mathbf{\Gamma}_2\cdot\mathbf{v}_2$, $(\mathbf{H}_0\times\mathbf{\Gamma}_2)\cdot\mathbf{v}_2$ or $[\mathbf{H}_0\times(\mathbf{H}_0\times\mathbf{\Gamma}_2)]\cdot\mathbf{v}_2$. (For further details see the Appendix.)

Jancel and Kahan prefer to split the terms in $[\mathbf{H}_0\times(\mathbf{H}_0\times\mathbf{\Gamma}_2)]\cdot\mathbf{v}_2$ into components of type $\mathbf{\Gamma}_2\cdot\mathbf{v}_2$ or $\mathbf{H}_0\cdot\mathbf{v}_2$. In both their treatment and ours the total current is written in terms of $\mathbf{\Gamma}_2$, $(\mathbf{H}_0\times\mathbf{\Gamma}_2)$ and $[\mathbf{H}_0\times(\mathbf{H}_0\times\mathbf{\Gamma}_2)]$, viz.:

$$\begin{aligned}I=n_2e_2\bar{\mathbf{v}}_2=\frac{4\pi}{3}e_2\{&J_1\mathbf{\Gamma}_2+J_2(\mathbf{H}_0\times\mathbf{\Gamma}_2)\\ &+J_3[\mathbf{H}_0\times(\mathbf{H}_0\times\mathbf{\Gamma}_2)]\} \qquad (5)\end{aligned}$$

As we shall see later, the fundamental dielectric tensor elements ϵ_{I}, ϵ_{II}, and ϵ_{III} are most naturally associated with the directions of the vectors $\mathbf{\Gamma}_2$, $(\mathbf{H}_0\times\mathbf{\Gamma}_2)$, and $[\mathbf{H}_0\times(\mathbf{H}_0\times\mathbf{\Gamma}_2)]$ (see equation 24). It thus appears somewhat more sensible physically to retain our ordering mode. This does not affect the algebraic expressions for $f_2^{(0)}$, α_2, β_2, ξ_2, η_2, γ_2, and δ_2, which upon proper substitution agree identically with those of Jancel and Kahan. We prefer to give these expressions the following terms, which are

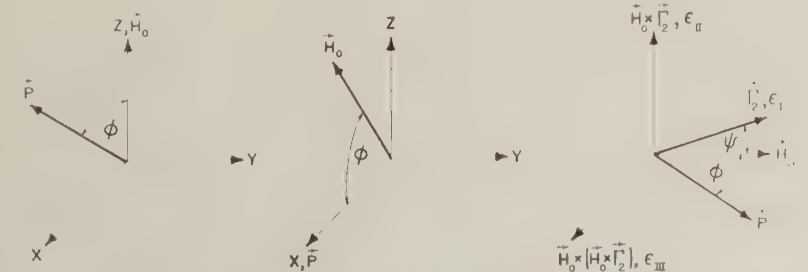

(a) (b) (c)

Fig. 1. Various coordinate systems utilized in the discussion of the form of the dielectric tensor, ϵ. (For further details see text.)

somewhat simpler than those of Jancel and Kahan:

$$\alpha_2 = \frac{-\nu}{\nu^2 + \omega^2} \frac{1}{v_2} \frac{\partial f_2^{(0)}}{\partial v_2}$$

$$\beta = \frac{-\omega}{\nu^2 + \omega^2} \frac{1}{v_2} \frac{\partial f_2^{(0)}}{\partial v_2}$$

$$\xi_2 = \frac{e_2}{m_2} \frac{(\nu^2 + s^2 - \omega^2)}{[\nu^2 + (\omega + s)^2][\nu^2 + (\omega - s)^2]} \frac{1}{v_2} \frac{\partial f_2^{(0)}}{\partial v_2}$$

$$\eta_2 = \frac{2e_2}{m_2} \frac{\omega\nu}{[\nu^2 + (\omega + s)^2][\nu^2 + (\omega - s)^2]} \frac{1}{v_2} \frac{\partial f_2^{(0)}}{\partial v_2}$$

$$\gamma_2 = \frac{s^2}{H_0^2} \frac{1}{(\nu^2 + \omega^2)} \frac{\nu(3\omega^2 - \nu^2 - s^2)}{[\nu^2 + (\omega + s)^2][\nu^2 + (\omega - s)^2]} \frac{1}{v_2} \frac{\partial f_2^{(0)}}{\partial v_2}$$

$$\delta_2 = \frac{-s^2}{H_0^2} \frac{1}{[\nu^2 + \omega^2]} \frac{\omega(s^2 - \omega^2 + 3\nu^2)}{[\nu^2 + (\omega + s)^2][\nu^2 + (\omega - s)^2]} \frac{1}{v_2} \frac{\partial f_2^{(0)}}{\partial v_2}$$

where the gyrofrequency of the electrons is $s = e_2 H_0 / m_2$.

Finally, we have

$$f_2^{(0)} = A \exp\left\{-\int_0^{v_2} \frac{m_2 v_2 \, dv_2}{kT + F(v_2)}\right\} \tag{7}$$

(for further details see Appendix), where

$$F(v_2) = \frac{\Gamma_2^2}{6} \frac{m_1(1 - C)}{\nu^2 + \omega^2}$$

and

$$C = \frac{s^2(\nu^2 + s^2 - 3\omega^2) \sin^2 \psi}{[\nu^2 + (\omega + s)^2][\nu^2 + (\omega - s)^2]}$$

The angle between the vectors $\mathbf{\Gamma}_2$ and $\mathbf{H}_0$ i designated by ψ.

The total velocity distribution function, to the first order of approximation in $\mathbf{\Gamma}_2$, is then

$$f_2 = f_2^{(0)} + \mathbf{f}_2^{(1)} \cdot \mathbf{v}_2 \tag{8}$$

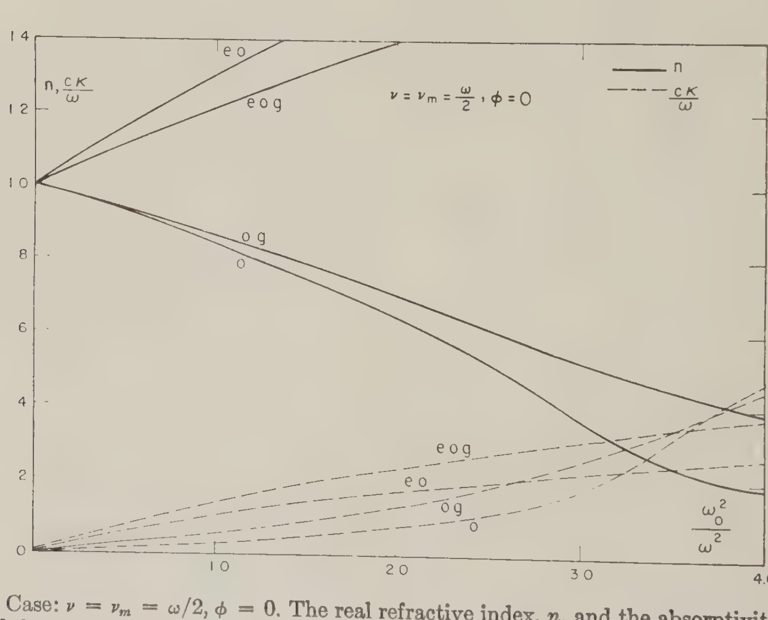

Fig. 2. Case: $\nu = \nu_m = \omega/2$, $\phi = 0$. The real refractive index, n, and the absorptivity, $c\kappa/\omega$, as a function of the square of the ratio of the plasma frequency, ω_0, to the wave frequency, ω, for longitudinal propagation ($\phi = 0$). Here o. = ordinary ray (classical theory), e.o. = extraordinary ray (classical theory), o.g. = ordinary ray (generalized theory), e.o.g. = extraordinary ray (generalized theory).

,

$= (\alpha_2 \cos \omega t + \beta_2 \sin \omega t)\mathbf{\Gamma}_2$

$\xi_2 \cos \omega t + \eta_2 \sin \omega t)(\mathbf{H}_0 \times \mathbf{\Gamma}_2)$

$\gamma_2 \cos \omega t + \delta_2 \sin \omega t)[\mathbf{H}_0 \times (\mathbf{H}_0 \times \mathbf{\Gamma}_2)]$

can be shown that $f_2^{(0)}$ determines the ber density and $\mathbf{f}_2^{(1)}$ determines the current ity. If we take the direction of $\mathbf{f}_2^{(1)}$ as the s of spherical coordinates, then

$$\iiint (f_2^{(0)} + f_2^{(1)} v_2 \cos \theta) v_2^2 \, dv_2$$

$$\cdot \sin \theta \, d\theta \, d\varphi = \int_0^\infty f_2^{(0)} 4\pi v_2^2 \, dv_2 \qquad (9)$$

provides the normalization condition for constant of integration, A, in equation 7. urthermore,

$$)_x = \iiint v_2 \sin \theta \cos \varphi (f_2^{(0)} + f_2^{(1)} v_2 \cos \theta) v_2^2 \, dv_2 \sin \theta \, d\theta \, d\varphi = 0$$

$$)_y = \iiint v_2 \sin \theta \sin \varphi (f_2^{(0)} + f_2^{(1)} v_2 \cos \theta) v_2^2 \, dv_2 \sin \theta \, d\theta \, d\varphi = 0 \qquad (10)$$

$$_2)_z = \iiint v_2 \cos \theta (f_2^{(0)} + f_2^{(1)} v_2 \cos \theta) v_2^2 \, dv_2 \sin \theta \, d\theta \, d\varphi = \int_0^\infty f_2^{(1)} \frac{4\pi}{3} v_2^4 \, dv_2$$

hus for *any* orientation of the axes

$$n_2 \bar{\mathbf{v}}_2 = \frac{4\pi}{3} \int_0^\infty \mathbf{f}_2^{(1)} v_2^4 \, dv_2 \qquad (11)$$

he total current is then

$$\mathbf{I} = n_2 e_2 \bar{\mathbf{v}}_2 = \frac{4\pi}{3} e_2 \int_0^\infty \mathbf{f}_2^{(1)} v_2^4 \, dv_2 \qquad (12)$$

as previously stated,

$$= \frac{4\pi}{3} e_2 \{ J_1 \mathbf{\Gamma}_2 + J_2 (\mathbf{H}_0 \times \mathbf{\Gamma}_2) + J_3 [\mathbf{H}_0 \times (\mathbf{H}_0 \times \mathbf{\Gamma}_2)] \} \qquad (5)$$

re

$$= \int_0^\infty (\alpha_2 \cos \omega t + \beta_2 \sin \omega t) v_2^4 \, dv_2$$

$$= \int_0^\infty (\xi_2 \cos \omega t + \eta_2 \sin \omega t) v_2^4 \, dv_2 \qquad (13)$$

$$= \int_0^\infty (\gamma_2 \cos \omega t + \delta_2 \sin \omega t) v_2^4 \, dv_2$$

So far we have not specified a coordinate system for the propagation of the electromagnetic wave. We choose a right-handed rectangular system with the Oz axis along $\mathbf{H}_0$. The direction of propagation falls in the xOz plane (see Fig. 1a). Then the generalized expression, σ_g for the conductivity tensor in this coordinate system becomes

$$\sigma_g = \frac{4\pi}{3} \frac{e_2^2}{m_2} \begin{vmatrix} (J_1 - H_0^2 J_3) & (-H_0 J_2) & 0 \\ H_0 J_2 & (J_1 - H_0^2 J_3) & 0 \\ 0 & 0 & J_1 \end{vmatrix} \qquad (14)$$

It is worth noting that this expression is the pivotal point in any generalization of the Appleton-Hartree formulas. The generalization thus consists of a proper averaging of the conductivity tensor elements taking into account the velocity dependence of the collision frequency. The above expression, equation 14, is valid for *any* velocity distribution function, Maxwellian or non-Maxwellian.

The formalism originally developed by Jancel and Kahan, and herein rephrased and reinterpreted, yields results identical to several other independent lines of research. We would like in particular to mention that the formalism in microwave diagnostics by *Allis* [1956] yields an identical expression for the above conductivity tensor, although their theory is based upon a method of expansion of the velocity distribution function which is different from the Chapman-Enskog method. Also *Bayet, Delcroix, and Denisse* [1954] arrive at an identical expression for the conductivity tensor, although subsequently their expression for the velocity distribution function differs from that of other workers.

The generalized velocity distribution function of equation 7 agrees under suitably simplifying assumptions with those derived by a number of

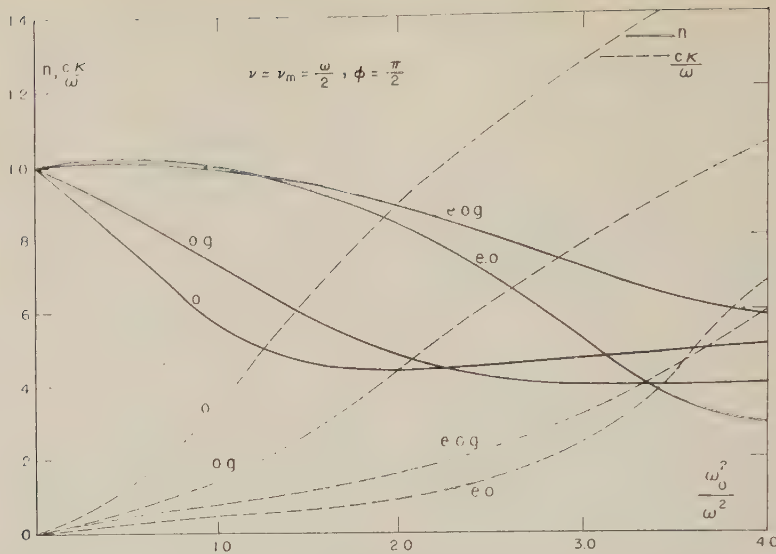

Figure. 3. Case: $\nu = \nu_m = \omega/2, \phi = \pi/2$. The real refractive index, n, and the absorptivity, $c\kappa/\omega$, as a function of the square of the ratio of the plasma frequency, ω_0, to the wave frequency, ω, for transversal propagation ($\phi = \pi/2$). Here o. = ordinary ray (classical theory), e.o. = extraordinary ray (classical theory), o.g. = ordinary ray (generalized theory), e.o.g. = extraordinary ray (generalized theory).

earlier investigators. We single out the following important cases:

(a) For $\omega = 0$ and $\mathbf{H}_0 \perp \mathbf{E}$ the results agree with the expression given by *Chapman and Cowling* [1958, p. 350].

(b) For $\mathbf{H}_0 = 0$ the results agree with that derived by *Margenau* [1946].

(c) For $\mathbf{H}_0 = 0$, $\omega = 0$, $kT \ll \Gamma_2^2$ the results agree with those derived by *Druyvesteyn* [193-].

It is interesting to note that, parallel to these developments, research along similar lines was carried out in Russia, especially at the Lebedev Physical Institute, Moscow, by *Alpert, Ginzburg, and Feinberg* [1953]. The Russian workers *Fain* [1955] and, independently, *Gurevich*

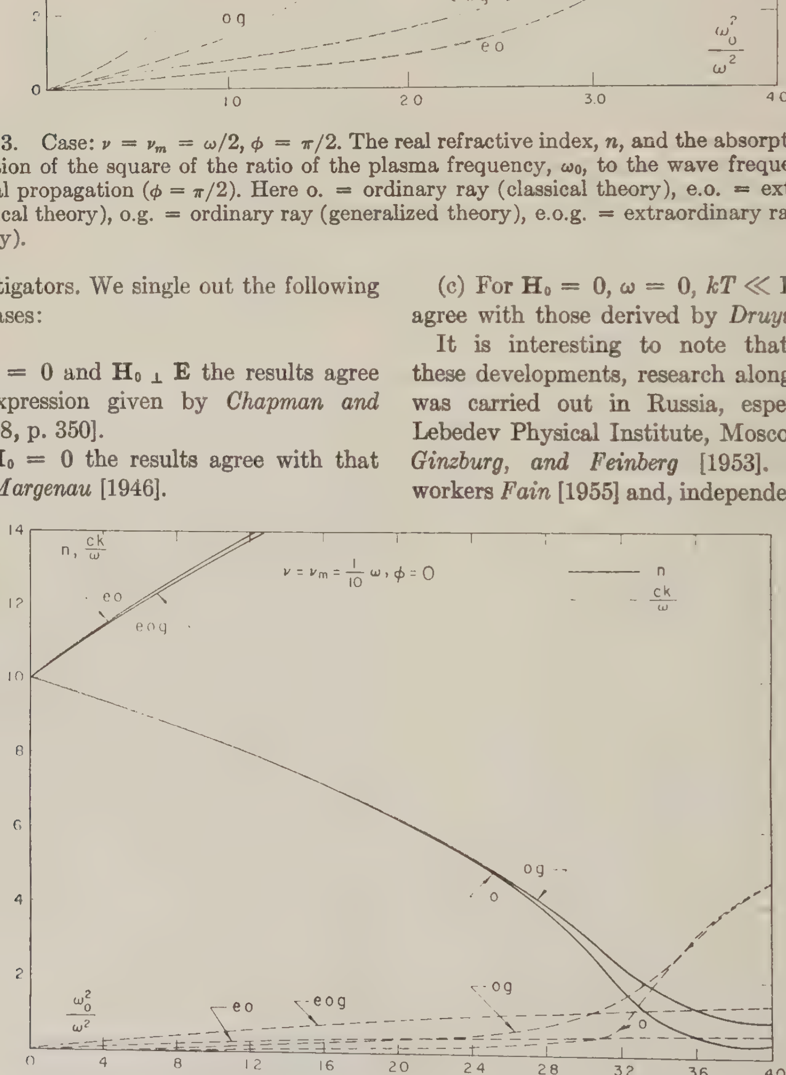

Fig. 4. Case: $\nu = \nu_m = \frac{1}{10}\omega$, $\phi = 0$. Symbols same as in Figure 2.

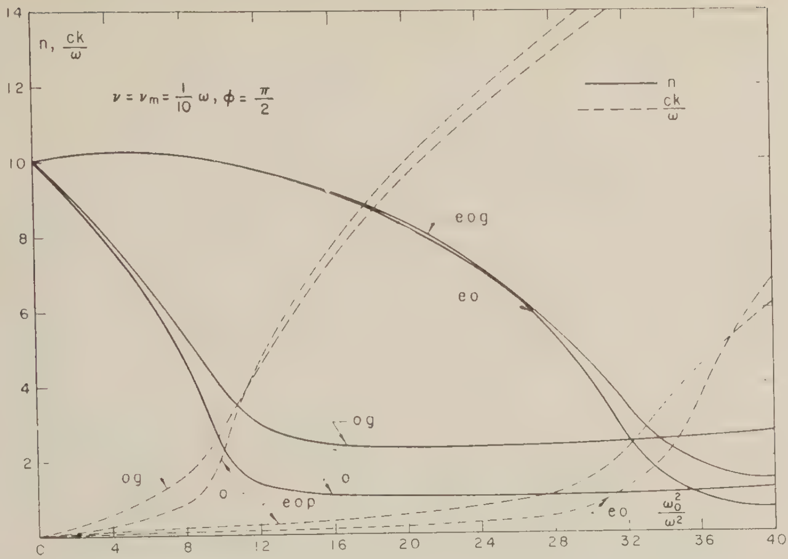

Fig. 5. Case: $\nu = \nu_m = \frac{1}{10}\omega$, $\phi = \pi/2$. Symbols same as in Figure 3.

.56] have also arrived at identically the same ›ression for the velocity distribution function expressed in our equation 7.

For the particular application to the problem radio-wave propagation in the ionosphere, e has generally the condition that the imposed ctric field energy, Γ_2^2, is negligible compared h the thermal energy, kT, and that the ctron velocity distribution is Maxwellian. In at follows we shall assume this to be the case.

A fundamentally different theoretical approach the conductivity of a slightly ionized plasma s been taken by *Huxley* [1951] in several ticles, and also independently by *Bayet* [1954]. eir work is based upon mean free path and ift velocity considerations. These methods ve been criticized by *Cowling* [1957] and also *Jancel and Kahan* [1955]. Recently, *Huxley* 957] has generalized his previous theory, which w appears in essential agreement with the sults based on the Boltzmann theory. The ean free path theories have not, however, been plied to derive the generalized velocity dis- ibution function (equation 7).

There is one important connecting link be- ween the results based on the Boltzmann quation and those based on the mean free th theory. They both arrive at the same pression for the conductivity tensor when = constant, i.e. when the collision frequency independent of the electron velocity. In that case the original Lorentz tensor appears in the following form:

$$\sigma_L = \frac{n_2 e_2^2}{m_2} \cdot \begin{vmatrix} \dfrac{\nu + i\omega}{(\nu + i\omega)^2 + s^2} & \dfrac{-s}{(\nu + i\omega)^2 + s^2} & 0 \\ \dfrac{s}{(\nu + i\omega)^2 + s^2} & \dfrac{\nu + i\omega}{(\nu + i\omega)^2 + s^2} & 0 \\ 0 & 0 & \dfrac{1}{\nu + i\omega} \end{vmatrix} \tag{15}$$

It can easily be shown that the generalized conductivity tensor, equation 14, reduces to this form when ν = constant. The mean free path arguments of *Bayet* [1954] lead to the same results. He has shown that this Lorentz tensor forms the basis for the Appleton-Hartree formulas of the complex refractive index and the polarization. Any generalized expression for the Appleton-Hartree formulas must reduce to these same formulas in the case of ν = constant. Huxley overlooked this result, which is easily deducible from his general formula for the conductivity tensor. He merely states that the Appleton-Hartree formula agrees with his general expression when $\nu = 0$.

The conductivity tensor having thus been generalized it remains to derive the generalized expression for the complex refractive index and

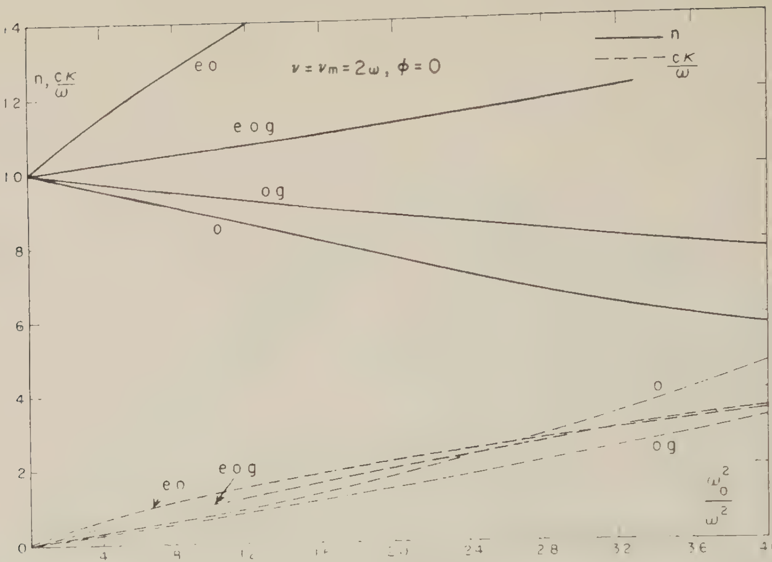

Fig. 6. Case: $\nu = \nu_m = 2\omega, \phi = 0$. Symbols same as in Figure 2.

the polarization valid for any velocity dependence of the collision frequency. It appears convenient to retain a coordinate system with orientations identical to those adopted in *Mitra* [1952, p. 195]. It is equivalent to our previously introduced coordinate system (Fig. 1*a*) rotated an angle $(\pi/2) - \varphi$ about the y axis (see Fig. 1*b*). The direction of propagation falls along the x axis. This is the direction of the wave normal, **N**.

$\mathbf{H}_0$ will lie in the xOz plane, forming an angle φ with the x axis.

The dielectric tensor in air is simply related to the conductivity tensor

$$||\epsilon|| = 1 + 4\pi/i\omega\, ||\sigma|| \tag{16}$$

and, in the above coordinate system (Fig. 1*b*), $||\epsilon||$ has the form

$$||\epsilon|| = \begin{vmatrix} \left(1 + \frac{\sigma_1}{i\omega}\sin^2\varphi + \frac{\sigma_2}{i\omega}\cos^2\varphi\right) & \left(-\frac{\sigma_3}{i\omega}\cos\varphi\right) & \left(\frac{\sigma_1}{i\omega} - \frac{\sigma_2}{i\omega}\right)\sin\varphi\cos\varphi \\ \frac{\sigma_3}{i\omega}\cos\varphi & \left(1 + \frac{\sigma_2}{i\omega}\right) & \left(-\frac{\sigma_3}{i\omega}\sin\varphi\right) \\ \left(\frac{\sigma_1}{i\omega} - \frac{\sigma_2}{i\omega}\right)\sin\varphi\cos\varphi & \frac{\sigma_3}{i\omega}\sin\varphi & \left(1 + \frac{\sigma_1}{i\omega}\cos^2\varphi + \frac{\sigma_2}{i\omega}\sin^2\varphi\right) \end{vmatrix} \tag{17}$$

where the Lorentz tensor elements of equation 15 are written in the form

$$\begin{aligned} \sigma_1 &= \frac{\omega_0^2}{\nu + i\omega} \\ \sigma_2 &= \frac{\omega_0^2(\nu + i\omega)}{[(\nu + i\omega)^2 + s^2]} \\ \sigma_3 &= \frac{\omega_0^2 s}{[(\nu + i\omega)^2 + s^2]} \end{aligned} \tag{18}$$

and the plasma frequency is $\omega_0^2 = 4\pi n_2 e_2^2/m$

By introducing the above dielectric tens[...] into the equation of propagation (1*a*) an[...] decomposing the vector equation into indi[...] vidual coordinate components, we obtain th[...] following equations:

$$\begin{aligned} -(\epsilon_{xx}E_x + \epsilon_{xy}E_y + \epsilon_{xz}E_z) &= 0 \\ \frac{c^2}{u^2}E_y - (\epsilon_{yx}E_x + \epsilon_{yy}E_y + \epsilon_{yz}E_z) &= 0 \\ \frac{c^2}{u^2}E_z - (\epsilon_{zx}E_x + \epsilon_{zy}E_y + \epsilon_{zz}E_z) &= 0 \end{aligned} \tag{19}$$

This system of equations has compatible solutions for **E** when the determinant vanishes

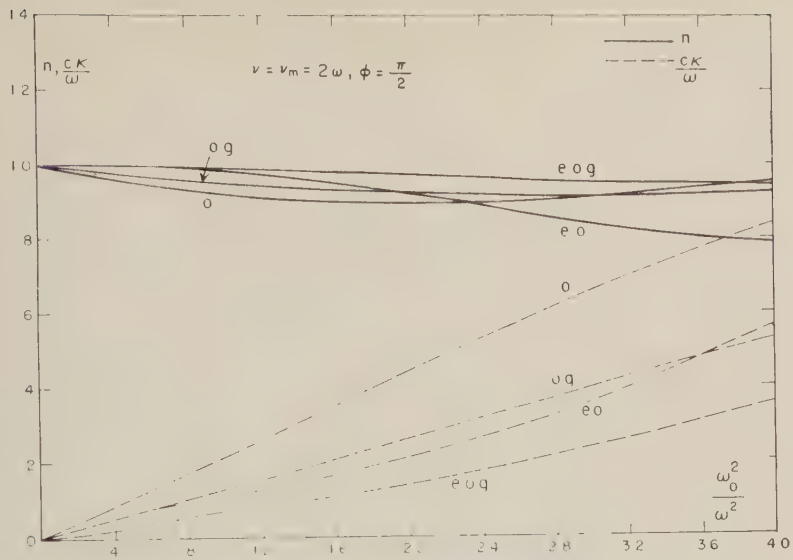

Fig. 7. Case: $\nu = \nu_m = 2\omega$, $\phi = \pi/2$. Symbols same as in Figure 3.

tically, wherefrom we have the condition

$$\begin{vmatrix} -\epsilon_{xx} & -\epsilon_{xy} & -\epsilon_{xz} \\ -\epsilon_{yx} & \left(\frac{c^2}{u^2} - \epsilon_{yy}\right) & -\epsilon_{yz} \\ -\epsilon_{zx} & -\epsilon_{zy} & \left(\frac{c^2}{u^2} - \epsilon_{zz}\right) \end{vmatrix} \tag{20}$$

Substituting from equation 17 and solving the complex refractive index, c^2/u^2, yields Appleton-Hartree formula

$$= 1 + \cfrac{1}{-\frac{\omega^2}{\omega_0^2} + \frac{i\nu\omega}{\omega_0^2} - \frac{\omega^2 s^2 \sin^2\varphi}{2\omega_0^2(\omega_0^2 - \omega^2 + i\nu\omega)} \pm \sqrt{\frac{\omega^4 s^4 \sin^4\varphi}{4\omega_0^4(\omega_0^2 - \omega^2 + i\nu\omega)^2} + \frac{\omega^2 s^2 \cos^2\varphi}{\omega_0^4}}} \tag{21}$$

For further comparisons we will write this the form

$$= 1$$

$$\frac{1}{B'' + C'' \sin^2\varphi \pm \sqrt{D'' \sin^4\varphi + E'' \cos^2\varphi}} \tag{22}$$

ere

$$B'' = \frac{-(\omega^2 - i\nu\omega)}{\omega_0^2}$$

$$C'' = \frac{-\omega^2 s^2}{2\omega_0^2(\omega_0^2 - \omega^2 + i\nu\omega)}$$

$$D'' = \frac{\omega^4 s^4}{4\omega_0^4(\omega_0^2 - \omega^2 + i\nu\omega)^2} \tag{23}$$

$$E'' = \frac{\omega^2 s^2}{\omega_0^4}$$

The above expressions are valid for ν = constant. It appears natural to generalize the above Appleton-Hartree formula by a simple introduction of the generalized dielectric tensor of equation 14 instead of the Lorentz dielectric tensor into the component equations of propagation (19). The generalized complex index of refraction is then a solution of the determinant equation involving the generalized dielectric tensor.

A very natural and convenient mode of

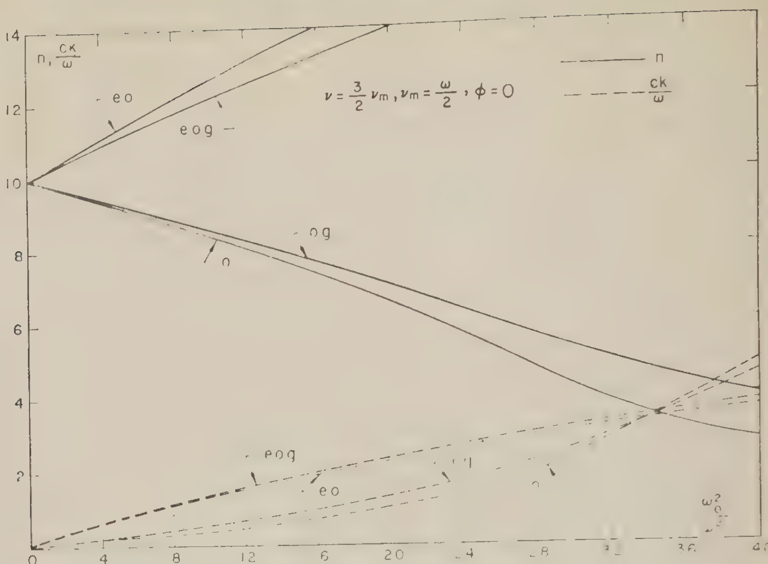

Fig. 8. Case: $\nu = \frac{3}{2}\nu_m$, $\nu_m = \omega/2$, $\phi = 0$. Symbols same as in Figure 2.

representation for the generalized dielectric tensor arises from the utilization of the current flow axes associated with $\mathbf{\Gamma}_2$, $(\mathbf{H}_0 \times \mathbf{\Gamma}_2)$ and $[\mathbf{H}_0 \times (\mathbf{H}_0 \times \mathbf{\Gamma}_2)]$. We define three fundamental dielectric tensor elements ϵ_{I}, ϵ_{II}, and ϵ_{III} associated with these axes in the following manner:

$$\epsilon_{\mathrm{I}} = 1 - \frac{4\pi i}{3\omega}\omega_0^{\,2} J_1'$$
$$\epsilon_{\mathrm{II}} = -\frac{4\pi i}{3\omega}\omega_0^{\,2} H_0 J_2', \tag{24}$$
$$\epsilon_{\mathrm{III}} = -\frac{4\pi i}{3\omega}\omega_0^{\,2} H_0^{\,2} J_3'$$

where ω_0 is the plasma frequency, $J_1 = n_2 J_1'$, $J_2 = n_2 J_2'$, $J_3 = n_2 J_3'$, and J_1, J_2, J_3 are written in their complex forms

$$J_1 = e^{i\omega t}\int_0^\infty \left(\alpha_2 + \frac{\beta_2}{i}\right) v_2^{\,4}\, dv_2$$
$$J_2 = e^{i\omega t}\int_0^\infty \left(\xi_2 + \frac{\eta_2}{i}\right) v_2^{\,4}\, dv_2 \tag{25}$$
$$J_3 = e^{i\omega t}\int_0^\infty \left(\gamma_2 + \frac{\delta_2}{i}\right) v_2^{\,4}\, dv_2$$

It is important to note that for J_1', J_2', and J_3' we have renormalized the velocity distribution function so that

$$\int_0^\infty 4\pi v_2^{\,2} f_2^{(0)}\, dv_2 = 1.$$

This is done in order to utilize n_2 for the int[...] tion of the plasma frequency, $\omega_0^2 = 4\pi n_2 e$[...] In Figure 1c is represented the *oblique* coor[...] system based on axes in the direction[...] $(\mathbf{H}_0 \times \mathbf{\Gamma}_2)$, and $[\mathbf{H}_0 \times (\mathbf{H}_0 \times \mathbf{\Gamma}_2)]$. $\mathbf{H}_0$, [...] $[\mathbf{H}_0 \times (\mathbf{H}_0 \times \mathbf{\Gamma}_2)]$ lie in the same plan[...] $(\mathbf{H}_0 \times \mathbf{\Gamma}_2)$ is perpendicular to this plane.

Generally this oblique coordinate s[...] rotates about the direction of propagati[...] as the $\mathbf{\Gamma}_2$ vector rotates about this axis. [...] $\mathbf{\Gamma}_2$ falls in the xOz plane in Figure 1*a*, th[...] $(\mathbf{H}_0 \times \mathbf{\Gamma}_2)$ axis coincides with the y ax[...] $[\mathbf{H}_0 \times (\mathbf{H}_0 \times \mathbf{\Gamma}_2)]$ with the x axis.

Saha and Banerjee [1945] were the fi[...] point out that the concept of principal die[...] axes as defined in crystal optics could be u[...] as a coordinate system. *Westfold* [1949] rigo[...] formalized this approach and showed tha[...] real principal axis, ϵ_1, lies along the ma[...] field. The two complex axes ϵ_2 and ϵ_3 m[...] matically represent rotations in opposi[...] rections about the real axis, ϵ_1.

The coordinate system in Figure 1*a* [...] to the following form for the dielectric [...] (cf. equation 14);

$$||\epsilon|| = \begin{vmatrix} (\epsilon_{\mathrm{I}} + \epsilon_{\mathrm{III}}) & -\epsilon_{\mathrm{II}} & 0 \\ \epsilon_{\mathrm{II}} & (\epsilon_{\mathrm{I}} + \epsilon_{\mathrm{III}}) & 0 \\ 0 & 0 & \epsilon_{\mathrm{I}} \end{vmatrix}$$

The oblique coordinate system in Figu[...]

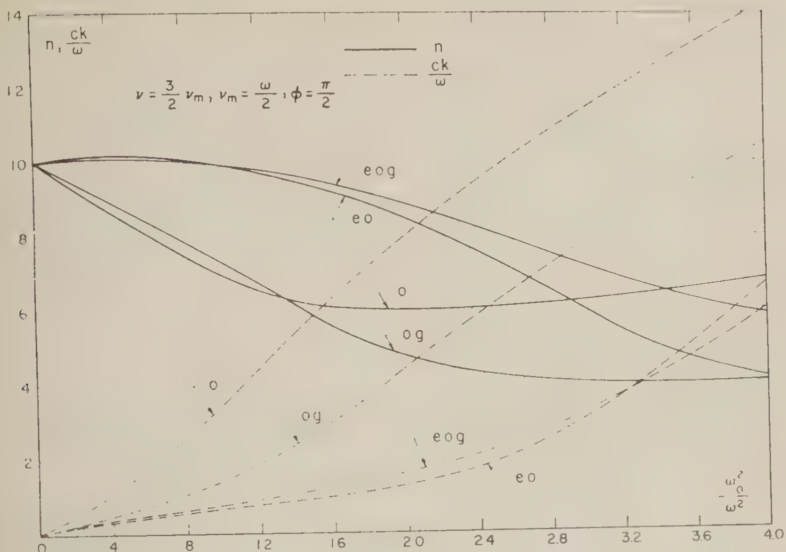

Fig. 9. Case: $\nu = \frac{3}{2}\nu_m$, $\nu_m = \omega/2$, $\phi = \pi/2$. Symbols same as in Figure 3.

...s to a diagonal dielectric tensor of the form:

$$||\epsilon|| = \begin{vmatrix} \epsilon_{\mathrm{I}} & 0 & 0 \\ 0 & \epsilon_{\mathrm{II}} & 0 \\ 0 & 0 & \epsilon_{\mathrm{III}} \end{vmatrix} \tag{26b}$$

...an be shown that the diagonalization of ...nsor in (26a) leads to the dielectric tensor ... with the principal axes as defined by ...stfold, where

$$||\epsilon|| = \begin{vmatrix} \epsilon_3 & 0 & 0 \\ 0 & \epsilon_2 & 0 \\ 0 & 0 & \epsilon_1 \end{vmatrix} \quad \text{and} \quad \begin{aligned} \epsilon_1 &= \epsilon_{\mathrm{I}} \\ \epsilon_2 &= \epsilon_{\mathrm{I}} + \epsilon_{\mathrm{III}} + i\epsilon_{\mathrm{II}} \\ \epsilon_3 &= \epsilon_{\mathrm{I}} + \epsilon_{\mathrm{III}} - i\epsilon_{\mathrm{II}} \end{aligned} \tag{26c}$$

We note that these principal axes are formally identical to the expressions for the complex refractive index for longitudinal and transverse propagation (see section on numerical applications, equations 39 and 44).

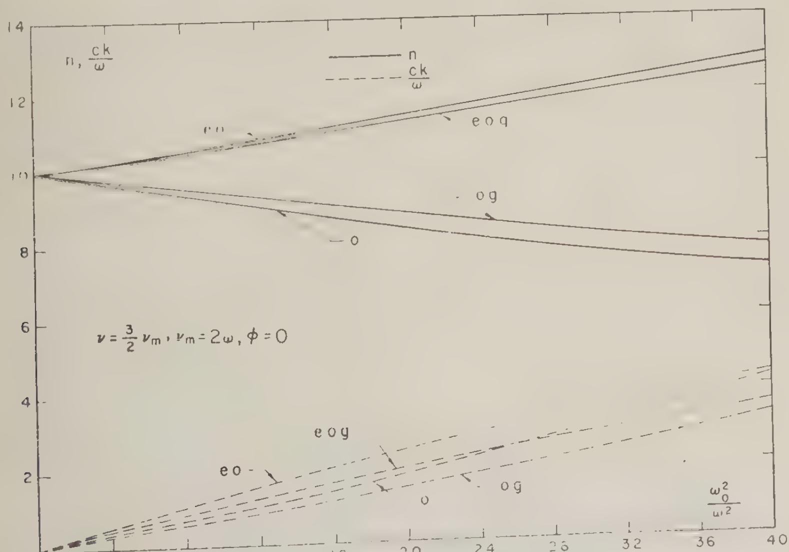

Fig. 10. Case: $\nu = \frac{3}{2}\nu_m$, $\nu_m = 2\omega$, $\phi = 0$. Symbols same as in Figure 2.

The formal advantage of utilizing the principal axes ϵ_1, ϵ_2, and ϵ_3 is that the dielectric tensor reduces to a diagonal matrix in a *rectangular* coordinate system (albeit introducing complex numbers); the fundamental axes $\epsilon_{\rm I}$, $\epsilon_{\rm II}$, and $\epsilon_{\rm III}$ also provide a diagonal matrix but only in the *oblique* coordinate system of Figure 1*c*. However, to us the association of $\epsilon_{\rm I}$, $\epsilon_{\rm II}$, and $\epsilon_{\rm III}$ with the current flow axes $\mathbf{\Gamma}_2$, $(\mathbf{H}_0 \times \mathbf{\Gamma}_2)$ and $[\mathbf{H}_0 \times (\mathbf{H}_0 \times \mathbf{\Gamma}_2)]$ appears physically more significant, and we prefer to retain this concept of fundamental elements $\epsilon_{\rm I}$, $\epsilon_{\rm II}$, and $\epsilon_{\rm III}$ in what follows.

With the same orientation of the coordinate axes as in the derivation of the Appleton-Hartree formula (Fig. 1*b*), the generalized dielectric tensor becomes

$$||\epsilon|| = \begin{vmatrix} (\epsilon_{\rm I} + \epsilon_{\rm III} \cos^2 \varphi) & -\epsilon_{\rm II} \cos \varphi & -\epsilon_{\rm III} \sin \varphi \cos \varphi \\ \epsilon_{\rm II} \cos \varphi & \epsilon_{\rm I} + \epsilon_{\rm III} & -\epsilon_{\rm II} \sin \varphi \\ -\epsilon_{\rm III} \sin \varphi \cos \varphi & \epsilon_{\rm II} \sin \varphi & \epsilon_{\rm I} + \epsilon_{\rm III} \sin^2 \varphi \end{vmatrix} \qquad (2$$

A substitution of this dielectric tensor into the wave equation 19 leads to the following generalized expression for the complex refractive index:

$$\frac{c^2}{u^2} = \left(n - \frac{ic\kappa}{\omega}\right)^2$$

$$= \frac{A + B \sin^2 \varphi \pm \sqrt{B^2 \sin^4 \varphi - C^2 \cos^2 \varphi}}{D + E \sin^2 \varphi} \qquad (27)$$

where

$$\begin{aligned} A &= 2\epsilon_{\rm I}(\epsilon_{\rm I} + \epsilon_{\rm III}) \\ B &= \epsilon_{\rm III}(\epsilon_{\rm I} + \epsilon_{\rm III}) + \epsilon_{\rm II}^2 \\ C &= 2\epsilon_{\rm I}\epsilon_{\rm II} \\ D &= 2\epsilon_{\rm I} \\ E &= 2\epsilon_{\rm III} \end{aligned} \qquad (28)$$

Equation 27 is identical with the expression originally derived by Jancel and Kahan. They were able to show that in the case of $\nu \ll \omega$ this reduces to the ordinary Appleton-Har formula with $\nu = 0$. However, in view of Bay demonstration any generalized expression the complex refractive index must rigoro reduce to the Appleton-Hartree formula in case $\nu =$ constant.

In order to show this more clearly we proc to transform the general expression 27 int form reminiscent of the classical one, viz.,

$$\frac{c^2}{u^2} = 1 + \frac{1 + A' \sin^2 \varphi}{B' + C' \sin^2 \varphi \pm \sqrt{D' \sin^4 \varphi + E' \cos}} \qquad ($$

where

$$A' = \frac{[\epsilon_{\rm III}(1 - \epsilon_{\rm I} - \epsilon_{\rm III}) - \epsilon_{\rm II}^2]}{\epsilon_{\rm I}[(1 - \epsilon_{\rm I} - \epsilon_{\rm III})^2 + \epsilon_{\rm II}^2]}$$

$$B' = \frac{-(1 - \epsilon_{\rm I} - \epsilon_{\rm III})}{[(1 - \epsilon_{\rm I} - \epsilon_{\rm III})^2 + \epsilon_{\rm II}^2]}$$

$$C' = \frac{-[\epsilon_{\rm III} + \epsilon_{\rm III}(1 - \epsilon_{\rm I} - \epsilon_{\rm III}) - \epsilon_{\rm II}^2]^2}{2\epsilon_{\rm I}[(1 - \epsilon_{\rm I} - \epsilon_{\rm III})^2 + \epsilon_{\rm II}^2]} \qquad ($$

$$D' = \frac{[\epsilon_{\rm III}(\epsilon_{\rm I} + \epsilon_{\rm III}) + \epsilon_{\rm II}^2]}{4\epsilon_{\rm I}^2[(1 - \epsilon_{\rm I} - \epsilon_{\rm III})^2 + \epsilon_{\rm II}^2]^2}$$

$$E' = \frac{-\epsilon_{\rm II}^2}{[(1 - \epsilon_{\rm I} - \epsilon_{\rm III})^2 + \epsilon_{\rm II}^2]^2}$$

The new coefficients A', B', C', D' and are considerably more complicated function $\epsilon_{\rm I}$, $\epsilon_{\rm II}$, and $\epsilon_{\rm III}$ than the original coeffici A, B, C, D, and E. However, equation 29 the advantage of showing how the generali expression is identical with the Appleton-Har formula in its angular dependence on φ exc for a new term $A' \sin^2 \varphi$.

In the case $\nu =$ constant, the integral pressions J_1', J_2', and J_3' reduce simply to forms

$$
\begin{aligned}
{}_0J_1' &= \frac{3}{4\pi} e^{i\omega t} \frac{1}{\nu + i\omega} \\
{}_0J_2' &= \frac{3}{4\pi} e^{i\omega t} \frac{(-s)}{[(\nu + i\omega)^2 + s^2]} \qquad (31) \\
{}_0^2J_3' &= \frac{3}{4\pi} e^{i\omega t} \frac{s^2}{(\nu + i\omega)[(\nu + i\omega)^2 + s^2]}.
\end{aligned}
$$

and the fundamental dielectric tensor elements become

$$
\begin{aligned}
\epsilon_{\mathrm{I}} &= 1 + \sigma_1/i\omega \\
\epsilon_{\mathrm{II}} &= \sigma_3/i\omega \qquad (32) \\
\epsilon_{\mathrm{III}} &= (\sigma_2/i\omega) - (\sigma_1/i\omega)
\end{aligned}
$$

where σ_1, σ_2, and σ_3 are the previously defined Lorentz tensor elements of equation 18. Upon introducing these expressions for σ_1, σ_2, and σ_3 into the coefficients A', B', C', D', and E' one finds that A' *becomes identically zero* and the other coefficients reduce to B'', C'', D'' and E''. Thus the proof is completed that, for the case ν = constant, the generalized formula 29 reduces to the ordinary Appleton-Hartree formula. It provides incidentally also a check on the internal consistency of the formalism developed in this paper.

Similar considerations can be made regarding the polarization studies of the electromagnetic wave. Following *Mitra* [1952, p. 186] we define:

$$
R = \frac{H_z}{H_y} = \frac{-E_y}{E_z} = -\frac{1}{\sqrt{E''}\cos\varphi} \cdot \left[\frac{1}{c^2/u^2 - 1} - B''\right] \qquad (33)
$$

After ordering terms using equation 22 we have

$$
R = -\frac{i[C''\sin^2\varphi \pm \sqrt{D''\sin^4\varphi + E''\cos^2\varphi}]}{\sqrt{E''}\cos\varphi} \qquad (34)
$$

This is then the complete expression for the state of polarization in the Appleton-Hartree case. In the generalized theory it can be shown that the state of polarization becomes

$$
R = -\frac{[B\sin^2\varphi \mp \sqrt{B^2\sin^4\varphi - C^2\cos^2\varphi}]}{C\cos\varphi} \qquad (35)
$$

As expected, when ν = constant this generalized expression reduces to the Appleton-Hartree formula when the conductivity tensor elements σ_1, σ_2, and σ_3 as defined by equation 18 are introduced into B and C. No new angular dependent terms analogous to $A'\sin^2\varphi$ appear in the generalized expression for the state of polarization. On the other hand, the generalized coefficients B and C may well alter the state of polarization as compared with the ordinary Appleton-Hartree case.

3. Numerical Applications

Clearly the generalization is of no interest when ν is negligible compared with ω, i.e., when absorption measures are not involved. However, as our calculations will show even for $\nu = 0.1\omega$, certain significant differences begin to appear between the absorptions calculated by the generalized expression and those by the Appleton-Hartree formula. In the case when the collision frequency is comparable to the wave frequency, the differences can no longer be overlooked in any precise work involving absorption measurements.

We have studied two limiting cases of propagation: (*a*) longitudinal propagation along the magnetic lines of force, $\varphi = 0$; and (*b*) transverse propagation across the magnetic lines of force, $\varphi = \pi/2$. These should represent minimum and maximum departures from the classical formula in view of the collisional absorption effects. The two cases also conveniently bracket the results of *Gobeau's* [1935] calculations for $\varphi = 30°$.

It is worth noting that our generalized expression for the complex refractive index leads, under the same simplifying assumptions as used by *Phelps and Pack* [1959], to an expression, Q, identical with the one derived by them for longitudinal propagation in *Kane's* [1959] D-layer problem. The above authors evaluate the quantity Q defined by the following equation:

$$
Q \equiv \frac{\kappa_x - \kappa_o}{(1 - n_x) - 1.4(1 - n_o)} = \frac{\frac{5}{2}\left\{\mathcal{C}_{5/2}\left(\frac{\omega + s}{\nu_m}\right) - \mathcal{C}_{5/2}\left(\frac{\omega - s}{\nu_m}\right)\right\}}{\left(\frac{\omega - s}{\nu_m}\right)\mathcal{C}_{3/2}\left(\frac{\omega - s}{\nu_m}\right) + 1.4\left(\frac{\omega + s}{\nu_m}\right)\mathcal{C}_{3/2}\left(\frac{\omega + s}{\nu_m}\right)}
$$

κ = absorption coefficient; x = extraordinary ray; n = real refractive index; O = ordinary ray. (36)

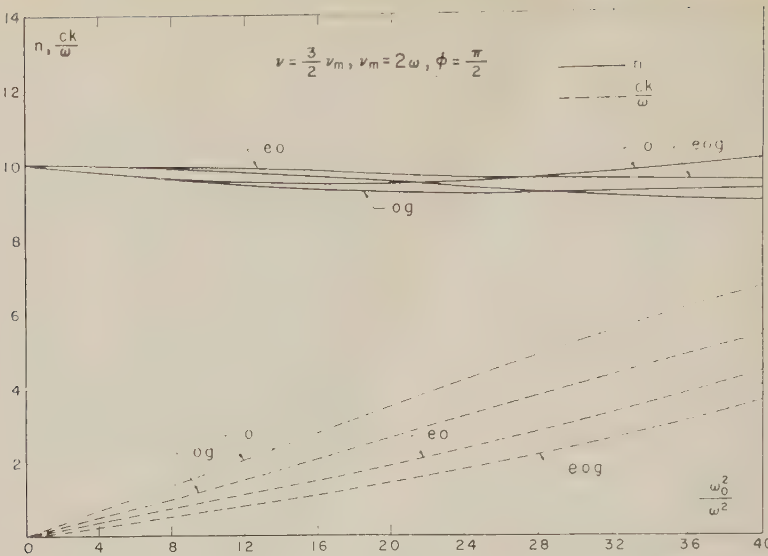

Fig. 11. Case: $\nu = \frac{3}{2}\nu_m$, $\nu_m = 2\omega$, $\phi = \pi/2$. Symbols same as in Figure 3.

Here

$$\mathcal{C}_p(x) \equiv \frac{1}{p!}\int_0^\infty \frac{\epsilon^p e^{-\epsilon}\, d\epsilon}{\epsilon^2 + x^2} \tag{37}$$

$\epsilon = m_2 v_2^2/2kT \qquad v_2 = \text{electron velocity}$

These C script integrals form a very convenient basis for the numerical applications of the generalized expression for the complex refractive index in air. The integrals have been tabulated by *Dingle, Arndt, and Roy* [1957].

The whole class of A, B, C, D script integrals as given by *Dingle, Arndt, and Roy* [1957] allows one to take into account any velocity dependence for the collision frequency as long as it is expressible in the form

$$\nu = \sum_{i=0}^{n} a_i v^i \tag{38}$$

In principle it can be shown that the resulting tensor element integrals are reducible to the cases ν = constant, $\nu \propto v$, $\nu \propto v^2$. Thus the general theory developed herein should be applicable to microwave propagation in other gases besides nitrogen, where the velocity dependence for the collision frequency may be different from that of nitrogen. In the ionospheric case of nitrogen and air, we adopt the findings of *Phelps and Pack* [1959], viz., that

$$\nu = \nu_m \epsilon = \nu_m \frac{m_2 v_2^2}{2kT}$$

Before proceeding with the actual numeric results we will give the requisite expressions f the complex refractive index in terms of t C script integrals.

Case I, $\varphi = 0$. *Longitudinal propagatio*

$$\frac{c^2}{u^2} = \left(n - \frac{i c \kappa}{\omega}\right)^2$$

$$= \epsilon_{\mathrm{I}} + \epsilon_{\mathrm{III}} \pm i\epsilon_{\mathrm{II}} = \epsilon_2 \quad \text{or} \quad \epsilon_3 \qquad (3$$

(cf. equation 26*c*).

Ordinary ray (classical formula).

$$\left(\frac{c^2}{u^2}\right)_o = \left\{1 - \frac{\omega_0^2(\omega - s)}{\omega[(\omega - s)^2 + \nu^2]}\right\} - i\left\{\frac{\omega_0^2 \nu}{\omega[(\omega - s)^2 + \nu^2]}\right\} \qquad (4$$

Ordinary ray (generalized formula).

$$\left(\frac{c^2}{u^2}\right)_o = \left\{1 - \frac{\omega_0^2(\omega - s)}{\omega \nu_m^2}\, \mathcal{C}_{3/2}\left(\frac{\omega - s}{\nu_m}\right)\right\} - i\left\{\frac{5\omega_0^2}{2\omega\nu_m}\, \mathcal{C}_{5/2}\left(\frac{\omega - s}{\nu_m}\right)\right\} \qquad (4$$

Extraordinary ray (classical formula).

$$\left(\frac{c^2}{u^2}\right)_x = \left\{1 - \frac{\omega_0^2(\omega + s)}{\omega[(\omega + s)^2 + \nu^2]}\right\} - i\left\{\frac{\omega_0^2 \nu}{\omega[(\omega + s)^2 + \nu^2]}\right\} \qquad (4$$

Extraordinary ray (generalized formula).

$$\left(\frac{c^2}{u^2}\right)_x = \left\{1 - \frac{\omega_0^2(\omega + s)}{\omega \nu_m^2}\, \mathcal{C}_{3/2}\left(\frac{\omega + s}{\nu_m}\right)\right\} - i\left\{\frac{5\omega_0^2}{2\omega\nu_m}\, \mathcal{C}_{5/2}\left(\frac{\omega + s}{\nu_m}\right)\right\} \qquad (43)$$

ase II, $\varphi = \pi/2$. Transversal propagation.

$$\left(\frac{c^2}{u^2}\right) = \left(n - \frac{ic\kappa}{\omega}\right)^2 = \epsilon_I \quad \text{or} \quad \frac{(\epsilon_I + \epsilon_{III})^2 + \epsilon_{II}^2}{\epsilon_I + \epsilon_{III}} \qquad (44)$$

f. equation 26c as $\epsilon_1 = \epsilon_I$)

Ordinary ray (classical formula).

$$\left(\frac{c^2}{u^2}\right)_o = \left\{1 - \frac{\omega_0^2}{\omega^2 + \nu^2}\right\} - i\left\{\frac{\omega_0^2 \nu}{\omega(\omega^2 + \nu^2)}\right\} \qquad (45)$$

rdinary ray (generalized formula).

$$\left(\frac{c^2}{u^2}\right)_o = \left\{1 - \frac{\omega_0^2}{\nu_m^2}\, \mathcal{C}_{3/2}\left(\frac{\omega}{\nu_m}\right)\right\} - i\left\{\frac{5\omega_0^2}{2\omega\nu_m}\, \mathcal{C}_{5/2}\left(\frac{\omega}{\nu_m}\right)\right\} \qquad (46)$$

xtraordinary ray (classical formula).

$$\left(\frac{c^2}{u^2}\right)_x = 1 + \omega_0^2 \frac{[(\omega_0^2 - \omega^2)(\omega^2 - \omega_0^2 - \nu^2 - s^2) + \nu^2(\omega_0^2 - 2\omega^2)]}{[\omega^2(\omega^2 - \omega_0^2 - \nu^2 - s^2)^2 + \nu^2(\omega_0^2 - 2\omega^2)^2]} - i\,\frac{\omega_0^2 \nu}{\omega} \frac{[(\omega_0^2 - \omega^2)^2 + \omega^2(\nu^2 + s^2)]}{[\omega^2(\omega^2 - \omega_0^2 - \nu^2 - s^2)^2 + \nu^2(\omega_0^2 - 2\omega^2)^2]} \qquad (47)$$

xtraordinary ray (generalized formula).

$$\left(\frac{c^2}{u^2}\right)_x = 2\,\frac{[(a'^2 + b'^2)c' + (c'^2 + d'^2)a']}{[(a' + c')^2 + (b' + d')^2]} + \frac{2i[(a'^2 + b'^2)\, d' + (c'^2 + d'^2)b']}{[(a' + c')^2 + (b' + d')^2]} \qquad (48)$$

here

$$\begin{aligned} a' &= 1 - \frac{\omega_0^2(\omega - s)}{\omega\nu_m^2}\, \mathcal{C}_{3/2}\left(\frac{\omega - s}{\nu_m}\right) \\ b' &= -\frac{5\omega_0^2}{2\omega\nu_m}\, \mathcal{C}_{5/2}\left(\frac{\omega - s}{\nu_m}\right) \\ c' &= 1 - \frac{\omega_0^2(\omega + s)}{\omega\nu_m^2}\, \mathcal{C}_{3/2}\left(\frac{\omega + s}{\nu_m}\right) \\ d' &= -\frac{5\omega_0^2}{2\omega\nu_m}\, \mathcal{C}_{5/2}\left(\frac{\omega + s}{\nu_m}\right) \end{aligned} \qquad (49)$$

The real refractive index, n, and the absorption factor $c\kappa/\omega$ were evaluated from the relations

$$\frac{c^2}{u^2} = \left(n - \frac{ic\kappa}{\omega}\right)^2 = L - iM$$

and thus rigorously

$$\begin{aligned} n &= \frac{1}{\sqrt{2}} \sqrt{L + \sqrt{L^2 + M^2}} \\ \frac{c\kappa}{\omega} &= \frac{1}{\sqrt{2}} \sqrt{-L + \sqrt{L^2 + M^2}} \end{aligned} \qquad (50)$$

Gobeau's [1935] values for ω, ν, and s were initially adopted as representative quantities in our numerical applications

$$\begin{aligned} \omega &= 3.86 \times 10^6 \\ \nu = \nu_m &= \omega/2 = 1.93 \times 10^6 \\ s &= 8.81 \times 10^6 \end{aligned} \qquad (51)$$

In Figure 2, for longitudinal propagation, n and $c\kappa/\omega$ are plotted as functions of ω_0^2/ω^2, where ω_0 is the plasma frequency. Figure 3 represents the same quantities for transverse propagation.

In general the effect of the velocity dependence of the collision frequency in air appears to be a *decrease* in the birefringent properties of the medium as evidenced from the curves of the real refractive index, n, in the ordinary and extraordinary modes of ray propagations.

The absorption factors, $c\kappa/\omega$, in the range of interest of ω_0^2/ω^2, differ anywhere from 30 up to 100 per cent, but mostly in the vicinity of 100 per cent. As expected the absorption factor for transverse propagation is considerably larger than for longitudinal propagation.

Identical calculations have been carried out for $\nu = \nu_m = \frac{1}{10}\omega$ and $\nu = \nu_m = 2\omega$. The same conclusions regarding n and $c\kappa/\omega$ hold, as evidenced from Figures 4, 5, 6, and 7. Even in the case $\nu = \nu_m = \frac{1}{10}\omega$ the corrections to the classical Appleton-Hartree formula for the absorption cannot be neglected.

However, the above calculations have been

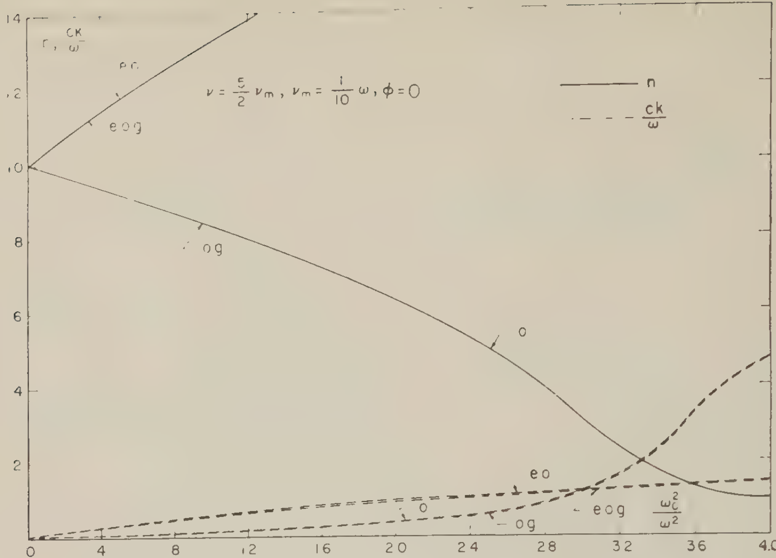

Fig. 12. Case: $\nu = \frac{5}{2}\nu_m$, $\nu_m = \frac{1}{10}\omega$, $\phi = 0$. Symbols same as in Figure 2.

carried out under the assumption that the collision frequency ν utilized in the classical formula and the parameter ν_m in the generalized theory represent the same quantity. It can be shown that ν_m represents the mean collision frequency associated with the square of the 'most probable speed.' The quantity ν does not necessarily have to be this same concept. In the original derivation of the Appleton-Hartree formula one is at liberty to choose any type of mean collision frequency and identify it with the 'friction' factor g. One can then well associate ν with the square of the 'root-mean-square speed.' *In the case* $\nu = \frac{3}{2}\nu_m$.

New calculations were carried out in the Appleton-Hartree case with $\nu = \frac{3}{2}\nu_m$ and the same values of ω, ν_m, and s as cited above, equation 51. Figures 8 and 9 give the results for respectively longitudinal and transverse propagations. Considerable improvement shows in the longitudinal case where the residual differences in the absorption factors are reduced from 100 per cent to at the most 30 per cent. For the extraordinary ray there is practically overlap between the generalized absorption curve and the Appleton-Hartree curve. In the case of transverse propagation there is also an improved agreement but not so complete. The residual difference between the two absorption curves for the ordinary ray still amount to about 100 per cent while for the extraordinary ray a difference of 30 per cent remains. Calculatio[ns] have also been carried out with $\nu = \frac{3}{2}\nu_m$ wh[en] $\nu_m = 2\omega$, and similar conclusions hold, as e[vi]denced from Figures 10 and 11.

In the case $\nu_m = \frac{1}{10}\omega$ we are approaching [an] important asymptotic limit, viz., when $\nu \ll$ [ω]. *Pfister* [1954] has shown that in this case wh[en] $\nu \propto v_2$ the Appleton-Hartree formula can [be] retained provided that ν is replaced by $\frac{4}{[3]}$[...] The general case, $\nu = av_2^{2n}$, easily follows fr[om] the theory developed in this paper. Wh[en] $\nu \ll \omega$ the generalized conductivity tens[or] elements reduce simply to the *form* of t[he] classical Lorentz tensor element (i. e., witho[ut] integral signs) *provided* that ν_{AH} is replaced [by] a new mean collision frequency defined [...]

$$\bar{\nu} = \frac{\int_0^\infty \nu e^{-\alpha v_2^2} v_2^4 \, dv_2}{\int_0^\infty e^{-\alpha v_2^2} v_2^4 \, dv_2} \qquad \alpha = \frac{m_2}{2kT} \qquad (5$$

while ν_{AH} can be defined as

$$\nu_{AH} = \frac{\int_0^\infty \nu e^{-\alpha v_2^2} v_2^2 \, dv_2}{\int_0^\infty e^{-\alpha v_2^2} v_2^2 \, dv_2} \qquad (5$$

Inserting $\nu = av_2^{2n}$ and upon evaluation of t[he] integrals we find quite generally that

$$\bar{\nu}/\nu_{AH} = (2n + 3)/3 \qquad (5$$

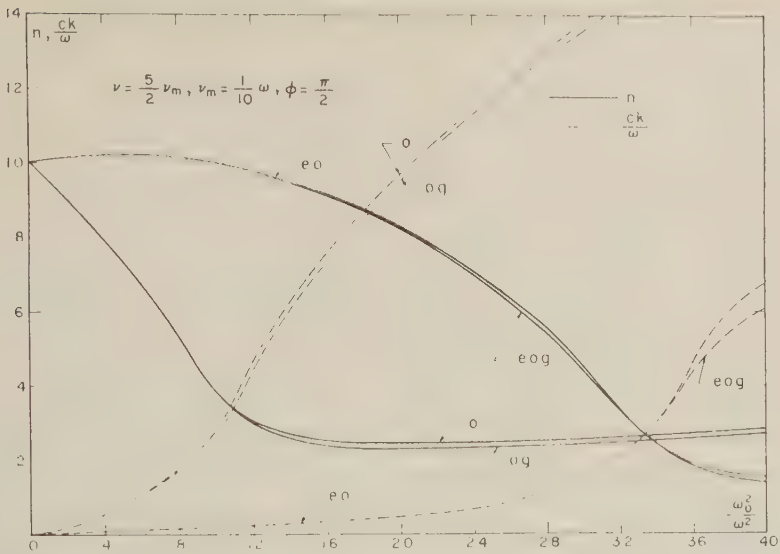

Fig. 13. Case: $\nu = \frac{5}{2}\nu_m$, $\nu_m = \frac{1}{10}\omega$, $\phi = \pi/2$. Symbols same as in Figure 3.

When $\nu = a v_2^2$, as in air, one should replace ν_{AH} by $\frac{5}{3}\nu_{AH}$. Consequently the case $\nu_m = \frac{1}{10}\omega$ was recalculated with $\nu = \frac{5}{3}\nu_{AH} = \frac{5}{3}\cdot\frac{3}{2}\nu_m = \frac{5}{2}\nu_m$. The results, shown in Figures 12 and 13, fully confirm the theory. All the curves for n and κ/ω show at the most 5 per cent disparity between the generalized theory and the Appleton-Hartree formula. We conclude that for $\nu < 0.1\omega$ the Appleton-Hartree formula can be retained provided that $\nu_{AH} = \frac{5}{2}\nu_m$. The factor $\frac{5}{2}$, incidentally, also appears in the same manner in the work of *Phelps and Pack* [1959].

The other asymptotic limit is that of $\nu \gg \omega$. In like manner it can be shown that the Appleton-Hartree formula can be retained provided that $\nu_{AH} = \frac{3}{2}\nu_m$.

For cases intermediate between the above two asymptotic limits one could try to choose a numerical factor relating ν_{AH} and ν_m so as to optimize the agreement between the two theories. This appears somewhat artificial and has little physical justification. Furthermore, as evidenced from Figures 8, 9, 10, and 11, there does not appear to exist any *one* factor of proportionality between ν_{AH} and ν_m which simultaneously optimizes the agreement for all modes of ray propagation. This optimizing factor will also vary with the ω/ν_m and $(\omega \pm s)/\nu_m$ factors.

In our opinion the simplest expedient is to retain the use of the generalized complex refractive index in the form of equation 27.

General case, III. $\phi \neq \pi/2$ or 0.

$$\frac{c^2}{u^2} = \left(n - \frac{i\kappa}{\omega}\right)^2 = \frac{A + B\sin^2\varphi \pm \sqrt{B^2\sin^4\varphi - C^2\cos^2\varphi}}{D + E\sin^2\varphi} \tag{27}$$

where

$$\begin{aligned} A &= 2\epsilon_{\mathrm{I}}(\epsilon_{\mathrm{I}} + \epsilon_{\mathrm{III}}) \\ B &= \epsilon_{\mathrm{III}}(\epsilon_{\mathrm{I}} + \epsilon_{\mathrm{III}}) + \epsilon_{\mathrm{II}}^2 \\ C &= 2\epsilon_{\mathrm{I}}\epsilon_{\mathrm{II}} \quad D = 2\epsilon_{\mathrm{I}} \quad E = 2\epsilon_{\mathrm{III}} \end{aligned} \tag{28}$$

In this general case we define:

$$\begin{aligned} a &= \frac{\omega_0^2}{\nu_m^2}\,\mathcal{C}_{3/2}\left(\frac{\omega}{\nu_m}\right) \\ b &= \frac{5\omega_0^2}{2\omega\nu_m}\,\mathcal{C}_{5/2}\left(\frac{\omega}{\nu_m}\right) \\ c &= \frac{\omega_0^2(\omega - s)}{\omega\nu_m^2}\,\mathcal{C}_{3/2}\left(\frac{\omega - s}{\nu_m}\right) \\ d &= \frac{5\omega_0^2}{2\omega\nu_m}\,\mathcal{C}_{5/2}\left(\frac{\omega - s}{\nu_m}\right) \\ e &= \frac{\omega_0^2(\omega + s)}{\omega\nu_m^2}\,\mathcal{C}_{3/2}\left(\frac{\omega + s}{\nu_m}\right) \\ f &= \frac{5\omega_0^2}{2\omega\nu_m}\,\mathcal{C}_{5/2}\left(\frac{\omega + s}{\nu_m}\right) \end{aligned} \tag{55}$$

Then the fundamental elements ϵ_{I}, ϵ_{II}, and ϵ_{III} of the generalized dielectric tensor are expressed as follows:

$$\begin{aligned}\epsilon_{I} &= (1 - a) - ib \\ \epsilon_{II} &= \tfrac{1}{2}(f - d) + (i/2)(c - e) \\ \epsilon_{III} &= [a - \tfrac{1}{2}(c + e)] + i[b - \tfrac{1}{2}(f + d)]\end{aligned} \tag{56}$$

The procedure of computation of n and $c\kappa/\omega$ in the general case of the generalized theory is then quite straightforward. For a given geographical location and experimental instrumentation the quantities φ, ω, and s are specified. We assume that ω_0 and ν_m can be specified with reasonable accuracy. The following scheme may then be expedient:

1. Calculate ϵ_{I}, ϵ_{II}, and ϵ_{III}, which in general are complex numbers.
2. Calculate D, E, C, C^2, A, B, B^2, which also will be complex numbers.

Upon ordering and rearranging the complex and real parts of equation 27 we finally derive n and $c\kappa/\omega$ from equation 50. These calculations of n and $c\kappa/\omega$ are then perfectly rigorous with no simplifying assumptions involved in their deduction from the generalized theory. With modern electronic computers ray tracings based on the generalized theory should also not be unduly cumbersome.

Acknowledgments. It is a pleasure to acknowledge the aid of Mr. Y. Trève in the mathematical details of the series expansion for the $\mathfrak{C}$ integrals, and the help of Mr. A. Shickman in the actual computations. We are indebted to Dr. Pfister and Dr. Phelps for several fruitful discussions.

Appendix I[1]

The Boltzmann equation for the electrons in a uniform Lorentz plasma in a homogene[ous] magnetic field and an oscillating external elect[ric] field is

$$\frac{\partial f_2}{\partial t} + \left[\mathbf{\Gamma}_2 \cos\omega t + \frac{e_2}{m_2}(\mathbf{v}_2 \times \mathbf{H}_0)\right] \text{grad}_{\mathbf{v}_2} \ldots$$
$$= \iiint (f_1'f_2' - f_1 f_2) g\, db\, d\epsilon\, d\mathbf{v}_1$$

where the symbols are as previously defined, [in] particular

$$\mathbf{\Gamma}_2 = \frac{e_2}{m_2}\mathbf{E}$$

The electron velocity distribution function [is] expanded in the form:

$$\begin{aligned}f_2 = f_2^{(0)} &+ \mathbf{\Gamma}_2\cdot\mathbf{v}_2(\alpha_2 \cos\omega t + \beta_2 \sin\omega t) \\ &+ (\mathbf{H}_0 \times \mathbf{\Gamma}_2)\cdot\mathbf{v}_2(\xi_2 \cos\omega t + \eta_2 \sin\omega t) \\ &+ [\mathbf{H}_0 \times (\mathbf{H}_0 \times \mathbf{\Gamma}_2)]\cdot\mathbf{v}_2(\gamma_2 \cos\omega t + \delta_2 \sin \ldots\end{aligned}$$

We substitute (2) in (1) and separate the sca[lar] terms in Γ_2^2, $\mathbf{\Gamma}_2\cdot\mathbf{v}_2$, $(\mathbf{H}_0 \times \mathbf{\Gamma}_2)\cdot\mathbf{v}_2$ and $[\mathbf{H}_0 \times (\mathbf{H}_0 \times \mathbf{\Gamma}_2)]\cdot\mathbf{v}_2$, so

$$\begin{aligned}\Gamma_2^2 \cos\omega t\Bigg[&(\alpha_2 \cos\omega t + \beta_2 \sin\omega t) \\ &+ \tfrac{1}{3}v_2\left(\frac{\partial\alpha_2}{\partial v_2}\cos\omega t + \frac{\partial\beta_2}{\partial v_2}\sin\omega t\right) \\ &- H_0^2 \sin^2\psi\left\{(\gamma_2 \cos\omega t + \delta_2 \sin\omega t) \right.\\ &\left.+ \tfrac{1}{3}v_2\left(\frac{\partial\gamma_2}{\partial v_2}\cos\omega t + \frac{\partial\delta_2}{\partial v_2}\sin\omega t\right)\right\}\Bigg] \\ = \iiint & (f_1'f_2'^{(0)} - f_1 f_2^{(0)}) g\, db\, d\epsilon\, d\mathbf{v}_1\end{aligned}$$

where ψ is the angle between $\mathbf{\Gamma}_2$ and $\mathbf{H}_0$.

$$\frac{\mathbf{\Gamma}_2\cdot\mathbf{v}_2}{v_2}\left[\omega v_2(-\alpha_2 \sin\omega t + \beta_2 \cos\omega t) + \frac{\partial f_2^{(0)}}{\partial v_2}\cos\omega t\right]$$
$$= \iiint [f_1'(\alpha_2 \cos\omega t + \beta_2 \sin\omega t)(\mathbf{\Gamma}_2\cdot\mathbf{v}_2') - f_1(\alpha_2 \cos\omega t + \beta_2 \sin\omega t)(\mathbf{\Gamma}_2\cdot\mathbf{v}_2)] g\, db\, d\epsilon\, d\mathbf{v}_1$$

$$\begin{aligned}(\mathbf{H}_0 \times \mathbf{\Gamma}_2)\cdot\mathbf{v}_2\Big[&\omega(-\xi_2 \sin\omega t + \eta_2 \cos\omega t) + (e_2/m_2)(\alpha_2 \cos\omega t + \beta_2 \sin\omega t) \\ &- \frac{e_2}{m_2}H_0^2(\gamma_2 \cos\omega t + \delta_2 \sin\omega t)\Big] = \iiint \{f_1'(\xi_2 \cos\omega t + \eta_2 \sin\omega t)[(\mathbf{H}_0 \times \mathbf{\Gamma}_2)\cdot\mathbf{v}_2'] \\ &- f_1(\xi_2 \cos\omega t + \eta_2 \sin\omega t)[(\mathbf{H}_0 \times \mathbf{\Gamma}_2)\cdot\mathbf{v}_2]\} g\, db\, d\epsilon\, d\mathbf{v}_1\end{aligned}$$

[1] This work (unpublished) was performed by one of us (H. K. S.) while at Hughes Aircraft Corporation, Culver City, California.

$$\Gamma_0 \times (\mathbf{H}_0 \times \mathbf{\Gamma}_2)]\cdot \mathbf{v}_2[\omega(-\gamma_2 \sin \omega t + \delta_2 \cos \omega t) + (e_2/m_2)(\xi_2 \cos \omega t + \eta_2 \sin \omega t)]$$

$$= \iiint \{f_1'(\gamma_2 \cos \omega t + \delta_2 \sin \omega t)[(\mathbf{H}_0 \times (\mathbf{H}_0 \times \mathbf{\Gamma}_2))\cdot \mathbf{v}_2']$$

$$- f_1(\gamma_2 \cos \omega t + \delta_2 \sin \omega t)[(\mathbf{H}_0 \times (\mathbf{H}_0 \times \mathbf{\Gamma}_2))\cdot \mathbf{v}_2]\}\, gb\, db\, d\epsilon\, d\mathbf{v}_1 \qquad (6)$$

ultiply (3) by $d\mathbf{v}_2 = 4\pi v_2^2\, dv_2$ and integrate om 0 to v_2; then

$$\Gamma_2^2 \cos \omega t\, v_2^3[\alpha_2 \cos \omega t + \beta_2 \sin \omega t$$

$$- H_0^2 \sin^2 \psi(\gamma_2 \cos \omega t + \delta_2 \sin \omega t)]$$

$$= \iiiint (f_1'f_2'^{(0)} - f_1 f_2^{(0)})gb\, db\, d\epsilon\, d\mathbf{v}_1\, d\mathbf{v}_2 \qquad (7)$$

he integral on the right-hand side of (7) has en evaluated by *Chapman and Cowling* [1958, . 348]. Equation 7 thus reduces to

$$\Gamma_2^2 \cos \omega t\, v_2^3[\alpha_2 \cos \omega t + \beta_2 \sin \omega t$$

$$- H_0^2 \sin^2 \psi(\gamma_2 \cos \omega t + \delta_2 \sin \omega t)]$$

$$= \frac{kT}{m_1\lambda} v_2^3 \frac{\partial f_2^{(0)}}{\partial v_2} + \frac{m_2 v_2^4}{m_1\lambda} f_2^{(0)} \qquad (8)$$

here $\lambda(v_2)$ is the mean free path of the electron f velocity v_2. The right-hand side of (8) does ot depend on time. Taking the mean value of e left-hand side with respect to time, we have

$$\Gamma_2^2 v_2^3[\alpha_2 - \gamma_2 H_0^2 \sin^2\psi]$$

$$= \frac{kT}{m_1\lambda} v_2^3 \frac{\partial f_2^{(0)}}{\partial v_2} + \frac{m_2 v_2^4}{m_1\lambda} f_2^{(0)} \qquad (9)$$

The integrals in (4), (5), and (6) are also evaluated in *Chapman and Cowling* [1958, p. 348]. The Lorentz gas approximation is sufficient here $v_2' = v_2 = g$ and $f_1(v_1)$ is Maxwellian t temperature T of gas. Thus we can write (4), 5), and (6) in the following forms:

$$\omega v_2(-\alpha_2 \sin \omega t + \beta_2 \cos \omega t) + \frac{\partial f_2^{(0)}}{\partial v_2} \cos \omega t$$

$$= -\frac{(\alpha_2 \cos \omega t + \beta_2 \sin \omega t)}{\lambda} v_2^2 \qquad (10)$$

$$\omega(-\xi_2 \sin \omega t + \eta_2 \cos \omega t)$$

$$+ \frac{e_2}{m_2}(\alpha_2 \cos \omega t + \beta_2 \sin \omega t)$$

$$- \frac{e_2}{m_2} H_0^2(\gamma_2 \cos \omega t + \delta_2 \sin \omega t)$$

$$= -\frac{(\xi_2 \cos \omega t + \eta_2 \sin \omega t)}{\lambda} v_2 \qquad (11)$$

$$\omega(-\gamma_2 \sin \omega t + \delta_2 \cos \omega t)$$

$$+ \frac{e_2}{m_2}(\xi_2 \cos \omega t + \eta_2 \sin \omega t)$$

$$= \frac{-(\gamma_2 \cos \omega t + \delta_2 \sin \omega t)}{\lambda} v_2 \qquad (12)$$

Equating the terms in $\cos \omega t$ and $\sin \omega t$ in (10), (11), and (12), we have

$$\omega v_2 \alpha_2 = \beta_2 v_2^2/\lambda \qquad (10')$$

$$\omega v_2 \beta_2 + \partial f_2^{(0)}/\partial v_2 = -\alpha_2 v_2^2/\lambda \qquad (10'')$$

$$-\omega\xi_2 + (e_2/m_2)(\beta_2 - H_0^2\, \delta_2) = -(\eta_2/\lambda)v_2 \qquad (11')$$

$$\omega\eta_2 + (e_2/m_2)(\alpha_2 - H_0^2\gamma_2) = -(\xi_2/\lambda)v_2 \qquad (11'')$$

$$-\omega\gamma_2 + (e_2/m_2)\eta_2 = -(\delta_2/\lambda)v_2 \qquad (12')$$

$$\omega\delta_2 + (e_2/m_2)\xi_2 = -(\gamma_2/\lambda)v_2 \qquad (12'')$$

Solving equations 10′ through 12″ leads to the following expression for α_2, β_2, ξ_2, η_2, γ_2, and δ_2:

$$
\begin{aligned}
\alpha_2 &= \frac{-\lambda}{(\lambda^2\omega^2 + v_2^2)} \frac{\partial f_2^{(0)}}{\partial v_2} \\
\beta_2 &= \frac{-\lambda^2\omega}{(\lambda^2\omega^2 + v_2^2)} \cdot \frac{1}{v_2} \cdot \frac{\partial f_2^{(0)}}{\partial v_2} \\
\xi_2 &= \frac{e_2\lambda^2(v_2^2 + \lambda^2 s^2 - \lambda^2\omega^2)}{m_2[v_2^2 + \lambda^2(\omega + s)^2][v_2^2 + \lambda^2(\omega - s)^2]} \cdot \frac{1}{v_2} \cdot \frac{\partial f_2^{(0)}}{\partial v_2} \\
\eta_2 &= \frac{2e_2}{m_2} \cdot \frac{\lambda^3\omega}{[v_2^2 + \lambda^2(\omega + s)^2][v_2^2 + \lambda^2(\omega - s)^2]} \cdot \frac{\partial f_2^{(0)}}{\partial v_2} \\
\gamma_2 &= \frac{\lambda^3 s^2(3\lambda^2\omega^2 - v_2^2 - \lambda^2 s^2)}{H_0^2[\lambda^2\omega^2 + v_2^2][v_2^2 + \lambda^2(\omega + s)^2][v_2^2 + \lambda^2(\omega - s)^2]} \cdot \frac{\partial f_2^{(0)}}{\partial v_2} \\
\delta_2 &= \frac{-\lambda^4\omega s^2[\lambda^2(s^2 - \omega^2) + 3v_2^2]}{H_0^2[\lambda^2\omega^2 + v_2^2][v_2^2 + \lambda^2(\omega + s)^2][v_2^2 + \lambda^2(\omega - s)^2]} \cdot \frac{1}{v_2} \cdot \frac{\partial f_2^{(0)}}{\partial v_2}
\end{aligned} \tag{13}
$$

where $s = (e_2/m_2)H_0$. If we introduce the collision frequency $\nu(v_2) = v_2/\lambda(v_2)$, formulas 6 of the main paper are retrieved.

To evaluate the electron velocity distribution function, $f_2^{(0)}$, we have to solve the integro-differential equation 9. Substitute the expressions for α_2 and γ_2 from (13) into (9), and this reduces to

$$
-\left[\tfrac{1}{6}\Gamma_2^2 \frac{(1 - C)}{(\omega^2 + \nu^2)} + \frac{kT}{m_1}\right] \frac{\partial f_2^{(0)}}{\partial v} = \frac{m_2 v_2}{m_1} f_2^{(0)} \tag{14}
$$

where

$$
C = \frac{s^2(\nu^2 + s^2 - 3\omega^2)}{[\nu^2 + (\omega + s)^2][\nu^2 + (\omega - s)^2]} \times \sin^2\psi
$$

Equation 14 can be solved by separation of variables, giving

$$
f_2^{(0)} = A \exp\left\{-\int_0^{v_2} \frac{m_2 v_2\, dv_2}{kT + F(v_2)}\right\}
$$

where A is an integration constant and

$$
F(v_2) = \frac{\Gamma_2^2}{6} \cdot \frac{m_1}{(\nu^2 + \omega^2)} \cdot \left\{1 - \frac{s^2 \sin^2\psi(\nu^2 + s^2 - 3\omega^2)}{[\nu^2 + (\omega + s)^2][\nu^2 + (\omega - s)^2]}\right\}
$$

which agrees with equation 7 in the main article.

References

Allis, W. P., *Handbuch der Physik, 21*, 413, Springer-Verlag, Berlin, 1956.

Alpert, Ia. L., V. L. Ginzburg, and E. L. Feinberg, *The Propagation of Radiowaves*, Moscow, 1953.

Appleton, E. V., *URSI Repts.*, Washington, 1927.

Appleton, E. V. and F. W. Chapman, *Proc. Phys. Soc., London, 44*, 246, 1932.

Bayet, M., *J. Phys. Radium, 15*, 258, 1954.

Bayet, M., J. L. Delcroix, and J. F. Denisse, *J. Phys. Radium, 15*, 795, 1954.

Chapman, S., and T. G. Cowling, *The Mathematical Theory of Non-Uniform Gases*, 2d, ed., Cambrid 1958.

Cowling, T. G., *Proc. Roy. Soc. London, A, 1* 453, 1944.

Dingle, R. B., D. Arndt, and S. K. Roy, *Ap Sci. Research, 6B*, 155, 1957.

Druyvesteyn, *Physica, 10*, 61, 1930, *1*, 1003, 19

Fain, V. M., *J. Exptl. Theoret. Phys. USSR,* 422, 1955.

Gobeau, G., *Hochfreq. Technik u. El. Akustik,* 183, 1935.

Goldstein, S., *Proc. Roy. Soc. London, A, 121,* 2 1928.

Gurevich, A. V., *J. Exptl. Theoret. Phys. USSR,* 1112, 1956.

Hartree, D. R. *Proc. Cambridge Phil. Soc., 25,* 1929.

Huxley, L. G., *Phil. Mag., 23*, 210, 442, 19

Huxley, L. G., *Phil. Mag., 25*, 148, 388, 19

Huxley, L. G., *Proc. Phys. Soc. London, B, 64,* 8 1951.

Huxley, L. G., *Australian J. Phys., 10*, 118, 2 1957.

Huxley, L. G., *J. Atmospheric and Terrest. Ph 16*, November 1959.

Jancel, R., and T. Kahan, *Nuovo cimento, 12*, 5 1954.

Jancel, R., and T. Kahan, *J. Phys. Radium,* 136, 824, 1955.

Kane, J. A., *J. Geophys. Research, 64*, 133, 19

Lorentz, H. A., *Theory of Electrons*, Teubn Leipzig, 1909.

Margenau, H., *Phys. Rev., 69*, 508, 1946.

Mitra, S. K., *The Upper Atmosphere*, Asia Society, Calcutta, 1952.

Molmud, P., *Phys. Rev. 114*, 29, 1959.

Pfister, W., *The Physics of the Ionosphere*, p. 3 Cambridge, 1954.

Phelps, A. V., and J. L. Pack, *Phys. Rev. Letters* 340, 1959.

Saha, M. N., and B. K. Banerjee, *Indian J. Ph 19*, 159, 1945.

Westfold, K. C., *Australian J. Sci. Research,* 168, 1949.

Westfold, K. C., *Phil. Mag., 44*, 711, 1953.

(Manuscript received September 20, 1960.)

An Approximate Method of Estimating the Size and Shape of the Stationary Hollow Carved Out in a Neutral Ionized Stream of Corpuscles Impinging on the Geomagnetic Field

V. C. A. FERRARO

Queen Mary College, University of London
London, England

Abstract. Using a formula which I derived in 1952 an approximate method is developed for estimating the size and shape of the stationary hollow carved out when a solar corpuscular stream impinges on the geomagnetic field. It is also shown that in a two-dimensional magnetic field, the breadth of the hollow at infinity is finite and is given by $(2\pi I^2/\rho v^2)^{1/2}$ where I is the current flowing in a permanent inducing system, ρ the density, and v the velocity of the stream.

Introduction. *Ferraro* [1952] pointed out t the form of the stationary hollow carved by the geomagnetic field in a neutral ionized ır corpuscular stream could be obtained from simple relation expressing the fact that in steady state the component of the dynamical ssure of the stream particles normal to the face of the hollow is equal to the normal pres- e of the magnetic tubes of force on the sur- e.

Denoting by ρ the density of the undisturbed eam, by v the undisturbed speed of the parti- s, by H_s the total (tangential) magnetic field the surface of the stream, and by $\pi/2 - \phi$ angle made by the normal at any point of surface of the hollow with the direction of tion of the particles, this relation is

$$v^2 \sin^2 \phi = \frac{H_s^2}{8\pi} \qquad (1)$$

ıe to an oversight the trigonometric factor was en in the present notation as sin ϕ instead of $^2\phi$ in my 1952 paper.

The magnetic field H_s at the stream surface is sum of the permanent magnetic field H_p and magnetic field H' due to the currents induced the stream surface. In general, this field will pend on the shape of the hollow and a self- sistent field method of solution would be re- ired. So far this has proved difficult and ap- oximate methods of solution must be resorted . One such solution has recently been given by *ard* [1960]. Some years ago the present au- or concluded that in certain cases a fair ap- oximation would be to assume that H_s is equal a constant multiple $2f$ of the resolute of the permanent magnetic field parallel to the surface. This approximation appears to be particularly suited to two-dimensional cases, and the purpose of this note is to give as an illustrative example the instance in which the permanent field is due to an infinite current line set perpendicular to the direction of motion of the stream. It is also shown that for two-dimensional motion the breadth of the hollow at infinity is finite and of amount $(2\pi I^2/\rho v^2)^{1/2}$, where I is the total cur- rent flowing in the permanent systems.

2. *A Particular Solution.* In Figure 1, PQ denotes an arc of the section of the stream sur- face by a plane perpendicular to the line-current whose trace is represented by the point O, the origin of cartesian coordinates (x, y). Ox is taken to coincide with the axis of the normal section of the hollow which is thus parallel to the un- disturbed direction of motion of the stream particles. The tangent to the surface of the hollow at P makes an angle ϕ with Ox and θ denotes the angle XOP. Since the direction of

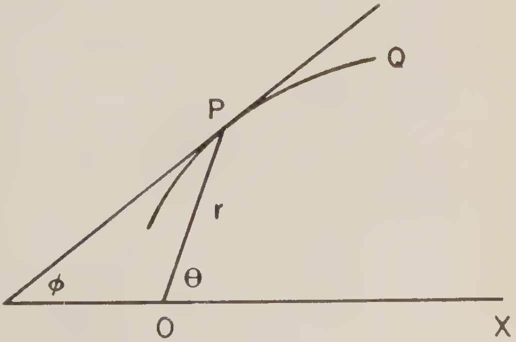

Fig. 1.

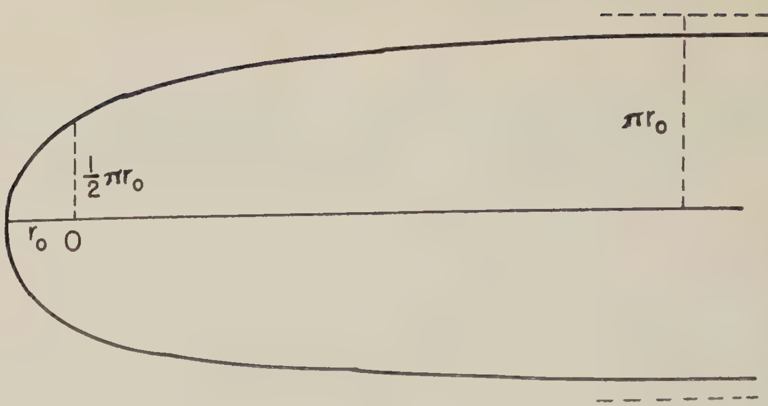

Fig. 2.

the line of force at P due to the line current is perpendicular to OP, its tangential resolute is $H_p \sin(\theta - \phi)$.

Denoting by I the current flowing in the wire, the magnitude of the magnetic field at P is

$$H_p = 2I/r$$

where $r = OP$. The simplifying assumption made in section 1 may now be written as

$$H_s = \frac{4fI}{r} \sin(\theta - \phi) \tag{2}$$

and equation 1 becomes

$$\frac{\sin(\theta - \phi)}{\sin\phi} = \frac{r}{r_0} \tag{3}$$

where

$$r_0^2 = \frac{2I^2f^2}{\pi\rho v^2} \tag{4}$$

Clearly r_0 is the distance of the apex of the hollow from the line current. Denoting by (x, y) the coordinates of P, and using the relations

$$\frac{dy}{dx} = \tan\phi, \quad x = r\cos\theta, \quad y = r\sin\theta \tag{5}$$

(3) may be written

$$y\frac{dx}{dy} - x = \frac{x^2 + y^2}{r_0^2} \tag{6}$$

the solution of which is

$$\tan^{-1}\frac{x}{y} = \frac{y}{r_0} + \text{const} \tag{7}$$

Since $x = -r_0$ when $y = 0$, $x/y \to -\infty$ as $y \to 0$ and the const $= -\pi/2$. Hence fi the equation of the hollow is

$$x = -y\cot(y/r_0)$$

or writing $x = r_0\xi$, $y = r_0\eta$,

$$\xi = -\eta\cot\eta$$

The shape of the curve is thus independen the density and velocity of the stream part and of the intensity of the current. A sketc the normal section is shown in Figure 2. note that $\xi = 0$ when $\eta = \pi/2$ so that the 'l rectum' of the section is πr_0; and since $\eta \to$ c $\eta \to \pi$, it follows that $\eta = \pm\pi$ are asymp of the section. The breadth of the sectio infinity is thus $2\pi r_0$.

3. *Estimation of the factor f.* The fact can be estimated by calculating the magn field produced at the apex by the currents f ing in the surface of the hollow (a cur sheet). This magnetic field is the sum of magnetic field due to an infinite elemen strip near the apex which has the values

$$H_1' = \pm 2If/r_0$$

on the two opposite sides of the strip, toge with the magnetic field H'_2 due to the remai of the sheet. Taking the sense of the curre to be into the plane of the paper, that of currents induced in the sheet will be out o plane of the paper. The current at any p per unit length of the section of the sheet is

$$j = H_s/4\pi$$

or by (1) and (4)

$$j = -\frac{If}{\pi r_0} \sin \phi \qquad (12)$$

ice, using (12), the magnetic field at the x due to the remainder of the sheet is found be

$$\gamma_2' = \frac{4If}{\pi r_0} \int_0^{\pi r_0} \frac{r_0 + x}{(r_0 + x)^2 + y^2} \, dy \qquad (13)$$

e $ds \sin \phi = dy$, ds being an element of arc Q. Expressing the variables under the integral n in terms of ξ and η we find

$$' = -\frac{4If}{\pi r_0}$$

$$\int_0^{\pi} \frac{\sin \eta \, (\sin \eta - \eta \cos \eta)}{\sin^2 \eta - 2\eta \sin \eta \cos \eta + \eta^2} \, d\eta \qquad (14)$$

$$= -0.9367 \, fI/r_0 \quad \text{approximately}$$

e total magnetic field produced by the in-ced current at the back and front of the sheet the apex is thus $-2.937 \, If/r_0$ and 1.063 r_0. The former must cancel the permanent gnetic field $2I/r_0$ at the back of the sheet. nce $f = 1/1.468 = 0.68$ approximately. The gnetic field in front of the sheet at the apex thus increased by the amount $0.724 \, I/r_0$, that just over 37 per cent greater than the per-nent field.

4. *The total induced current.* One interest-g and exact result which holds for any two-mensional magnetic field due to unidirectional rrents is that the breadth of the hollow b is ite at infinity. This follows at once from (1) d (10). In fact, the current per unit length the section of the sheet is

$$j = -(\rho v^2/2\pi)^{1/2} \sin \phi \qquad (15)$$

that the total current is

$$-\left(\frac{\rho v^2}{2\pi}\right)^{1/2} \int ds \sin \phi = -\left(\frac{v^2}{2\pi}\right)^{1/2} \int dy \qquad (16)$$

integration being over the contour of the hollow. Since this must be equal and opposite to the total current I of the inducing field, the breadth of the stream is thus

$$\left(\frac{2\pi I^2}{\rho v^2}\right)^{1/2} \qquad (17)$$

and so is finite.

For the special case of an infinite line current, using (4), this may be written $\pi r_0/f$ or $1.468 \, \pi \, r_0$ adopting the estimate of f derived in section 3. The value of b derived in section 2 is $2\pi \, r_0$ so that there is a discrepancy of about 30 per cent in these two estimates of the breadth of the hollow. Thus the assumption that f is constant is much too crude; nevertheless the method provides a fair estimate of the shape and size of the hollow. It must be stressed, however, that the method is not applicable generally.

It is of interest to illustrate the orders of magnitude involved in connection with the theory of geomagnetic storms, and we note that for a moderate storm producing a main phase decrease of 100γ the current flowing outside the earth at the distance a few earth radii is of the order of 5 million amperes. If we take the streaming velocity of the particles to be 1000 km/sec, and the density of the stream is n protons/cc, (17) gives the breadth of the hollow as $15 \, n^{-1/2}$ earth radii. This result agrees fairly well with current estimates of r_0, the distance of closest approach of the stream to the earth.

References

Ferraro, V. C. A., *J. Geophys. Research, 57,* 15–49, 1952.

Beard, D. B., *Phys. Rev. Letters, 5,* 89–91, 1960.

(Manuscript received September 6, 1960.)

On the Effect of a Magnetic Field on the Spectrum of Incoherent Scattering

THOMAS LAASPERE

Center for Radiophysics and Space Research
Cornell University
Ithaca, New York

Abstract. The effect of an applied magnetic field is analyzed at scales of scattering smaller than the Debye length. If the scattering wave vector is directed everywhere perpendicular to the magnetic field vector, and each electron is assumed to gyrate unperturbed about a magnetic line of force, the spectrum of scattering will, in the first approximation, consist of lines. The separation of the lines is equal to the electron gyromagnetic frequency. If the average radius of gyration of the electrons is large compared to the scale of scattering, the envelope of the line spectrum is given simply by the thermal Doppler-spectrum curve that would exist in the absence of any magnetic field. As the average radius of gyration is decreased, however, an increasing fraction of power appears in the central line. Curves given in the paper reveal that the line spectrum gets smeared rapidly as the angle between the scattering wave vector and the magnetic lines of force is decreased from 90 degrees.

troduction. Approximately two years ago as recognized by *Gordon* [1958] that the ır techniques and powerful equipment of the would permit the detection of incoherent ıomson) scattering by individual electrons in ionosphere as well as in the adjacent space. n afterward scattering of this type was in detected by *Bowles* [1958, 1959], whose obations have now been confirmed and exled by those of *Pineo, Kraft,* and *Briscoe* 60].

The theory of such scattering in the absence of a magnetic field has recently been considered by a number of authors [*Dougherty and Farley,* 1960; *Fejer,* 1960; *Renau,* 1960; *Salpeter,* 1960*a*, 1960*b*]. A step in the direction of determining the effect of the magnetic field has now been taken by the writer [*Laaspere,* 1960], who has analyzed in detail the case in which electrostatic interactions between charged particles can be neglected. (This implies that in the case of backscatter, the author's results are re-

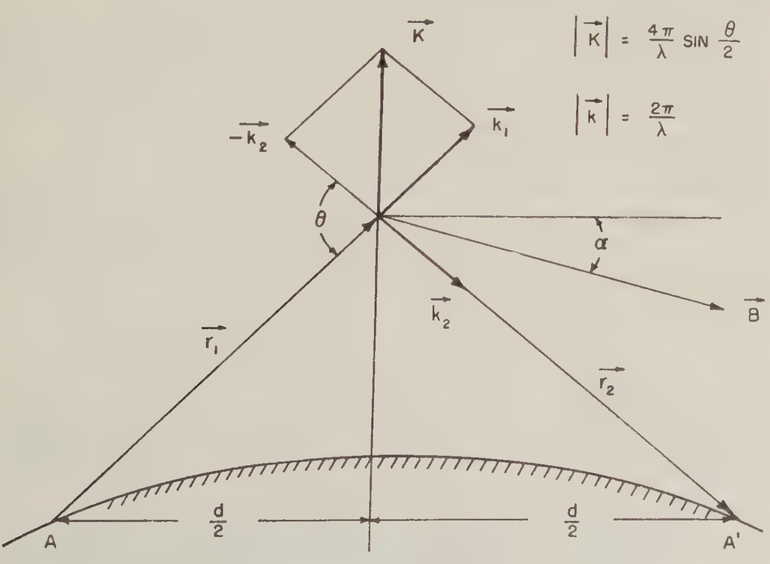

Fig. 1. Geometry of scattering.

stricted to wavelengths that are smaller than 4π times the Debye length.)

Analysis. The fundamental idea of the analysis is quite simple. Each electron is assumed to gyrate freely about a magnetic line of force at its thermal velocity. The gyration of an electron will have the effect of modulating sinusoidally the phase of the radiation scattered by that electron. If the frequency of the incident electric field is much higher than both the gyromagnetic as well as the plasma frequency of the electrons, then the magnetic field has little effect on the component of the electron's motion that is due to the incident electric field. The result is that if in Figure 1 the transmitted wave is assumed to be of the form

$$\mathbf{E}_1 = \frac{\mathbf{E}_0}{r_1} \sin (\omega_T t - kr_1 + \phi_1) \qquad (1)$$

then the electric field of scattering from the gyrating electron at the receiving site A′ at the time t is given by

$$\mathbf{E}_2(t) = \sigma_e^{1/2} \frac{E_0 \mathbf{n}}{r_1 r_2} \sin$$
$$\cdot \{\omega t - 2k'R \sin (\omega_b t + \phi_2) + \phi_3\} \qquad (2)$$

where

σ_e	= scattering cross section of a single electron ($\sigma_e = 7.95 \times 10^{-30} \times \sin^2 \chi$ square meters, χ being the angle between the direction of the incident electric field and that of scattering).
ω_T	= $2\pi f_T$ = the transmitted radian frequency.
λ	= the transmitted wavelength.
k'	= $k \cos \alpha \sin \theta/2 = (2\pi/\lambda) \cos \alpha \sin \theta/2$.
$\mathbf{n}$	= unit vector in the direction of $\mathbf{r}_2 \times \{\mathbf{r}_2 \times \mathbf{E}_1\}$.
R	= radius of gyration of the electron.
ω_b	= $2\pi f_b$ = radian gyromagnetic frequency.
ϕ_1, ϕ_2, ϕ_3	= constant phase angles

In equation 2 the symbol ω denotes the Doppler-shifted radian frequency

$$\omega = \omega_T + \frac{4\pi}{\lambda} v \sin \alpha \sin \theta/2 \qquad (3)$$

where v is the drift velocity of the electron along the magnetic field in that direction which y[ields] a component along the negative direction o[f the] scattering wave vector **K**.

Equation 2 can be expanded by steps al[...] known to those acquainted with the theo[ry of] frequency and phase modulation. We find [that] the power spectrum of radiation from the [elec]tron consists of lines at $f \pm nf_b$, $n = 0,$ [1, 2,] . . . . The average power density at the [fre]quency $f + nf_b$, or $f - nf_b$, is equal to

$$S_n = \sigma_e \frac{E_0^2}{2\rho r_1^2 r_2^2} J_n^2(2Rk')$$

watts per square meter, where J_n $(2Rk')$ [de]notes the Bessel function of the first kind, [order] n, and argument $2Rk' = (4\pi/\lambda) R \cos \alpha \sin$ [...] and ρ is the characteristic impedance of [free] space. The spectrum resulting from scatt[ering] by all the electrons of the scattering volum[e is a] superposition of such line spectra and ca[n be] determined if the distribution of the ele[ctron] velocities (and thus also of the radii of gyra[tion]) is known. If the spatial distribution of elec[trons] is assumed to be random and the electro[n ve]locity distribution to be that of a gas in th[ermal] equilibrium at a temperature T, the result [can] be shown to be as follows.

Results. If the scattering wave vector [in] Figure 1 is directed perpendicular to the [mag]netic field vector **B** in the whole scatterin[g vol]ume, the spectrum consists of lines tha[t are] located at $f_T \pm nf_b$, $n = 0, 1, 2, \ldots$, wh[ere f_T] is the transmitted frequency and f_b the [gyro]magnetic frequency of the electrons. The [frac]tion of the total power contained in bot[h the] line at $f_T + nf_b$ and the line at $f_T - nf_b$ is [equal] to

$$e^{-x} I_n(x)$$

where $I_n(x)$ denotes the modified Bessel [func]tion of the first kind, order n, and argum[ent x.] In (5)

$$x = 0.01429/\gamma_\theta^2$$

where

$$\gamma_\theta = \frac{\lambda_{\text{meters}} B_{\text{gauss}}}{\sin \theta/2 \sqrt{MT_{abs}}}$$

The symbol M denotes the ratio of the m[ass of] an electron to the mass of an atom o[f unit] atomic weight. If the average radius of gy[ration] of the electrons is large compared to the[...]

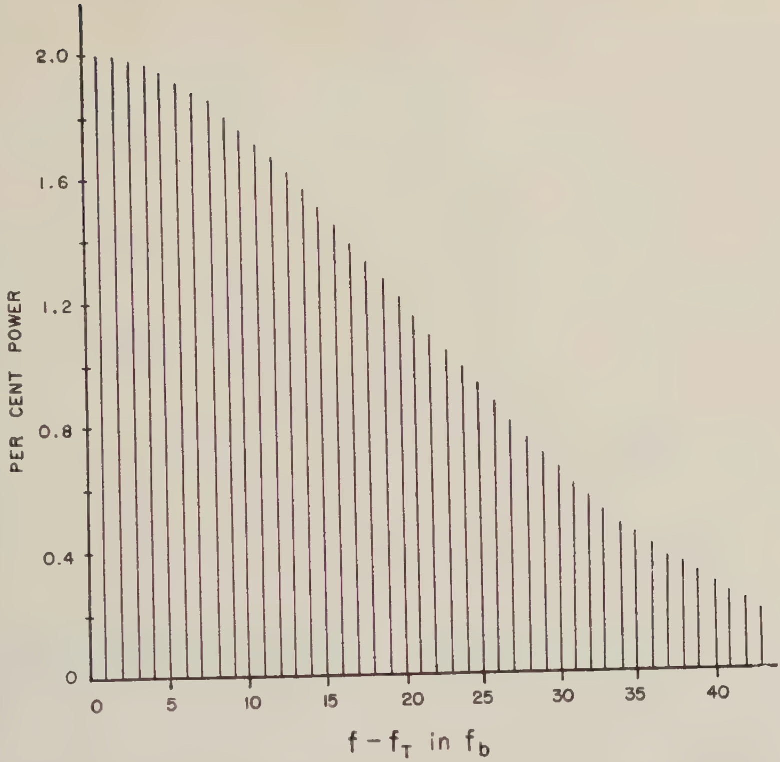

Fig. 2. One wing of the symmetrical line spectrum for $\gamma_\theta = 0.5975 \times 10^{-3}$. The envelope can be taken to be that of the Gaussian Doppler spectrum with practically no error.

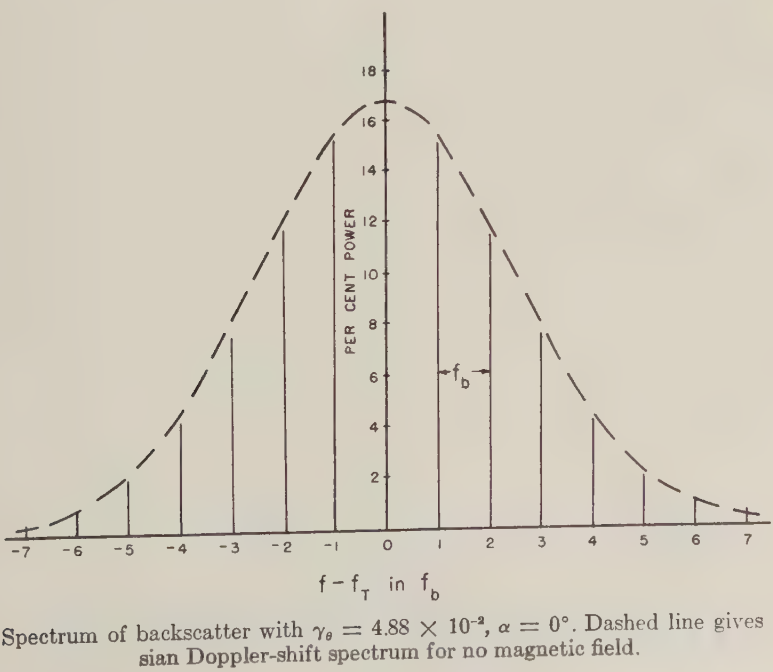

Fig. 3a. Spectrum of backscatter with $\gamma_\theta = 4.88 \times 10^{-2}$, $\alpha = 0°$. Dashed line gives the Gaussian Doppler-shift spectrum for no magnetic field.

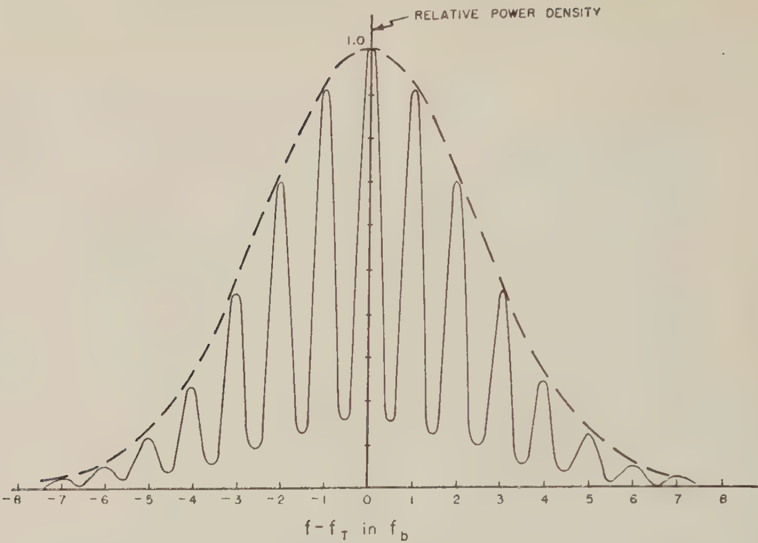

Fig. 3*b*. Spectrum of backscatter with $\gamma_\theta = 4.88 \times 10^{-2}$, $\alpha = 5°$.

of scattering, the envelope of this line spectrum turns out to be given simply by the thermal Doppler-spectrum curve that would have existed in the absence of any magnetic field. As the average radius of gyration is decreased, however, an increasing fraction of power appears in the central line.

If the angle α between the wavefronts the magnetic field is different from zero (**K** perpendicular to **B**), the resultant spectrum be computed by considering it to be a su position of Gaussian spectra that are cent at each of the frequencies $f_T \pm nf_b$, $n = 0$, ... The component spectrum located at f

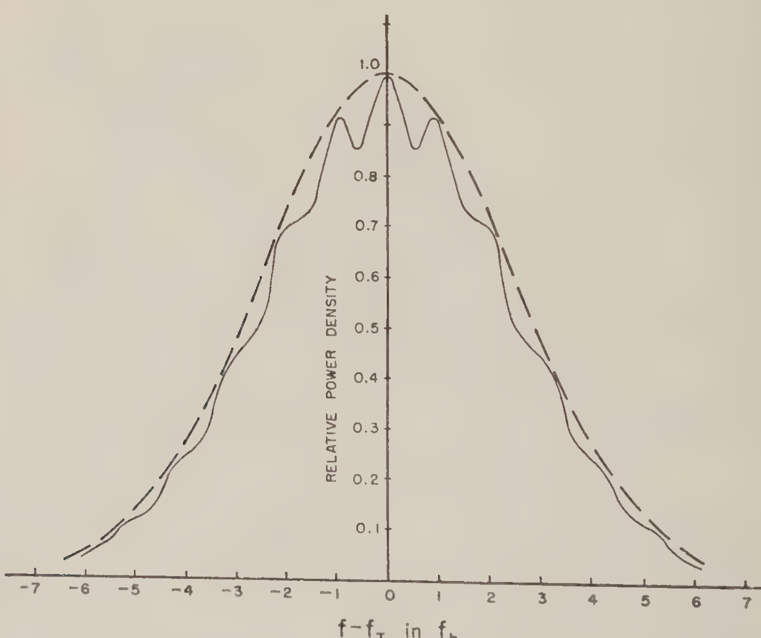

Fig. 3*c*. Spectrum of backscatter with $\gamma_\theta = 4.88 \times 10^{-2}$, $\alpha = 10°$.

f_b is given by

$$I_n(f) = Ae^{-z}I_n(z) \cdot \exp\left(-\left\{\frac{f - f_T \mp nf_b}{258(1/\lambda'')\sqrt{T/M}}\right\}^2\right) \quad (8)$$

where

$$\lambda'' = \frac{\lambda_{\text{meters}}}{\sin\alpha \sin\theta/2} \quad (9)$$

and A is a constant of proportionality, which is the same for all component spectra. The parameter z is equal to

$$z = 0.01429/\gamma_{\theta,\alpha}^2 \quad (10)$$

where

$$\gamma_{\theta,\alpha} = \frac{\lambda_{\text{meters}}}{\cos\alpha \sin\theta/2} \frac{B_{\text{gauss}}}{\sqrt{MT}} \quad (11)$$

Some sample spectra are given in Figures 2 and 3. Figure 2, drawn for $\gamma_\theta = 0.5975 \times 10^{-2}$, should apply for backscatter in the ionosphere somewhere in the height range from about 1000 km to 3000 km, if a wavelength $\lambda = 0.03$ meters (10,000 Mc/s) is used. Some smearing of the line spectrum will occur if the magnetic field of the earth does not lie in the surfaces of constant phase of backscatter. Other possible causes of smearing have been discussed by the author [*Laaspere*, 1960].

Figure 3 shows the effect on the spectrum of incoherent backscatter of increasing the angle α between the surfaces of constant phase and the magnetic field from 0 to 10 degrees. The results apply for $\gamma = 4.88 \times 10^{-2}$. If we use $\lambda = 0.7$ meters (430 Mc/s), we obtain $B/\sqrt{T} = 1.62 \times 10^{-3}$, which might correspond to conditions existing at a height of about 3000 km above the surface of the earth. At that height the condition $4\pi l_D > \lambda$, where l_D is the Debye length, might also be satisfied. The significant feature of Figure 3 is that it shows a rapid smearing of the spectrum as the angle α is increased. A curve was also calculated for $\alpha = 15°$, but is not reproduced, since it would be indistinguishable from the Gaussian Doppler-shift curve that would apply in the absence of any magnetic field.

Acknowledgments. Thanks are due a number of people at Cornell University, and in particular Professor W. E. Gordon. This work was made possible by funds from a United States Steel Foundation Fellowship and from a summer research assistantship on a project sponsored by the Advanced Research Projects Agency through Air Force Cambridge Research Center.

References

Bowles, K. L., Observations of vertical incidence scatter from the ionosphere at 41 Mc/sec, *Phys. Rev. Letters, 1,* 454–455, 1958.

Bowles, K. L., Incoherent scattering by free electrons as a technique for studying the ionosphere and exosphere: Observations and theoretical considerations, *NBS Report No. 6070,* September 18, 1959.

Dougherty, J. P., and D. T. Farley, A theory of incoherent scattering of radio waves by a plasma, *Proc. Roy. Soc. A,* 1960 (in press).

Fejer, J. A., Scattering of radio waves by free electrons, *Canad. J. Physics,* 1960 (in press).

Gordon, W. E., Incoherent scattering of radio waves by free electrons with applications to space exploration by radar, *Proc. IRE, 46,* 1824–1829, 1958.

Laaspere, T., An analysis of the effect of an imposed magnetic field on the spectrum of incoherent scattering, *Res. Rep. RS 15,* Cornell University, July 15, 1960.

Pineo, V. C., L. G. Kraft, and H. W. Briscoe, Some characteristics of ionospheric backscatter observed at 440 Mcps, Report 30G-0008, Lincoln Laboratory, Massachusetts Institute of Technology, July 6, 1960.

Renau, J., Scattering of electromagnetic waves from an ionized gas in thermal equilibrium, Paper presented at the Spring meeting of URSI–IRE in Washington, D. C., May, 1960.

Salpeter, E. E., Scattering of radio waves by electrons above the ionosphere, *J. Geophys. Research, 65,* 1851–1852, 1960*a*.

Salpeter, E. E., Electron density fluctuations in a plasma, *Phys. Rev.,* 1960*b* (in press).

(Manuscript received September 14, 1960.)

The Latitudinal Distribution of Magnetic Activity in Canada

K. WHITHAM, E. I. LOOMER, AND E. R. NIBLETT

Dominion Observatory
Ottawa, Canada

Abstract. Hourly ranges in the principal horizontal field component have been measured for sixteen Canadian IGY magnetic observatories and variation stations. The latitudinal variation of disturbance measured by this index has been determined seasonally and as a function of disturbance. One station, Alert, at the northern end of Ellesmere Island, confirms the existence in these longitudes of an apparently narrow zone or area of enhanced magnetic activity, as defined by this measure of disturbance. Semipersistent structure is also apparent in the principal auroral zone in the meridian sections of magnetic activity.

Diurnal occurrence patterns, amplitude-frequency plots, the diurnal variation of the mean disturbance field, and the physical significance of this range index have been investigated in an attempt to explain this apparent inner maximum of magnetic activity. More homogeneous very high latitude data are required to determine the morphology of the anomalous region found.

Introduction. The distribution and density of magnetic observatories and variation stations in Canada during the IGY were sufficient, for the first time, for an investigation of the latitudinal variation of magnetic disturbance using homogeneous data. The diurnal and seasonal variations of irregular magnetic activity have been determined, and the relationship of irregular magnetic disturbance to the daily variation of the disturbance field studied, in an attempt to assess the significance of the observational evidence for the existence of an inner zone of enhanced magnetic activity.

The outstanding feature of Canadian magnetograms is the high level of irregular magnetic activity more or less continuously present, though, of course, enhanced at the time of magnetic storms. The precise identification of such events as bays, sudden impulses, and crochets is not possible without data from lower latitudes, and the storm-time characteristics usually considered in the formulation of magnetic storm theory [see, for example, *Dessler and Parker*, 1959] are smaller than the average background of wide-band, large-amplitude noise visible on the magnetograms.

Distribution of IGY magnetic observatories and variation stations in Canada. Table 1 shows the position of the stations used at one time or another in this study: the geomagnetic coordinates shown are those calculated assuming the position of the north geomagnetic pole to be 78.3°N, 69.0°W. Except for Agincourt observatory, the observatories lie close ($<\pm 20°$) to geomagnetic longitude, $\Lambda = 302°$E. The majority of the variation stations are near the auroral zone in central Canada.

A measure of magnetic activity. The problem of defining the optimum objective measure of magnetic activity is very difficult since such an index is a function of latitude and the use to which the data is put. In this work, the index chosen for representing the irregular magnetic activity was one widely used by Russian workers, the hourly range in the principal horizontal or some other magnetic field component. The advantages in choosing this index rather than K or Q indices are:

(*a*) A direct comparison with Nikolski's work is possible for longitudes ~180° different: in particular the suggestions of *Alfvén* [1955] and of *Nikolski* [1956] regarding an inner zone of maximum magnetic activity can be tested with homogeneous data, thereby avoiding some of the uncertainties implicit in Nikolski's treatment, because of the large seasonal changes of activity at high latitudes.

(*b*) The K and Q indices are quasi-logarithmic, and when data are averaged, quasi-geometric means are obtained that can be misleading. Furthermore, the interval for the K index (3-hours) are rather longf or investigation of diurnal variation, and that for the Q index (15 minutes) so short that a prohibitive amount of manual scaling is required. Essentially the K index is

TABLE 1. Coordinates of Canadian IGY Magnetic Observatories and Variation Stations

Observatory	Abbreviation	Principal Horizontal Component	Geographic		Geomagnetic	
			Latitude North	Longitude West	Latitude North	Longitude East
			°	°	°	°
Victoria	Vi	H	48.5	123.4	54.3	292.7
Agincourt	Ag	H	43.8	79.3	55.2	346.9
Meanook	Me	H	54.6	113.3	61.9	300.7
Churchill	Ch	X	58.8	94.1	68.8	322.5
Yellowknife	Yk	X	62.4	114.4	69.1	292.8
Baker Lake	BL	X	64.3	96.0	73.9	314.8
Resolute Bay	RB	Y	74.7	94.9	83.1	287.7
Variation Station						
Ottawa	Ot	H	45.4	75.7	57.0	351.3
Swift Current	SC	X	50.3	108.0	58.7	309.4
Winnipeg	Wi	H	49.9	97.4	59.8	322.5
Saskatoon	Sa	X	52.1	106.6	60.6	310.2
The Pas	TP	X	53.9	101.1	63.2	316.1
Goose Bay	GB	X	53.3	60.4	64.8	12.1
Bird	Bi	X	56.5	94.2	66.6	323.7
Ennadai Lake	EL	X	61.3	101.2	70.3	310.7
Alert	Al	Y	82.5	62.5	85.7	168.7

not designed for morphological work. The selection of the lower limit of $K = 9$, different at different observatories in order to normalize, so far as possible, the frequency distribution of K's, simplifies the calculation of a world-wide index of solar particle activity, K_p, while complicating the study of magnetic disturbance throughout a limited region. In Canadian latitudes the hourly-range index primarily measures the dominant irregular activity and is approximately proportional to the rms value of the magnetogram noise in each hour [*Whitham and Niblett*, 1961].

(*c*) The hourly-range index is easily measured and requires no determination of the absolute level of the normal curve, thereby being usable with records obtained from electrical recording magnetometers of the saturable core type. Such records are the only ones available at nine out of the sixteen Canadian stations.

The disadvantages of the hourly-range index adopted are:

(*a*) No precise separation of the disturbance field into the mean daily disturbance variation, storm-time disturbance, or irregular activity is possible.

(*b*) It has not been widely used, except by Russian workers, so that comparison with indic[...] published by American or Danish stations a[...] not easily made.

Uncertainties in the determination of the hour[...] range. The measurement of ranges on th[...] standard run, standard sensitivity photograph[...] variometers is straightforward since the a[...] propriate scale constants are generally know[...] to better than 1 per cent, and base-line drif[...] and uncompensated temperature effects in an[...] one hour are negligible.

At the variation stations, the electrical r[...] cording magnetometers used have drift rates [...] the order of 1 γ/hr, temperature effects in th[...] vertical field component of about 3 γ/C°, and [...] chopper-bar type of recording system that r[...] duces the peak-to-peak values of the high[...] amplitude, shorter-period, irregular fluctuation[...] recorded. The nominal scale value depends on[...] on the magnitude of a precision resistance in th[...] feedback loop and the solenoid constant of th[...] magnetic detector and was thought to be 1[...] mv/γ ± 1 per cent, equivalent to 8.3 ± 1 pe[...] cent γ/mm, with the recording system used[...] Nonlinearity of the meters used prohibits suc[...] accuracy in practice. Careful comparisons wit[...] photographic magnetograms at Yellowknif[...]

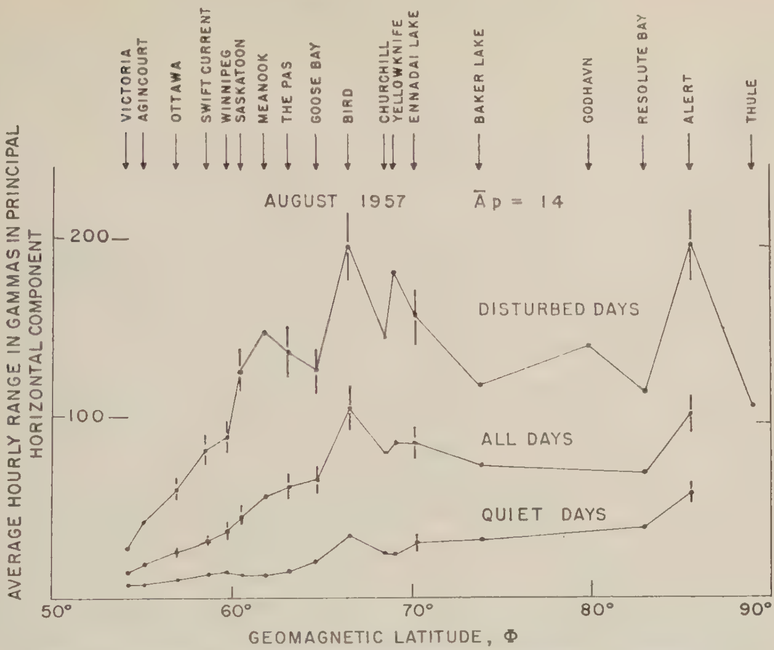

Fig. 1. Meridian section of irregular magnetic activity in August, 1957.

ker Lake, and Resolute Bay observatories owed that a more realistic scale value was γ/mm ± 3 per cent sd in any one instrument, d that an approximate correction of +6 per nt to the ranges deduced from the records ould be applied to compensate for the chopping tion. The latter correction is rather arbitrary ce the true correction is a function of the equency spectrum of the irregular fluctuations. llowing the procedure outlined above, however, it is clear that the ranges in gammas rived from electrical recording magnetometers, rforming satisfactorily under field conditions, e reliable to better than ±10 per cent.

Latitudinal distribution of magnetic activity in nada. The average hourly range in the principal horizontal field component (the numerically rgest component H, X, or Y recorded) is own for 4 months for all days, for the 5 intertional quiet days, and for the 5 international sturbed days as a function of geomagnetic titude in Figures 1 to 4. The months illustrated e August, September, December, 1957, and ne, 1958, and on each plot the mean monthly anetary amplitude index A_p in units of 2 γ is own. Error flags in Figures 1 to 3 indicate the ±10 per cent maximum uncertainty discussed ove at variation stations. Disturbed-day data re available for two Danish high-latitude observatories (Godhavn and Thule) for August and December, 1957, and quiet-day data for September, 1957. The data are essentially homogeneous, though, on occasion, equipment failures necessitate corrections (usually based on the nearest stations) for short periods of time. Figure 4 also shows for comparison the average hourly range in gammas for June, 1958 in the vertical field component.

These meridian sections immediately illustrate:

(1) There is a pronounced maximum of intensity throughout the auroral region in all seasons: this result is well known and was expected.

(2) There is strong evidence for persistent structure in the main zone. This is examined further below.

(3) Using horizontal field components, the Alert station apparently confirms Nikolski's inner zone of enhanced magnetic activity at the geomagnetic latitude, $\Phi \simeq 86°$. This is discussed below and is a persistent effect since unpublished analyses of the disturbed days on 3 other months also exhibit the rise.

(4) There is a seasonal variation of magnetic activity in Canada which, also, will be considered further below.

Structure of the zone of maximum magnetic

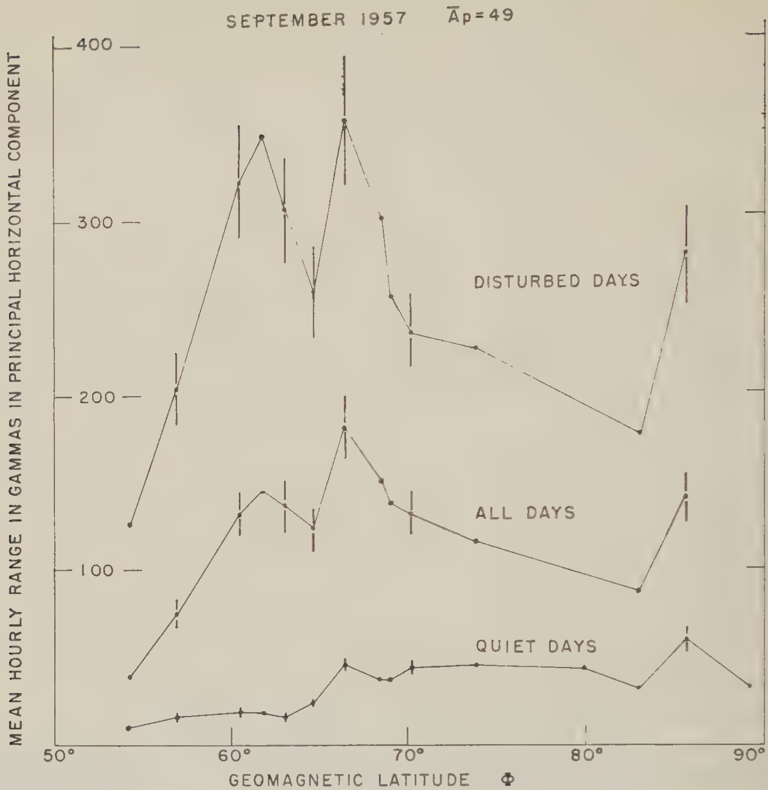

Fig. 2. Meridian section of irregular magnetic activity in September, 1957.

activity. Figures 1, 2, and 4 illustrate clearly the bifurcation of the zone in the summer and equinoctial months examined. This is not so evident in the winter data. The bifurcation becomes striking as the level of disturbance rises and is most apparent on the disturbed days of the most disturbed month (September, 1957). The main maximum always occurs near Bird ($\Phi = 66.6°$), and the subsidiary maximum is near Meanook ($\Phi = 61.9°$). Under the most disturbed conditions, the southern branch intensity equals that in the main branch.

The movement of auroral forms equatorward with increasing disturbance has long been recognized. There is evidence [*Obayashi*, 1959] that the shift during a magnetic storm is related to the depression of the geomagnetic field intensity, i.e., to the strength of any ring current. Movement to the south of the region of maximum irregular magnetic disturbance might therefore be expected, but the relative constancy in position of the principal and subsidiary maxima was not anticipated for months of such different over-all levels of activity. The correlation of irregular magnetic activity with the stati position of the auroral zone in Canada s therefore be attempted in order to resolv discrepancy.

The apparent bifurcation is unlikely to consequence of any longitude effect, sinc only (Goose Bay) of the two stations mediate between the maxima is displaced siderably from the mean longitude. Furthe certain preliminary results from Russian st (communicated privately by Nikolski) in no appreciable longitude effect.

On occasion, there is evidence for a nor branch centered on Yellowknife (Φ = The balance of evidence does not suggest ever, that irregular magnetic activity ex both north and south with increasing distur

Burdo [1955] has pointed out that no s attempts appear to have been made to data on irregular magnetic activity to the disturbance vector. The mean daily varia disturbance has been examined in det *Vestine and Chapman* [1938] and *Vestin porte, Lange, and Scott* [1947]. The diurna

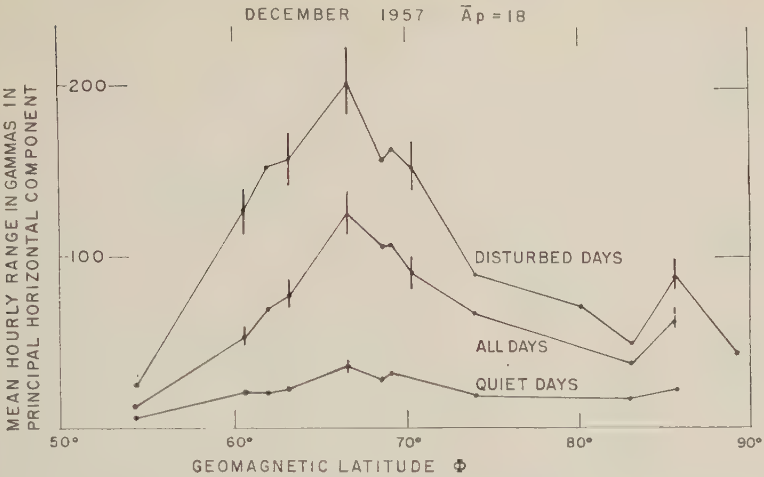

Fig. 3. Meridian section of irregular magnetic activity in December, 1957.

…ion of the D field across geomagnetic meridian … ~ 120° has been studied by *Harang* [1946], …d that across Λ ~ 300° by *Whitham and …omer* [1957*a*], using a rather larger range of …titude. The results of these investigations may … summarized by saying that the ΔH, ΔZ con…urs indicate two current systems in opposite …rections (westward on the AM side, eastward … the PM side), and that if the mean position … the lines of maximum $|\Delta H|$ and zero ΔZ is …sumed to represent the horizontal projection … a disturbing current system, this coincides …th the zone of maximum auroral frequency (near $\Phi = 67°$), at least at the hours of maximum disturbance. Seasonal and annual shifts in the position of the auroral zone and its motions as a function of increasing disturbance can all be followed in this manner. Making rather arbitrary corrections for induction inside the earth, approximate agreement with geomagnetic observation is possible with simple geometrical concepts such as a line current or narrow sheet at ionospheric altitudes.

The daily variation of disturbance in Canada has been examined with the increased number of stations. The curves of diurnal variation are

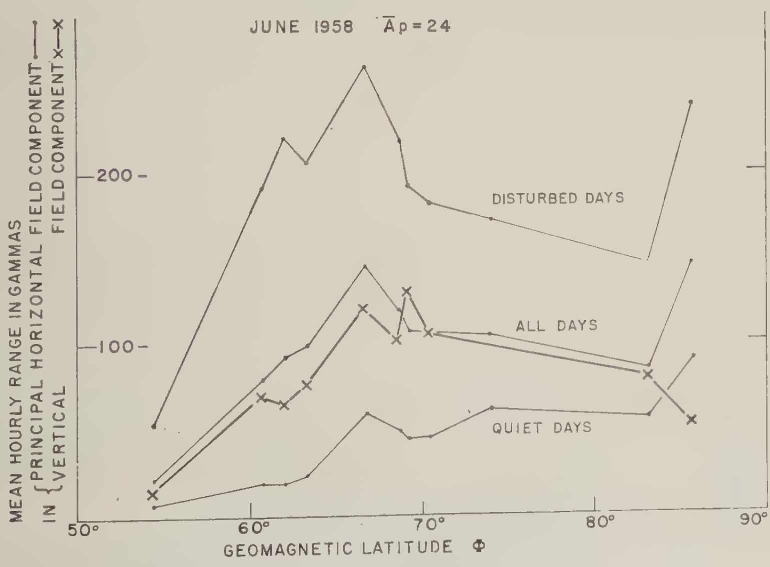

Fig. 4. Meridian section of irregular magnetic activity in June, 1958.

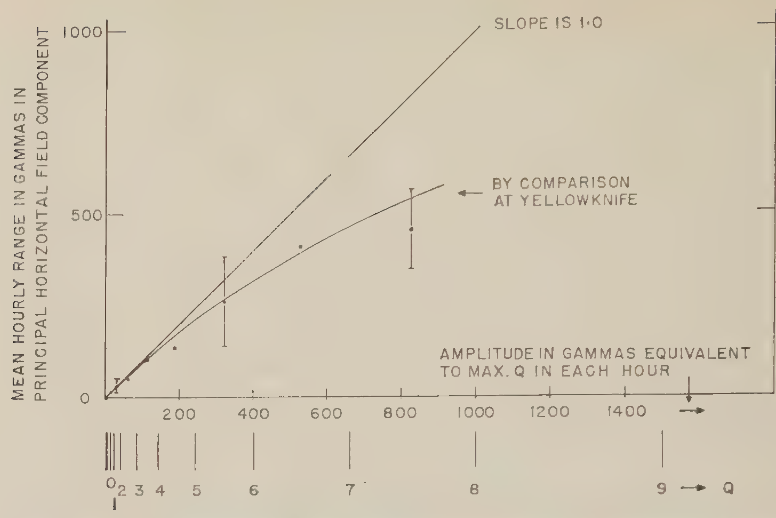

Fig. 5. Comparison of Q index with mean hourly-range index at Yellowknife, August, 1957.

not shown here because the conclusions drawn above are substantially confirmed. In August, 1957, for example, the average position of the AM branch is between Churchill and Bird and that of the PM branch north of Ennadai Lake. With increasing disturbance in September, 1957, both branches move south of Bird. The detailed correlation with the sections of irregular magnetic activity shown in Figures 1 and 2 is obscure; certainly fluctuations proportional to the mean level of disturbance do not explain the result. This can be proved by separately plotting meridian sections of the average disturbance between 10–22 hours LT and 22–10 hours LT for a winter and a summer month. The results are practically indistinguishable from the pl[...] shown in Figure 7. Occasionally the occurren[...] of a double maximum in ΔZ is used to determi[...] the mean latitude of the two branches, and her[...] the mean position of the auroral zone and [...] movements. No contradictions with the ear[...] results have been found if this method is adopt[...]

It should be noted that interpretation of [...] tail is very uncertain and depends somew[...] upon whether the data are considered in g[...] magnetic or geographic coordinates and ti[...] *Meek* [1955], for example, finds evidence for t[...] opposing spiral patterns.

The inner zone of enhanced magnetic activ[...] Figures 1 to 4 demonstrate immediately t[...]

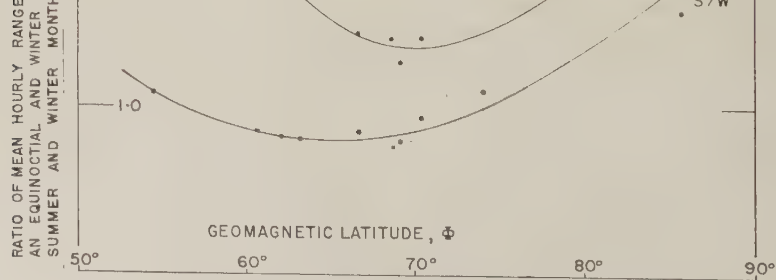

Fig. 6. The seasonal variation of magnetic activity in Canada.

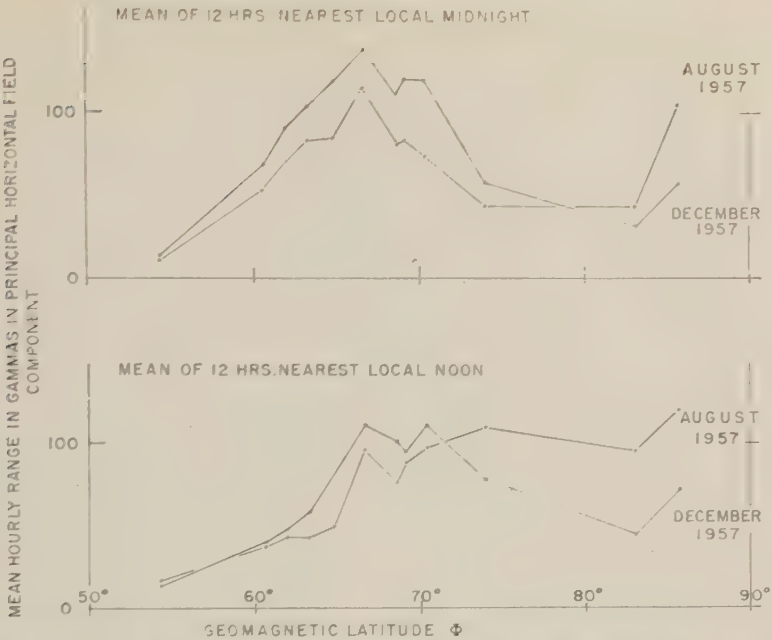

Fig. 7. Meridian sections of irregular magnetic activity in August and December, 1957 for two 12-hour intervals.

Alert ($\Phi = 85.7°$) shows an unexpected maximum of magnetic activity, as measured by this index. The effect is always present, but is relatively more important in the arctic summer when its magnitude, measured in this way, becomes equal to that at Bird in the main auroral zone. The relatively small amount of data presently available from Godhavn and Thule suggests an inner maximum rather than an increase towards the geomagnetic pole. No anomalous effect is evident at Resolute Bay ($\Phi = 83.1°$) confirming the earlier conclusions of *Whitham and Loomer* [1956] who were unable to detect the existence of an inner zone from analysis of magnetic disturbance at Resolute Bay, though noting certain unusual diurnal characteristics.

The data suggest that if a zone, rather than an anomalous region, exists, such a zone is narrow and at a smaller colatitude than Alfvén's theoretical prediction, or Nikolski's suggested position; both these correspond to the position of Resolute Bay where, using Nikolski's method of determination and other investigations, no inner maximum is found. The narrowness of the apparent zone and other considerations may explain why the data of *Mayaud* [1956] provide no confirmation of its existence.

Two questions immediately arise about the Alert maximum: is its significance related to the particular index used, and is it a local anomalous effect without major significance?

That the existence of the Alert maximum depends on the use of an index involving horizontal components, and hence sensitive to overhead currents, is immediately obvious from an examination of Figure 4 where, for the vertical field fluctuations, the anomaly has disappeared. The only other index of solar particle precipitation accepted internationally, suitable for the study of overhead currents, is the Q index proposed by *Bartels and Fukushima* [1956]. This index is a quasi-logarithmic range index (10 numeric and 2 alphabetic points) and measures in each 15 minutes the total deviation from a normal curve in the most disturbed horizontal component. Equivalent ranges deduced from Q indices are therefore greater than or equal to the usual range defined in this study; in particular, when longer period bay-like phenomena, or enhanced DS occur, equivalent Q ranges become greater than the ranges adopted in this study. This is illustrated in Figure 5 for Yellowknife in August, 1957. The Q indices published by *Loomer, Whitham, and Niblett* [1960] were examined, the maximum of the eight values of Qx and Qy in each hour selected, and the corresponding range used

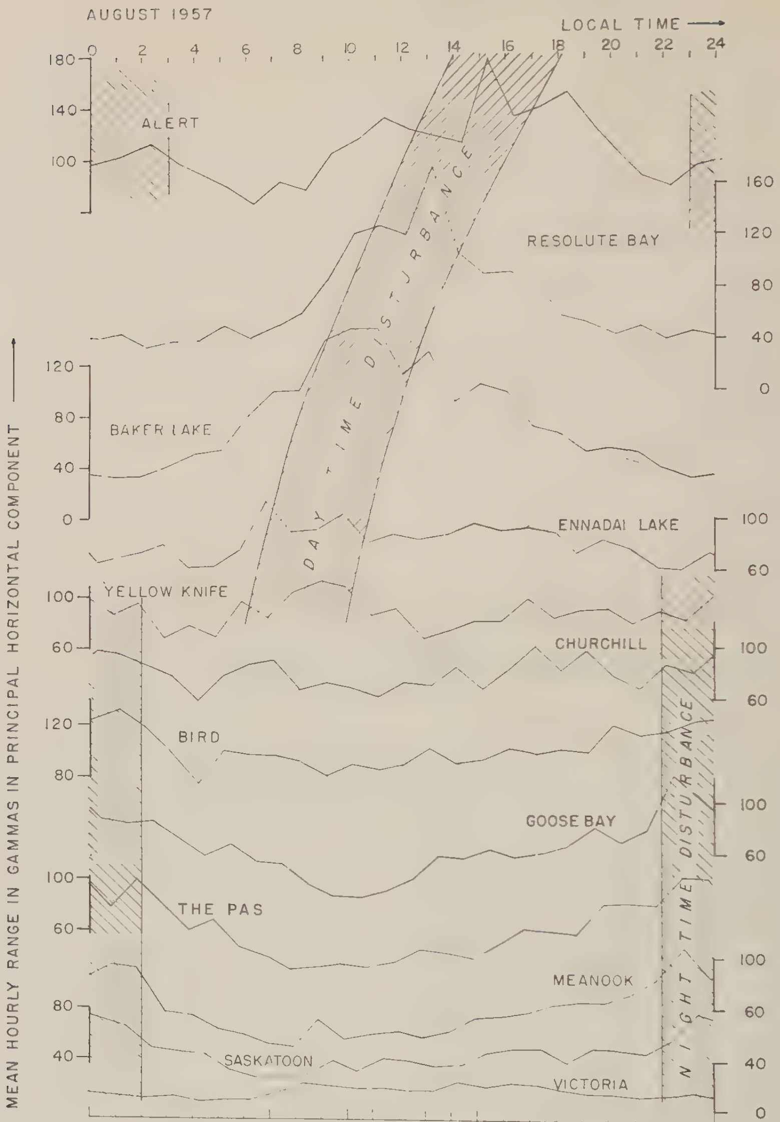

Fig. 8. The diurnal variation of irregular magnetic activity in Canada, August, 1957.

in this study noted. The mean ranges for $Q = 0$, 1, 2, etc., were calculated and plotted against the equivalent Q index. The results are identical up to $Q = 4$ (i.e., slope = 1), but at larger values of disturbance, the equivalent Q ranges are much larger. Since the most probable value of Q is 3, and the mean value, in general, less than 4 at high latitudes, it appears certain that an inner maximum would also be indicated if Q values were available. The correlation between the average value of Q for a day and the logarithm of the daily average hourly range in the principal horizontal field component for August, 1957, [illegible] Yellowknife, is 0.92. Figure 5 demonstrates [illegible] weakness of the simple hourly-range index [illegible] the study of quasi-regular long-period p[illegible]nomena, and may explain some of the appar[illegible] lack of detailed correlation between irregu[illegible] fluctuations and the average disturbance field[illegible]

Anomalous conductivity in either the crust[illegible] the mantle, or both, near Alert might produ[illegible] the anomalous range increase noted there. Su[illegible] effects have been found in Japan [*Rikitake*, 19[illegible]] and in Germany [*Siebert and Kertz*, 1957], [illegible]

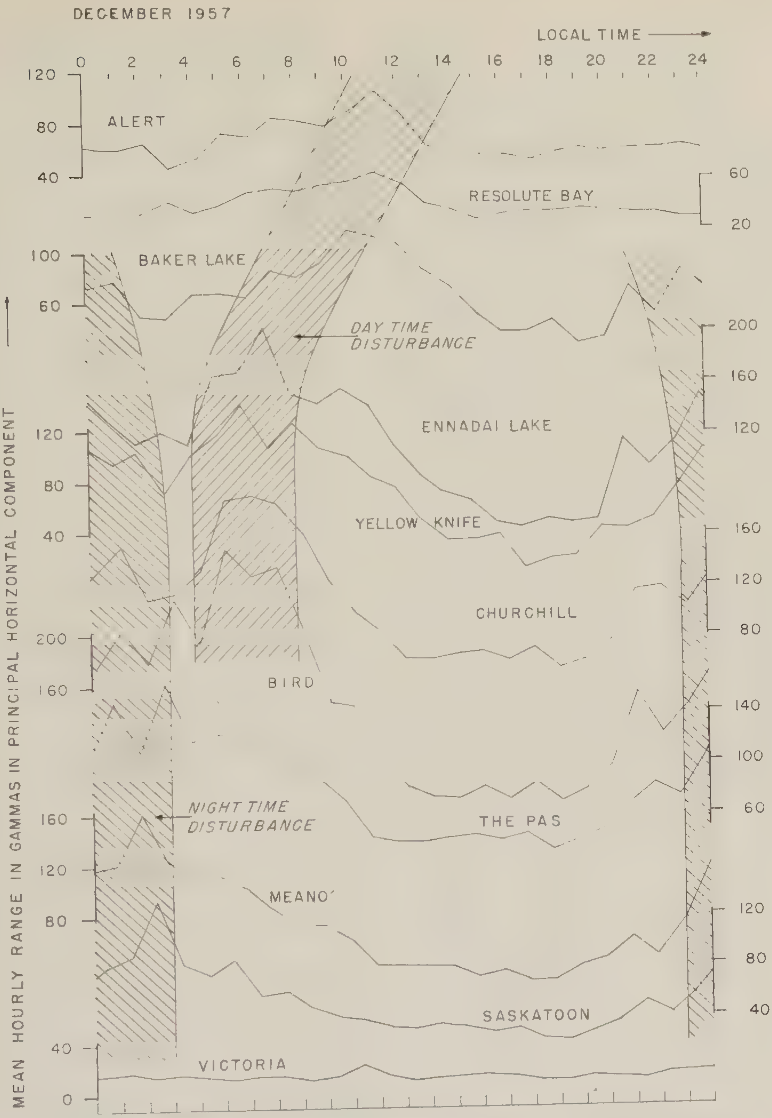

Fig. 9. The diurnal variation of irregular magnetic activity in Canada, December, 1957.

no general prediction of the sign of such an effect seems possible. The size of the increase in range at Alert, together with its seasonal variation and certain other characteristics discussed later, suggests that a local effect is unlikely. Furthermore, in at least one of the two well-demonstrated cases, that in Japan, the effect on horizontal component ranges is comparatively slight whereas vertical component ranges are enhanced. Figure 4 does not show this effect. Finally, the influence of polar ice and the sea could conceivably produce marked localization of magnetic activity [see, for example, *Senko*, 1958], but large effects are considered unlikely in the frequency range discussed here.

Obviously more data from Thule and Godhavn in vertical field component fluctuations would be of interest, and a more detailed confirmation of this suggested inner zone is required experimentally. By using the logistic facilities and geophysical personnel of the newly formed Polar Continental Shelf Project of the Canadian Department of Mines and Technical Surveys it is hoped to obtain magnetograms for short periods of time from several of the northern arctic islands, while maintaining in operation the

observatory at Resolute Bay and re-equipping Alert to observatory standards for a limited period.

An examination of the relation of this inner maximum to the daily variation of the disturbance field, similar to that described above in the main auroral zone, has been attempted. The latitudinal variation of the vertical component disturbance field inside the polar cap provides the best test for the existence of a concentrated current path near Alert. The results indicate only a gradual decrease in the magnitude of the amplitude of the AM and PM peaks in $|\Delta Z|$ from Baker Lake northward through Resolute Bay and Alert. Examination of the published daily-variation curves for Thule for a different period of time [*Vestine, Laporte, Lange, and Scott*, 1947] supports this conclusion. The most reasonable interpretation of the data is still a current sheet return-path (directed towards the 10^h meridian) which perhaps may not be very uniform. Again there is no evidence of an inner maximum in a horizontal component, but rather a flattening out of the amplitude corresponding to entry under a sheet flow. More precise data of observatory standard from Alert, without the temperature effects of the saturable core magnetometer used there during the IGY, is definitely required. Again, at high latitudes the problem of the best coordinate system to use is even more pressing; unpublished data from field surveys in Ellef Rignes Island indicate that in Z, at any rate, the diurnal variation in high latitudes in Canada is similar to that at Resolute on a local time basis.

Seasonal variation of magnetic activity in Canada. This has been previously outlined by *Whitham and Loomer* [1957*b*] using the sparse network of permanent observatories. The denser IGY network confirms the earlier analysis. Figure 6 illustrates the large seasonal variation as a function of geomagnetic latitude: clearly interstation comparisons should be made using only contemporaneous data or data from which the seasonal variation has been removed. Relative to the winter level, equinoctial activity increases more to the north and south of the main auroral zone than in the zone itself, whereas in the arctic summer a large increase in activity is found inside the polar cap only. The seasonal variation in activity can be clarified by considering the diurnal variation of magnetic activity. The latitudinal variation of the seasonal activity is a consequence of two effects: (*a*) The daytime peak in activity evident in the nort of the auroral zone and dominant inside th polar cap moves south in the arctic winte season. This result is in agreement with th *Nikolski* [1947] Siberian analyses. (*b*) The night time peak in activity evident throughout th auroral zone and a little to its south moves nort in the winter months. This result was show much earlier by *Stagg* [1935]. This can be see in Figure 7 where the average hourly range fo the 12 hours nearest local noon and neares local midnight are shown separately for Augus and December, 1957, as a function of geomag netic latitude. *Mayaud* [1956] has shown tha antarctic seasonal behavior is similar.

Diurnal variation of irregular magnetic activit in Canada. The two regimes of activity ar clearly illustrated in Figures 8 and 9, which show the diurnal variation of the average hourl range in the principal horizontal field componen as a function of local time, for a number o locations for a summer month (August, 1957) and a winter month (December, 1957) of ap proximately the same over-all level of disturb ance. The two regimes are indicated broadly b hatching without attempting to specify the pre cise times of maximum. Figures 8 and 9 clearl demonstrate the existence of two diurnal peak to the north of the auroral zone (Stagg's tran sition region). An analogous mode apparentl reappears at Alert, at least in the summe month.

Burdo [1957] has published plots showing thre distinct linear relationships between the geo magnetic time of occurrence of maxima of geo magnetic activity and geomagnetic latitude. In general, it appears from our results that clea definition of the times of maxima is not possibl without either a very large number of data such that smoothing is unnecessary, or a valid basi for smoothing. Thus Figures 8 and 9 represen unsmoothed data, and Figure 10 compares th diurnal variation (in universal time) of the range index for three different months at four typica locations. The significance of certain maxima is to say the least, obscure, and unambiguous plots of the type suggested by Burdo not justified with Canadian data. It is clear, however, tha the time of the maximum of the daytime activity becomes later with increasing geomagnetic lati tude, and changes from $\sim$6 hours LT at $\Phi \sim 67$ to $\sim$14 hours LT at $\Phi \sim 86°$. The time of th nighttime maximum is within a few hours o

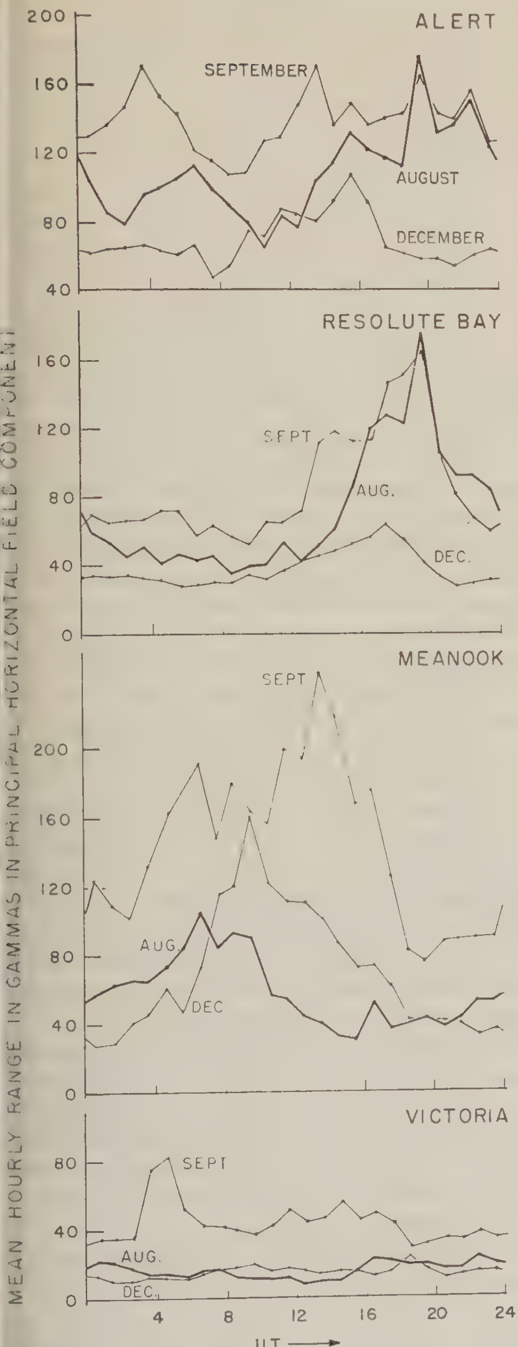

Fig. 10. Illustrating the variability of the diurnal variation of irregular magnetic activity in Canada.

local midnight throughout the entire region, with possibly a slight tendency to occur earlier at higher latitudes. Up to and including Resolute Bay, the difference between local time and local geomagnetic time is less than the ambiguities in the time of maxima; at Alert local geomagnetic noon is near local midnight.

Although the earlier pattern of Mayaud is largely confirmed, the three maxima of magnetic activity discussed by *Nikolski* [1958] and *Burdo* [1955] are not apparent. Furthermore, the Alert results do not agree with the predictions of Nikolski's spiral isolines of the morning disturbance maximum; the UT of the maximum is 18 ± 3 hours, and the spiral prediction, 10 hours. South of Resolute Bay, agreement is satisfactory when the morning maximum can be identified.

Lassen [1959] has pointed out that the daytime class of magnetic activity is very poorly—or not at all—correlated with aurora. He has directed attention to a population of auroras which appears to form an inner auroral zone—between $\Phi = 75°$–$80°$—occupied in early morning hours irrespective of disturbance in the main auroral zone. Possibly therefore, reappearance of the nighttime activity at Alert is highly significant and when auroral data become available correlations with this should be sought.

Finally there is little doubt that daytime and nighttime magnetogram noise are somewhat different; visual examination suggests that the spectral distribution may be shifted toward shorter periods during the daytime.

Over-all correlation of magnetic activity in Canada. Whitham and Loomer [1956] have shown that the correlation of magnetic activity between a polar cap observatory, Resolute Bay, and a transition zone one, Baker Lake, is very high. Figure 11 shows the correlation of the daily mean hourly range for August and September, 1957, between Alert and stations to the north, center, and south of the main auroral zone. The pronounced curvature of the correlation plotted against the geomagnetic latitude separation arises from the change in the relative magnitudes of daytime and nighttime activity. The correlation obtained is a function of the season, since the seasonal dependence of the daytime high latitude activity (maximum in summer) is different from that of the nighttime activity (maximum in equinoxes).

Further investigation of the inner maximum at Alert. By constructing amplitude-frequency histograms, it was clearly shown that the Alert rise is not a consequence of comparatively few large-amplitude range values; in fact, at Alert, the number of large amplitude ranges (say

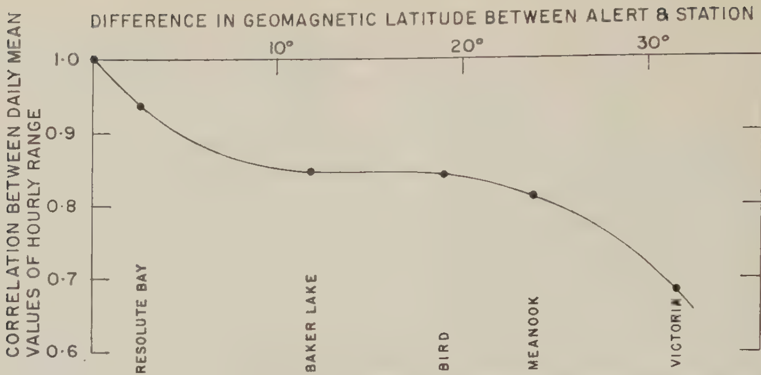

Fig. 11. The correlation between the daily mean level of irregular magnetic disturbance at Alert and stations to the south.

>300 γ) is less than in the auroral zone. At Alert the most probable range is between 50 and 100 γ; at all other stations, between 0 to 50 γ.

The ten most disturbed days in each month for August, September, and December, 1957, at each station were selected and ranked, using as a criterion the daily range sum. Although most days of disturbance were common throughout the auroral zone and in the polar cap, on certain days (noticeably August 3, 4, 29; September 13, 22; December 17, 1957) disturbance inside the polar cap was relatively more marked than in the auroral zone, i.e., on these days the ranking level became increasingly higher from Baker Lake through Resolute Bay to Alert. Only two of these days appear in the lists of five international disturbed days each month, whereas in the auroral zone the international disturbed days are in general the local disturbed days selected by this criterion. The opposite effect is suggested on August 6, 13, 21; September 23; December 1, 5, 31, 1957; on these days the order of ranking in the auroral zone is appreciably higher than in the polar cap. August 13 is interesting in that a very clear sudden commencement in the auroral zone and to its south was not observable at Resolute Bay. All but two of the latter days are included in the internationally selected days.

These different days, which correspond to days of pronounced storms or polar storms, have been examined in an attempt to deduce a systematic reason for the difference. Such an effect as daytime enhancement of storms commencing in the morning hours might be responsible for the first class. No clear conclusion appears possible, though this may provide a partial explanation.

Hakura and Goh [1959] have published a list of outstanding solar-terrestrial phenomena during the IGY including events with a pre-SC pola cap blackout. Only two of the outstandingly disturbed polar cap days are associated with days of absorption of cosmic noise as determined by the riometer in the polar cap. September 1 is an example. *Hakura, Takenoshita, and Otsuki* [1958] have examined this event when Type-3 absorption appeared in the polar cap ~20 hours before the onset of the geomagnetic storm, and the abnormal ionization spreads through the auroral zone towards lower latitudes as the storm develops.

The possible relationship of abnormal polar cap magnetic activity to Type-3 absorption is therefore far from clear. *Reid and Collins* [1959] point out that Type-3 absorption sets in within a few hours of the onset of a major solar flare, usually persists for 2–3 days, is predominantly a daytime phenomena and shows little if any correlation with K_p. High-energy protons (>1 Mev) are considered responsible, and the density of protons in the incident stream is thought to be insufficient to produce appreciable magnetic disturbance; precipitation apparently occurs in the whole polar cap, and if Störmerian orbits are assumed the particles must arrive equally from all directions [*Obayashi*, 1959].

In contrast, the anomalous inner zone is apparently localized, and although the daytime regime of activity is dominant there is evidence for the reappearance of the nighttime mode. However, the use of K_p to specify very high latitude magnetic disturbance can on occasion be misleading. In fact, a comparison of hourly range measurements with the monthly mean A_p for the 4 months investigated shows that the planetary-amplitude index is equivalent to the range at $\Phi = 58° \pm 1°$ in all seasons.

Vestine [1960] has shown that the use of adiabatic invariants to study the drift motion of particles trapped in the earth's magnetic field may be useful in considering the geometrical form of auroral isochasms and the averaged direction of auroral arcs. He has published curves of equal adiabatic invariants, calculated using 48 terms of the spherical harmonic analysis of the geomagnetic field, and it is interesting to note that these curves are essentially centered near Alert. Such a result might be expected from the presence of the centers of maximum field intensity in central Canada and northern Siberia. The significance of this coincidence is uncertain since particles are not found experimentally to be trapped in orbits thought to correspond to such high latitudes. At the latitude of Alert, the magnetic field lines cross the equator at $\sim 10^2$ earth radii and the intensity of the field is $\sim 10^{-2}$ γ only. North of the auroral zone and well south of Alert, the lines of force of the geomagnetic field are usually regarded as completely disrupted by solar streams at a distance greater than a few earth radii, and may on occasion link up with solar-stream field lines providing a preferred path of precipitation in the polar cap. Again isotropy is inferred. It may also be remarked that if the geomagnetic latitude is replaced as an isopleth of irregular magnetic activity by magnetic latitude, or an effective latitude based upon an effective pole at Alert, no improvement in presenting the data of Figures 1 to 4 is found. *Hatherton and Midwinter* [1960] have suggested, however that geomagnetic latitude may not be a satisfactory isopleth of auroral and magnetic behavior at high latitudes.

Quenby and Webber [1959] have suggested that for cosmic rays a satisfactory isopleth is $\bar{\lambda}$ which is an effective latitude that can be calculated for any point on the earth's surface from a knowledge of its geographical position, the $n = 1$ terms in the spherical harmonic analysis of the field and the actual regional field components. $\bar{\lambda}$ was calculated for all the Canadian stations. For Alert, using X instead of H in Quenby and Webber's approximation, $\bar{\lambda} = 88°$, and for Thule, $\bar{\lambda}$ is only fractionally higher. No satisfactory smoothing of the data occurs on using $\bar{\lambda}$ as the abscissa. Since very high latitude regional field data are given little weight in spherical harmonic analyses, the formulas given by Quenby and Webber for $\bar{\lambda}$ may be considerably in error at very high latitudes.

Nikolski's [1957] interpretation of an inner zone in terms of Störmer's theory may be summarized as follows. Following Störmer, four regions on the spiral belt of auroras in which particles impinge more densely are assumed, and the latitude of the inner zone corresponds to that of the inner auroral zone. Qualitative arguments and presumably unpublished data are used to suggest that the actual inner zone is somewhat distorted from a geomagnetic latitude. In fact, at different times [*Nikolski*, 1956; 1957] the position and form of the proposed zone have been modified somewhat. The usual well-known objections can be raised. However, neglecting the effects of an external ring current, protons of velocity 10^3 km/sec ($H\rho = 10^4$) largely precipitate at a geomagnetic colatitude of 7°. Is it possible that a steady background of solar particles, possibly self-focused, do indeed follow classical Störmer theory paths and precipitate at very high latitudes? Since in these regions deviations from the dipole field are large, some curious anomalies might be expected.

Suggestions for further work. A clearer idea of the morphology of an inner zone of enhanced magnetic activity should be possible if all high-latitude data are examined; homogeneous data and indices should be used. Such an investigation should be quite straightforward after World Data Center collections are complete.

In Canada magnetograms from the region between Resolute Bay and Alert are required; a program to acquire this data is now underway. A satellite station to Alert (say within 50 miles) is urgently needed to verify the Alert result.

Modern magnetohydrodynamic storm theories which can explain averaged storm features should be extended to a consideration of the two regimes of magnetic activity and their variation with latitude. The auroral zone structure may be related to the formation of a magnetic tail on the night side of the earth suggested in some formulations [*Piddington*, 1960].

In general, the relation of irregular magnetic disturbance to auroral occurrence requires re-examination in areas north of the auroral zone. Storm time effects at very high latitudes may also be anomalous [*Whitham and Loomer*, 1957*a*].

References

Alfvén, H., On the electric-field theory of magnetic storms and aurorae, *Tellus* 7, 50–64, 1955.

Bartels, J., and N. Fukushima, A Q-index for geomagnetic activity in quarterly hour intervals,

Proc. Acad. Sci., Göttingen, sp. ed. 2, Part 2, 1956.
Burdo, O. A., Re certain laws of magnetic disturbance in the high latitudes, *Trans. Conf., Comm. Solar Research*, 22–24, 1955; or Academy of Sciences Press, Moscow, 159–166, 1957. Available as *Defence Research Board Translation T 321-R* (translator E. R. Hope).
Dessler, A. J., and E. N. Parker, Hydromagnetic theory of geomagnetic storms, *J. Geophys. Research*, *64*, 2239–2252, 1959.
Hakura, Y., Takenoshita, Y., and T. Otsuki, Polar blackouts associated with severe geomagnetic storms on Sept. 13, 1957, and Feb. 11, 1958, *Rept. Ionosphere Research Japan*, *12*, 459–468, 1958.
Hakura, Y., and T. Goh, Pre-SC polar cap ionosphere blackout and type IV solar radio outburst, *J. Radio Research Lab. Japan*, *6*, 635–650, 1959.
Harang, L., The mean field of disturbance of the polar earth magnetic storm, *Terrest. Magnetism and Atmospheric Elec.*, *51*, 353–380, 1946.
Hatherton, T., and G. G. Midwinter, Observations of the Aurora Australis at New Zealand antarctic stations during IGY, *J. Geophys. Research*, *65*, 1401–1411, 1960.
Lassen, K., Existence of an inner auroral zone, *Nature*, *184*, 1375–1377, 1959.
Loomer, E. I., K. Whitham, and E. R. Niblett, Record of observations at Yellowknife Magnetic Observatory, 1957-58, *Publ. Dom. Obs. Ottawa*, *24*, 9, 1960.
Mayaud, P. N., Magnetic activity in the polar regions, *Ann. géophys.*, *12*, 84–101, 1956.
Meek, J. H., The location and shape of the auroral zone, *J. Atmospheric and Terrest. Phys.*, *6*, 313–321, 1955.
Nikolski, A. P., Dual laws of the course of magnetic disturbance and the nature of mean regular variations. *Terrest. Magnetism and Atmospheric Elec.*, *52*, 147–173, 1947.
Nikolski, A. P., Geographic distribution of magnetic disturbance in the circumpolar region of the Arctic, *Doklady Akad. Nauk SSSR*, *109*, 939–942, 1956. Available as *Defence Research Board Translation T 232-R* (translator, E. R. Hope).
Nikolski, A. P., The world-wide distribution of magneto-ionospheric disturbance and aurora, *Doklady Akad. Nauk, SSSR*, *115*, 84–87, 1957. Available as *Defence Research Board Translation T 266-R* (translator, E. R. Hope).
Nikolski, A. P., Magnetic disturbance in circumpolar regions of the Arctic, *Problems of the North*, *1*, 116–132, 1958.
Obayashi, T., Entry of high energy particles into the polar ionosphere, *Rept. Ionosphere Research Japan*, *13*, 201–219, 1959.
Piddington, J. H., Geomagnetic storm theor *J. Geophys. Research*, *65*, 93–106, 1960.
Quenby, J. J., and W. R. Webber, Cosmic ra cut-off rigidities and the earth's magnetic fiel *Phil. Mag.*, *4*, 90–113, 1959.
Reid, G. C., and C. Collins, Observations of a normal VHF radio-wave absorption at mediu and high latitudes, *J. Atmospheric and Terres Phys.*, *14*, 63–81, 1959.
Rikitake, T., Anomaly of geomagnetic variatio in Japan, *Geophys. J. RAS*, *2*, 276–287, 195
Senko, P. K., Usual localized character of magnet variation in the Mirny Region, *Inf. Bull. Sovi Ant. Exp.*, 'Morskoi Transport' Press, Leningra 81–82, 1958. Available as *Defence Researc Board Translation T 319-R* (translator E. R Hope).
Siebert, M., and W. Kertz, On the analysis of local magnetic field of disturbance into extern and internal parts, *Nachr. Akad. Wiss.*, Götting *Math-Phys. Kl.*, *2a*, 87–112, 1957.
Stagg, J. M., The diurnal variation of magnet disturbance in high latitudes, *Proc. Roy. So London, A*, *149*, 298–311, 1935.
Vestine, E. H., and S. Chapman, The electr current system of geomagnetic disturbance *Terrest. Magnetism and Atmospheric Elec.*, *4* 307–382, 1938.
Vestine, E. H., L. Laporte, I. Lange, and W. E Scott, The geomagnetic field, its descriptio and analysis., *Carnegie Inst. Washington Pub 580*, 1947.
Vestine, E. H., Geomagnetic control of auror phenomena, *Proc. Symp. on Sun-Earth Env* Defence Research Board, Ottawa, Canada DRTE Publ. 1025, 157–164, 1960.
Whitham, K., and E. I. Loomer, A comparison o magnetic disturbance at Resolute Bay an Baker Lake, Canada, *Tellus*, *8*, 276–278, 195
Whitham, K., and E. I. Loomer, Characteristic of magnetic disturbance at the Canadian Arcti observatories, *Pub. Dom. Obs., Ottawa*, *18* 289–346, 1957*a*.
Whitham, K., and E. I. Loomer, Irregular magneti activity in northern Canada with special referenc to aeromagnetic survey problems, *Geophys.*, *22* 646–659, 1957*b*.
Whitham, K., and E. R. Niblett, The diurna problem in aeromagnetic surveying in Canad *Geophys.*, *26*, 1961.

(Manuscript received July 14, 1960; revise August 26, 1960.)

On a Sensitive Method for the Recording of Atmospheric Ozone

VICTOR H. REGENER

Department of Physics, University of New Mexico
Albuquerque, New Mexico

Abstract. A device is described which uses the luminescence of a dry substance in the presence of ozone for the automatic quantitative determination of minute concentrations of atmospheric ozone. The sensitivity of the device is extremely high and the response is instantaneous. Since there are no liquid chemicals, the method can be used at extreme heights in the atmosphere, and it is equally applicable to the continuous monitoring of ozone near the earth's surface.

Introduction. The need for a simple device ich would determine atmospheric ozone quan- atively and automatically in the highest lay- s of the atmosphere as well as near the surface l to the development of the described instru- ent. Chemical ozone recorders and sondes of e type designed by *Brewer, Milford, and iggs* [1960] and by *Regener* [1957, 1959] ke use of aqueous solutions of chemicals. ndes of this type are therefore limited to alti- des at which the solution does not boil. Opti- l ozone sondes of the spectro-photographic pe and of the spectro-photoelectric type, on e other hand, measure the integral amount of mospheric ozone above the sonde and there- re will never be capable of resolving the fine ructure of the vertical ozone distribution to e same extent as an instantaneously respond- g chemical sonde. The sonde described below dry, it is insensitive to NO_2, it requires no reparation before the flight other than a quick libration, and it responds instantly to varia- ons in ozone density. It lends itself to the con- nuous telemetering of the ozone density in ich a manner that ozone can be read directly n the record chart along with other meteoro- gical parameters.

The instrument. Figure 1 gives a schematic iagram of the ozone sonde in its present form. ize and weight of the sonde are 5 × 5 × 6 ches and 1100 grams, respectively, without hermal insulation. The power consumption is .4 watts. Air is aspirated from the outside at *A*, passes between the chemiluminescent disk *B* nd the sensitive face of the photomultiplier ibe *C*, and it enters a 'breather' pump consist- ng of a stationary external dish *D* and an internal dish *E*. A thin rubber sheet *F* seals dish *E* against dish *D*. The lever *G*, whose right-hand end rides on the rotating cam *H*, raises the dish *E* at a constant rate during the intake stroke. Ozone is measured by the constant amount of light emitted by the disk *B* during the 15-second duration of the intake stroke, which aspirates 100 cm³ of air. The luminescent reaction of the ozone is complete, a fact which is borne out by the absence of a signal during the return stroke of the valveless breather pump.

Disk *B* is coated with the luminescent material. It consists essentially of silica gel, upon which Luminol has been adsorbed from an alkaline solution. The silica gel used for this purpose

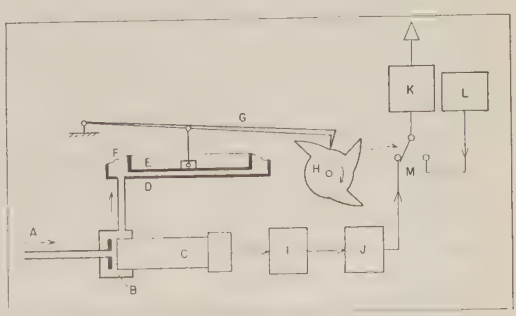

Fig. 1. Schematic diagram of dry chemiluminescent ozone sonde. *A*, air intake; *B*, chemiluminescent disk; *C*, photomultiplier tube (Dumont 6467); *D*, breather pump, outside dish; *E*, breather pump, inside dish; *F*, rubber sheet; *G*, lever; *H*, cam, 0.5 rpm; *I*, amplifier; *J*, audio-frequency modulator, 40 to 200 cps, controlled by ozone; *K*, radiosonde transmitter; *L*, radiosonde modulator, controlled by pressure, temperature and humidity; *M*, switch, operated by cam drive every 15 seconds.

is in the form of a fine powder. After the treatment with Luminol it is mixed with a small amount of a binder and a little water to form a paste which is applied to the plastic disk *B*. After drying, the white surface can be smoothed with sand paper.

The consumption of the active chemical on the luminescent disk is so slow that air containing about 200 micrograms of ozone per cubic meter can be aspirated past the disk at a rate of 500 cm³ per minute for several days without a substantial decrease of the light output. The quoted density of ozone is about 5 times larger than that found on the average in the atmosphere near the earth's surface, and about half as large as that found in the ozone maximum in the stratosphere. The Luminol appears to play the role of converting the energy made available by the destruction of the ozone molecule into photons, without being oxidized itself during the process at the expected rate. This is in contrast to the experience of *Bernanose and Réné* [1959], who attempted to use paper moistened by an alkaline solution of Luminol for the same purpose. Further work is planned to clear up this point.

The sensitivity of the luminescent disk to NO_2 was tested by adding this gas at a known rate to an air stream from which ozone had been removed previously. It was determined that there is luminescence with NO_2 also. However, the density of NO_2 in the air stream had to be 500 times larger than that of ozone to furnish the same amount of light. The response to atmospheric NO_2 is therefore negligibly small.

Changes of the temperature and of the relative humidity of the air containing the ozone do not appear to affect the sensitivity of the device substantially. Further work is planned to determine the extent of this independence on temperature and humidity.

The output of the photomultiplier tube is of the order of 0.5 microamperes at a potential difference of 110 volts between dynodes, when air containing 50 micrograms of ozone per cubic meter is drawn past the disk at a rate of 500 cm³/min. For balloon-borne ozone sondes, this signal is applied to a small electrometer tube which constitutes amplifier *I* in Figure 1. The output from this tube controls the audio frequency of the blocking oscillator *J*, and this audio signal is used to modulate the standard Weather Bureau radiosonde transmitter *K*. The

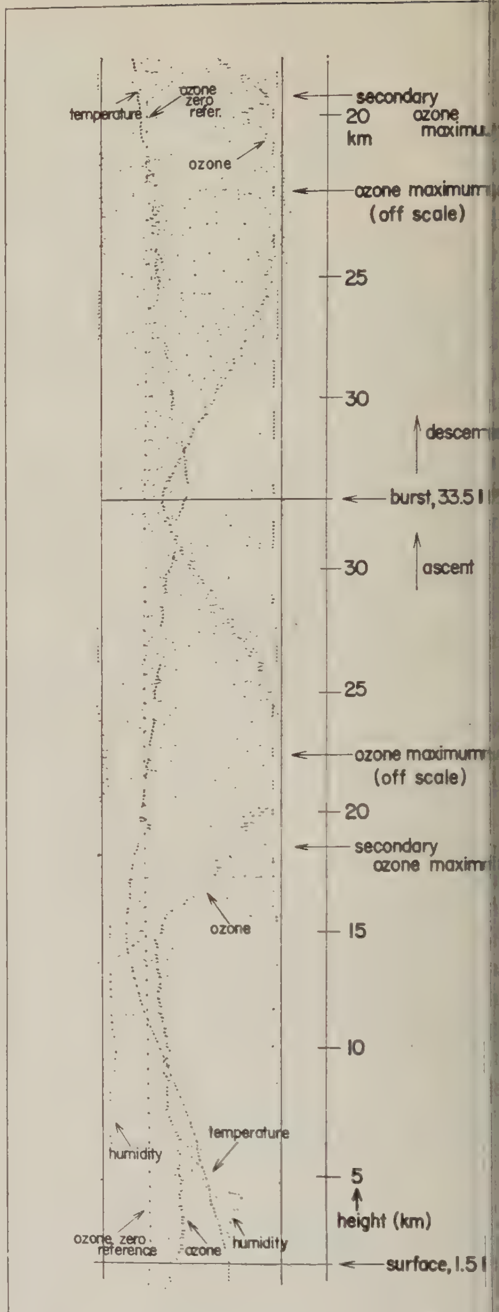

Fig. 2. Reproduction of original reco chart from balloon flight of July 6, 1960 Albuquerque, N. M. The principal ozon maximum at a height of approximately km is off scale. A narrow secondary maximu can be seen at a height of 18 km on ascen and descent. The ozone density is read fro left to right, starting at the 'ozone zero refe ence' line. The ozone density at the surfa was approximately 50 micrograms/m³.

eorological modulator unit L of the radio-le is connected to the transmitter K in al-ation with the ozone-controlled modulator very 15 seconds by means of the switch M. e switching sequence is accomplished by the or drive for the cam H in such a way that switch M connects the transmitter to the ne modulator J during the intake stroke of breather pump, whereas it connects the nsmitter to the meteorology modulator L at er times. Since the cam H rotates once in 2 nutes and since it has three instead of four n rises on its circumference, there will be ee ozone measurement periods of 15-seconds ation during every 2 minutes. During the ssing fourth ozone period the transmitter is o modulated by the photoelectric tube, but hout air being aspirated past the disk B. is procedure serves to transmit the 'ozone o reference' modulator frequency for one 15-ond period during every 2 minutes, as a eck on the proper functioning of the photo-ctric tube and the associated circuitry.

The flight record. Figure 2 is a photograph the original record chart obtained on July 6, 60, at Albuquerque, N. M. This is one of 15 t flights made so far. It reached a maximum itude of 33.5 km, as determined from the essure transmitted by the barograph. The nsitivity adjustment of the unit was somewhat gh on this particular flight, and the ozone ding went off scale in the region of the ozone aximum. The chart shows a considerable nount of detail of the vertical ozone distribu-on in the troposphere. Above the tropopause, e ozone density begins to rise. There is a condary ozone maximum at a height of 18 km during the ascent as well as during the descent. The slight shift in altitude on the two occasions is probably the result of barograph hysteresis. This secondary ozone layer is only 1 km thick in the vertical direction. It should be noted that during this particular flight the deflection on the chart is linear with respect to ozone density only up to one-half of the chart width. Beyond that, the sensitivity decreases as a result of the electrometer tube characteristic, and the right-hand edge of the chart was made to coincide with the maximum possible deflection, regardless of ozone density. In future sondes, the deflection will be made proportional to ozone density.

Acknowledgments. I appreciate the cooperation of Charles E. Williams. This work is sponsored by the Geophysics Research Directorate, Air Force Cambridge Research Laboratories, Air Research and Development Command, U.S.A.F.

References

Bernanose, A. J., and M. G. Réné, Oxyluminescence of a few fluorescent compounds of ozone, *Ozone Chemistry and Technology,* American Chemical Society, Washington, D. C., 7–12, 1959.

Brewer, A. W., J. R. Milford, and M. Griggs, An electrochemical ozone sonde, *IUGG Monograph 3,* 20–21, 1960.

Regener, V. H., Chemical telemetering sonde for balloon soundings of atmospheric ozone, *Sci. Rept. 1, contract AF 19 (604)–1950,* Air Force Cambridge Research Center, December 26, 1957.

Regener, V. H., Automatic chemical determination of atmospheric ozone, *Advances in Chemistry, Ser. 21,* American Chemical Society, Washington, D. C., 124–127, 1959.

(Manuscript received July 21, 1960; presented at the 12th General Assembly of the IUGG, August 4, 1960, Helsinki, Finland.)

The Coalescence of Water Drops in an Electric Field

GEORGE FREIER

School of Physics, University of Minnesota
Minneapolis, Minnesota

Abstract. Measurements have been made on large, freely falling drops interacting in a strong electric field. The measurements show definite coalescing effects due to the electric field, and the results can be interpreted as being due to induced dipole interactions. The effective radius of the drop can become 30 per cent greater than the geometrical drop radius when interactions take place in electric fields between 1 stat volt/cm and 10 stat volts/cm.

troduction. *Lord Rayleigh* [1879, 1882] rmed many experiments describing the na- of jets of water running in an electric field. pointed out that similar phenomena might ribute to processes involved in rainfall. *egut, Moore, and Botka* [1959] made stud- f this process carried out in nature. *Lang-* [1948] considered the hydrodynamics of s in relative motion through a viscous um and introduced the concept of collec- efficiency. Measurements such as those by *n and Hitschfeld* [1951] verified Langmuir's k, but measurements were made in the ab- e of an electric field. *Sartor* [1954] per- ed detailed model studies on colliding drops suggested a mechanism for drop charging would aid coalescence. *Sartor* [1960] made her computations on small droplets in rela- motion in an electric field and found that e should be enhanced coalescence in an elec- field. The experiment described in this paper one in which direct measurements were le on drops freely falling in air and sub- ed to strong electric fields.

heory. If a stream of droplets of uniform is projected obliquely upward into the air, y will travel in a parabolic trajectory of zontal range s and height h. If the drops are jected at regular intervals of time τ, the cing between the drops will be large where velocity is large and smaller near the top ere the velocity reaches a minimum. If the ps do not interact, the spacing along the h will increase on the descending branch of parabola. If there is an attractive short- ge interaction between the drops, there will a tendency for the drops to form pairs. The first drop in a sequence will pull the second drop closer to it and away from the third drop, and the third drop can repeat the process with the fourth drop, etc. A study of this pairing should give some insight into the nature of the force producing the pairing. The process described above is shown in Figure 1.

Any pair of these drops may then be approximately treated as a dynamic system. If each drop were projected with a vertical component of velocity v_{y0}, then at any time t after projection, its vertical component of velocity would be $v_y = v_{y0} - gt$. The second drop which is projected at a time τ later will have a vertical velocity of $v_y = v_{y0} - g(t - \tau)$. If the two drops are of equal mass, the vertical velocity of the center of mass of these two drops is $v_{cm} = v_{y0} + (g\tau/2) - gt$. With respect to this center of mass, the first drop will have a vertical velocity of $-g\tau/2$, while the second drop has a vertical velocity of $+g\tau/2$. If m is the mass of each drop, the kinetic energy available in the interaction is $m(g\tau/2)^2$, since no energy associated

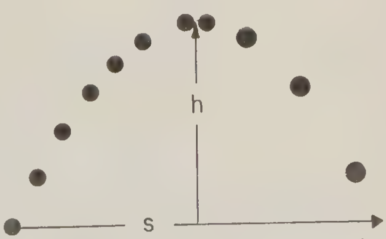

Fig. 1. Sketch of parabolic path having range s and height h. The sketch shows how the drops tended to pair and then coalesce at the top so that there are half as many drops on the descending branch as on the ascending branch.

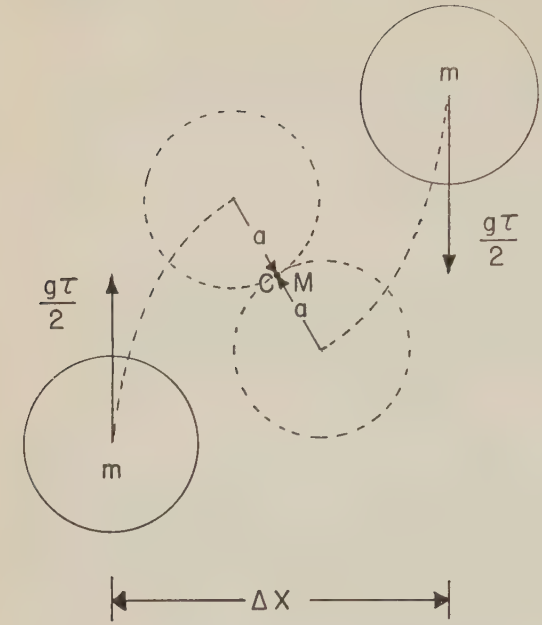

Fig. 2. Interaction of two drops as seen from the center-of-mass coordinate system. Each drop of mass m has a velocity of $g\tau/2$. The initial energy of the two-drop system is $m(g\tau/2)^2$, and the initial angular momentum is $m\Delta x\ g\tau/2$. An attractive force could produce the collision course shown in dashed lines.

with the motion of the center of mass is available in the interaction.

In the horizontal direction each drop has an initial velocity v_{x0}, which is also the horizontal velocity of the center of mass of the two drops. The interaction is internal to the two-drop system and cannot change the horizontal motion of the center of mass. The original horizontal spacing between the drops is $\Delta x = v_{x0}\tau$. We may then consider a process as shown in Figure 2 in which the motions are all designated with respect to the center of mass. The fact that we are in a coordinate system having an acceleration g will make the two drops weightless.

A force that would make the pair of drops coalesce will bend their trajectories toward the center of mass until they collide. If the original horizontal separation Δx is greater than $2a$, where a is the radius of the drop, and if we observed coalescence, then we could infer that there was some attractive force between the drops. A measurement of $\Delta x/2a$ would give some insight regarding the strength and range of the force.

If this interaction takes place in a st[…] electric field, we would expect the drops to [...] the induced dipole moments given by *Joos* [1[…] p. 291], $M = a^3E_o\ (K-1)/(K+2) \simeq$ [...] where a is the drop radius, E_o is the ap[…] field, and K is the dielectric constant of the [...] terial of the drop. The above equation is fo[…] isolated drop in the field, and a second drop [...] certainly alter the equation, but for simpl[…] in describing the experiment we shall ass[…] that the equation holds. To this approxima[…] two interacting drops will have their di[…] moments parallel to each other and parall[…] the applied field E_o. The potential between [...] such drops is given by *Smythe* [1939]: [...] $(M_1M_2/r^3)\ (1 - 3\cos^2\theta)$, where θ is the a[…] between the moments or field and the ra[…] vector r connecting the two drops. This po[…] tial leads to a radial force, $F_r = (3M_1M$[…] $(1 - 3\cos^2\theta)$, and a force in the direction o[…] creasing θ, $F_\theta = (6M_1M_2/r^4)\ \cos\theta$ si[…] These equations for the forces, although [...]

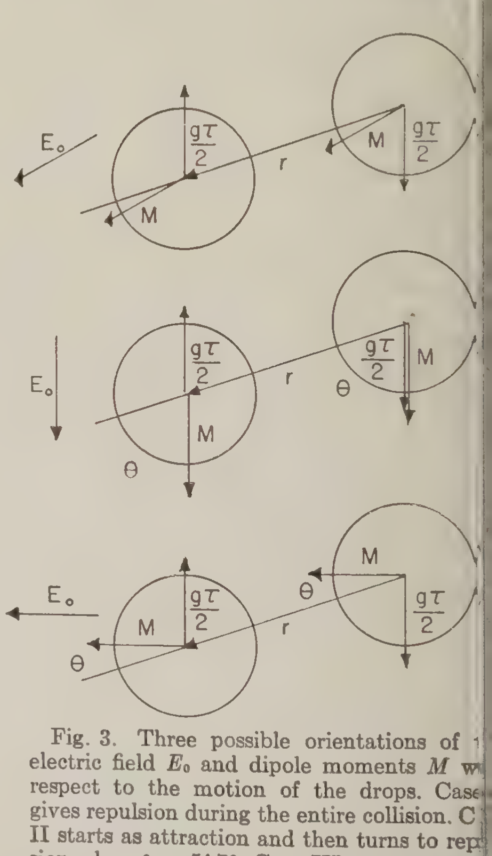

Fig. 3. Three possible orientations of [...] electric field E_0 and dipole moments M w[…] respect to the motion of the drops. Case [...] gives repulsion during the entire collision. C[…] II starts as attraction and then turns to rep[…] sion when $\theta = 54.7°$. Case III starts as rep[…] sion and then turns to attraction at $\theta = 54$[…]

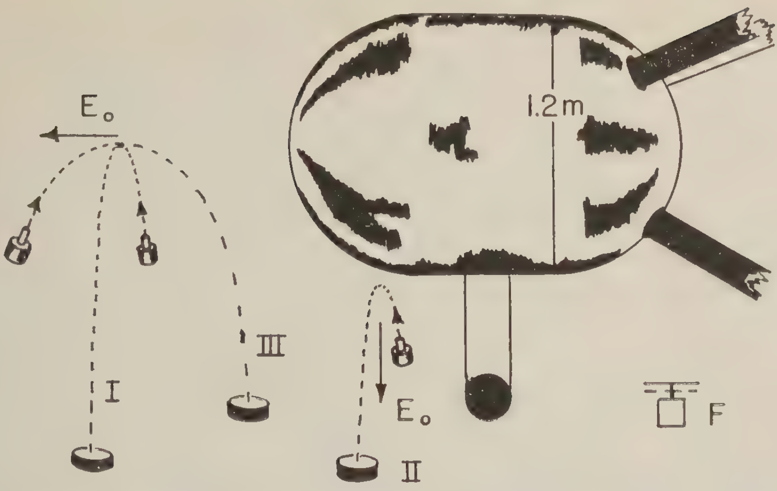

Fig. 4. Diagram showing how data were taken at various points around the machine. Case I has the electric field perpendicular to the plane of the trajectories and perpendicular to the radius vector between any two interacting drops. Case II has the electric field parallel to the relative motion of the drops and in the plane of the trajectory. Case III has the electric field perpendicular to the relative motion of the drops and in the plane of the trajectory.

antitatively applicable at small distances, can used qualitatively to determine three different nbinations of attractive and repulsive forces tween the drops during their interaction in e electric field. Figure 3 shows the three cases at can be studied for the pairs of interacting ops. Case I shows both moments perpendicu-r to the plane of the trajectories. In this case e radial force is repulsive throughout the in-raction, because $\theta = 90$ for all relative posi-ns of the two drops. Case II shows both oments parallel to the direction of motion. re θ is initially small, so the radial force is tially attractive. When $\theta = 54.7°$ the force anges from attractive to repulsive. Case III ows the moments at right angles to the direc-n of motion but in the plane of motion. Here is initially at 90°, so the force is initially re-lsive. At $\theta = 54.7°$ the force changes from pulsive to attraction. The more complex prob-m of calculating the forces down to small parations has been done for a special case by *rtor* [1959].

Experimental arrangement. To produce all e theoretical conditions, we applied an elec-ic field over a region of space sufficiently large allow us to set up parabolic trajectories of ater. An open-air electrostatic generator with hell 1.2 meters in diameter was placed in a gh-ceilinged room. The shell had a cylindrical section between the hemispherical ends where the charging belt could be placed without disturbing the approximately spherically-symmetrical ends. The geometry of the machine and the orientation of the trajectories in the three cases is shown in Figure 4. A field mill at *F* measured the field at that position, and field values at other points were calculated by the inverse square law. The field varied throughout the trajectory of the water drops, but most of the interaction occurred at the top of each trajectory where the drops were close together. Quoted values of the field are for the point determined by the vertex of the parabolic trajectory, and care was taken to have sufficiently large trajectories so that field distortions caused by the projecting nozzles would be minimized. The trajectory ran sufficiently close to the machine to make the field at the trajectory vertex be primarily determined by the geometry of the end of the machine. Errors in the field measurement are estimated to be ±20 per cent. These close trajectories also made it easy to test for no charging of the drops, as charging of the drops became apparent by the drops following a different trajectory when the field was turned on.

The drops were projected by a shaker as shown schematically in Figure 5. A 110-volt solenoid with a soft iron core was driven by a

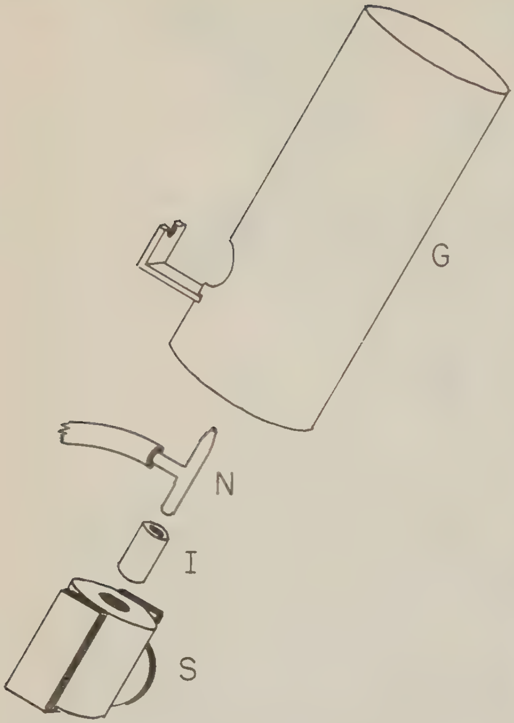

Fig. 5. Diagram of shaker. The solenoid S holds the iron slug I which in turn carries the glass nozzle N. The shield G prevents charging of the drops by induction as they leave the nozzle in the electric field of the machine.

variac. The iron core was counter-bored to hold a sealed end of a glass T. The other end of the T was drawn to a nozzle with a 1.6-mm-diameter hole. The side arm on the T was connected to a jug of water maintained at constant water level. When the parabola height had been chosen, the variac was adjusted to give a stream of drops of uniform size at a rate of 120/sec, so $\tau = 1/120$ sec. The stream was shielded by a screen cylinder 15 inches long and 3 inches in diameter. This shielding prevented charging of drops by induction processes.

In producing a jet such as this, there is a tendency to get small drops between the large drops. With no field, these small drops have a slightly different trajectory from that of the large main drops and cause a ragged or fuzzy beam. As soon as the field reaches about 0.15 stat volts/cm, the large drops absorb most of the small drops before the strong interaction takes place between the large drops at the top of the trajectory. If the beam is viewed wi
fast stroboscope very few of the small drop
seen in the region near the top of the trajec
The general appearance of the beam is tha
much tighter and well defined when this
field is applied. Observations with zero fiel
subject to a much greater error and are n
cluded in the report.

The pairing of the drops and coalescence
nomena were detected by viewing throu
rotating disk cut as shown in Figure 6. The
was driven at 1800 rpm, so that when vi
through the four-opening circle the stream
seen 120 times per second; and while vi
through the two-opening circle the stream
seen 60 times per second. By moving one's
slightly, the viewing frequency could be ch
from 120 to 60 cps. If the drops coalesced a
top of the trajectory, the number per unit l
of the path would be half as great on the d
ward branch of the parabola. The viewing
cps appears the same as the viewing at 12
when there is no coalescence. When the
coalesce in pairs, a sharp contrast betwee
viewing at 120 cps and at 60 cps is seen.

The data were taken in the following
The rate of flow was adjusted to make the
est point of the parabola at the desired
in the field of the machine. The shaker was
adjusted to give a good clean beam of indi
drops. With the machine turned on, the sh
the trajectory was varied until we just ob

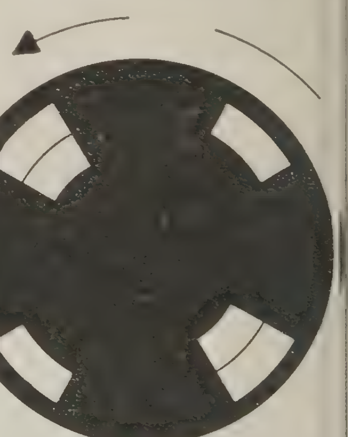

Fig. 6. Viewing disk which was rotate
30 rev/sec. The stream could be seen
times per second through the outer circl
openings and 60 times per second through
inner circle of openings.

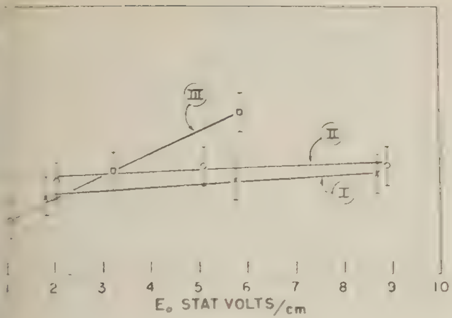

ig. 7. Typical results for measurements of /2a as a function of the electric field strength nits of stat volts/cm.

scence at the top of the trajectory. The neters, s and h, of the trajectory were then ured. When the field of the machine was , the parameters, s and h, of the la were readjusted until coalescence oc- d in the same way as that for the lower . In all cases the parabola had to have a r trajectory for a higher field, but the unt of flattening was different for the dif- t cases.

hroughout the experiment, $\tau = 1/120$ sec, is was the only frequency at which sufficient r to drive the shaker could be obtained. drop size was obtained by measuring the me rate of flow f, the radius of the drop then given by $a = (3f\tau/4\pi)^{1/3}$. The initial ontal distance Δx between the drops was n by $\Delta x = (\tau s/2)(g/2h)^{1/2}$. The value of 2a was then calculated and found to be a measure of the effectiveness of the coalescing forces.

The absence of charge on the drops could be detected by no additional deflection of the trajectory in the strong electric fields. A secondary test was made by letting the drops fall into a special counter connected to a model 100 amplifier which drove a model 200 pulse height analyzer [*Elmore and Sands*, 1949]. The charge on any one drop was not greater than 10^3 electronic charges.

Results. Typical results are shown graphically in Figure 7 and listed in Table 1, for each of the three cases. Each of the curves could have been shifted up or down slightly, depending on the criteria selected for coalescence, but once the criteria were determined for any set of runs the slope of the curve remained the same. Most of the measurements were made with tap water, since no difference in the results was detected for distilled water or water containing ammonia. There is no physical reason for drawing straight lines through the data points.

A poor assumption in the handling of the data is that the drops are spherical. When drops are produced by a shaker, they vibrate with rather large amplitude, and this oscillation persists throughout the trajectory. However, the amount of oscillation is the same for any one sequence of data points, so the coalescing observations due to the electric field should be independent of the oscillations.

Discussion. It is difficult to obtain the value of the force directly from the measurements,

TABLE 1. A Set of Typical Values for the Three Types of Measurements

Case	s, cm	h, cm	f, cm³/sec	a, cm	Δx, cm	E, st volts/cm	$\Delta x/2a$
I	37.3	34.5	7.35	0.245	0.585	2.0	1.19
	38.0	34.4	7.34	0.245	0.597	5.1	1.22
	38.0	34.3	7.31	0.245	0.597	7.9	1.22
II	37.6	36.8	7.53	0.247	0.571	1.8	1.16
	38.4	36.6	7.43	0.246	0.585	5.8	1.19
	39.0	36.6	7.50	0.246	0.595	8.7	1.21
III	42.0	48.1	8.07	0.251	0.557	1.0	1.11
	45.5	47.5	8.10	0.251	0.609	3.2	1.21
	48.5	45.0	8.13	0.251	0.665	5.8	1.33

= range of trajectory; h = height of trajectory; f = flux of water from nozzle; a = radius of drop; = horizontal spacing of drops; E_0 = value of electric field at top of the trajectory.

since the drops coalesce after following different trajectories for different values of the field. In the center-of-mass coordinate system, the kinetic energy at large separation of the drops is $m(g\tau/2)^2$. The potential energy V is a function of both r and θ but should be proportional to E_0^2 and a^6; this results from the product of the induced dipole moments. The collisions take place at a definite value of $r = R$ for all trajectories, but θ may be different for each collision trajectory. If v is the velocity of the drops at the point of collision, the energy equation would be $m(g\tau/2)^2 = mv^2 + V$. The angular momentum before the collision is $m\Delta x g\tau/2$, and the angular momentum at the collision point should be mvR. The nonradial forces may change the angular momentum by the amount ΔJ, so the angular momentum equation becomes $m\Delta x g\tau/2 + \Delta J = mvR$. If this equation is solved for v and substituted into the energy equation, we obtain

$$m\left(\frac{g\tau}{2}\right)^2 = m\left(\frac{\Delta x\ g\tau}{2R} + \frac{\Delta J}{mR}\right)^2 + \frac{E_0^2 a^6}{R^3}(1 - 3\cos^2\theta)$$

Even if ΔJ is small, we can see why the value of $\Delta x/R$ is not simply proportional to E_0^2. The oscillations of the drops will undoubtedly make $R > 2a$, so with this further uncertainty it seemed that a more detailed analysis was not warranted.

Rather large amounts of energy are released when two drops of equal size coalesce. If we assume that the drops before collision were spheres of radius a, the surface energy of each drop would be $4\pi a^2\Gamma$, where Γ is the surface tension. The coalesced drop would have a surface energy of $4\pi a'^2\Gamma$, where $a' = 2^{1/3}a$. The difference of these energies plus $m(g\tau/2)^2$ can show up as rotational energy, vibrational energy, or heat energy in the coalesced drop. (In separate experiments on freely falling, oscillating drops I have found that the energy of oscillation is not readily converted to heat energy of the drop.) *Lord Rayleigh* [1945] solved the problem of oscillating drops, and for the lowest mode of vibration the radius of the drop may be written as $r = a_0 + A\cos\omega t P_2(\cos\theta)$, where $P_2(\cos\theta)$ is a second Legendre polynomial giving the shape of the drop and $\omega = (8\Gamma/\rho a^3)^{1/2}$. The total energy W of the oscillating drop in the

TABLE 2. Table of Various Forms of Energy Corresponding Amplitude of Oscillation To Be pected if Drop Oscillates in Its Lower Mod

a, cm	$4\pi a^2\Gamma$, ergs	a', cm	W, ergs	A, cm	$m(g$ er
0.245	54.2	0.308	22.2	0.248	1.
0.246	54.2	0.310	21.2	0.248	1.
0.251	56.9	0.316	23.3	0.252	1.

lowest mode is $W = (8\pi\Gamma/5)A^2\cos^2\omega t + (\pi a^3/$ $\sin^2\omega t$. If the difference in surface tension en all goes into oscillation of the lowest mod can evaluate the amplitude A:

$$\frac{8\pi\Gamma A^2}{5} = 4\pi a^2[2 - 2^{2/3}]\Gamma \quad \text{or}$$

$$A = 1.01a = 0.$$

These energies have been calculated for drops used in this experiment and are list Table 2. The value of A is equal to 0.80 t the radius of the drop, and this violates so the assumptions in the derivation of the a equations. In any case, the fact that the os tions are very large was verified by obs tion with a fast stroboscope. The drops w retain the energy of oscillation throughou remainder of their fall without flying apart with undetectable damping of the amplitu

The uncertainties in the measurements d allow any definite conclusions to be d about case I or case II, in which the forces are primarily repulsive during the i action. In case III the potential energy is likely negative at the time of coalescen $\simeq 0$), and the effects of the electric fiel definite.

The fact that none of the curves extrap to $\Delta x/2a = 1$ at $E_0 = 0$ can be explain part by the fact that the oscillations o drops make $R > 2a$.

We might argue that, since high fields c spond to flatter trajectories, the drops are s ing more time in the higher fields. The ti flight actually becomes less for the flatte jectories. Also, in the center-of-mass coor system, the relative velocities of the drop completely independent of the shape o trajectory.

Conclusion. The measurements show freely falling drops tend to coalesce in an

field and that electric fields which are nsverse to the relative motion of the drops in the plane of the relative motion are most ctive in producing coalescence. Furthermore, coalescence is accomplished over distances separation which increase with increasing ld strength. The oscillations of drops can conute to the collision cross section even at zero ld.

cknowledgments. I wish to thank Mr. R. B. rness for aid in construction of equipment and Paul Hill for aid in taking the data.

his work was supported in part by grants from Ohio Oil Company and the National Science ndation.

References

ore, W., and M. Sands, *Electronics,* McGraw-Iill Book Co., New York, 417 pp., 1949.

n, K., and W. Hitschfeld, A laboratory investiation of coalescence between large and small ater drops, *J. Meteorol., 8,* 7–16, 1951.

s, G., *Theoretical Physics,* G. E. Stechert and ompany, 748 pp., 1934.

gmuir, I., The production of rain by a chain reaction in cumulus clouds at temperatures above freezing, *J. Meteorol., 5,* 175–192, 1948.

Rayleigh, Lord, The influence of electricity on colliding water drops, *Proc. Roy. Soc. London, 28,* 406–409, 1879.

Rayleigh, Lord, Further observations upon liquid jets, *Proc. Roy. Soc. London, 34,* 130–145, 1882.

Rayleigh, Lord, *Theory of Sound,* vol. II, Dover Publications, New York, 504 pp., 1945.

Sartor, J. D., A laboratory investigation of collision efficiencies, coalescence, and electrical charging of simulated cloud droplets, *J. Meteorol., 11,* 91–103, 1954.

Sartor, J. D., The mutual attraction of cloud droplets in the electrostatic field of the atmosphere, *RAND Corp., P-1824,* 1959.

Sartor, J. D., Some electrostatic cloud-droplet collision efficiencies, *J. Geophys. Research, 65,* 1953–1957, 1960.

Smythe, W. R., *Static and Dynamic Electricity,* McGraw-Hill Book Co., New York, 560 pp., 1939.

Vonnegut, B., C. B. Moore, and A. T. Botka, Electrification and precipitation in thunderstorms, *J. Geophys. Research, 64,* 347–357, 1959.

(Manuscript received August 17, 1960; revised September 22, 1960.)

Fission Product Radioactivity in the Air along the 80th Meridian (West) During 1959

L. B. LOCKHART, JR., R. L. PATTERSON, JR.,
A. W. SAUNDERS, JR., AND R. W. BLACK

U. S. Naval Research Laboratory
Washington, D. C.

Abstract. The program of measurement of the fission product concentration in the air at ground level at sites along the 80th meridian was continued during 1959. During this period no fresh nuclear debris was added to the atmosphere, with the result that seasonal changes in deposition rates from stratospheric sources were more apparent.

The radioactivity levels in the northern hemisphere reached the highest average during the operation of this network (started May 1956) in the spring of 1959. Radiochemical analyses indicated that the bulk of this debris was introduced into the stratosphere during the October 1958 series of high-yield nuclear tests held in the arctic region of the Soviet Union.

Evidence has been obtained of a definite seasonal dependence for stratospheric deposition, with debris in the arctic stratosphere being more strongly influenced than that in the tropic stratosphere. No such definite conclusions can be made from radioactivity collected in the southern hemisphere.

Evidence is presented that mixing of the stratospheric sources in the northern hemisphere was not complete by the end of 1959; and though radioactivity levels in the two hemispheres were approaching unity in late 1959, the isotopic composition of the collections indicated that the average age of the debris in the southern hemisphere was much greater.

INTRODUCTION

he program of measurement of the fission duct radioactivity in the air at ground el along the 80th meridian, initiated in 1956 l conducted during 1958 as part of the ernational Geophysical Year Program on nospheric Nuclear Radiation, was continued ing 1959 as part of the International Geo- ysical Cooperation–1959 Program.

Studies of atmospheric radioactivity and out made at the U. S. Naval Research boratory [*Lockhart, Baus, Patterson, and unders*, 1960] and elsewhere during the past v years have disclosed that a stratospheric rce of radioactive debris from large yield clear weapons exists. A number of questions ve been raised about the residence time of s debris in the stratosphere before it appears the lower atmosphere (and as fallout) and out the mechanism by which the mixing urs. It has been strongly suggested from t studies that variation in deposition is sonal; however, the presence of tropospheric tamination from other nuclear tests has vented any unambiguous results from being tained. The moratorium on nuclear tests, beginning in November 1958 and extending throughout 1959, has afforded an opportunity for a definitive study.

EXPERIMENTAL PROCEDURE

Daily samples were collected at each cooperating site along the 80th meridian by the filtration of about 1200 cubic meters of air during a 24-hour period. These samples were returned by air to NRL where they were ashed at 650°C in a furnace, compressed into pellets, and assayed for gross β activity two weeks after collection. Radiochemical analyses were performed on monthly collections from each of several representative sites.

Well-tested radiochemical separation and purification procedures were employed and standard β-counting equipment and techniques were used [*Baus, Gustafson, Patterson, and Saunders*, 1957]. The counting error was kept as small as was practical by the use of long counting times and, on occasion, by the use of low-background counters of high sensitivity. The statistical error in counting was usually maintained at less than ± 1 per cent (standard deviation). The cases in which this error was exceeded were

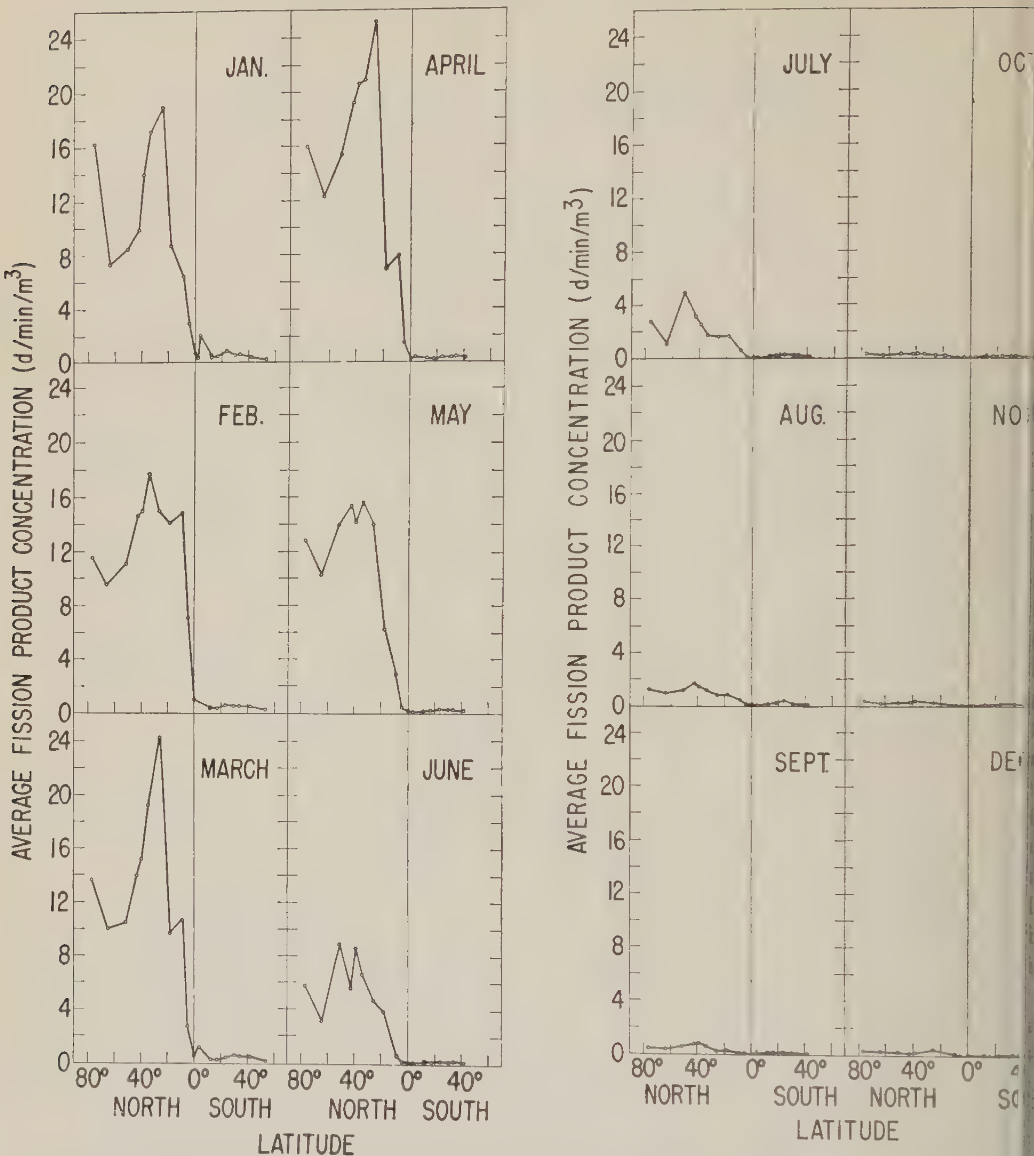

Fig. 1. Profiles of gross fission products in the air along the 80th meridian during 1959: (a) January–June; (b) July–December.

due principally to the absence of sufficient activity in the sample at the time of counting to give the desired accuracy; rarely, low chemical recoveries of the isotope have been the cause of the low activity.

All additional sources of error were held to a minimum: air flow rates were known to within ±3 per cent, chemical recoveries were determined to within ±0.2 per cent and corrections made for the fraction of sample counted, and equipment standardization was estimated to within ±10 per cent of the absolute (relative to one another, counts of a isotope remeasured at different times an different equipment agreed within the exp statistical variation of counting rates). C to the shortage of time and the lack of sui samples, no extensive series of replicate ana were made. However, the similar pattern activity encountered in samples from neighb

s and the corresponding consistency in ous counting-rate ratios indicated a high r of reliability in the analytical results.

Results

ross fission product concentrations in the air. nthly profiles of gross fission product con- trations in the ground-level air along the h meridian are shown in Figure 1. The ivity in the northern hemisphere during uary and February continued at the high els reached following the fall 1958 series of s in the Soviet Union. March and April wed progressive increases in airborne fission duct radioactivity, with April having the hest levels recorded in the north temperate e since this network was established in 1956. ere was an abrupt change in May, with the ivity beginning a rapid decline. This decrease m May through September was at the rate about 50 per cent per month, giving an ctive maximum residence half-time of 30 ys for tropospheric debris. The occurrence of y stratospheric leakage at all during this riod would have implied that the actual idence half-time for tropospheric debris due normal deposition processes is less than 30 ys during this season of the year. This depletion e was evident in the air concentration of such her activities as Sr^{90}, Cs^{137}, and Ce^{144}. In cember 1959 and in early 1960 there were lications of the beginning of another seasonal rease in radioactivity.

In the southern hemisphere, fission product tivity levels became progressively smaller as e year advanced; during the last part of the ar they were so low that reliable measure- ents could not be made. In January–March 59 there were indications that northern- misphere activity had penetrated as far south Quito, Ecuador, and Iquitos, Peru, east of e Andes. However, in April and May there s a sharp gradient near the equator with corresponding radioactivity south of the uator. Recently reported measurements of ^{90} in soil and bone samples from Ecuador *rench*, 1960] indicate higher values east of e Andes, a possible indication of greater netration of northern-hemisphere air into this gion.

Radiochemical analyses. The results of the diochemical analyses of composite monthly r-filter collections made during 1959 are tabulated elsewhere [*Lockhart, Patterson, Saunders, and Black*, 1960*b*].

Strontium 90 in the air. For several successive spring seasons there has been a peak in the air concentration of Sr^{90} in the northern hemisphere. Because, before 1959, the occurrence of nuclear testing usually coincided with this period of high Sr^{90} activity, it was impossible to assign the increased activity to a purely stratospheric source. Following the moratorium on nuclear testing, effective November 3, 1958, a strong maximum in the concentration of Sr^{90} in the ground-level air in the spring of 1959 was observed, and it is unambiguously assignable to a stratospheric source. Monthly changes in the air concentration of Sr^{90} at sites in the north temperate zone during 1958 and 1959 are shown in Figure 2. The high concentration of Sr^{90} in 1959, nearly twice as high as in 1958, was due primarily to the Soviet arctic series of tests of September 30–November 3, 1958. This assignment has been made on the basis of Sr^{89}/Sr^{90} activity ratios.

The rapid decrease in Sr^{90} concentration in the ground-level air after May 1959 corresponded to that observed for the gross fission products. Residence half-times for gross fission products and for several radioisotopes in the air of the north temperate zone have been calculated for the periods May–July and May–September on the assumption that no debris from a strato-

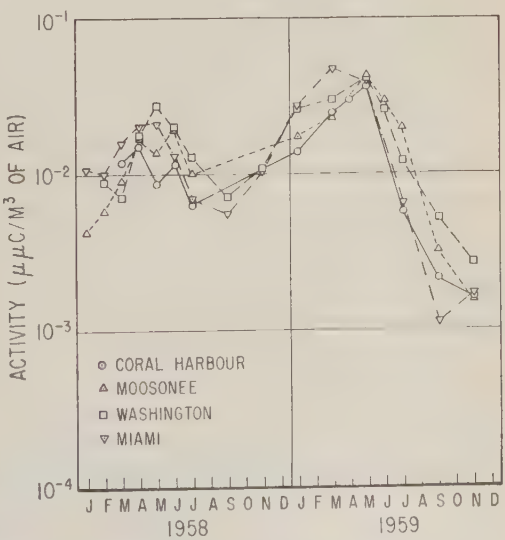

Fig. 2. Monthly changes in the Sr^{90} concentration in the air of the north temperate zone.

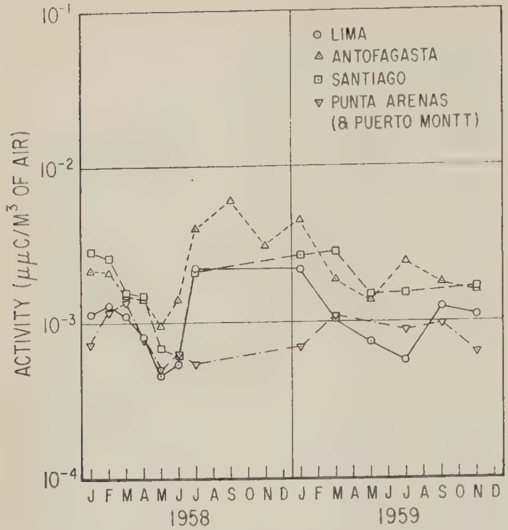

Fig. 3. Monthly changes in the Sr^{90} concentration in the air of the southern hemisphere.

spheric source entered the troposphere after May 1959. Although this is certainly an oversimplification of the actual processes, it does allow an estimate to be made of a maximum residence time for tropospheric debris or, equivalently, a minimum rate for the normal deposition processes acting during this period. The results shown in Table 1 indicate about a 30-day residence half-time for fission products in the troposphere during this season. The W^{185} results indicate a somewhat longer residence half-time, which implies the continued leakage of Hardtack debris into the troposphere after the effective cutoff date of entry of the bulk of the fission products. (Hardtack debris was tagged uniquely with W^{185} [*Lockhart, Baus, Patterson, and Saunders*, 1959]. Since debris from Hardtack was a minor contributor to the radioactivity in the northern hemisphere in May 1959 [*Lockhart, Patterson, Saunders, and Black*, 1960*a*], the fission products associated with this W^{185} would not greatly affect the apparent residence time of the fission product conglomerate). These data, then, indicate a strong seasonal variation in downward mixing from the stratospheric source, with the seasonal effect more pronounced in arctic than in tropic regions. This interpretation is consistent with the atmospheric circulation processes described by *Machta and List* [1958].

Monthly changes in the Sr^{90} concentration in

TABLE 1. Residence Half-Time of Tropospl[...]
Debris in the Northern Hemisphere during [...]
the Summer of 1959

		Half-Time in Days*			
Station	Season	Gross β	Sr^{90}	Cs^{137}	Ce^{144}
Coral	May–July	21	23	24	24
Harbour	May–Sept	30	30	28	27
Moosonee	May–July	52	56	58	53
	May–Sept	30	33	35	30
Washing-	May–July	28	35	35	32
ton	May–Sept	36	42	39	36
Miami	May–July	22	24	27	21
	May–Sept	23	24	25	22

* Corrected for radioactive decay (half-life [...] months assumed for gross fission products).

the air of the southern hemisphere are presen[...] in Figure 3. The expected spring maximum[...] 1958 was obscured by contamination from [...] U. S. Hardtack tests and, particularly, fi[...] British tests held in the Christmas Island a[...] in August and September 1958. During 1[...] there was no consistency in the pattern [...] change in the Sr^{90} concentration at the vari[...] sites in South America, which would substant[...] the existence of a seasonal effect there.

Contribution of Sr^{90} to the gross fission pro[...] activity in the air. The fission product mixt[...] that results from the detonation of a nuc[...] device exhibits an initially rapid decay wh[...] decreases in rate as the shorter-lived fiss[...] products die out. Since Sr^{90} is long lived, [...] fractional contribution to the total activity [...] the mixture increases with the age of the deb[...] The effect of this aging process is shown [...] Figure 4, in which the measured contribut[...] of the Sr^{90}–Y^{90} pair to the gross β activity [...] plotted against the month of collection. [...] spite of rather large variations within eit[...] hemisphere, the grouping of the curves indic[...] a decided difference in Sr^{90}–Y^{90} content ([...] hence in age) of airborne debris in the [...] hemispheres, with the oldest debris appea[...] south of the equator.

The scale on the right in Figure 4 indic[...] an apparent age in days which is based on [...] calculated contribution of Sr^{90}–Y^{90} to the g[...] fission product mixture at various times a[...] fission. The age assignments appear reasona[...] in light of the possible sources of the fiss[...]

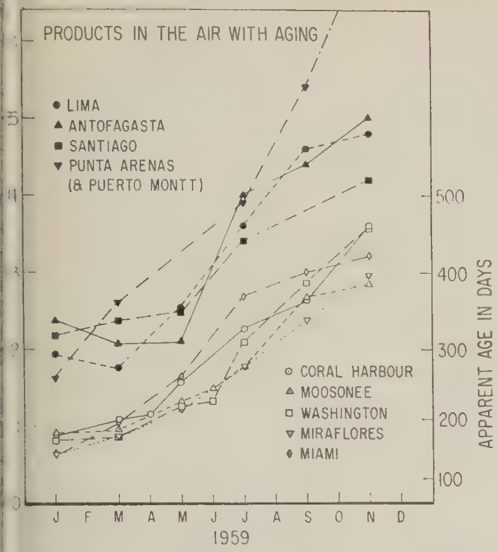

Fig. 4. Progressive increases in the contribution of Sr^{90}–Y^{90} to the gross fission products in the air with aging.

bris; however, this appearance of correctness ay be fortuitous.

Age of fission product debris in the air near ound level. Fission product ratios can gener-y be employed to give reasonably accurate timates of the time of fission when the kind material under going fission and the reaction nditions are known. However, the presence of bris from several sources of unannounced aracter and the ever-present possibility of actionation (deposition of different isotopes at fferent rates) makes difficult any such dating nuclear debris collected from the atmosphere. here are times, though, when debris from a ngle source (or a short series separated in time om other such series) may be so prominent relation to the background activity that ssion product ratios can be useful for dating e series.

The Sr^{89}/Sr^{90} activity ratio is particularly eful in dating, since this ratio is relatively sensitive to the conditions of fission and to actionation (both isotopes have gaseous pre-ursors and are identical chemically) and be-ause the Sr^{89} has a convenient half-life (51 ays). The changes in this activity ratio at ur sites in the north temperate zone during 59 are shown in Figure 5. During the spring d early summer this ratio decayed with the xpected half-life of 51 days, indicating that uring this period a single source or a well-mixed conglomerate from two or more sources in a fixed proportion was supplying the activity. The contribution of the most recent source of activity can be estimated by extrapolating the 51-day decay curve shown back to the value expected at zero time, i.e., the date of fission. On October 15, 1958, roughly the midpoint of the fall Soviet series in the Arctic, the extrapolated value of the Sr^{89}/Sr^{90} activity ratio was 140, which may be compared to a ratio of 182 for the fast neutron fission of U^{238} [*Katcoff*, 1958]. If the contribution of Sr^{89} from sources prior to the Soviet series of September 30–November 3, 1958, is neglected, an estimate is obtained that 75 to 80 per cent of the Sr^{90} activity appearing in the northern hemisphere during the spring of 1959 was produced in this series. The activity ratios for January and September indicate the presence of a higher percentage of old debris at these times; results to be discussed later show the contribution of Hardtack debris to have been more significant at these times.

The Sr^{89}/Sr^{90} activity ratios at four sites in the southern hemisphere (Fig. 6) show an entirely different pattern. A great influx of younger debris was evident during the period March–July 1959, with a resulting increase in the Sr^{89}/Sr^{90} ratio followed by a slower rate of influx during September–November 1959. From

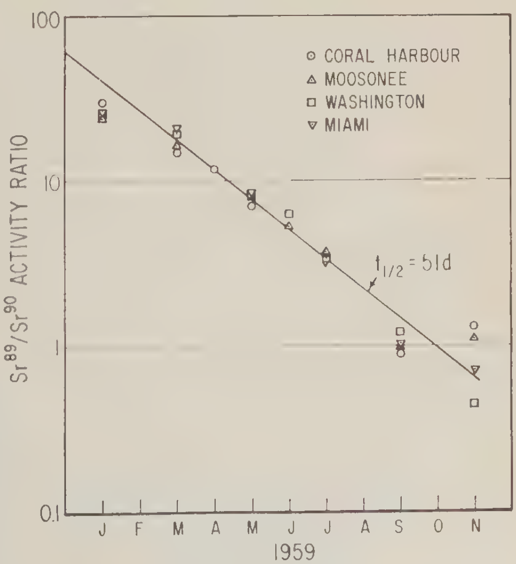

Fig. 5. Monthly changes in the Sr^{89}/Sr^{90} activity ratio in the air of the north temperate zone.

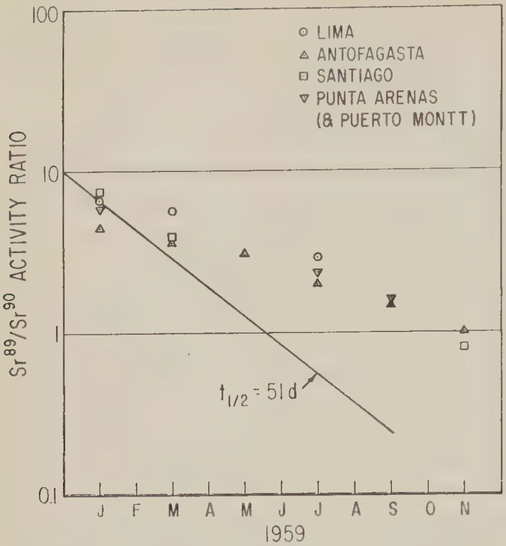

Fig. 6. Monthly changes in the Sr^{89}/Sr^{90} activity ratio in the air of the southern hemisphere.

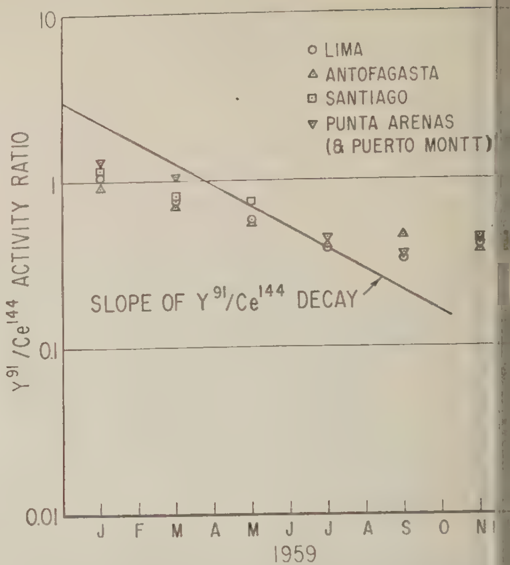

Fig. 8. Monthly changes in the Y^{91}/Ce^{144} activity ratio in the air of the southern hemisphere.

this information it is not possible to conclude whether the source of this younger activity is the tropospheric contamination in the northern hemisphere or debris (U. S. Hardtack or U. K. Christmas Island tests of 1958) from a stratospheric source in the southern hemisphere. If the sequence of events in the northern hemisphere has been correctly interpreted, an o[...]of-phase relationship should exist in the south[...] hemisphere—thus debris from a tropical stra[...]spheric source should become more promin[...] during the fall season for the southern he[...]sphere. This tropical stratosphere should [...] relatively rich in debris from the U. S. a[...] U. K. tests of 1958, and the polar stratosph[...] should contain the oldest debris. The activ[...] ratios presented in Figure 6 are consist[...] with this interpretation.

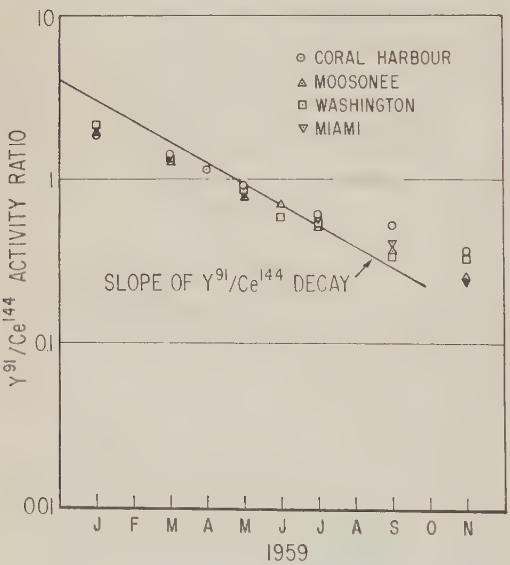

Fig. 7. Monthly changes in the Y^{91}/Ce^{144} activity ratio in the air of the north temperate zone.

Similar interpretations can be obtained fr[...] studies of the Y^{91}/Ce^{144} ratios. These are sho[...] in Figures 7 and 8. Reasonable dating is [...] possible, however, because of lack of inform[...]tion on Y^{91} yields from fast neutron fission[...] U^{238}. It should be noted that there was apparen[...] an additional influx of younger debris in b[...] hemispheres during September and Novembe[...] not a real effect but one due to the contribut[...] of the Pm^{147} (2.65 year half-life) compon[...] of the activity collected by the yttrium carr[...] which assumed relatively more importance [...] the shorter-lived Y^{91} (58-day half-life) d[...] appeared through radioactive decay.

In Figure 9, the plot of the monthly chan[...] in the Ce^{144}/Sr^{90} activity ratios during 19[...] shows at least three definite groupings of poi[...] The first group is composed of activity ra[...] at northern-hemisphere sites during the spr[...]

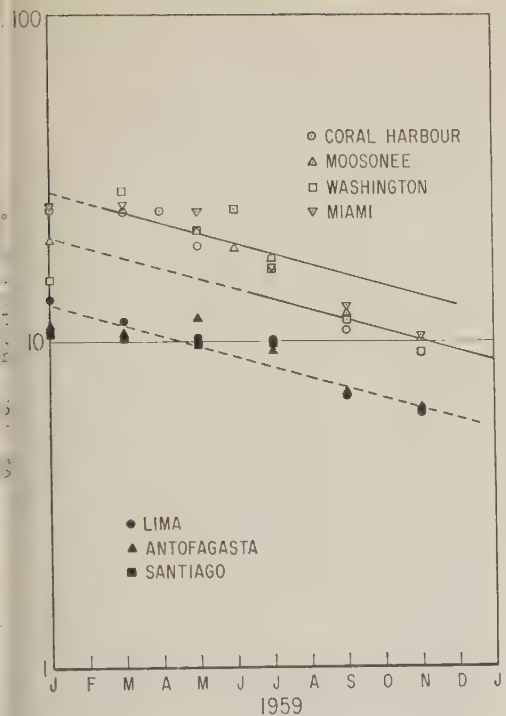

Fig. 9. Monthly changes in the Ce^{144}/Sr^{90} activity ratio during 1959.

nd early summer of 1959; the second consists f the older northern-hemisphere mixture present efore and after this period; the third consists f debris in the southern hemisphere, where n influx of younger debris during the fall season or the southern hemisphere is evident. If ission yields of Ce^{144} and Sr^{90} as given by *Katcoff* 1958] are used, data for U^{235} fission by thermal eutrons give effective dates of generation of hese sources as about September 30, 1958, May 17, 1958, and October 25, 1957, respectively. Data for U^{238} fission by fast neutrons give the inrealistic fission dates of April 1958, December 1957, and May 1957, respectively. The possiility of fractionation of Ce ^{144} relative to Sr^{90} annot be overlooked.

Tungsten-containing debris in the air near ground level. Soon after its production and injection into the atmosphere during the U. S. Hardtack series of tests at the Pacific Proving Grounds, W^{185} appeared in the air near ground level at all sites along the 80th meridian (west) in both hemispheres, initially appearing in highest concentration in the tropical regions of the southern hemisphere [*Lockhart, Baus, Patterson, and Saunders*, 1959, 1960]. At a removal rate of only 50 per cent per month, by January 1959 the concentration of Hardtack debris would have been reduced to less than 2 per cent of the original tropospheric contamination by the normal deposition processes operating in the atmosphere. Since this would be negligible compared with the actual tungsten-containing debris found in January 1959, a stratospheric source is indicated for the W^{185} found in the air during 1959.

The latitudinal variations of W^{185} in the air at ground level along the 80th meridian at bimonthly intervals during 1959 are shown in Figure 10. Very strong maxima in the mid-latitudes of both hemispheres are evident in early 1959, with that in the north being 4 to 5 times that south of the equator. After July, sufficiently accurate data to draw complete W^{185} profiles could not be obtained because of low activity levels. The month-to-month decay of the W^{185} is evident, though it is affected to some extent by the different rates of deposition from the stratospheric source at various times. By the end of 1959, W^{185} activity levels in the two hemispheres were nearly equal, probably as the result of the seasonal variations in downward mixing from the stratosphere (minimum in the northern hemisphere, maximum in the

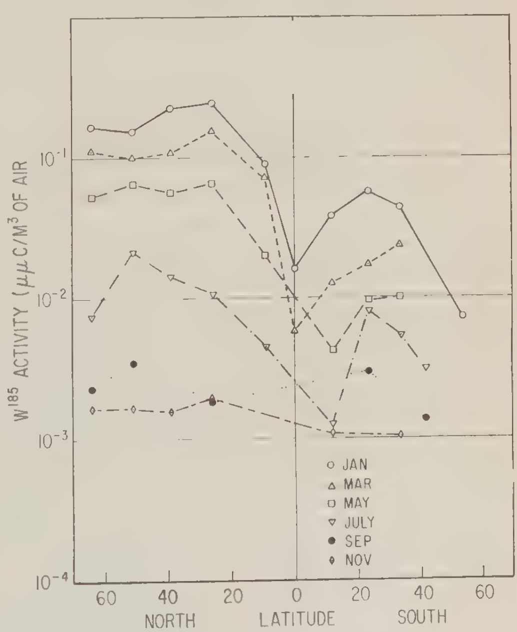

Fig. 10. Profiles of W^{185} concentration in the air along the 80th meridian during 1959.

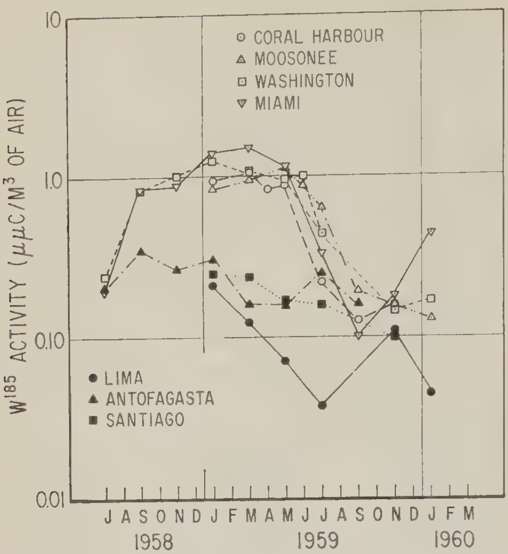

Fig. 11. Seasonal changes in the W^{185} concentration in the ground-level air along the 80th meridian.

southern hemisphere) rather than because of complete mixing of debris in the stratosphere. If January is taken as a 'neutral' month, when seasonal effects would be at a minimum, the relative W^{185} activity at ground level in the two hemispheres indicates that of the stratospheric component of the Hardtack debris about 80 per cent resides above the northern hemisphere and 20 per cent above the southern hemisphere.

In Figure 11, changes in the air concentration of W^{185}, arbitrarily corrected for decay to July 15, 1958, are shown for several sites along the 80th meridian. The progressive increase in W^{185} in the northern-hemisphere air at ground level during 1958 is the result of the spread of debris northward in both the stratosphere and troposphere, with the stratospheric source becoming dominant by November 1958. A well-defined spring maximum is present, with the possibility of another spring rise for 1960 being indicated by the data for Miami. Unfortunately, owing to the loss of W^{185} through radioactive decay as well as through normal attrition processes, it appears unlikely that this tracer can be followed throughout another cycle unless much larger samples can be acquired.

In the southern hemisphere the transition from tropospheric to stratospheric deposition of W^{185} is smooth, with no clear evidence of seasonal effects.

Contribution of Hardtack debris to atmosph contamination during 1959. Data presen previously in Figures 2 and 11 indicate str seasonal variations in both the Sr^{90} and W activities in the ground-level air of the north hemisphere. The curves in Figure 12 show monthly changes in the W^{185}/Sr^{90} ratio a indicate that the seasonal variation of W^{185} considerably less than that of the Sr^{90}. T implies that the lower atmosphere of the north hemisphere is being supplied with debris fr a minimum of two stratospheric sources contamination, both having different compo tions and deposition rates but being influen by a seasonal variation (spring maximum) i mixing into the troposphere. There is so indication that a similar effect is taking pl in the southern hemisphere, out of phase w that in the north, but the seasonal variatio not so pronounced.

By employing an assumption discussed i previous report [*Lockhart, Baus, Patterson, Saunders*, 1960], that a W^{185}/Sr^{90} activity ra of 500 (as of July 15, 1958) characterized deb from the U. S. Hardtack series of tests in Pacific, assignments have been made of contributions of Hardtack Sr^{90} to the total S in the air at the various sites. This was complished by dividing the measured W concentration by 500, after correcting for de to July 15, 1958, to obtain the Sr^{90} associa

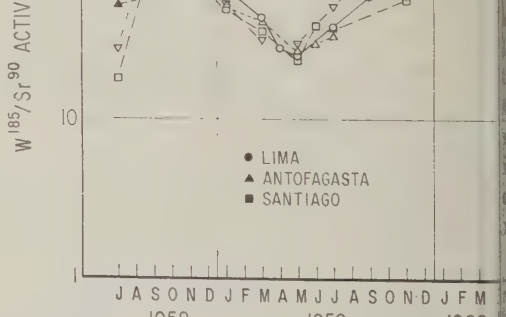

Fig. 12. Seasonal changes in the W^{185}/Sr^{90} activity ratio in the ground-level air along the 80th meridian.

BLE 2. Contribution of Sr^{90} from the U. S. Hardtack Tests to the Total Sr^{90} in the Air during 1959

	Hardtack Sr^{90}, percentages of total Sr^{90}					
tation	Jan	Mar	May	July	Sept	Nov
rthern hemisphere						
oral Harbour	13.4	8.8	4.9	7.7	11.9	20.0
oosonee	9.9	8.4	5.4	6.6	12.1	21.2
ashing-on	9.7	7.1	4.8	7.3	...	11.2
iami	10.3	6.4	5.9	10.2	17.6	21.6
iraflores	11.1	5.5	6.8	8.3	...	...
athern hemisphere						
ma	19.6	24.6	19.4	13.5	...	19.8
ntofa-gasta	14.1	17.9	24.4	20.2	18.4	...
antiago	18.7	17.0	22.8	22.0	...	12.2

h the Hardtack debris, and then comparing s value with the measured Sr^{90} in the same sample. The results, presented in Table 2, arly show two effects: (*a*) Hardtack was a nor source of Sr^{90} contamination in the rthern hemisphere during the spring of 1959, t it became increasingly important after the ssation of mixing from the arctic source; (*b*) ring most of 1959, Hardtack debris con-buted a considerably larger fraction of Sr^{90} the air of the southern hemisphere, but it ll was a minor source of the total Sr^{90} activity ere.

On the basis of the information contained in able 2 and the indication that the north-south lit of Hardtack debris was 80/20, as suggested W^{185} analyses of January 1959 collections, e Hardtack contribution to the world-wide atospheric reservoir of Sr^{90} is estimated to ve been about 10 per cent during January 59. Implicit in this calculation is the assump-on that, during January, deposition from the o stratospheric sources occurred at the same te. Measurements made in January 1960 dicate a relative increase in the contribution Hardtack debris due in part to the higher te of deposition of Soviet debris during 1959.

Nonhomogeneity of the stratospheric reservoir. l the monthly changes in the activity ratios the various fission products presented in the eceding figures indicate that the stratospheric ervoir of activity is far from homogeneous. is lack of uniform mixing is shown most clearly in Figure 13 by the monthly changes in the Sr^{89}/W^{185} activity ratios. Because of its relatively short half-life, Sr^{89} is most representative of the last high-yield test series, whereas W^{185} is characteristic of the Hardtack series. When or if mixing is complete, the Sr^{89}/W^{185} ratio should decay with a composite half-life of 165 days; deviations from this decay rate would indicate a contribution of debris from more than one source. As may be seen in Figure 13, a Sr^{89}–rich source was contributing progressively more heavily to the lower atmosphere of the northern hemisphere during early 1959; after May 1959, contributions from a Sr^{89}-poor or W^{185}-rich source caused the ratio to decrease faster than was expected for a homogeneous mixture. Even at the end of 1959 there is no indication that the rate of decrease of the Sr^{89}/W^{185} ratio has stabilized. At this time, however, the low activity levels associated with both these radioisotopes make accurate determinations impossible. At Antofagasta, in the southern hemisphere, there is again evidence of nonuniformity and, as might be expected, an inverse relationship to trends in the northern hemisphere.

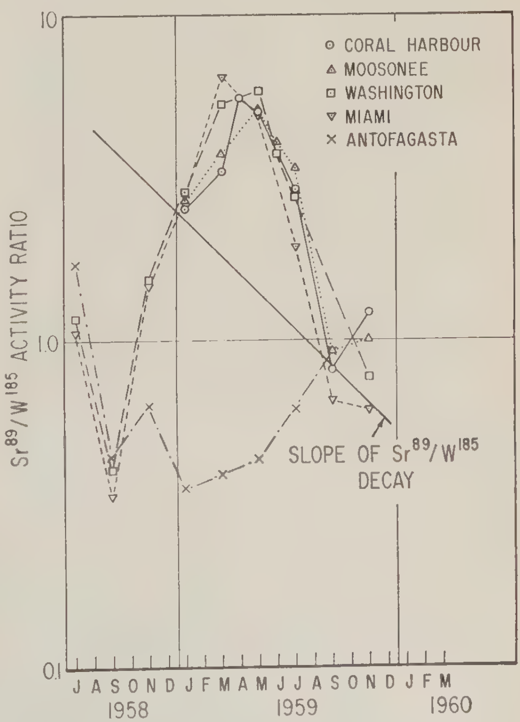

Fig. 13. Seasonal changes in the Sr^{89}/W^{185} activity ratio in the air during 1959.

A special effort has been made to point out the nonuniformity of the stratospheric deposition of fission products throughout 1959 as deduced from ground-level air measurements, particularly in regard to the existence of different deposition rates for different stratospheric locations and the presence of discrete stratospheric sources. The existence of these relatively unmixed sources in the stratospheric has been shown previously by stratospheric sampling with high-altitude aircraft [*HASP*, 1960] and by balloon-borne air filters [*Hardy and Klein*, 1960]. Contrary to a recent report [*Harley*, 1960], there seems to be no evidence from measurements made here of nuclear debris in the air at ground level to indicate that complete mixing of U. S. and Soviet debris occurred within six months or, indeed, that it had occurred by the end of 1959, more than a year following the last nuclear tests.

On the basis of the study of fission product changes in the ground-level air during the past year, a re-evaluation of the meaning of Ba^{140}/Sr^{90} activity ratios described by *Martell* [1959] is in order. His explanation of the rate of decay of Ba^{140}/Sr^{90} activity ratios in rain collections during the spring of 1958, assigning both Ba^{140} and Sr^{90} to a stratospheric source, could be correct in light of the present information. However, the radioactivity appearing later in the year, immediately following the U. S. Hardtack and fall USSR nuclear tests, must be principally tropospheric in origin rather than stratospheric. It now appears reasonable to conclude that debris introduced into the arctic regions immediately prior to or during the early spring months of any year would be mixed downward into the troposphere at such a rapid rate that there would be no distinction between tropospheric and stratospheric contaminants. After about May, however, this mixing path appears to be effectively terminated until the following spring; thus any debris introduced above the arctic tropopause, or migrating there, would be held in storage until such time as the process recommences. Because of the negligible stratospheric deposition during this period, the Ba^{140}/Sr^{90} activity ratios should be expected to extrapolate to the date of the associated nuclear tests contributing directly to the tropospheric contamination. It should be noted that a change by a factor of 2 in this ratio would result in an error of less than 2 weeks in the assigned date. The principal di ence between this interpretation and tha Martell is the assignment of the debris tropospheric and stratospheric sources, res tively.

A further observation by *Martell* [1959], debris having different Ba^{140}/Sr^{90} ratios contained in rainfall associated with air ma having their origin in polar and tropical regi is supported, in part, by the deposition me nism postulated here. However, Martell's m urements were made at a time when d tropospheric contamination of the air probably dominant. Such short-term meas ments made on air or rain samples during should have disclosed similar differences b and after the passage of polar or tropical fro if this mechanism is correct; these short-t changes would be masked by the samp technique employed here, which effecti averages the activity level over a month- period. If there is a single point of entry, as through the tropopause break in the latitudes, there should be no such differentia of polar and tropic air masses. The lack of great north-to-south variations in the $W^{185}/$ and Sr^{89}/W^{185} ratios at sites in the nort hemisphere at any given time suggests e that there is only a single point of entry or debris is generally well mixed in the u troposphere before appearing at ground l

Conclusions

During April 1959 fission product radioact in the ground-level air along the 80th meri at all sites within the north temperate reached the maximum concentration reco during any month since inauguration of 80th meridian network in 1956. The bulk of radioactivity was produced in the serie nuclear tests held in the Soviet Union du the preceding fall (September 30 to Novemb 1958).

There is strong evidence that mixing incomplete within either the northern or sout hemispheres during 1959, since isotope r showed decay rates not compatible with concept. Transequatorial mixing in either stratosphere or troposphere was apparently an important factor during this time.

Spring maxima in stratospheric depositio debris from both arctic and tropic sourc activity in the northern hemisphere occ

959, with the former showing the strongest onal dependence. No such definite seasonal t was noted in the southern hemisphere. adioactivity measurements at sites in the hern hemisphere indicated a sudden decrease tratospheric mixing after May 1959, with naximum residence half-time of about 30 s for tropospheric debris. Tungsten-con- ing debris from a tropic source was not as ngly affected by the sudden cutoff in mixing, cating that year-round leakage through ions of the tropopause takes place. A con- uting factor to the decrease in deposition he arctic stratospheric debris may have been letion of the arctic source.

ross fission product levels in the northern isphere were 50 to 100 times those in the thern hemisphere during April 1959; this o decreased to about a factor of 2 by October. ratios varied from 20–30 to 1 in May to than 2 to 1 in December 1959.

cknowledgment. This work was carried out as t of the International Geophysical Coopera- n-1959 program and was supported by the U. S. vy and the U. S. Atomic Energy Commission; vould not have been possible, however, without cooperation of the U. S. Weather Bureau and erested groups in the other countries near the h meridian who have conscientiously operated collection equipment and returned the samples the U. S. Naval Research Laboratory for assay.

References

us, R. A., P. R. Gustafson, R. L. Patterson, Jr., nd A. W. Saunders, Jr., Procedure for the se- uential radiochemical analysis of strontium, ttrium, cesium, cerium and bismuth in air- ilter collections, *U. S. Naval Research Lab. Mem. Rept. 758,* November 1957.

French, N. R., Strontium-90 in Ecuador, *Science, 131,* 1889-1890, 1960.

Hardy, E. P., Jr., and S. Klein, *Health and Safety Laboratory Fallout Program Quarterly Summary Report, USAEC HASL-84,* 66–90, April 1960.

Harley, J. H., Quarterly summary of monthly fall-out deposition data, in *Health and Safety Laboratory Fallout Program Quarterly Summary Report, USAEC HASL-84,* 140–141, April 1960

HASP High Altitude Sampling Program—A Special Report to the Government of Argentina, *Defense Atomic Support Agency Rept. DASA 532,* June 1, 1960.

Katcoff, S., Fission product yields from U, Th and Pu, *Nucleonics, 16,* 78–85, 1958.

Lockhart, L. B., Jr., R. A. Baus, R. L. Patterson, Jr., and A. W. Saunders, Jr., Contamination of the air by radioactivity from the 1958 nuclear tests in the Pacific, *Science, 130,* 161–162, 1959.

Lockhart, L. B., Jr., R. A. Baus, R. L. Patterson, Jr., and A. W. Saunders, Jr., Radiochemical analyses of fission debris in the air along the 80th meridian, west, *J. Geophys. Research, 65,* 1711–1722, 1960.

Lockhart, L. B., Jr., R. L. Patterson, Jr., A. W. Saunders, Jr., and R. W. Black, Contribution of Hardtack debris to contamination of the air during 1959, *Science, 132,* 154, 1960*a*.

Lockhart, L. B., Jr., R. L. Patterson, Jr., A. W. Saunders, Jr., and R. W. Black, Fission product radioactivity in the air along the 80th meridian (west) during 1959, *U. S. Naval Research Lab. Rept. 5528,* August 1960*b*.

Machta, L., and R. J. List, Meteorological interpretation of strontium-90 fallout, in *Environmental Contamination from Weapons Tests, USAEC HASL-42,* 327–338, 1958.

Martell, E. A., Atmospheric aspects of strontium-90 fallout, *Science, 129,* 1197–1206, 1959.

(Manuscript received July 21, 1960; revised September 9, 1960.)

RNAL OF GEOPHYSICAL RESEARCH VOLUME 65, NO. 12 DECEMBER 1960

Atmospheric Radioactivity in South America and Antarctica

LUTHER B. LOCKHART, JR.

U. S. Naval Research Laboratory
Washington, D. C.

Abstract. Information on the concentration of the major natural radioactive species and of gross-fission-product β activity in the ground-level air at several sites in South America and Antarctica is reported. These data have been obtained through a cooperative program between the U. S. Naval Research Laboratory and groups at the various collecting sites utilizing equipment designed and supplied by NRL.

Fission products have been found to be minor contributors to the radioactivity of the air in the southern hemisphere, except that in Antarctica (and presumably at some island sites) it assumes relatively more importance because of the low concentrations of natural activity there.

Seasonal variations in one or more of the radioactive components of the atmosphere are evident at each of the various sites.

INTRODUCTION

In view of the sparsity of data on atmospheric lioactivity levels in the southern hemisphere, was decided several years ago that valuable ormation could be obtained by operating its of the U. S. Naval Research Laboratory -monitor equipment at various sites below e equator. Therefore, as the NRL program of easurements in the northern hemisphere was rtailed, units were transferred to various sites South America and to one site in Antarctica r operation by cooperating groups there.

The NRL air-monitor equipment was degned to detect the presence of fission products low concentration in spite of the much larger ckground of natural radioactivity in the air d without an excessive delay in time. This uipment had been operated at a number of es in the northern hemisphere starting as rly as December 1949; additional equipment as in operation during the U. S. Greenhouse sts in the Pacific in 1951. Though much of this twork has been abandoned, several units are ill in operation.

As was mentioned above, this equipment was signed for the detection of fission products in e air. It has been possible, however, to analyze e data in such a way as to obtain reasonably antitative estimates of the concentrations of don, thoron, and gross-fission-product β acvity in the air. Because the units are all of the me design and because the same operating and calibrating procedures are used at all sites, the relative activity levels at the various sites should be reliable.

The sources of the fission products in the air are, of course, the atomic explosions that have taken place at the various nuclear testing grounds. Radon and thoron, however, are naturally occurring radioisotopes that result from the radioactive decay of radium and thorium in the soil. These chemically inert gases enter the atmosphere by diffusion from the soil or rock source or else are injected into the air by the energetic recoil that takes place when an α particle is ejected from the parent atom. Recoil of the solid daughters of radon (RaA, 3-minute half-life) or thoron (ThA, 0.16-second half-life) on emission of α particles could similarly contribute to the measured RaB and ThB in the air. These recoil processes must be relatively more important in the case of ThB activity because the short half-life of the thoron gas (54 seconds) gives only a limited opportunity for diffusion to occur before it is transformed into a solid.

EXPERIMENTAL PROCEDURE

The concentrations of radon, thoron, and gross fission products in the air were obtained from the measured changes over a 16-hour period in the rate of β decay of radioactive particulate matter collected on efficient filters through which 900–1300 cubic meters of air had

TABLE 1. Typical Data for Southern Hemisphere Stations, December 1959

	Average β-Counting Rates*				Fission Product Activity in 16th hr Count	Calculated β Activity at Zero Time			Count Efficien (towar UX₂
	Initial, c/min	6th hr, c/min	16th hr, c/min	Ratio 6th/16th	%	Fission Products, c/min	ThB + C, c/min	RaB + C, c/min	%
Lima	567	236.0	128.6	1.835	9.5	12.2	319	236	10.6
Chacaltaya	759	81.1	42.7	1.900	2.0	0.9	115	643	14.2
Rio de Janeiro									
(*a*) Pontificia Universidade Catolica do Rio de Janeiro	1160	473	251	1.886	3.4	8.5	665	486	14.8
(*b*) Instituto Nacional de Tecnologia	1490	512	270	1.893	2.7	7.3	723	760	15.2
South Pole	28.5	12.0	11.8	1.02	98	11.6	0.6	16.3	13.7

* Background subtracted.

passed during the previous 24 hours [*Lockhart*, 1959; *Lockhart, Baus, Patterson, and Blifford*, 1958]. Originally, the contributions of fission products and thoron were calculated from the observed half-life of this mixture after decay of the 26.8-minute RaB(RaC) component. Presently, the analysis for the three major components (radon, thoron, and fission products) is based on the counting rates at zero time (initial count on filter after removal from the air stream), at 6 hours (average count rate between the 5th and 6th hours) and at 16 hours (average count rate between the 15th and 16th hours). Corrections have been made for changes in air flow during the collection (from measured changes in the pressure drop across the filter), in the counting efficiency (based on daily counting of a U_3O_8 standard), and for the filter efficiency (100 per cent for fission products; 75 per cent for natural radioactivity). A correction has also been applied for the differences in β energy between the collected isotopes (assuming an average β energy of 1 Mev for fission products) and the standard (UX_2).

Filters were changed daily at about 1600 hours local time, when the radon levels should have been at a minimum in the diurnal cycle. The thoron and fission-product levels are more nearly representative of the average concentration during the preceding 24 hours.

In the calculations, secular equilibrium has been assumed between radon and its daughters (RaA, RaB, and RaC) and between thoron and its daughters (ThA, ThB, ThC, etc.), and the results are reported in terms of the concent[ra]tion of the parent activity. Actually, the resu[lts] apply equally well to the concentrations of [the] longer-lived daughters, RaB (26.8-minute ha[lf-]life) and ThB (10.6-hour half-life).

Results

The average counting rates recorded dur[ing] the decay measurements of samples collected [at] the four southern-hemisphere sites during De[cember] 1959 are shown in Table 1. The cal[cu]lated contributions of gross fission produc[ts,] thoron decay products (ThB+C), and ra[don] decay products (RaB+C) to the initial cou[nt]ing rate of the filter are also shown. The coun[ting] efficiency (including geometry factor) tow[ard] the UX_2 standard is listed and may be employ[ed] to convert the measured counting rates to dis[in]tegration rates for comparison. It is evid[ent] that in all these cases the contribution of fiss[ion] products to the total radioactivity of the ai[r is] negligible. The background count varied fr[om] about 25 counts/min (Lima) to about [...] counts/min (Chacaltaya) and imposed a li[mit] to the accuracy with which the determinati[on] could be made.

The averages of the radon, thoron, and gr[oss] fission products are reported in Table 2 [for] collections made at Lima, Peru; Chacalta[ya,] Bolivia; Rio de Janeiro, Brazil; and Antarct[ica] (Little America V, 1956–1958, Amundsen-Sc[ott] station at South Pole, 1959–1960). Mont[hly] variations in these activities are presented [in] Figures 1 to 4. The results for Little America

TABLE 2. Summary of Atmospheric Radioactivity Measurements in South America and Antarctica

Site	Period of Observation	Number of Measurements	Radioactivity in $\mu\mu C/m^3$		
			Radon	Thoron	Fission Products
na, Peru	May–Dec 1959	153	36.3	1.28	0.035
	Feb–Apr 1960	89	22.2	1.43	0.027
acaltaya, Bolivia	Sept–Dec 1958	86	35.5	0.70	0.65
	Jan–Dec 1959	323	39.4	0.54	0.016
	Jan–Apr 1960	90	39.7	0.34	0.002
o de Janeiro, Brazil					
(a) Pontificia Universidade Catolica					
	Aug–Dec 1958	106	40.3	2.26	0.23
	Jan–Nov 1959	115	46.1	2.80	0.054
	Jan–Apr 1960	99	37.0	2.11	0.012
(b) Instituto Nacional de Tecnologia					
	Jan–Dec 1958	182	71.3	2.94	0.24
	Jan–Dec 1959*	87	56.6	2.89	0.042
	Jan–Apr 1960	56	57.8	2.50	0.008
ttle America V	Apr–Dec 1956	179	2.0	(0.008)	0.021
	Jan–Dec 1957	230	2.2	(0.006)	0.019
	Jan–Oct 1958	290	3.1	(0.006)	0.019
uth Pole	Feb–Dec 1959	186	0.49	(0.003)	0.036
	Jan–Apr 1960	116	0.64	(0.007)	0.016

* No data for period February–July 1959.

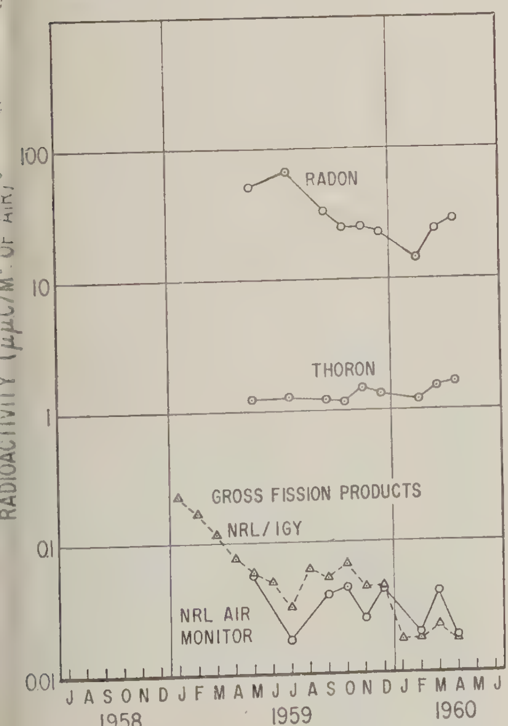

Fig. 1. Atmospheric radioactivity at Lima, Peru.

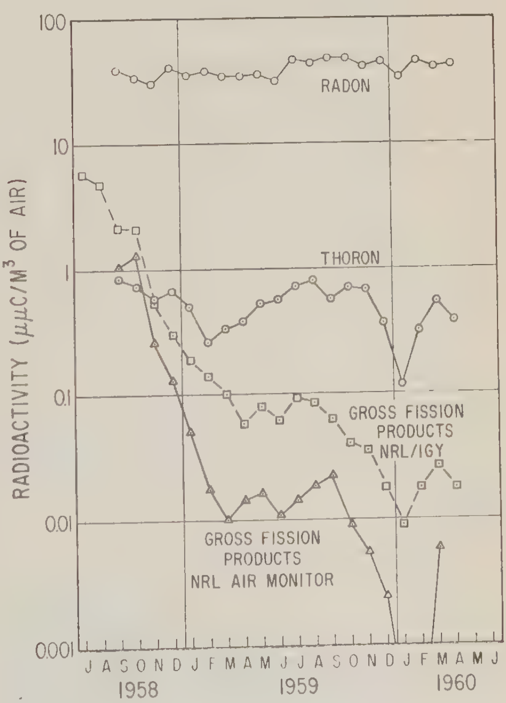

Fig. 2. Atmospheric radioactivity at Chacaltaya, Bolivia.

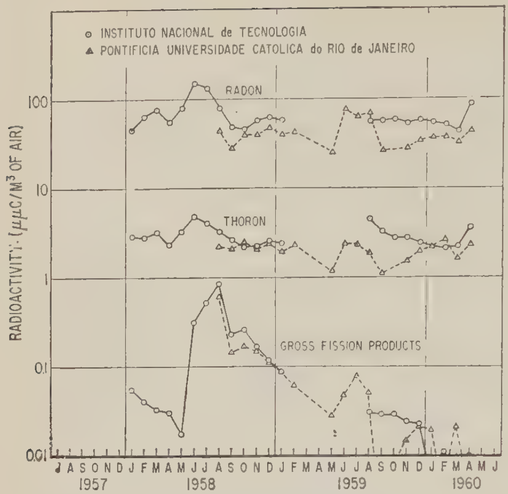

Fig. 3. Atmospheric radioactivity at Rio de Janeiro, Brazil.

are slightly at variance with those reported earlier [*Lockhart,* 1958; *Lockhart, Baus, Patterson, and Blifford,* 1958]. The former results were deduced from information received via dispatch; these have been calculated directly from the actual daily data sheets.

Continuous recordings of the activity collecting on the filters during sampling show that strong diurnal effects are present at all sites except Antarctica; the activity levels there are so low that no useful information of this type has been obtained. Although such diurnal variations in the radon concentration would not be expected in the arctic and antarctic regions, they have been observed at all other sites where this equipment has been operated [*Blifford, Friedman, Lockhart, and Baus,* 1956].

Wilkening [1959] made a thorough study of the diurnal changes in the radon content of the air and showed that these changes can be explained in terms of the vertical mixing caused by eddy diffusion in the lower atmosphere. No such detailed study of the NRL data has been undertaken.

Discussion

The average radon content of the air was about equal at the three sites in South America where measurements were made, in spite of the differences in climate, altitude, and location relative to the ocean winds. The radon concentration resembles that found at coastal sites in the northern hemisphere but is markedly lower th that recorded for the Washington, D. C., a [*Lockhart,* 1958]. The low radon concentrati in Antarctica are to be expected in view of snow and ice covering that would seal the rad activity in the ground long enough for it to transformed through decay into the long-li RaD (22-year Pb^{210}).

Thoron concentrations are highly varia from site to site, and, on the basis of the limi information available, thoron appears to c tribute generally a much larger fraction of total activity than it contributes at northe hemisphere sites. This suggests that the relat concentrations of thorium to uranium (or dium) in the soil in these areas must theref be several-fold higher than that at sites in northern hemisphere where similar measu ments have been made.

Fission products are minor contributors the radioactivity of the air at all sites in Sou America, although at the start of the measu ments at Chacaltaya following the U. S. a U. K. Pacific tests of 1958, the average gro fission-product concentration exceeded that the thoron in the air. At the south pole t fission-product concentration, though very lo constitutes a relatively large fraction of t total atmospheric radioactivity.

Lima (*Ancon*), *Peru.* As indicated in Fi ure 1, in the 1 year of data collected at Lim Peru (May 1959–April 1960), there is a sugge tion of a yearly cycle in the radon concentr tion with a minimum in the southern-hemisphe summer. No periodicity is evident in the thor concentration or in the gross-fission-product co tent of the air.

The gross-fission-product concentration of t air, obtained through operation of other equi ment at Lima (Limatambo Observatory) in continuation of the IGY and IGC-59 progran is also plotted in Figure 1 and shows this sam variability. The disagreement in the absolu magnitude of the fission-product activity is a sociated with the different counting equipme employed in the two methods and the wi range of β energies associated with mixed fissi products. This problem has been considered detail and reported elsewhere [*Lockhart a Patterson,* 1960].

Chacaltaya, Bolivia. The monthly averag of the radon, thoron, and fission-product co

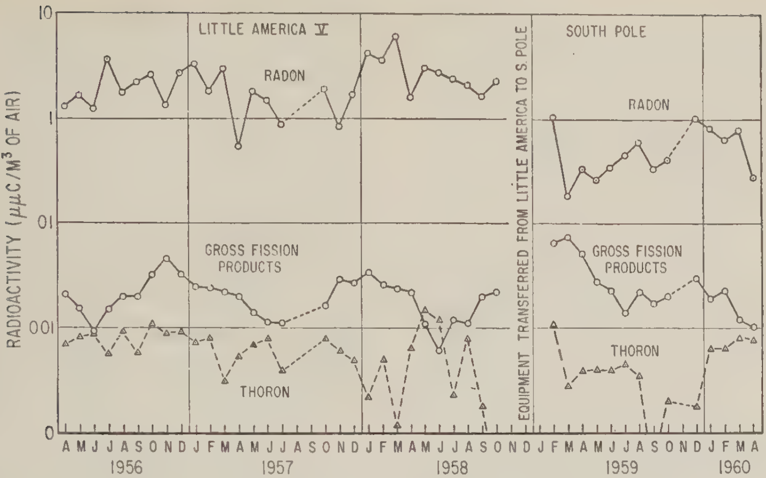

Fig. 4. Atmospheric radioactivity in Antarctica.

itrations in the air at the site of the Lab-atorio de Fisica Cosmica de Chacaltaya (eleva-n 5220 meters) during the period of operation this air-monitor equipment are shown in Fig-e 2. The gross-fission-product concentration as termined by the method employed during the Y is also shown for comparison.

Here the average radon concentration does t appear to be unusually variable or to un-rgo seasonal changes. On the other hand, e thoron content does have minima in each the two summer seasons covered in this study. ie gross-fission-product concentration shows a pid decrease from the relatively high concen-ation encountered following the U. S. and . K. tests in the Pacific during 1958. There is i indication of a spring maximum in the fission-oduct concentration, but it is not as clear-cut that found in the northern hemisphere. The ssion-product concentration as determined by ie IGY procedure is several times as high as iat determined by this procedure. Part of the fficulty is due to the different techniques used, s mentioned previously; a large part is no oubt due to the inaccuracy inherent in meas-ring the extremely low levels of fission-product tivity encountered.

Rio de Janeiro, Brazil. Two NRL air-moni-or units are in operation at Rio de Janeiro, one t the Instituto Nacional de Tecnologia and one t the Pontificia Universidade Catolica do Rio e Janeiro. The latter system is operated on the ime time schedule and in the same manner as the equipment located at the other sites; that at the Instituto Nacional de Tecnologia, however, is operated on a shorter time schedule (generally 2000–1600 hours) because of the higher dust loading in the air at that location. Furthermore, in this latter equipment the filter (Staplex type TFA 2133) is different from that used elsewhere (U. S. Army Chemical Corps type 5). In the data presented in Figure 3 the same efficiency has been assumed for the two filters; the differences encountered may be due in part to the filters but perhaps, more significantly, to the different locations of the stations or the different heights of the intake stacks above the ground. Recent work [*Moses, Stehney, and Lucas,* 1960] has indicated the extreme dependence of the radon concentration on the elevation of the sampling point above the ground.

Although the available data are insufficient to document the seasonal changes in the activity levels, there are definite indications of maxima in the radon and thoron concentrations at Rio de Janeiro during the southern-hemisphere winter season. These may be associated with weather patterns which bring a larger proportion of continental air than of maritime air into the area during this season.

The fission products are at all times minor contributors to the atmospheric radioactivity here. The maximum concentration was recorded in the winter of 1958 (June–August) following U. S. nuclear tests at the Pacific Proving

Grounds. The secondary peak in October of that year is probably related to the U. K. tests in the Christmas Island area during August and September 1958. There is a suggestion of a seasonal rise in the winter of 1959. In late 1959 and early 1960 the fission product levels were so low that their accurate determination by this method was impossible.

Antarctica. During the period of increasing interest in Antarctica which preceded the IGY by several years, the opportunity occurred to send an NRL air-monitor unit to Little America. This equipment, operated by personnel of the Polar Operations Project, U. S. Weather Bureau, obtained the first information on the radioactivity of the air in this large area of the world. The NRL air-monitor equipment was operated at Little America V for nearly three years (1956–1958) before being transferred to the Amundsen-Scott Station at the south pole, following the decision to abandon the former base.

As is shown in Figure 4, the radon content at Little America was extremely variable and averaged only a few per cent of that found at the other southern-hemisphere sites. It is possible that the source of this activity is, in part, associated with materials brought to this site and is not due entirely to natural sources there. Radon levels encountered at the South Pole station were even lower, as would be expected. The thoron content at both locations was so low that no reasonable measurements have been possible. In spite of the curve for thoron shown in Figure 4, it is reasonable to say only that the thoron content does not exceed 0.01 $\mu\mu C/m^3$ of air.

On several occasions during equipment checks at Little America the radioactivity in room air rather than outside air was determined. As may be seen from data presented in Table 3, unusually high thoron concentrations were found indoors (radon and fission products were normal), indicating that some of the supplies or construction materials brought into Little America contained thorium. This is not unusual, since thorium is widely distributed in nature; what is unusual is that the radon concentration was not similarly affected, since uranium is equally widely distributed.

The gross fission products in the air in Antarctica have been measured with reasonable accuracy in spite of their low concentrations because of the absence of any interfering long-

TABLE 3. Comparison of the Radioactivity Indoor and Outdoor Air at Little America during July 1956

Source of air	Date	Activity in $\mu\mu C/m^3$ Radon	Thoron	Fissi Produ
Indoors	July 8	3.1	1.07	0.00
	July 21	2.0	0.32	0.00
Outdoors	July average	3.7	(0.006)	0.01

lived activity (thoron daughters) there. S sonal changes in the fission-product concent tion, with maxima in the southern hemisph in late spring or summer and minima in winter for each of the years during which t equipment has been in operation, are evide The peak during the summer of 1958–19 seems to be displaced; however the absence data for the period November 1958–Janu 1959, while the equipment was being mov makes any interpretation subject to uncertain It may be of some significance that data fr air-filter collections made at Punta Arenas, Cl (53°S), and Puerto Montt, Chile (41°S), sh maxima in the gross fission products in the at about this same time.

The variations in the air concentration of sion products in Antarctica must be related the proposed seasonal cycles of downward m ing of stratospheric air into the troposphere p marily in the polar regions [*Machta,* 1959]. T principle, though not the mechanistic details its operation, appears to be well documented the result of recent studies of fission products the air of the northern hemisphere [*Lockha Patterson, Saunders, and Black,* 1960]. It thought unlikely that the peaks at Little Am ica in November 1956 and November 19 January 1958 could be related to tropospher contamination from U. K. tests in Austra since the activity levels at Punta Arenas w not noticeably affected by the 1957 tests. Si lar studies in the northern hemisphere have dicated the weakness of the poleward drift tropospheric activity introduced at Eniwe (11°N) and Nevada (37°N) by the low sponses encountered at Kodiak, Alaska (58°N to tests at these sites [*Blifford, Friedman, Lo hart, and Baus,* 1956].

The only other reported measurements of at-
spheric radioactivity in the Antarctic were
de by the Belgian Antarctic Expedition at
se Roi Baudouin near the coast of Antarctica
icciotto, 1958]. The reported activities dur-
; early 1958 were: RaB 1 $\mu\mu C/m^3$, ThB 0.05
C/m^3, and fission-product β activity 0.01–
4 $\mu\mu C/m^3$. The results are in essential agree-
nt with those reported here for Little Amer-
. V during the same period. Interestingly, the
lgians also considered the possibility of con-
nination of the outside air by building ma-
ials brought to the site because of the finding
enhanced RaB and ThB activity indoors.

Summary

The first extensive series of measurements of
e natural radioactivity of the air in South
nerica has been presented. It shows, for the
w sites covered, the radon content to be gen-
ally less than that at similar sites in North
nerica. Furthermore, evidence is presented
at thorium is relatively more prevalent in the
rface soils there than in North America. In
ntarctica the natural radioactivity of the air
s been found to be extremely low, with thoron
ing a negligible contributor to this activity.

Fission products are minor contributors to the
dioactivity of the air in the southern hemi-
here, except in the Antarctic (and presumably
some island sites) where it assumes relatively
ore importance because of the low natural ac-
vity present.

Seasonal changes in one or more of the radio-
tive components of the atmosphere are evi-
nt at each of the sites. Changes in the natural
tivity levels are probably related to such
eteorological factors as wind direction and
rbulence, kind and quantity of rainfall, and
e location of soils rich in the parent radioac-
ve element (uranium or thorium), while
hanges in the fission product concentration are
lated to seasonal changes in the mixing rate of
ratospheric and tropospheric air masses.

Acknowledgments. The U. S. Naval Research
aboratory and the author wish to express their
ppreciation to the various groups that have con-
ibuted to the success of this program: Father
. X. Roser, Department of Physics, Pontificia Universidade Catolica do Rio de Janeiro; Dr. Arthur Aron and Dr. Bernhard Gross, Divisao de Medidas Electricas, Instituto Nacional de Tecnologia, Rio de Janeiro, Brazil; Dr. Ismael Escobar V., Director, and Ing. Raoul Weil, Laboratorio de Fisica Cosmica de Chacaltaya, Universidad Mayor de San Andres, La Paz, Bolivia; Mr. Chester B. Cunningham, NASA Satellite Tracking Station, Lima, Peru; and Messrs. C. E. Twombley, S. A. Wilson, C. E. Williams, T. E. Smith (U. S. Navy), and H. F. Thomas of the U. S. Weather Bureau who operated the equipment under adverse conditions at the Little America and the South Pole stations.

References

Blifford, I. H., Jr., H. Friedman, L. B. Lockhart, Jr., and R. A. Baus, Geographical and time distribution of radioactivity in the air, *J. Atm. and Terr. Physics, 9,* 1–17, 1956.

Lockhart, L. B., Jr., Concentrations of radioactive materials in the air during 1957, *Science,* 128, 1139, 1958.

Lockhart, L. B., Jr., Atmospheric radioactivity levels at Yokosuka, Japan, 1954–1958, *J. Geophys. Research, 64,* 1445–1449, 1959.

Lockhart, L. B., Jr., R. A. Baus, R. L. Patterson, Jr., and I. H. Blifford, Jr., Some measurements of the radioactivity of the air during 1957, *U. S. Naval Research Lab. Rept. 5208,* October 1958.

Lockhart, L. B., Jr., and R. L. Patterson, Critical analysis of measurements of the gross fission product activity in the air at ground level, *U. S. Naval Research Lab. Rept. 5440,* February 1960.

Lockhart, L. B., Jr., R. L. Patterson, Jr., A. W. Saunders, Jr., and R. W. Black, Fission product radioactivity in the air along the 80th meridian (west) during 1959, *J. Geophys. Research, 65,* 3987–3997, 1960.

Machta, L., Hearings before the Special Subcommittee on Radiation of the Joint Committee on Atomic Energy, Congress of the United States, 86th Congress, first session on Fallout from Nuclear Weapons Tests, May 5–8, 1959, Vol. 1, U. S. Government Printing Office, Washington, 778–806, 1959.

Moses, H., A. F. Stehney, and H. F. Lucas, Jr., The effect of meteorological variables upon the vertical and temporal distributions of atmospheric radon, *J. Geophys. Research, 65,* 1223–1238,1960.

Picciotto, E., Measurement of the radioactivity of the air in the Antarctic, *Nuovo cimento,* 10, 190–191, 1958.

Wilkening, M. H., Daily and annual courses of natural atmospheric radioactivity, *J. Geophys. Research, 64,* 521–526, 1959.

(Manuscript received July 21, 1960.)

A Preliminary Investigation of the Heat Flux from the Ocean to the Atmosphere in Antarctic Regions

JAMES D. KANGOS [1]

U. S. Weather Bureau
Washington, D. C.

Abstract. Estimates have been made for the summer and fall seasons of the sensible and latent heat flux for 5° latitudinal zones from 40°S to 70°S eastward between 20°E and 180°. Results indicate that there are large variations in the total heat flux from summer to fall and from zone to zone, the largest seasonal variations occurring in the zones 40° to 45°S (183 cal/cm²/day) and 65° to 70°S (187 cal/cm²/day). A minimum in the total heat flux for both summer (16 cal/cm²/day) and fall (−54 cal/cm²/day) is found in the zone 50° to 55°S, the approximate mean position of the Antarctic Convergence. Annual evaporation values were determined, revealing a minimum (15 cm) in the zone 50° to 55°S with a secondary minimum (32 cm) along the coast.

troduction. There has been a recent and uraging re-emphasis of investigations of the strial heat budget, and the steady accumu- n of investigations on the subject has ght proof that many meteorological and cli- ological problems can be solved wholly or ially through the consideration of energy esses. A detailed treatment of evaporation sensible heat flux for the region south of 3 seems nonexistent. Although *Albrecht* 51] obtained bimonthly charts of evapora- for the Pacific and Indian oceans, they rtunately show little detail in the high lati- s. Means for latitudinal zones which just h the regions to be discussed here have published by *Sverdrup* [1951], *Reichel* 52], and *Wüst* [1954].

evaporation studies, one of the aims has been the establishment of relationships that ld permit the computation of latent heat from meteorological elements such as wind city, humidity, and sea surface temperature. h this in mind, *Sverdrup* [1938] and *Jacobs* 51] both derived formulas for the determi- on of evaporation using the above-mentioned eorological elements as parameters. *Swin- k* [1959] developed a formula after a thor- h investigation of the methods of determin- latent heat flux, and the results of his nula are approximately 10 per cent larger than results obtained using Jacob's formula. However, Swinbank's formula was derived to yield instantaneous values of evaporation, whereas Jacobs' and Sverdrup's formulas were developed to yield mean values of evaporation. Results of the Sverdrup formula and the Jacobs formula agree within ±8 per cent and, for this reason and for computational ease, Jacobs' formula will be used in continuing and future contemplated studies of evaporation over the Antarctic Ocean.

[1] Now at Travelers Weather Research Center, velers Insurance Company, Hartford, Connecti-

Method. Using Jacobs' evaporation formula in conjunction with the *Bowen* [1926] ratio, one can obtain the sensible heat flux from the ocean to the atmosphere. The sensible heat flux is determined in the following manner. Knowing Jacobs' evaporation formula,

$$E = 0.143(e_w - e_a)w \qquad \text{mm/day} \qquad (1)$$

where

e_w = vapor pressure of the sea water in millibars,
e_a = vapor pressure of the air in millibars,
w = wind speed in m/sec,

the latent heat flux is obtained by

$$Q_e = EL_t \qquad \text{cal/cm}^2\text{/day} \qquad (2)$$

where E = evaporation (g/cm²/day).

$$L_t = 585 \text{ cal/g at standard temperature (15°C) and pressure (1013 mb).} \qquad (3)$$

Therefore

$$Q_e = 8.36(e_w - e_a)w \qquad \text{cal/cm}^2\text{/day} \qquad (4)$$

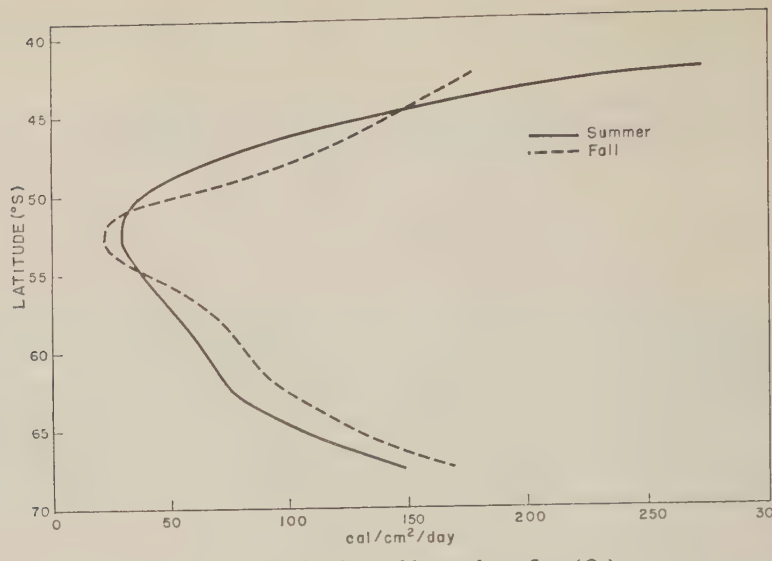

Fig. 1. Zonal values of latent heat flux (Q_e).

The error introduced by assuming the latent heat of vaporization at standard temperature and pressure is 1 to 3 per cent and may be neglected in comparison with the observational errors. Using the Bowen ratio,

$$R = 0.66 \frac{(t_w - t_a)}{(e_w - e_a)} \frac{p}{1000} \qquad (5)$$

where

t_w = water temperature (°C).
t_a = air temperature (°C).
e_w = vapor pressure of water (mb).
e_a = vapor pressure of the air (mb).
p = air pressure (mb).

By definition the ratio of sensible heat (Q_c) to latent heat (Q_e) equals the Bowen ratio

$$R = Q_c/Q_e \qquad (6)$$

hence we obtain the sensible heat flux from ocean to the atmosphere,

$$Q_c = 0.66 \frac{(t_w - t_a)}{(e_w - e_a)} \frac{p}{1000} Q_e$$

$$\text{cal/cm}^2\text{/day}$$

By assuming that $p = 1000$ mb

$$Q_c = 5.53(t_w - t_a)w \qquad \text{cal/cm}^2\text{/day}$$

where the temperature is in °C and the velocity in m/sec. The error introduced b[y] assumption $p = 1000$ mb is ±1 per cent a[...] approximate range of the surface pressure i[...] to 1010 mb over the Antarctic Ocean. This [...] is small in comparison with observational er[...] thus the assumption will be used. The tota[l] [en]ergy exchange (Q_a) between the sea and [the] atmosphere is

TABLE 1. Latitudinal Distribution of Quantities Used in Determining Latent and Sensible Heat Flux

	Summer				Fall			
Latitude	T_a	T_w	$e_w - e_a$	w	T_a	T_w	$e_w - e_a$	w
40–45°S	13.4	14.7	3.6	9.1	13.8	13.5	1.6	13[...]
45–50	10.2	9.1	1.0	9.1	8.7	8.9	1.3	10[...]
50–55	5.2	4.8	0.6	5.8	6.4	5.3	0.2	12[...]
55–60	0.7	1.1	1.0	6.2	2.1	1.7	0.6	13[...]
60–65	−1.1	0.2	1.3	6.9	−2.5	0.6	1.6	7[...]
65–70	−0.6	−1.1	2.1	8.5	−3.8	−1.4	1.9	10[...]

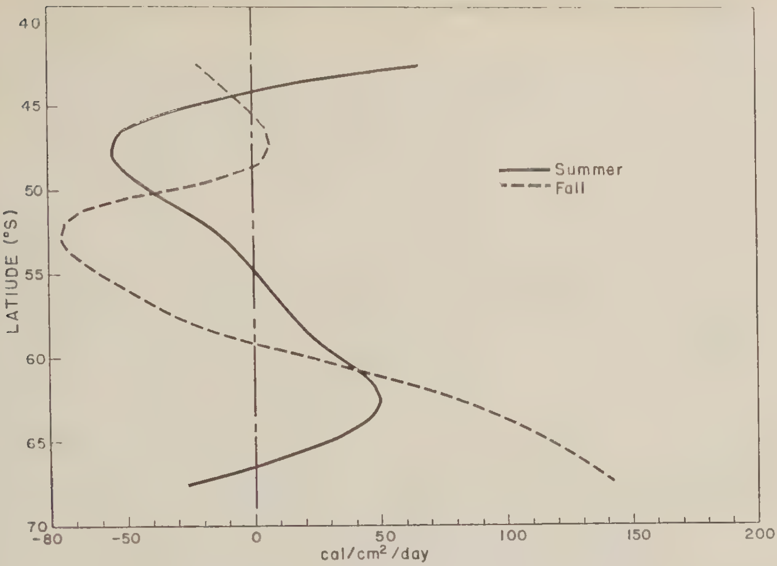

Fig. 2. Zonal values of sensible heat flux (Q_c).

$$Q_a = Q_c + Q_e \quad (9)$$

echt [1951] determined evaporation values g Sverdrup's formula, and the results indi- that evaporation is greater in the eastern fic than in the western Pacific and Indian ans, the annual evaporation being 41 cm in eastern Pacific as compared with 35 cm in western Pacific and Indian Oceans for the 50° to 60°S, and 17 to 12 cm in the zone to 70°S for both Pacific and Indian Oceans. *ett* [1958] obtained some seasonal evapora- values using Jacobs' formula in the vicinity he Falkland Islands and in the eastern Pa-. His values are of the order of 72 cm per r, with generally higher values in autumn winter than in summer. No recent values of poration for the South Atlantic seem to exist. *ott* [1944] and *Wüst* [1954] both gave an ual mean of 22 cm for the belt 50° to 60°S 7 cm for the belt 60° to 70°S.

brief study of the heat flux (latent, sensi- and total) in the eastern Antarctic Ocean m 40°S to Antarctica, and from 20°E to °) using the above formulas was conducted the months December through May. Mean es of the air temperature, relative humidity, wind speed were used which were obtained n 1224 observations taken aboard the fol- ing ships: *Atka* (1956–1957), *Balaena* (1946–7), *Ob* (1955–1956), and the *Umitaka-Maru* (1956–1957). The individual reports were grouped into two seasons, summer (Dec., Jan., Feb.) and fall (Mar., Apr., May), and means were computed over 5° latitudinal belts. Due to the sparsity of data in the Antarctic Ocean (south of 40°S) the representativeness of the sample of data is unknown, and at present it is impossible to compute the two-dimensional distribution of heat flux. However, since the main area of activity is in the immediate vicinity of the coast, the density of observations increases towards higher latitudes. Thus, latitudinal means were used to determine the energy fluxes.

Results. The results indicate that the mean latent heat flux for both seasons, summer (Dec., Jan., Feb.) and fall (Mar., Apr., May), is positive with a minimum in the belt 50° to 55°S, the approximate mean position of the Antarctic Convergence. As can be seen in Figure 1 the greatest changes of the latent heat flux from summer to fall occur north of 50°S. Table 1 is a summary of the latitudinal distribution of the quantities used in determining the latent heat flux and sensible heat flux.

According to Table 1 and Figure 1, increases or decreases in the vapor pressure differences from summer to fall for all latitudinal zones (except 55° to 60°S and 65° to 70°S) have resulted in corresponding increases or decreases of the latent heat flux. Zones 55° to 60°S and 65° to

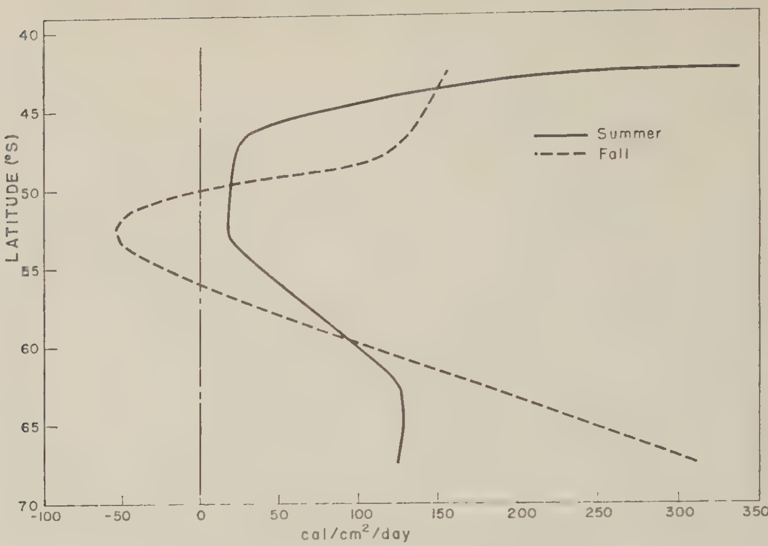

Fig. 3. Zonal values of total heat flux (Q_s).

70°S will be discussed in detail in an effort to illustrate the degree of predominance of either the wind speed or the vapor pressure differences in the determination of the latent heat flux. In all cases the wind speed increased from summer to fall, which should have the effect of increasing the latent heat flux (Fig. 1). As this did not occur in all cases (belts 40° to 45°S and 50° to 55°S), the implication is that the vapor pressure differences are predominant. In the belt 55° to 60°S the latent heat flux increased from summer (52 cal/cm²/day) to fall (68 cal/cm²/day) (Fig. 1), the vapor pressure difference decreased by 40 per cent, and the wind speed increased by 54 per cent. In the region 65° to 70°S, the latent heat flux increased by 14.1 per cent from summer (149 cal/cm²/day) to fall (170 cal/cm²/day), the vapor pressure difference decreased 9.5 per cent and the wind increased 20.6 per cent. It is evident that in these two cases the percentage increase of the wind was greater than the percentage decrease of the vapor pressure difference. Since the formula used to determine the latent heat flux is linear, it must follow that for a given percentage increase of the wind speed or vapor pressure difference there must be the same percentage decrease of vapor pressure difference or wind speed to maintain the same latent heat flux.

The minimum found in the belt 50° to 55°S for both the summer and fall seasons is the result of small vapor pressure differences betw the water and air. A possible explanation for small vapor pressure differences may be presence of the 'Antarctic Divergence' [*We* 1959]. If the convergence is a divergence Wexler has stated, then there will be a zon cold water at the surface due to upwelling. T there will be relatively lower vapor pressure the zone. This zone of relatively cold water not be detected when means over 5° latitude used, as the zone is only about 2° latitud width.

The sensible heat flux is not positive in latitudinal belts, as was the latent heat flux both seasons. During the summer season a m mum is found in the latitudinal belt 45° to 5 with a secondary maximum in the belt 60 65°S. Figure 2 shows that during the fall sea there is a minimum in the belt 50° to 55°S, a secondary maximum from 45° to 50°S. A c parison of the sensible heat flux of both sea reveals a decrease from summer to fall in latitudinal belts 40° to 45°S and 50° to 6 with a large increase in the belt 45° to 5 The decrease of the sensible heat flux in the 40° to 45°S is a result of a rather large decr in the mean water temperature (Table 1) f summer to fall, the cause of which is unkn owing to the sparsity of synoptic and oce graphic data. As can be seen in Table 1, t was an increase in the mean water tempera

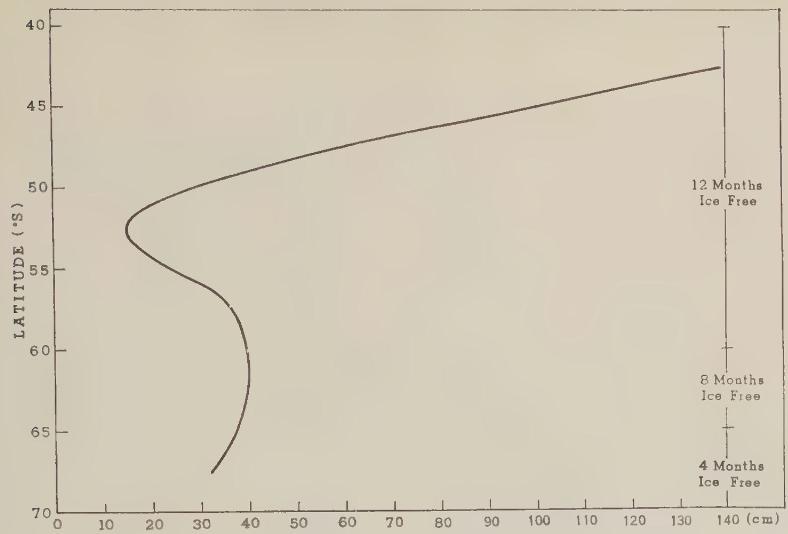

Fig. 4. Zonal values of annual evaporation (E).

n summer to fall in the zone 50° to 60°S— increase which is to be expected because the ans reach their maximum temperature in fall. wever, the rise in the mean air temperature this zone is unexplainable owing to lack of optic data. Thus, the increases of the mean and water temperatures have resulted in decrease of the sensible heat flux. During the nmer season the sensible heat flux along the st (65° to 70°S) is negative (−24 cal/cm²/); in the mean, therefore, the air tempera- e is warmer than the water temperature. wever, during the fall season the sensible t flux along the coast (65° to 70°S) is ongly positive (142 cal/cm²/day); thus, in mean, the air temperature is considerably der than the water temperature. This latter iation is to be expected along the coast, as air blowing off the shore is much colder in than in summer, whereas the difference in ter temperature between summer and fall is te small (0.3) in comparison with the differ- e in air temperature (3.2). The total heat ($Q_s + Q_e$), Figure 3, shows a decrease from nmer to fall in the belts 40° to 45°S and 50° 60°S and an increase in the regions 45° to S and south of 60°S, with the greatest in- ase occurring along the coast, the reason be- that the offshore winds are colder in fall n in summer.

An estimate of annual evaporation was de- mined for the 5° latitudinal belts by using two assumptions and weighting factors. It was first assumed that the evaporation during the spring and winter seasons is the same as it is during the summer and fall seasons and, second, that there is no evaporation from the ice surface which extends outwards to approximately 60°S during the winter season. Data are lacking for evaporation over both the open ocean and the ice shelf for the spring and winter seasons. The weighting factors used were determined by the number of months that the sea surface within the zone is ice free. The region 40° to 60°S was considered to be ice free the year round. The belt 60° to 65°S is ice free 8 months of the year, and 65° to 70°S is clear 4 months of the year. Thus, from the above-mentioned assumptions, the seasonal evaporation values (Table 2) as determined from the latent heat flux, and the weighting factors, an estimate of the annual evaporation was obtained.

TABLE 2. Seasonal Evaporation Values

Zone	Summer E, cm	Fall E, cm
40–45°S	42.2	27.4
45–50	11.7	16.9
50–55	4.5	3.2
55–60	8.0	10.5
60–65	11.5	15.2
65–70	22.9	26.2

The annual evaporation (Fig. 4) decreased

rather sharply from the belt 40° to 45°S (139 cm) to the belt 50° to 55°S (15 cm). There was an increase from the belt 50° to 55°S to the belt 60° to 65°S (40 cm) and then a slight decrease to 32 cm along the coast (65° to 70°S). As the ice shelf increases outward from the continent during the winter, it is quite likely that the evaporation also increases towards the lower latitudes, since the cold, dry air penetrates farther north. Thus, the estimates of annual evaporation presented in this paper are rather crude as a result of the assumptions imposed owing to lack of data.

Acknowledgments. The author is grateful to Mr. Morton J. Rubin for the stimulating discussions of this research, and to the National Academy of Sciences, USNC-IGY, and the National Science Foundation, under whose contract this work was supported.

References

Albrecht, F., Monatskarten der Verdunstung und Wasserhaushaltes des Indischen und Stillen Ozeans, *Ber. deut. Wetterdienstes U. S. Zone,* Bad Kissingen, no. 29, 1951.

Bowen, I. S., The ratio of heat losses by conduction and evaporation from any water surface, *Phys. Rev., 27,* no. 6, 1926.

Jacobs, W. C., The energy exchange betwee sea and the atmosphere and some of its c quences, *Bull. Scripps Inst. Oceanog.,* Calif., 1951.

Privett, D. W., The exchange of heat acros sea surface, *Marine Observer, 28,* no. 179,

Reichel, E., Der Stand des Verdunstungsprob *Ber. deut. Wetterdienstes, U. S. Zone,* Bad singen, no. 35, 1952.

Schott, G., *Geographie des Atlantischen O* 3 ed., Hamburg, 1944.

Sverdrup, H. U., On the evaporation from oceans, *J. Marine Research, Sears Found. 1,* 1938.

Sverdrup, H. U., Evaporation from the ocea *Compendium of Meteorology,* Am. Met Soc., Boston, 1951.

Swinbank, W. C., Evaporation from the o *Sci. Rept. 12, contract AF 19(604)-2179,* of Meteorology, Univ. of Chicago, 1959.

Wexler, H., The Antarctic Convergence—or D gence? in *Rossby Memorial Volume,* Rocke Inst. Press and Oxford Univ. Press, New 1959.

Wüst, G., Gesetzmassige Wechselbeziehungen schen Ozean und Atmosphere in der Z Verteilung von Oberflachensalzgehalt, Ve stung und Niederschlag, *Arch. Meteorol. phys. u. Bioklimatol., Ser. A, 7,* Vienna, 1

(Manuscript received August 8, 1960.)

Chlorine-36 Radioactivity in Rain

O. A. SCHAEFFER, S. O. THOMPSON, AND N. L. LARK

Chemistry Department
Brookhaven National Laboratory
Upton, Long Island, New York

Abstract. Cosmic rays and nuclear explosions are adding radioactivity to the atmosphere from which it is then removed by rainfall. The investigation of these activities furnishes a means of obtaining new information of significance in geological problems as well as in the understanding of the hazards of nuclear fallout. Chlorine-36 is an interesting isotope for such a study as it has a relatively long half-life, 308,000 years, and at the same time is very soluble in water. Relatively high levels of Cl^{36} activity have been found in rain. The levels are several orders of magnitude above the level to be expected from cosmic-ray production. The Cl^{36} is almost surely the result of neutron irradiation of sea water by nuclear explosions.

ıtroduction. The presence of radioactive ıs in the earth's atmosphere is due principally ıree causes: (1) the interaction of cosmic-ray icles with nuclei of the atmosphere; (2) ear explosions; and (3) the entering into atmosphere of radioactive nuclei from estial and extraterrestrial sources. Most of radioactivities are washed out of the atmosre by rainfall. In recent years H^3 [*Faltings Harteck*, 1950], Be^7 [*Arnold and Al-Salih*, 5], P^{32} and P^{33} [*Lal, Narasappaya, and shi*, 1957], Na^{22} [*Marquez, Costa, and Almeida*, 7], and S^{35} [*Goel*, 1956] have been isolated ı rain in measurable amounts and have been ibed to the interactions of cosmic rays with atmosphere. The S^{35} has also been attributed tly to the effects of nuclear explosions *, Rama, and Zutshi*, 1960]. In the production phosphorus and sulfur the interactions are ı the argon of the atmosphere and in the ium and beryllium production the interacıs are with the oxygen and nitrogen. A large ıber of radioactivities have been found that the result of nuclear explosions. The longd radioactivities introduced into the rain by mic bombs could be used as a means of lying the migration of surface and underınd water as well as processes taking place he atmosphere, such as mixing between the tosphere and troposphere.

'or a study of ground water movement the ivity should be one of the ions which is not ly removed by the soil and rocks or by poration. A good isotope for such studies is Cl^{36}, which in addition to being one of the most soluble anions also has a long half-life, 308,000 years.

With these thoughts in mind a study was made of the possible Cl^{36} content of rain water. It was found that rain does indeed contain Cl^{36} in measurable amounts that may be useful for further studies.

Experimental procedures. To detect Cl^{36} produced in the atmosphere and concentrated by rain, very large samples were needed. Samples of 1000–2000 gallons were readily obtained by collecting the runoff from a 5000-square-foot roof. The solid and organic matter swept from the roof was allowed to settle. The clear liquid was passed through a filter and pumped through an ion-exchange column where the chlorides and other anions were complexed and concentrated.

The exchange column was a stainless steel container 6 inches in diameter and 5 inches long, filled with 50–100 mesh Nalcite–SAR–10 per cent D.V.B. The resin was prepared by converting it to the hydroxyl form with 10 per cent sodium hydroxide solution and removing excess alkali with distilled water. This column was able to completely remove chloride and other anions from rain at through-put rates up to 150 gallons per hour.

The chloride and other anions were eluted from the column with one to two gallons of 10 per cent sodium hydroxide solution. Barium nitrate was added to the eluent to precipitate sulfate and carbonate ions. The clear filtrate

TABLE 1. Fission Product Radionuclides Concentrated by Rains

Radio-nuclide	Radi-ation	Cumulative Thermal Fission Product Yields of U^{235}*	Half-life
Pu^{239}	α	...	24,000 yr
Sr^{90}	β	5.8%	27.7
Cs^{137}	β, γ	6.2	26.6
Pm^{147}	β	2.7	2.64
Ce^{144}	β, γ	6.0	285 d
Zr^{95}	β, γ	6.2	65 d
Y^{91}	β	5.4	58 d
Sr^{89}	β	4.8	51 d
Ru^{103}	β	3.0	40 d
Nb^{95}	β, γ	6.3	35 d
Ba^{140}	β, γ	6.3	13 d
I^{131}	β, γ	3.1	8 d
Ru^{106}	β	0.38	1 yr

* *Katcoff*, [1958].

was acidified to pH 1 with nitric acid, and silver nitrate was added to precipitate silver chloride.

After being filtered and washed, the silver chloride was dissolved in several hundred ml of 15 N. Forty mg of sodium iodide carrier was dissolved in the solution and an equivalent amount of silver nitrate was added to precipitate silver iodide. The solution was filtered, boiled to remove ammonia, and then acidified to reprecipitate the chlorine as silver chloride. The steps described so far in this paragraph were repeated once. Then the silver chloride was dissolved once more in ammonia and the silver was removed by precipitation with hydrogen sulfide. Evaporation of the solution to dryness gave ammonium chloride and a small amount of free sulfur.

The ammonium chloride was treated with sulfuric acid in an air-free distilling system and the hydrogen chloride that was evolved was dissolved in distilled water in a quartz vessel. The hydrogen chloride solution was neutralized with aqueous ammonia.

It was essential to establish unquestionably the radiochemical purity of the chlorine since no measurements were made of either the half-life or the energy of the radiation. A list of the more abundant long-lived fission products is given in Table 1. To remove the possibility of contamination by these and other products of nuclear explosions, carriers for the following elements were added before the hydrogen chloride distillation step: Ba, Ce, Cs, Mn, Nb, Ru, Sr, and Zr. It was established by a separate test that none of these elements is carried [illegible] into the hydrogen chloride solution when [illegible] mg of each carrier and 15 g of ammon[illegible] chloride are treated with sulfuric acid.

The evolution step of the ammonium chlo[illegible] purification was carried out three times and [illegible] resulting ammonium chloride was evapor[illegible] until the solution became saturated. The [illegible] was rapidly crystallized out by the addi[illegible] of 100–200 cc of absolute ethyl alcohol. [illegible] resulting slurry was applied to a steel liner [illegible] a spinning process previously described [*D*[illegible] *and Schaeffer*, 1955]. The ammonium chlo[illegible] was counted in a screen-wall counter in a[illegible] coincidence with an annular ring of Ge[illegible] counters. The electronics and counting proce[illegible] have been described elsewhere [*Davis* [illegible] *Schaeffer*, 1955].

In Table 2 the Cl^{36} contents of several [illegible] samples are listed as well as a value for the [illegible] content of a Vermont stream and Long Is[illegible] ground water.

Discussion. As seen from Table 2, the [illegible] activity in rain is measurable with low-l[illegible] counting techniques. The problem now is [illegible] determine the source of this activity. The [illegible] most likely sources are cosmic rays and nuc[illegible] devices. As the amount of activity one m[illegible] expect from these two sources is likely to [illegible] orders of magnitude different it is possibl[illegible] infer the origin of the Cl^{36} by estimating [illegible] relative production rate of Cl^{36} by cosmic [illegible] and by nuclear explosions.

The amount of Cl^{36} produced by cosmic [illegible] interactions with the atmosphere can be [illegible] mated by a slight modification of the calcula[illegible] made by Lal [*Lal, Malhortra, and Peters*, 1[illegible] for S^{35}. In the atmosphere, S^{35} and Cl^{36} [illegible] produced by simple reactions of cosmic [illegible] from argon. The productions can be relate[illegible] the occurrence of stars in photographic emuls[illegible] exposed to cosmic rays. The nuclear ev[illegible] are recorded by the tracks originating at [illegible] atom interacting with the cosmic ray. E[illegible] charged particle coming out of the interac[illegible] is shown by a track. As sulphur is two cha[illegible] less than argon, sulfur will be produced in [illegible] and two pronged stars, one pronged if the ch[illegible] of the particle is +2 and two pronged if [illegible] particles are protons. On the other hand, chlo[illegible] being only one charge less than argon, will [illegible] be produced by single-pronged stars, one p[illegible] of charge one. The probability P_S and P_{Cl} [illegible]

TABLE 2. Chlorine-36 in Rain and Surface Water

Sample*	Date Collected	Amount Collected, liters	Cl Content, mg/liter	Cl^{36} Activity, d/m-g Cl	Atoms Cl^{36}, per ml of water
No. 2	Aug. 1957	4500	1.1	3.0	770,000
No. 3	Sept. 1957	8300	0.85	9.2	1,830,000
No. 5	April 1959	8500	0.24	4.3	240,000
No. 6	May 1959‡	6800	0.004	12.2	10,200
No. 7	Feb. 1960	3900	1.4	0.80	263,000
Island Well	Aug. 1957	2500	2.7	1.02	640,000
ont Stream	Sept. 1957	2800	0.27	0.56	35,000
Ronkonkoma	Sept. 1960	6040	4.1	0.28	268,000

he rain samples are composite samples of several rain falls over a two to four week period.
t the end of a long rainy period.

ıcing respectively sulfur and chlorine is . in terms of the relative probabilities n_1 n_2 of the occurrence of single- and double-ged events by:

$$P_S = n_1(1 - p) + n_2p^2 \quad (1)$$

$$P_{Cl} = n_1p$$

e p represents the probability that a given is single charged, and $1 - p$ is the then ıbility that a given track is double charged. ng $p = 0.83$ and $n_1/n_2 = 5/3$ [*Lal, Mal-a, and Peters*, 1958] one computes $P_{Cl}/P_S =$ or the relative production of chlorine to r. Then using an interpolation formula for lating the isotopic distributions with the ants given by *Rudstam* [1955], one computes 30 per cent of the chlorine production is and that 34 per cent of the sulfur production . The production ratio of Cl^{36}/S^{35} is then The production has been integrated [*Lal, ıortra, and Peters*, 1958] on a world-wide taking into account the variation of ic rays with latitude and altitude. The l production rates obtained in this way for and S^{35} are listed in Table 3 along with values for Cl^{36} obtained by multiplying the alues by 1.2.

ıe observed Cl^{36} activity is about 3,000 s higher than the estimated cosmic-ray uction rate. On the other hand, the same od of estimation gives reasonable agree- for the calculated and observed value of and S^{35} content of rain. This suggests that Cl^{36} has a different origin than the P^{32} or probably nuclear explosions. It is unlikely enough Cl^{36} could be produced by fission

TABLE 3. Global Average Production of P^{32}, S^{35}, and Cl^{36} by Cosmic Ray Interactions with Atmospheric Argon

Isotope	Atmospheric Production Rate 10^3 atoms per cm^2 column-year: Troposphere	Stratosphere	Total	Average found in rain
P^{32}	4.4	8.8	13	
S^{35}	8.1	15	23	
Cl^{36}	10	18	28	80,000*

* Average value at 40° latitude which is near the average production rate.

so the Cl^{36} is most likely the result of neutron irradiation of sea water by marine nuclear explosions.

Dyrssen and Nyman [1955] have computed the relative slow neutron induced radioactivity produced in sea water by a nuclear explosion. They estimate the ratio of atoms of Cl^{36}/S^{35} to be 230, while the value found is 3300 (based on comparison of 1957 rains in India and on Long Island) [*Goel, Narasappaya, Prabhakara, Rama, and Zutshi*, 1959] roughly 15 times higher. The high Cl^{36} activity can be understood if most of the S^{35} has decayed before the activity comes down in rain. This is certainly the case in the rains of 1959 which were collected some time after bomb testing had stopped. A very likely model is that after a burst the part of the activity in the troposphere is washed out in a relatively short time, of the order of a month; then the part of the activity which was blown into the stratosphere remains there long enough that most the S^{35} decays and the ratio

of Cl^{36} to S^{35} is higher than at production.

The Cl^{36} has been added to the atmosphere in a relatively short time and serves as a spike for studying geological problems. If bomb testing is not resumed the Cl^{36} will gradually leave the stratosphere and will enter the ground water and, finally, into the sea, where it will essentially be lost because of the large amount of stable chloride in the sea. Indeed, we have already detected Cl^{36} in ground waters. By a careful sampling procedure it should be possible to study the processes involved in the storage of water underground.

Acknowledgment. Research for this paper was performed under the auspices of the U. S. Atomic Energy Commission.

References

Arnold, J. R., and H. Al-Salih, *Science, 121,* 451, 1955.
Davis, R., and O. A. Schaeffer, BNL (340) 1955.
Dyrssen, D., and P. O. Nyman, *Acta Radiolc* *43,* 421, 1955.
Faltings, V., and P. Harteck, *Nature,* London 1109, 1950*a*.
Faltings, V., and P. Harteck, *Z. Naturforsch* 438, 1950*b*.
Goel, P. S., *Nature, 178,* 1458, 1956.
Goel, P. S., N. Narasappaya, C. Prabhakara, Rama, and P. K. Zutshi, *Tellus, XI,* 91, 1959
Katcoff, S., *Nucleonics, 16,* 78, 1958.
Lal, D., P. K. Malhortra, and B. Peters, *J. mospheric and Terrestrial Phys., 12,* 306, 19
Lal, D., N. Narasappaya, and P. K. Zutshi, *clear Phys., 3,* 69, 1957.
Lal, D., Rama, and P. K. Zutshi, *J. Geo Research, 65,* 669, 1960.
Marquez, L., N. L. Costa, and I. G. Alm *Nuova cimento, 6,* 1292, 1957.
Rudstam, S. G., *Phil. Mag., 46,* 344, 1955.

(Manuscript received August 31, 1960.)

Reliability of Hourly Precipitation Data[1]

ARNOLD COURT[2]

Pacific Southwest Forest and Range Experiment Station
Forest Service, U. S. Department of Agriculture
Berkeley, California

Abstract. Properly exposed, calibrated, and evaluated, the customary 8-inch-diameter weighing rain gage yields hourly precipitation values with standard errors of about .01 inch, so that reliability within .02 inch can be assumed. But two identical gages 10 feet apart on a windy ridge top can differ consistently in catch by 50 per cent of the smaller. Four pairs of identical gages, exposed side by side at four sites in Santa Barbara County, California, January-April 1959, were studied.

ntroduction. Reliability within .02 inch for rly precipitation amounts, obtained from ghing rain gages operated and evaluated in a ine manner, is indicated by the records for pairs of gages operated in the mountains of hern California during 1959. The gages, all nch-capacity dual-traverse (Friez) weighing gages 8 inches in diameter, had been lent by U. S. Weather Bureau to the Department Vater Resources of the State of California.

'he gages were installed, calibrated, mained, and read by the Department of Water ources personnel in the customary manner, pt that calibrations were monthly and were le with bucket in place rather than with the of a 'bucket weight.' This procedure, though e tedious, was found by the staff meteorolts to give more reproducible results. The rt drums revolved every 24 hours, but would from 7 to 10 days on one winding. Charts e changed weekly by experienced meteorolts, Harold Vedera and Herbert G. Dorsey, Jr. 'he installations were part of the elaborate -gage network operated in and around Santa bara County for evaluation of the effects of d seeding with silver iodide from grounded generators. The four twin gage sites were:

Location	Gage Nos.		Lat. N.	Long. W.	Elevation, ft
Cachuma Saddle	T-23	T-36	34° 43.5	119° 55.1	3100
Potrero Seco	T-27	T-37	34 38.3	119 25.6	4840
Horse Canyon	T-17	T-35	34 37.1	119 51.1	1465
T-V Peak	T-7	T-31	34 31.5	119 57.5	3990

All are within 30 miles of Santa Barbara (Fig. 1). T-V Peak is in the coastal mountains, 5 miles from the ocean; the other three sites are north of the Santa Ynez River, which flows westward north of the coastal mountains. Three of the four locations are within the Los Padres National Forest, the fourth (Horse Canyon) is on an adjacent ranch. The photographs of the four sites (Figs. 2–6) were taken on March 4 and April 2, 1959.

At each location, a single recording gage had been operated during two previous winters. A second gage at each location was installed to help insure continuity of record, in case of clock stoppage or other gage malfunction. Hourly precipitation data from the four sites were vital to the analysis of the results of the cloud seeding experiment.

Actually, at two of the four sites one of the paired gages did not operate for one or more days during the period. At Cachuma Saddle, paper expansion forced the clip off the drum of the older gage (T-23), causing loss of its record from February 7 to 11. During this period the newer gage (T-36) caught 5.32 inches in 46 hours. Total catches of the two gages, by special volumetric check, differed by only .02 inch. At

---

[1] This report is the outgrowth of a cooperative rt of the Experiment Station with the Statisti- Laboratory of the University of California and Department of Water Resources of the State California.

[2] Now at Applied Climatology Branch, Geosics Research Directorate, U.S.A.F., Bedford, ss.

Fig. 1. Santa Barbara County, Calif., and adjacent areas. Dots indicate locations of recording rain gages used in evaluating effects of cloud seeding whose primary target (inside dotted line) was drainage area of Santa Ynez River above Cachuma Dam. Locations of four pairs of duplicate gages are shown by larger dots, and labeled.

Potrero Seco, the pen was knocked below the clock flange of the newer gage (T-37), perhaps by wind or the splash of heavy precipitation, causing loss of the record on February 11 and 12, when the older gage (T-27) caught 1.50 inches in 27 hours. No volumetric check could be made because colder weather after the storm had frozen the accumulated precipitation in the buckets. Both these periods were omitted the following analysis of the reliability o individual gage readings.

Discussion. Almost all the precipitation ing the winter of 1959 at these four sites f rain; snowfall was negligible. Charts from eight gages were evaluated routinely along those from 42 similar gages. Gages are c

Fig. 2. Cachuma Saddle, toward SSE. ewer gage (T-36) at left, older (T-23) at ht. Helicopter used in servicing gages is hidn behind trees and brush at left.

d by number, and evaluators usually were aware that certain gages were side by side, at preliminary evaluation was independent such pairing. Later, checks were made o days of precipitation, but not hourly unts.

each location the second gage caught less the original one, but only at one station, Peak, was the difference significant. Here it striking: the new gage caught only about -thirds as much rain as the old one. This rence was consistent from hour to hour (Fig. and day to day (Table 1). The correlation veen the hourly catches of these two gages 0.97.

iewed from the east (Fig. 5), the two record- gages on T-V Peak seem to have almost tical exposures. But the view from the th (Fig. 6) shows that the older gage (T-7) the lee of a clump of chamise and ceanothus, le the newer gage (T-31) is much less pro- ed. The older gage caught 30.80 inches dur- 4 months while the newer one recorded only 0 inches. But an 8-inch standard Weather eau gage, even closer to the chaparral clump n the older gage, caught 22.85 inches, only a e more than the newer, more exposed gage. dings of this gage, made at 5 P.M. daily by staff of the nearby television station, and y amounts for the two recording gages for same period, are given in Table 1.

Vhat was the true precipitation on T-V Peak ing these 4 months? Presumably it varied

TABLE 1. Daily Rainfall Catches, at 5 P.M., of Three Gages on T-V Peak, Santa Barbara County, Calif., Jan.–Apr. 1959, in inches

Date	Std.	Old	New	New/Old
Jan. 5	.70	.65	.43	.66
6	4.68	6.52	4.95	.76
7	.05	.11	.10	.91
8				
9	T			
10		.07	.05	.71
11				
12		.01		
13	.37	.45	.34	.75
...				
25	.10	.17	.06	.35
...				
Feb. 1	T			
...				
7	.43	.58	.39	.67
8		.14	.12	.86
9				
10	5.00	6.51	3.90	.60
11	1.37	2.58	1.43	.55
12	.19	.20	.07	.35
...				
15	.18	.29	.21	.72
Feb. 16	2.83	4.57	3.00	.66
17				
18	3.50	3.52	2.50	.71
19	.03		.01	
20				
21	1.48	1.76	1.50	.85
...				
Mar. 23	.05	.06	.04	.67
24	.04			
...				
Apr. 24	T	.04	.02	.50
25	1.55	2.39	1.69	.71
26	.30	.18	.19	1.05
...				
Total	22.85	30.80	21.00	.68

from point to point almost as much as did the catches of these three gages. These results emphasize the difficulties of rain-gage operation in windy sites, and the need for adequate wind shelter.

At the other three pairs of gages, differences in hourly catches were less than .08 inch, except for 2 hours at each gage. These hours were consecutive at two of the gages, and separated by an hour at the third. Such differences apparently arise when a heavy burst of rain falls just at the hour. Then a lag of only a few minutes in the clock, or even slight differences in pen friction, can transfer rain from one hour to the next.

The number of hours in which the new gage differed from the old by various small amounts (in hundredths of an inch) were:

Diff., new − old	−7	−6	−5	−4	−3	−2	−1	0	1	2	3	4	5	6
Cachuma Saddle	1		1	2	4	11	27	38	20	9	3	2	1	
Potrero Seco				2	1	18	32	50	30	7	3			
Horse Canyon		1	1		4	14	42	42	37	7	3	1	1	
T-V Peak	6	12	6	11	15	23	43	18	30	8	3	1		1

Differences greater than 0.07 inch are shown clearly on the scatter diagrams of Figure 7, but the large numbers of small departures could not be clearly indicated there.

At each of the first three places, more than two-thirds of the differences were between +0.01 and −0.01 inch. Except for the extremes, the differences were independent of the actual amounts caught, as shown in the scatter diagrams of Figure 7. They were also independent of the hour of the day, and of the month.

How reliable is an individual gage reading of hourly precipitation? Since gages in each pair were identical in construction, each is presumably as reliable as the other. Hence the best estimate of the precipitation at each site is the mean of the readings of the two gages. This assumption, and the further assumption that the errors of any one gage reading have a normal statistical distribution, permit the standard deviation of an individual reading to be estimated. It is obtained by squaring and adding the hourly differences, dividing by twice the number of observations, and extracting the square root. (The factor of 2 enters because the difference between two readings is twice as great as departure of either one from the presumed value.)

Fig. 3. Potrero Seco, toward WNW. Newer gage (T-37) at left, older (T-27) on right.

The mean differences between gages, and standard deviations, were computed (A) fo hours at each site, and (B) for all hours ex the two that differed most, due to clock irr larities. Results, in hundredths of an inch, w

	Number of Hours		Mean Difference between Gages		Stanc Devia
	A	B	A	B	A
Cachuma Saddle	123	121	1.67	1.28	2.67
Potrero Seco	145	143	1.08	0.92	1.34
Horse Canyon	155	153	1.21	1.06	1.44
T-V Peak	220	218	5.04	4.68	6.34

Neglecting the one extreme pair of hour each site reduced the standard deviations ap ciably. The standard deviation of a single ho rainfall figure from a recording gage, prop exposed—or rather properly sheltered from wind—is about 0.02 inch when all data are u and slightly over 0.01 inch when major data ferences due to clock adjustment are igno But the standard deviation is several ti larger for data from a gage that is improp exposed to the rain-bearing winds.

Comparison. Despite the increasing us weighing precipitation gages in the United S in the past 20 years, no similar determinatio the operational accuracy of such gages app to have been published. The extensive studi the San Dimas Experimental Forest [*Hami* 1954], in very similar terrain about 100 mil the east, involved different methods of expo tilting, and support, so that no two adja gages were identical. In a similar study, *Hel* [1954] exposed two weighing (recording) two standard (nonrecording) gages side by on a steep, windy slope; one weighing and standard gage had stereo orifices, the other had horizontal orifices; the weighing gages shielded, the standard gages unshielded. In

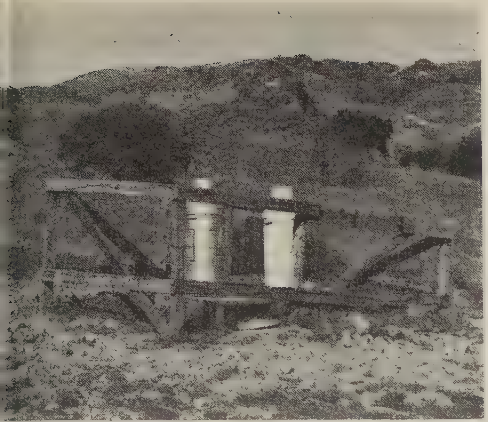

Fig. 4. Horse Canyon, toward NNE. Newer ıge (T-35) at left, older (T-17) on right. This ıte, on San Marcos Ranch, is the only one of ıe four not on the Los Padres National Forest ınds proper, and hence was fenced to protect he gages from range cattle.

Fig. 5. T-V Peak, toward WSW. Rain gages are, from left to right, Weather Bureau standard 8-inch, old recorder (T-7), new recorder (T-31). Precipitation totals for the four months, Jan.-April 1959, were, respectively, 22.85, 30.80, and 21.00 inches. (Photograph taken on March 4, 1959, by Harold Vedera.)

borate Thunderstorm Project in Ohio a 'netrk of 55 precipitation gages spaced on apximately two-mile centers' over a 10 x 22 e area was used [*Linsley and Kohler*, 1951], no site was replicated.

Near Austin, Texas, 'four tipping-bucket, two ıtinuous-wire, one weighing gage, and two p-size gages were distributed uniformly along 1,000-ft. attenuation measurements path' during 1955–1957 [*Gerhardt*, 1958]. For the next season these, and eight modified tipping-bucket gages, were placed in two parallel 1500-ft lines for 2 months, thereafter in a single line, with '400 simple totalizing gages located at 40-foot intervals.' South-to-north movement of showers, and 'significant horizontal variations in the rate' of rainfall were found, but no two

Fig. 6. T-V Peak, toward south. Older recording gage (T-7) and 8-inch standard gage, at left, are partially sheltered by chamise and ceanothus from southerly rain-bearing winds; newer gage (T-31) at right is more exposed to winds.

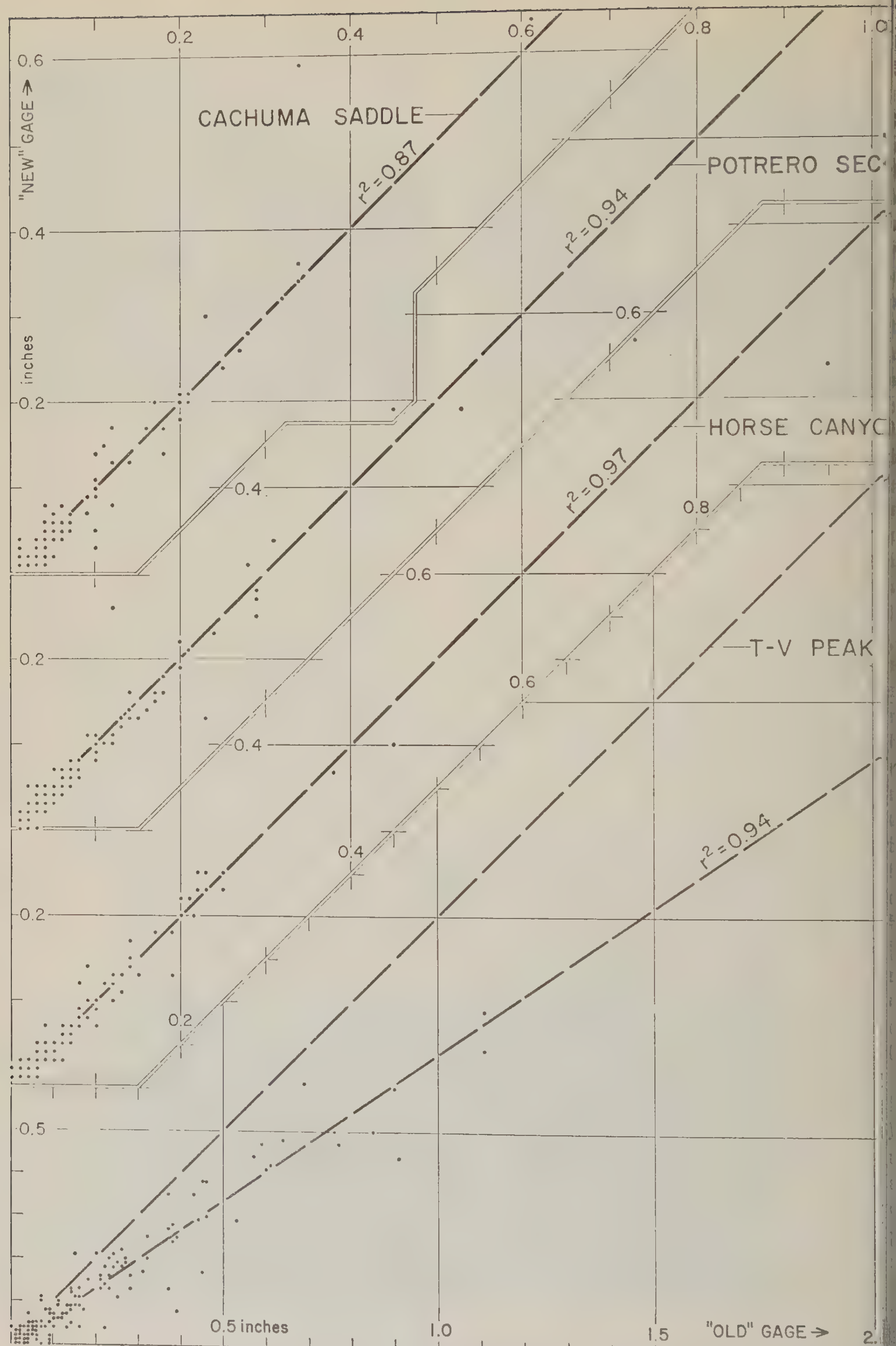

Fig 7. Hourly precipitation catches of duplicate gages at four sites in Santa Barbara County, January–April 1959.

ntical gages were close enough together to stitute instrumental replication.

.t the Central Sierra Snow Laboratory in ifornia during the 1947–1948 winter, seven es were exposed 'only a few feet apart, hav- been located in general as close as seemed sible without obstructing one another,' but y had 'different combinations of shielding, e of gage, etc.' [*Wilson,* 1954]. A correlation 0.98 was found between the daily (not hourly) als of a Friez gage on a 20-foot tower and a vens gage on a 15-foot tower 20 feet away; h were shielded. 'The scatter shows differ- es due to the different positions of the gages the forest clearing, differences in the gage pe and mechanism, differences in reading the arts, capping of one or the other gage at times rors due to capping may affect timing as well total storm catch), missing record, different ality of servicing from time to time, and addi- nal influences that might be suggested,' Wil- n said. 'The standard error of estimate is about 4 inch.'

Nine standard British (5-inch-diameter) non- cording gages 30 feet apart in a 3 × 3 grid, ad daily for 20 months, showed individual vari- ions from the group means of 4.5 per cent onthly total 0.33 inch) to 0.8 per cent onthly total 3.79 inches); *Watkins* [1955] tributed the differences to exposure rather an to gage errors. In Iowa, eight gages made om 6-inch-diameter No. 10 cans fitted with nnels 1.5 inches below the rims were mounted pipes 3 feet apart in a cross, with a standard eather Bureau 8-inch gage in the middle *Jrsic and Thames,* 1958]. In 63 storms total- g 43 inches from April to December 1957, two- irds of the can readings were within 0.01 inch that of the standard gage—and hence within 02 inch of each other.

Extensive replication of identical gages a few et apart was employed by the Illinois State ater Survey in its exhaustive study of rainfall easurement and characteristics. Pairs of stand- d (not recording) 8-inch gages were installed feet apart at the corners, center, and mid- oints of the 600-foot sides of a square on a level eadow at the University of Illinois airport *Huff,* 1955*a*]. The average difference between e storm totals (not hourly or daily amounts) ught by the pairs of gages were, by storm sizes *Huff,* 1955*b*]:

Storm avg., inch	.01–.19	.20–.49	.50–.99	1.00–2.00
Number of storms	46	19	15	13
Avg. diff., inch	.003	.005	.009	.020

For comparison, the average differences (regardless of sign) of the hourly amounts at three pairs of gages (excluding T-V Peak) in the Santa Barbara experiment were 0.017, 0.011, and 0.012 inch, for a grand average of 0.013. These values are somewhat larger than Huff's, presumably because they apply to hourly totals rather than to storm totals.

Conclusions. Hourly precipitation amounts obtained from a standard 8-inch-diameter weighing rain gage, operated routinely in accordance with instructions, apparently are reproducible within 0.02 inch most of the time. This range of error is comparable to that due to the type of chart paper in use. At Santa Barbara, Vedera found that, with increasing humidity, the chart paper expands by about 0.05 inch in 6 inches (1 per cent) at the center of the chart, less at the ends where it is held by the clip. Presumably, adjacent identical gages undergo similar paper expansion, so that this effect is not reflected in the differences found in the present study.

The largest source of error connected with rain-gage readings lies in the assumption that they represent the actual precipitation at the site. As was found for T-V Peak, in exposed places precipitation varies markedly in distances of 6 to 10 feet. But at more sheltered locations, such as the other three sites studied, hourly rainfall totals are about the same at places a few feet apart. Whether these totals represent the actual rainfall on the ground, or are merely proportional to it, is not established. For measuring the amount of rain falling into a funnel, hour by hour, the 8-inch-diameter weighing rain gage, in a sheltered location, seems acceptably reliable.

References

Gerhardt, J. R., Observations of small-scale rainfall-rate time variations with sensitive rainfall recording instruments, *Bull. Am. Meteorol. Soc., 39,* 189–194, 1958.

Hamilton, E. L., Rainfall sampling on rugged terrain, *U. S. Dept. Agr. Tech. Bull. 1096,* 41 pp., Dec. 1954.

Helmers, E., Precipitation measurements on wind-

swept slopes, *Trans. Am. Geophys. Union, 35,* 471–474, 1954.

Huff, F. A., Comparison between standard and small orifice raingages, *Trans. Am. Geophys. Union, 36,* 689–694, 1955*a*.

Huff, F. A., A micrometeorological study of rainfall variability, *Bull. Am. Meteorol. Soc., 36,* 489–490, 1955*b*.

Linsley, R. K., and M. A. Kohler, Variations in storm rainfall over small areas, *Trans. Am. Geophys. Union, 32,* 245–250, 1951.

Ursic, S. J., and J. L. Thames, An inexpensive ra gage, *J. Soil and Water Conserv., 13,* 231–2 1958.

Watkins, L. H., Variation between measureme of rainfall made with a grid of gauges, *Meteo Mag., 84,* 350–354, 1955.

Wilson, W. T., Analysis of winter precipitation servations in the cooperative snow investi tions, *Monthly Weather Rev., 85,* 183–199, 19

(Manuscript received July 29, 1960.)

The Drainage of Liquids from Porous Materials

E. G. YOUNGS

Agricultural Research Council Unit of Soil Physics
Huntingdon Road, Cambridge, England

Abstract. An equation is derived to describe the yield of liquid at a given time from a freely draining column of initially saturated porous material in a gravitational field by using a capillary tube model. The equation is supported by experimental evidence.

Introduction. The theory of land drainage at e present time is handicapped by our inability take into account the time-dependent drainage the unsaturated region above the water table ring nonsteady-state conditions except in the nplest approximate way [*Childs*, 1960]. *Day d Luthin* [1956] have shown that the numeril procedure of solving the equation of liquid w in unsaturated porous materials [*Richards*, 31; *Childs and Collis-George*, 1950; *Klute*, 52] for the simpler one-dimensional case of a eely drained column of porous material, inilly saturated, is long and tedious for acceptble accuracy in the final solutions. Another proach is used here to investigate this parcular problem.

Although the capillary tube model of porous aterials has met with only moderate success in lculations of permeability [*Childs and Collis-eorge*, 1950], infiltration equations based esntially on the model of a column of porous aterial as a capillary tube have been introduced predict the infiltration into soils [*Green and mpt*, 1911; *Philip*, 1954]. It is of interest to e what success attends the use of such a model r the case of the unimpeded drainage of inially saturated columns of porous material.

The drainage from a capillary tube. Conder a capillary tube of radius r and length L itially full of liquid of density ρ and intercial tension γ with an angle of contact with e surface of the tube θ. Further, let r be small that inertia effects during the drainage may e neglected. Let the capillary tube start draing freely in a gravitational field αg at zero me. By Poisseuille's law the flow at time t is escribed by the equation

$$-\pi r^2 \frac{dz}{dt} = \frac{\pi r^4}{8\eta} \cdot \frac{\Phi}{z} \tag{1}$$

where η is the viscosity of the liquid and Φ the difference in potential between the meniscus of the liquid at a height z above the bottom of the tube and the base of the tube. The potential difference Φ is the sum of that due to the height of the liquid and that arising from the surface forces at the meniscus. Thus

$$\Phi = z\rho\alpha g - 2\gamma \cos \theta / r \tag{2}$$

If h is the height of liquid left in the capillary tube after infinite time, then the last term of equation 2 becomes $\rho\alpha gh$ and equation 1 becomes

$$-\frac{dz}{dt} = \frac{r^2}{8\eta} \frac{(z - h)\rho\alpha g}{z} \tag{3}$$

Integrating equation 3

$$\frac{r^2 \rho\alpha g t}{8\eta} = L - z - h \ln\left(\frac{z - h}{L - h}\right) \tag{4}$$

If there are n tubes per unit cross section, then the initial flux F_0 from the base of the bundle of tubes is $n\pi r^4(L - h)\rho\alpha g/8\eta L$, and the total quantity of liquid Q removed after a time t is $n\pi r^2(L - z)$. Equation 4 can be rewritten after rearrangement

$$\frac{F_0 t}{Q_\infty} = -\ln(1 - Q/Q_\infty) - \frac{1}{2}\left(\frac{Q}{Q_\infty}\right)\left(\frac{Q}{R}\right) - \frac{1}{3}\left(\frac{Q}{Q_\infty}\right)^2\left(\frac{Q}{R}\right) - \cdots \tag{5}$$

where $Q_\infty = n\pi r^2(L - h)$, the quantity of liquid drained after infinite time, and $R = n\pi r^2 L$, the total quantity held initially in the tubes. If the series terms can be neglected, equation 5 becomes

$$1 - Q/Q_\infty = e^{-\tau} \tag{6}$$

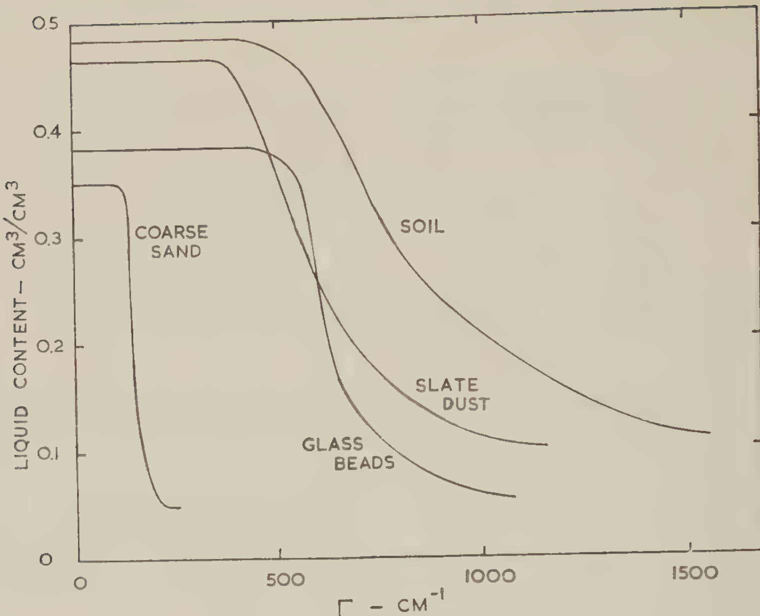

Fig. 1. The liquid content–suction relationships for the porous materials used in the experiments.

where $\tau = F_0 t/Q_\infty$. By differentiating Q/Q_∞ with respect to τ, the ratio of the flux at a given time to that at zero time is obtained.

The drainage from columns of porous material. In the model of a column of porous material used in deriving the infiltration equation, the suction in the soil at the wetting front is taken as constant, corresponding to the interfacial tension effect at the meniscus in a capillary tube. In the drainage case here considered, we assume the 'drainage front,' the fairly sharp demarcation observed between the saturated porous material and that which is partially drained, to be at a constant suction and to act in a similar fashion to the meniscus in a capillary tube. Equation 5 then holds for columns of porous material if it is also assumed that an equal quantity of water drains for an equal advance of the drainage front. This concept is very similar to that of a constant specific yield assumed in the approximate theory of the nonsteady state in land-drainage studies, the difference being that here the fall of the top of the capillary fringe in the column is considered instead of the fall of the water table which is at the base of the column throughout the drainage. The errors involved in such an assumption have been well explained by *Childs* [1960]. It follows from Childs' arguments that with (5) the ra[illegible] Q/Q_∞ during the initial period of time of t[illegible] drainage of a column will be overestimated. T[illegible] mathematical approximations leading to ([illegible] cause an underestimate of the ratio Q/Q_∞ at [illegible] given time as given by (5). Thus the physi[illegible] model and the mathematical simplification [illegible] troduce errors of the opposite sign, and ther[illegible] fore (6) may describe the drainage more a[illegible] curately than (5).

In the case of the drainage of liquids fr[illegible] initially saturated columns of porous materia[illegible] the quantities F_0 (equal to dQ/dt at the sta[illegible] of the drainage) and Q_∞ in the dimensionless e[illegible] pressions in (6) can be obtained from a plot [illegible] the yield of liquid Q from a given colum[illegible] against the time. They can also be obtain[illegible] from a knowledge of the permeability and t[illegible] relationship between the liquid content and t[illegible] suction for the particular porous material.

The liquid content–suction relationships f[illegible] the porous materials used in the experimen[illegible] study are given in Figure 1. The materials us[illegible] were a coarse sand consisting of particles b[illegible] tween 1.0 mm and 0.25 mm in diameter, sm[illegible] glass beads less than 0.1 mm in diameter, a sla[illegible] dust containing particles between 0.125 and 0.[illegible] mm in diameter, and a disturbed soil mater[illegible]

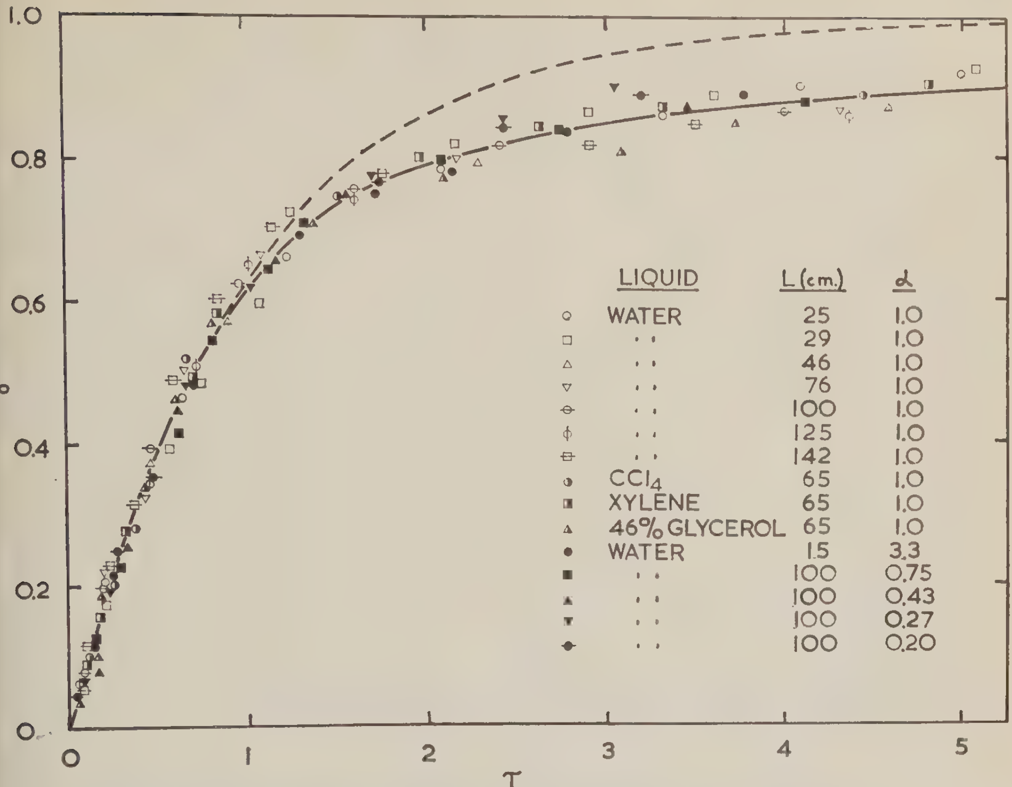

Fig. 2. The variation of Q/Q_∞ with τ for the experiments with the coarse sand. The broken line is that given by equation 6.

rom a fen silt profile consisting mainly of parti-les between 0.2 mm and 0.02 mm. In Figure 1 he suction is plotted in a form that is inde-endent of the liquid used and dependent only n the size of the pore by putting

$$\Gamma = \rho\,\alpha g H / 2\gamma \cos\theta \tag{7}$$

vhere H is the suction expressed in centimeters f the given liquid. The relationships were btained for samples of the porous materials ontained in Haine's apparatuses with water s the liquid; the angle of contact of water vith the surfaces of the particles was assumed o be zero so that $\cos\theta$ was unity.

In all the porous materials it is observed that o liquid drains until a certain value of the uction corresponding to a value Γ_0 is reached, ppropriate to the emptying of the largest ores in the material. The suction at the surface f the column of porous material must therefore each a value $2\gamma\Gamma_0 \cos\theta/\rho\alpha g$ before appreciable rainage starts. The porous material has a uniform permeability while it is saturated, so that at the beginning of the drainage there is a uniform potential gradient down the column equal to $(\rho\alpha g L - 2\gamma\Gamma_0 \cos\theta)/L$, where L is the length of the column. The initial flux out of the base of the column is

$$F_0 = \frac{(\rho\alpha g L - 2\gamma\Gamma_0 \cos\theta)K_s}{\eta L} \tag{8}$$

where K_s is the saturated permeability of the porous material for a hypothetical liquid of unit viscosity. Values of K_s were 0.0093, 0.00059, 0.00019 and 0.00010 cgs units for the coarse sand, the glass beads, the slate dust, and the soil, respectively.

The quantity Q_∞ can be obtained directly from the area above the liquid content–suction relationship between $\Gamma = 0$ and $\Gamma = \Gamma_m$ (Γ_m is defined later). After infinite time the suction H is equal to the height above the base of the column. Thus

$$\rho\alpha g z = 2\gamma\Gamma \cos\theta \tag{9}$$

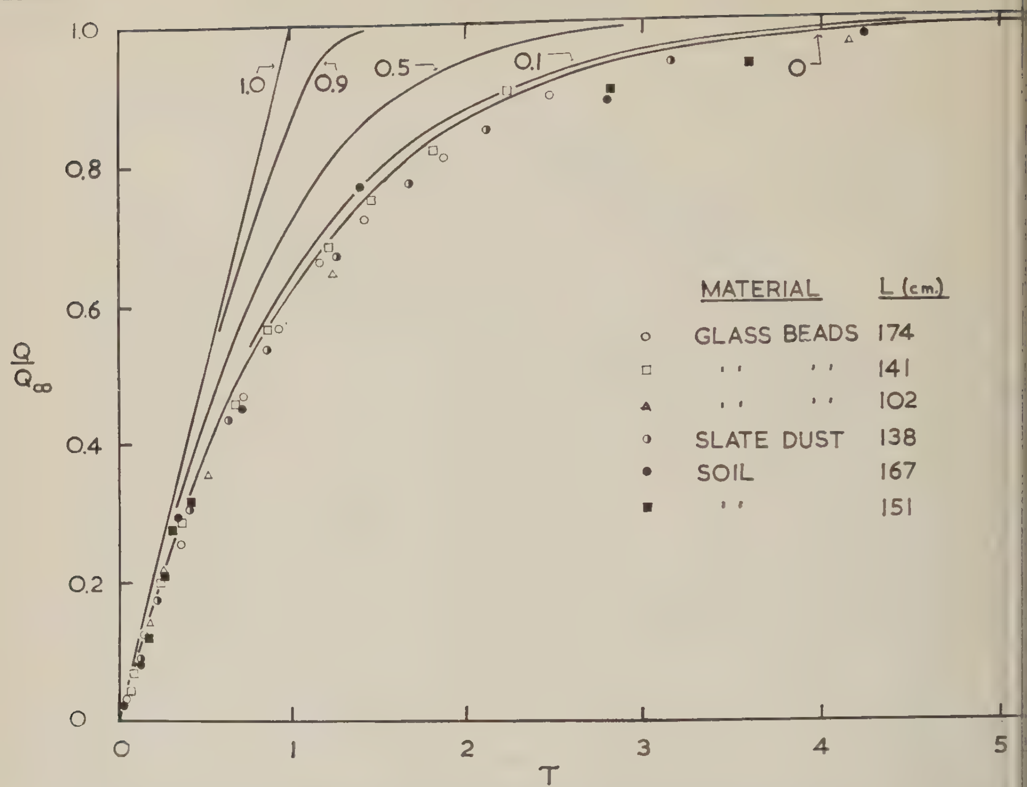

Fig. 3. The variation of Q/Q_∞ with τ for the experiments with the finer porous materials. The curves are the relationships given by equation 5 for different values of Q_∞/R. When $Q_\infty/R = 0$, the curve is the same as that given by equation 6.

where z is measured upwards from the base. Q_∞, the yield after infinite time per unit cross section of the column, is given by

$$Q_\infty = \int_0^L (c_s - c)\, dz$$

$$= \int_0^L (c_s - c)\, d\left(\frac{2\gamma\Gamma \cos\theta}{\rho\alpha g}\right)$$

$$= \frac{2\gamma \cos\theta}{\rho\alpha g} \int_0^{\Gamma_m} (c_s - c)\, d\Gamma \qquad (10)$$

where c is the liquid content and the subscript s indicates saturation, and $\Gamma_m = \rho\alpha g L/2\gamma \cos\theta$.

Experimental procedure. Experiments with columns of porous materials were conducted to investigate the yield of liquid as a function of time for the unimpeded drainage from saturated columns for the following conditions: (a) various lengths of column with various porous materials under a gravitational field of g; (b) various liquids with different values of density, in[...] facial tension, and viscosity; (c) various gr[...] tational fields.

For the first series of experiments, glass t[...] of diameter 4.0 cm and 1.2 cm and of len[...] between 170 cm and 25 cm were filled with[...] dry porous material, being tapped continu[...] during the filling to obtain uniform pack[...] The porous material was contained at the [...] tom of the tube by means of a sintered plat[...] greater permeability than the porous mate[...] Water was used as the liquid. The columns [...] saturated by infiltrating water from a po[...] surface. Infiltration was continued until w[...] started draining from the base of the colu[...] It was then stopped, and, at the moment w[...] the water disappeared from the surface, m[...] urement of the yield from the base of the [...] umn with increasing time was begun. The m[...] urement could be done automatically wit[...] modified rainfall recorder with a 1-day c[...] mechanism. It was found that the flux of w[...]

suing from the base of the column showed a scontinuity with time as the column changed om percolation with the surface ponded to ainage; this gives confirmation to the argu- ents leading to equation 8.

Another series of experiments was done to de- rmine what effect a change in density, inter- cial tension, and viscosity would have on the eld as a function of time. The other liquids ed besides water were carbon tetrachloride, lene and a 46 per cent solution of glycerol in ater. Listed in this order, the densities were 0, 0.87, and 1.12 g cm^{-3}, the interfacial ten- ns were 27, 30, and 70 dynes cm^{-1}, and the scosities were 0.0097, 0.0062, and 4.95 poises, mpared with values for water of 1.0 g cm^{-3}, 73 nes cm^{-1}, and 0.01 poise. Columns 75 cm long the coarse sand were used in this investigation d the procedure adopted in the experiments as the same as in the previous experiments th water.

Finally, experiments were conducted to in- stigate the effect of a change in the gravita- nal field causing the drainage. For values of e gravitational field less than g, the column the porous material was inclined at an angle to the horizontal. The gravitational field down e column was then αg, where $\alpha = \sin \beta$. Values α of 0.75, 0.43, 0.27, and 0.20 were obtained this way with experiments on the drainage of ater from columns of coarse sand 100 cm long. he experiments were otherwise conducted in a milar manner as before. A value of $\alpha = 3.3$ as obtained by centrifuging. Columns of coarse nd, 15 cm long, were mounted horizontally at e end of arms 61 cm long after first being turated in a vertical position. No water drained it from the column after the cessation of in- tration in the vertical position because the ngth of the column was such that the critical lue Γ_0 could not be reached. The arms of the ntrifuge were then rotated at a rate of 75 rpm. t intervals during the experiment, the rotation as stopped and the column weighed in order to sess the drainage from the columns. For the mputation of α, the gravitational field at the idpoint of the column was calculated; thus an verage value of α was obtained over the length the column.

Discussion of results. In Figure 2 Q/Q_∞, the tio of the yield at a given time to the total nal yield of the draining column, is plotted against values of τ ($= F_0 t/Q_\infty$) for the experiments with the coarse sand. It is observed that all the experimental points lie on one curve, indicating that Q/Q_∞ is a unique function of τ for the drainage of different liquids from different lengths of column in various gravitational fields. It is seen that the curve fits the plot of equation 6 for values of τ up to $\tau = 1$ when the fractional yield $Q/Q_\infty = 0.63$. For higher values of τ, Q/Q_∞ values are lower than predicted by the equation. In Figure 3 are given some results for the drainage of water from saturated columns of other porous materials made up of finer particles. The fractional yield obtained with these as a function of τ is seen to follow closely the algebraic relationship of (6).

We noted previously that the physical assumptions of the capillary tube model for a column of porous material which led to (5) might be offset by the mathematical approximations which were introduced to obtain the dimensionless equation 6; this is upheld in the experiments. In Figure 3 are given the theoretical relationship between Q/Q_∞ and τ for the capillary tube model as given in (5) for various values of Q_∞/R. This latter ratio is dependent on the experimental variations employed in the experiments. For a given value of τ, the value of Q/Q_∞ is always greater than that given by (6), the opposite effect to what is observed in the experiments with columns of porous material. The experiments thus give support to the caution which must be used in assuming a constant specific yield, implicit in the capillary tube model, in nonsteady-state drainage calculations.

It is concluded from these experiments that equation 6 is useful in predicting the yield from a column of porous material which is draining freely. Q_∞ and F_0 can be obtained from simple preliminary experiments as indicated in equations 8 and 10, and the relationship between the yield Q and the time t obtained for the given column.

References

Childs, E. C., The nonsteady state of the water table in drained land, *J. Geophys. Research, 65*, 780–782, 1960.

Childs, E. C., and N. Collis-George, The permeability of porous materials, *Proc. Roy. Soc. London, A, 201*, 392–405, 1950.

Day, P. R., and J. N. Luthin, A numerical solution of the differential equation of flow for a vertical drainage problem, *Soil Sci. Soc. Am. Proc., 20,* 443–447, 1956.

Green, W. H., and G. A. Ampt, Studies in soil physics, 1, Flow of air and water through soils, *J. Agr. Sci., 4,* 1–24, 1911.

Klute, A., A numerical method for solving the flow equation for water in unsaturated materials, *S[illegible] Sci., 73,* 105–116, 1952.

Philip, J. R., An infiltration equation with physi[illegible] significance, *Soil Sci., 77,* 153–157, 1954.

Richards, L. A., Capillary conduction of liqu[illegible] through porous mediums, *Physics, 1,* 318–[illegible] 1931.

(Manuscript received May 17, 1960.)

Water Level Control in Evaporation Pans[1]

BESSEL D. VAN'T WOUDT

Hawaii Agricultural Experiment Station, College of Agriculture
University of Hawaii, Honolulu, Hawaii

Abstract. An attempt has been made to develop a fixed-water-level pan evaporimeter utilizing the Mariotte principle and flanged overflow nozzles for rejecting rain. Owing to temperature effects, frictional losses in conduits, and surface tension effects, the Mariotte principle proved to be only partially satisfactory. The overflow nozzles showed curious meniscus behavior, depending on the shape of the rim. They were unsuited for the purpose and have been replaced by a float-operated ball and valve system. If a fixed water level in a pan is maintained, a shallow depth of water is necessary. This shallow depth causes the daily pattern of evaporation to closely follow daily air temperature fluctuation.

Introduction. There are two possible errors in conventional pan evaporation measurement: (1) the assumption that the rainfall collected by a pan is the same as the rainfall measured by a nearby rain gage and (2) a fluctuating water level in the pan.

Rain intercepted by evaporation pans. Rain recorded by a nearby rain gage is used on successive days to correct the readings from standard Weather Bureau pans. Data collected by a recording evaporation pan developed by D. C. Cox of the Experiment Station of the Hawaiian Sugar Planters' Association [*H.S.P.A.*, 1958, pp. 35–39] were used for assessing the effect of this procedure. The water level in this pan was kept constant by allowing continuously circulating water to overflow through a plastic nozzle placed in a stilling well in the center of the pan. Evaporation from this pan and addition of water to it from rain were measured in a nearby supply tank by a float recorder as a drop or rise in water level. The pan used had standard Weather Bureau pan dimensions: diameter, 4 feet; height, 10 inches; and a water level 2 inches below the rim.

Table 1 shows the results of nearly 8 months of measurement. (The measurements were discontinued because of the difficulties experienced in keeping the required small pump continuously operating under field conditions.) In this table evaporation from a standard Weather Bureau pan and from the described recording pan are compared, as well as the rain measured by a standard Weather Bureau rain gage and by the recording pan. During heavy rain, measurements from the Weather Bureau pan and the recording pan were not reliable and adequate data during such periods are lacking. A particularly large error may be introduced during these periods, and it is for this reason that evaporation data from a Weather Bureau pan are often rejected on days of heavy rain.

Fluctuating water level in evaporation pans. The effect of a fluctuating water level in a standard Weather Bureau pan is unavoidable. The water level should be kept between 2 and 3 inches below the rim. (*Boynton* [1950] recorded a difference in evaporation of 15 per cent as the water level varied by 2 inches.) Either rain or water-level fluctuation thus introduces an error in pan evaporation measurement.

Although the significance of pan evaporation for meteorological considerations has been debated, the usefulness of these data in irrigation practice has been recognized. For this reason it seemed appropriate to attempt to refine the measurement. As will be described below, to accomplish this, a pan operating on the Mariotte principle in combination with an overflow nozzle was tried [*Stark and Whitfield*, 1930; *Reeve and Furr*, 1941]. Other attempts (unpublished) to use these principles have been made elsewhere, and it seems worth while to point out the limitations of this technique as established by the experimental work reported below.

The Mariotte principle. The Mariotte principle is illustrated in Figure 1. In this system

[1] Hawaii Agricultural Experiment Station Technical Paper No. 484.

TABLE 1. Evaporation from a Weather Bureau Pan and a Recording (HSPA) Pan and Rainfall Measured by a Standard Rain Gage and by the Recording Pan (all instruments a few feet apart)

Period 1958	No. of Days	Evaporation		Rain Measured by		Wind at	
		USWB Pan	HSPA Pan	Gage	HSPA Pan	USWB Pan	HSP. Pan
		inches		inches		total miles*	
4/8–4/30	23	4.488	4.388	0.71	0.741		
5/1–5/31	31	6.347	6.394	1.37	1.479		
6/1–6/4							
6/6–6/30	29	7.181	6.636	1.63	1.57	1741.7	1842.
7/1–7/21							
7/26–7/31	27	5.596	4.894	3.07	2.692	1668.1	1536.
8/1							
8/10–8/27	19	5.726	4.594	0.50	0.448	1287.3	1335.
9/8–9/30	23	5.513	4.650	1.24	1.074	1483.9	1542.
10/1–10/22							
10/28–10/31	26	4.779	4.678	1.10	0.97	1544.6	1507.
11/1–11/30	30	4.393	4.16	0.96	0.92		
12/1–12/31	31	4.47	4.026	2.48	2.457		
	239	48.493	44.420	13.06	12.35	7725.6	7764.

* Wind was measured at 1 foot above pan level.

the difference between atmospheric pressure and that in a volume of air above the water surface within a supply tank causes a column of water to be held above the water level in a connected outside reservoir exposed to the air. The water level in the outside reservoir is determined by the level of the bottom end of an air vent protruding below the water surface inside the supply tank. This is a simple and widely known principle used in bird baths and ink wells; however it apparently has not been described in texts.

One limitation of this method arises from the

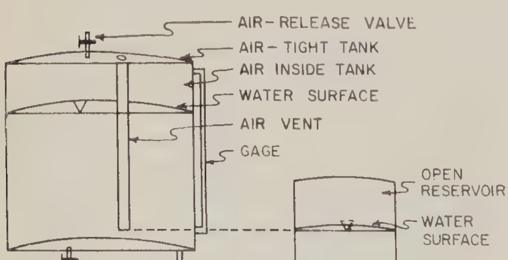

Fig. 1. Example of supply tank with Mariotte principle for maintaining a 'fixed' water level in a connected reservoir open to the atmosphere (in cross section).

need to keep the air temperature in the sup tank constant. Even though the daily temp ture under the conditions of testing did not v more than 15°F, it proved to be a factor wh caused water to be pushed out of the sup tank upon expansion of the air above the w and to re-enter the supply tank from the side reservoir when the air cooled.

For the equipment used in the tests (a s ply tank 2 feet in diameter and an air vol varying from 1 to 40 inches in height, and outside reservoir 4 feet in diameter), a temp ture change of 15°F gives a calculated maxim water-level fluctuation in the outside reser of 0.30 inch and a minimum one of 0.007 i

To reduce the temperature effect, the sup tank was insulated with two 1-inch layers fiberglas wool, over which additional plastic terial was applied, and the outside was pai with aluminum paint. However, water temp ture in the supply tank still fluctuated by during the day. The fluctuation in air temp ture within the tank remained unknown but probably greater. One-degree temperature f tuation still caused the water level in the side reservoir to vary from 0.03 to 0.0004 i For this particular type of instrument it considered impracticable to provide additi

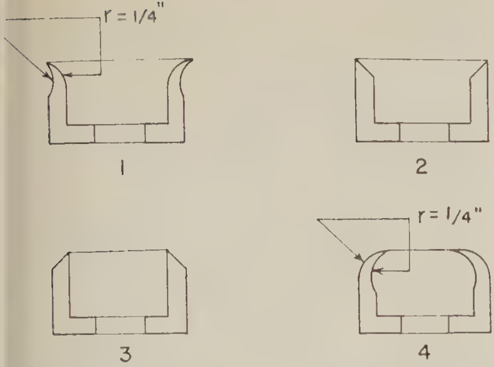

Fig. 2. Cross section through overflow nozzles used for draining rainfall from evaporation pan.

ısulation aimed at eliminating the last trace of ·mperature effect, because of other weaknesses s discussed below.

Minute friction losses in the conduit between ıe supply tank and the reservoir require a nall differential head to initiate flow from the ıpply tank to the reservoir. This is evidenced y the observation that increasing the diameter f the connecting tubing from ¼ to ½ inch auses bubbling (entry of air through the air ent in the supply tank) to be more frequent nder comparable conditions. However, by iminating flow through any conduit in a metal ıodel with plastic windows it was found that ıtermittent bubbling is not related to frictional ·sistance in conduits alone. In the field instruıent, bubbling occurred at intervals, after about 00 ml (0.0015 inch) had been removed from ıe reservoir. In the laboratory model, bubbling as induced after about 300 ml had been reıoved from the reservoir.

The air vent in the model was then so adısted that the bottom end of it could be made p of glass tubes, varying in diameter from ¼ ı 1 inch. The size of the tubing did not have ny discernible effect on the interval between ubblings. Through the plastic window, hower, it could be seen that, as water removal rom the reservoir was started, the water ıeniscus gradually rose within the air-filled air ent. Renewed bubbling apparently did not tart until after a sufficient pressure difference ad built up to overcome the surface tension of ıe water at the bottom of the air vent. Once ubbling started it continued till the original water level in the reservoir had been restored. The agitation of the water due to the bubbling or the inertia of the moving water might account for the continuation of bubbling as a result of a temporary lowering of the interfacial tension [*van't Woudt*, 1959]. Independent of the size of the air vent, the average air bubble had a volume of 17 ml, as determined by water displacement.

TABLE 2. Meniscus Behavior during Overflow over the Nozzles Shown in Figure 2.

Nozzle	Height of Meniscus at Time Overflow Starts, inches $\times 10^{-3}$	Difference between Heights of Meniscus at which Overflow Starts and Stops, inches $\times 10^{-3}$
1	130	113
	145	126
	139	112
	149	123
average	141	118
2	172	120
	162	120
	164	117
	168	116
average	166	118
3	192	69
	180	67
	189	69
	192	75
average	188	70
4	189	50
	185	45
	185	50
	193	50
average	188	49

Overflow nozzles. Small fluctuations in water level in a reservoir due to temperature changes, frictional losses, and presumed surface tension effects become significant when rainfall in the reservoir needs to be drained. Such drainage was attempted by overflow nozzles of the type shown in Figure 2. The nozzles were machined from the same piece of stainless steel. Their curious behavior under field conditions led to the testing of a model from which the observations given in Table 2 are derived. The difference in behavior was obviously due to the shape of the nozzle. The data show that the height of the meniscus at overflow increases in

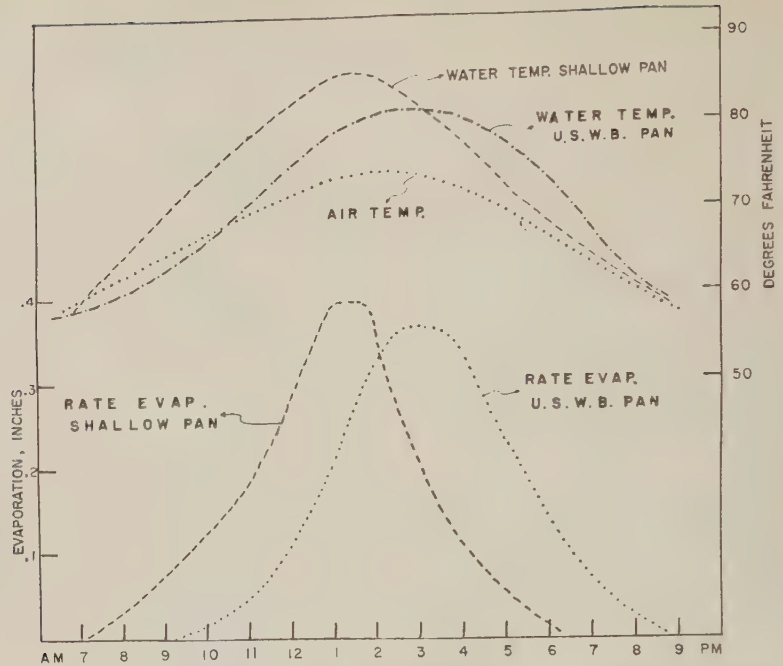

Fig. 3. Typical daily air and pan water temperatures and daily pattern of evaporation from an evaporation pan with 1 inch (shallow pan) and 8 inches (U. S. Weather Bureau pan) depth of water.

passing from a divergent, flanged nozzle, to those with an inside and outside 45° angle, to a convergent, flanged nozzle. However, overflow stops at varying meniscus levels. The meniscus drop on overflow is lowest for nozzle 4 and this nozzle should thus be most satisfactory for rain rejection as long as a correction of 0.049 inch is made for each rainfall. Unfortunately, little reliance can be placed on this figure under field conditions. Minute particles at the water surface change the meniscus height, and if a particle lodges across the nozzle rim, the water level in the reservoir may fall below the level of the rim as a result of capillary siphoning.

This type of overflow system thus proved quite unsatisfactory. The negative results are, however, recorded here because of the curious behavior of the different types of nozzle tested. An extensive review of the literature did not reveal a record of similar behavior. It is probable that an explanation could be given on the basis of nozzle geometry. This has not been attempted, as it was felt to be beyond the scope of this study.

A more satisfactory solution for controlling overflow from a reservoir following rain was found to be the use of large carburetor val attached to a small float in a stilling well. Th allowed control of the water level to within 0 inch. However, under field conditions, corros and dirt interfered with this mechanism in long run. Consequently, the carburetor syst was replaced by a Teflon ball fitting int nylon valve seat, similarly controlled by a fl at the water surface. This system has been erated for several months under field conditio and the same principle has recently been u to control inflow more accurately than is p sible by utilizing the Mariotte principle. Ho ever, even this system still presents proble under field conditions, and a long-term fi testing program is still in progress.

Meanwhile, accepting an error ranging fr 0.01 to 0.03 inch introduced by each rainf the Mariotte principle, in combination with ball and valve seat mechanism, has been plied for more than a year for approxim measurement of pan evaporation in two isola areas in the Hawaiian Islands where only wee or fortnightly readings can be made.

The effect of water depth. Drainage of r necessitating the setting of a sharply defi

tflow level, makes it necessary to use a shal- v pan. The 8-inch depth of water in a stand- d Weather Bureau pan gives a fluctuation in ter level due to thermal expansion over a nge from, say, 58° to 90° F (20° to 30° C) of 019 inch. For that reason a shallow pan (2 hes deep) was used, having the same diameter the Weather Bureau pan (4 feet). In this pan e water depth was kept to 1 inch. With this pth of water, thermal expansion over the ove temperature range causes a fluctuation of 023 inch only, which is considered acceptable.

Changing the depth of water from 8 inches to inch alters the heat storage in the water. gure 3 shows typical daily data for 1-inch and inch water depth in the 2-inch pan under test d a 10-inch Weather Bureau pan. The total aporation per 24 hours is the same, but in the allow pan evaporation starts soon after sun- e and stops after sunset. In line with this, the ily pattern of water temperature in the shal- w pan follows the pattern of air temperature ore closely than in the deep pan. In the deep n heat accumulation in the water after sunrise accounts for a delay in evaporation and a continuation of evaporation after sunset, apparently at the expense of the stored heat. Because of insignificant heat storage in plant tissue, a thin layer of water in a shallow pan gives a daily pattern of evaporation which follows more closely that of daily transpiration than is given by a thicker layer of water in a deep pan.

References

Boynton, C. W., Evaporation studies using some South Australian data, *Trans. Roy. Soc. S. Australia, 73,* 198–219, 1950.

H.S.P.A., Report of the Hawaiian Sugar Planters' Association Experiment Station, 1958.

Reeve, J. O., and J. R. Furr, Evaporation from a shallow black pan evaporimeter as an index of soil moisture extraction by mature citrus trees, *Proc. Am. Soc. Hort. Sci., 39,* 125–132, 1941.

Stark, O. K., and C. J. Whitfield, An improved evaporimeter, *Ecology, 11,* 288–292, 1930.

van't Woudt, B. D., Particle coatings affecting the wettability of soils, *J. Geophys. Research, 64,* 263–267, 1959.

(Manuscript received May 11, 1960; revised September 15, 1960.)

Water Flow through a Soil Profile as Affected by the Least Permeable Layer[1]

DALE SWARTZENDRUBER

Purdue University, Lafayette, Indiana

Abstract. Water movement through a water-saturated soil profile is analyzed on the basis of Darcy's law for a sectionally continuous hydraulic conductivity along a one-dimensional, downward flow path. The resulting relationships are used to assess the effect of the least permeable layer on the flow through the profile. It is shown that the hydraulic conductivity of the least permeable layer does not of itself control the flow.

A second analysis, based on a quantity defined as the hydraulic resistance, shows that the hydraulic resistance of the least permeable layer controls the flow through the profile with much less error than does the hydraulic conductivity. Furthermore, the error becomes negligible as the hydraulic resistance of the least permeable layer increases.

INTRODUCTION

.. statement frequently encountered among scientists is that the flow of water through ..turated soil profile is limited by the hydrau- ..conductivity of the least permeable layer. .. essence of this statement appears in the ..ly used text of *Baver* [1948, p. 243] and is ..d on data of Wollny in which a 1-cm ..tum of loam was placed in a 50-cm column ..and; 50-fold reductions in flow through the ..mn were reported. In a later edition [*Baver,* ..6, p. 272] the statement is somewhat modi- .., but the exemplary data and their inter- ..ation remain the same. An application of idea appears in the work of *Nelson and ..kenhirn* [1941], who concluded that their ..hod of measuring infiltration rates was valid ..use the resulting values compared favor- .. with rates measured on soil cores taken .. the least permeable horizon.

..he beginning statement of the preceding ..graph is often interpreted in an extreme ..e, to the extent of implying that the hydrau- ..conductivity of the least permeable layer ..pletely controls flow through the profile. This ..eme interpretation will hereinafter be called limiting-layer concept. It is the purpose of .. paper to investigate the validity of this con- .. on the basis of Darcy's law. A mathemati- development follows immediately, in which several key formulas are derived. The limiting-layer concept is then evaluated with these formulas.

FLOW THROUGH LAYERED SYSTEMS

Hydraulic conductivity approach. Consider the steady-state, one-dimensional flow of water through the profile of a saturated porous medium of depth L, as shown in Figure 1. A constant level of water is maintained on the surface $z = 0$; outflow occurs into the very highly (infinitely) permeable stratum at the bottom of the profile. The hydraulic conductivity, $K(z)$, is constant in the lateral directions at any given value of z, but varies continuously with z in the interval $(0, L)$. Darcy's law is written in derivative form as

$$Q = -K(z) A \, dh/dz \tag{1}$$

where Q is the volume flow rate, A is the constant cross-sectional area of the profile, and h is the hydraulic head. Separating variables and integrating yields

$$Q \int_0^L \frac{dz}{K(z)} = -A \, \Delta h \tag{2}$$

where h_0 and h_L are the hydraulic heads at the inlet ($z = 0$) and outlet ($z = L$) surfaces, respectively, and $\Delta h = h_L - h_0$.

For a profile of variable hydraulic conductivity, the flow per unit area per unit over-all average hydraulic gradient can be calculated and defined as the equivalent hydraulic conductivity

---

[1] Contribution from the Department of Agron- ..y. Journal Paper No. 1646 of the Purdue Uni- ..sity Agricultural Experiment Station.

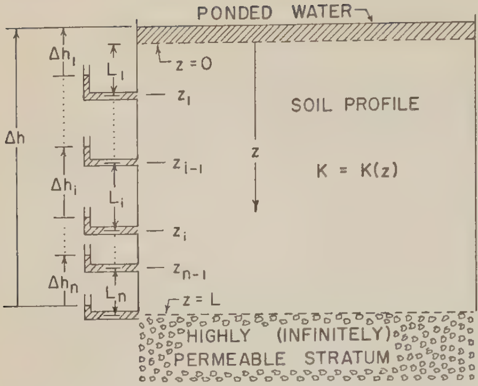

Fig. 1. Diagram of water flow through a saturated soil profile.

K_e of the entire profile, namely

$$K_e = -\frac{Q}{A\ \Delta h/L} \tag{3}$$

Combining equations 2 and 3 yields

$$K_e = \frac{L}{\displaystyle\int_0^L \frac{dz}{K(z)}} \tag{4}$$

Mathematically, K_e is simply the reciprocal of the average value of $1/K(z)$ over the interval $(0, L)$.

If $K(z)$ is continuous throughout the whole interval $0 \leq z \leq L$, it is continuous through any part. Thus, for the ith section we can write

$$K_i = \frac{L_i}{\displaystyle\int_{z_{i-1}}^{z_i} \frac{dz}{K(z)}} \tag{5}$$

where K_i is the equivalent hydraulic conductivity of the ith section and L_i is its depth. The denominator of equation 4 can be written

$$\int_0^L \frac{dz}{K(z)} = \sum_{i=1}^{n} \int_{z_{i-1}}^{z_i} \frac{dz}{K(z)} \tag{6}$$

Hence, using equations 4, 5, and 6, we find

$$K_e = \frac{L}{\displaystyle\sum_{i=1}^{n} L_i/K_i} \tag{7}$$

Equation 7 will apply even if $K(z)$ is only sectionally continuous. This is observed by noting that the order of addition in equations 6 and 7 is immaterial. Hence, the sections i (1 to n) could be rearranged in any desired flow sequenc and this introduces the condition of section continuity with discontinuities at the junctio of the sections. Hence, equation 7 is valid f any conceivable pattern of hydraulic condu tivity variation likely to be encountered in soil profile.

Note that the form of the conductivity add tivity relationship, equation 7, is a direct cons quence of the mathematical form of Darcy law. The same basic mathematical form appli to the flow of electricity, heat, and gas (ma movement), and to diffusion processes. Henc similar analyses for these phenomena wou yield additivity relationships mathematically t same as equation 7.

A special case of equation 7 arises when $K($ is sectionally constant; that is, $K(z) = k_i$ whe $z_{i-1} < z < z_i$, but the constants, k_i, are n necessarily equal. Putting this condition in equation 5 leads to equation 7, but with replacing K_i. Such an equation was derived b *Terzaghi* [1943, p. 244], presented without t derivation by *Fireman* [1941], and repeate later by *Russel* [1947]. It is felt that the Te zaghi-Fireman equation is unnecessarily restri tive, and that it is desirable to be aware of t general validity of equation 7.

Hydraulic resistance approach. For the pr file of Figure 1 let us define dR, the differenti

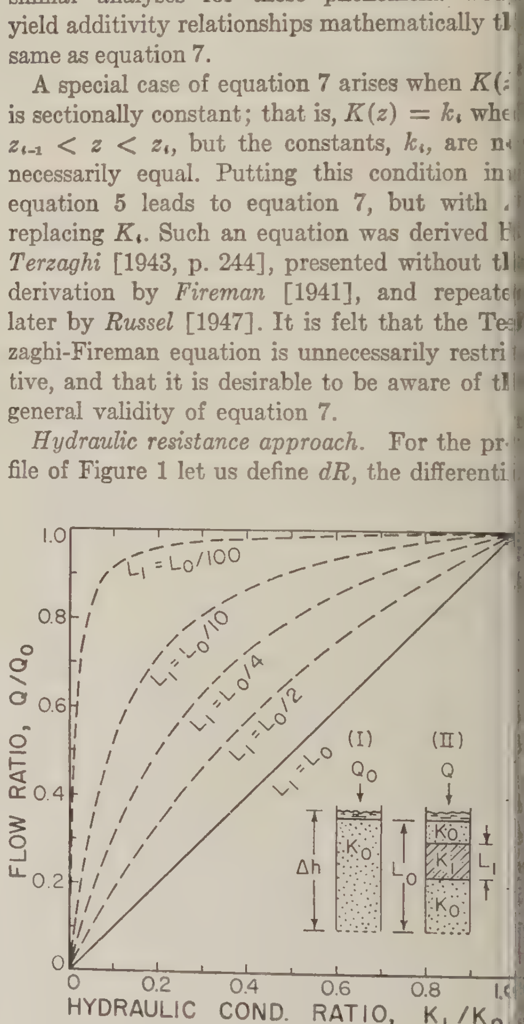

Fig. 2. Curves of flow ratio versus hydraulic conductivity ratio. Flow and soil profile conditions are shown diagramatically in (I) and (II).

the hydraulic resistance, to be

$$dR = \frac{dz}{AK(z)} \tag{8}$$

egration of this expression yields

$$R_e = \frac{1}{A}\int_0^L \frac{dz}{K(z)} \tag{9}$$

ere R_e is the equivalent resistance of the ole profile, and similarly

$$R_i = \frac{1}{A}\int_{z_{i-1}}^{z_i} \frac{dz}{K(z)} \tag{10}$$

ere R_i is the equivalent resistance of the ith tion. Combining equations 9 and 2 leads to e flow law

$$QR_e = -\Delta h \tag{11}$$

ich is completely analogous to Ohm's law for e flow of electricity. In differential form, equa- ns 8 and 1 combine to yield $QdR = -dh$. Substituting equations 9 into 4, and 10 into 5, lds, respectively,

$$R_e = L/AK_e \tag{12}$$

d

$$R_i = L_i/AK_i \tag{13}$$

en, if equations 12 and 13 are substituted to equation 7, the resistance additivity rela- nship becomes

$$R_e = \sum_{i=1}^{n} R_i \tag{14}$$

ich is completely analogous to the familiar rmula for the addition of electrical resistances. Note that the hydraulic resistance as defined equation 8 has a capacity aspect contributed the depth and cross-sectional area, as well an intensity aspect contributed by the hy- aulic conductivity. Its dimensions are time r unit area. Also, if the hydraulic conductiv- is constant in a profile, a calculation as uation 9 would yield $r = L/Ak$, where k is e constant hydraulic conductivity and r is e hydraulic resistance which no longer needs be designated as equivalent. However, the athematical form is unchanged from equa- n 12.

Limiting-Layer Concept Examined

On the basis of hydraulic conductivity. Consider a profile of length L_0, cross-sectional area A, and hydraulic conductivity K_0. (From here on the adjective 'equivalent' is being dropped for convenience, but the reader is reminded that the analysis is valid whether the conductivities are equivalent or not.) Water is ponded on the soil surface with a total head difference Δh, and the flow rate is Q_0. Compare with this the flow Q through a second profile containing a section L_1 of hydraulic conductivity K_1, where K_1 is less than K_0. In this second case, Δh, A, and total profile length L_0 are unchanged. The setups are diagrammed as I and II of Figure 2.

Applying Darcy's law to these two profiles and taking ratios yields

$$\frac{Q}{Q_0} = \frac{-K_e A\ \Delta h/L_0}{-K_0 A\ \Delta h/L_0} = \frac{K_e}{K_0} \tag{15}$$

Expressing K_e by equation 7 and rearranging yields

$$\frac{Q}{Q_0} = \frac{K_1/K_0}{L_1/L_0 + (K_1/K_0)(1 - L_1/L_0)} \tag{16}$$

Now the limiting-layer concept requires that the flow ratio Q/Q_0 equal the conductivity ratio K_1/K_0; from equation 16 it is seen that this is not so, in general. The nature of the relationship can be visualized more easily by plotting Q/Q_0 against K_1/K_0 for selected values of L_1, as is shown by the curves of Figure 2. There are three special circumstances under which Q/Q_0 is actually equal to K_1/K_0. These are for the trivial cases of $K_1 = 0$, in which no flow occurs; for $L_1 = L_0$, in which the whole profile has a conductivity of K_1; and finally for $K_1 = K_0$, in which there is no layer of reduced conductivity. For all other values of K_1/K_0 and $L_1 < L_0$, the actual flow is in excess of that expected by the limiting-layer concept, and the excess increases as L_1/L_0 decreases.

Since all curves of Figure 2 approach zero with K_1/K_0, one might expect the limiting-layer concept to be more correct as K_1/K_0 becomes small. This may be approached graphically by plotting the curves of Figure 2 on log-log paper, as is done in the upper left-hand part of Figure 3. The curve for $L_1 = L_0$, which is the expectation of the limiting-layer concept, is still the 45° diagonal as in Figure 2. It is clear that the

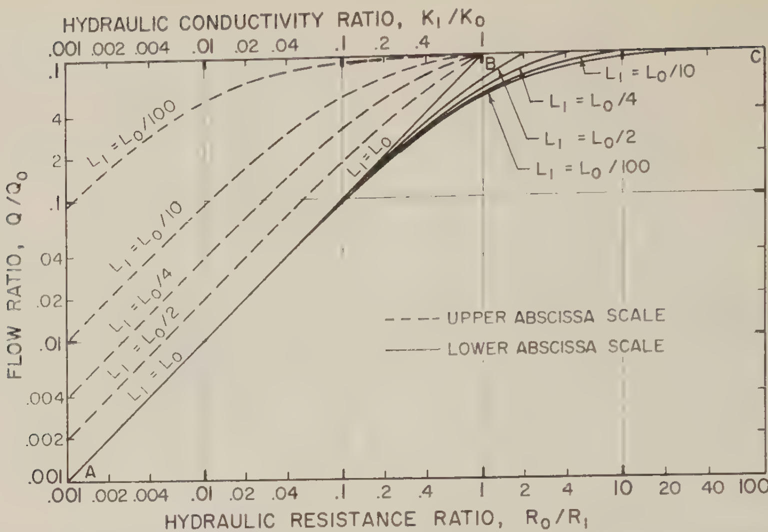

Fig. 3. Flow ratio versus hydraulic conductivity ratio (upper abscissa) and hydraulic resistance ratio (lower abscissa), all scales logarithmic.

curves for $L_1 < L_0$ do not approach the curve for $L_1 = L_0$ as K_1/K_0 becomes small. This can also be verified analytically from equation 16, in which it is seen that Q/Q_0 approaches $(K_1/K_0)(L_0/L_1)$ as K_1/K_0 becomes small, rather than approaching K_1/K_0 alone.

Thus, it is seen that the limiting-layer concept, when formulated in terms of hydraulic conductivity, fails rather badly on two counts. First, it is exact only under trivial circumstances; second, its failure becomes progressively worse as the hydraulic conductivity and the thickness of the least permeable layer become small. For all nontrivial circumstances, the actual flow always exceeds that predicted on the basis of the limiting-layer concept.

The physical mechanism causing failure of the limiting-layer concept may be visualized in I and II of Figure 2 by considering the total profile average hydraulic gradient $\Delta h/L_0$ and the sectional average gradient $\Delta h_1/L_1$. In I, $\Delta h/L_0$ produces a flow of Q_0, but in II it yields a flow of Q, less than Q_0, simply because the layer of lower conductivity has been introduced. But with $Q < Q_0$, less gradient is required to drive water through the sections that still have a conductivity of K_0 (thickness $L_0 - L_1$ in II). However, since the total gradient is still $\Delta h/L_0$, the gradient, $\Delta h_1/L_1$, through the least permeable layer is increased. Hence, the introduction of the least permeable layer causes in turn an increase in hydraulic gradient across it, thus partia[lly] compensating for its lower conductivity. Mat[he]matically, this is demonstrated by evaluati[ng] the gradient ratio, $(\Delta h_1/L_1)/(\Delta h/L_0)$. Usi[ng] Darcy's law and equations 7 and 15, and r[e]membering that $Q = Q_1$, where Q_1 is the fl[ow] through the least permeable layer, we find th[at] the result is

$$\frac{\Delta h_1/L_1}{\Delta h/L_0} = \frac{L_0}{L_1 + (K_1/K_0)(L_0 - L_1)} \qquad (1$$

which shows that $\Delta h_1/L_1$ exceeds $\Delta h/L_0$ for [K_1] less than K_0.

On the basis of hydraulic resistance. T[he] form of the flow law represented by equation [...] is applied to I and II of Figure 2 to obtain

$$\frac{Q}{Q_0} = \frac{-\Delta h/R_e}{-\Delta h/R_0} = \frac{R_0}{R_e} \qquad (1$$

where R_0 and R_e are the respective hydrau[lic] resistances of profiles I and II. From equati[on] 14 it follows that $R_e = R_1 + R_2$, where R_1 is t[he] resistance of the section of thickness L_1 (the lea[st] permeable layer), and R_2 is the resistance of t[he] remainder of the column, so that

$$\frac{R_0}{R_e} = \frac{R_0}{R_1 + R_2} = \frac{R_0/R_1}{1 + R_2/R_1} \qquad (1$$

From equation 13 it follows that $R_2 = (L_0 - L_1)/AK_0$ and $R_0 = L_0/AK_0$, which in turn le[ads]

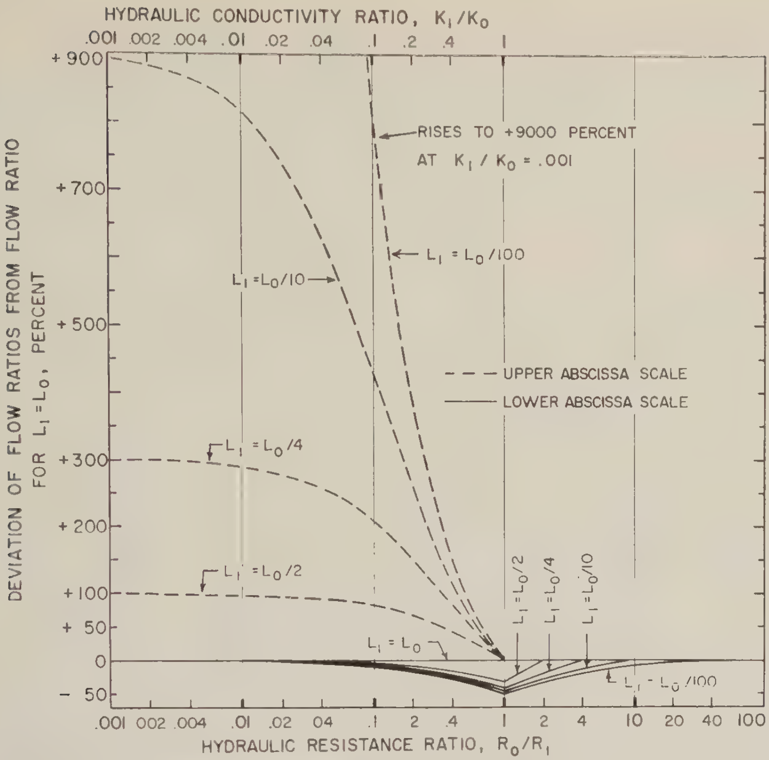

Fig. 4. Deviation of flow ratios from flow ratio for $L_1 = L_0$, for both the conductivity and resistance approaches.

$R_2 = (L_0 - L_1)R_0/L_0$. Putting this result into ɥuation 19 finally yields

$$\frac{Q}{Q_0} = \frac{R_0/R_1}{1 + (R_0/R_1)(1 - L_1/L_0)} \tag{20}$$

hich is the resistance counterpart of equation 3.

The resistance ratio R_0/R_1, in equation 20 has ›en chosen to decrease as the resistance of the ast permeable layer, R_1, increases; this facili-tes comparison between the conductivity and sistance approaches. Strict equality between $/Q_0$ and R_0/R_1, which is the requirement of the niting-layer concept, again is not always ob-ined unless $L_1 = L_0$. This is demonstrated by ie 45° diagonal in Figure 3, where log-log plots Q/Q_0 against R_0/R_1 are shown for the same ılues of L_1 used previously in the hydraulic nductivity approach.

For $L_1 < L_0$, unit flow ratios are obtained only r resistance ratios properly in excess of unity. his is a consequence of the hydraulic resistance ›pending on both thickness and conductivity. However, it is seen that the flow ratio–resistance ratio curves follow the curve ABC much more closely than the flow ratio–conductivity ratio curves follow the line AB. Furthermore, equation 20 shows that Q/Q_0 becomes indistinguishable from R_0/R_1 as the latter becomes small. This is shown in Figure 3 by the merging of all flow ratio–resistance curves for $R_0/R_1 < 0.01$, regardless of the value of L_1. This is in sharp contrast with the behavior of the curves of the hydraulic conductivity approach.

A further comparison of the two approaches is given in Figure 4. Here the standard of comparison is the expected flow ratio of the limiting-layer concept, which is line AB of Figure 3 for the hydraulic conductivity approach and line ABC for the resistance approach. On the linear-scale ordinate of Figure 4, there is plotted the percentage deviation of the actual flow ratio from the flow ratio for $L_1 = L_0$, defined as 100 $[(Q/Q_0) - (Q/Q_0)_1]/(Q/Q_0)_1$, where $(Q/Q_0)_1$ is the flow ratio for $L_1 = L_0$. From the figure it is clear that the error in the hydraulic resistance

formulation of the limiting-layer concept is zero for $R_0/R_1 < 0.01$; and, for the range of L_1 here considered, it is never more than -50 per cent for any resistance ratio. On the other hand, when formulated in terms of hydraulic conductivity, the limiting-layer concept is in error by generally more than $+50$ per cent, and it goes as high as $+9000$ per cent.

Discussion

It is not the purpose of this paper to insist that the limiting-layer concept must always carry the extreme connotation used here. It is believed, however, that the analysis shows quite definitely that we must not use the extreme connotation when a limiting-layer concept is formulated in terms of hydraulic conductivity. If, on the other hand, the concept is formulated in terms of hydraulic resistance, we could state, for saturated conditions, that the flow of water through a soil profile is limited by the hydraulic resistance of the least permeable layer. Even the most extreme interpretation of this statement does not result in an error magnitude of more than 50 per cent for $L_1 \geq L_0/100$, and as R_0/R_1 becomes small the error decreases. For $R_0/R_1 <$ 0.1, the error is small and the extreme interpretation becomes exact for most practical purposes. Furthermore, in terms of hydraulic resistance, the flow truly is 'limited' in the sense that actual flows are less than expected flows. This is demonstrated in Figure 3 by line *ABC*, which forms an upper limit for all flow ratio–resistance ratio curves. This is not true of the conductivity approach. Instead, the line *AB* [in] Figure 3 is a lower limit for all flow rat[io–] conductivity ratio curves.

Thus, it is recommended that statements [of] the nature of the opening sentence of this pa[per] be avoided, unless the necessary qualificati[ons] are added to ensure that an extreme interpre[ta]tion will not be made. An acceptable qualifi[ca]tion would be the inclusion of the thickness [of] the least permeable layer along with its hydr[au]lic conductivity, in the manner of *Russel* [194[7]] and *Adams, Kirkham, and Scholtes* [195[8]]. However, this qualification is simply and c[on]cisely included if the statement is formula[ted] in terms of hydraulic resistance.

References

Adams, J. E., D. Kirkham, and W. H. Schol[tes], Soil erodibility and other physical properties [of] some Iowa soils, *Iowa State Coll. J. Sci.*, [32,] 485–540, 1958.

Baver, L. D., *Soil Physics*, John Wiley & Sons, N[ew] York, 2nd ed., 398 pp., 1948; 3rd ed., 489 [pp.,] 1956.

Fireman, M., Permeability measurements on [dis]turbed soil samples, *Soil Sci.*, *58*, 337–353, 19[44].

Nelson, L. B., and R. J. Muckenhirn, Field per[co]lation rates of four Wisconsin soils having dif[fer]ent drainage characteristics, *J. Am. Soc. Agr[on.]*, *33*, 1028–1036, 1941.

Russel, J. C., The movement of water in soil [col]umns and the theory of the control section, *[Soil] Sci. Soc. Am. Proc.*, *11*, 119–123, 1947.

Terzaghi, K., *Theoretical Soil Mechanics*, J[ohn] Wiley & Sons, New York, 510 pp., 1943.

(Manuscript received July 26, 1960.)

URNAL OF GEOPHYSICAL RESEARCH VOLUME 65, NO. 12 DECEMBER 1960

Oxygen-Isotope Ratios in the Blue Glacier, Olympic Mountains, Washington, U.S.A.[1]

ROBERT P. SHARP, SAMUEL EPSTEIN, AND IRENE VIDZIUNAS

California Institute of Technology
Pasadena, California

Abstract. The mean per mil deviation from a standard (average ocean water) in the O^{18}/O^{16} ratio of 291 specimens of ice, firn, snow, and rain from the Blue Glacier is −12.4; extremes are −8.6 and −19.2. This is consistent with the moist temperate climatological environment. The O^{18}/O^{16} ratio of snow decreases with declining temperature of precipitation, and it also decreases with increasing altitude at 0.5/100 meters.

Analyses of the three principal types of ice, coarse-bubbly, coarse-clear, and fine, composing lower Blue Glacier, show that ratios for coarse-clear ice are generally lower and for fine ice they are mostly higher than the ratios for coarse-bubbly ice. This indicates that the fine ice represents masses of firn and snow recently incorporated into the glacier by filling of crevasses or by infolding in areas of severe deformation. Coarse-clear ice masses may represent fragments of coarse-bubbly ice within a breccia formed in the icefall. Because of unfavorable orientation, these fragments could have undergone exceptional recrystallization with reduction in air bubbles and, possibly, a relative decrease in O^{18}.

A longitudinal septum in the lower Blue Glacier is characterized by higher than normal O^{18}/O^{16} ratios. These values are consistent with an origin for this feature involving incorporation of much surficial snow and firn near the base of the icefall. Samples from longitudinal profiles on the ice tongue suggest that ice close to the snout comes from high parts of the accumulation area. Analyses from the light and dark bands of ogives are compatible with the concept that the dark bands represent greatly modified insets of firn-ice breccia filling icefall crevasses.

The range in ratios of materials is much greater in the accumulation area than in the ice tongue. This is attributed to homogenization, much of which takes place during the conversion of snow to glacier ice. This is supported by comparative analyses of snow layers when first deposited and months later after alteration. Refreezing of rain and meltwater percolating into underlying cold snow is an important mechanism as shown by analyses of ice layers and lenses in the firn formed in this manner.

Introduction. Some potential uses of oxygen-otope data in glaciological research have been lustrated by analyses of samples from the askatchewan and Malaspina glaciers [*Epstein nd Sharp,* 1959]. Other uses will be demon-rated by analyses of materials from Green-nd [*Benson,* 1960; *IGY Bull.,* 1959, pp. 82–83] nd Antarctica, to be published shortly. The sefulness of the stable isotopes of oxygen and ydrogen in glaciological research rests on the act that their range of abundance in snow is elatively large, far exceeding analytical errors f ±0.1 in the ratio values. The value and range f O^{18}/O^{16} ratios in glaciers depend principally pon meteorological conditions, especially upon he temperature at the time of snowfall. Thus he ratio varies with the storm, the season, the levation, and other factors. The accumulation area of a glacier acquires patterns in the distribution of O^{18}/O^{16} ratios which can be used as natural tracers. Although the ratios are modified during conversion of snow to ice and during subsequent flow within the glacier, this does not destroy their value as tracers. Among the modifying influences are freezing of meltwater and rain, capture of snow in crevasses, and homogenization by other unidentified processes. Thus the O^{18}/O^{16} ratios tell something about the original conditions of accumulation and reflect the influence of modifying processes during a subsequent history.

Oxygen-isotope studies of glaciers are still in a formative stage. The usefulness of this approach varies with the nature of a glacier, its environment, and the problems chosen for study. For example, the O^{18}/O^{16} ratios in snow on the Greenland ice sheet display simple relationships useful in stratigraphic correlation. In contrast, it

[1] Contribution No. 967, Division of Geological ciences.

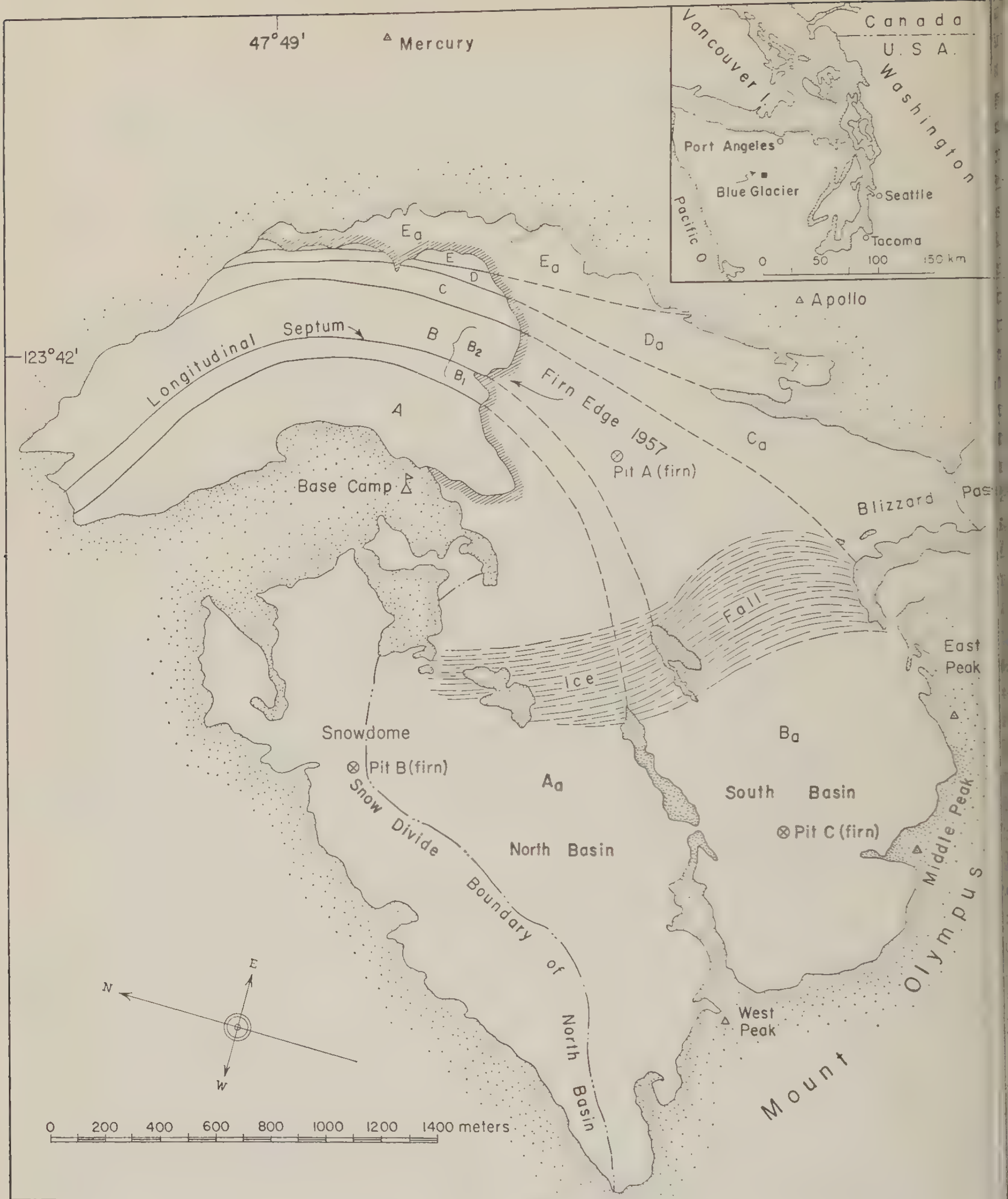

Fig. 1. Location, setting, shape and principal components of Blue Glacier.

appears that icefalls and temperate conditions with copious meltwater and rapid exchange of material lead to complications difficult to interpret. In investigations to date, the applicability of oxygen-isotope studies to all types of glaciers has not been satisfactorily defined. The present investigation was made in an attempt to determine the usefulness of the oxygen-isotope method on a small temperate glacier with a large material budget [*LaChapelle*, 1959, pp. 443–446].

The Blue Glacier was selected because it is relatively small, geometrically simple, and easily accessible; its constitution and structure ar

own [*Allen, Kamb, Meier, and Sharp*, 1960], d associated glaciological and meteorological idies contribute to an understanding of oxy- n-isotope relationships. The principal items estigated are (1) the range and mean value O^{18}/O^{16} ratios as related to general environ- ntal conditions and to the theory of oxygen- tope fractionation; (2) the influence of alti- de and temperature on O^{18}/O^{16} ratios; (3) anges in isotope ratios within firn layers dur- g alteration; (4) differences in isotope ratios the three principal types of ice, coarse-bubbly, arse-clear, and fine, composing this glacier d their bearing on the origin and history of ese types of ice; (5) differences in isotope tios of ice coming from various accumulation eas; (6) variations in isotope ratios along ngitudinal profiles on the surface of the ice ngue below the firn edge and their relation to w lines within the glacier; (7) differences in otope ratios of the materials composing ogive nds as an aid in understanding the origin of is structure; and (8) changes in oxygen-iso- pe ratios, if any, produced by recrystallization, anges of state, and other processes related to lid flow.

A general program of glaciological research as begun on Blue Glacier in the summer of 57; it has extended through 1960 and will be ntinued, with the permission of the National ark Service. It was preceded by Park Service servations in the 1940's and early 1950's and aciological and glacio-meteorological work dur- g 1955 and 1956 [*Hubley*, 1957], and it has een accompanied by glacio-meteorological re- arch on upper Blue Glacier from 1957 to 1959 *LaChapelle*, 1958, 1959]. Samples for oxygen- otope analyses were collected during the win- r of 1957–1958 and in the summers of 1958 d 1959.

Physical setting and constitution of the Blue lacier. The Blue Glacier is a small ice stream at rises high on the northeastern slope of ount Olympus (2413 m) in the heart of the lympic Mountains of northwestern Washing- n (Fig. 1). This glacier is 4.3 km long and km wide at the firn edge; it covers 4.3 km² d descends from a maximum elevation of 375 m to a terminus at 1265 m. The firn edge as an approximate elevation of 1600 m, and e bare ice tongue extends 2 km farther down e valley. A major icefall, 300 m high, 0.8 km upglacier from the edge of the firn, separates lower Blue Glacier from its principal accumulation basins, termed 'upper Blue Glacier.' The Blue Glacier, supposedly temperate, has a high rate of mass exchange owing to heavy accumulation and strong ablation [*LaChapelle*, 1959, p. 445].

The climatological environment is strongly maritime, that is, relatively warm and moist. Records from the Snowdome station at 2070 m on upper Blue Glacier [*LaChapelle*, 1958, p. 12] for the period August 1, 1957, to July 31, 1958, show a mean annual temperature of 1.6°C (34.9°F), a mean for the coldest month (March) of −6.1°C (+21.1°F), and a mean minimum for March of −8.9°C (16.1°F). The lowest temperature recorded was −15°C (5°F) and the highest 21.7°C (71°F). Total precipitation was 378 cm (148.9 inches) of water, of which 305 cm (119.7 inches), or 80 per cent, fell as snow. This period of observation was unusually warm and dry, judging from records at other meteorological stations in northwestern Washington, and the above figures are not representative of long-range means. In an average year the mean annual precipitation on Snowdome may exceed 500 cm (200 inches) of water.

Lower Blue Glacier consists of two major and three minor ice streams, each originating in separate accumulation areas (Fig. 1). Only major streams A and B extend to the snout; minor streams C, D, and E terminate along the east margin. Ice stream B consists of two currents below the icefall separated by an intensely foliated, structurally complex zone, the longitudinal septum, which is unusually rich in fine ice and coarse-clear ice. This septum separates two arc-shaped foliation patterns displayed by composite ice streams A + B_1 and B_2 + C (Fig. 1). Ice stream A also displays a series of weak ogives of the internal variety. Details of these and other structures are given elsewhere [*Allen, Kamb, Meier, and Sharp*, 1960].

Sampling and analysis. The method of analysis has been described elsewhere [*Epstein and Mayeda*, 1953, p. 214] and will not be reviewed here. In this paper, the result of an analysis is expressed as a relative, per mil deviation of the O^{18}/O^{16} ratio of the sample from the ratio of a standard—in this instance, mean ocean water. This value, termed δ, is calculated in the following manner.

TABLE 1. Oxygen-Isotope Ratios in Ice of a Core Taken 150 Meters below the Firn Edge in Ice Stream B, August 22, 1958

Depth, cm	δ Value of O^{18}/O^{16} Ratio
30.5	−12.5
61.0	−12.5
91.5	−12.3
122.0	−12.8
152.5	−12.8
183.0	−12.8
213.5	−12.9
244.0	−12.5
274.5	−12.4
305.0	−12.5
Average	−12.6

$$\delta = \left[\frac{H_2O^{18}/H_2O^{16}(\text{sample})}{H_2O^{18}/H_2O^{16}(\text{mean ocean water})} - 1\right] \times 1000$$

In such an arrangement the δ for mean ocean water is zero. Since the O^{18}/O^{16} ratio of all natural precipitation is lower than that of mean ocean water, the δ of such precipitation is always negative in this arbitrary system.

Accurate analyses of the materials composing a glacier are of limited value unless the significance of the specimen is fully understood in terms of the field relations. A clear understanding of structural relations and a recognition of the different types of ice on the Blue Glacier proved necessary for intelligent sampling, and specimens had to be collected with specific objectives in view.

The practice has been to dig to fresh-looking ice 10 to 20 cm beneath the surface before taking a sample, in order to eliminate possible surface effects. The data of Table 1 suggest that the near surface samples are reasonably representative of ice to a depth of at least 3 m. Data from core samples to that depth display a relatively high degree of homogeneity, the range in δ values being only 0.6 (−12.3 to −12.9). This compares nicely with a detailed surface traverse of similar dimensions on the Saskatchewan Glacier [*Epstein and Sharp*, 1959, p. 100], where the difference was 0.5 (−20.1 to −20.6).

Proper care of samples is necessary. It is particularly important that evaporation subsequent to collection be prevented. Our practice has been to place enough material in small-mouth plastic bottles to make 25 to 50 cc of wa[ter] when melted. The bakelite caps should be test[ed] for tightness several times after collection. P[os]sible evaporation can be observed by referen[ce] to lines drawn at water level on the outside [of] the bottles or by indenting the bottles sligh[tly] with the fingers before capping. If the inden[ta]tion remains, the cap is obviously tight. Samp[les] should be transferred to glass bottles in th[e] laboratory if they are to be stored for a co[n]siderable length of time.

Oxygen-isotope ratios in relation to the c[li]matological environment. The mean δ of 2[..] specimens from all parts of the Blue Glaci[er] representing glacier ice, firn, snow, and rain, [is] −12.4. This is not a truly representative figu[re] as it does not give weight in proper proportio[n] to the different materials; nonetheless it is [a] reasonable figure. The extremes recorded a[re] −8.6 and −19.2. These values confirm the ba[sic] hypothesis concerning fractionation of oxyg[en] isotopes in natural precipitation [*Epstein a[nd] Mayeda*, 1953, p. 220]. The Olympic Mountai[ns] lie in a moist, temperate environment that [is] not exceptionally cold even in winter. As theo[ry] predicts, these conditions yield only moderate[ly] low δ values as compared with much low[er] values from glaciers in truly cold environmen[ts].

Until 1957–1958 essentially nothing was know[n] from direct measurement of the meteorologic[al] conditions prevailing on Mount Olympus in wi[nter]

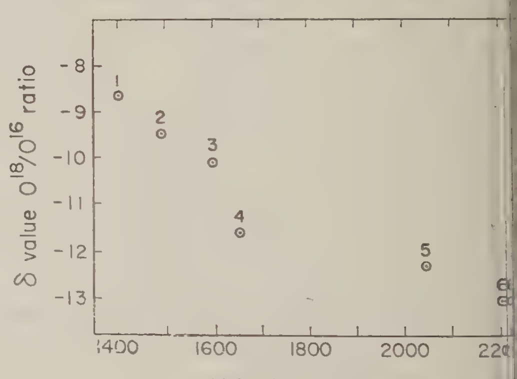

Fig. 2. Relationship between altitude and δ values of O^{18}/O^{16} ratio in snow and firn on Blue Glacier. 1, snow in crevasse; 2, snow on glacier; 3, snow bank; 4, average of 13 samples of 1957–1958 snow, pit A; 5, average of 18 samples of 1958–1959 snow, pit B; 6, average of 45 samples of 1958–1959 snow, pit C.

BLE 2. Changes in O^{18}/O^{16} Ratio with Altitude at Various Localities

Locality	Latitude and Longitude	Change in δ Value of O^{18}/O^{16} Ratio per 100-m Altitude
rthwestern Greenland	70–78°N; 40–65°W	0.6
katchewan Glacier, Alberta, Canada	52°08′N; 117°12′W	0.2
rra Nevada, Calif.	39°N; 120°W	0.3
rra Madre Mountains), Calif.	34°30′N; 118°W	0.2
ue Glacier, Wash.	47°49′N; 123°42′W	0.5

. The upper Blue Glacier study [*LaChapelle*, 58, p. 12] now provides such information, and e oxygen-isotope ratios are compatible with ese meteorological data.

Effects of altitude. The altitude at which condensation occurs in clouds affects the O^{18}/O^{16} ratio of the precipitate [*Epstein*, 1959, pp. 224–228], the δ becoming lower with increasing altitude. Measurements would best be made on samples collected at various elevations during corresponding stages of a single storm. On Blue Glacier this was not possible, and samples were taken from remnants of snow found at various elevations. This procedure is open to criticism, as it does not eliminate seasonal variations. Nonetheless, the data (Fig. 2) show a reasonably consistent relation between δ and altitude. The value becomes lower with increasing altitude at a rate of 0.5 per 100 meters. As is shown in Table 2, this is a steeper gradient than that recorded in some areas, but it is not as steep as the one in Greenland. Since the magnitude of the altitudinal effect must also be influenced by temperature gradient, altitude gradient, and the nature of individual storms, it is hardly likely to be the same in different places.

Current precipitation. Glacier ice is old in the sense that it consists largely of material ac-

TABLE 3. Samples of Current Precipitation

ature of aterial	Date and Hour Collected	Location	Temperature at Time of Collection, °C	Comments	δ Value of O^{18}/O^{16} Ratio
now	1/ 7/58, 1400	Snowdome	−2	Fresh, wind-blown	−10.2
now	1/ 8/58, 1000	Snowdome	−5	Fresh, wind-blown	−11.5
now	1/ 8/58, 1600	Snowdome	−8	Probably fresh, wind-blown	−13.5
now	1/ 9/58, 0930	Snowdome	−4	Fresh, wind-blown	−13.9
now	1/10/58, 1000	Snowdome	−3	Fresh, wind-blown	−13.1
now	1/11/58, 1000	Snowdome	−6	Wind-blown, probably reworked	−17.4
now	1/12/58, 0930	Snowdome	−4.5	Fresh, wind-blown	−15.7
now	1/13/58, 0930	Snowdome	−7	Wind-blown, reworked	−15.3
now	1/15/58, 1000	Snowdome	−2	Fresh, from surface	−9.1
now	1/16/58, 0900	Snowdome	0	Fresh, from surface	−14.3
now	2/ 9/58, 1130	Snowdome	−4.4	Fresh, from surface	−16.7
now	2/17/58, 1430	Snowdome	0	Fresh, from surface	−13.9
now	3/ 6/58, 1004	Snowdome, east slope	−11.1	Fresh powder snow	−13.4
now	3/ 6/58, 1127	Snowdome, SW of center	−1.1	Fresh powder snow	−11.0
now	3/ 8/58, 0900	Snowdome	−10.0	Fresh from surface	−14.1
now	3/28/58, 1330	Snowdome	−1.0	Wind-blown	−11.9
now	3/30/58, 0830	Snowdome	−7.0	From surface, worked by wind	−19.2
now	4/21/58, 1300	Snowdome	−5.5	Fresh, from surface	−12.5
now	4/24/58, 1330	Snowdome	−3.3	Fresh, from surface	−17.2
ain	8/18/59, 1600	Caltech base camp	+7 (est.)		−9.1
ain	8/22/59, 0600	Caltech base camp	+3 (est.)		−10.6

cumulated tens, hundreds, or even thousands of years ago. By way of comparison it is worth looking at oxygen-isotope ratios in current precipitation on the Blue Glacier, chiefly in the form of new-fallen snow, collected during the winter of 1957–1958 by the group on Snowdome.

The δ for rain samples from the Caltech base camp are higher (Table 3) than those for snow on Snowdome. This is to be expected because the elevation of the Caltech camp is 445 m lower and because the samples from the camp were collected in the summer and those from Snowdome were collected in the winter. Values for the snow samples decrease with declining temperature of precipitation. It is also apparent (Table 3) that a number of the snow layers deposited during windy periods have lower values than snow not blown by wind. The mean δ of ten wind-blown samples is −14.2, compared with −13.5 for eight noneolian specimens. Even though this difference is small, it may be significant. Temperature does not seem to be the controlling influence, as it was slightly higher during accumulation of the wind-blown material (4.8°C as compared with 4.6°C). There is no basis in theory for thinking that evaporation associated with wind action would reduce the relative amount of O^{18}, and condensation could either raise or lower the value depending upon the nature of the condensing moisture. The true explanation may lie in basic differences in windy storms and in their histories of precipitation prior to their arrival on Mount Olympus.

The average δ for snow from Snowdome is somewhat lower (−13.9) than the average for all samples from the ice tongue (−12.1). Furthermore, the range of values for the snow (−9.1 to −19.2) is much greater than for the materials of the ice tongue (−10.3 to −14.1), as is shown by bars *S* and *E* in Figure 3. These data suggest a considerable homogenization, much of which occurs during conversion of snow to glacier ice and which probably continues at a reduced rate during the subsequent history of ice in the glacier (compare *D* of Fig. 3 with *A*, *B*, and *C*). A moderate relative enrichment in O^{18} also takes place. This could be brought about either by adding O^{18} or by removing O^{16}. The analyses do not indicate that old, far-traveled ice has been enriched in O^{18}, as compared with young, less-traveled ice (Fig. 5). Actually, they suggest the reverse, although the interpretation

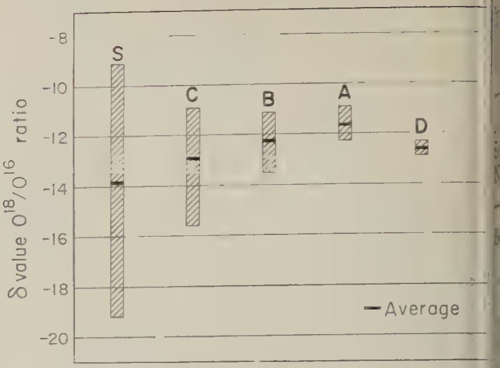

Fig. 3. Range of δ values in materials [at] following sites: *S*, specimens of fresh sno[w] collected on Snowdome, winter of 195[7]–1958. *A*, pit in firn on lower Blue Glacier [at] elevation 1654 m as sampled August 7, 195[8]. *B*, pit in firn on Snowdome at elevation 20[..] m as sampled August, 18, 1958. *C*, pit in Sou[th] Basin (Fig. 1) at elevation 2205 m as sample[d] on August 9 and 18, 1958. *D*, 3-meter co[re] hole in ice 150 m below firn edge as collecte[d] August 22, 1958. *E*, all samples from ice tong[ue] below edge of the firn. Black bar indicat[es] average δ value.

is complicated by the fact that the older [ice] probably originated at a higher altitude an[d] δ values should be somewhat lower for t[his] reason. Changes occurring within the firn [are] probably a more likely cause of relative enr[ich]ment in O^{18} and also of much of the homogen[iza]tion. It seems unlikely that the difference[s in] average δ values of samples from Snowd[ome] and from the ice tongue reflect a secular clim[atic] change, in view of the relatively small sec[ular] change in temperature in this region over [recent] decades [*Hubley*, 1956, p. 673; *Landsberg*, 1[...] p. 1520].

One possible mechanism of homogeniza[tion] and O^{18} enrichment is the refreezing of the m[elt] water and rain water that percolate into c[old] underlying snow or firn. In an annual laye[r of] snow, before the melting season, the part t[hat] accumulates in winter has the greatest reser[ve] of cold and, on the average, the lower δ val[ues]. This winter snow is initially overlain by sp[ring] and possibly early-summer snows which [were pre]cipitated under warmer conditions and co[nse]quently have high δ values. Meltwater t[hat] percolates into the cold winter layers co[mes] from these surface snows of high δ values. [The] difference in δ is probably even more marke[d in] the instance of rain water, although much

ABLE 4. Changes in O^{18}/O^{16} Ratio of Specific Snow Layers with Time for Samples from Snowdome

mple umber	Date Collected	Description	δ Value of O^{18}/O^{16} Ratio
ries I			
1	2/9/58	Surface of a deep layer of new snow, marked for recovery	−16.4
2	6/22/58	Collected from the same layer as sample 1 now re-exposed at surface (from open snow surface)	−12.8
3	6/22/58	Same layer as sample 1, protected by a tin can	−12.9
4	6/22/58	Same layer as sample 1, protected by 1 sq ft of aluminum foil	−13.1
ries II			
5	2/17/58	Surface of new snow layer	−13.9
6	6/16/58	Same layer as sample 5, from open exposed surface	−13.2
7	6/16/58	Same layer as sample 5, protected by tin can	−14.6
8	6/16/58	Same layer as sample 5, protected by aluminum foil	−14.3
ries III			
9	3/8/58	Surface of new snow layer	−14.1
10	6/5/58	Same layer as sample 9, not protected	−13.5
11	6/5/58	Same layer as sample 9, protected by tin can	−13.9

e cold reserve in the snow has probably been iminated before much rain falls. Refreezing of ercolating meltwater, and to a limited degree rain, in the cold winter snows is believed to an important factor in the homogenization d relative enrichment in O^{18} within the snow at survives the ablation season. This is the aterial, of course, that ultimately makes up e ice tongue. Homogenization may continue ter the firn is raised to the freezing tempera-re through exchange of oxygen between the n and percolating water. This should be a slow process, and it has not been evaluated by actual measurements.

An attempt to measure the rate of homogenization was made through cooperation of the Snowdome group by sampling layers of snow when they first accumulated and resampling them months later after they had undergone considerable alteration. The results (Table 4), though interesting, are not entirely consistent or compelling. For example, the snow layer that accumulated on February 9, 1958, had a decidedly higher δ when resampled on June 22, 1958. Part of this may have been due to its free-water content in June, which could have been in the neighborhood of 10 per cent by weight (LaChapelle, personal communication), but most of the difference was presumably due to the refreezing of water percolating down from the surface in late spring. An attempt to evaluate the effects of percolation was made by protecting part of the same snow layer by means of impermeable coverings. The difference in the samples so protected is consistent with a reduced percolation, but it is not of great magnitude. It may be that the percolating waters gained considerable access to the covered snow through lateral capillary channels and that the protection was only partly effective.

The δ values for the snow layers of February 17 and March 8 (Table 4) had also become higher when resampled on June 16 and June 5, respectively, but the change was much less than that in the snow layer of February 9. The shielded part of the March 8 layer showed a smaller change than the unshielded material, which would be expected if it had received less meltwater. However, the shielded samples of the February 17 layer had lower δ values than the original snow. This is an unexpected result for which no satisfactory explanation has yet been found. The sampling procedure may be at fault. It is known that the δ for ice layers and lenses in firn sections (Table 5) is generally higher than that in the adjacent firn layers. Since the ice bodies are formed by refreezing of percolated meltwater, they indicate that relative enrichment of O^{18} by this mechanism does occur.

Oxygen-isotope ratios in firn. Knowledge of oxygen-isotope ratios within the firn of the accumulation area is valuable, as this is the source of the material composing the ice tongue of the glacier. In August 1958, samples were taken

TABLE 5. Oxygen-Isotope Ratios in 1957–1958 Firn from Pits on Blue Glacier

Depth, cm		δ Value of O^{18}/O^{16} Ratio
	Pit A, elevation 1654 m, sampled August 7, 1958	
0 - 5.5		−11.8
5.5– 11.0		−11.9
11.0– 17.0		−11.3
17.0– 23.0		−11.2
20.0	0.5-cm ice layer	−11.2
23.0– 28.5		−11.7
28.5– 34.5		−11.3
34.5– 40.0		−11.7
40.0– 45.5		−12.0
40.5	0.5-cm ice layer	−10.9
45.5– 51.5		−12.3
51.5– 57.0		−12.0
67.0	old, water-saturated firn	−11.5
	Average	−11.6
	Max. range	1.4
	Pit B, elevation 2045 m, sampled August 18, 1958	
0 - 7.5		−12.1
7.5– 15.0		−12.4
15.0– 23.0		−12.4
23.0– 30.5		−12.2
30.5– 38.0		−12.3
38.0– 45.5		−12.5
45.5– 53.5		−13.5
53.5– 61.0		−13.3
61.0– 68.5		−13.0
68.5– 76.0		−12.3
76.0– 84.0		−12.1
84.0– 91.5		−12.2
89.0	1-cm ice layer	−11.1
91.5– 99.0		−12.7
99.0–106.5		−12.0
101.5	5-cm ice layer	−13.1
106.5–114.5		−11.3
114.5–122.0		−11.3
	Average	−12.3
	Max. range	2.4
	Pit C, elevation 2205 m, sampled August 9 and 18, 1958	
0 - 7.5		−12.1
15.0– 23.0		−14.7

TABLE 5. Continued

Depth, cm		δ Value of O^{18}/O^{16} Ratio
30.5– 38.0		−13.5
45.5– 53.5		−12.1
61.0– 68.5		−13.1
63.5	ice layer	−11.9
68.0– 76.0		−10.9
73.5	ice layer	−11.2
76.0– 84.0		−13.2
91.5– 99.0		−15.4
106.5–114.5		−15.6
122.0–129.5		−14.9
137.0–145.0		−14.3
152.5–160.0		−13.6
167.5–175.0		−12.7
183.0–190.5		−11.2
198.0–205.5		−13.7
213.5–221.0		−13.9
228.5–236.0		−13.8
244.0–251.5		−13.5
259.0–267.0		−13.9
274.5–282.0		−12.9
289.5–300.0		−13.4
307.5–315.0		−13.9
322.5–330.0		−13.6
338.0–345.5		−13.6
353.0–361.0		−13.2
368.5–376.0		−13.4
376.0–383.5		−13.0
386	1-cm ice layer	−10.9
383.5–391.0		−11.8
391.0–399.0		−12.6
406.5–414.0		−12.8
421.5–429.0		−13.0
437.0–444.5		−12.6
452.0–460.0		−12.9
467.5–475.0		−12.3
482.5–490.0		−12.2
498.0–505.5		−12.5
513.0–520.5		−12.5
528.5–536.0		−12.5
543.5–551.0		−12.4
559.0–566.5		−12.8
566.5	2.5-cm ice layer	−13.0
566.5–574.0		−12.5
	Average	−13.0
	Max. range	4.7

from pits in the 1957–1958 annual firn layer at three sites spanning the maximum possible vertical (550 m) and horizontal (1.4 km) range. Continuous channel sampling was used, each specimen representing a thickness between 5.5 and 7.5 cm. Ice layers and lenses within the firn were separately sampled. The sections sampled do not represent a complete annual layer, much material had been lost at the top throu ablation. The section at pit C (altitude 2205 was by far the thickest and most complete (F 4) and had unquestionably undergone the le alteration.

The data (Table 5) confirm the trend

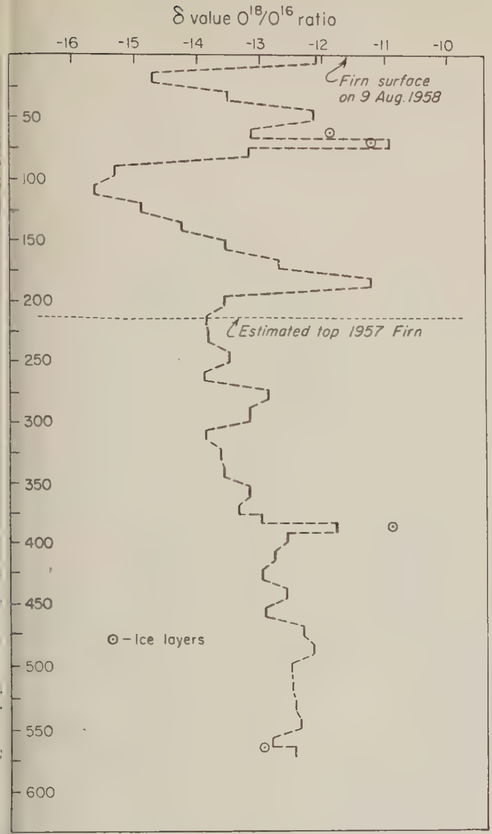

Fig. 4. O^{18}/O^{16} ratios in firn and ice layers of pit *C*, elevation 2205 m.

neral magnitude of the altitudinal influence on $^8/O^{16}$ ratios (Fig. 3). The range in δ values so increases with altitude, being 1.4 at pit A 654 m); 2.4 at pit B (2045 m), and 4.8 at t C (2205 m). Since the range of values in w-fallen snow collected near the site of pit B still greater, 10.1 (Table 5), the conclusion is rmissible that the decrease in range at lower titudes is at least in part a matter of increas- g homogenization. The firn at lower elevations s simply been permeated by greater amounts meltwater over a longer interval of time. Five the specimens from pit C have a lower δ than y sample from the ice tongue, and it seems at during the process of homogenization a rela- ve increase of O^{18} in the materials of the tongue s occurred. These relationships are borne out aphically in Figure 4, which shows that the equency and range of variations within the 58 layer clearly exceed those in the underly- g firn. Furthermore, a small but steady enrichment in O^{18} with depth is indicated. A comparison of 'new' firn (−11.2) and 'old' firn (−10.6) at the firn edge shows the same trend.

Ice layers and lenses in firn are formed by the refreezing of water that percolates down from the surface and spreads out along a particularly stratigraphic layer [*Sharp*, 1951, p. 613; *Benson*, 1960, pp. 38–40]. For reasons already discussed, these ice bodies should have δ values higher than those in the adjacent firn. This proved to be the case for six out of eight ice layers and lenses in the firn pits of the Blue Glacier. The exceptions constitute an unsolved problem similar to that encountered in pits on Saskatchewan Glacier [*Epstein and Sharp*, 1959, p. 94]. It may be that the original snow layers had such low δ values that permeation with meltwater did not bring the value up to that of the adjacent layers.

Types of ice. The tongue of lower Blue Glacier consists principally of three types of ice, arbitrarily identified as coarse bubbly, coarse clear, and fine.[2] The fine ice is also bubbly, and all three types are described in more detail elsewhere [*Kamb*, 1959, p. 1893; *Allen, Kamb, Meier, and Sharp*, 1960]. In many instances, closely associated specimens of these types of ice display significant differences in δ values (Fig. 6, Table 6) which may reflect differences in genesis and history. In most places coarse-bubbly ice constitutes at least 90 per cent of the exposed material. It is considered to be the 'normal' or 'average' ice, and its δ provides a datum for comparison with other types of ice.

Coarse-clear ice occurs in close association with both coarse-bubbly and fine ice. In some places it is in sharply defined masses, and in others the transition into coarse-bubbly ice is gradual. At most localities the δ values for coarse-clear ice are distinctly lower than the values obtained for adjacent coarse-bubbly ice. The mean difference in the values for 30 closely associated coarse-bubbly and coarse-clear ice pairs is −0.4, and the maximum is −2.0. In 6 out of the 30 pairs the δ of coarse-clear ice was higher, but in 3 of these the difference was only +0.1. The δ of coarse-clear ice is also lower than that of associated fine ice in nearly all instances, although one striking exception was

[2] This or similar material has been called granulated ice [*Epstein and Sharp*, 1959, p. 99] or firn ice (Firneis) [*Klebelsberg*, 1948, p. 39–40].

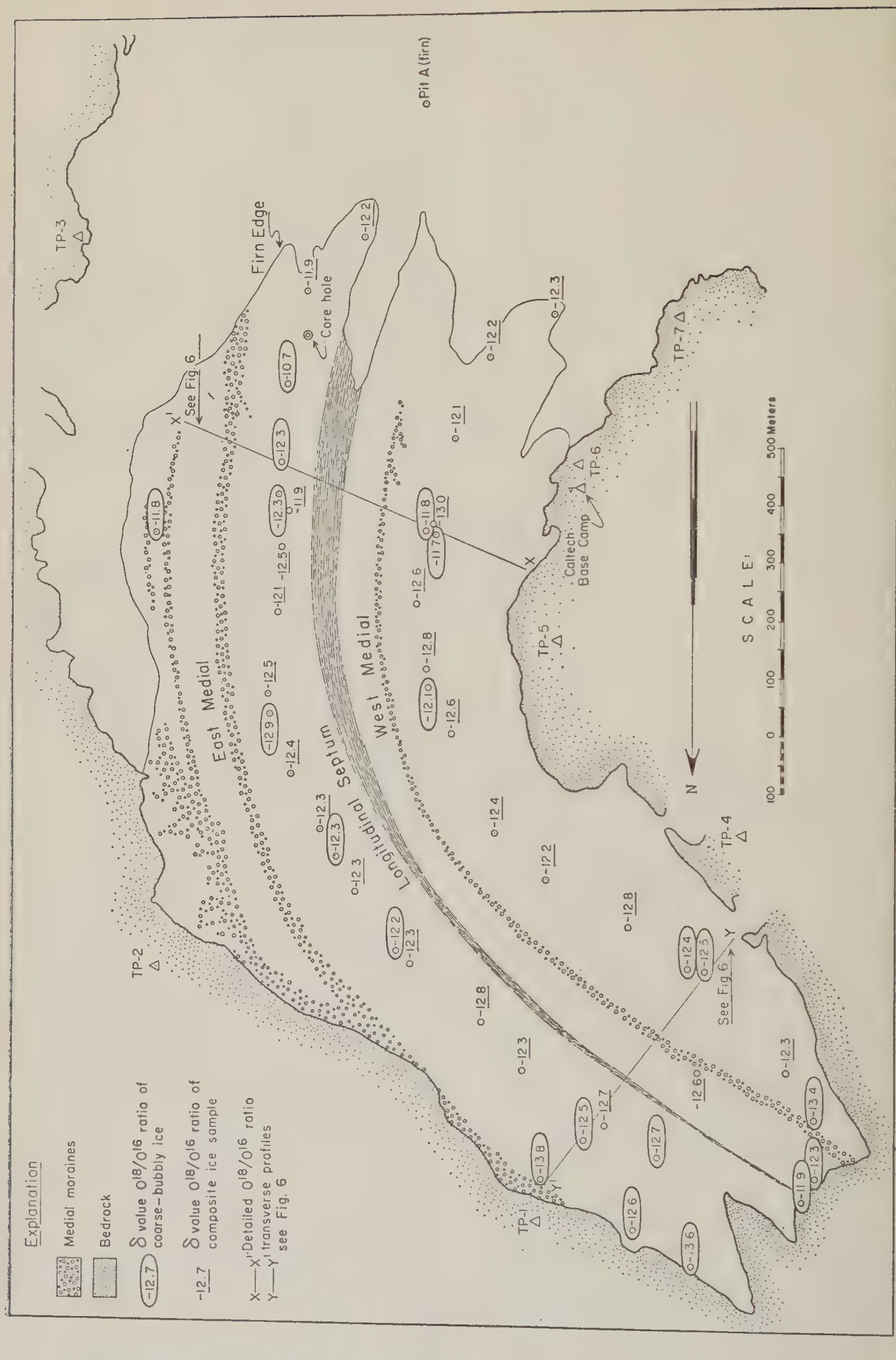
Explanation
Medial moraines
Bedrock
δ value O18/O16 ratio of coarse-bubbly ice
δ value O18/O16 ratio of composite ice sample
X—X' Y—Y' Detailed O18/O16 ratio transverse profiles see Fig. 6
East Medial
West Medial
Longitudinal Septum
Firn Edge
Core hole
Pit A (firn)
Caltech Base Camp
See Fig 6
TP-1
TP-2
TP-3
TP-4
TP-5
TP-6
TP-7
N
SCALE
0 100 200 300 400 500 Meters

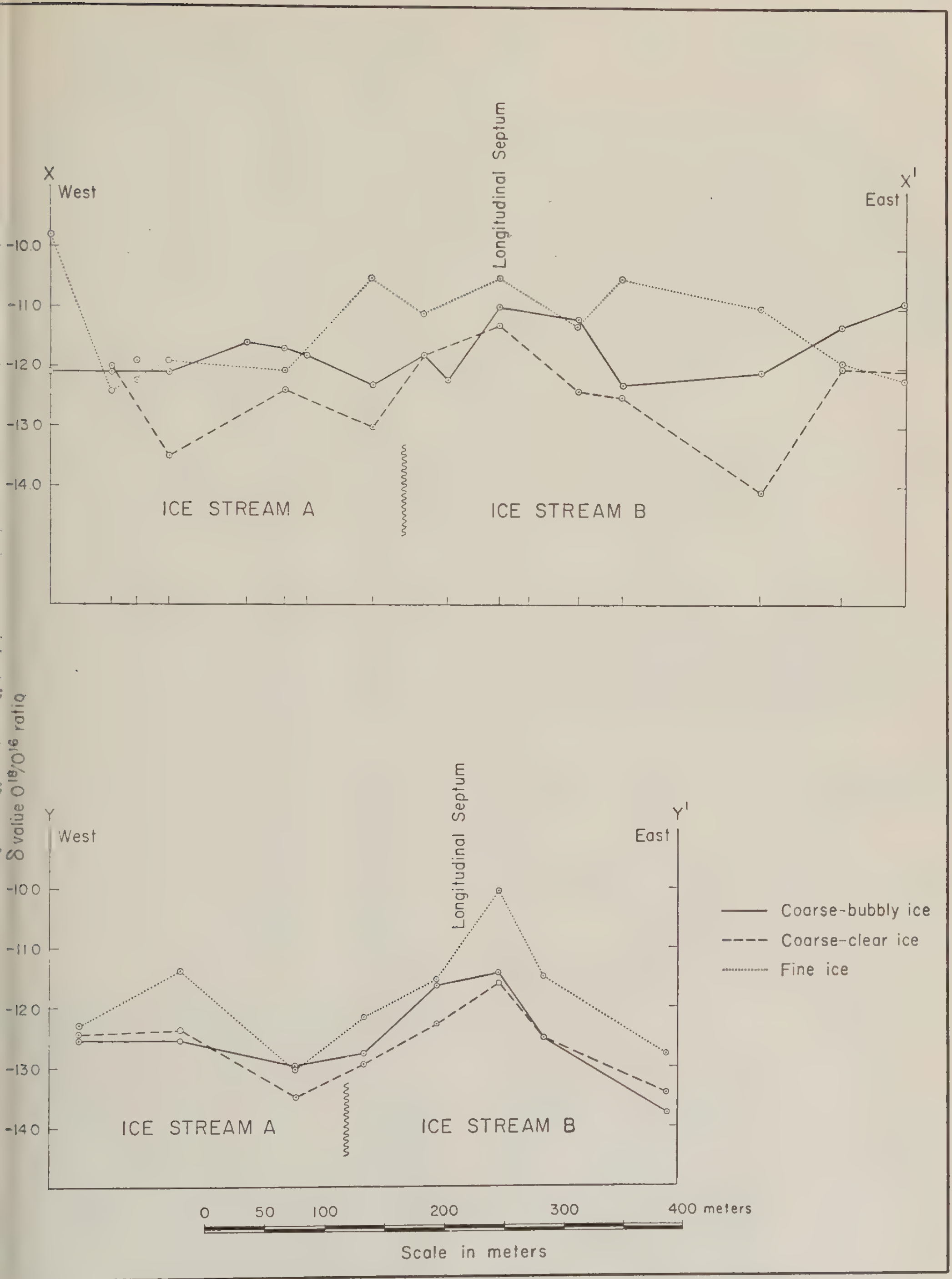

Fig. 6. Plots of oxygen-isotope variation in samples of coarse-bubbly, coarse-clear, and fine ice along transverse profiles across lower Blue Glacier; Fig. 5 for location.

TABLE 6. The δ Values for Coarse-Bubbly, Coarse-Clear, and Fine Ice

Location	Coarse-Clear Ice	Fine Ice	Coarse-Bubbly Ice	Difference	
				CCI − CBI	FI − CBI
At base of western icefall		−11.6	−11.8		+0.2
6 m downglacier from icefall	−13.3		−12.4	−0.9	
225 m downglacier from icefall	−13.5	−11.4	−12.1	−1.4	+0.7
Dark ogive band opposite base camp	−13.1	−11.3	−12.3	−0.8	+1.0
White ogive band opposite base camp	−12.5	−13.0	−12.2	−0.3	−0.8
Dark ogive band opposite base camp	−14.1	−11.3	−13.7	−0.4	+2.4
White ogive band opposite base camp	−10.5	−11.7	−12.1	+1.6	+0.4
Dark ogive band opposite base camp	−12.7	−11.5	−12.7	0	+1.2
Longitudinal septum opposite base camp		−10.7	−12.5		+1.8
6 m from west rock wall below TP-5 (Fig. 5)		−9.8	−12.1		+2.3
	−12.0	−12.4	−12.1	+.1	−0.3
	−13.5	−11.9	−12.0	−1.5	+0.1
	−12.4	−12.0	−11.7	−0.7	−0.3
	−13.0	−10.5	−12.3	−0.7	+1.8
	−11.8	−11.1	−11.8	0	+0.7
Upper transverse profile XX' (Fig. 5)	−11.3	−10.5	−11.0	−0.3	+0.5
	−12.4	−11.3	−11.2	−1.2	−0.1
	−12.5	−10.5	−12.3	−0.2	+1.8
	−14.1	−11.0	−12.1	−2.0	+1.1
	−12.0	−11.9	−11.3	−0.7	−0.6
		−12.2	−10.9		−1.3
Center of ice stream A opposite TP-5 (Fig. 5)	−13.0	−12.4	−12.1	−0.9	−0.3
East edge of stream B opposite TP-5	−13.4	−11.0	−14.0	+0.6	+3.0
Center of stream A opposite TP-4 (Fig. 5)	−12.6	−12.0	−12.4	−0.2	+0.4
West part of stream B opposite TP-4	−12.3	−11.1	−11.4	−0.9	+0.3
East part of stream B opposite TP-4	−13.0	−11.1	−12.8	−0.2	+1.7
	−12.4	−12.3	−12.5	+0.1	+0.2
	−12.4	−11.4	−12.5	+0.1	+1.1
	−13.5	−13.0	−13.0	−0.5	0
Lower transverse profile YY' (Fig. 5)	−13.0	−12.2	−12.8	−0.2	+0.6
	−12.3	−11.5	−11.6	−0.7	+0.1
	−11.6	−10.0	−11.4	−0.2	+1.4
	−12.5	−11.5	−12.5	0	+1.0
	−13.4	−12.8	−13.8	+0.4	+1.0
West medial moraine 300 m above terminus		−11.7	−12.6		+0.9
East margin 200 m above terminus		−12.2	−12.6		+0.4

found in a pod of coarse-clear ice with a δ of −8.6 completely surrounded by fine ice with a ratio of −9.8.

On the basis of δ values and field relations, it is suggested that the masses of coarse-clear ice may originate in at least two ways: (1) Coarse-clear ice with a δ higher than that of the associated ice may represent local bodies of material that gradually recrystallized while soaked with water. Since most meltwater and rain water are richer in O^{18} than most of the underlying snow, firn, or ice, incorporation of such water by recrystallization would produce a higher δ. Reference is not made here to refrozen pools of water filling moulins, crevasses, or other depressions. Bodies of ice formed in this manner, although relatively abundant, are so readily recogniz[ed] by their distinctive form and crystal structu[re] that there is little chance of confusing the[m] with the masses of coarse-clear ice under co[n]sideration. (2) Bodies of coarse-clear ice w[ith] δ values lower than those of the associat[ed] coarse-bubbly ice may represent chunks [of] deeper and older ice which became mixed w[ith] surficial material in the icefall. Ice breccias co[n]taining fragments of coarse-grained bluish ice [in] a matrix of firn and fragmented ice have be[en] observed near the base of the fall. If the blu[e] ice of the breccia represents deeper material, [it] should have a lower δ because it comes fr[om] higher in the accumulation basin.

The masses of coarse-clear ice in the ice tong[ue]

much less bubbly than the breccia frag-nts. This could be due to an unusual degree recrystallization experienced by these frag-nts because the orientation of their crystals s not well suited to the direction of stress at base of the icefall. Recrystallization is principal means by which ice grains in the ccia fragments could be reoriented and the rity of the ice increased by reduction of air bbles. This interpretation is supported by the t that nearly all the ice near the glacier ut, which presumably has experienced much rystallization, is much clearer than most ice ther upglacier. Ice along lateral margins of glacier, where large crystals suggest consider-e recrystallization, is also relatively clear.

Most fine ice has higher δ values than the ociated coarse-bubbly ice, but in a few in-nces the values are the same or even lower able 6). The mean difference in 35 coarse-bbly and fine ice pairs is +0.7, and the maxi-m is +3.0. Statistical analysis shows that s difference is not due to chance. In 8 out of 35 pairs, the δ of fine ice is lower.

At some locations it is clear from direct ob-vation that the fine ice represents insets of w or firn filling crevasses. However, it is not ar from the field relationships that all fine ice lower Blue Glacier originated in this manner. ne of the fine-ice bodies are lenses or pods, ers are highly irregular in shape, and many thin folia intimately associated with the er types of ice. If all the fine ice represents et bodies of firn, the geometrical relations ve been so greatly modified and the fine ice so sely incorporated into the prevailing foliation ucture of the glacier that the inset mode of gin is no longer obvious. We have entertained thought that some of the fine ice may be und-up or recrystallized [*Kamb*, 1959, pp. 6–1900] coarse-bubbly ice, but the δ values not generally support these ideas. The δ ues of fine ice in thin folia are roughly the e as the values for firn fillings in crevasses. n general, snow filling a crevasse would be ected to have a higher δ than the ice of the vasse walls, which represents material that imulated at higher elevations. However, vari-ns in the O^{18}/O^{16} ratio among individual w storms are considerable (Table 3), and it ossible that snow accumulating in a crevasse occasionally have about the same or even a lower δ than the adjacent ice. Thus, even fine ice with δ values lower than those in the associated coarse-bubbly ice may originate as insets of snow. The same explanation might also hold for the one example of fine ice with a δ lower than the coarse-clear ice mass it enclosed.

Transverse profiles. Variations in oxygen-isotope ratios along profiles extending transversely across a glacier should reveal differences in the site of accumulation of the material composing individual ice streams. Samples were taken along two principal transverse profiles and along several shorter traverses across parts of the ice tongue of lower Blue Glacier. The uppermost profile (XX', Fig. 5) is 150 to 250 meters below the firn edge. It starts at the west wall and crosses ice streams A, B, and C (Fig. 1). An apron of firn covers most of ice streams D and E, so they were not sampled. The lower profile (YY', Fig. 5) is 450 m above the snout and extends completely across the glacier from wall to wall. It involves only ice streams A and B, the other streams having terminated farther upglacier. Data from the miscellaneous shorter traverses are not discussed, but they are consistent with results from the longer profiles.

Separate samples of coarse-bubbly, coarse-clear, and fine ice were taken at each collection site along the principal transverse profiles. The δ values of these samples are plotted in Figure 6. One relationship immediately apparent is the difference in δ values of the three types of ice already discussed. If fine ice actually represents insets of firn, the difference in δ values between it and the accompanying coarse-bubbly ice should be greater along the lower profile because the coarse ice of the lower profile comes from higher in the accumulation basin. This proves to be the case.

The difference in the average δ of coarse-bubbly and coarse-clear ice is less on the lower profile than on the upper profile, −0.2 compared with −0.7. This is consistent with the greater similarity in appearance of these two types of ice in the lower reach of the glacier and with the general evidence of homogenization, but the reasons for the relative changes in δ values are not known.

Useful comparisons of the different ice streams can be made on the basis of δ values in coarse-bubbly ice alone. Along profile XX' these values have only a small range within ice stream A and

are about the same in both ice streams A and B. This is to be expected, as both streams originate in accumulation basins having a similar morphology and essentially the same elevation. The only marked departure is within ice stream B at the crossing of the longitudinal septum where the δ values are distinctly higher than average (Fig. 6). This is consistent with the preferred hypothesis of origin for this feature involving the incorporation of a large amount of snow and firn in and at the base of the icefall [*Allen, Kamb, Meier, and Sharp*, 1960].

Samples from the lower profile show essentially the same features as the upper profile, including higher δ values in the longitudinal septum. The low δ at the east end of the lower profile (*YY′*, Fig. 6) may be due to excessive marginal ablation, which exposes relatively deeper ice. Lack of a correspondingly low value at the west end of the profile could be due to a much lower ablation related to shaded exposure and to protection afforded by residual snow banks. In general, ice along the margins would be expected to have somewhat lower δ values because of the slower velocity, which gives opportunity for exposure of deeper ice by greater melting.

Longitudinal profiles. Deductions concerning longitudinal lines of flow in a valley glacier suggest that ice appearing on the surface at positions progressively farther below the firn edge came from successively higher parts of the accumulation area. If this is correct, the δ values should become progressively lower from firn edge to glacier terminus.

To explore this relation, a series of composite samples[3] was collected in 1958 along the center flow lines of ice streams A and B. In 1959, samples of coarse-bubbly ice alone were taken along the center flow line of ice stream B. The δ values of these samples are shown on the map (Fig. 5), and the values for the coarse-bubbly ice alone are plotted in Figure 7.

The composite samples collected along the longitudinal profiles show no consistent trend in δ values (Fig. 5). Considering the possible origins of fine and coarse-clear ice, this is perha[ps] not surprising. However, the samples of coars[e-] bubbly ice do show a somewhat irregular b[ut] unmistakable decrease in δ downglacier (Fig. 7). Irregularities in these curves probably refle[ct] local inhomogeneities within the ice left ov[er] from the firn. Although physical aspects of indi[-] vidual firn layers may be obscured within th[e] glacier tongue, it is hardly likely that the con[-] siderable differences in δ values for individu[al] firn layers (Fig. 4) are completely eliminate[d]. Furthermore, variations related to secular cl[i-] matic changes may exist and must involve lar[ge] masses of ice. If allowances are made for su[ch] inhomogeneities, the case for a modest decrea[se] in δ is acceptable.

A more reliable evaluation is perhaps afford[ed] by comparison of the mean δ for all samples [of] coarse-bubbly ice taken along the two tran[s-] verse profiles, *XX′* and *YY′* (Fig. 6). The mea[n] value along the lower profile (−12.5) is low[er] than the mean value along the higher pro[file] (−11.9). Other δ values for coarse-bubbly [ice] on the surface of the glacier, but not located [on] the longitudinal profiles (Fig. 5), confirm in ge[n-] eral the trend toward lower values downglaci[er]. Thus, data from Blue Glacier offer modest su[p-] port to the deductions of *Reid* [1896, p. 91] concerning flow lines in a valley glacier.

Oxygen-isotope ratios in ogives. The ogi[ves] of lower Blue Glacier appear as lunate, altern[ate] white and darker bands on the surface of [ice] stream A below the firn edge. The white ba[nds] average roughly 25 m in width, the dar[ker] bands 5 m. These bands represent the outc[rop] traces of layers of material within the glac[ier]. The white bands are 90 to 95 per cent coa[rse-] bubbly ice, and the darker bands are a m[ore] heterogeneous mixture of coarse-bubbly, f[ine] (up to 35 per cent), and coarse-clear ice (up [to] 10 per cent). The origin of these ogives i[s a] matter of speculation, but one hypothesis [*Al[len,] Kamb, Meier, and Sharp*, 1960] is that [the] darker bands represent insets of ice breccia t[hat] accumulated in icefall crevasses. It is interest[ing] to see what light the O^{18}/O^{16} ratios can throw [on] the origin of these structures.

The samples analysed came from two differ[ent] but closely associated sets of ogives, represe[nt-] ing two white and three darker bands. Th[e] values for fine and coarse-clear ice display w[ide] variations (Table 7), presumably for reas[ons]

[3] A composite sample consists of small chips of ice taken at ten separate spots distributed over an area not exceeding 10 to 12 m in radius. The three common types of ice are included in roughly the estimated proportions exposed on the surface at the sampling site.

ABLE 7. Oxygen-Isotope Ratios of Materials Composing Ogive Bands of Blue Glacier

	Type of Band	Nature of Material	δ Value O^{18}/O^{16}
ve set 1		Composite*	−12.2
		Coarse-bubbly ice	−12.1
	White (1*w*)	Fine ice	−11.7
		Coarse-clear ice	−10.5
		Composite*	−12.4
		Coarse-bubbly ice	−12.7
	Dark (1*d*)	Fine ice	−11.5
		Coarse-clear ice	−12.7
ve set 2		Coarse-bubbly ice	−12.3
	Dark (2*d*)	Fine ice	−11.3
		Coarse-clear ice	−13.1
		Coarse-bubbly ice	−12.2
	White (2*w*)	Fine ice	−13.0
		Coarse-clear ice	−12.5
		Coarse-bubbly ice	−13.7
	Dark (2*d*)	Fine ice	−11.3
		Coarse-clear ice	−14.1

A composite sample consists of small chips of aken at ten separate locations within a radius) to 12 meters, representing the three types of n approximately their estimated abundance.

ady discussed. The δ of coarse-clear ice in e band 1*w* is higher and the δ of fine ice in e band 2*w* is lower than would normally be ected. The significance of this is not readily arent. The δ of coarse-bubbly ice is lower in darker bands than in the white bands, the aged difference being 0.7. A possible expla- on of this is that the insets of ice breccia ain considerable deep ice which has lower alues. Possibly, this could come about by anching and crevasse-wall calving in the ll.

immary and conclusions. The oxygen-iso- data from Blue Glacier lead to some rela- y straightforward, definite conclusions and support to certain interpretations and ulations, but they also raise many questions hich there are as yet no clear answers. This t unexpected in view of the complexities of 3lue Glacier environment and the formative of oxygen-isotope studies of glacier ma- ls.

e Blue Glacier analyses show the usual de- e in δ with increasing altitude, the rate being 0.5/100 m. This behavior is not unique to snow, as it characterizes many types of precipitation [*Epstein*, 1956]. The Blue Glacier data also show that homogenization of oxygen isotopes begins shortly after snow accumulates, and significant effects are evident within a few months. It appears that much homogenization is effected in the accumulation area through refreezing of downward percolating water derived from melting of surface snow and from rain. The effects of vapor transfer and diffusion of oxygen are matters of speculation. Further homogenization occurs within the ice tongue during flow, but the processes causing it are not known. They may involve recrystallization, changes of state, and diffusion. The homogenization is of local extent and does not destroy large-scale heterogeneities in δ values which can be used to study and interpret glacier structure and behavior.

Differences in O^{18}/O^{16} ratios proved to be a useful aid in understanding some of the structures within the ice tongue of the Blue Glacier. They indicate that thin layers of fine ice in the foliation pattern represent greatly drawn out masses of firn incorporated into the glacier by infolding or insetting, largely within and at the base of the icefall. The O^{18}/O^{16} ratios support the interpretation that creation of the longitudinal septum, a major structural feature, occurs near the base of the icefall and involves the incorporation of large amounts of snow and firn. The hypothesis that ogive dark bands represent greatly modified insets of firn-ice breccia filling icefall crevasses is supported by the oxygen-isotope data. Variations in δ values also attest to the probable validity of deductions concerning longitudinal flow lines within a valley glacier by showing that ice near the terminus probably comes from the higher parts of the accumulation area.

On the other hand, the present studies do not contribute significantly to an understanding of the fundamental control of O^{18}/O^{16} ratios exercised by various aspects of the meteorological environment. Processes of homogenization, particularly within the ice tongue, remain largely unknown. Study of other glaciers in different climatological environments is in order. They should be of simple geometry with the least number of complicating influences. Sampling constitutes a major problem which cannot be

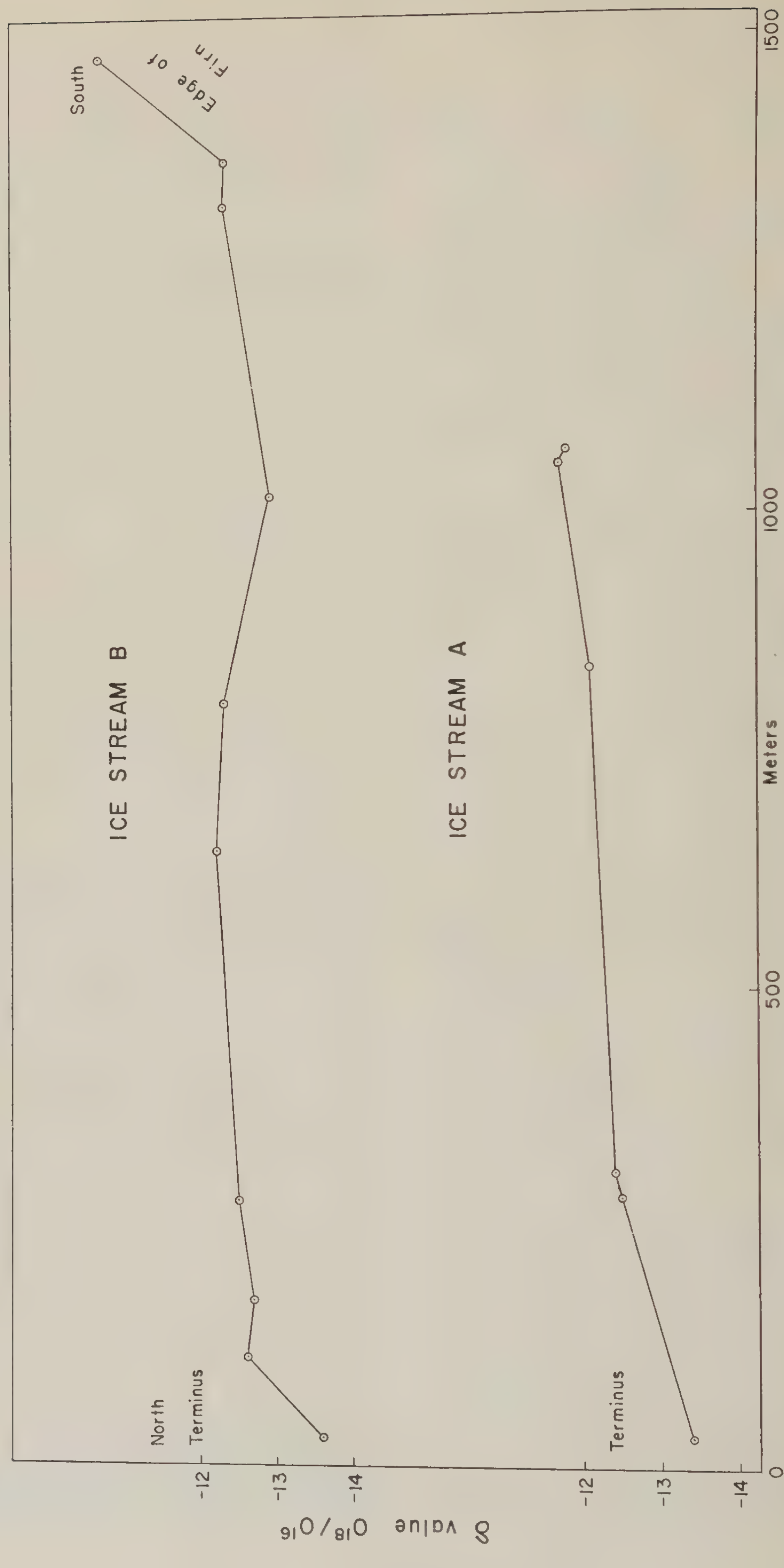

Fig. 7. Plots of O^{18}/O^{16} ratios of ice along longitudinal profiles in ice streams *A* and *B*, lower Blue Glacier.

lligently handled without a thorough under-ıding of the structure and constitution of glacier. Analyses of samples from properly ated deep core holes in valley glaciers could significant. Ultimately, a classification of iers in terms of the value and range of $O^{18}/$ ratios should be possible. This is something the future, and a number of glaciers in dif-nt environments must be studied first.

cknowledgments. The work of 1957 and 1958 Blue Glacier was an International Geophysical r activity under the auspices of the U. S. Na-al Committee. The investigation was contin- in 1959 with support from the National Sci- Foundation. The mass spectrometer used oxygen-isotope analyses is the property of the mic Energy Commission. The National Park ice graciously granted permission to make the ly and aided in many ways. Supplies and equip-it were carried to the glacier by the U. S. Air ce and the U. S. Coast Guard. Equipment was ied by the Snow, Ice and Permafrost Research ablishment of the U. S. Army Engineers and the Office of Naval Research (contract 896-00). Personnel of the Snowdome project on er Blue Glacier collected samples of snow dur-the winter of 1957–1958. Field colleagues C. R. n and J. C. Savage aided in the collection of er samples. William R. Fairchild of the Angeles ing Service provided superb logistical support. n Nye, Henri Bader, and Edward Anders have lly offered critical and much appreciated com-its on the manuscript, but they do not neces-ly endorse any statements made in this paper.

References

n, C. R., W. B. Kamb, M. F. Meier, and R. P. harp, Structure of the lower Blue Glacier, Vashington, in press, 1960.

son, C. S., Stratigraphy in snow and firn of the reenland ice sheet, Ph.D. thesis, Calif. Inst. of echnology, 213 pp., 1960.

tein, Samuel, Variation of the O^{18}/O^{16} ratio of fresh water and ice, *Publ. 400, U. S. Natl. Acad. Sci.*, 20–28, 1956.

Epstein, Samuel, The variation of the O^{18}/O^{16} ratio in nature and some geologic implications, *Researches in Geochemistry,* John Wiley & Sons, New York, 217–240, 1959.

Epstein, Samuel, and T. Mayeda, Variation of O^{18} content of waters from natural sources, *Geochim. et Cosmochim. Acta, 4,* 213–224, 1953.

Epstein, Samuel, and R. P. Sharp, Oxygen-isotope variations in the Malaspina and Saskatchewan glaciers, *J. Geol., 67,* 88–102, 1959.

Hubley, R. C., Glaciers of the Washington Cascades and Olympic Mountains; their present activity and its relation to local climatic trends, *J. Glaciol., 2,* 669–673, 1956.

Hubley, R. C., Glacier research on Mt. Olympus, Olympic National Park, Washington, Arctic Institute of North America, mimeographed, 12 pp., 1957.

IGY Bulletin, Oxygen isotope studies, *Trans. Am. Geophys. Union, 40,* 81–84, 1959.

Kamb, W. B., Ice petrofabric observations from Blue Glacier, Washington, in relation to theory and experiment, *J. Geophys. Research, 64,* 1891–1909, 1959.

Klebelsberg, R. v., *Handbuch der Gletscherkunde und Glacialgeologie,* 1, Springer, Vienna, 403 pp., 1948.

LaChapelle, E. R., Blue Glacier, preliminary report on the scientific investigations, *USNC-IGY Project 43,* Dept. Meteorol. Climatol., Univ. Washington, mimeographed, 28 pp., 1958.

LaChapelle, E. R., Annual mass and energy exchange on the Blue Glacier, *J. Geophys. Research, 64,* 443–449, 1959.

Landsberg, H. E., Note on the recent climatic fluctuation in the United States, *J. Geophys. Research, 65,* 1519–1525, 1960.

Reid, H. F., The mechanics of glaciers, *J. Geol., 4,* 912–928, 1896.

Sharp, R. P., Features of the firn on upper Seward Glacier, St. Elias Mountains, Canada, *J. Geol., 59,* 599–621, 1951.

(Manuscript received July 9, 1960.)

The Deep Water Circulation in the Southwest Indian Ocean[1]

XAVIER LE PICHON

Lamont Geological Observatory
(Columbia University)
Palisades, New York

Abstract. The 'core method,' together with geostrophic computations, is used to make a tentative interpretation of the circulation of the deep water in the southwest Indian Ocean. A deep current towards the north, having the characteristics of a western boundary current, is shown to be deflected and weakened by the complex system of ridges. The existence of a homogeneous body of water, east of 60°*E*, is attributed to the mixing of the Atlantic deep water with Antarctic waters, the salinity being kept constant by a small inflow of deep water of north Indian Ocean origin.

INTRODUCTION

his study is limited to the region of the hwest Indian Ocean between 20° and 70°E itude and 20° and 50°S latitude. The south- boundary is marked by the approximate tion of the Antarctic convergence, where deep water begins to change its characteristics ng its steep ascent to the surface [*Deacon*, 7]. Hydrologically, the whole deep water ulation below 2000 meters is determined by inflow of Atlantic deep water. Above 2000 ers, water of north Indian Ocean origin is by the Agulhas current through the Mozam- ie Channel. These two inflows of water with bably a notable amount of north Indian an deep water contribute to the formation mass of water of constant characteristics ipying the depths of the Reunion basin. ince the Agulhas current and its return ent are well defined and deep, the influence he bottom topography is of primary impor- ce. A rough bathymetric map (Fig. 1) has constructed, making preliminary use of *Vema* data which have confirmed the con- ity of the mid-oceanic ridge, as inferred from location of earthquake epicenters by *Ewing Heezen* [1956, 1960]. For convenience, the valley is not shown. Maps of potential om temperatures (Fig. 2) and bottom ities (Fig. 3) have also been constructed. se maps define the boundaries of the different ns and give a picture of the circulation of the om water. From the Agulhas basin an important flow of Antarctic bottom water enters the basin situated between Africa and the Madagascar ridge (isotherm 0.25°C, isohaline 34.70° per mil). It is very probable that the Antarctic bottom water similarly enters the Kerguelen basin between Kerguelen Island and Marion Crozet plateau (isotherm 0.25°C, isohaline 34.70° per mil) and that it flows from this basin into the eastern part of the Reunion basin, the sill depth being about 4500 meters. Another solution is that this water comes into the Reunion basin through a gap between the Madagascar ridge and the mid-oceanic ridge, the sill depth being about 4000 meters. The small basin between Africa and the Madagascar ridge appears to have a hydrological unity; for convenience it will be called 'northern Agulhas basin.'

From a hydrological point of view the main feature of the topography is the mid-oceanic ridge, which runs from the southwest to the northeast and is probably connected with the Madagascar ridge as shown by the map of *Stocks* [1960]. This results in the delimitation of three main units, the Agulhas basin and its northern prolongation, the Reunion basin, and the Kerguelen basin.

Deacon [1937], gave a comprehensive review of the work that had been done on the deep water circulation of the Indian Ocean. He showed the importance of the inflow of the Atlantic deep water, which goes eastwards along the continental slope of South Africa and then turns southeast and finally south between 50°E and the Kerguelen–Gaussberg ridge. Using the *Discovery* stations along the Mozambique

[1] Lamont Geological Observatory Contribution 455.

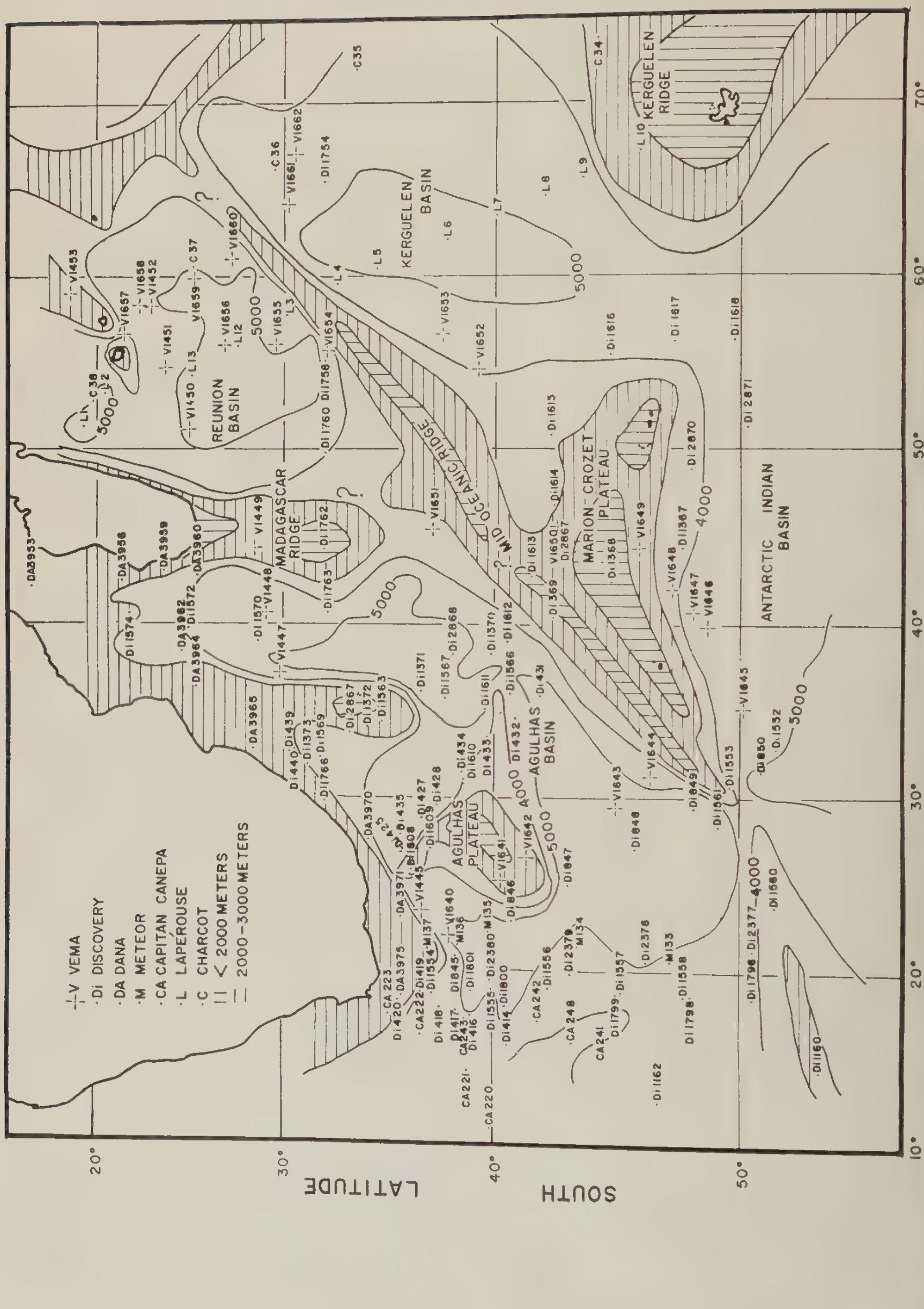
V VEMA
Di DISCOVERY
DA DANA
M METEOR
CA CAPITAN CANEPA
L LAPÉROUSE
C CHARCOT
< 2000 METERS
2000–3000 METERS
REUNION BASIN
MADAGASCAR RIDGE
KERGUELEN BASIN
KERGUELEN RIDGE
MID OCEANIC RIDGE
MARION-CROZET PLATEAU
AGULHAS BASIN
AGULHAS PLATEAU
ANTARCTIC INDIAN BASIN
EAST LONGITUDE
SOUTH LATITUDE
5000
4000

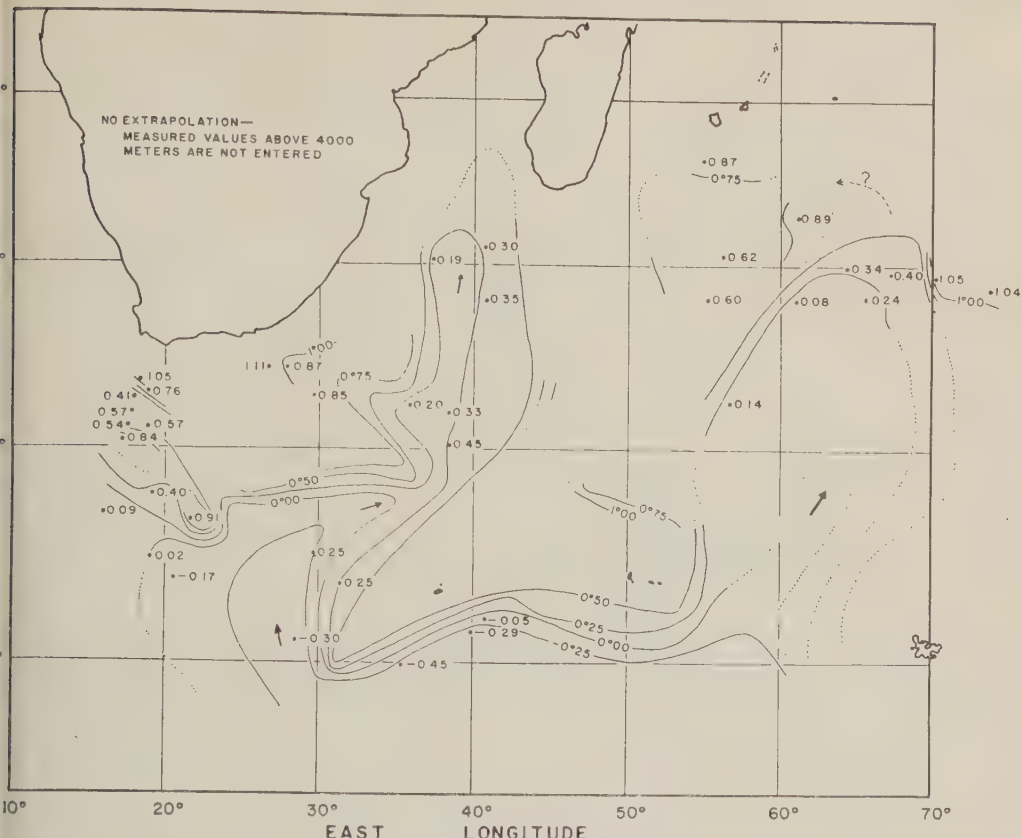

Fig. 2. Potential bottom temperature.

nnel, he showed that the Arabian Sea water still detectable as far as 40°S as a layer of ly oxygenated water spreading above the ntic deep water. In more recent work, *rnia, Lacombe, and Le Floch* [1951] of the oratoire d'Oceanographie Physique in Paris ted out that the influence of the Arabian water is limited to the 34.80 per mil isohaline bout 20°S in the Mozambique Channel. consider that the last traces of Arabian water disappear here and that only a slug- flow continues towards the south. However, suggest that there is a formation of deep r on the hydrological barrier which obstructs propagation of the Antarctic intermediate r towards the north and the Arabian Sea r towards the south. A mixing of these waters d contribute to the formation of deep water h would flow southwards [*Tchernia, Lacombe, Guibout*, 1958].

nce the work of *Deacon* [1937], a number of *very* stations have been occupied in this area. There are some *La Perouse* and *Charcot* stations near Kerguelen Island, but the *Charcot* stations are shallow and the values of the salinity given by the *La Perouse* stations generally do not appear to have the precision required for this kind of work. Lately, during two cruises, the R.V. *Vema* occupied 42 stations, the results of which have just been reported. A few stations of *Capitan Canepa* and *Meteor* west of 20°E together with the *Dana* stations in the Mozambique Channel have also been used. The stations examined for this study are shown on the bathymetric map. Very few of these stations were occupied during the northern summer, and they were not taken into account in drawing the core maps. However, they do not show any systematic seasonal change either in the content of oxygen or in salinity, with one exception: west of 30°E the deep water is at least 0.30 ml/l less oxygenated during the northern summer. Furthermore, according to *Di* 1796, the 34.80 per mil isohaline contour reaches much farther

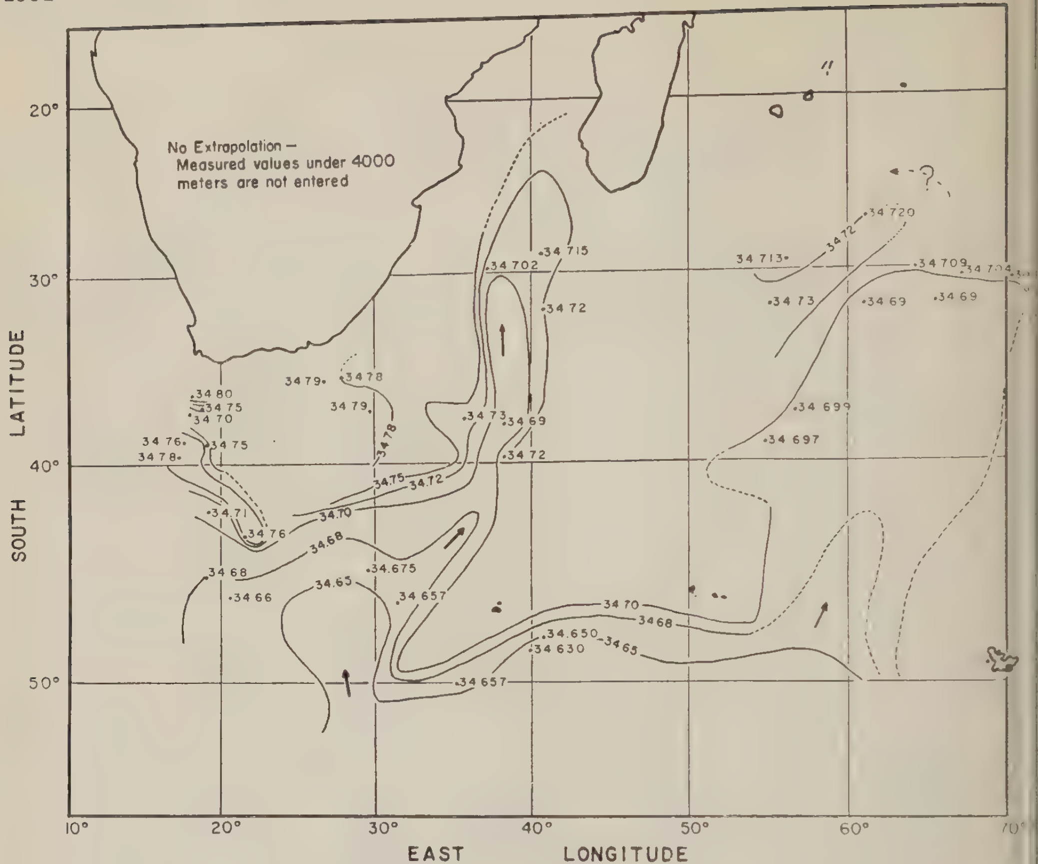

Fig. 3. Bottom salinities.

south (50°S) on 19°E and, according to *Di* 2379, farther north (43°S) on 20°E. Owing to the very small number of stations, there is a possibility that the changes are not seasonal but depend on the year and are caused by differences in the transport of the Agulhas current and the development of large eddies [*Deacon*, 1937; *Sverdrup, Johnson, and Fleming*, 1946]. The discrepancy between the *Di* 179 series and the *Di* 237 series is in favor of this last hypothesis.

Maximum Salinity Layer

T-S relationship. To trace the propagation of the Atlantic deep water, the distribution of the salinity is determined in the layer of maximum salinity. The main currents are then indicated by the shape of the isohalines. In the use of this 'core method' the recommendations of *Wüst* [1936] were followed; only measured values were used and they were checked against the temp[...] ture-salinity diagram. For this diagram (Fi[...] the potential temperature was used. The [...] tionship appears to be linear. The incom[...] water on 20°E and 40°S has the follo[...] characteristics:

$$\Theta = 2.30° \quad S = 34.86‰ \quad \sigma_\Theta = 27.8[...]$$

and at the other end, in the Madagascar b[...]

$$\Theta = 1.60° \quad S = 34.735‰ \quad \sigma_\Theta = 27.[...]$$

Θ is the potential temperature, S the salin[...] $\sigma_\Theta = 10^3(d - 1)$, d being the density of [...] water if it were adiabatically brought bac[...] the surface. The same kind of relationship [...] a decrease of density was found by *Wüst* [1[...] for the circulation of the Atlantic deep w[...] in the Atlantic Ocean. The values given by[...] *Vema* 16 stations to Australia along 30°S s[...] that the points stay on this same line betw[...]

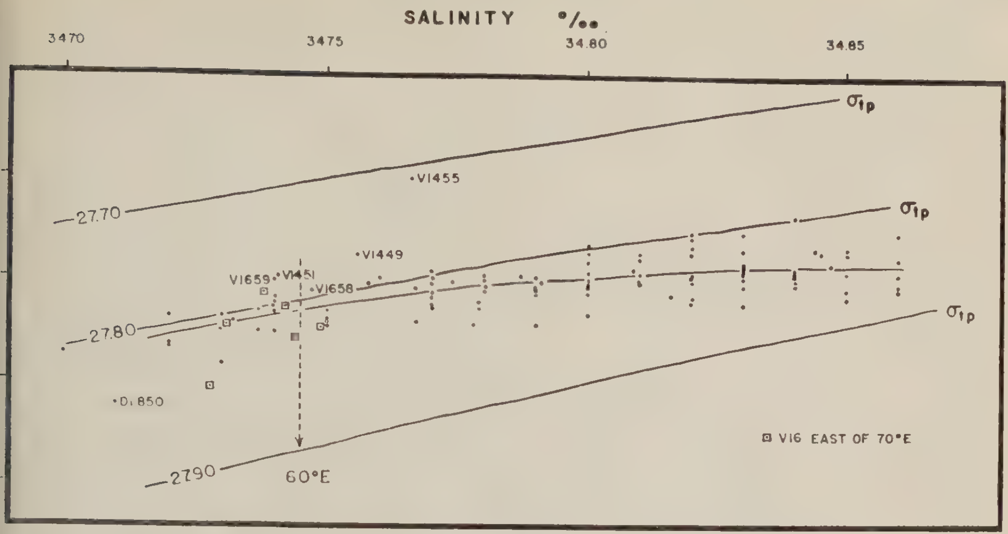

Fig. 4. Potential temperature-salinity diagram of maximum salinity.

ities of 34.73 and 34.76 per mil. This indi-s that the role of the Atlantic deep water he formation of the south Indian Ocean water is probably still important in the heast Indian Ocean and that east of 60°E ate of equilibrium is reached in the mixing the Atlantic deep water with Antarctic rmediate and bottom waters as well as with er of north Indian Ocean origin. The fact the mixing of the Atlantic deep water rds the south is along the same line as it is rds the east indicates that the influence of Antarctic waters is predominant. But an ission of north Indian Ocean water is ssary to maintain the salinity [*Deacon*, 1937]. more detailed study of the role of the north an Ocean deep water is possible in the nion basin. The potential temperatures for layer of maximum salinity of the stations ted in the Reunion basin are slightly high. re seems to be a very small increase of salinity rds the north.

V 16 60	27°S	61°E	34.737 ‰
V 16 59	25°S	60°E	34.741 ‰
V 16 58	22°S	58°E	34.747 ‰

hese changes may be significant, since the surements were made on board with a ity bridge [*Paquette*, 1958], and the same ence water was used. Considering the follow- *V* 14 stations, we see that there is no imum between 20°S and 10°S.

V 14 50	25°S	51°E	34.76 ‰
V 14 51	23°S	54°E	No maximum
		Knudsen method (accuracy of only ±0.04)	
V 14 53	18°S	59°E	34.740 ‰ at 2500 m—no maximum
V 14 54	13°S	64°E	34.738 ‰ at 1600 m—34.737 ‰ at 3000 m—no maximum
V 14 55	10°S	68°E	34.766 ‰ at 1700 m, 34.738 ‰ at 2700 m

The *T-S* diagrams (Fig. 5) show that below 2000 meters, for all these stations, there is a homogeneous body of water of salinity 34.74 per mil. Above, at 1600 meters, a maximum appears on 10°S that can be attributed to the formation of deep water by the process suggested by *Tchernia, Lacombe, and Guibout* [1958] (see above). Therefore, it seems probable that there is a slight admission of this water into the Reunion basin which contributes to an increase of salinity. On the other hand, the influence of the Atlantic deep water can be traced to 20°S, where the maximum of salinity disappears. The homogeneous mass of water which occupies the depths of the Reunion basin is a result of these two influences. We do not know what kind of exchange takes place between

Madagascar and Reunion Island, and it is possible that here, on the contrary, there is a sluggish flow of deep water towards the north, if we can rely on *V* 14 50.

Core map. The core map obtained by drawing the isohalines in the layer of maximum salinity

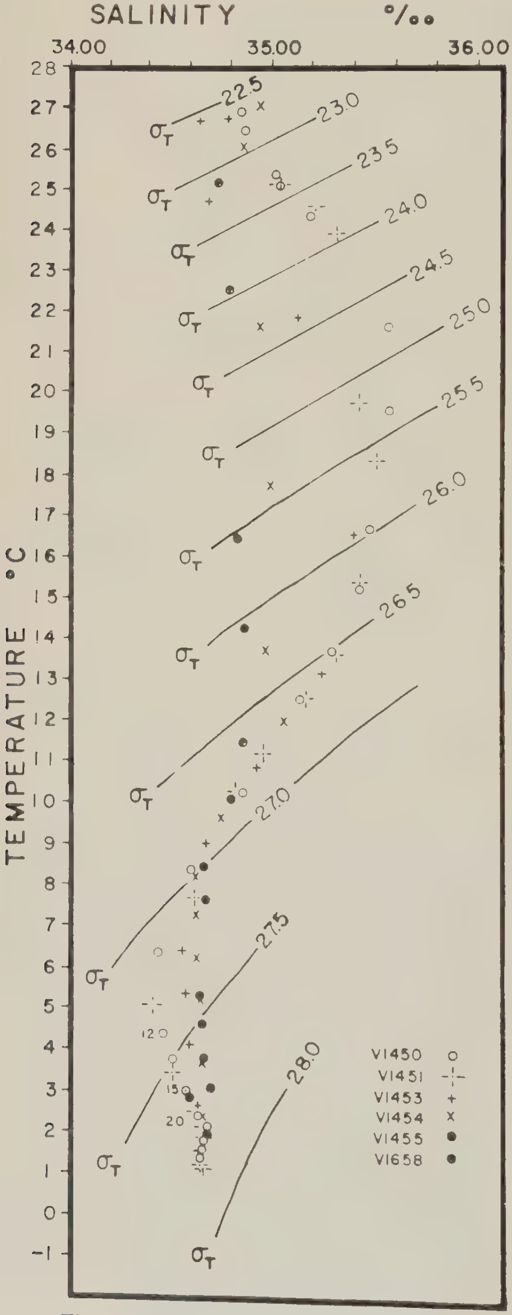

Fig. 5. Temperature-salinity diagrams.

(Fig. 6) shows the main flow of the Atla deep water running along the continental s of Africa, first deflected by the Agulhas plat then deflected southeast by the prolonga of the African shelf at 35°E, finally recur south-eastwards across the mid-oceanic ri and going south between the Kerguelen r and 50°E. The different deflections are to expected from the theory of Ekman about influence of the topography, [*Deacon*, 19 However, some new features appear. F the 34.82 per mil isohaline clearly shows a curr towards the north under the Agulhas curr This current probably cannot pass the Moz bique Channel and has to come back southw along the Madagascar ridge. It has the cha teristics of a western boundary current defle from the continental slope by the topogra Second, the influence of the Atlantic deep w seems to be particularly important on the o side of the Madagascar ridge, immedi north of the mid-oceanic ridge, in the so western part of the Reunion basin, as is indic by the bending of the 34.78 per mil isoha (*V* 16 51 and *Di* 1760). The 34.75 per mil. haline can be considered the limit of this s Indian Ocean deep water mass, the chara istics of which have been shown to be f constant east of 60°E. West of 30°E, in area below South Africa where the Agu current recurves eastwards, the interpreta is very difficult. A number of large eddie less saline water may account for the ra large variations (see above) and the sout limit of the 34.85 per mil isohaline must yearly (*Di* 84 series compared with *Me* 13 s and *V* 16 42).

Corresponding oxygen distribution. A ma the oxygen content in the layer of maxi salinity has also been constructed (Fig It is much less accurate because of uncertai in the determination of the oxygen con and because the oxygen is not a truly conserv property. Furthermore, oxygen content is a able for fewer stations than is sali Particularly, the *Vema* 16 stations were used, as the oxygen values are substan higher than the *Discovery* or *Vema* 14 va which are fairly consistent. The values o oxygen content seem to vary seasonally of 30°E (see above). The only deep *Dana* st in the Mozambique Channel (taken in Jan is 0.30 ml/l higher than the nearby *Di*

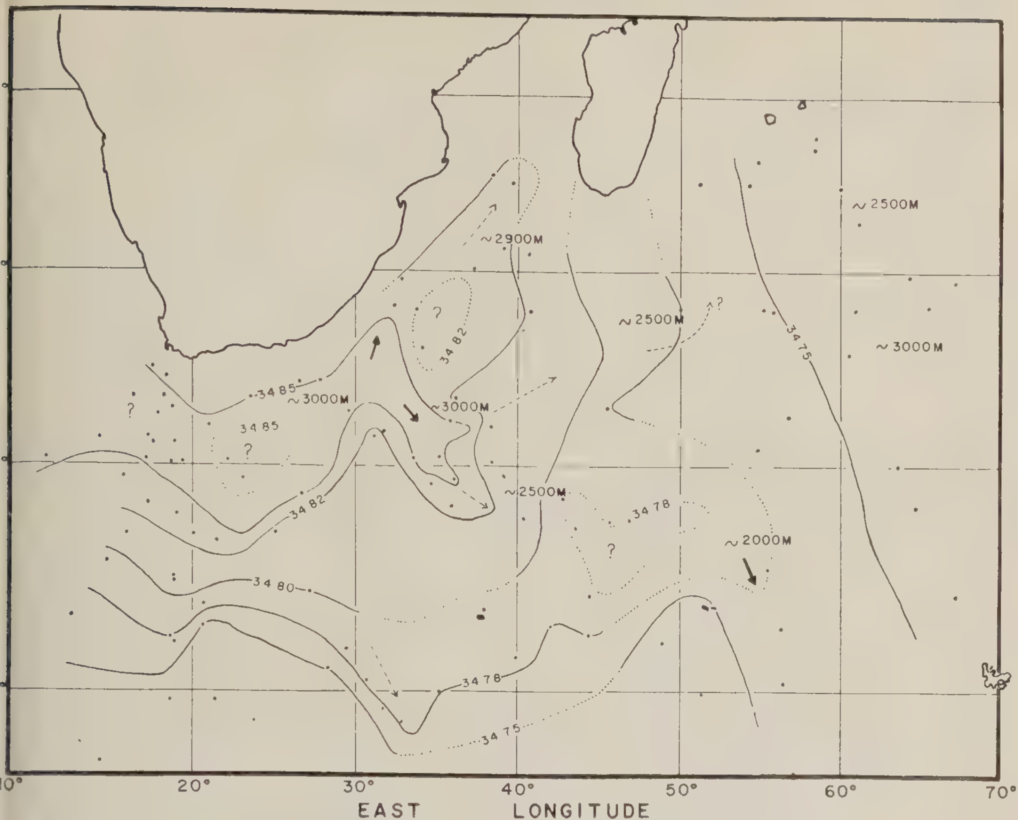

Fig. 6. Layer of maximum salinity, November through May.

:en in May). But in the whole median part :e is no apparent seasonal change.

.owever, even when we keep in mind the ortant limitations of the oxygen distribution, ı a map confirms and sometimes complements maximum of salinity core map. The deep ent towards the north in the northern lhas basin is very conspicuous (isopleth ml/l). The main stream bending over the -oceanic ridge is also very clear, but the ving is rather hypothetical owing to the ll number of stations. A possible secondary n stream appears at 50°S between 20°E and E. This map also gives a good picture of the ılation in the Reunion basin. A definite ease of oxygen appears towards the north- , where a small inflow of north Indian Ocean water has been shown to be probable. ion *V* 14 50 suggests that the influence of Atlantic deep water is more effective on west side and that some flow of water ırds the north takes place between Reunion ıd and Madagascar. *Di* 1756 and *Di* 1754 show that the 3.50 and 3.75 ml/l isopleths bend towards the east above the mid-oceanic ridge. This is confirmed by the preliminary *V* 16 values (which apparently are 0.25 ml/l too high, possibly because of the calibration of the burette) shown below.

North of the ridge			
V 16 58	22°S	58°E	3.57 ml/l
V 16 59	25°S	59°E	3.66 ml/l
V 16 60	27°S	61°E	3.68 ml/l
South of the ridge			
V 16 61	30°S	64°E	3.99 ml/l
V 16 62	30°S	67°E	3.99 ml/l

It is apparent that the influence of the Atlantic deep water is predominant south of the ridge, whereas the influence of the north Indian Ocean deep water is important in the Reunion basin.

A characteristic of the Atlantic deep water gives a method of checking this map: As this water enters the Indian Ocean it has a well-defined maximum of oxygen which progressively disappears towards the east where there is a

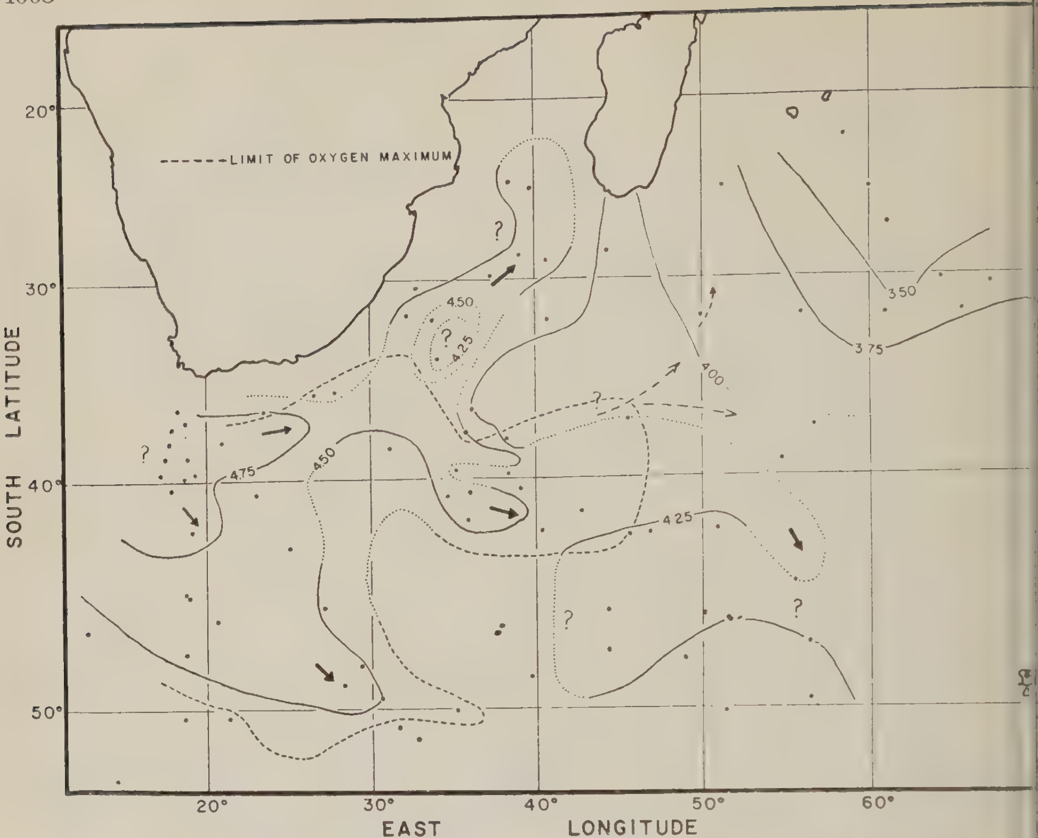

Fig. 7. Oxygen in the layer of maximum salinity, November through May.

constant increase down to the Antarctic bottom water. The dashed line shows the approximate limit of this maximum. The results are in good agreement with the preceding conclusions except towards the Mozambique Channel where no such maximum is found. This apparent disagreement is resolved when we consider the distribution of Antarctic bottom water. As there is an important northward flow of this water in the northern Agulhas basin, the bottom water is much colder, less saline, and more oxygenated than that along the continental slope south of Africa. This results in a relative decrease of salinity and an increase of oxygen content in the lower part of the Atlantic deep water, owing to vertical mixing. It consequently appears that the flow of Atlantic deep water is strengthened by a similar flow of Antarctic bottom water.

Minimum Oxygen Layer

In accordance with the concept of Thomsen and Deacon, the layer of minimum oxygen [illegible] been used to trace the spreading of water [illegible] north Indian Ocean origin (Fig. 8). This wa[illegible] may have completely lost, by mixing, the [illegible] traces of genuine Arabian Sea water. Howe[illegible] the core map (Fig. 8) shows that the water [illegible] north Indian Ocean origin is very poorly o[illegible] genated and it spreads all over the south[illegible] Indian Ocean north of 40°S, distributed by [illegible] Agulhas current and its return current. Th[illegible] shown in particular by the isopleths for [illegible] and 3.75 ml/l. The limitations of the use [illegible] oxygen values already cited apply to t[illegible] conclusions. Furthermore, there is a very str[illegible] objection because the layer of minimum oxy[illegible] is generally a level of very slow motion [illegible] this map would be only an indication of [illegible] layer. But such an explanation cannot accoun[illegible] the form of the isopleths, which suggest[illegible] well-defined current all along the path of [illegible] Agulhas current. If there is a 'level of no moti[illegible] and there must be one if the deep cur[illegible]

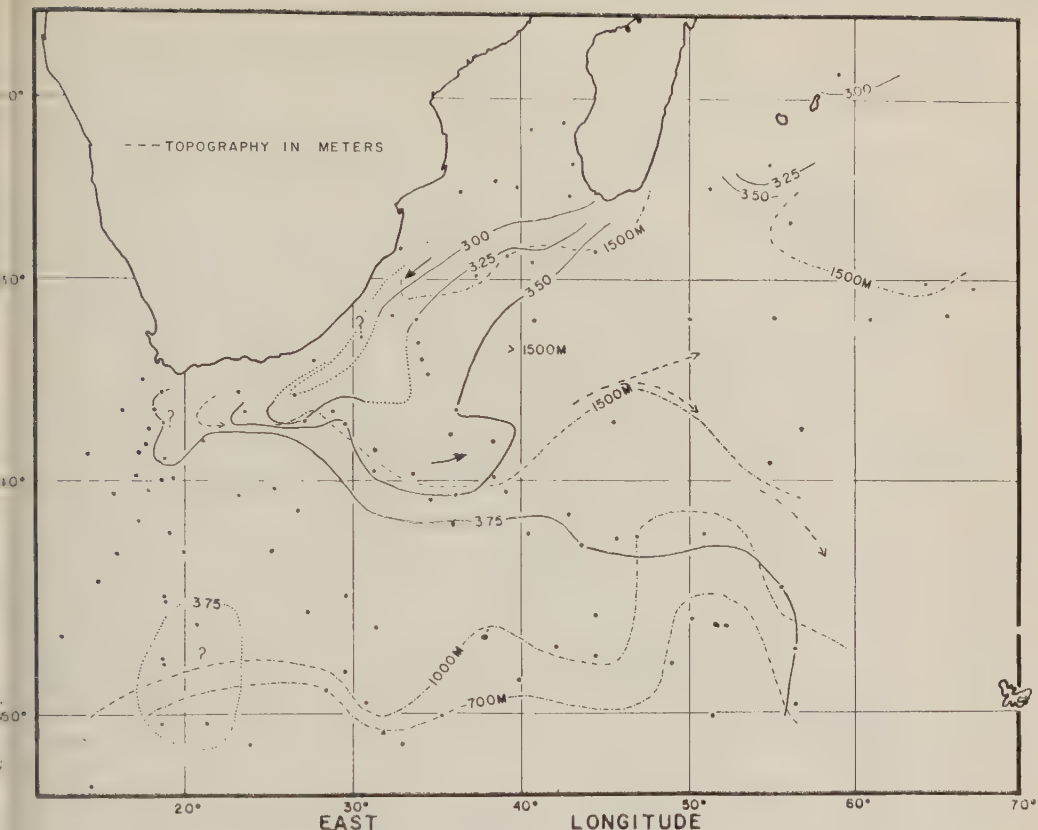

Fig. 8. Layer of minimum oxygen.

vards the north detected by the core method real, this layer is situated between the layers minimum oxygen and of maximum salinity—ıt is, between 1500 and 2800 meters.

It is interesting to note that the whole of union basin is covered by a layer having an ygen content of 3.50 to 3.60 ml/l, which licates that the only large inflow of water m the north at this depth takes place through Mozambique Channel and that a state of iilibrium maintains this value constant. The er in this area probably moves very slowly d the oxygen content is constant.

Geostrophic Interpretation

In 1951 Lacombe gave a geostrophic interpre- ion of the circulation in the whole Indian ean. He was able to show three important ts:

1. The existence of a region of strong current ıerally located between the Antarctic and subtropical convergences. This branch of strong current is very well defined on the meridian of Madagascar, where it is pressed by the Agulhas return current against the mid-oceanic ridge.

2. The great northward extension of the eastern current.

3. The striking influence of the topography.

It was possible that a more regional study of the geostrophic currents at the surface would confirm the topography inferred from the deep water circulation, owing to the far-reaching effect of the topography on such well-defined currents. In particular, the supposed complete junction between the Madagascar ridge and the mid-oceanic ridge is likely to have important effects. Furthermore, a geostrophic interpretation of the deep currents might add something to the core analysis.

Consequently, the anomalies of dynamic height were computed for the *Vema* stations and some *Discovery* stations (reference water

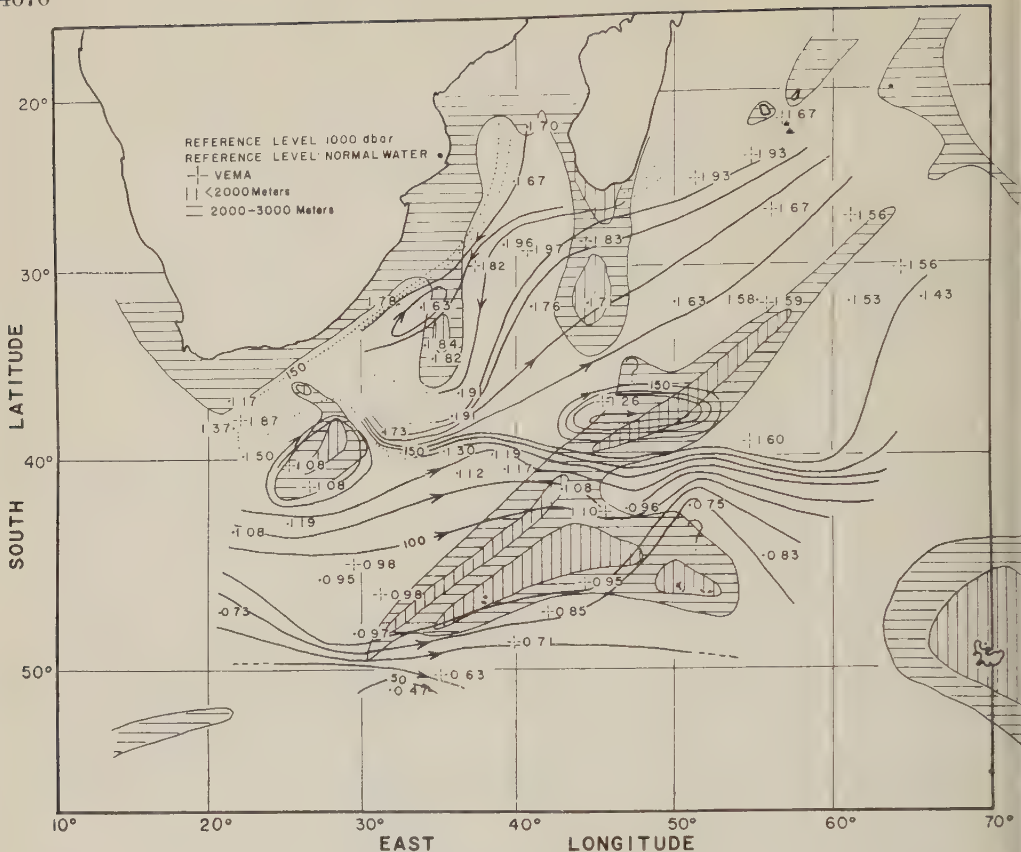

Fig. 9. Dynamic topography.

S = 35.00 per mil, T = 0°). Four *Meteor* stations and *Di* 847 to 850, for which the anomalies of dynamic height had been published, were also used. All these stations were taken from March to June except the *V* 16 and the *Di* 161 series. The *V* 16 stations taken in January nevertheless agree with the others, as is shown by *Di* 848, *V* 16 43 and *Di* 1758, *V* 16 44. The *Di* 161 series was taken in November. However, the only large discrepancy is between *V* 16 50 and *Di* 1614 because at a reference level of 1000 dbar the anomalies of dynamic height are 110 cm for *V* 16 50 and 96 cm for *Di* 1614. But *V* 16 50 was immediately north of the subtropical convergence. The bathythermograph shows at 200 meters an increase of temperature from 4°C 40 miles south of the station to more than 11° at the station. The temperature at 200 meters at *Di* 1614 is 5.72°. *Di* 1614 is on the other side of the convergence, this convergence having been about 1° higher when *Di* 1614 was taken. Consequently, we did not use *Di* 1614 but used others, knowing that their probably slightly lo dynamic height would explain the very impor bending at *Di* 1615.

Surface current. The map (Fig. 9) of topography of the surface (reference 1000 db) agrees fairly well with the correspon map by Lacombe. There is a zone of st current immediately north of the subtrop convergence. This convergence, which has found at 43°S during the two crossings by *Vema*, is approximately shown by the 100 contour. Between the 100-cm and 90-cm tours there is a large region without cur and a second region of strong current app to be connected with the Antarctic converge

If we consider the distribution of tempera at 200 meters, using the *Vema* bathythermog and the different stations available, we find the 10°C isotherm coincides with the 100 contour and the 3°C isotherm with the 9

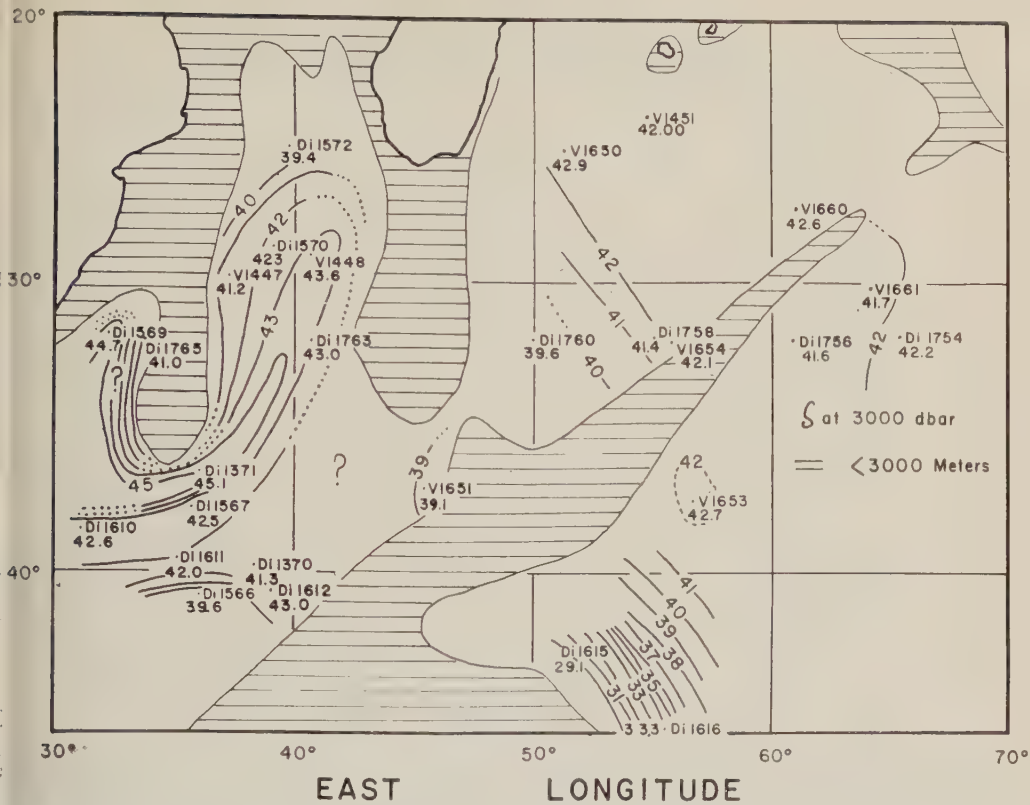

Fig. 10. Specific volume anomaly at 3000 dbar.

tour. South of the 10°C isotherm, which icates the subtropical convergence, there is ecrease of 5 or 6° in less than 50 miles. This rly indicates that the current is driven by distribution of temperatures [*Tchernia, combe, and Le Floch,* 1951] and that the main eams are related to the two convergences. e large region of very weak current between 90-cm and 100-cm contours is related to the rion Crozet plateau.

Regional studies of the Agulhas current near petown and of the circulation in the Mozamue Channel have been undertaken lately. nsequently, no attempt has been made to e a good picture of the currents in this area. wever, the following facts appear: There is a inite effect of the small ridge on 35°E. The ulhas plateau causes a large divergence and return current shows the deflection *cum sole* then *contra solem* on the upper part. This urn current joins the current which follows subtropical convergence, crosses the midanic ridge, and turns southeastwards. This crossing apparently results in the formation of a huge divergence centered on the axis of the mid-oceanic ridge. This is shown by the bathythermograms between *V* 16 50 and *V* 16 51, and *V* 16 51 and *V*16 52. The temperature at 200 meters, which was over 11° at *V* 16 50, first increased to 17° at 40°S and then decreased to 8° at 38°S before increasing again to nearly 12° at *V* 16 51. Between *V* 16 51 and *V* 16 52, the temperature first increased to nearly 16° and then decreased to 10° at 48°S before increasing again to 16°, where it remained nearly constant at about 15° to *V* 16 52. The anomalies of dynamic height are

V 16 50	42°	39S	45°	40E	110 cm
V 16 51	37°	09S	45°	30E	126 cm
V 16 52	39°	11S	54°	48E	160 cm

This enormous eddy, which may be related to the branching of the Madagascar ridge, has consequently been drawn. Like the deep current, the surface current apparently crosses the mid-oceanic ridge mainly between 40°S and

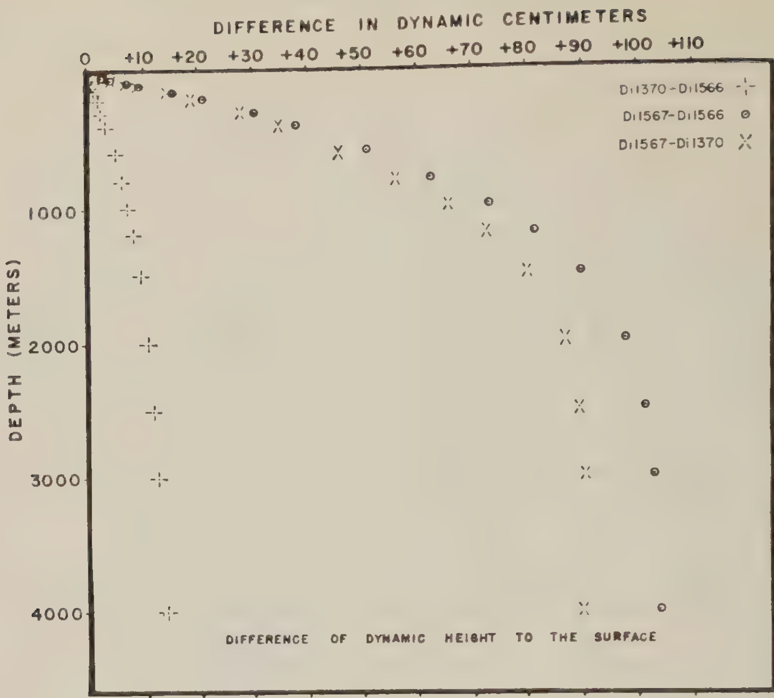

Fig. 11.

42°S. This is a possible indication of a lowering of the ridge similar to the one determined from the bathymetric map.

Deep current. The distribution of the anomaly of specific volume at 3000 meters (which is the average depth of the maximum salinity under the Agulhas current) first indicates that the whole Reunion basin contains a homogeneous deep water (Fig. 10). The error on the anomaly being probably less than $\pm 1.0 \times 10^{-5}$ cm^3/g (0.04° and 0.01 per mil), we see that the anomaly stays constant at 42×10^{-5} cm^3/g. This is in agreement with the conclusions from the core analysis. However, in the Agulhas basin the anomalies give the impression that a current running north turns southwards above 28°S, but if the reference level is below 3000 meters, the current must go north on the east side and south on the west side, an interpretation which is difficult to believe.

In this area of marked topography, the method of Defant may give some indication as to the choice of this reference level. Two groups of stations have been used, one at about 40°S and 37°E in the well-defined current towards the east (as indicated by the core analysis, Fig. 11), the other at about 29°S and 40°E in the supposed current towards the north (Fig. 12). It is q obvious that this will not give any decis conclusion owing to the limitations of the meth the very small number of stations used, and small differences of dynamic height involv However, *Di* 1567–1566 and *Di* 1566–1370 sh that the current is apparently constant direction and still detectable at 3000 me (Fig. 11). Between *Di* 1567 and *Di* 1370 current appears below 2500 meters.

If we look at the differences of dyna heights in the northern group of stations (Fig. we see that at least a marked point of inflex appears between 2000 and 2500 meters. Suc reference level agrees very well with the c analysis. It still indicates an appreciable curr in the layer of minimum oxygen and allow current towards the north below 2500 met west of 41° east. However, these conclusi do not agree with the surface of no motion determined in this area by *Mamayev* [195

Conclusions

The core analysis and the geostrophic int pretation seem to be in good agreement. B indicate the existence of a homogeneous a nearly stationary mass of deep water in

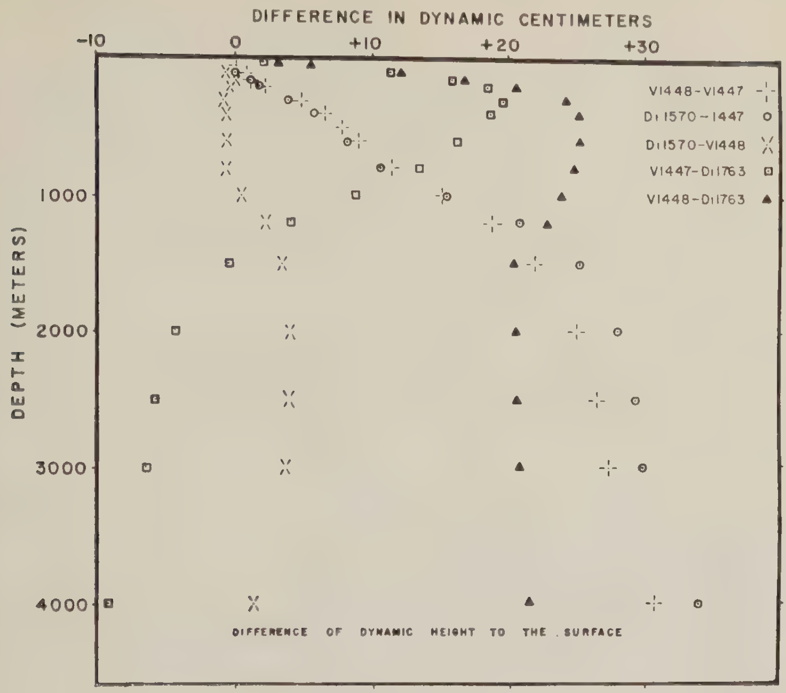

Fig. 12.

inion basin, except in the southwestern part, re there is a definite influence of Atlantic water. Both confirm the very important ct of the system of ridges. The agreement the northward deep current is certainly not clusive. This interpretation is only probable. h a flow of deep water towards the north was posed by *Stommel* [1957] and *Stommel and ns* [1960]. This 'deep western boundary rent,' detected by the core method and gested by the geostrophic interpretation, has y peculiar features. It seems to be a much per current than the one flowing beneath the f Stream; the layer of no motion had to be ced at approximately 1500 meters, in such ay that a definite current appears towards the th in the layer of minimum oxygen. Further-re, its flow is disturbed by a complex system ridges. The Atlantic deep water goes north ng the continental slope, then is deflected n it by the small ridge connected to the lf along 35°E, and is finally forced back to south by the shallow Mozambique Channel. ere is some evidence that part of this water nages to pass across the Madagascar ridge, nly immediately north of the mid-oceanic ge, having joined the upper part of the eastward deep current. Once in the Reunion basin, it seems to move slowly towards the north on the west side. The complete junction of the Madagascar ridge to the mid-oceanic ridge would explain the weakening of the current.

Many questions are still unsolved, the most important being that of the existence of important seasonal or annual changes in the deep water circulation. A more homogeneous network of stations, together with a topographic survey of the Madagascar ridge, would check what has been suggested here, especially in the Agulhas basin and its northern part, this being the key area for a better understanding of the deep water circulation in the Indian Ocean.

Acknowledgments. I gratefully acknowledge the help of Dr. Maurice Ewing, who initiated this study. I wish to thank Robert Gerard, Saul Friedman, and Charles Fray, who carried out the program of stations of the *Vema* and authorized the use of these very valuable data prior to publication.

This research was jointly sponsored by the National Science Foundation, the Office of Naval Research, Department of the Navy, and the National Committee for the International Geophysical Year, National Academy of Sciences, under an IGY grant of the National Science Foundation.

I also wish to acknowledge the support of the Higgins Fellowship at Columbia University.

References

No attempt has been made to give a complete bibliography, since one can be found in *Clowes and Deacon* [1935], *Deacon* [1937], and *Tchernia, Lacombe, and LeFloch* [1951].

Clowes, A. J., and G. E. R. Deacon, The deep water circulation of the Indian Ocean, *Nature, 136*, 936–938, 1935.

Deacon, G. E. R., The hydrology of the southern ocean, *Discovery Reports*, v. 15, Cambridge Univ. Press, 96–99, 1937.

Ewing, M., and B. C. Heezen, Some problems of antarctic submarine geology, *Antarctica in the International Geophysical Year, AGU Monograph No. 1*, 75–81, 1956.

Ewing, M., and B. C. Heezen, Continuity of mid-oceanic ridge and rift valley in southwestern Indian Ocean confirmed, *Science, 131*, 1677–1679, 1960.

Mamayev, O. I., Vertical turbulence in the sea and the surface of no motion, Intern. Oceanog. Congr. Preprints, 410–412, 1959.

Paquette, R., A modification of the Wenner-Smith-Soule salinity bridge for the determination of salinity in sea water, *Univ. Wash. Tech. Rept. 61*, 58–14, 1958.

Stocks, T., Zur Bodengestalt des Indischen Ozeans, *Erdkunde, 14*, 3, Bonn, 1960.

Stommel, H., The abyssal circulation, *Deep-Sea Research, 5*, 80–82, 1957.

Stommel, H., and A. B. Arons, On the abyssal circulation of the world ocean, 2: An idealized model of the circulation pattern and amplitude in oceanic basins, *Deep-Sea Research, 6*, 217–233, 1960.

Sverdrup, H. U., M. W. Johnson, and R. H. Fleming, *The Oceans, Their Physics, Chemis* *and General Biology*, 696 pp., 1946.

Tchernia, P., H. Lacombe, and J. LeFloch, C tribution a l'étude de l'Océan Indien et secteur adjacent de l'Océan Antarctique, *B inform. COEC, 3*(10), 65 pp., 1951.

Tchernia, P., H. Lacombe, and T. Guibout, quelques observations hydrologiques, relati à la région équatoriale de l'Océan Indien, *B inform. COEC, 10*(3), 115–143, 1958.

Wüst, G., Die stratosphare, *Deutsche Atlantis Exped. Meteor 1925–1927*, 109–288, 1936.

Research Vessel Reports

Capitan Canepa. Operacion Oceanografica Atlant Sur—Resultados Preliminares, 1959.

Charcot. Bull. inform. COEC, 3(10), 1951.

Dana. Hydrographical Observations made dur the *Dana* Expedition 1928-1930, *Dana Rept.* 1937.

Discovery II Discovery Reports, Cambridge Un Press.

La Perouse. Bull. inform. COEC, 9(10), 19

Meteor. Wissenschaftliche Ergebnisse der Deutsch Atlantischen Expedition Auf Dem Forschun Und Vermessungsschiff, Meteor, 1925-19 Herausgegeben im Auftrage der Notgeme schaft der Deutschen Wissenschaft, Von Defant, Band IV, Zweiter Teil; Dr. George W (1932).

Vema. Oceanographic data obtained in the Indi Ocean, Gulf of Aden, and the Red Sea dur Cruise Vema 14 and Vema 16, *Tech. Re CU-10-60 (AT 30-1) 1808*, 1960.

(Manuscript received July 5, 1960; revised Aug 16, 1960.)

Double, Triple, and Higher-Order Dimples in the Profiles of Wind-Generated Water Waves in the Capillary-Gravity Transition Region

ALLEN H. SCHOOLEY

U. S. Naval Research Laboratory
Washington 25, D. C.

Abstract. Photographs of short-fetch wind-generated water waves are used to show examples of 'double-dimple' wave profiles in the region of 2.44-cm wavelength as predicted by *Wilton* [1915]. Additional experimental profiles are presented to suggest that double-dimple waves are the start of the phenomenon of 3, 4, 5, etc., dimples of capillary waves of appropriate wavelength riding in front of the crest of gravity waves having the same velocity.

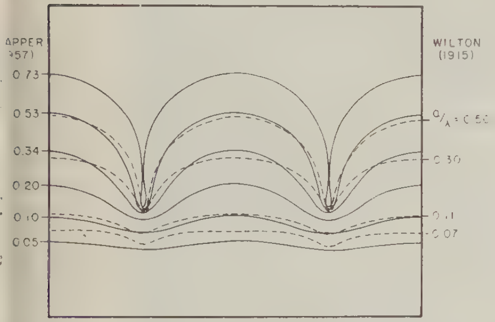

Fig. 1. Two wavelengths of single-dimple profiles theoretically predicted by Wilton and Crapper.

Introduction. *Crapper* [1957] theoretically pre-...ted that pure capillary waves have profiles ...t peak or dimple downward, which is the ...erse of the case of gravity waves. *Schooley* ...58] confirmed Crapper's theory by taking ...h-speed motion pictures of short-fetch wind-...erated water waves. Examples were also ...en by means of pictures which showed that ...rt capillary waves of appropriate wavelength, so as to have the same velocity as gravity waves, often rode just in front of the start of the crests of the gravity waves.

Pierson and Fife [in press] have recently extended the theoretical work of *Wilton* [1915], who predicted wave profiles similar to those predicted by Crapper. In addition, Wilton's theory predicts conditions of single- and double-dimple wave profiles at 2.44-cm wavelength. Wilton noted that he was 'tempted to say' that the double-dimple wave is 'probably unstable.' In his theoretical treatment he took gravity and viscosity into account, as well as surface tension.

It is the purpose of this paper to show by means of enlarged pictures of short-fetch wind-generated waves that double-dimple wave profiles are observable in the capillary-gravity transition region. Furthermore, pictures are used to show that triple, quadruple, etc., dimpled waves are also observed under proper conditions. It is suggested that the double-dimple wave that Wilton predicted at 2.44-cm wavelength is the start of the phenomenon of capillary ripples riding in front of gravity waves.

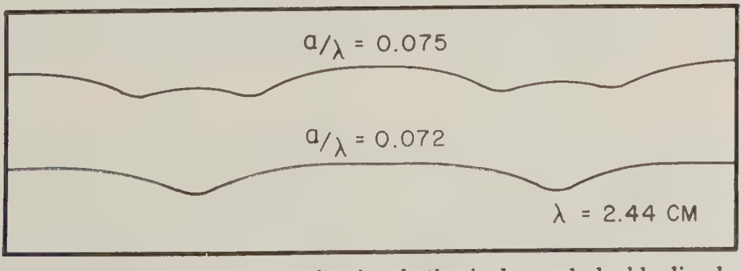

Fig. 2. Theoretical profiles of Wilton showing both single- and double-dimple profiles at 2.44-cm wavelength.

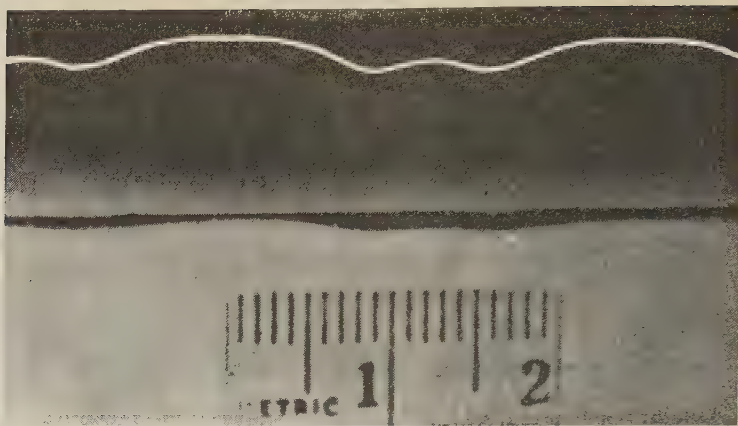

Fig. 3. Actual double-dimple water wave profile compared with theoretical profile.

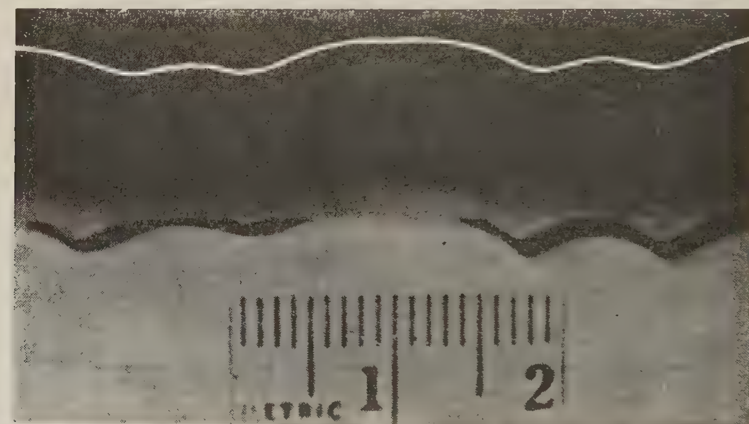

Fig. 4. Higher-amplitude double-dimple profile compared with theoretical profile.

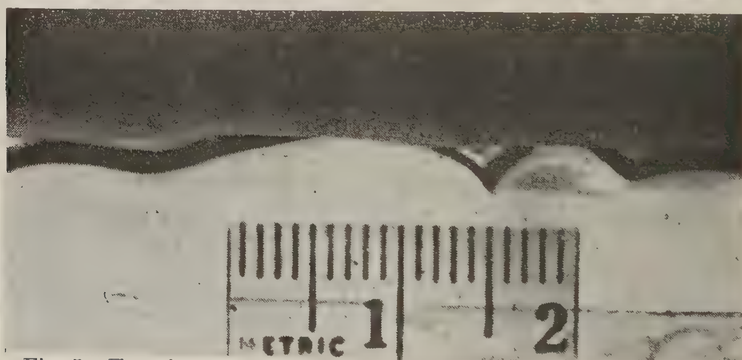

Fig. 5. Experimental double-dimple profile with a third just starting.

Theoretical and experimental profiles. In Figure 1 wave profiles predicted by Wilton (dashed curves) are compared with those predicted by Crapper (solid curves) for various values of amplitude-to-wavelength ratios (α/λ). In general, the troughs appear to be narrower and the crests flatter for Wilton's profiles. Figure 1 shows two wavelengths and omits the doubl dimple profile. This profile is shown in Figure as the upper curve. Underneath it is the singl dimple profile that Wilton's theory indicates ca also exist at the unique wavelength of 2.44 c

Figure 3 shows the double-dimple profile Figure 2 drawn to scale above an actual doubl

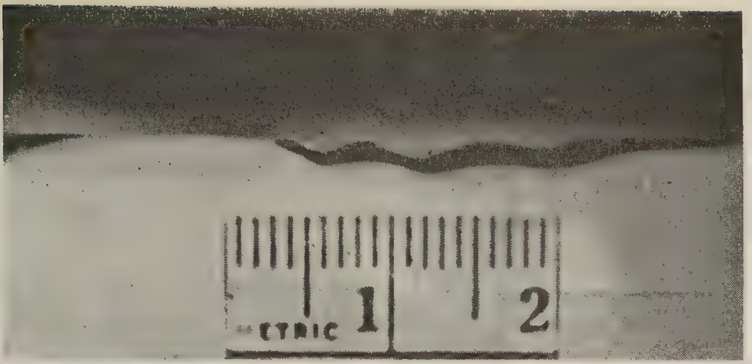

Fig. 6. Triple-dimple wave in front of the developing gravity wave as the wind velocity is increased.

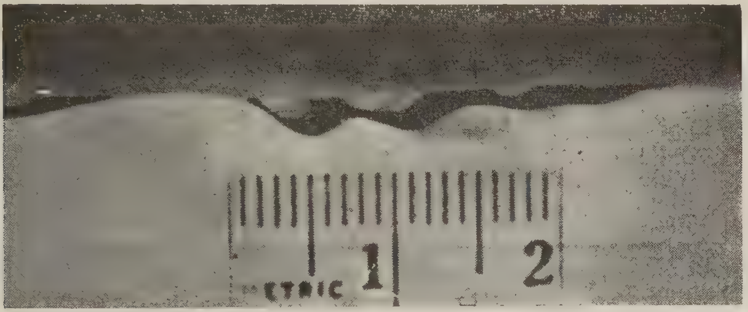

Fig. 7. Quadruple-dimple wave.

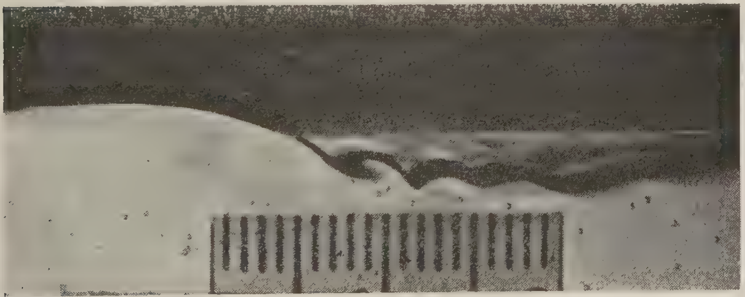

Fig. 8. Five or six capillary dimples riding in front of the crest of a gravity wave.

mple profile of a wind-generated water wave a small transparent water-wind tunnel. The ater in the bottom half of the picture appears ght because underwater lighting was used. he air above appears dark except for a slight aze just above the water surface. The narrow ack band just above the water surface is the ptical effect of the water meniscus that clings the transparent wall of the channel. The tch was about 14 inches with the wind blowing om left to right. The picture is a selected ame from a 16-mm motion picture film taken at 72 frames per second. The wave velocity was measured and found to be very nearly 30 cm/sec. This was determined by the distance the wave traveled between frames, as measured by referring to the 20-mm scale in the picture.

Figure 4 is similar to Figure 3 except that in it the wind velocity is now 12 knots. The wave velocity was found to be very nearly 30 cm/sec. The amplitude-to-wavelength ratio (α/λ) for Figure 4 is 0.08. For Figure 3 it was 0.04. The Wilton theoretical double-dimple profile has an α/λ = 0.075, which is between the measured

Fig. 9. At least seven capillary waves propagating with the accompanying gravity wave.

α/λ values of Figure 3 and 4. In neither case do the dimples in the water surface perfectly match the dimples of the Wilton profile, but the resemblance is close enough to indicate that Wilton's double-dimple waves actually do exist in nature.

Figure 5 is another 12-knot wind-generated wave profile with two dimples and a hint of a third. In Figure 6 the wind velocity is 14 knots and three dimples in front of the now more developed gravity wave are quite evident. Figure 7, also for a 14-knot wind, shows four capillary waves riding in front of the gravity wave.

In Figure 8 a 16-knot generated wave consisting of perhaps five or six capillary waves in front of the crest of the gravity wave is shov Figure 9 is the profile of part of a 20-kı generated wave with at least seven capilla dimples. The film of water clinging to the side the channel above the capillary waves in Figu 8 and 9 may distort the apparent shape of th waves but their existence is unquestionable.

The double-dimple points at 2.44-cm wa length which were obtained from Figures 3 ar 4, together with data given by *Schooley* [195 are plotted in Figure 10. The two points f substantially on top of each other and a represented by the large solid circle. Th data fit well with the earlier experimental da In this figure the dashed curve is approximat the experimental average and is about 30 p

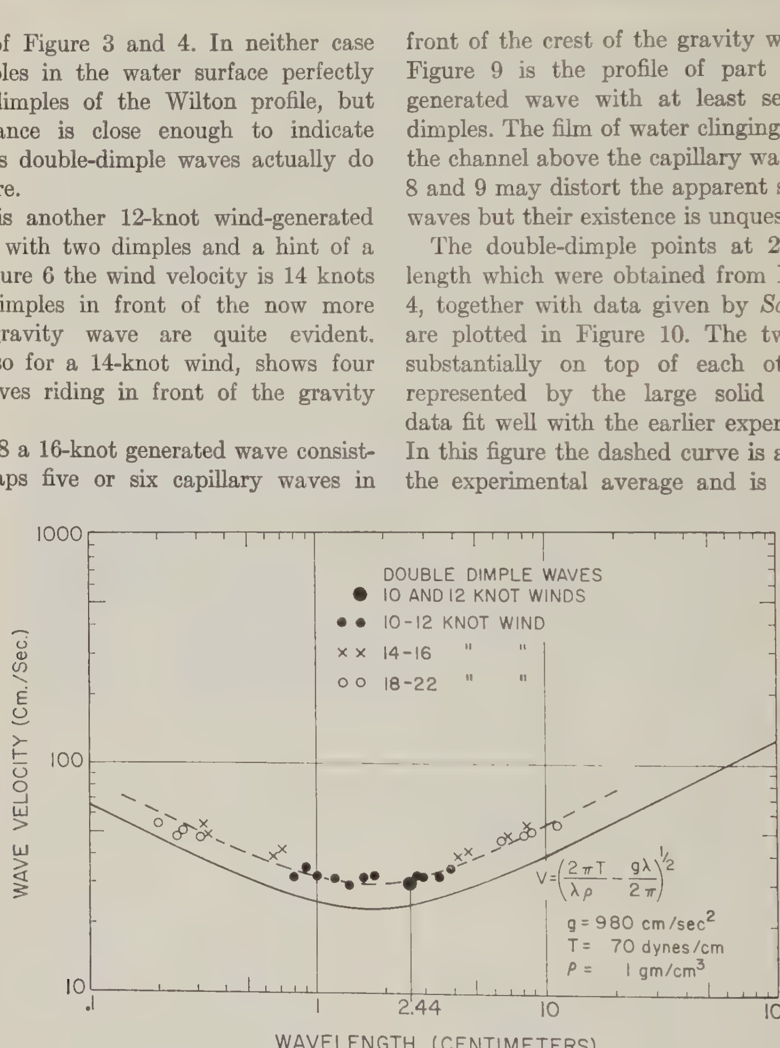

Fig. 10. Experimental and theoretical curves relating wavelength to propagation velocity. Data on double-dimple waves are included.

t higher than the solid theoretical curve. is discrepancy may be due to the wind forcing waves to a higher velocity than would be case for mechanically generated waves in l air.

Conclusions.

. A few examples of double-dimple profiles the 2.44-cm wavelength region in short-fetch nd-generated water waves have been observed.

2. It is suggested that double-dimple waves the start of the phenomenon that is charac- ized by 3, 4, 5, etc., dimples of capillary ves of appropriate wavelength riding in nt of the crest of gravity waves having the ne velocity.

3. From the experimental evidence it is ncluded that Wilton's theory is more complete an Crapper's. This is expected because Wilton alyzed the interaction of gravity, surface tension, and viscosity in his study. Crapper considered surface tension the sole restoring force.

REFERENCES

Crapper, G. D., An exact solution for progressive capillary waves of arbitrary amplitude, *J. Fluid Mech., 2,* 532–539, 1957.

Pierson, W. J., Jr., and Paul Fife, Some nonlinear properties of long-crested periodic waves with lengths near 2.44 centimeters, *J. Geophys. Research,* in press, 1961.

Schooley, A. H., Profiles of wind-created water waves in the capillary-gravity transition region, *J. Marine Research, Sears Foundation, 16,* 100–108, 1958.

Wilton, J. R., On ripples, *Phil. Mag., 29,* 688–700, 1915.

(Manuscript received September 2, 1960; presented at the Forty-first Annual Meeting of the American Geophysical Union, Washington, D. C., April, 1960.)

Variation in Sea Temperature off La Jolla

ROBERT S. ARTHUR

Scripps Institution of Oceanography
University of California
La Jolla, California

Abstract. Hour-to-hour and seasonal changes in temperature were measured by bathythermograph at 32°52′30″N, 117°16′50″W during the IGY period. The temperature-depth traces for 21 series, each extending over 6 to 9 hours, show important hour-to-hour variations at all seasons as a result of internal waves. The median value of the ranges in mean temperature from surface to 100 meters for the 21 series is 0.8°C. The corresponding sampling error in charts of relative topography of the sea surface is about ±1 centimeter. Longer-term variations result from horizontal and vertical (upwelling) advection as well as local heating and cooling.

Introduction. As a part of the oceanographic ogram during the recent International Geo- ysical Year, observations of sea level were tiated over a network of island observatories d coastal stations in the Pacific [*Pattullo,* in ess]. Observations of temperature and salinity re also made every two weeks to permit cal- lation of changes in the *steric* level which is termined from the vertical distribution of nsity by application of the hydrostatic equa- n. The writer undertook to monitor the field ocedures and performance of equipment by cupying a station off La Jolla every few weeks. by-product of the observations is information the variation of temperature in the area and the significance of a single temperature trace om a bathythermograph (BT). The recorded riations in temperature, particularly the hour- -hour changes, are considered in the present per. The relation of the observations to anges in sea level will be discussed elsewhere *attullo,* in press].

Methods. Some notes on the instrumentation d procedures are given to indicate the accu- cy of the measurements and the feasibility of taining hydrographic observations in coastal eas from a small skiff with light-weight equip- ent.

Two standard (135 m) BT's and two deep 70 m) BT's were used for the temperature easurements. The original new standard in- rument was lost on October 7, 1958, when the re parted. Replacement was made with a conditioned instrument. The first deep instru- ent was replaced after October 28, 1958, because of indications that the bellows was beginning to deteriorate.

Checks were made on the temperature readings from the BT's by simultaneous lowerings of two BT's, by simultaneous lowerings of a BT and the temperature element of an electrical resistance thermometer, and by comparisons between BT's and a mercury thermometer in a stirred bath in the laboratory. The results indicated that with the usual calibration procedure [*LaFond,* 1951] the absolute accuracy of the BT readings could not be guaranteed to better than ±0.4°C. Corrections have been applied from the laboratory checks in an attempt to maintain the temperatures reported here to an accuracy of ±0.2°C. Results are better with respect to reproducibility. Identifiable features on traces from repeated lowerings on the same day show a precision of about ±0.1°C. It is to be emphasized that these instruments were handled much more carefully than is possible in ordinary shipboard use.

The customary reading of the bucket thermometer was made in conjunction with each lowering of a BT for calibration purposes [*LaFond,* 1951]. On a number of occasions the temperature at a depth of 1 to 2 m was more than 0.5°C lower than the temperature at the depth of 20 to 30 cm, as determined with the bucket thermometer suspended from a cork float. The effect was naturally most pronounced on relatively calm, clear days during the early afternoon. The recording of the thin, warm layer at the surface is usually obscured on the BT trace by the temperature variations which occur when

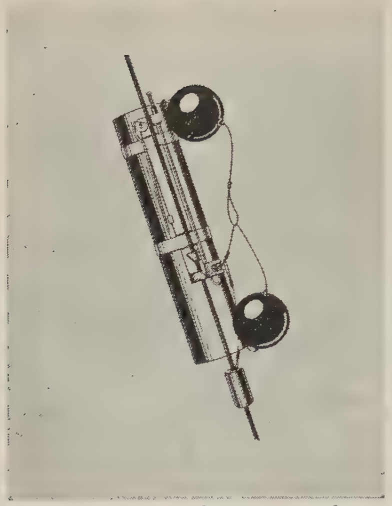

Fig. 1. Sketch of water sampler.

the instrument is put in and taken out of the water. An erroneous calibration comparison may frequently result because the tendency is to assume that the deeper isothermal layer extends to the depth at which temperature is measured with the bucket thermometer. When observations are made from a skiff the difficulty may be eliminated by holding the BT over the side and allowing the temperature element to equilibrate with water at a depth of 20 to 30 cm before the stylus is released. The observation is then made and the stylus is lifted before the BT is taken out of the water. With a sharp stylus and gold-plated slides it was routinely possible to obtain a thin, unobscured trace at the surface.

A check was made on the depths recorded by the BT's. The wire was marked with nylon thread at the maximum depths to which the standard and deep BT's were to be lowered. The wire angle was maintained at less than 10° as estimated visually. The depth recorded by the standard BT was always within ±2 m of wire length at 135 m. The depth element of the deep BT did not remain so accurate. After 15 lowerings the trace showed a depth of less than zero at the surface and a depth greater than the wire length at 245 m. The recorded depth interval from the top to the bottom of the trace was 5 to 10 m too great, and the results indicated deterioration of the bellows. A replacement BT performed satisfactorily for the subsequent lowerings.

The plastic water samplers (Fig. 1) were d[e]signed by J. D. Frautschy as a modification of sampler described by *Van Dorn* [1956]. T[he] salinities of some water samples collected belo[w] 135 m appeared to be anomalously low, and [it] seemed probable that the sampler was exchan[g]ing water during the return to the surface. T[he] hollow ball closures had been provided with [a] vent, so that the pressure inside the ball cou[ld] equalize with the pressure outside. Comparis[on] samples were taken at 135 and 245 m with t[he] plastic bottles before and after an additional ve[nt] of ⅛-inch diameter was provided. Samples we[re] also collected with a Nansen bottle. The resul[ts] showed that the original vent was adequate [...] collected below 135 m after the enlarged ven[ts] were provided are reported. It was also foun[d] that the plastic tubing in the samplers could g[et] out of round and the seat at the ends for the ba[ll] closure could become worn. It is necessary [to] take routine comparative samples with the[se] collectors and a Nansen bottle at the maximu[m] depth.

In a check on the titrations, salinities of du[...]plicate samples from the same bottle and fro[m] closely spaced bottles (1- to 2-meter interva[ls]) agreed within ±0.04 per mil. All samples we[re] collected at depths determined by measure[d] lengths marked on the wire, and the wire angl[es] were small enough so that sample depths a[re] accurate to within about 2 per cent.

Observations. The station was located 2[...] km from shore on the axis of La Jolla Canyo[n] (32°52′30″N, 117°16′50″W), where depth wa[s] about 300 m. On station the standard BT and [a] water sampler were lowered to 135 m with thre[e] additional samplers attached between the su[r]face and the BT. Six to eight subsequent lowe[r]ings of the BT without samplers were made a[t] intervals of about an hour. On many days one o[r] two additional sets of water samples were co[l]lected. When the deep BT was available it wa[s] used immediately after the first lowering of th[e] standard BT, and water samples were collecte[d] below 135 m. A second lowering of the deep BT was made on some days.

Observations were made on 26 days betwee[n] August 1, 1957, and March 31, 1959. All th[e] bathythermograms were read and curves of tem[...]perature against depth and salinity against dept[h] were drawn for each day. A selection of 18 o[f] the 26 days has been made, and the curves fo[r]

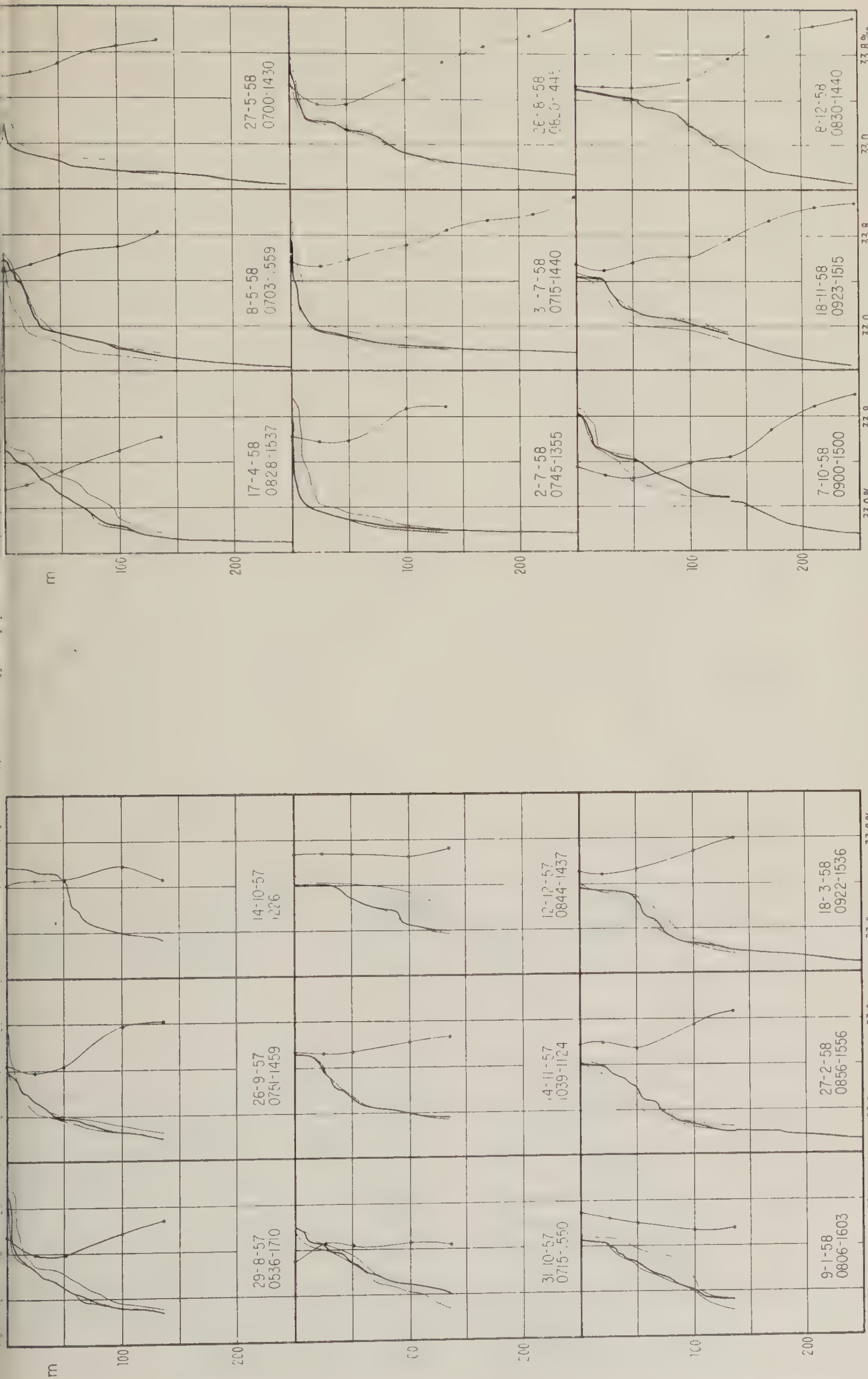

Fig. 2. Temperature (heavy line) and salinity (thin line with points) as functions of depth. The shaded area shows the range of temperature from additional BT lowerings between the times (PST) indicated below the date.

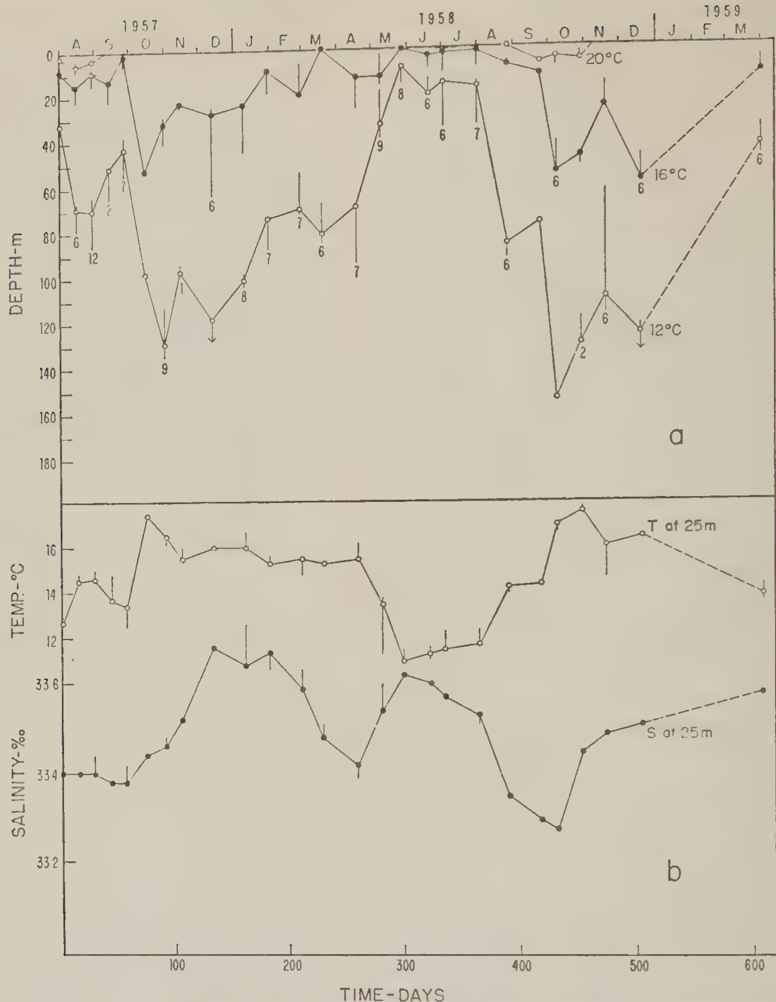

Fig. 3. (*a*) Depth of isotherms as a function of time from a single BT on each day. Vertical lines show range of depth from additional BT's extending over the number of hours indicated (to nearest hour). (*b*) Temperature and salinity at 25 meters as functions of time. Vertical lines show range of variation. In the case of salinity, only one or two additional samples were taken on each of 10 days.

these representative days are shown in Figure 2. In general, the temperature curve to 135 m has been taken from the first lowering of the standard BT on the day. The shaded area shows the range of temperature from subsequent lowerings on the same day. The curve below 135 m is taken from the first lowering of the deep BT. The two curves do not always match at 135 m because of the difference in time (about 30 minutes) and errors in the measurement. The shape of each curve was drawn to follow the actual BT trace in all major features. Salinities from the samples corresponding to the temperature curves were plotted and curves draw through the points.

Points which represent the depths of particula isotherms have been plotted in Figure 3*a* fro a single BT lowering for each day. Vertical lin through the points indicate the range of dept variation for each isotherm as obtained from ad ditional BT lowerings for the same day. Th temperature at 25 m from a single lowering an the range for each day are shown in Figure 3 Salinity at 25 m is also represented with th range for those days when additional water sam ples were collected.

ABLE 1. Range of Variation in Temperature (°C) at Standard Depths

pth, m	Min	Max	25%	50%	75%
urface	0.2	2.2	0.5	0.7	1.2
10	0.2	3.9	0.4	1.0	2.0
20	0.2	3.4	0.4	0.6	1.0
30	0.2	1.8	0.4	0.5	0.8
50	0.3	2.1	0.5	0.7	1.3
75	0.2	2.1	0.5	0.8	1.2
00	0.2	2.9	0.4	0.5	0.8
T_{0-100}	0.5	1.6	0.6	0.8	1.2

)iscussion. Important hour-to-hour varia-ns in temperatures were present at all seasons ing the months of observations. These short-m variations are considered to be associated marily with internal waves. Such waves have n observed [*Reid*, 1956; *Leipper*, 1955; *Ar-ur*, 1954] or are now being observed [*LaFond*, 50] off the California coast. The range of tical movement of three isotherms (12°, 16°, °C) is shown in Figure 3*a*. The extreme oc-rred on November 18, 1958, when the depth the 12°C isotherm ranged from 63 to 117 m. e inadequacy of a sample consisting of a gle temperature trace is apparent.

The variations in temperature at standard pths from surface to 100 m are summarized Table 1. The basis for the summary consists 21 intervals of time during each of which the ies of BT observations extended over 6 to 9 urs. During 17 of the 21 intervals the ob-rvations extended over 6 to 7 hours. The mini-um range is 0.2°C and the maximum is 3.9°C. spection of the individual BT traces has shown at greater ranges tend to occur where the rtical temperature gradient is greater. These ported values are undoubtedly less than the tal ranges of variation produced by the in-rnal waves. The energy in internal waves is stributed from periods of minutes to many urs, but tidal periods are very prominent in e records [*Reid*, 1956: *Arthur*, 1954]. Hourly servations over intervals of at least 12 hours e required to cover the full range of tempera-re variation.

The influence of the temperature variations on e relative topography of the sea surface may estimated from entries in the last row in able 1. Let ΔT denote the difference between e minimum and maximum temperatures at any depth during one of the BT series. The mean value of ΔT between the surface and 100 m, denoted by $\overline{\Delta T}_{0-100}$, has been determined for each of the 21 series. Some 50 per cent of the series have a mean difference greater than 0.8°C and 25 per cent greater than 1.2°C. An approximate value of the coefficient of thermal expansion of sea water is 0.0002/°C^{-1} and the corresponding variation in height of the surface relative to 100 m is 1.6 and 2.4 cm, respectively. These values are probably an underestimate of the variation in height of the sea surface for three reasons: (1) the BT series have not extended over complete tidal periods, (2) the temperature oscillations extend below 100 m, and (3) salinity tends to increase with depth and would add to the variation. The variations are comparable to those found by *Reid* [1956]. They may be regarded as representing the sampling error which exists when stations occupied at different times are used in constructing a chart of relative topography [*Wooster and Taft,* in press]. In view of the magnitude of about 2 cm for the range, the use of a contour interval of 2 cm or less in such charts for the waters off California is certainly inappropriate. Various factors enter into the determination of contour interval, but these results on short-term variation suggest that perhaps 5 cm is a permissible minimum interval

The location of the station over a submarine canyon raises the question whether the observed temperature variations are representative. The curves of temperature and salinity with depth at the IGY station are similar to corresponding curves at a station about 25 km to the west which was occupied seven times during the IGY period. Internal wave activity in much more shallow water close to shore has been shown to be similar with or without the presence of a canyon [*Arthur*, 1954]. It is, therefore, believed that the observed variations are representative of the area off the California coast, particularly in view of *Reid's* [1956] similar results north of Point Conception.

Some longer-term variations, e.g. seasonal, which have been discussed previously [*e.g., Reid, Roden, and Wyllie,* 1958], may be noted in Figures 2 and 3:

1. During the fall months, the temperature and salinity at depths below about 25 m show an increase, with the cumulative effect reaching

a maximum in December. The seasonal inshore countercurrent is important in introducing warmer, more saline southern water at these depths.

2. A more transient variation occurred in October 1957 (Fig. 2, Oct. 14, 1957). A single observation was made within a few hours of the passage of a front which was preceded by relatively strong southerly winds and followed by westerly winds. Warmer water from offshore apparently flooded the water column to a depth of 50 m. For nearshore stations, the onshore movement of surface water is of at least occasional importance during the fall season.

3. Below the surface, e.g. at a depth of 25 m, the lowest temperatures occur in May, June, and July (note Fig. 3, especially). The greater salinity of the cold water suggests the influence of late spring and early summer upwelling at the station.

Acknowledgments. This paper represents the results of research carried out by the Scripps Institution of Oceanography, University of California, under contract with the Office of Naval Research and an IGY grant through the National Science Foundation. Reproduction in whole or in part is permitted for any purpose of the United States Government. The author is indebted to Earl D. Murray for his assistance with all of the observations. Helmuth Sandstrom assisted with the analysis. The scientific program for the IGY observations of sea level was developed by June G. Patt[illegible] and Jeffrey D. Frautschy.

References

Arthur, R. S., Oscillations in sea temperature [illegible] Scripps and Oceanside Piers, *Deep-Sea Resear[illegible]* *2*, 107–121, 1954.

LaFond, E. C., Processing oceanographic d[illegible] *U. S. Navy Hydrograph. Office Publ. 614*, Wa[illegible]ington, D. C., 1951.

LaFond, E. C., Isotherm follower (abstract), *Geophys. Research, 65*, 2505–2506, 1960.

Leipper, D. F., Sea temperature variations as[illegible]ciated with tidal currents in stratified shal[illegible] water over an irregular bottom, *J. Marine R[illegible]search, Sears Foundation, 14*, 234–252, 1955.

Pattullo, J. G., Seasonal variation in sea level [illegible] the Pacific Ocean during the International G[illegible]physical Year, 1957–1958. *J. Marine Resear[illegible] Sears Foundation*, in press.

Reid, J. L., Observations of internal tides in Oc[illegible]ber 1950, *Trans. Am. Geophys. Union, 37*, 2[illegible] 286, 1956.

Reid, J. L., Jr., G. I. Roden, and J. G. Wyll[illegible] Studies of the California Current System, *M[illegible]rine Research Comm., Calif. Cooperative Ocea[illegible] Fisheries Invest., Progr. Rept., 1 July 1956 to January 1958*, The State Printer, Sacramen[illegible] 1958.

Van Dorn, W. G., Large-volume water sample[illegible] *Trans. Am. Geophys. Union, 37*, 682–684, 1956.

Wooster, W. S., and B. A. Taft, On the reliabili[illegible] of field measurements of temperature and sali[illegible]ity in the ocean. *J. Marine Research, Sea[illegible] Foundation, 17*, in press.

(Manuscript received July 28, 1960.)

Geophysical Measurements in the Western Caribbean Sea and in the Gulf of Mexico[1]

J. EWING, J. ANTOINE, AND M. EWING

Lamont Geological Observatory
(Columbia University)
Palisades, New York

Abstract. The data from 48 seismic refraction profiles in the western Caribbean Sea and in the Gulf of Mexico are presented in the form of structure sections crossing the Colombian basin, Nicaraguan rise, Cayman trough, Cayman ridge, Beata ridge, Yucatan basin, Campeche bank, and Sigsbee deep. The Cayman trough has a remarkably thin crust, which suggests that it is a tensional feature. Although parts of the basins have a relatively thin crust, similar to the oceanic type, the shallower areas are intermediate or almost continental in structure. In the Gulf of Mexico the main basin is similar to typical ocean basins in structure except that the high-velocity crust is overlain by very thick sediments. The depth to the mantle is appreciably greater in the Gulf than in an ocean basin. This may be partly the result of loading by the sediments, but large scale tectonic activity is a more likely cause. The Sigsbee escarpment, the northern boundary of the main basin, appears to be the surface expression of a fault or sharp flexure in the layers beneath the unconsolidated sediments.

WESTERN CARIBBEAN SEA

roduction

)uring the past few years a large number of ;mic refraction measurements have been de in the Caribbean area. The purpose of king these measurements has been to study crustal structure in an island arc–deep sea nch province and its relationship to ocean in and continental structure. Results have n published on the Lesser Antilles, Puerto o and the Virgin Islands, Aves swell, iezuelan basin, Barbados ridge, and Puerto o trench [*Worzel and Ewing*, 1948; *Officer, ing, Edwards, and Johnson*, 1957; *Ewing, rzel, and Shurbet*, 1957; *Officer, Ewing, nnion, Harkrider, and Miller*, 1959; *Talwani, ton, and Worzel*, 1959]. The present report ls with the western Caribbean, including the ata ridge, Colombian basin, Nicaraguan rise, yman trough, and Yucatan basin.

The techniques used in making these measurents have been described in detail in the papers erred to above. Figure 1 shows the locations the profiles and of the structure sections. e travel-time graphs and the topography ng the profiles are shown in the Appendix. Receiving positions are designated by circles and the track over which the shots were fired by heavy lines. Also in the Appendix is a table which summarizes the results.

[1] Lamont Geological Observatory Contribution . 456.

Discussion of Results

Seismic refraction measurements. (1) Section *C–D*. This section, the lower part of Figure 2, runs from stations *V* 1–10 and 11 in the Yucatan basin southeasterly across the Cayman trough, the Nicaraguan rise, and the Colombian basin, to station *V* 8–16 on the continental slope off Cape Augusta, Colombia. The average water depth in the Yucatan and Colombian basins is about 4 km; in the Cayman trough it is about 5 km, deepening to almost 7 km in the Bartlett deep. The section crosses the Nicaraguan rise in the saddle between Rosalind bank and Pedro bank. The average depth of water along this part of the rise is about 1 km. The Cayman ridge was crossed between Grand Cayman and Little Cayman where the minimum sounding was 1.2 km.

The structure along this cross section is widely variable, as might be expected in an area where the physiography includes broad basins, prominent ridges, and a deep-sea trench. There is reasonably good correlation between topography and crustal thickness: a thin crust under

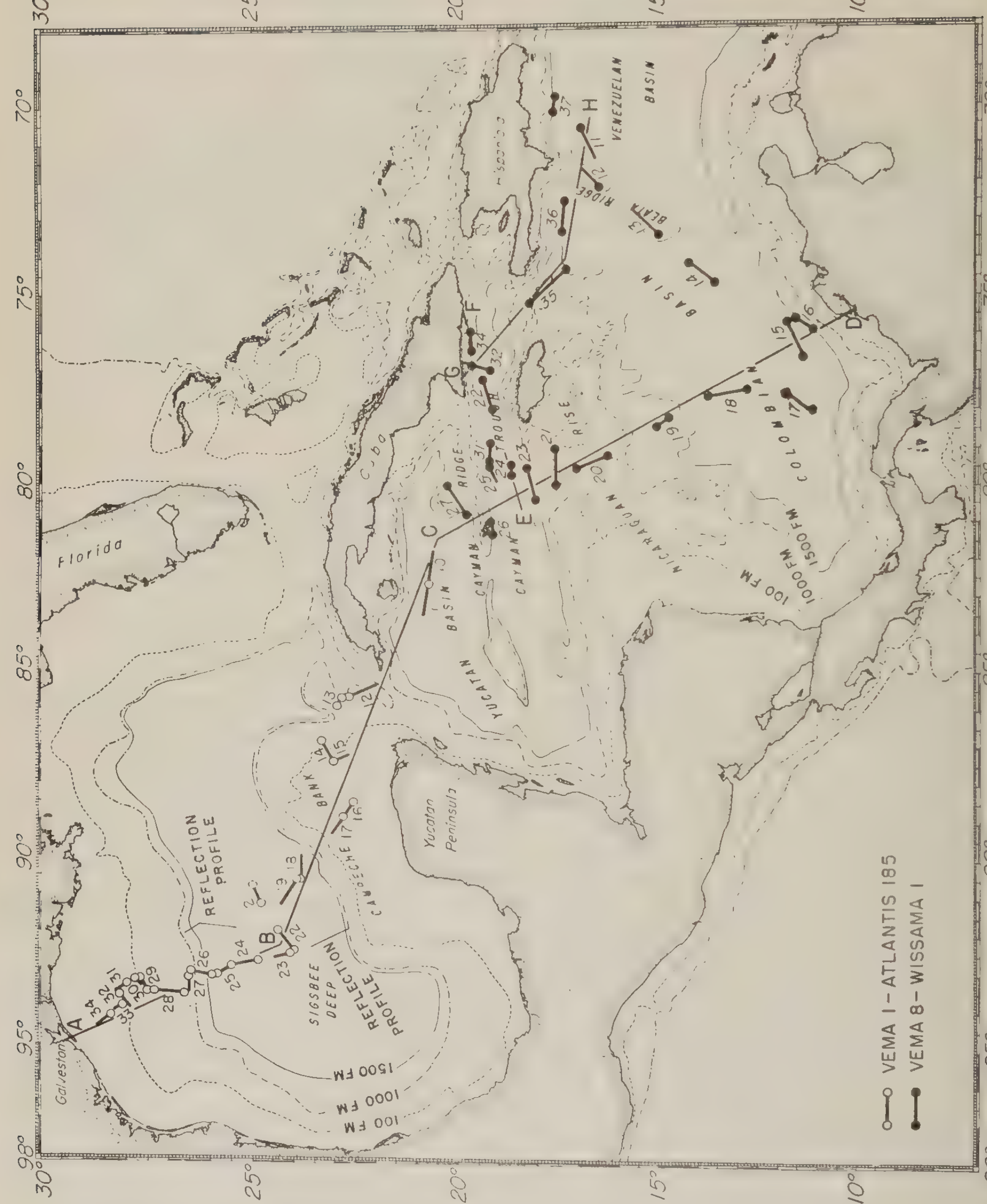

Fig. 1. Area chart showing locations of profiles and section lines

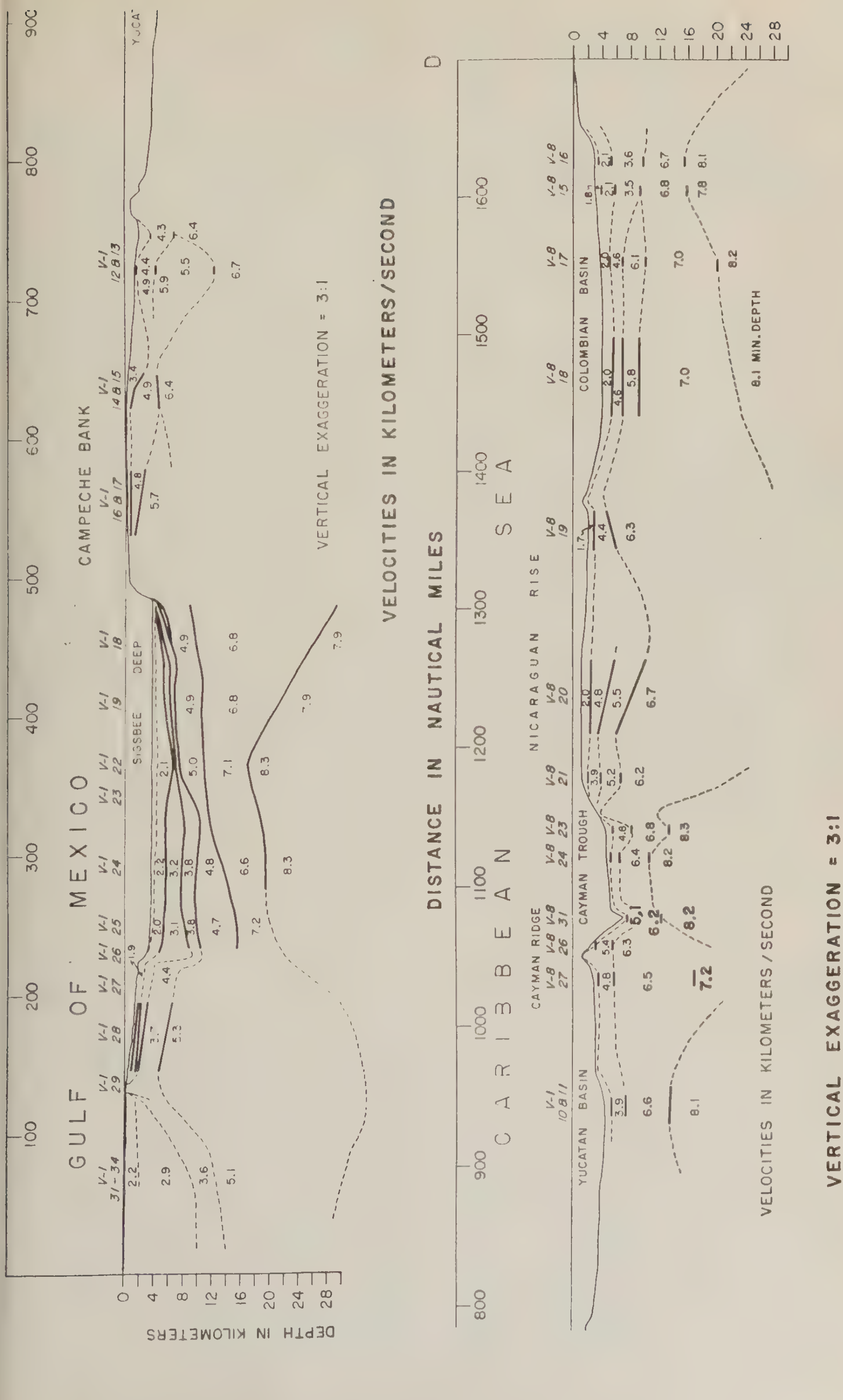

Fig. 2. Structure section *A–D* from Galveston, Texas (*A*), to Cartegena, Colombia (*B*).

the Cayman trough, intermediate under the basins, and thick under the ridges. The entire crustal section was measured only in the Yucatan basin, the Cayman trough, and the southern part of the Colombian basin. The mantle is 10 to 11 km below sea level in the Cayman trough and 15 to 20 km in the basins. The mantle depth under the ridges, by extrapolation and minimum depth computations, is at least 20 to 25 km.

The velocities in the main crustal layer range from 5.8 to 7.2 km/sec, the higher velocities appearing at greater depth in the layer. The material overlying the main crustal layer is widely variable in velocity, and it is often difficult to correlate some of the layers between profiles, owing to wide spacing. The upper part of the section, judging by the seismic velocities, consists of sedimentary layers, some unconsolidated and others somewhat more compacted or lithified. At greater depth, velocities are found that can be associated with metamorphic, volcanic, or intrusive rocks. The material above the main crustal layer is thickest on the Nicaraguan rise, intermediate in thickness in the basins, and thinnest in the Cayman trough.

A prominent structural feature in this section is the thin crust under the Cayman trough. It is also notable that the high-velocity crustal rocks are relatively thin in the Yucatan basin and in the southern part of the Colombian basin. These thin areas are accentuated by the very thick sections nearby under Cuba, the ridges, and the South American continent. The differences between crustal structure in the basin areas and in a typical oceanic section are small.

In the middle of the Colombian basin the crustal rocks are at least twice as thick as the average oceanic crust, even though the water depth is only about 1 km less. Similar results were obtained in the Venezuelan basin [*Officer, Ewing, Hennion, Harkrider, and Miller*, 1959], where the crust was found to be thick except in the southern and central parts. Many of those measurements clearly showed that the velocity increases with depth in the crust from 6.0 to 6.5 km/sec in the upper part to 7.0 to 7.5 at the bottom. This suggests that the density of the deeper part of the Caribbean crust is high, and, despite the extra thickness of the crust and the moderately deep water, approximate isostatic balance is achieved.

At the southern end of the Colombian ba[sin] the high-velocity crustal layer is thinner th[an] in other parts of the basin and is overlain [by] a sedimentary section approximately 7 [km] thick. These sediments are part of an enormo[us] accumulation which fills a broad crustal trou[gh] north of the Colombian and Venezuelan coas[ts]. The eastward extension of the trough has be[en] shown by seismic studies in the vicinity of [the] Netherlands Antilles (Hennion and Ew[ing], unpublished manuscript) and indicated [by] gravity measurements [*Ewing, Worzel, a[nd] Shurbet*, 1957]. On three traverses where bo[th] gravity and seismic measurements have be[en] made, a strong gravity minimum coincides w[ith] the sediment-filled trough.

The Cayman ridge was measured by o[nly] two profiles, one south and one north of Gra[nd] Cayman Island. These indicate that the ric[ge] is principally an expression of the 4.8- [to] 5.4-km/sec layer. The main crustal layer h[as] a velocity of 6.3 to 6.5 km/sec, increasing [to] 7.2 km/sec at a depth of 17 km. The absence [of] intense short-period magnetic anomalies ([see] Fig. 5) indicates that there is little, if any, ba[sic] intrusive or volcanic material near the surfa[ce].

Although there are too few measurements [to] determine it positively, there is a definite in[di]cation that the high-velocity crust is arched [or] folded up into two ridges under the Nicaragu[an] rise—one near the northern and the other ne[ar] the southern edge. Overlying and betwe[en] these ridges is a great amount of the int[er]mediate-velocity material (4 to 5 km/sec) wh[ich] is found almost everywhere in the Caribbea[n], particularly along the ridges.

(2) Section *G–H*. This section, shown [in] Figure 3, runs northwest to southeast fro[m] the Oriente deep, across the Nicaraguan ri[se] between Jamaica and Haiti, across the northe[rn] arm of the Colombian basin, across the Bea[ta] ridge, and into the Venezuelan basin. Th[e] northwest end of this section is a few mil[es] west of the western limit of the deep abyss[al] plain of the Oriente deep [*Hersey and Rutste[in]*, 1958]. Between the Nicaraguan rise and th[e] Beata ridge, the section crosses the 2350-[fm] (4.3-km) abyssal plain in the northern arm [of] the Colombian basin. Profile 36 is partially [on] the plain and partially on a topographic prom[i]nence which extends into the basin from th[e] southern coast of Haiti.

Although this section is short and the da[ta]

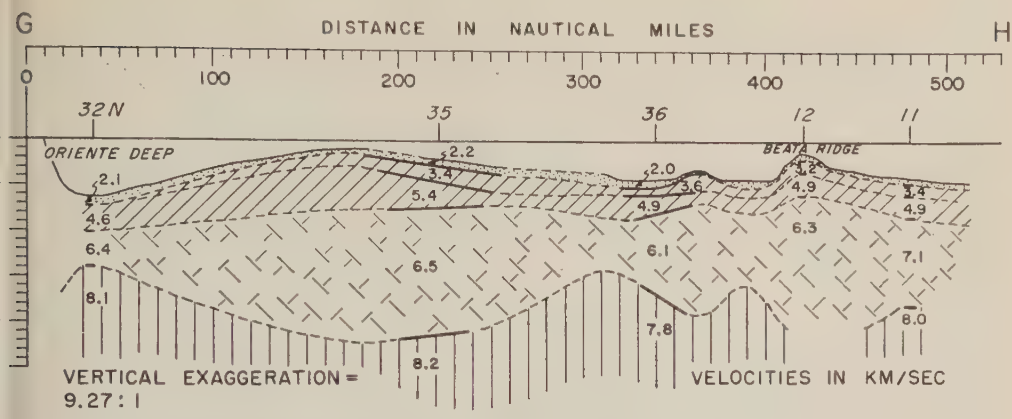

Fig. 3. Structure section G–H from Cuba (G) to the Venezuelan basin (H).

ıly five profiles are used, it demonstrates ationship between crustal thickness and · depth. Profiles 32, 35, and 36 measured ·ntire crustal section, giving depths of 14 o the mantle in the Oriente deep, 17 km e Colombian basin, and 22 km under the ·aguan rise. Although profile 35 by itself not give a good measurement of crustal ness, the results shown are substantiated ıdditional data in preparation (Hennion Ewing, unpublished manuscript). Profiles ıd 12 are unreversed. The fact that they shot in opposite directions on approxi- ly the same azimuth gives some reason to ve that the true velocity in each layer is t the average of the apparent velocities.

Profile 37 is not included in any of the sections. It was shot on the slope south of Ciudad Trujillo, Dominican Republic, on about the 1400-fm (2.5-km) curve. The main crustal layer and a layer with velocity of 2.8 km/sec are reasonably well determined. The other layers, 2.0 km/sec and 4.4 km/sec, were not observed but were assumed to be present because of their occurrence in other profiles in the area.

(3) Section E–F. Figure 4 is a section along the Cayman trough beginning with profile 24, south of the Bartlett deep, and continuing to profile 34, south of Santiago, Cuba. The section cuts obliquely across the eastern end of the Oriente deep at a depth of about 3600 fm (6.6 km) and ends at about the 1800-fm (3.3-km)

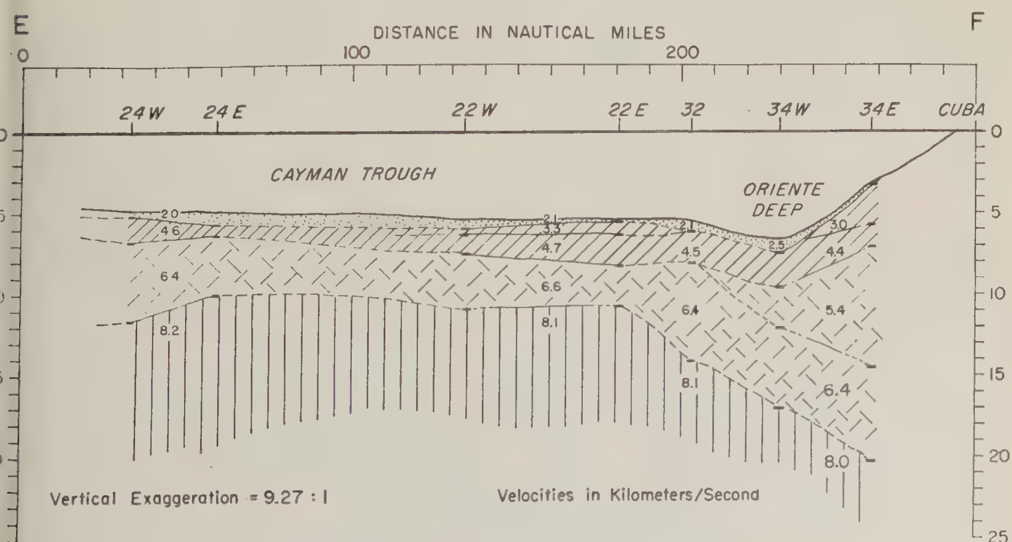

Fig. 4. Structure section E–F along the Cayman trough.

SCALE
0
1000
GAMMAS
500 FM
1000 FM
1500 FM
2000 FM
60
65
70
75
80
85
20
15
10

Fig. 6. Physiographic chart of the Gulf of Mexico [after *M. Ewing, D. Ericson, and B. Heezen*, 1958] showing locations of seismic refraction and reflection profiles.

e south of Santiago. In water depth and ture, the western part is closely comparable n ocean basin. The most significant differ- is a slightly thinner high-velocity crust possibly a greater thickness of the upper s. In the eastern part of the section the thickens somewhat under the Oriente and becomes very thick on the slope south uba. A large part of the increased thickness ue to a 5.4-km/sec layer. This velocity ably corresponds to the intrusive and nic rocks of the Sierra Maestra. The m/sec layer was not measured but assumed present, masked by the 5.4-km/sec layer. r the most part, the profiles in the Cayman h have strong ground-wave arrivals, and nterpretation of the data is straightforward, ing simple ocean-type structure. The veloci- and thickness are well determined, and results clearly show that the mantle is 11 to 12 km below sea level, the shallowest ded in any part of the Caribbean.

There is a distinct structural contrast between the Cayman trough and the Puerto Rico trench, where the depth to the mantle is 18 to 20 km [*Officer, Ewing, Hennion, Harkrider, and Miller*, 1959; *Talwani, Sutton, and Worzel*, 1959]. The Cayman trough is approximately in isostatic balance [*Ewing and Heezen*, 1955], the Puerto Rico trench is not [*Worzel and Shurbet*, 1955]. These contrasts may indicate either different tectonic origins, different ages, or both.

Profiles 25 and 31 in the Bartlett deep and profiles 32 and 34 in the Oriente deep show that the floor of the trench in these places is covered by 0.5 to 1 km of unconsolidated sediments. This amount is approximately the same as that found in the South Sandwich trench [*Ewing and Ewing*, 1959], more than that reported by *Raitt, Fisher, and Mason* [1955] for the Tonga trench and much less than that found in the Puerto Rico trench [*Ewing and Worzel*, 1954, *Officer, Ewing, Hennion, Harkrider, and Miller*, 1959; *Talwani, Sutton, and Worzel*, 1959]. Turbidity

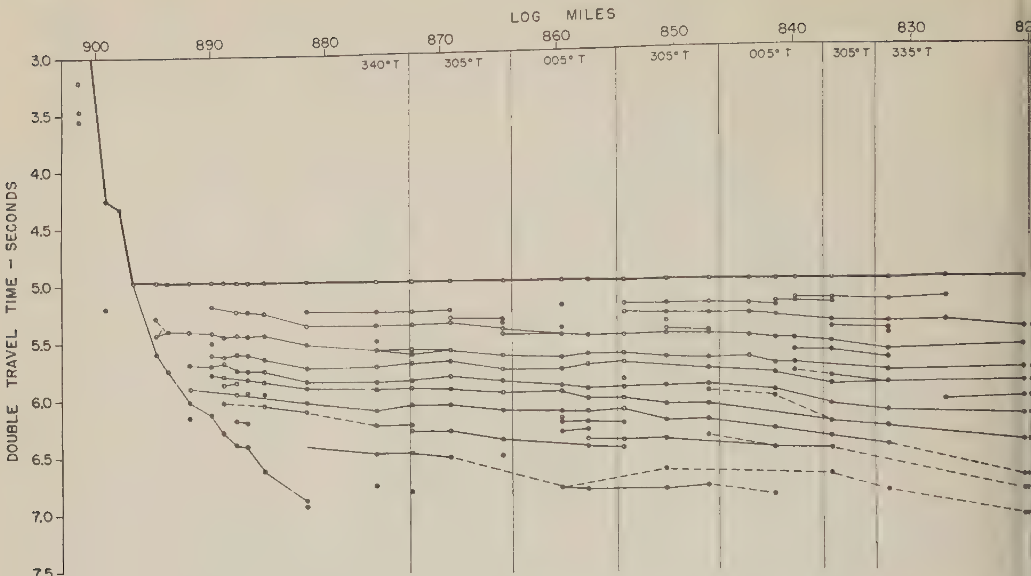

Fig. 7. Reflection profile north of the Campeche escarpment. Vertical lines indicate course changes.

current deposition has been suggested as the agent in the formation of the abyssal plains in both the Puerto Rico trench and the Cayman trough [*Ewing and Heezen*, 1955; *Hersey and Rutstein*, 1958]. The latter authors estimated the thickness of low-velocity sediments to be 0.35 to 0.45 km in the Oriente deep, from the results of seismic reflection shots.

The abyssal plain in the Bartlett deep is very narrow compared with its length. South of Grand Cayman Island it is less than a mile in width at a depth of 3760 fm (6.9 km).[2] Toward the east, the depth increases at the rate of approximately 1 fm per mile to a maximum of 3867 fm (7.1 km) south of Cayman Brac. In this area the plain is 2 to 4 miles wide; farther eastward, it apparently becomes narrower and shallower. The soundings are less detailed in the eastern than in the western part.

Magnetic measurements. Variations of total magnetic intensity along several traverses in the western Caribbean are shown in Figure 5. These data were obtained with a fluxgate magnetometer of self-orienting type. Allowance for regional variations has been made by simply drawing an average base line through the measured intensities on each of the long traverses.

[2] The water depths given in this paper have been corrected for velocity of sound in the water but have not been corrected for bottom slope.

The slopes of the resulting 'regional correctio were compared with those published by *Vest LaPorte, Lange, and Scott* [1947] and found agree reasonably well. For shorter traver the regional slope from *Vestine and others* [19 was used. The magnitude of the corrections then taken from an intersecting profile available) or from the mean intensity on given profile. Most of the track was covered w an airborne instrument, flown at an eleva of 1500 to 2000 ft; the remainder was measu with the sea magnetometer towed behind Ve The only object in showing these results is indicate areas of rough and smooth magn field. Without question, the over-all res show that the Venezuelan basin has an appr ably smoother field than the Colombian b and is remarkably smoother than the rid submerged and emerged. The ridges characterized by short-period disturbances t are believed to indicate shallow-seated variati in magnetic susceptibility, probably due volcanic or near-surface intrusive activity, near-surface structural irregularities in a mate with relatively high susceptibility. Particul noticeable changes in the character of magnetic field are seen in traverses across edges of the Venezuelan basin. These sl definite anomalies associated with Puerto R the Aves swell, the Netherlands West In

nain, and the Beata ridge. The field over the Nicaraguan rise and the Cayman ridge is also s rough as that over the southern peninsula f Haiti and the Sierra Maestra of Cuba. Owing o the generally rough field on each side, it is ifficult to say whether the Cayman trough has characteristic magnetic anomaly associated ith it.

A close correlation between the character of ne magnetic field and crustal structure, as etermined by seismic measurements, is not bvious, and it is entirely possible that the ctor or factors responsible for a rough field ay vary from place to place. In the present ork, the most apparent relationship is in the ype of material above the main high-velocity rustal layer, i.e., the material with velocities ss than about 6 km/sec. In general, velocities r the upper crust are no higher than about 5 to 4.0 km/sec in the areas of smooth field, hereas velocities in the range 4.5 to 5.5 km/sec re characteristic of the rough areas. Even if is relationship is significant, it cannot be xpected to be without exception. A velocity 5 km/sec, for example, can correspond to mestone in one place and to igneous or volcanic ock in another.

In the Caribbean area, the magnetic field is noothest in the southern part of the Colombian asin, in most of the Venezuelan basin, in the obago trough, and in the region east of the indward Islands. (The Yucatan basin is not nsidered here owing to scarcity of data, both ismic and magnetic.) In these areas the velocies above the main crustal layer are low. In e Gulf of Mexico, on the other hand, the eld is smooth [*Miller and Ewing*, 1956] and upper crustal layer with a velocity range of 7 to 5.3 km/sec is found in every profile.

mmary

These measurements have shown that the ustal structure in the western Caribbean Sea widely varied. Parts of the Colombian and ucatan basins have near-oceanic structure, sharp contrast with the submarine ridges which e almost continental in crustal structure and ickness. A prominent feature is the Cayman ough, a relatively narrow strip with very deep ater and a thin crust, closely bounded by the ayman ridge on the north and the Nicaraguan e on the south. Geophysical data on the Cayan trough were presented by *Ewing and Worzel* [1954] in the form of a gravity profile across this area. Their deduction that the crust is thin under the trough is confirmed by these seismic measurements. Their conclusion that the structure resulted from tension seems to remain valid in the light of the present measurements. The structure found here is different from that in the Puerto Rico trench [*Officer, Ewing, Hennion, Harkrider, and Miller*, 1959] where the high-velocity crust and the mantle are much deeper and are covered by a thicker section of low-velocity, and presumably low-density, material. This difference in structure of the two trenches is also indicated by the gravity anomalies. The free-air anomalies are 100 to 150 mgal more negative in the Puerto Rico trench than in the Cayman trough.

The tectonic development of the Caribbean has been discussed by many writers. One of the hypotheses that is interesting to consider in the light of the present data is that supported by *Hess and Maxwell* [1953], *Bucher* [1952], and others in which the Cayman trough is considered to be a great tear fault or strike-slip fault zone along which the Caribbean basin, Jamaica, Hispaniola, and Puerto Rico moved eastward relative to the Yucatan basin, Cuba, and the Bahama Islands. Another is that proposed by *Eardley* [1954] in which the Cayman trough might be considered a graben developed in the cooling, radioactively heated column, which is postulated as the main epeirogenic agency in his theory of uplift, orogeny, and subsidence.

The seismic results reported here show that the crust in the trough is thin even when compared with oceanic crust and particularly so when compared with the nearby submarine ridge areas. There would appear to be three possible explanations of the thin crust. One is that the trough is a great crack, into which the mantle material flowed laterally and vertically, accompanied by the differentiation and ascent of the crustal material—or, as the case may be, the establishment of the phase boundary believed by some to be the discontinuity between crust and mantle. Another explanation might be that the Cayman trough is simply a slightly stretched remnant oceanic area, not drastically different from many parts of the Yucatan, Colombian, and Venezuelan basins. The other possibility is that the trough is a graben.

Geological evidence pertinent to the origin of the Cayman trough is found in southeastern

Cuba where 'the Paleocene and Eocene pyroclastics are coarser southward, and flows are more numerous in the same directions, indicating a southward source' [*Woodring*, 1954, p. 727]. Judging by the crustal structure (Fig. 2), this source could hardly have been the Cayman trough, nor could lava flows from the Nicaraguan rise, the most obvious source south of Cuba, have crossed the trough. Therefore, unless these volcanic rocks are of local origin, which is apparently contrary to geologic evidence, the natural conclusion to be drawn is that sometime during or after middle Eocene, the Nicaraguan rise was pulled away from Cuba, and the Cayman trough was formed in the process.

Eardley and others have postulated that the submarine ridges in the Caribbean are remnants of old orogenic belts, dating back to Paleozoic. From seismic evidence alone, there is no outstanding difference between the submerged ridges and the island ridges. Generally speaking, they are thickened, raised welts of high-velocity crustal rocks overlain by layers of varying thickness with velocities that are usually associated with intrusive, volcanic, and metamorphic rocks. It seems reasonable to assume, as have other writers, that parts of the now submerged ridges were land areas at some time and that they were the sites of the volcanoes which produced the large volumes of Cretaceous and Paleocene-Eocene pyroclastics present in the Caribbean islands. Geophysical evidence that the ridges are volcanic is that they have characteristic magnetic anomalies that are usually associated with intrusive or volcanic rocks.

Gulf of Mexico

Introduction

All the seismic refraction measurements in the Gulf of Mexico used in this report are presented in the upper part of section *A–D* (Fig. 2), which runs from Galveston, Texas, to Cartegena, Colombia. A preliminary analysis of six of the profiles, numbers 16, 21, 22, 24, 28, and 29, has been published previously [*Ewing, Worzel, Ericson, and Heezen*, 1955]. The present study has produced a revised interpretation of some of the results; hence all the profiles are presented in the present paper. For a recent description of the topography and the sediments of the Gulf of Mexico, the reader is referred to *Ewing, Ericson, and Heezen* [1958]. Figure 6 is a reproduction of their chart showing the physiographic provinces of the Gulf. On it are shown the locations of the seismic refraction profiles discussed here.

Discussion of Results

Seismic refraction measurements. The part of the structure section, *A–D*, from Galveston to the Yucatan Channel, is based on the results of profiles 12–34 from cruise *V*–1, *A*–185. At the northern end, the thickness of 14 km for the sedimentary column given by *Colle, Cooke, Denham, Ferguson, McGuirt, Rudy, and Weaver* [1953] has been used. Between the Texas coast and the Sigsbee escarpment, the control on the section is not good. Profiles 31–34 are unreversed and are not long enough or shot heavily enough to give positive results. For this reason, a single computation of layer thicknesses was made from average slopes and intercepts taken from the four travel-time graphs. Obviously this gives only a very rough estimate of the structure, but the velocities obtained in this way are similar to those found in the other profiles, and we are reasonably certain that the total thickness of material above the 5.1-km/sec layer is at least approximately correct.

Profile 28 on the upper continental slope measures the structure down to a layer at about 6-km depth which has a velocity of 5.- km/sec. This velocity is similar to that found at about 12-km depth in the profiles farther north. The velocity was not accurately measured owing to the fact that shots at the longer ranges failed to produce ground wave arrivals. In the earlier paper, this high attenuation in the 5-km/sec layer was interpreted on the assumption that the layer was thin and presumably underlain by more low-velocity layers. After examination of all the data, it now appears more likely that the 5-km/sec material is part of a large ridge which separates the Sigsbee deep from the Gulf geosyncline. The structure section, Figure 2, is drawn according to this view.

It was not possible to determine the structure accurately at profile 29 (the travel-time graph and further discussion are given in the Appendix). Our interpretation of the results is that the profile crossed a major structural feature, possibly a salt dome. Although neither of the shooting tracks in profile 29 showed any topographic evidence for the structure, profile 30 which was shot just north of 29, crossed a ree

ike feature in the same general area. Unfortu-
ately, neither of the profiles gives positive nformation about the feature. In profile 29, he structure appears to be in a layer whose elocity is about 3.7 km/sec; i.e., a sharp rise n the 3.7- km/sec material from a depth of bout 1 km to the sea floor would produce the bserved behavior of the points on the travel-ime graph. On the other hand, the data could ndicate a dome or ridge in some deeper layer which rises to the surface at this point.

Profiles 25, 26, and 27 constitute a reversed tation; 26 extends across the Sigsbee escarp nent, and end-to-end unreversed profiles 25 nd 27 extend to either side. Although the nterpretation is uncertain, this group of profiles s judged to indicate that the Sigsbee escarpment s the expression of a large fault or flexure which s the southern edge of the ridge between the Gulf Coast geosyncline and the main basin of he Gulf of Mexico.

Profiles 18–25 are in the basin of the Gulf of Mexico, the southern part of which is commonly alled the Sigsbee deep. The top of the high-elocity crust, 6.9 km/sec average velocity, s at a depth of approximately 9 km in the south ear the Campeche escarpment and slopes to depth of 15-16 km in the north near the Sigsbee scarpment. The overlying layers of sediments nd sedimentary rocks resemble a wedge, apered toward the south. The low-velocity edimentary layers appear to be impounded, s would be expected if turbidity currents riginating at the Mississippi delta supply the major portion of the sediments of the Sigsbee asin, as proposed by *Ewing, Ericson, and Heezen* 1958]. Measurements of total crustal thickness ndicate that the mantle is at a depth of 16 to 17 m near the center of the Sigsbee deep and is ppreciably deeper both to the north and to ne south. The crust-mantle interface north of ne Sigsbee deep has been drawn, speculatively, eeper under the upper continental slope than nder the Texas-Louisiana coastline on the asis of recorded seismic velocities and con-deration of isostatic equilibrium.

Profiles 12–17 were recorded between the ucatan channel and the Campeche escarp-ent. It is not apparent how the layers measured y these profiles relate to the layers found in e main basin of the Gulf of Mexico or to ose in the Yucatan basin, and no attempt as been made to connect the interfaces to those toward the north or south. It is noteworthy that relatively high velocities, near 6 km/sec; are found to be shallower in this area than at any other point along the structure section. These high velocities might correspond to crystalline rocks or to high-velocity limestones or dolomites. The 5.7-km/sec layer found at stations 16 and 17 on the Campeche bank slopes upward toward the northwest, and extrapolation of the slope in this direction would bring the top of the layer to the surface approximately at the lip of the escarpment. This extrapolation is not unduly speculative, since the measurements were made not far from the escarpment. Another possibility is that the 5.7-km/sec layer reverses its direction of dip and outcrops on the escarpment at a depth of about 1 km, where the break in slope suggests a change in material.

Seismic reflection measurements. In Figure 7 are shown the results of about 30 seismic reflection shots, recorded with a 6-element reflection string, spaced over a distance of approximately 90 miles at the southern edge of the Sigsbee deep. The location of the profile is shown in Figure 1. The last few shots are on the slope of the Campeche escarpment. The bottom is almost perfectly flat at a depth of 2050 fm (3.7 km) at the northern end of the line and rises gently as the escarpment is approached. Although a closer shot spacing would have been advantageous, the correlation of reflections is reasonably certain. The results show that the reflecting horizons are nearly horizontal, sloping upward to the south at a low angle. This is in agreement with the conclusions of *Ewing, Ericson, and Heezen,* [1958] that the basin of the Gulf of Mexico has been filled with turbidity-current deposits.

Another reflection profile approaching the Sigsbee escarpment is shown in Figure 8. Correlation over the entire distance is less certain than in the profile near the Campeche escarpment. Several groups of records can be correlated, however, and these indicate that, except for those that are very near the escarpment, the beds are nearly flat-lying here, as they are in the southern part of the Sigsbee deep. Other reflection profiles in the deep areas of the Gulf show similar results, i.e., correlations of reflection can usually be made with groups of records indicating near-horizontal bedding, but a single horizon cannot be traced for more than a few tens of miles. This type of layering is to be

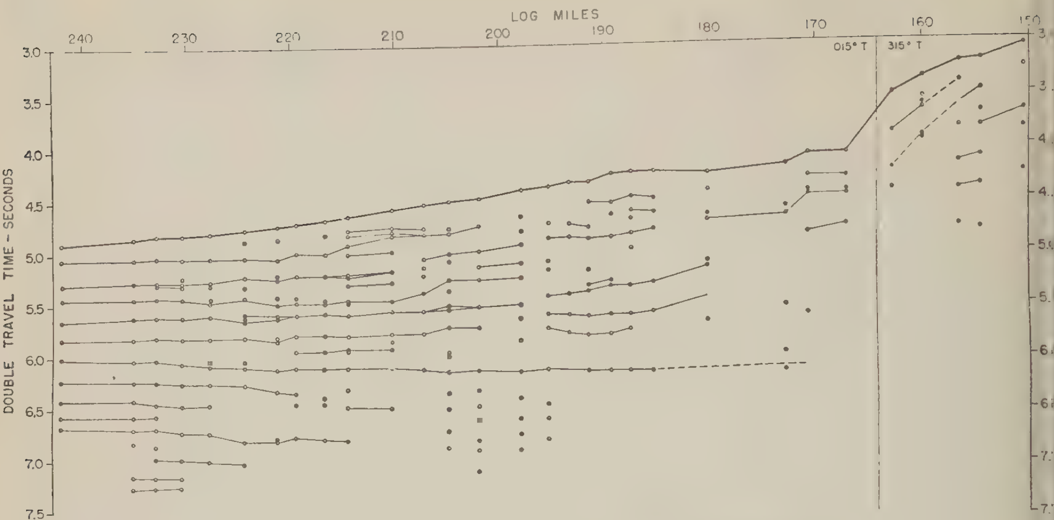

Fig. 8. Reflection profile south of the Sigsbee escarpment.

expected in areas where turbidity-current deposition is predominant.

Summary

The main basin of the Gulf of Mexico is typically oceanic in structure, except that the high-velocity crustal layer is covered with a greater than normal amount of sedimentary material, and the main crustal layer (average velocity 6.8 km/sec) and the mantle are appreciably deeper here than in an average ocean basin. Although the upper layers of sediment are nearly flat-lying, the main crustal layer in the Sigsbee deep dips northward from the Campeche escarpment to the Sigsbee escarpment. Thus, in a north-south section, the sedimentary material is in the form of a wedge, thick at the north and thinner at the south.

In the northern part of the Gulf of Mexico is the well-known Gulf Coast geosyncline, which has a sedimentary thickness estimated to be about 14 km. The refraction results presented here indicate that in the south this geosyncline is bounded by a ridge on the order of 100 miles wide, the southern edge of which is approximately coincident with the 1500-fm (2.7-km) contour. *Ewing and Heezen* [1955] pointed to the aseismic nature of the area including the Sigsbee escarpment as strong evidence that the origin of the escarpment is limited to processes in the sediments and is not controlled by tectonic activity in the basement. Magnetic measurements in the Gulf which show no anomali connected with the escarpment [*Miller an Ewing*, 1956] are cited as additional evidence It thus appears that the ridge was cause either by folding of the older sediments or b uplift of a trough or trench which had bee filled. It is suggested that this ridge migh represent a continuation of the Appalachia system which trends toward this point at lea as far south as eastern Mississippi [see *Kin* 1959, pp. 69–70].

Acknowledgments. The research in this pap was supported by the U. S. Navy Bureau of Ship contract Nobsr 64547, and the Office of Naval R search, contract N6-onr-266(13). The assistan and cooperation extended by the commandi officers and personnel of the U. S. Naval statio at Coco Solo, Panama, and Guantanamo Ba Cuba, were important to the expeditions. It a pleasure to acknowledge the assistance of Bentley, A. Stockel, C. Hubbard, J. L. Worz J. Hennion, B. C. Heezen, and M. Landisman, wi participated in the field work.

In addition to government contract support, w wish to acknowledge financial assistance gene ously given by the following private industries a individuals: California Research Corporation, Gu Oil Corporation, Shell Development Compa Standard Oil Development Company, The A lantic Refining Company, Magnolia Petroleu Company, Ohio Oil Company, Kennecott Copp Corporation, E. De Golyer, and L. J. Buck.

For the magnetic measurements shown here, are indebted to several members of the scienti staff of Lamont Observatory. We wish particula to acknowledge the work of Julius Hirshman.

Appendix—Discussion of Profiles

Vema-8, Wissama-1

Profile 11 is an unreversed station received in the Venezuelan basin with the shot line running along the flank of the Beata ridge. The line representing the 1.8-km/sec layer is assumed. That representing the 8.0-km/sec layer is little better than an assumed line, although the two second arrivals which fall on it are good. The line is at least significant for computing the minimum thickness of the crustal layer. The line representing the 3.4-km/sec layer is drawn principally on the basis of strong sub-bottom reflections, shown by x's in the travel-time graph. Both the 6.7- and the 4.7-km/sec layers are well determined.

Profile 12 is an unreversed profile along the axis of the Beata ridge, 32 miles south of Point Beata. Apparent velocities of 3.2, 4.9, and 6.3 km/sec were recorded. A sedimentary layer with a velocity of 1.8 km/sec was assumed. Both refracted and reflected arrivals were received from the 3.2-km/sec layer. Topographic corrections were applied for an assumed horizontal datum plane at a depth of 1500 fm (2.7 km).

Profile 13 is an unreversed profile shot along the axis of the Beata ridge about 110 miles southwest of profile 12. A horizontal datum plane at a depth of 1700 fm (3.1 km) was assumed for topographic corrections. Although some large corrections were required, the corrected points are reasonably well aligned, determining three layers with apparent velocities of 2.9, 4.9, 5.4, and 6.5 km/sec. A velocity of 1.8 km/sec was assumed for the sediments. Since this is an unreversed profile, the layer thicknesses were computed by using true velocities from more recent nearby stations, (Hennion and Ewing, in preparation). This account for the discrepancies in the slopes of the lines shown on the travel- time graph and the velocities listed in Table 1.

Profile 14 is in the Colombian basin southwest of the Beata ridge. The water depth was almost constant at about 4 km, and no topographic corrections were applied. The most satisfactory alignment of the points on the travel-time graph requires an offset of approximately 0.6 seconds near the middle of the profile in the line that determines the 6.3-km/sec layer. This represents a fault or flexure with the southwest side being down relative to the northeast side. The uncorrected travel-time data indicated that there is appreciably more low-velocity sediment at the southwest end of the profile than at the northeast end. Allowing a 0.7-km offset in the interface between the sediments and the 4.3-km/sec layer, we still require a 2.0-km offset in the next deeper interface (that between the 4.3- and the 6.3-km/sec layer) to account for for the total offset in the G_3 lines. The G_4 lines, representing the mantle, are drawn assuming no offset in the crust-mantle interface, and the points are fitted satisfactorily. The location of the fault or flexure determined by the *Vema* profile does not agree with the location given by the *Wissama* profile. This discrepancy is understandable, however, owing to the fact that the drift rate was high and the time required to shoot the reversed profile was 14 hours. Good sub-bottom reflections were received from the top of the 4.3-km/sec layer.

Profile 15 is on the continental rise 80 miles northwest of Cape Augusta, Colombia, in approximately 1700 fm (3.1 km) of water. Five layers with velocities of 2.1, 3.5, 6.8, and 7.8 km/sec were measured, and 1.8 km/sec was assumed for the upper sediments. The velocity of 6.8 km/sec is well determined. The velocities of 3.5 and 7.8 km/sec are less accurate. The line representing the 2.1-km/sec layer was drawn principally on the basis of strong sub-bottom reflections recorded at both ends of the profile.

Profile 16 is on the continental rise, 60 miles northwest of Cape Augusta, Colombia. The velocities measured are 1.8, 2.1, 3.6, 6.7, and 8.1 km/sec. There are only a few relatively weak arrivals from long-range shots, and, although the break from 6.7 km/sec to a higher velocity is definitely indicated, an accurate velocity cannot be assigned to the deeper layer. The velocity shown is appropriate for the mantle.

Profile 17 is located 180 miles northeast of Colon, Panama, in the southwestern edge of the Colombian basin. The velocities in the upper layers (1.8 and 4.2 km/sec) are not precisely determined, but there is little doubt that these layers are present. The 6.1-km/sec layer is well determined by a good first-arrival line in the *Vema* profile, but it is apparently very thin at the *Wissama* end and is less clearly indicated there. The velocity of 7.0 km/sec is measured by long lines on both sides. Second arrivals, exceptionally strong in the *Wissama* profile, are identified as mantle arrivals. These indicate a velocity of 8.2 km/sec at a depth of about 19 km.

Profile 18 was shot in the western part of the Colombian basin. It is 62 miles long, and the arrivals are strong for the entire length of the profile. The velocity in the unconsolidated sedimentary layer was measured in the *Vema* profile and assumed in the *Wissama* profile. Although there is some indication of the next deeper layer (4.6 km/sec) in the close shots, the principal reason for showing it is its appearance in almost all other Caribbean profiles. There is little doubt about the presence of the 5.8- and 7.0-km/sec layers. Unlike profile 17, which had several strong second arrivals interpretable as mantle waves, this profile gives, at best, only a lower limit for crustal thickness. A minimum thickness of 13 km was computed for the 7.0-km/sec material, assuming that insufficient shot distance rather than insufficient charge size accounts for the failure to see first-arrival mantle waves. The resulting depth of 22 km to the M discontinuity seems excessive for a basin area. The explanation for this may lie in the proximity of the profile to the Nicaraguan rise or the Isthmus of Panama. Additional measurements in this area would be very useful, since both profiles (17 and 18) in the western part of the basin show an unusually thick section of high-velocity

crust compared with other areas having similar water depth.

Profile 19 is on the flank of the Nicaraguan rise south of Jamaica in approximately 1200 fm (2.2 km) of water. The profile is 26 miles long and measures three layers, with velocities of 1.7, 4.4, and 6.3 km/sec. All three layers are well determined in the *Wissama* profile. Although no sedimentary arrivals were recorded by *Vema*, the other two layers were satisfactorily determined.

Profile 20 was shot southeast to northwest on the Nicaraguan rise, between Pedro Bank and Rosalind Bank. Four layers were measured with velocities of 2.0, 4.8, 5.5, and 6.7 km/sec. The 4.8-km/sec layer is best determined by the *Vema* profile, the 5.5-km/sec layer by the *Wissama* side. The uncertainties in the last two points of the *Vema* profile are the result of poor time breaks.

Profile 21 is an east-west profile on the Nicaraguan rise west of Jamaica. The upper part of the section consists of three layers totaling about 5 km in thickness, with velocities of 1.8, 3.9, and 5.2 km/sec. Underneath is a thick layer with a velocity of 6.2 km/sec and possibly a 7.6-km/sec-layer. The 6.2-km/sec layer is well determined, particularly in the *Wissama* profile, which has first arrivals appearing for a distance of 40 miles, with little scatter. The 7.6-km/sec layer is determined in the *Wissama* profile by several strong second arrivals and one strong first arrival, but it is not seen in the *Vema* profile, possibly because of weaker records. The assumed line in the *Vema* profile has been drawn to indicate approximately constant thickness of the 6.2-km/sec layer across the profile. It is possible that the interface is deeper at the east end and the velocity beneath it higher than 7.6 km/sec.

Profile 22 was shot in the Cayman trough, south of the western end of the Oriente deep. The uncorrected travel times show that there is about 0.5 km of unconsolidated sediment in the level area at *Vema's* end and none on the rise. Topographic corrections were made using a 2960-fm (5.4-km) datum level. Four layers were measured with velocities of 3.3, 4.7, 6.6, and 8.1 km/sec, and a 2.1-km/sec sedimentary layer was assumed.

Profile 23 was shot in the edge of the Cayman trough near the west end of Jamaica. The eastern end and the major portion of the profile are in the Cayman trough. Westward the profile extends onto the Nicaraguan rise, and *Wissama's* receiving position was on the slope, near the top of the rise. Three layers were measured with velocities of 4.6, 6.4, and 8.3 km/sec, and a velocity of 2.1 km/sec was assumed for the layer of unconsolidated sediments. The sediments, which are almost 1 km thick in the trough, pinch out on the flank of the ridge. In making the topographic corrections, this variation in the thickness of the sediments, as well as the bottom topography, was taken into account. The travel-time graph is the result of correcting ground-wave travel times for deviations from a horizontal datum plane at the level of the base of the low-velocity sediments at the eastern end of the profile. The water waves (R_1 curves), if corrected to this same datum, would appear approximately 1 second later than shown.

Profile 24 was shot approximately parallel to the axis in the Cayman trough a few miles south of the Bartlett deep. Only part of the profile was reversed, leaving some uncertainty about the subcrustal velocity, but there are probably no large errors. The velocities measured are 2.0, 4.6, 6.4, and 8.2 km/sec.

Profile 25 is in the Bartlett deep of the Cayman trough. Although the profile is unreversed, the receiving position near one end of reversed profile 31 provided a useful check because of the conditions imposed by an end-to-end profile arrangement. In this profile, only the crustal layers were measured with any precision. The line corresponding to the mantle was drawn through the end point, which is slightly low, with an intercept appropriate to the depth measured in profile 31. The apparent velocities measured here are 4.1, 5.0, 6.8, and 8.0 km/sec. The velocity in the unconsolidated sediments was assumed to be 2.0 km/sec.

Profile 26 was shot on the slope south of Grand Cayman Island. The water depth varies between 1100 and 1700 fm (2–3.1 km). In each half of the profile the first arrivals can be fitted with a single line which corresponds to a velocity of 6.0 km/sec. Although it is not possible to correlate later arrivals from shot to shot, they are present in some of the seismograms and are suggested in others by the character of the signals. Hence the layer with assumed velocity of 3.8 km/sec has been included in the computations and in the section. Reasonable limits for the velocity in it are 3 to 5 km/sec.

Profile 27 is on the flank of the Cayman ridge, northwest of Little Cayman Island. The water depth was relatively constant at about 1500 fm (2.7 km). Three layers are measured with velocities of 4.8, 6.5, and 7.2 km/sec, and the sediments were assumed to have a velocity of 2.0 km/sec. The 7.2-km/sec layer is drawn on the basis of second arrivals, which are particularly strong in *Vema's* profile.

Profile 31 was shot in the Bartlett deep, starting at *Vema's* receiving position in the abyssal plain and extending slightly onto the slope of the southern wall. Three layers were determined, with velocities of 5.1, 6.2, and 8.2 km/sec. The layer of unconsolidated sediments, assumed velocity 2.0 km/sec, is about twice as thick in the abyssal plain as on the slope where *Wissama* received. Topographic corrections were made by assuming that the first high-velocity layer has the same angle of dip beneath the plain as on the slope. Some inaccuracy in the results can be expected here owing to the uncertainty about corrections for buried topography, but there seems to be little doubt that the crust is thin, probably thinner than in any other place that has been measured to date.

Profiles 32 and 33 were shot across the Oriente deep of the Cayman trough. The receiving position common to both profiles was near the axis of

the deep. The reverse of profile 32 was received between the deep and Jamaica. Profile 33 was unreversed. In the travel-time graph shown for these profiles, topographic corrections have been made using 2600 fm (4.8 km) as the datum level. As usual, the depths and thicknesses have been readjusted for the actual topography for listing in Table 1 and for inclusion in the sections. Velocities of 4.6 and 6.4 km/sec were measured for the first two layers beneath the sediments. The velocity in the upper of these is not well determined, but the presence of a layer having approximately this velocity is indicated. At *Wissama's* end of profile 32 an apparent velocity of 8.1 km/sec was measured, probably representing the mantle. This layer may be indicated in *Vema's* profile by the low, scattered points at the longer ranges, but it could not be positively identified owing to weak and noisy records.

Profile 34 was shot from the eastern end of the Oriente deep to a point on the slope of Cuba about 15 miles south of Santiago. The water depth varied from 3700 fm (6.8 km) in the deep to 1300 fm (2.4 km) on the slope. Velocities of 2.5, 3.0, 4.4, 5.4, 6.4, and 8.0 km/sec were found. The 6.5-km/sec layer is masked but is indicated by a few scattered second arrivals. None of the upper layers is accurately measured, but all are indicated on at least one side of the profile. The discrepancy in reverse points for the high-velocity lines can be explained as the result of drift. During the time required to shoot the profile, both ships were set approximately 10 miles toward the west. The effect in this case would be higher reverse points for *Vema's* profile than for *Wissama's,* as is observed. The depth to the mantle is about 17 km in the Oriente deep and 21 km on the slope at *Wissama's* receiving position. In the abyssal plain, a strong sub-bottom echo was recorded by the echo sounder, the depth varying from 2.5 to 3.0 fms below the bottom. This is presumably the same sub-bottom horizon reported by *Hersey and Rutstein* [1958].

Profile 35 runs southeast from a point near Navassa Island. The water depth varied between 500 and 1600 fm (0.9–2.9 km) over the length of the profile. The measured velocities are 3.4, 5.4, and 6.5 km/sec, and a velocity of 2.2 km/sec was assumed for the upper sediments. The 5.4-km/sec layer is determined principally in the *Vema* profile. The longest shots of the *Vema* profile indicate a break into a high velocity assumed to be the mantle, but the velocity cannot be determined from the present data. With the support of more recent measurements in this area (Hennion and Ewing, in preparation) a velocity of 8.2 km/sec is taken for the mantle, and the depth to it is computed to be about 21 km.

Profile 36 was shot west to east just south of Haiti and west of the Beata ridge. The first 30 miles of the profile crossed a 2350-fm (4.3-km) abyssal plain. The last 23 miles was shot over hills with the minimum depth occurring at *Wissama's* receiving position, where the depth was approximately 1800 fm (3.3 km). Five layers were measured with velocities of 2.0, 3.6, 4.9, 6.1, and 7.8 km/sec. The uncorrected travel times showed that the abyssal plain had about 0.8 km of sediment, as compared with about 0.2 km at the receiving position in the hills. Therefore, in addition to the usual topographic corrections, the points were further corrected to allow for the variation in thickness of the sediments. The corrected points are shown in the travel-time graph. The thicknesses listed in Table 1 are adjusted to take the topography into account and are true values. Over most of the abyssal plain a strong sub-bottom horizon was recorded by the echo sounder, the depth varying from approximately 3 to 4 fm below the bottom.

Profile 37 is approximately 45 miles south of Ciudad Trujillo, Dominican Republic. Reasonably good lines in both profiles determine layers with velocities of 2.8 and 6.4 km/sec. The velocity in the unconsolidated sediments was assumed to be 2.0 km/sec. On the strength of its being found in other stations in the area, a layer with velocity of 4.4 km/sec is assumed to be present here. There is some second-arrival evidence for the layer, but at the range where first arrival from it would appear, the *Vema* profile had no shots and the *Wissama* profile had very weak records.

Vema-1, Atlantis-185

Profiles 10 and 11 are end-to-end in the Yucatan basin south of the Isle of Pines. The first 20 miles at the eastern end of the combined profile crossed hills; the remainder crossed an abyssal plain where the water depth increased smoothly from 2320 fm (4.2 km) in the east to 2460 fm (4.5 km) at the western end of the profile. The low-velocity sediments are approximately 1 km thick at the receiving position. If this thickness is approximately constant over the entire length of the profile, the travel-time graph shown is correct and indicates a break from crust to mantle velocity at a range of 25 to 30 seconds of water wave time. It is quite possible, however, that the sediments are appreciably thinner on the hills than on the plain. This would require extra positive topographic correction for the travel times on the shots at the eastern end of the profile, and the computations for this case would give a greater depth to the mantle. Therefore, the value given here (13.5 km) can probably be considered a minimum.

Profile 12 is an unreversed profile north of the Yucatan Channel. The apparent velocities of 4.4 and 5.5 km/sec indicated by first-arrival lines are probably reasonably accurate, because topographic corrections were applied for a horizontal datum plane. The second-arrival line corresponding to a velocity of 6.7 km/sec gives only approximate results at best.

Profile 13 for the *Atlantis* profile is weak, but the velocities determined are in reasonably good agreement with those from other profiles in this general area.

Reversed profile 14 is end to end with unre-

versed profile 15. Profiles 16 and 17 are similarly arranged. This gives good control of the data. The profiles were shot on the eastern edge and on top of Campeche Bank. Agreement of the results at the two sites is good except for the deepest layer. Profiles 14 and 15 give 6.4 km/sec as compared with 5.7 km/sec at 16 and 17. This difference in velocity is tentatively interpreted as indicating different materials (see Fig. 2). Many more measurements are needed in this area.

Profiles 18 to 24 are all in the main basin of the Gulf of Mexico. Owing to their approximate end-to-end arrangement, they provide mutual support and reasonably good control over the data across the basin. Most of the profiles provide good measurements of the main crustal layer (6.9 km/sec) and of the layer above it. The upper layers are well determined in some profiles, poorly determined or assumed in others. None of the profiles by itself provides a good measurement of the mantle, but the combined data from profiles 19–24 gives reasonably reliable results. The steep southward dip of the M discontinuity along profile 19 is not precisely determined, but from the mantle depth found at profiles 21 and 22 and the limitations imposed by the recorded arrivals in profile 19 it is difficult to arrive at a significantly different result. The continuation of the dip of the M discontinuity under profile 18 is based on the assumption that the true velocities in the crust and in the mantle are the same as in profile 19.

Profiles 25, 26, and 27 are a set consisting of reversed profile 26 with unreversed legs at each end. Profile 26 runs N-S and is approximately centered on the Sigsbee escarpment. Profile 25 extends southward into the Sigsbee deep, and profile 27 runs westward, parallel to the topographic contours. Owing to the great structural changes associated with the escarpment, the interpretation of the travel-time data for profile 26 is complicated and uncertain. However, the structure south of the escarpment is well determined by profiles 24 and 25, and that north of the escarpment is reasonably well determined by end-to-end profiles 26 and 27. These three profiles indicate that the structure associated with the escarpment is a large fault or flexure in the deeper layers, considerably covered over by the overlying sedimentary layers. The configuration can be determined only roughly for obvious reasons. In addition to ordinary complications arising from shooting a profile across a major structural feature, the problem is made even worse here because *Atlantis* drifted partially across the escarpment during receiving. All the arrivals are plotted on the travel-time graph. The reader is invited to make his own interpretation if the one shown is objectionable.

Profile 28 is on the continental slope north of the Sigsbee escarpment. Although the profile is relatively long, ground wave arrivals could not be recorded beyond a range of 15 to 18 miles. This may have been partially due to equipment trouble, but unusually high attenuation appears to have been a definite factor as well. In a preliminary report on this work [*Ewing, Worzel, Ericson, and Heezen*, 1955] the high attenuation in the 5.3-km/sec layer was tentatively interpreted as indicating that the layer was thin and underlain by more low-velocity sediments. In the interpretation that the 5.3-km/sec velocity is associated with a large tectonic ridge, the high attenuation would probably have to be attributed to scattering and absorption resulting from complex structure and inhomogeneities.

Profiles 29 and 30 were shot in the neighborhood of the 100-fm contour. The topography in profile 29 did not show any major features, although the refracted waves in the *Atlantis* profile indicate a rise of a moderately high velocity material to the approximate level of the sea floor. The shot line for profile 30 was slightly farther north and crossed a reef-like feature near the location of the offset in profile 29. This is undoubtedly one of the submarine mounds common in this area, possibly a salt dome [*Atwater*, 1959]. The mound is wider than is indicated by the topographic section shown for profile 30. This profile did not cross the mound; the longest shot was fired near the edge on a slightly different azimuth, not on the far side of the mound.

Profiles 31 to 34 are unreversed profiles shot in various directions on the continental shelf. Owing to the questionable quality of the data obtained from any one of them, a computation was made using average slopes and intercepts from all to give a rough approximation of thicknesses and velocities in the general area.

References

Atwater, G. I., Geology and petroleum development of the continental shelf of the Gulf of Mexico, *World Petrol. Congr. Proc., 5th Congr.* 1959.

Bucher, W. H., Geologic structure and orogenic history of Venezuela, *Geol. Soc. Am. Mem. 49*, 1952.

Colle, Jack, W. F. Cooke, R. L. Denham, H. C. Ferguson, J. H. McGuirt, Frank Rudy, and Paul Weaver, Sedimentary volumes in Gulf Coastal Plain of United States, 4, Volume of Mesozoic and Cenezoic sediments in Western Gulf Coastal Plain of United States, *Bull. Geol. Soc. Am. 63*, 1193–1200, 1953.

Eardley, A. J., Tectonic relations of North and South America, *Bull. Am. Assoc. Petrol. Geologists, 38*, 707–773, 1954.

Ewing, J., and M. Ewing, Seismic refraction measurements in the Scotia Sea and South Sandwich Islands arc, in *Preprints Intern. Oceanog. Congr.*, edited by M. Sears., Am. Assoc. Advance. Sci., Washington, D. C., 22–23, 1959.

Ewing, J. I., C. B. Officer, H. R. Johnson, and R. S. Edwards, Geophysical investigations in the eastern Caribbean–Trinidad shelf, Tobago trough, Barbados ridge, Atlantic Ocean, *Bull. Geol. Soc. Am., 68*, 897–912, 1957.

Ewing, M., D. B. Ericson, and B. C. Heezen, Sediments and topography of the Gulf of Mexico, in

Iabitat of Oil, Am. Assoc. Petrol. Geologists, ulsa, Okla., 995–1053, 1958.

ing, M., and B. C. Heezen, Puerto Rico trench opographic and geophysical data, in *Crust of he Earth,* edited by A. Poldevaart, *Geol. Soc. Am. Spec. Paper, 62,* 255–267, 1955.

ing, M., and J. L. Worzel, Gravity anomalies nd structure of the West Indies, 1 and 2, *Bull. Geol. Soc. Am., 65,* 165–174 and 195–200, 1954.

ing, M., J. L. Worzel, D. B. Ericson, and B. C. Heezen, Geophysical and geological investigaions in the Gulf of Mexico, 1, *Geophysics, 20,* –18, 1955.

ing, M., J. L. Worzel, and G. L. Shurbet, Gravty observations at sea in U. S. submarines Barracuda, Tusk, Conger, Argonaut, and Medegal; *Verhandel. Ned. Geol. Mijnbouwk. Genoot., Geol. Ser. 18,* 49–96, 1957.

rsey, J. B., and M. S. Rutstein, Reconnaissance urvey of the Oriente deep (Caribbean Sea) vith a precision echo sounder, *Bull. Geol. Soc. Am., 69,* 1297–1304, 1958.

ss, H. H., and J. C. Maxwell, Caribbean research project, *Bull. Geol. Soc. Am., 64,* 1–6, 953.

ng, P. B., *The Evolution of North America,* Princeton Univ. Press, Princeton, N. J., 1959.

ller, E. T., and M. Ewing, Geomagnetic measurements in the Gulf of Mexico and in the vicinty of Caryn Peak, *Geophysics, 21,* 406–432, 1956.

ficer, C. B., J. I. Ewing, R. S. Edwards, and H. R. Johnson, Geophysical investigations in the eastern Caribbean: Venezuelan basin, Antilles Island arc, and Puerto Rico trench, *Bull. Geol. Soc. Am., 63,* 359–378, 1957.

Officer, C. B., J. I. Ewing, J. F. Hennion, D. G. Harkrider, and D. E. Miller, Geophysical investigations in the eastern Caribbean: Summary of 1955 and 1956 cruises, *Physics and Chemistry of the Earth,* vol. 3, Pergamon Press, 17–109, 1959.

Raitt, R. W., R. L. Fisher, and R. G. Mason, Tonga Trench, in *Crust of the Earth,* edited by A. Poldevaart, *Geol. Soc. Am. Spec. Paper 62,* 237–254, 1955.

Talwani, M., G. H. Sutton, and J. L. Worzel, A crustal section across the Puerto Rico trench, *J. Geophys. Research, 64,* 1545–1555, 1959.

Vestine, E. H., L. Laporte, I. Lange, and W. E. Scott. The geomagnetic field, its description and analysis, *Carnegie Inst. Wash., Publ. 580,* 1947.

Woodring, W. P., Caribbean land and sea through the ages, *Bull. Geol. Soc. Am., 65,* 719–732, 1954.

Worzel, J. L., and M. Ewing, Explosion sounds in shallow water, *Geol. Soc. Am., Mem. 27,* 1–53, 1948.

Worzel, J. L., and G. L. Shurbet, Gravity interpretations from standard oceanic and continental crustal sections, *Bull. Geol. Soc. Am., 62,* 87–100, 1955.

(Manuscript received May 31, 1960; revised October 1, 1960.)

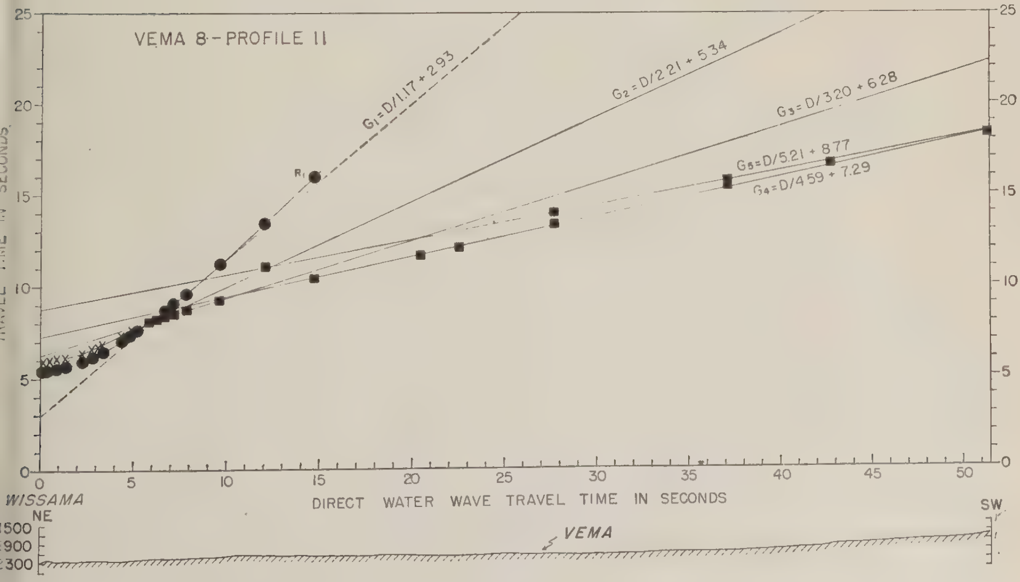

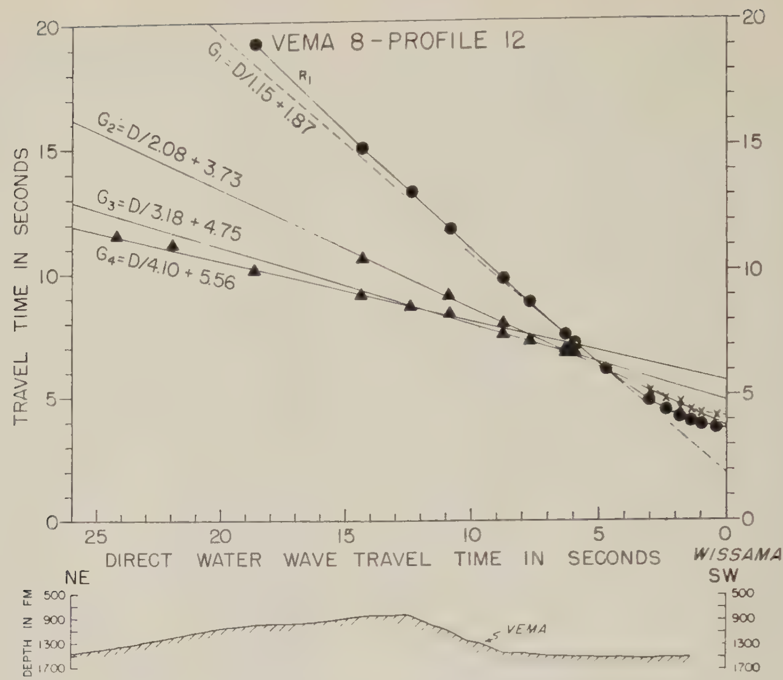
VEMA 8-PROFILE 12
$G_1 = D/1.15 + 1.87$
R_1
$G_2 = D/2.08 + 3.73$
$G_3 = D/3.18 + 4.75$
$G_4 = D/4.10 + 5.56$
TRAVEL TIME IN SECONDS
DIRECT WATER WAVE TRAVEL TIME IN SECONDS
NE
SW
WISSAMA
DEPTH IN FM
VEMA

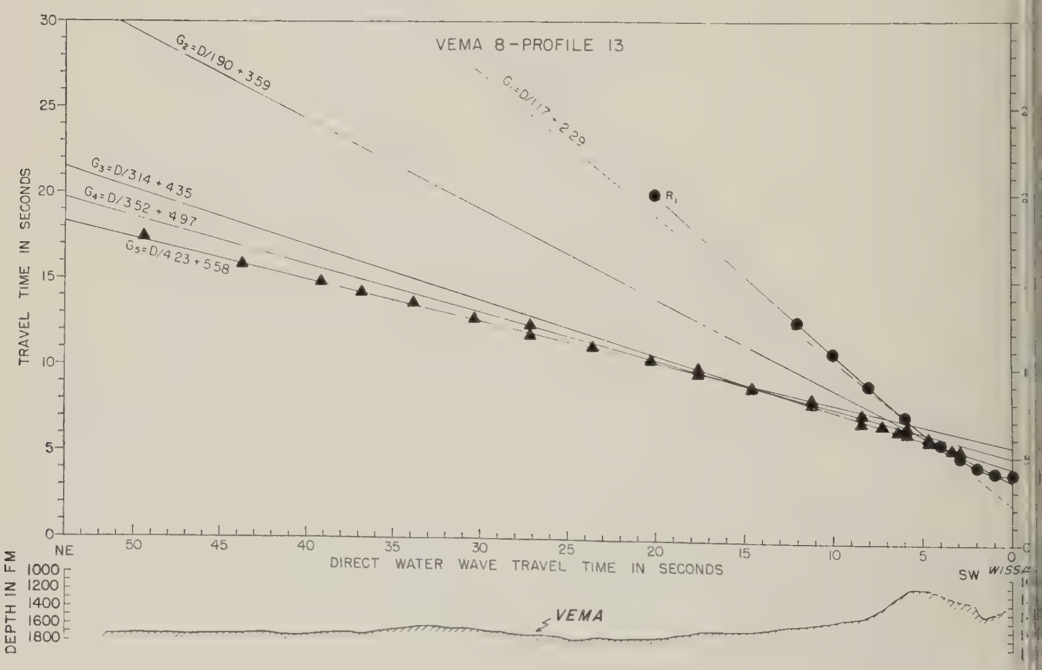
VEMA 8-PROFILE 13
$G_2 = D/1.90 + 3.59$
$G_1 = D/1.17 + 2.29$
R_1
$G_3 = D/3.14 + 4.35$
$G_4 = D/3.52 + 4.97$
$G_5 = D/4.23 + 5.58$
TRAVEL TIME IN SECONDS
DIRECT WATER WAVE TRAVEL TIME IN SECONDS
NE
SW
DEPTH IN FM
VEMA

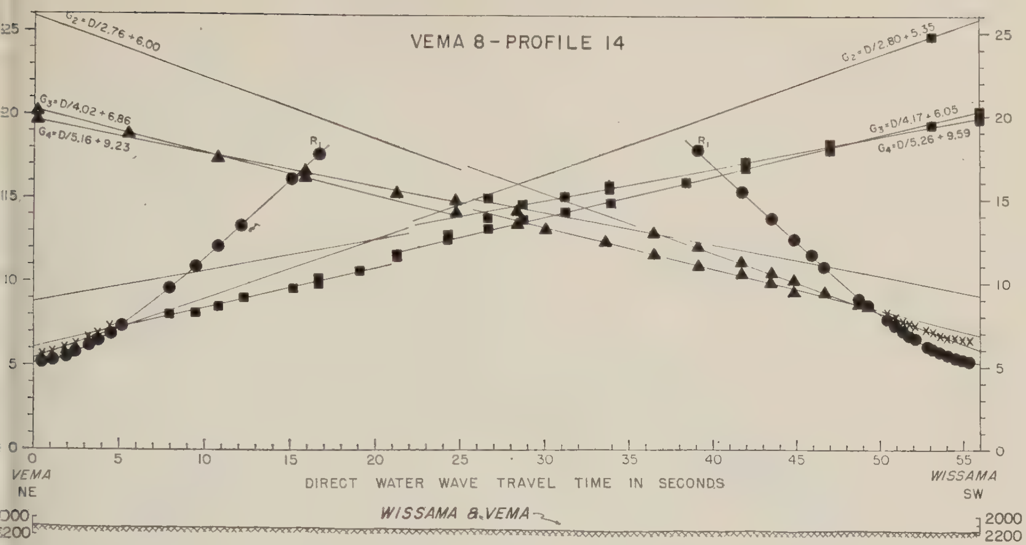
VEMA 8 - PROFILE 14
$G_2 = D/2.76 + 6.00$
$G_3 = D/4.02 + 6.86$
$G_4 = D/5.16 + 9.23$
$G_2 = D/2.80 + 5.35$
$G_3 = D/4.17 + 6.05$
$G_4 = D/5.26 + 9.59$
R_1
VEMA
NE
DIRECT WATER WAVE TRAVEL TIME IN SECONDS
WISSAMA
SW
WISSAMA & VEMA
2000
2200

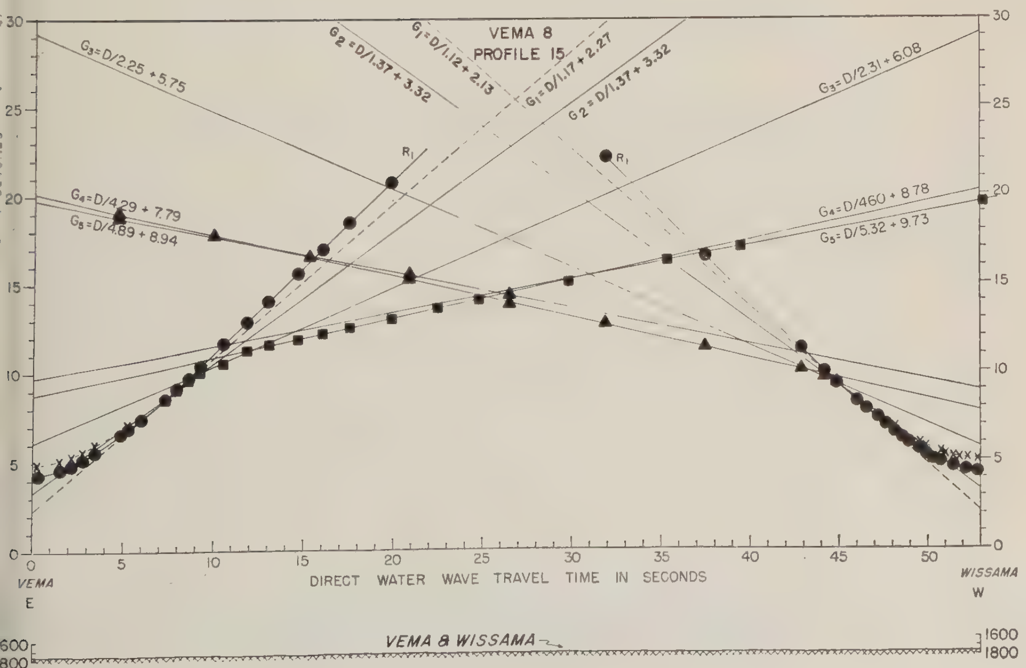
VEMA 8
PROFILE 15
$G_3 = D/2.25 + 5.75$
$G_2 = D/1.37 + 3.32$
$G_1 = D/1.12 + 2.13$
$G_1 = D/1.17 + 2.27$
$G_2 = D/1.37 + 3.32$
$G_3 = D/2.31 + 6.08$
$G_4 = D/4.29 + 7.79$
$G_5 = D/4.89 + 8.94$
$G_4 = D/460 + 8.78$
$G_5 = D/5.32 + 9.73$
R_1
VEMA
E
DIRECT WATER WAVE TRAVEL TIME IN SECONDS
WISSAMA
W
VEMA & WISSAMA
1600
1800

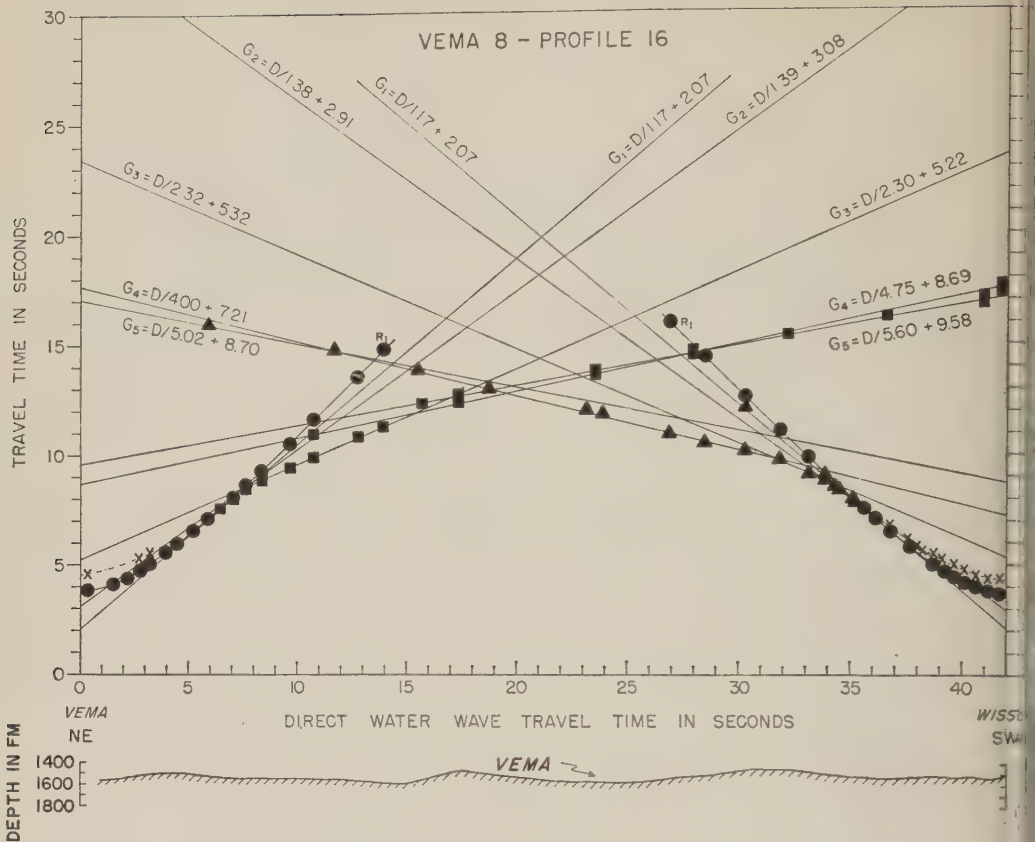
VEMA 8 - PROFILE 16
G2=D/1.38+2.91
G1=D/1.17+2.07
G1=D/1.17+2.07
G2=D/1.39+3.08
G3=D/2.32+5.32
G3=D/2.30+5.22
G4=D/4.00+7.21
G5=D/5.02+8.70
G4=D/4.75+8.69
G5=D/5.60+9.58
R1
TRAVEL TIME IN SECONDS
DIRECT WATER WAVE TRAVEL TIME IN SECONDS
VEMA
NE
DEPTH IN FM
1400
1600
1800

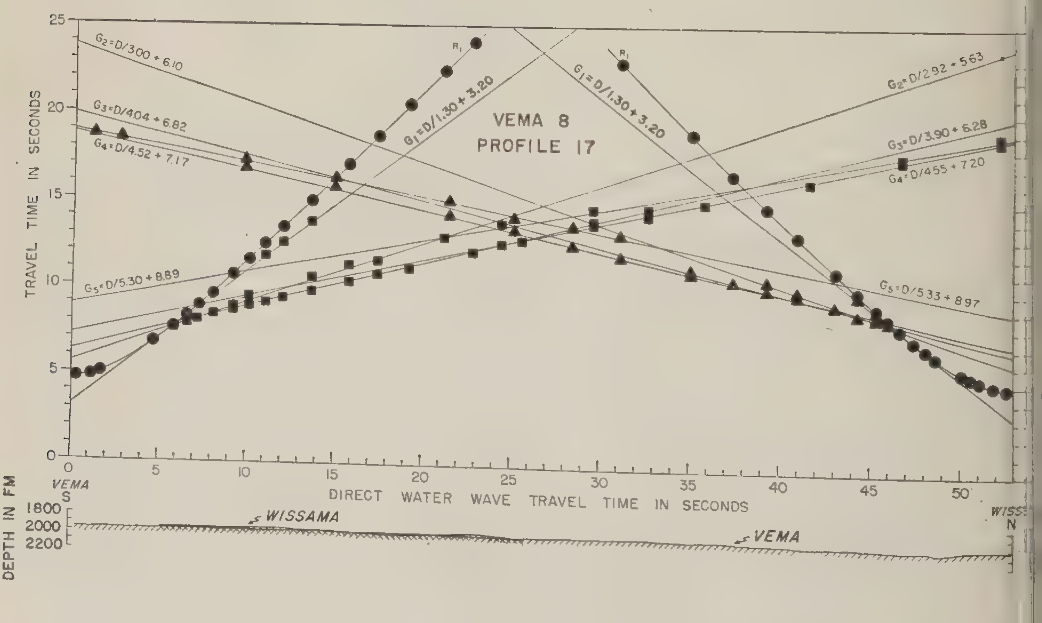
VEMA 8
PROFILE 17
G2=D/3.00+6.10
G3=D/4.04+6.82
G4=D/4.52+7.17
G5=D/5.30+8.89
G1=D/1.30+3.20
G1=D/1.30+3.20
G2=D/2.92+5.63
G3=D/3.90+6.28
G4=D/4.55+7.20
G5=D/5.33+8.97
R1
TRAVEL TIME IN SECONDS
DIRECT WATER WAVE TRAVEL TIME IN SECONDS
VEMA
S
N
WISSAMA
DEPTH IN FM
1800
2000
2200

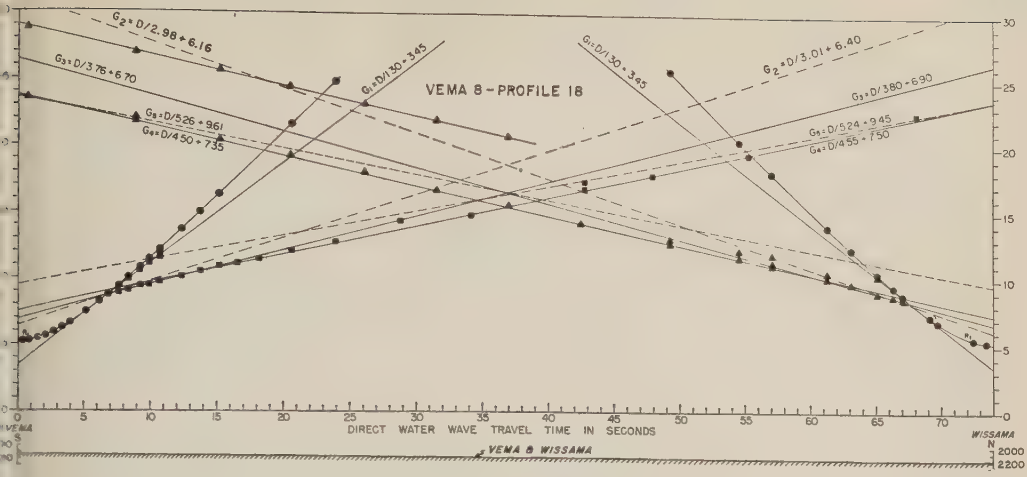
VEMA 8 - PROFILE 18
G2=D/2.98+6.16
G3=D/3.76+6.70
G5=D/5.26+9.61
G4=D/4.50+7.35
G1=D/1.30-3.45
G1=D/1.30+3.45
G2=D/3.01+6.40
G3=D/3.80-6.90
G5=D/5.24+9.45
G4=D/4.55+7.50
DIRECT WATER WAVE TRAVEL TIME IN SECONDS
VEMA
S
WISSAMA
N
VEMA & WISSAMA
2000
2200

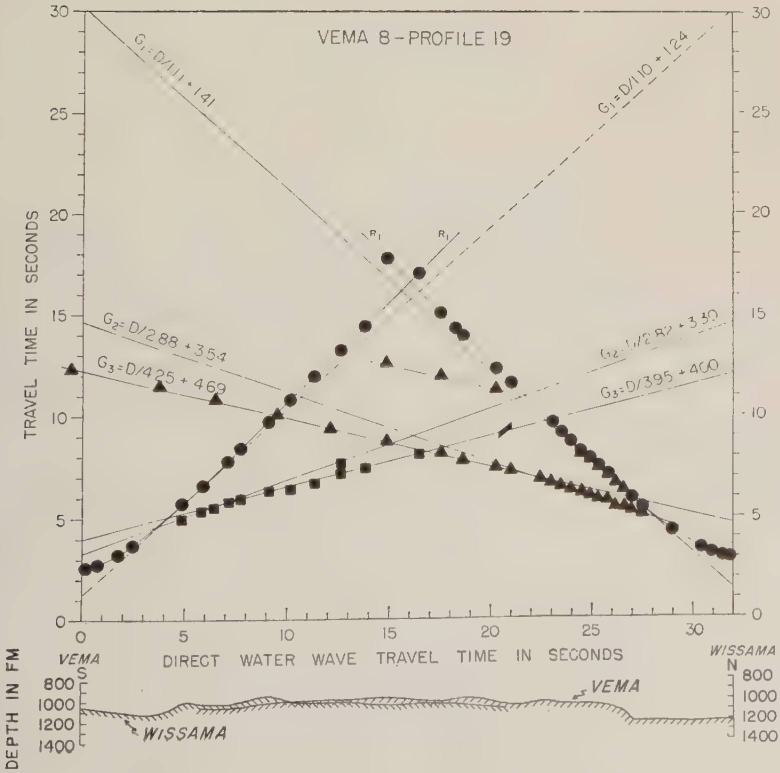
VEMA 8 - PROFILE 19
G1=D/1.11+1.41
G1=D/1.10+1.24
R1
R1
G2=D/2.88+3.54
G3=D/4.25+4.69
G3=D/3.95+4.00
TRAVEL TIME IN SECONDS
DIRECT WATER WAVE TRAVEL TIME IN SECONDS
VEMA
S
WISSAMA
N
VEMA
WISSAMA
DEPTH IN FM
800
1000
1200
1400

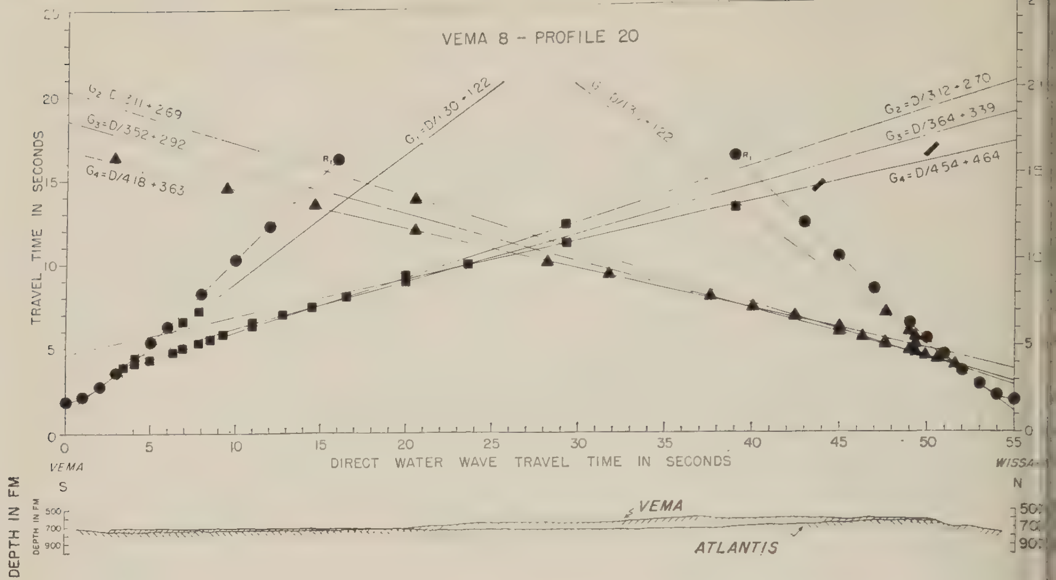
VEMA 8 - PROFILE 20
TRAVEL TIME IN SECONDS
DIRECT WATER WAVE TRAVEL TIME IN SECONDS
$G_3 = D/352 + 292$
$G_4 = D/418 + 363$
$G_2 = D/312 + 270$
$G_3 = D/364 + 339$
$G_4 = D/454 + 464$
R_1
VEMA
WISSAMA
S
N
DEPTH IN FM
VEMA
ATLANTIS

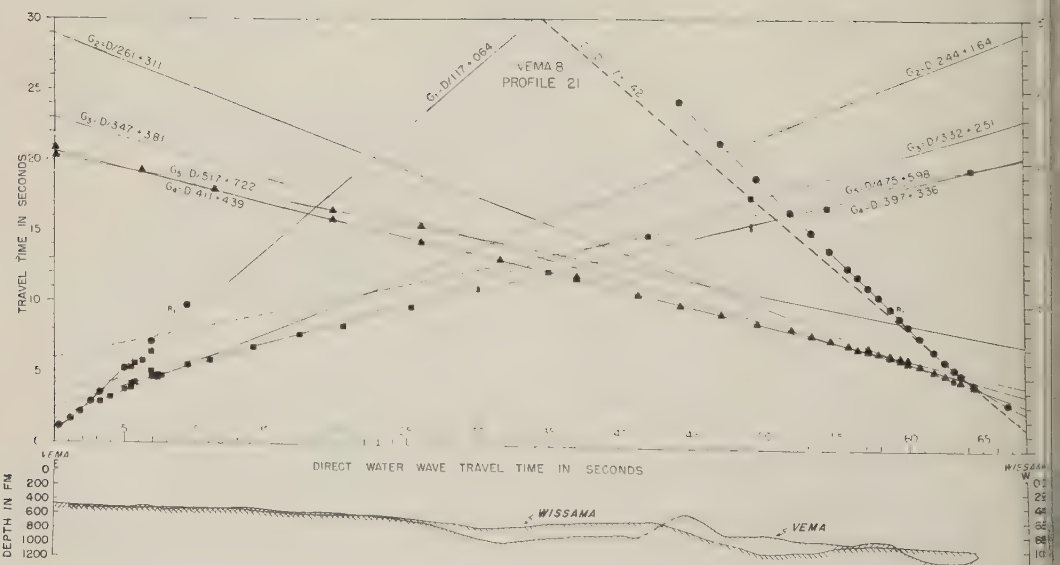
VEMA 8
PROFILE 21
$G_2 = D/261 + 311$
$G_1 = D/117 + 064$
$G_3 = D/347 + 381$
$G_5 = D/517 + 722$
$G_4 = D/411 + 439$
$G_2 = D/244 + 164$
$G_3 = D/332 + 251$
$G_5 = D/475 + 598$
$G_4 = D/397 + 336$
R_1
TRAVEL TIME IN SECONDS
DIRECT WATER WAVE TRAVEL TIME IN SECONDS
VEMA
WISSAMA
W
DEPTH IN FM
WISSAMA
VEMA

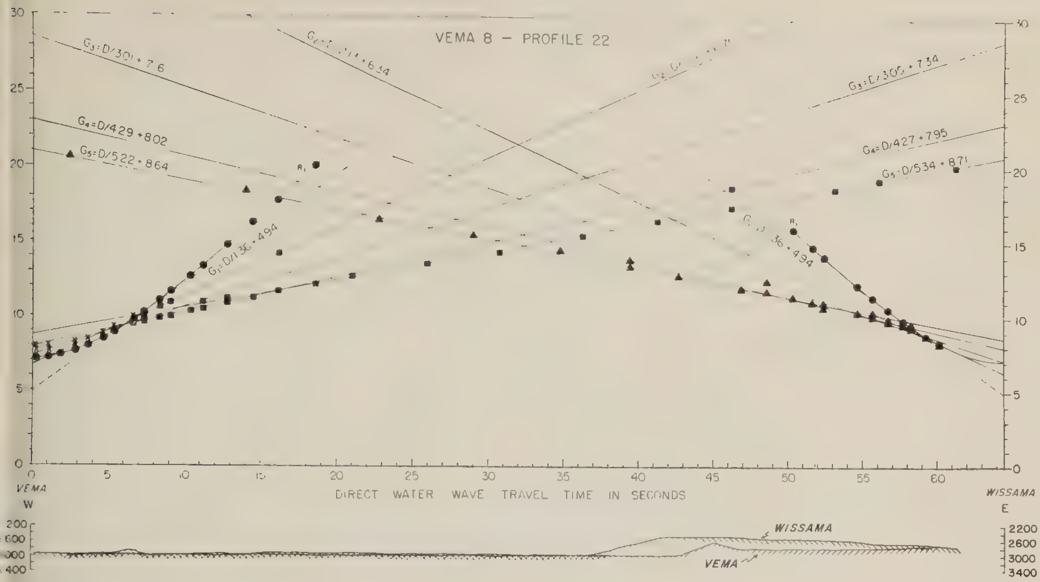
VEMA 8 — PROFILE 22
G_3=D/301+7.6
G_4=D/429+802
G_5=D/522+864
G_1=D/136+494
G_3=D/305+734
G_4=D/427+795
G_5=D/534+871
DIRECT WATER WAVE TRAVEL TIME IN SECONDS
VEMA
W
WISSAMA
E
WISSAMA
VEMA

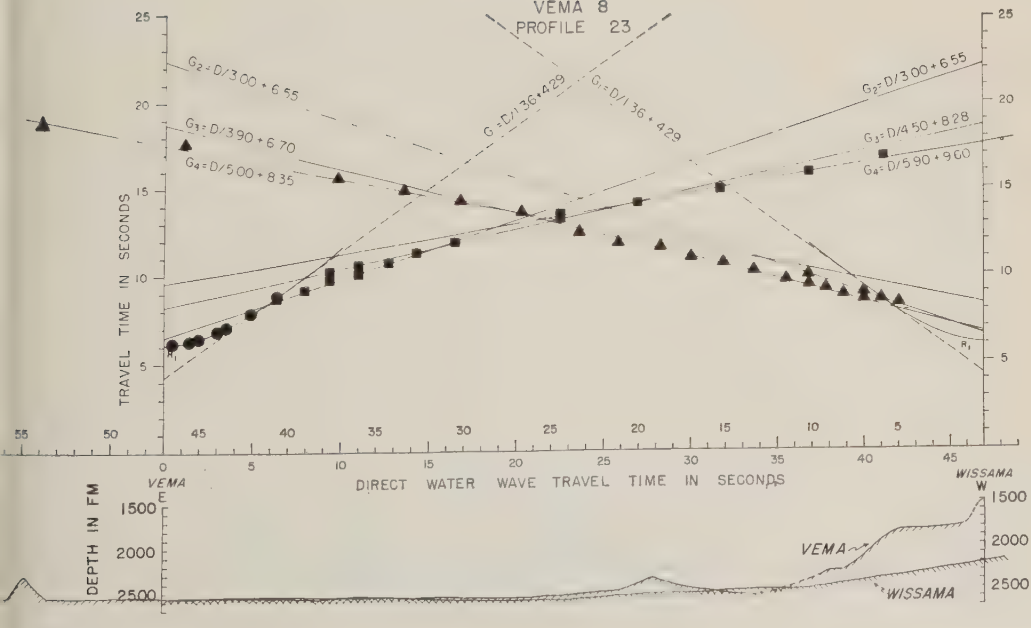
VEMA 8
PROFILE 23
G_2=D/3.00+6.55
G_3=D/3.90+6.70
G_4=D/5.00+8.35
G=D/1.36+4.29
G_1=D/1.36+4.29
G_2=D/3.00+6.55
G_3=D/4.50+8.28
G_4=D/5.90+9.60
TRAVEL TIME IN SECONDS
DIRECT WATER WAVE TRAVEL TIME IN SECONDS
VEMA
E
WISSAMA
W
DEPTH IN FM
VEMA
WISSAMA

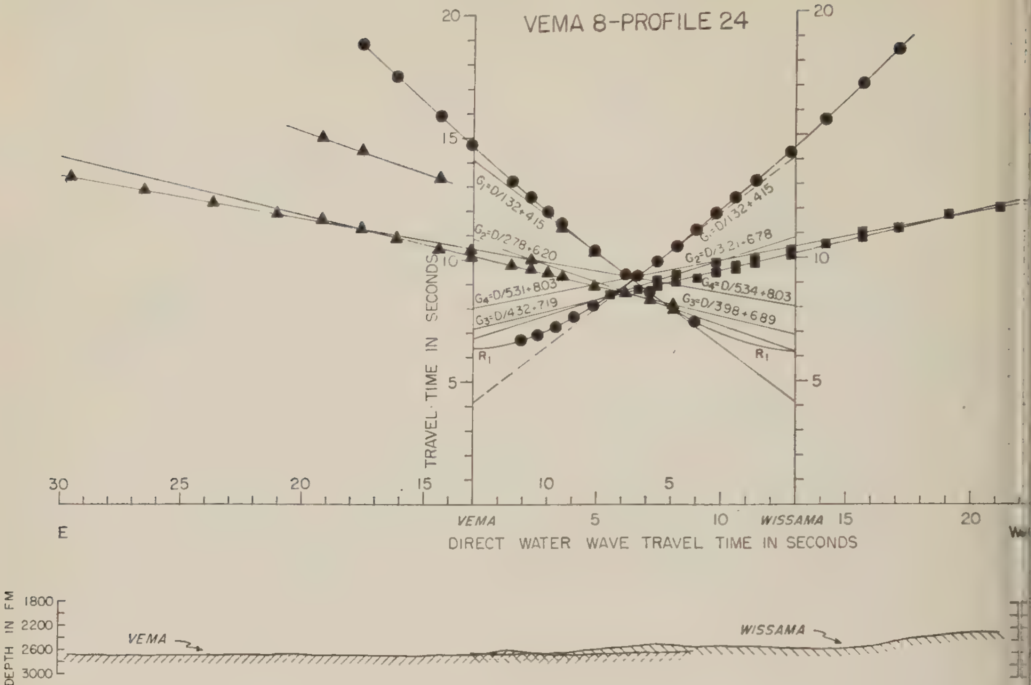
VEMA 8-PROFILE 24
TRAVEL TIME IN SECONDS
$G_1 = D/1.32 + 4.15$
$G_2 = D/2.78 + 6.20$
$G_4 = D/5.31 + 8.03$
$G_3 = D/4.32 + 7.19$
R_1
$G_1 = D/1.32 + 4.15$
$G_2 = D/3.21 + 6.78$
$G_4 = D/5.34 + 8.03$
$G_3 = D/3.98 + 6.89$
R_1
E
VEMA
WISSAMA
DIRECT WATER WAVE TRAVEL TIME IN SECONDS
DEPTH IN FM
VEMA
WISSAMA

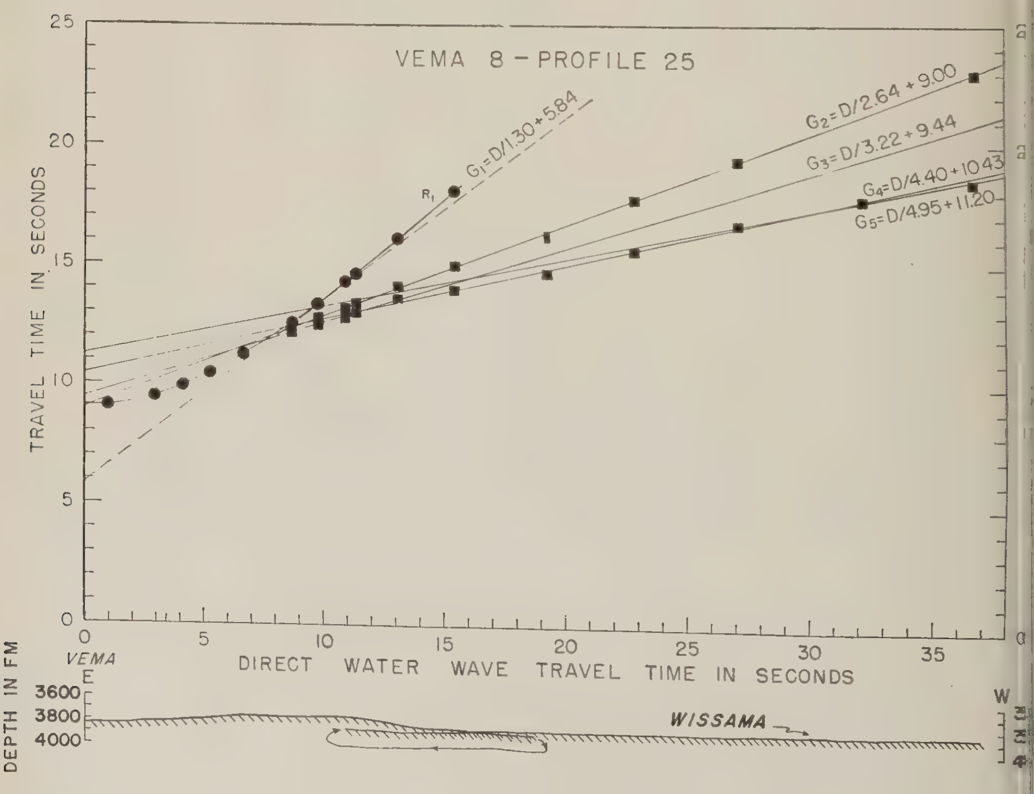
VEMA 8 - PROFILE 25
TRAVEL TIME IN SECONDS
$G_1 = D/1.30 + 5.84$
R_1
$G_2 = D/2.64 + 9.00$
$G_3 = D/3.22 + 9.44$
$G_4 = D/4.40 + 10.43$
$G_5 = D/4.95 + 11.20$
VEMA
E
DIRECT WATER WAVE TRAVEL TIME IN SECONDS
W
DEPTH IN FM
WISSAMA

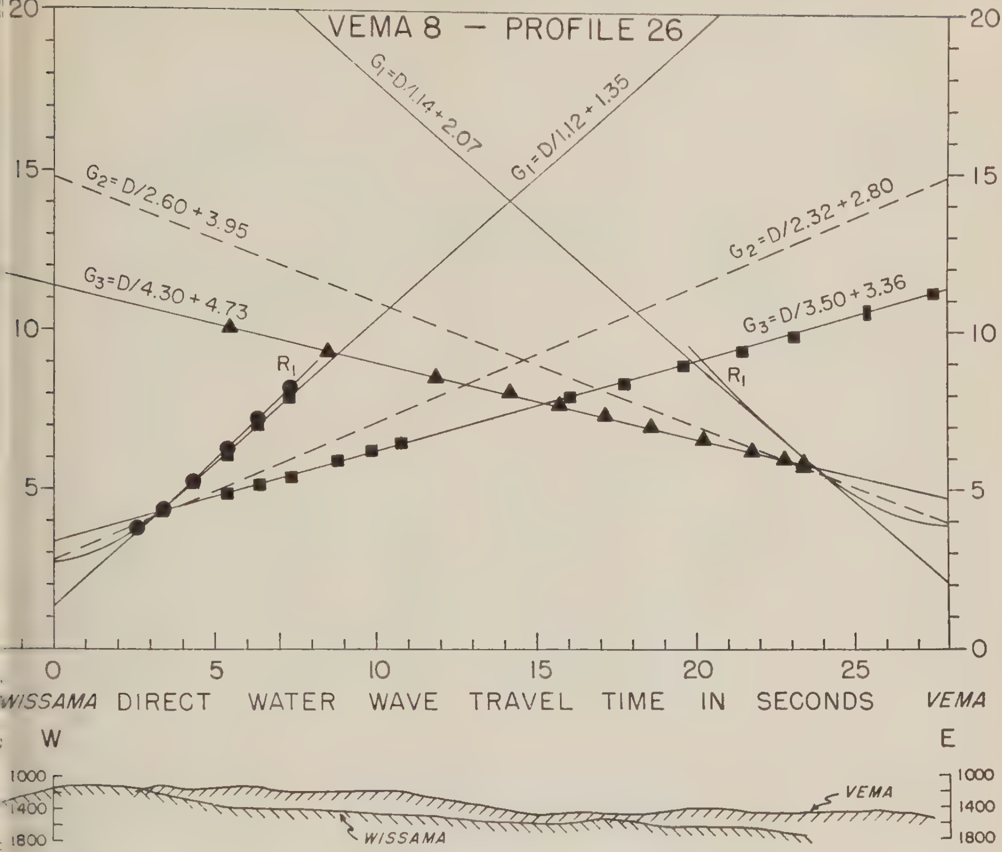
VEMA 8 — PROFILE 26
G1=D/1.14+2.07
G1=D/1.12+1.35
G2=D/2.60+3.95
G2=D/2.32+2.80
G3=D/4.30+4.73
G3=D/3.50+3.36
R1
R1
0
5
10
15
20
25
WISSAMA DIRECT WATER WAVE TRAVEL TIME IN SECONDS VEMA
W
E
1000
1400
1800
VEMA
WISSAMA

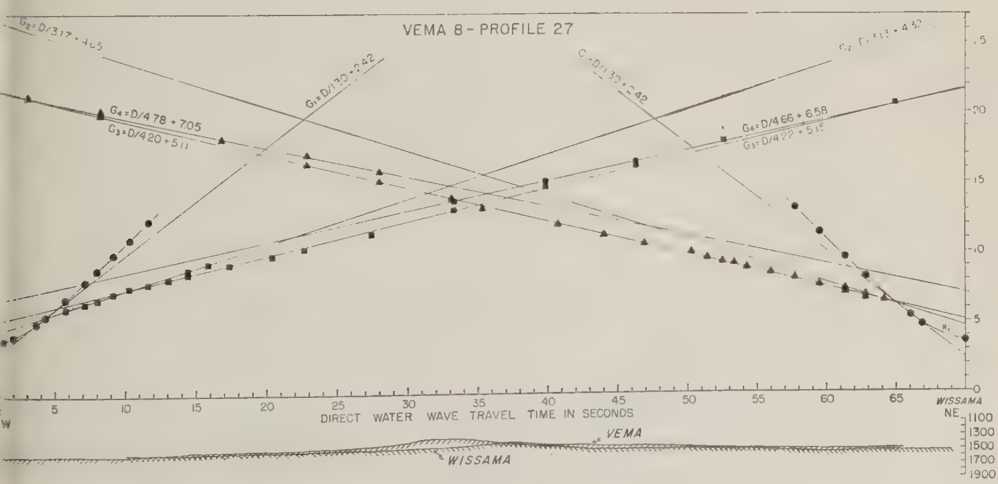
VEMA 8 - PROFILE 27
G4=D/4.78+7.05
G3=D/4.20+5.11
G4=D/4.66+6.58
5
10
15
20
25
30
35
40
45
50
55
60
65
DIRECT WATER WAVE TRAVEL TIME IN SECONDS
WISSAMA
NE
W
1100
1300
1500
1700
1900
VEMA
WISSAMA

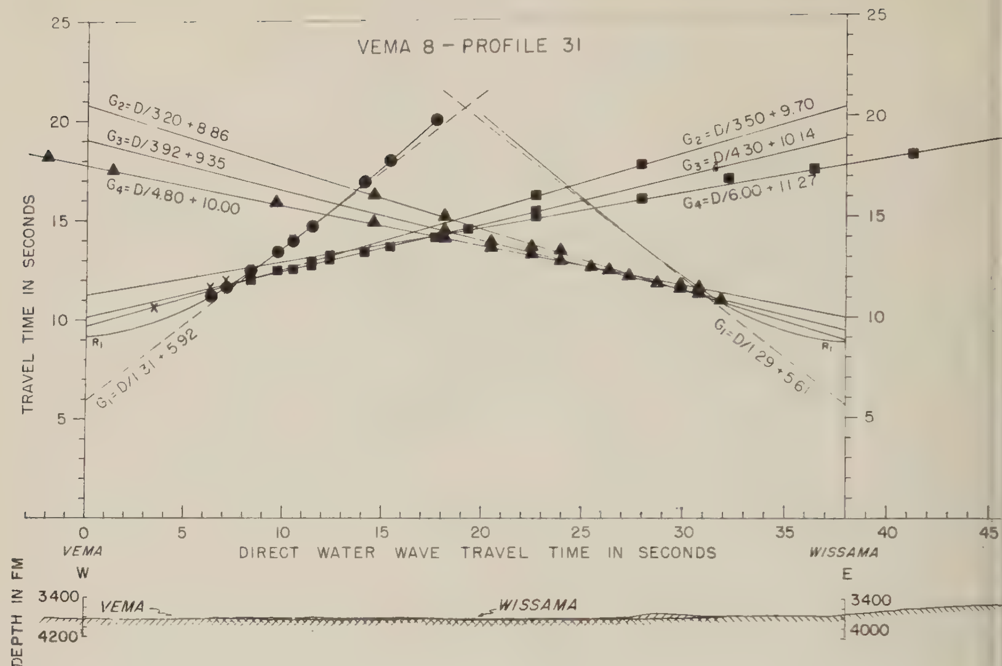
VEMA 8 - PROFILE 31
G2=D/3.20 + 8.86
G3=D/3.92 + 9.35
G4=D/4.80 + 10.00
G2=D/3.50 + 9.70
G3=D/4.30 + 10.14
G4=D/6.00 + 11.27
G1=D/1.31 + 5.92
G1=D/1.29 + 5.61
R1
TRAVEL TIME IN SECONDS
DIRECT WATER WAVE TRAVEL TIME IN SECONDS
VEMA
WISSAMA
W
E
DEPTH IN FM
3400
4200
4000

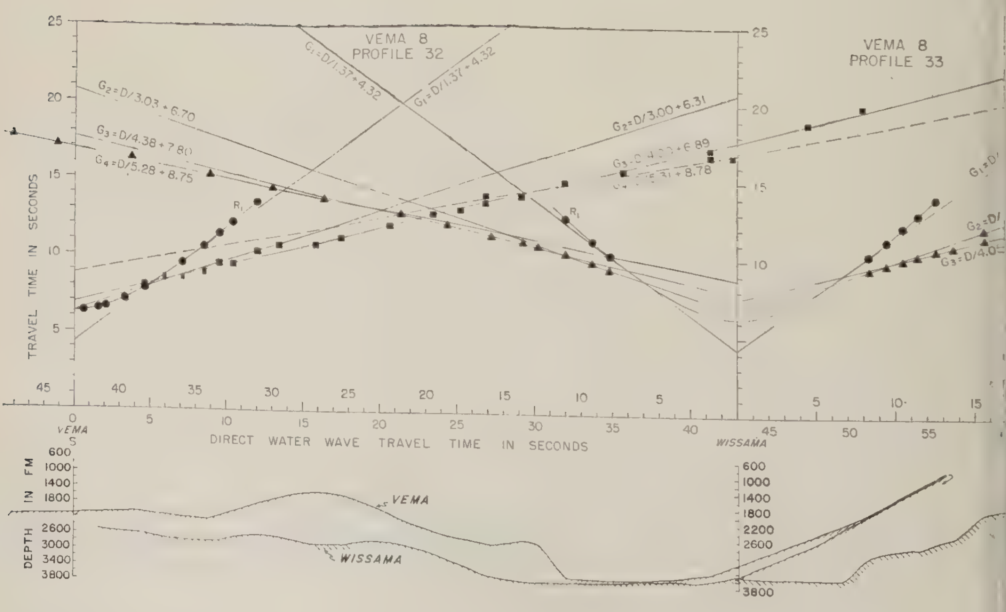
VEMA 8
PROFILE 32
VEMA 8
PROFILE 33
G1=D/1.37+4.32
G2=D/3.03+6.70
G3=D/4.38+7.80
G4=D/5.28+8.75
G2=D/3.00+6.31
R1
TRAVEL TIME IN SECONDS
DIRECT WATER WAVE TRAVEL TIME IN SECONDS
VEMA
WISSAMA
S
DEPTH IN FM

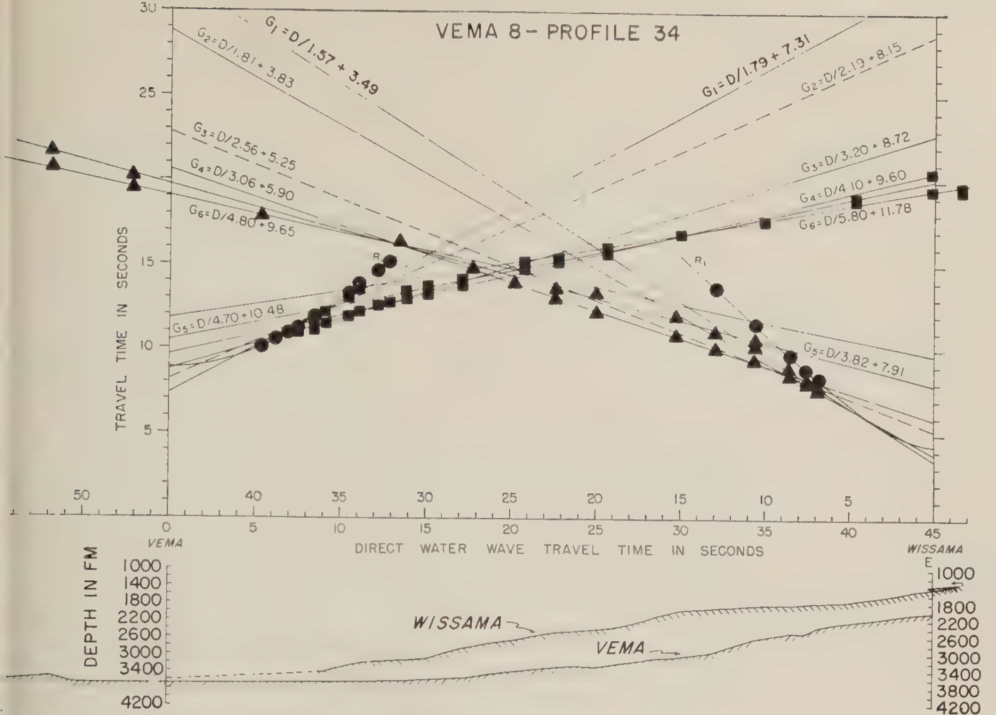
VEMA 8 - PROFILE 34
G1=D/1.57+3.49
G2=D/1.81+3.83
G3=D/2.56+5.25
G4=D/3.06+5.90
G6=D/4.80+9.65
G5=D/4.70+10.48
G1=D/1.79+7.31
G2=D/2.19+8.15
G3=D/3.20+8.72
G4=D/4.10+9.60
G6=D/5.80+11.78
G5=D/3.82+7.91
TRAVEL TIME IN SECONDS
DIRECT WATER WAVE TRAVEL TIME IN SECONDS
VEMA
WISSAMA
E
DEPTH IN FM
WISSAMA
VEMA

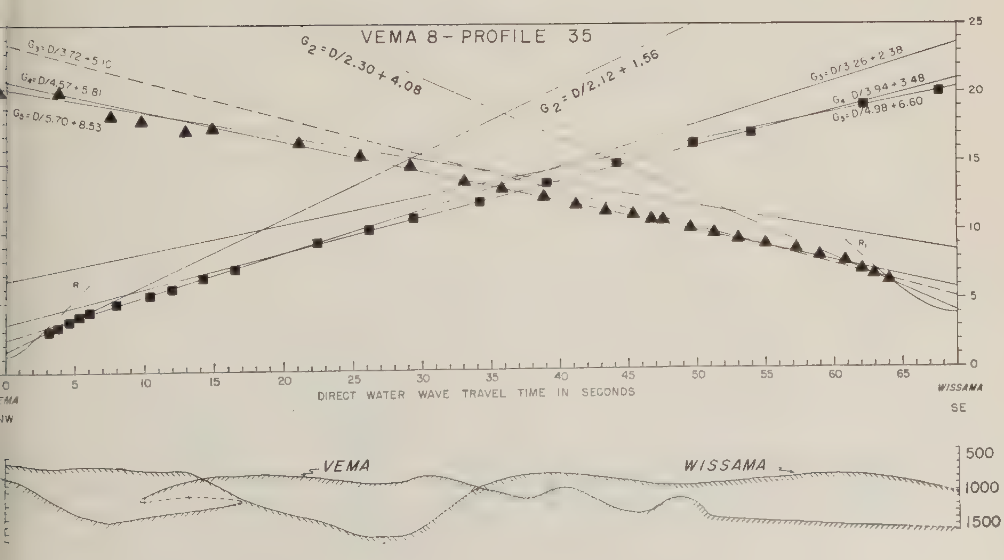
VEMA 8 - PROFILE 35
G3=D/3.72+5.10
G4=D/4.57+5.81
G5=D/5.70+8.53
G2=D/2.30+4.08
G2=D/2.12+1.56
G3=D/3.26+2.38
G4 D/3.94+3.48
G5=D/4.98+6.60
DIRECT WATER WAVE TRAVEL TIME IN SECONDS
WISSAMA
SE
NW
VEMA
WISSAMA

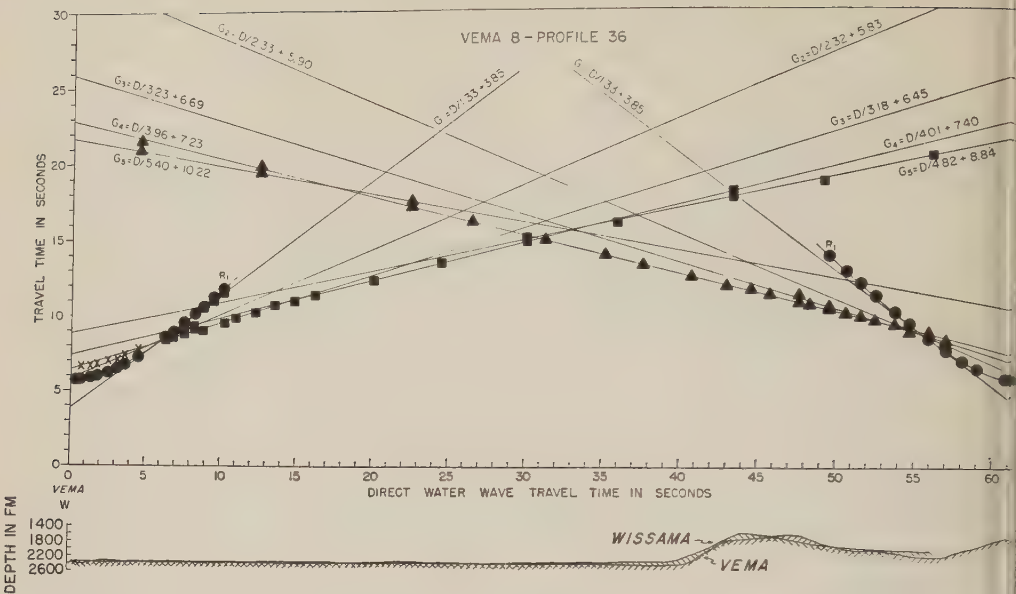
VEMA 8 - PROFILE 36
$G_2 = D/2.33 + 5.90$
$G_3 = D/3.23 + 6.69$
$G_4 = D/3.96 + 7.23$
$G_5 = D/5.40 + 10.22$
$G_1 = D/1.33 + 3.85$
$G_1 = D/1.33 + 3.85$
$G_2 = D/2.32 + 5.83$
$G_3 = D/3.18 + 6.45$
$G_4 = D/4.01 + 7.40$
$G_5 = D/4.82 + 8.84$
R_1
R_1
TRAVEL TIME IN SECONDS
DIRECT WATER WAVE TRAVEL TIME IN SECONDS
VEMA
W
DEPTH IN FM
1400
1800
2200
2600
WISSAMA
VEMA

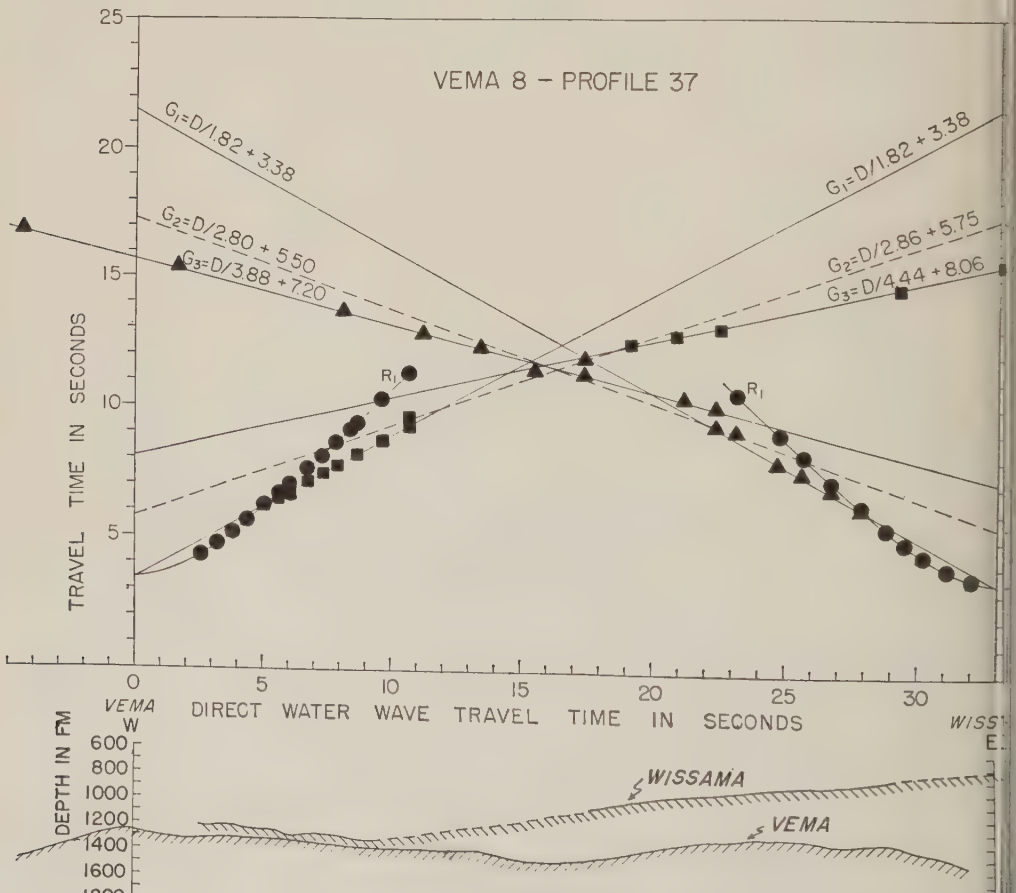
VEMA 8 - PROFILE 37
$G_1 = D/1.82 + 3.38$
$G_2 = D/2.80 + 5.50$
$G_3 = D/3.88 + 7.20$
$G_1 = D/1.82 + 3.38$
$G_2 = D/2.86 + 5.75$
$G_3 = D/4.44 + 8.06$
R_1
R_1
TRAVEL TIME IN SECONDS
DIRECT WATER WAVE TRAVEL TIME IN SECONDS
VEMA
W
DEPTH IN FM
600
800
1000
1200
1400
1600
1800
WISSAMA
VEMA

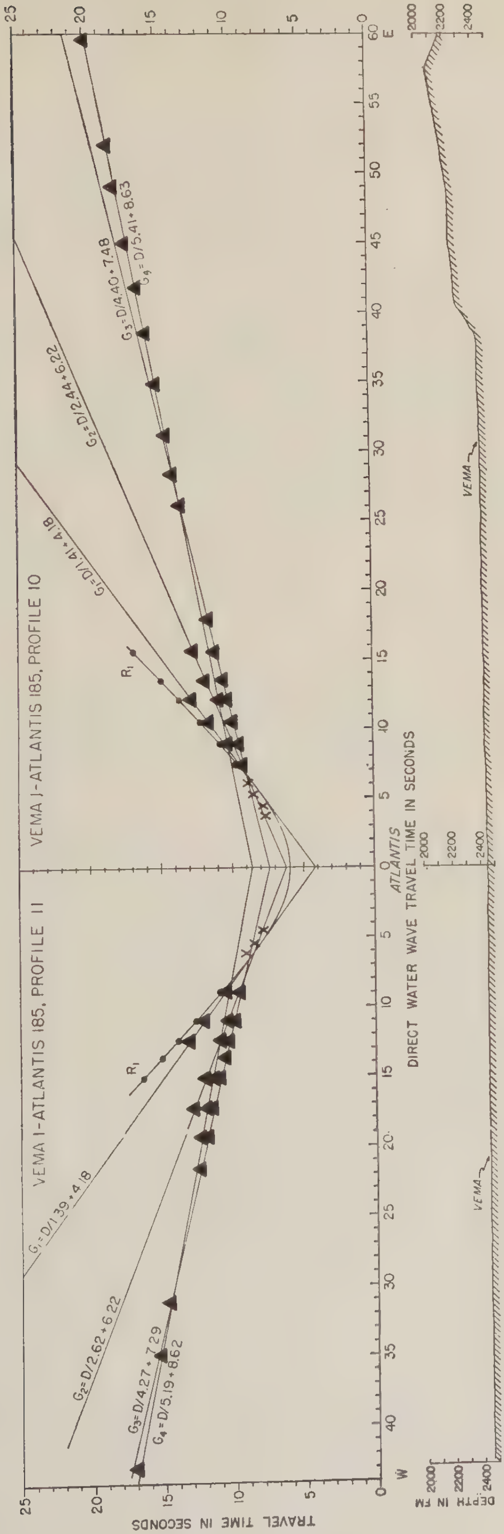
VEMA I-ATLANTIS 185, PROFILE 10
VEMA I-ATLANTIS 185, PROFILE 11
$G_1 = D/1.41 + 4.18$
$G_2 = D/2.44 + 6.22$
$G_3 = D/4.40 + 7.48$
$G_4 = D/5.41 + 8.63$
$G_1 = D/1.39 + 4.18$
$G_2 = D/2.62 + 6.22$
$G_3 = D/4.27 + 7.29$
$G_4 = D/5.19 + 8.62$
R_1
R_1
TRAVEL TIME IN SECONDS
DIRECT WATER WAVE TRAVEL TIME IN SECONDS
ATLANTIS
VEMA
VEMA
W
E
DEPTH IN FM

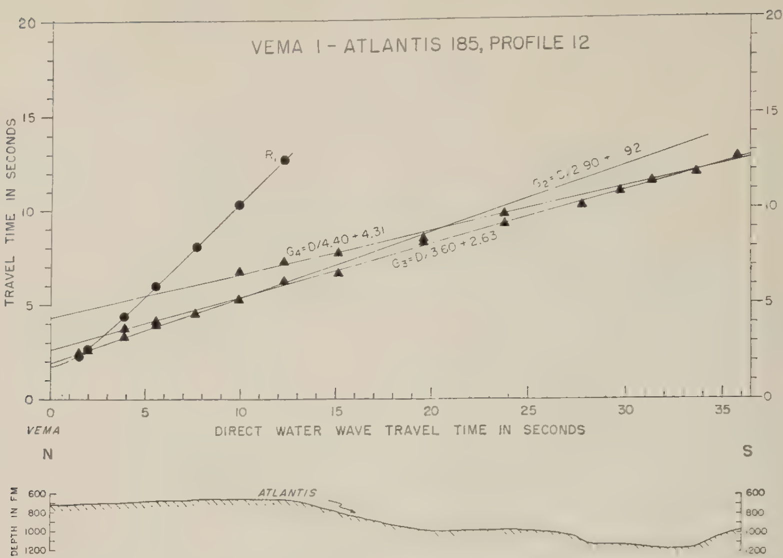
VEMA 1 - ATLANTIS 185, PROFILE 12
TRAVEL TIME IN SECONDS
DIRECT WATER WAVE TRAVEL TIME IN SECONDS
VEMA
N
S
R_1
G_4=D/4.40 + 4.31
G_3=D/3.60 + 2.63
DEPTH IN FM
ATLANTIS

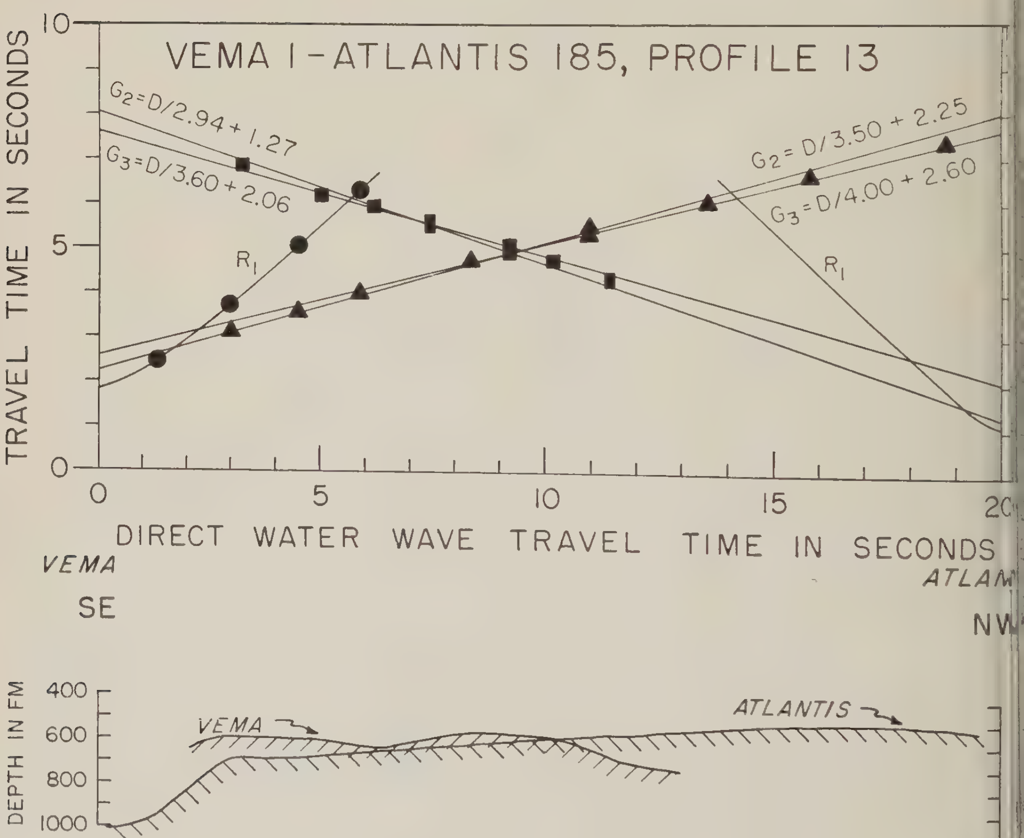
VEMA 1-ATLANTIS 185, PROFILE 13
TRAVEL TIME IN SECONDS
G_2=D/2.94 + 1.27
G_3=D/3.60 + 2.06
G_2 = D/3.50 + 2.25
G_3 = D/4.00 + 2.60
R_1
R_1
DIRECT WATER WAVE TRAVEL TIME IN SECONDS
VEMA
SE
DEPTH IN FM
VEMA
ATLANTIS

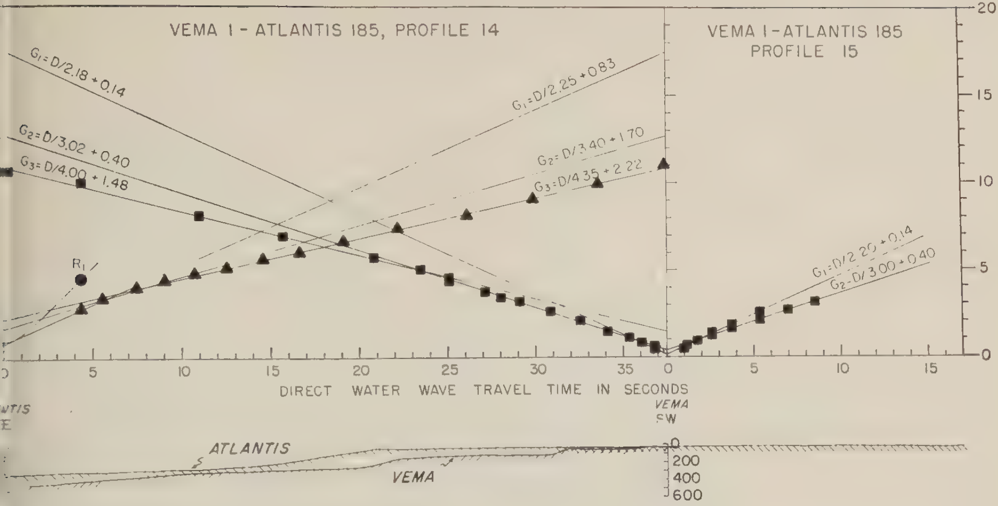
VEMA I - ATLANTIS 185, PROFILE 14
VEMA I-ATLANTIS 185
PROFILE 15
G1=D/2.18+0.14
G2=D/3.02+0.40
G3=D/4.00+1.48
G1=D/2.25+0.83
G2=D/3.40+1.70
G3=D/4.35+2.22
R1
G1=D/2.20+0.14
G2=D/3.00+0.40
DIRECT WATER WAVE TRAVEL TIME IN SECONDS
VEMA
SW
ATLANTIS
VEMA
200
400
600

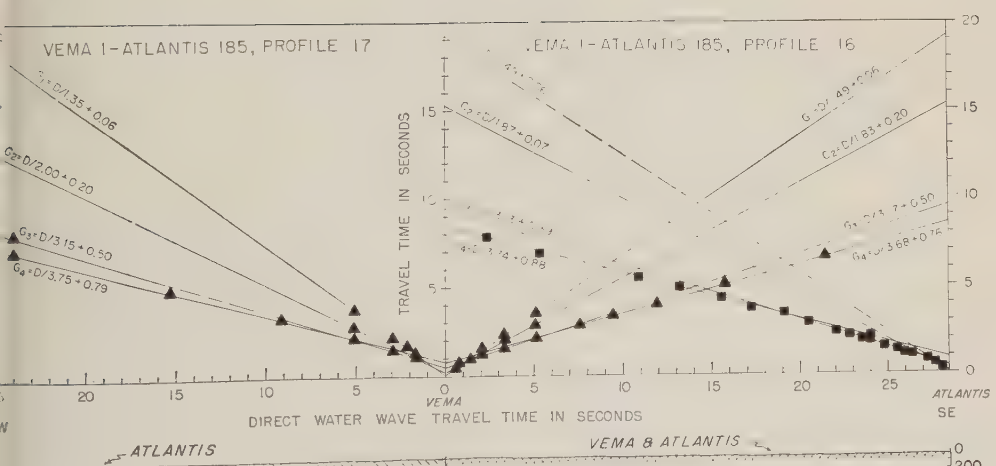
VEMA I-ATLANTIS 185, PROFILE 17
VEMA I-ATLANTIS 185, PROFILE 16
G1=D/1.35+0.06
G2=D/2.00+0.20
G3=D/3.15+0.50
G4=D/3.75+0.79
G2=D/1.87+0.07
G2=D/1.83+0.20
TRAVEL TIME IN SECONDS
DIRECT WATER WAVE TRAVEL TIME IN SECONDS
VEMA
ATLANTIS
SE
ATLANTIS
VEMA & ATLANTIS
200

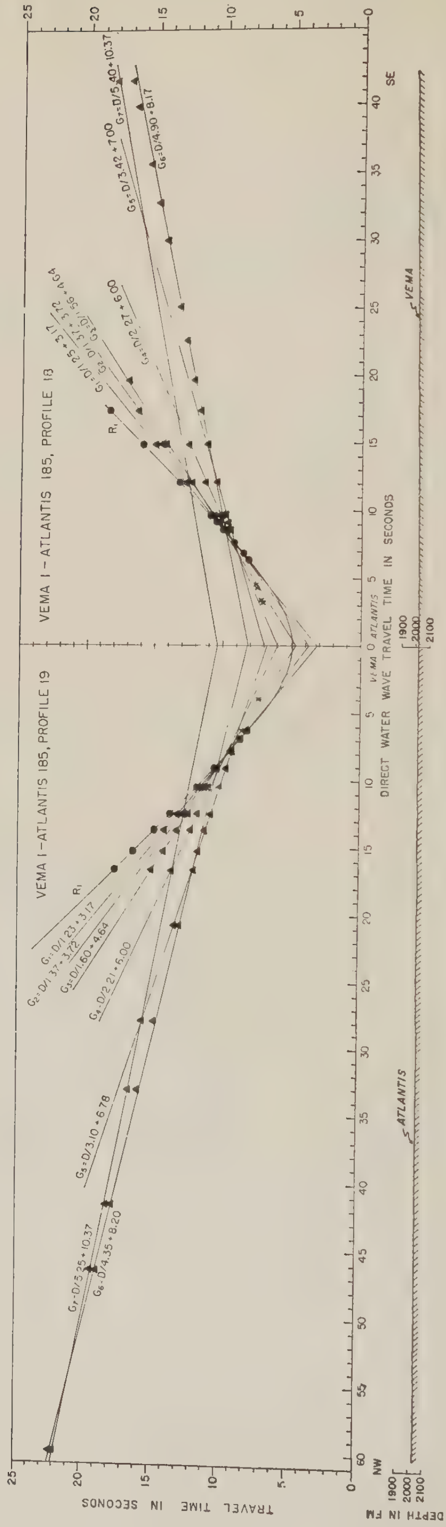
VEMA I - ATLANTIS 185, PROFILE 18
VEMA I-ATLANTIS 185, PROFILE 19
DIRECT WATER WAVE TRAVEL TIME IN SECONDS
TRAVEL TIME IN SECONDS
DEPTH IN FM
NW
SE
VEMA
ATLANTIS

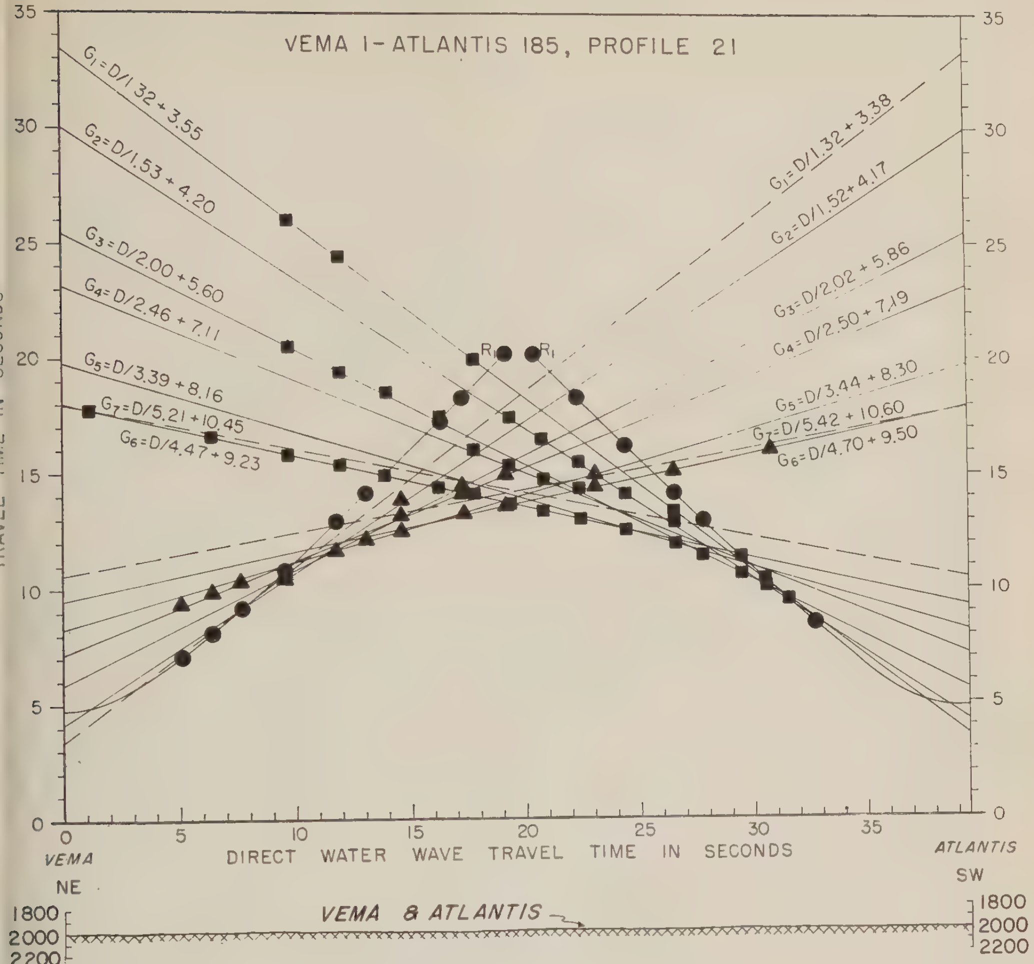
VEMA I-ATLANTIS 185, PROFILE 21
G1=D/1.32+3.55
G2=D/1.53+4.20
G3=D/2.00+5.60
G4=D/2.46+7.11
G5=D/3.39+8.16
G7=D/5.21+10.45
G6=D/4.47+9.23
G1=D/1.32+3.38
G2=D/1.52+4.17
G3=D/2.02+5.86
G4=D/2.50+7.19
G5=D/3.44+8.30
G7=D/5.42+10.60
G6=D/4.70+9.50
R1
DIRECT WATER WAVE TRAVEL TIME IN SECONDS
VEMA
NE
ATLANTIS
SW
VEMA & ATLANTIS
1800
2000
2200

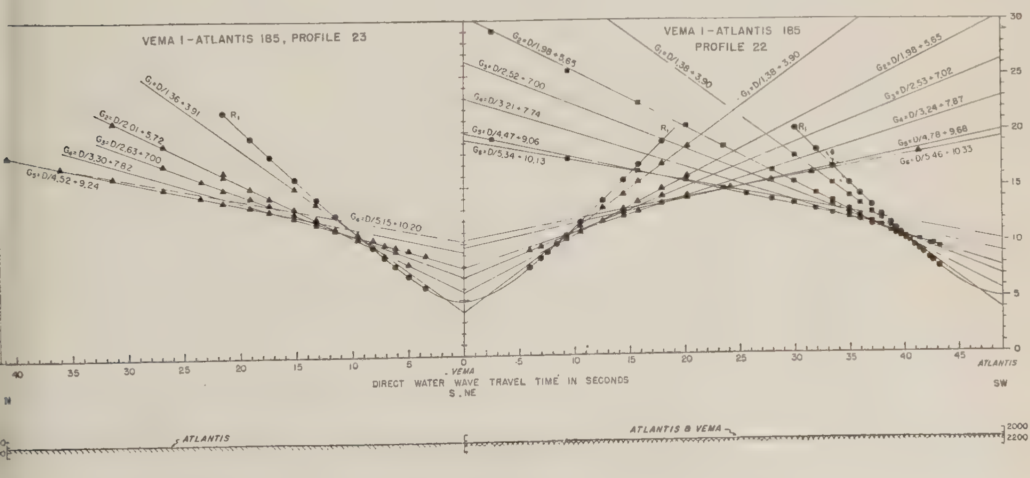
VEMA I-ATLANTIS 185, PROFILE 23
VEMA I-ATLANTIS 185
PROFILE 22
R1
DIRECT WATER WAVE TRAVEL TIME IN SECONDS
VEMA
S. NE
ATLANTIS
SW
ATLANTIS & VEMA
2000
2200

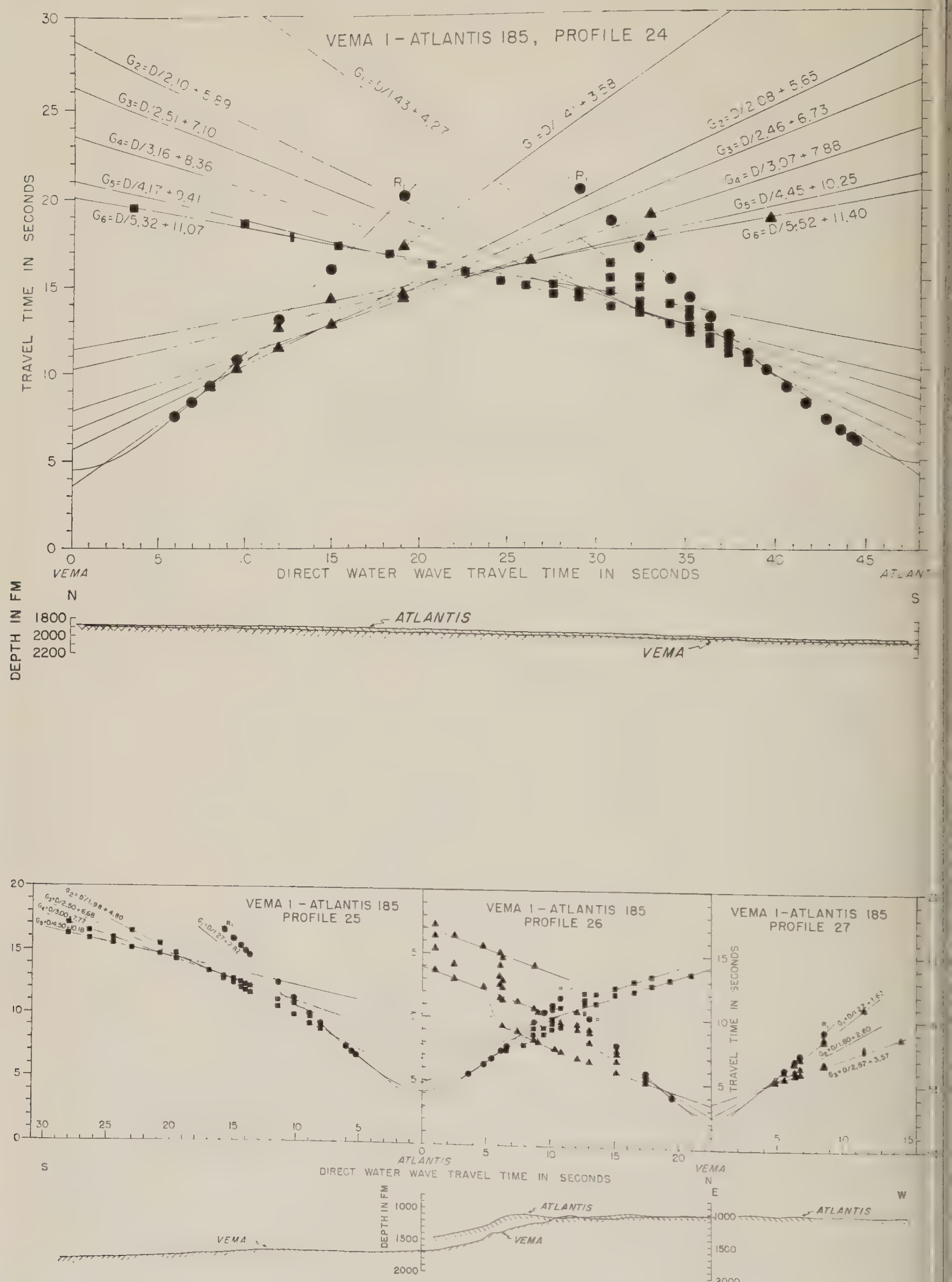
VEMA I - ATLANTIS 185, PROFILE 24
TRAVEL TIME IN SECONDS
DIRECT WATER WAVE TRAVEL TIME IN SECONDS
VEMA
DEPTH IN FM
ATLANTIS
VEMA I - ATLANTIS 185 PROFILE 25
VEMA I - ATLANTIS 185 PROFILE 26
VEMA I - ATLANTIS 185 PROFILE 27
DIRECT WATER WAVE TRAVEL TIME IN SECONDS

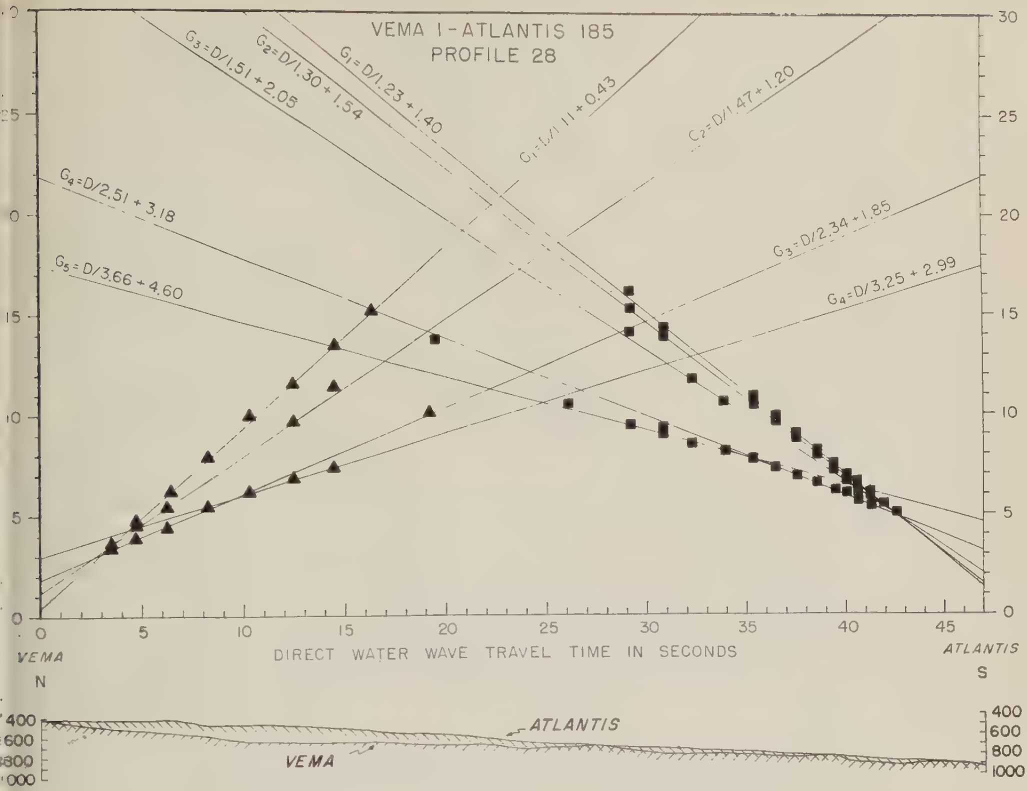
VEMA I-ATLANTIS 185
PROFILE 28
G_3=D/1.51+2.05
G_2=D/1.30+1.54
G_1=D/1.23+1.40
G_4=D/2.51+3.18
G_5=D/3.66+4.60
G_3=D/2.34+1.85
G_4=D/3.25+2.99
C_2=D/1.47+1.20
DIRECT WATER WAVE TRAVEL TIME IN SECONDS
VEMA
N
ATLANTIS
S
ATLANTIS
VEMA

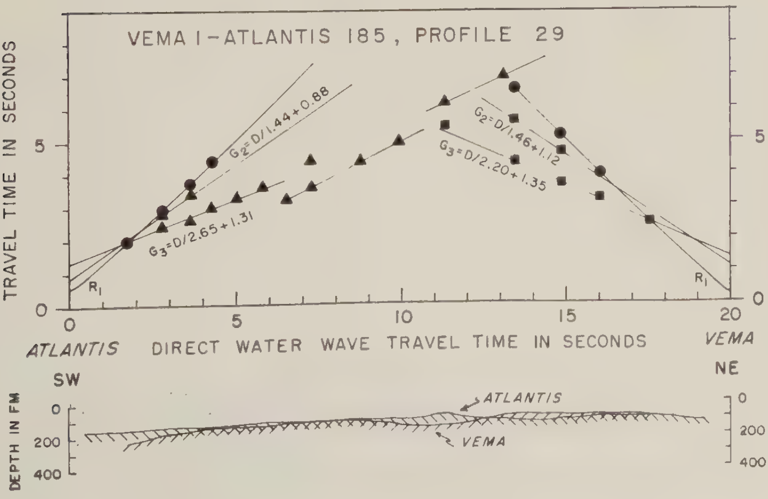
VEMA I-ATLANTIS 185, PROFILE 29
G_2=D/1.44+0.88
G_3=D/2.65+1.31
G_2=D/1.46+1.12
G_3=D/2.20+1.35
TRAVEL TIME IN SECONDS
DIRECT WATER WAVE TRAVEL TIME IN SECONDS
ATLANTIS
SW
VEMA
NE
DEPTH IN FM
ATLANTIS
VEMA

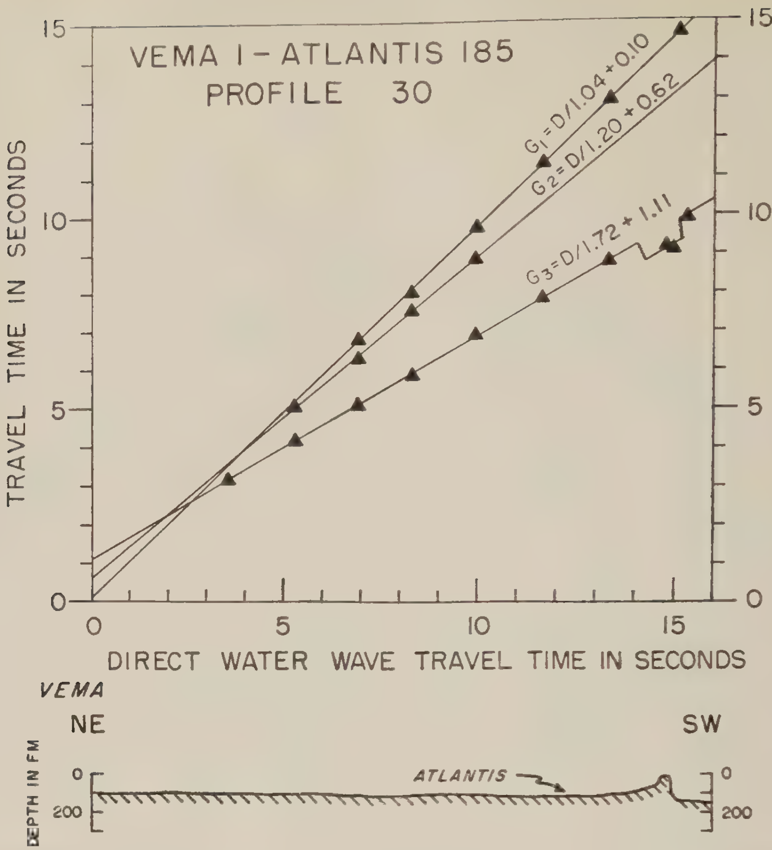
VEMA I - ATLANTIS 185
PROFILE 30
G1=D/1.04+0.10
G2=D/1.20+0.62
G3=D/1.72+1.11
TRAVEL TIME IN SECONDS
DIRECT WATER WAVE TRAVEL TIME IN SECONDS
VEMA
NE
SW
DEPTH IN FM
ATLANTIS

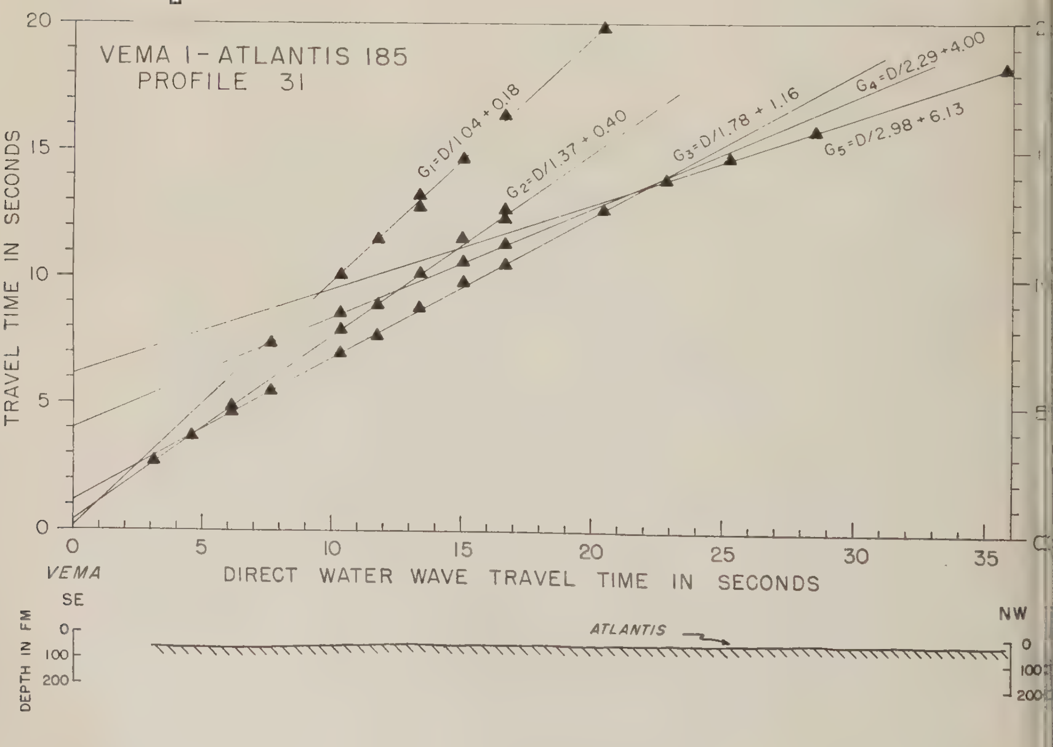
VEMA I - ATLANTIS 185
PROFILE 31
G1=D/1.04+0.18
G2=D/1.37+0.40
G3=D/1.78+1.16
G4=D/2.29+4.00
G5=D/2.98+6.13
TRAVEL TIME IN SECONDS
DIRECT WATER WAVE TRAVEL TIME IN SECONDS
VEMA
SE
NW
DEPTH IN FM
ATLANTIS

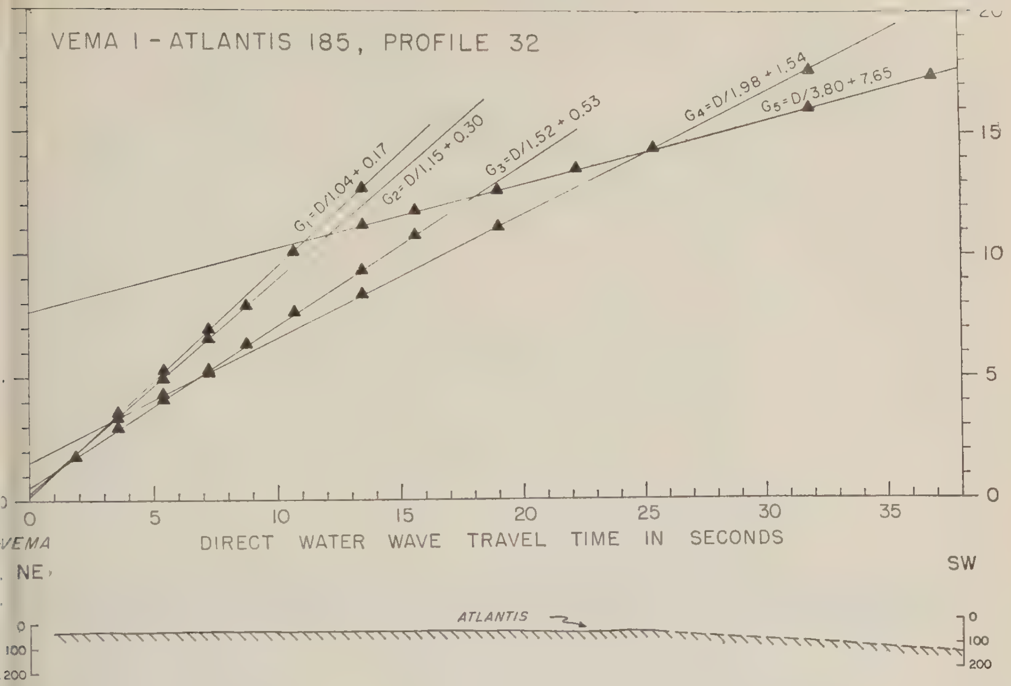
VEMA I - ATLANTIS 185, PROFILE 32
G1=D/1.04+0.17
G2=D/1.15+0.30
G3=D/1.52+0.53
G4=D/1.98+1.54
G5=D/3.80+7.65
DIRECT WATER WAVE TRAVEL TIME IN SECONDS
VEMA
NE
SW
ATLANTIS

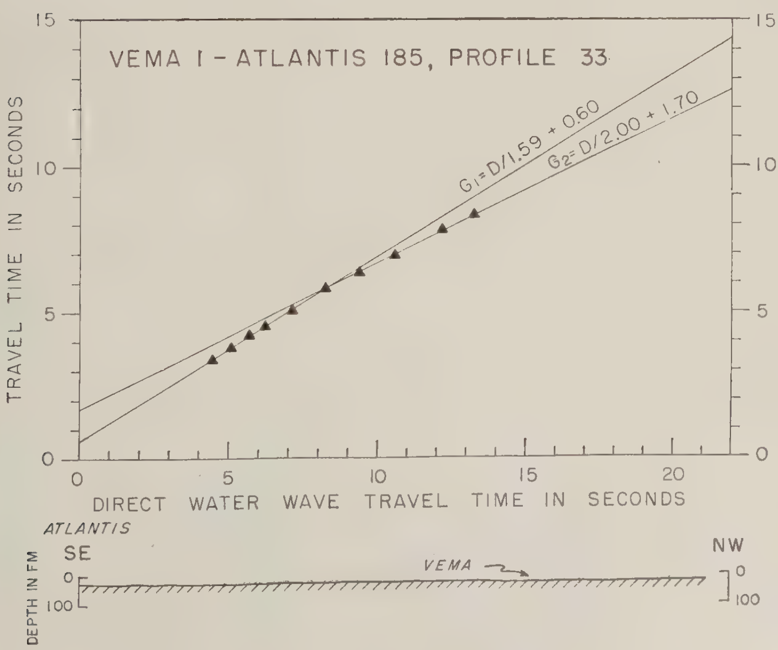
VEMA I - ATLANTIS 185, PROFILE 33
G1=D/1.59+0.60
G2=D/2.00+1.70
TRAVEL TIME IN SECONDS
DIRECT WATER WAVE TRAVEL TIME IN SECONDS
ATLANTIS
SE
NW
VEMA
DEPTH IN FM

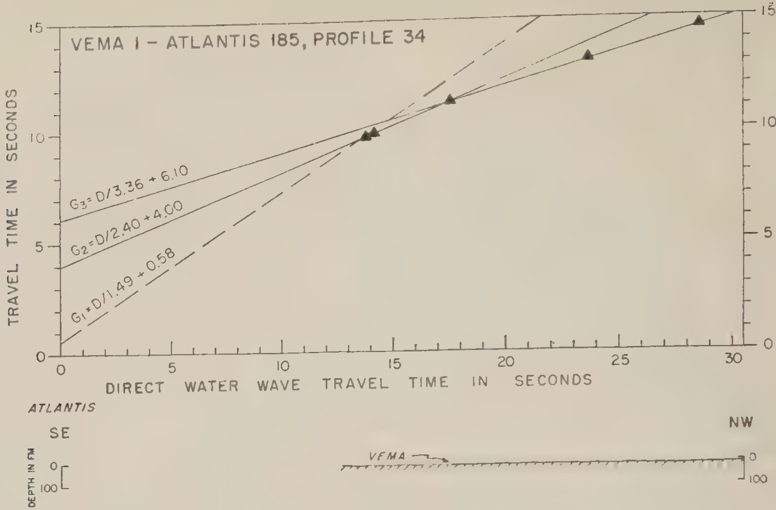

TABLE 1. Receiving Positions, Seismic Velocities, and Layer Thicknesses, Cruise *Vema* 8—*Wissama* 1[...] (Assumed velocities are indicated by asterisks, unreversed velocities by parentheses, and those from end-to-end profiles by *italics*. Others are true velocities determined by reversed profiles.)

		Velocity (km/sec)									Thickness (km)				
Profile	Receiving Position	Unconsolidated and Semiconsolidated Sediments		Consolidated Sediments and High-Velocity Rock A	B	C	D	E	Water		Unconsolidated and Semi consolidated Sediments		Consolidated Sediments and High-Velocity Rock A	B	C
11	16°55′N 70°35′W	1.8*		(3.4)	(4.9)	(7.1)	(8.0)		4.03		.58		1.4	2.5	10
12	16°29′N 72°12′W	1.8*		(3.2)	(4.9)	(6.3)			2.74		.53		1.5	2.4	
13	14°58′N 73°36′W	1.8*		(2.9)	(4.9)	(5.9)	(6.8)	(8.5)	2.56		.39		.04	2.3	2.6
14 NE	14°14′N 74°20′W	1.8*		4.3	6.3	8.0			4.02		.34		1.4	13	
SW	13°34′N 74°50′W								4.02		.99		2.9	9.0	
15 E	11°44′N 75°44′W	1.8*	2.1	3.5	6.8	7.8			3.27		.43	2.3	4.1	5.6	
W	11°19′N 76°39′W								3.07		.74	1.8	2.9	7.2	
16 NE	11°31′N 75°39′W	1.8	2.1	3.6	6.7	8.1			2.87		.71	1.5	6.1	3.8	
SW	11°04′N 75°56′W								2.78		.42	2.0	2.7	7.8	
17 S	11°13′N 77°49′W	2.0		4.6	6.1	7.0	8.2		3.58		1.2		1.6	5.0	8.7
N	11°45′N 77°36′W								3.73		1.7		1.8	1.4	11
18 S	12°45′N 77°31′W	2.0		4.6*	5.8	7.0	8.1*		3.94		1.6		1.3	2.3	12
N	13°45′N 77°40′W								4.02		1.3		1.4	2.5	14
19 S	14°43′N 78°14′W	(1.7)		4.4	6.3				1.95		.77		1.8		
N	15°01′N 78°29′W								2.22		.69		3.2		
20 S	16°14′N 79°15′W	2.0		4.8	5.5	6.7			1.39		1.0		3.2	4.5	
N	17°01′N 79°36′W								1.39		1.0		.93	2.6	
21 E	17°33′N 79°05′W	1.8*		3.9	5.2	6.2	7.6		.86		.59		2.3	3.3	12
W	17°31′N 80°04′W								1.92		.76		1.7	2.1	14

TABLE 1. Continued

...le	Receiving Position	Velocity (km/sec): Unconsolidated and Semiconsolidated Sediments	Velocity: Consolidated Sediments and High-Velocity Rock A	B	C	D	E	Water	Thickness (km): Unconsolidated and Semiconsolidated Sediments	Thickness: Consolidated Sediments and High-Velocity Rock A	B	C	D
	19°09′N 78°02′W	2.1*	3.3	4.7	6.6	8.1		5.41	.49	.37	1.2	3.4	
	19°23′N 77°14′W							5.05	0	.93	1.9	2.4	
	18°16′N 79°36′W	2.1*	4.6	6.4	8.3			4.65	.85	5.1	4.7		
	18°02′N 80°29′W							3.11	0	.20	7.9		
	18°39′N 79°32′W	(2.0)	4.6	6.4	8.2			4.81	.88	.63	3.6		
	18°38′N 79°47′W							4.68	.23	1.7	4.9		
	19°14′N 79°34′W	2.0*	*4.1*	*5.0*	*6.8*	*7.6*		6.97	.65	.67	2.4	4.7	
	19°07′N 81°24′W	(2.0)	5.4*	6.3				2.01	.66	2.1			
	19°11′N 81°03′W							2.93	.89	2.3			
W	19°46′N 80°52′W	2.0*	4.8	6.5	7.2			2.89	.92	2.6	9.4		
E	20°15′N 80°04′W							2.74	1.3	1.2	13		
	19°13′N 79°24′W	2.0*	5.1	6.2	8.2			7.04	1.0	1.2	4.2		
	19°10′N 78°55′W							6.68	.59	1.6	1.9		
	19°12′N 77°00′W	2.1*	4.6	6.4	(8.1)			4.76	.47	1.3	9.1		
	19°39′N 76°51′W							6.40	.93	3.0	3.7		
	19°39′N 76°51′W	2.1*	*4.7*	*6.5*				6.40	.93	3.0	3.7		
	19°39′N 76°29′W	1.8* 2.5	(3.0)	(4.4)	5.4	6.4	8.0	6.73	.19 .55	∼.40	2.5	3.3	4.2
	19°41′N 75°53′W							3.29	.01 .11	2.3	1.4	9.0	4.7
W	18°17′N 75°14′W	2.2*	3.4	(5.4)	6.5	8.2		.90	.70	1.4	4.7	15	
E	17°16′N 74°20′W							2.89	.88	2.1	1.3	14	
	17°23′N 73°21′W	(2.1)	3.6	4.9	6.1	7.8		4.30	.82	.78	3.2	5.3	
	17°19′N 72°31′W							3.29	.20	1.9	1.4	14	
	17°36′N 70°11′W	2.0*	2.8	4.4*	6.4			2.56	.70	3.5	5.5		
	17°34′N 69°44′W							2.56	.70	3.1	3.8		
					Cruise Vema 1—Atlantis 185								
1	20°41′N 82°44′W	*2.1*	*3.9*	*6.6*	*8.1*			4.45	1.0	1.9	6.1		
	22°38′N 85°42′W	2.0*	*4.4*	*5.5*	(6.7)			1.32	.29	2.5	7.0		
E	22°47′N 85°44′W	2.0*	4.9	5.9				1.38	.57	1.7			
W	22°55′N 85°56′W							.82	.25	3.1			
	23°17′N 86°51′W	2.0*	3.4	4.9	6.4			.73	0	1.9	1.4		
	23°00′N 87°25′W							.06	.10	.56	4.0		
	23°00′N 87°25′W	2.0*	*3.4*	*4.6*				.06	.10	.56			
E	22°32′N 88°44′W	2.3	(2.8)	4.8	5.7			.06	0	.54	2.2		
W	22°45′N 89°06′W							.06	.25	.40	1.1		
	22°45′N 89°06′W	*2.1*	*3.1*	*4.8*	*5.7*			.06	.17	.53	1.1		

TABLE 1. Continued

Profile	Receiving Position	Velocity (km/sec): Unconsolidated and Semiconsolidated Sediments		Velocity: Consolidated Sediments and High-Velocity Rock A	B	C	D	E	Water	Thickness (km): Unconsolidated and Semiconsolidated Sediments		Thickness: Consolidated Sediments and High Velocity Rock A	B	C
18	23°47′N 90°46′W	1.9*	2.1	2.4	3.3	4.9	6.8	7.9	3.63	.21	.09	0	.51	4.2
									3.73	.45	1.1	.55	1.1	3.0
19	23°54′N 90°45′W	1.9*	2.1	2.5	3.4	4.9	6.8	7.9	3.73	.43	.73	1.0	.62	3.9
									3.73	.64	2.3	.30	.31	3.5
21 E	24°58′N 90°54′W	2.0*	(2.3)	3.1	3.8	5.2	7.0	8.2*	3.67	.74	1.8	2.2	1.2	3.1
W	24°45′N 91°25′W								3.67	.58	1.4	2.8	.87	2.7
22 NE	24°21′N 92°07′W	1.9*	2.1	3.0	3.9	5.0	7.1	8.3	3.76	.38	1.3	2.3	1.1	4.6
SW	23°58′N 92°40′W								3.80	.38	1.3	2.3	.75	3.0
23	24°05′N 92°44′W	1.9*	2.1	3.1	4.1	5.2	7.0	8.3*	3.80	.42	1.2	2.0	1.3	3.8
									3.75	.75	.92	1.8	2.9	1.8
24 N	25°30′N 92°56′W	1.9*	2.2	3.2	3.8	4.8	6.6	8.3	3.44	.30	1.9	2.3	1.8	6.1
S	24°51′N 92°48′W								3.71	.76	.95	2.8	2.1	1.4
25	25°49′N 93°08′W	1.9*	2.0	3.1	3.8	4.7	7.2		3.42	.61	1.3	2.0	2.3	5.1
									3.07	.11	1.4	4.4	1.4	4.8
26 S	25°57′N 93°10′W	1.9		2.8	4.4				3.07	1.5		4.2		
N	26°28′N 93°04′W								1.86	.90		1.2		
27	26°31′N 93°14′W	1.9		2.8	4.4				1.86	.90		1.2		
28 N	27°21′N 93°36′W	(1.8)	2.0	2.3	3.7	5.3			.73	.16	.63	.34	3.0	
S	26°37′N 93°40′W								1.65	.13	.44	.84	3.6	
29 SW	27°31′N 93°36′W	1.8*	2.2	3.7					.37	.83	.05			
NE	27°40′N 93°15′W								.18	1.4	0			
30	27°48′N 93°16′W	(1.7)	(1.8)	(2.7)					.18	.79	.18			
31 32 33 34	27°59′N 93°25′W 28°09′N 93°41′W 28°05′N 94°00′W 28°21′N 94°14′W	(1.7)	(2.2)	(2.9)	(3.6)	(5.1)			.31	.31	1.2	5.5	4.3	

Development of the Earth and Tectogenesis

V. V. BELOUSSOV

Academy of Sciences of the USSR
Moscow

PRINCIPAL GEOTECTONIC REGULARITIES

n a number of earlier works the author has eady raised the question of the connections sting between the tectogenesis and the genl development of the earth [*Beloussov*, 1942–3; 1951; 1954*a*; 1954*b*]. There are grounds believing that by applying the latest data geophysics, geochemistry, and geotectonics may advance toward a solution of this prob and may combine in a general theory a er complex of deep and geotectonic processes n has been possible before. In this article author restricts himself to an account of a eral outline of such a theory, bearing in mind necessity of further elaboration of its many ects. As we shall see, the character of the ory enables us to elaborate it further, not y qualitatively but also quantitatively.

he following ideas about the tectonic deopment of the earth's crust are used as a is for further analysis.

ince folding is a phenomenon derived from tical oscillatory movements of the earth's st [*Beloussov*, 1958], we may limit ourselves considerations of such movements and not rch for some independent explanations for ling. Fault tectonic movements are mostly result of either oscillatory movements or ling. A certain group of fault phenomena, ever, the primary deep faults, do not ded on oscillatory movements or folding; they ear to play a primary part in the developnt of the deep processes and the earth's st. Arising in different regions, in some sucion, they create the block structure of the h's crust and are the paths of the ascent of p-lying material.

uite independent are magmatic phenomena, analysis of which is exceedingly important clarifying the relations between the movets of the earth's crust and deep processes. general theory must evidently provide an explanation for the succession of magmatic phenomena in geosynclines, on platforms, and in other conditions, while allowing for possible deviations that may be observed.

During a certain period in geological history the continental parts of the earth's crust evolved generally from geosynclinal conditions to the platform ones, i.e., from the conditions of contrast and intensive wavelike oscillatory movements to the conditions of extremely weakened movements of the same type. This evolution took place against the background of tectonic periodicity which is mainly caused by the development of the so-called general oscillations of the earth's crust—of its depressions and uplifts not compensated spatially and occuring in geosynclines and on platforms almost simultaneously, but evidently more strongly in the geosynclines and more weakly on the platforms. It is known that in their development oscillations reveal periodicity of different orders; the movements of the highest order with periodicity of the order of 150 to 200 millions of years determine what is called geotectonic cycles. It has been pointed out that at the end of the cycle in the epoch of general uplift an intensification of wavelike oscillatory movements, their extension both in widespread and in local zones, takes place against the background of this uplift [*Beloussov*, 1948; 1951].

In the latest geological time in some regions the phenomenon of 'postplatform activization' is observed, which is displayed in a new intensification of wavelike oscillatory movements of the earth's crust after the movements have subsided with the end of geosynclinal conditions.

The phenomenon of postplatform activization is most evidently manifested in the Tien Shan. At present, however, the concept of activization formulated earlier must be generalized to a considerable degree. In the vast territory of central

and east Asia we may observe a specific characteristic of the development of the earth's crust, where the postplatform activization proper is only a part of the whole phenomenon. In addition, to contrast tectonic division of the parts that have already become platforms (the Tien Shan, the Sayans, the Altai, a number of Chinese ridges, and others) we may observe here the elevation of such large plateaus as the Tibetan and Pamirs at sites of geosynclines of different age, including the Alpine; the formation of grabens of the Baikal type, of basins and uplifts of the Transbaikal type (widespread not only in the Transbaikal but in Mongolia as well), and formation of the west Siberian inner basin. These specific phenomena originated in different regions and at different times, but at any rate not before the beginning of the Mesozoic. Many of them are characteristic of the latest period of geological time, of Neocene and Quaternary.

We may believe that the whole complex of the phenomena mentioned essentially differing from what characterizes 'normal' development of geosynclines and platforms testifies to a specific new line of the development of the earth's crust which comes to replace the preceding geosynclinal-platform line.

We assume that formation of oceans and seas of the mediterranean type lies on the extension of the same line.

Oceans and inner seas of the mediterranean type are considered as new formations which began to develop not earlier than the Mesozoic and many of them much later. During the Cretaceous, Tertiary, and Quaternary periods oceans increased their area at the expense of the continents and greatly deepened.

Although geological data we have mentioned seem to be very convincing evidence for this point of view [*Beloussov*, 1955] the idea of secondary character and of the juvenility of modern oceanic basins has encountered some objections, so that the author thinks it necessary to dwell on the matter.

The objections do not concern geological facts proving the increase of the oceans in Mesozoic and Cenozoic; they follow another course. Our critics claim that this idea contradicts the differences in the structure of the earth's crust on the continents and under the oceans stated by geophysical methods [*Kropotkin*, 1956; *Kropot-*
kin, Lustikh, and Povalo-Shveikovskaya, 19
Lustikh, 1959; *Magnitsky*, 1955, 1956*b*]. In f
for the transformation of continents into oce
a radical transformation of the earth's crus
obviously necessary: it must become consi
ably thinner, and the so-called granite la
must somehow be liquidated. Lustikh in the
ticle cited says that these transformations
energetically impossible. Such assertions s
hazardous. First of all, we must make sure
the increase of the oceans and mediterra
seas at the expense of the continents is actu
observed according to geological data. If
phenomenon is indeed observed, we have
right to ignore it simply because we do
understand the process. Just the contrary. C
ing up any unjustified confidence about wha
and what is not possible on the earth, we m
do our best to find an explanation of this 'oce
zation' of the earth's crust, constantly bea
in mind that the properties of the deep mate
of the earth are still very little known.

As evidence of the late formation and a
ther development and deepening of the oce
and deep seas the author has previously m
tioned the following:

1. The traces of the earlier existence of la
where oceans are now. These lands have
played themselves as the sources of the te
genous rocks or as routes of the migration
plants and animals; for instance, land bri
between the continents of Gondwana existe
the upper Paleozoic; land bridges between
rope and North America, as well as betw
Indonesian islands and the continent, betw
the Japanese islands and the continent, and
tween New Zealand and Australia, existed
to the Neocene; the sources of terrigenous r
existed during the lower Paleozoic in the
lantic northwest of Scandinavia, during the M
dle and upper Paleozoic east of the Appal
ians in the Atlantic and in the beginning of
Mesozoic in the Atlantic west of the Co
basin.

2. Quite evident former spreading of
tinental sediments of the Karoo basin bey
the limits of the modern continent of Afr
granite boulders brought by upper Paleo
glaciers from regions now engulfed by the
dian ocean.

3. Undeniable paleogeographic data on
existence of land at the sites of the Mediter

and Caribbean seas which now have the th's crust of the oceanic type (in respect to se seas the works of *Behrmann* [1958] and *terlin* [1956] are of specific interest); unable paleogeographic data indicating the ence of land and shallow sea during a conous geological history in the Black Sea and southern part of the Caspian Sea, where e is now the crust of oceanic structure *gelyants, Galperin, Kosminskaya, and Kraka*, 1958; *Neprotchnov*, 1958; 1959].

Guyots in the Pacific and the Atlantic ns and also the results of drilling on atoll ds, indicating a comparatively recent (posttaceaus) deepening of the oceans.

General 'superimposed' character of the ntic and the Indian oceans as well as of y marginal and mediterranean seas in relato the structure of the continents and a ken off' form of the latter.

Shore flexures especially well observed on shores of the Atlantic Ocean (Greenland, ted States, Africa).

he majority of these data certainly are not and in recent time have been considered to quite sufficient proof of the secondary charr of oceans. A revision of this statement is ely connected with the establishment of the tioned difference in the deep structure of earth's crust under continents and under ns. However, since geological data are not roved and cannot be explained otherwise, ring them is completely unjustified. We not take seriously either of the extremely ficial explanations of these facts, as *Lustikh* 59], for instance, tries to do. This investir assumes that separate parts of the earth's t of the oceanic structure could remain for ng time in an uplifted position, in contradicto the conditions of isostasy. Then, he ases, they subsided, leading to isostatic bal. Apart from the fact that this abnormal tion for them has not been explained, it ld be extremely strange to suppose that isely in our epoch all these parts subsided that the general accordance with the isostaconditions that we observe has now been esished. We could further add that a single tworthy phenomenon of the 'oceanization' he earth's crust is sufficient to raise the probof transformation of the earth's crust ughout its volume. If in the Miocene granite pebbles were brought from the region of the Tyrrhenian Sea [*Behrmann*, 1958], while according to gravimetric data the crust under this sea is of a certain oceanic structure [*Kropotkin, Lustikh, and Povalo-Shveikovskaya*, 1958], or if similar changes are described for the Black and the Caribbean seas, the problem of 'oceanization' of the crust for each of these cases is in general the same problem as for the Pacific and, indeed, for all the oceans of the world. Since the conditions of isostasy exist, and since the structure of the earth's crust in the oceans somehow differs in shallow and deep parts of the basin, the fact of a simple deepening of the oceanic basin, established by guyots or by the results of drilling on coral reefs, is also quite sufficient to raise the same problem in all its importance.

Chemical Composition of the Crust and the Mantle

For discussing the questions facing us, it is first of all necessary to know something about the composition of the region in which the deep processes, now to be discussed, are going on.

The so-called 'granite layer' of the earth's crust includes sedimentary and metamorphic rocks, gneisses and granites, the gneisses and granites comprising the main part. The composition of the 'basaltic' layer is less certain. Some geophysical and geological data suggest basaltic or, to be more exact, gabbroic composition for this layer, but not unequivocally. If we agree that the origin of tectonic movements and basic sources of magma is below the earth's crust, which is to a considerable degree a passive object under the influence of deeper processes, the question of the composition of 'basalt' layer is not so urgent. The most likely assumption seems to be that in the upper part of this layer are mixed granites and gneisses and the basic rocks (gabbro), and that the largest part of it, consisting of basalts (or gabbro), is the region within the limits of which, depending on the changes of temperature and pressure, the Mohorovicic discontinuity migrates and reversible transitions between eclogite and basalt occur.

The question of the composition of the upper part of the earth's mantle is of extreme importance. In these layers, within the limits of some hundreds of kilometers from the surface, must be concentrated the causes of tectonic and

magmatic processes. Volcanic sources are marked at the depths of 60 to 200 km. Deep earthquakes are observed down to the depth of approximately 700 km.

Since the granites have been convincingly demonstrated to be of metamorphic origin, so that there is no necessity to assume their coming from the mantle in final composition, the mantle must be considered a source of basalt. The volume of basalt extruded from the mantle is enormous. The basalt extrusions on the bottom of the oceans are especially voluminous, but even on the continents the plateau basalt extrusions reach enormous amounts. A point to be stressed is the considerable homogeneity in chemical composition of basalts of different age and from different regions. None of the other magmatic rocks from ultrabasic to acid rocks can compare with basalt in volume; they can be adequately explained as the result of differentiation or 'contamination' by the rocks of the crust.

From these considerations it seems hardly probable that the upper part of the mantle consisted, as is often assumed, of such an ultrabasic rock as peridotite. Basalt certainly could be derived from peridotite for instance, by the melting of fusible components. But it is quite unlikely that melted products are so stable in composition, and it is not clear why the rock itself comes to the surface in so much smaller quantities than basalt.

In this connection, the hypothesis of the basaltic composition of the mantle seems more attractive, assuming, however, that the basalt in the mantle is in the form of eclogite. This hypothesis has been stated by Fermor, Goldschmidt, Holmes, and Birch. Quite recently it was advanced by *Lovering* [1958], who believes that it is in good accordance with new data on an intermediate composition of meteorites and on the physical properties of the upper part of the mantle. He assumes that the upper 60 per cent of the mantle may consist of eclogite under which are peridotite (35 per cent) and dunite (5 per cent). From this point of view the Mohorovicic discontinuity is considered not as a boundary between different materials but as a region of phase transition from basalt (or gabbro) of low pressures to eclogite of high pressures. The phase transition is determined mainly by the conversion of certain molecules
of feldspar into molecules of jadeite, ompha
and garnet. Since in this process the increas
pressure and the rise of temperature are ac
in the opposite directions, the rise of temp
ture at constant pressure or the fall of p
sure at constant temperature must caus
transition of part of the eclogite to ordin
basalt and the corresponding lowering of
Mohorovicic discontinuity. The volume of
material increases by approximately 15
cent, and the layers of basalt ascend. Upon a
crease in temperature or an increase in pres
some part of the basalt at the bottom of
crust must transform into eclogite, which m
lead to an elevation of the Mohorovicic dis
tinuity, a decrease in the volume, and a
pression of the overlying basalt. Thus,
elevation and subsidence of the Mohoro
discontinuity are not connected with the
placement, influx, and removal of the mate
but only with the transition of the material f
one phase to another one. This idea contrib
to the understanding of many deep proce

We think it probable that the eclogite c
position of the mantle remains the same d
to the depth at which a sharp change of
gradient of the increase of velocity of seis
waves with the depth takes place, i.e., 900
from the surface (the foot of the 'Golitsin la
or the C layer of the mantle).

Magnitsky [1956] assumed that a chang
physical properties in the C layer with de
which is inferred from the change in seis
waves velocities could be explained by the
teration of intermolecular bonds from the
type to the covalent type, the idea of the cha
in chemical composition of the material b
ignored. This assumption was supported by
ther researches [*Magnitsky and Kalinin*, 19
As for the source of ultrabasic rocks, the m
volumes that are observed on the earth's
face may be explained by local differentia
of material initially of basaltic composition,
curring in separate melted sources. An im
tant source of these rocks may be the sett
in the upper layer of melting and differentia
in the mantle, which will be discussed later.

Since we believe the interchange of the m
rials between the surface and the depths of
earth to be limited we do not dwell on the c
position of deeper layers of the mantle
even less on the composition of the earth's c

'FERENTIATION IN THE UPPER LAYER OF THE 'MANTLE BY MEANS OF SELECTIVE MELTING, AND ITS CONSEQUENCES

ı accordance with the universally recognized ory worked out by *Schmidt* [1957] in the SR and by *Urey* [1952] in the United States, earth was formed by the coalescence of l dust particles belonging to protoplanetary surrounding the sun. Accordingly, the earth first cold and quasihomogeneous, since the ticles constituting it were of different chemi- composition and dispersed fortuitously in it. 'he thermal history of the earth from this nt of view was considered in a number of ers by *Lubimova* [1958]. Both the probable istribution of radioactive sources of heat in process of differentiation and changes in t conductivity with depth and with change emperature were taken into account. Howr, the unreliability of the parameters that st be used in this theory makes the thermal iputations only provisional. A further source ıncertainty is that Lubimova took into acnt the transfer of heat only by means of ecular heat conductivity and radiation, comely disregarding the transfer of heat with material itself; as it will be seen below, we inclined to ascribe to this latter mechanism predominant role in the thermal processes de the earth. However, in spite of the tenta- nature of the computations, we believe t their principal result may serve as a basis further discussion.

'he principal result of Lubimova's compuons is first of all the establishment of ther- l autonomy of the interior parts of the th, beginning approximately from the depth 500 km. Owing to the low heat conductivity he material of the earth's mantle, radioactive t at depths greater than 500 km is not transed to the surface of the earth and so the p parts of the earth are subjected to heat- which is still going on.

s for the outer part of the earth's mantle, n to the depth of about 500 km, after conious heating the cooling process must comice. This process, according to Lubimova's iputations, began 1 or 2 million years ago se figures are extremely unreliable).

'he comparison of the distribution of temitures with the temperature of melting of the mantle material at different depths leads to the assumption that radioactive heating may cause the melting of the material, first in a certain layer in the upper part of the mantle (according to Lubimova, depths of 100 to 700 km). The position of this layer is determined by the combination of temperatures and pressure: at higher levels the temperatures are too low for melting, and at deeper levels the pressure is too high. It is plausible to assume that this layer of probable melting has some relation to the layer of decreased speeds of propagation of seismic waves located within the limits of 100 to 250 km of depth [*Gutenberg*, 1954; *Shirokova*, 1959].

Depending on local temperatures and pressures at different levels of this layer, either complete melting of the whole material, or partial melting of the more fusible components out of it, is possible.

Inside the melted layer, conditions are created favoring gravitational differentiation, during which lighter components are gathered at the top of the layer and heavier at the bottom.

The author has already suggested that differentiation of the material of the earth according to its density is the principal deep process and the main source of energy for tectonic movements and magmatism [*Beloussov*, 1943; 1951; 1954*a*]. At present we specify the mechanism of this differentiation, in which an important role is played by the process of partial melting of relatively fusible components which are also lighter in density. The great importance of selective melting in the history of the earth has been emphasized by *Vinogradov* [1959*a*; 1959*b*]; the same idea has been treated by *Magnitsky* [1955; 1956] and *Wilson* [1959] among others.

The author assumes that, under various conditions for differentiation at various depths, the differentiation develops, as it were, in layers, independently and at different speeds in different layers. We may consider the movements in the earth's mantle in at least two layers: the upper, which is characterized by a more energetic course of differentiation and which is a source of the movements of the earth's crust in geosynclines; and the lower, where the differentiation goes on much more slowly and which is the source of movements displayed on the platforms [*Beloussov*, 1951]. It must also be emphasized

that the 'platform' movements of the earth's crust are not limited by the platform but manifest themselves also in geosynclines where they are the background of, and to a considerable degree veiled by the more energetic geosynclinal movements proper. *Shatsky* [1948], however, cited examples in which deeper 'platform' movements are clearly 'seen through geosynclinal.' From this point of view the transition from geosynclinal to platform conditions is determined by cessation of differentiation in the upper layer, after which the processes of the deeper layer are clearly reflected on the surface.

These considerations must be kept in mind; they are in good accord with surface observations and with the theories about the mechanism of the processes presented here.

The products of differentiation, formed in the melted layer, lighter than those containing the mantle material (eclogite), tend to come to the surface, whereas the products of the same differentiation heavier than eclogite tend to sink. In the first group we include not only the light components that concentrate toward the top of the melted layer, but basalt as well, which is produced by complete melting of eclogite since the density of basalt is lower than that of eclogite.

The light material comes to the surface, as we believe, with the help of a mechanism similar to the mechanism of the surfacing of salt in salt domes. From the surface of the melted layer, columns composed of relatively light material grow upward. They intrude into the covering layer of heavier material, pull it apart, and it descends to the place that has become vacant.

We assume that an analogous process goes on in the lower part of the melted layer, where the material heavier than that containing eclogite is concentrated. Here also the heavy material appears to cover the lighter, so that conditions are identical to those existing toward the top of the melting layer. The underlying light material rises and the covering heavy material descends, exchanging places with each other.

The whole complex of processes under consideration—melting, differentiation, surfacing, and submerging of the material—must be essentially influenced by deep faults, since their opening leads to a decrease of pressure and, consequently, together with the increase of te perature, contributes to melting, differentiati and vertical displacements. Thus, the devel ment of deep faults together with the tempe ture regime influences the depth of the m ing layer, its thickness, the activity of vert exchange of the material, and also the ra and the form of vertical flows; it is natural assume that surfacing and submerging of mel products go on along developing deep fau taking the form of welts striking along faults but not the form of columns.

Differentiation at the top and bottom of melting layer takes place under different con tions. Material at the top is under less press and has a lower viscosity than material bel Therefore the differentiation above must velop more intensively than below, to wh tendency, as we shall see, the fact that deep fa evidently penetrate into the upper part of melting layer but do not reach the lower p also contributes. The high intensity of process of exchange of material toward top of the melting layer is expressed in a hig speed of vertical displacements and also in closer location of ascending columns and w of light material.

Differentiation in the Mantle and It Connection with the Earth's Crust Movements

The flow of light material upward and heavy material downward causes correspond elevations and subsidencies of the earth's cr The intensive differentiation in the upper p of the melting layer creates a contrasting di ion into intensive uplifts and subsidences ch acteristic of geosynclines. Vertical moveme of the material in the lower part of the melt layer occurring under conditions of con erably greater viscosity develop much m slowly and by larger flows; they are conside to be the cause of platform wavelike oscillat movements.

At first we assumed that cessation of differ tiation in the upper part with continuing ferentiation in the lower part, with which connected the transition from geosynclinal platform conditions, is caused by the fact t the quicker differentiation in the upper p leads to an earlier balance in the distribu of material. It was assumed that the differen

n was coming to an end because the material ources for it were exhausted.

Of course this reason must play some part in cessation of geosynclinal differentiation in upper layers: the further it develops the s become the means for its continuation. But may not be the main cause. Possibly a more portant cause is the cooling that is spread- downward in the mantle, the cooling that s stressed by *Lubimova* [1958]. This cooling, nnected with the general distribution of tem- rature in the deep parts of the earth, may at certain moment put a stop to the differentia- n and vertical exchange of the material in the per geosynclinal layers and cause a transition m geosynclinal to platform conditions at the rface.

It will be proper to emphasize here that, for e physics of the deep processes being con- lered it is extremely important that during ferentiation and vertical circulation in the intle heat moves to the surface much more ensively than it would simply by heat con- ctivity. The powerful vertical circulation of e material in the upper layers contributes to a nsiderable degree to their cooling, or 'freez- g.' At the same time, in the lower layer, where nperatures still remain sufficiently high, verti- l circulation is going on. Thus the transition m geosynclinal to platform conditions in our ew is linked with the process of 'secular' cool- g of the upper part of the mantle, intensified a powerful vertical circulation of material.

The assumed connection between wavelike cillatory movements of the earth's crust and e deep processes suggests an explanation of me essential peculiarities of these movements. explains why the regions of elevations and pressions on the platforms are notable for eater horizontal dimensions than the zones of evation and depressions in geosynclines; it so explains both for geosynclines and for plat- rms the phenomenon of mutual compensation space of elevations and subsidences occur- ng simultaneously.

A peculiarity of all post-Archean as well as at least certain Archean geosynclines (see *hoenmann* [1959] on ancient African geosyn- ines) is a linear distribution of zones of ele- tion and depression. For geosynclines of dif- rent age one prevailing strike of tectonic nes is very often maintained. An example is the northwestern strike predominant over the area from the eastern Sayan Mountains to the Apennines, and displayed in the upper Pro- terozoic (Baikal) geosyncline of the eastern Sayans, in the Caledonian geosyncline of the western Sayans and the Altai Mountains, in the Hercynian geosyncline of the Rudny Altai, in the Hercynian parageosyncline of central Ka- zakhstan and Karatau, in the Alpine geosyncline of Turkmeno-Horasan mountains, in the Cau- casus, Crimea, the eastern Carpathians, the Dinarides, and the Apennines.

At the same time ancient platforms are characterized by oval and irregular contours of subgeoanticlines and subgeosynclines without any expression of linearity.

The linearity of geosynclinal elevations and depressions may be explained by the influence of primary deep faults [*Hobbs*, 1911; *Peive*, 1956; *Sonder*, 1938]. A number of facts to which the author has already referred [*Belous- sov*, 1954*b*] show that the deep faults have their own history, that they are formed in different regions at different times and have different directions: although diagonal (north- eastern and northwestern) are evidently pre- dominant, there are also meridional and lati- tudinal directions. We have stressed that the meridional Caledonian strike in the western part of central Kazakhstan was replaced in the Hercynian cycle by the northwestern strike of the zones of elevation and subsidence which was connected with the appearance of a new net- work of deep faults. Schoenmann has pointed out a crossing of Archean geosynclines of dif- ferent ages in South Africa, which must be con- nected with the reorienting of active deep faults. On the whole, however, the history of primary faults has thus far been inadequately investi- gated.

Various theories of the origin of primary deep faults have been advanced. It is commonly stated that the origin of most such faults lies in tensions in the earth's crust and the mantle which may be induced by the change in the degree of compression along the axis of the earth as a result of gradual deceleration of the rota- tion of the earth under the drag influence of tidal forces [*Shatsky*, 1955]. However, nobody has showed any actual connection between deep faults and tensions of this type.

In the light of our theories we may suggest a

different explanation for the formation of primary deep faults. Such faults may be connected with the expansion of the interior parts of the earth under the influence of radioactive heating, and the tension and cracking of the upper layers of the earth caused by this expansion. It will then be necessary to analyze the possible spreading of tensions in the stretching mantle of the earth.

The fact that linearity is not displayed on ancient platforms indicates that primary deep faults of this type cut the geosynclinal level but do not penetrate to the platform level. Thus the usual depth of their penetration is measured by perhaps 100 to 150 km. This, however, does not mean that the other groups of deep faults may not have a smaller or a greater depth of penetration.

The absence of linearity in the structure of some Archean geosynclines (for instance, on the Baltic shield, where granite domes rounded or irregular in their contours abound) indicates that deep faults have not yet originated there.

One more difference between wavelike oscillatory movements on geosynclines and on platforms can be explained. The elevations and depressions formed in geosynclines and on the platforms by wavelike oscillatory movements of the earth's crust show two patterns. Sometimes the elevations are of regular geometric shape (usually an elongated oval) and the depressions fill the space between them, conforming to their outlines; in contrast, sometimes the depressions take a definite form (usually round) and the elevations fill the space between them. Depressions and elevations have not been extensively analyzed from the point of view of our theory, but in general we may say that the first pattern evidently prevails in geosynclines and the second on ancient platforms.

When the lighter material emerges inside the heavier and the heavier descends, two quite different distributions of ascending and descending flows may be observed. The light material may form ascending columns and welts of definite geometric outlines while the descending flows of heavy material fill in the spaces between them; or the opposite may happen—heavy material descending may form overturned columns or welts, while the emerging light material fills in the spaces between them.

Evidently the relative viscosities of the participating materials determine which happe
The lower-viscosity material forms ascendi columns and welts, while the flows of mo viscous material fill in the spaces between the

Proceeding from what has been said of th prevailing form of elevations and depressio in geosynclines and on ancient platforms, may conclude that the fluid light material the geosynclinal layers has not only lower de sity but also lower viscosity than the containi material. At a lower depth in the platfor lower viscosity characterizes the descendi heavier material. This somewhat unusual co relation of viscosities and densities needs spec consideration. It indicates that in the platfor layers the increase of pressure with depth fluences the viscosity of the material more th its density.

A certain regularity in the location of you (alpine) geosynclines on the surface of t earth has long been observed. On one side the geosynclines surround the Pacific; on the oth they stretch in approximately latitudinal dire tion from the Mediterranean across centr Asia, the Himalayas, and Indonesia. Geosy clines existed here earlier, but they were co siderably wider and occupied an area extendi beyond the limits of the mentioned zones. Th we must consider these zones as the most favo able for a more continuous retaining of ge synclinal conditions.

The explanation probably lies in the fact th conditions in these zones are favorable for ope ing deep faults, which moreover contributed melting, differentiation, and vertical displac ments in the mantle for long periods of tim Bucher's experiments with paraffin spheres su jected to an extension from inside [*Bucher*, 192 are pertinent. In these experiments a series fractures were obtained on the surface of t sphere closely resembling in their location t distribution of young geosynclines on the eart surface. Paleogeographic constructions indica that the Mediterranean-Himalayan Alpine ge synclinal zone corresponds approximately to t Mesozoic and Early Tertiary equator [*Rukh* 1959]. It would be quite reasonable to assum that centrifugal force, maximum at the equato made its contribution to the opening of de faults and the elevation of light material to t surface in the process of differentiation. This another matter needing quantitative study.

'rom the point of view of the theories being ussed it is unlikely that geosynclinal activi- could begin again in the newest stage of the ling of the upper layers of the mantle, where tform conditions have already been estab- ed. Theoretically, however, it might not be sidered entirely impossible. The appearance new deep faults could break up the balance he mantle and lead to a renewal of intensive tical circulation there, where the 'material' sibilities for it remain, that is where local lting in the fault zone still may cause differ- iation.

But at an earlier stage in the history of the th when heating enveloped the whole of it luding the upper layers of the mantle such henomenon was quite likely due to the ap- arance of new melting sources and to a com- ation of the network of deep faults. May we ume that the cases of crossing of geosyn- es and their 'regeneration' mentioned by *oenmann* [1959] for the Archean era are ated to this ancient stage of general heating?

According to the most recent data of abso- e geochronology in comparison with the analy- of tectonic history, a crucial turning point the development of the earth's crust occurred proximately 1500 million years ago (for nno-Sarmathia, with the transition from the relide cycle to the Gothide cycle). The first ble 'stabilization nuclei' were then formed in e earth's crust, and a successive extension of tforms and reduction geosynclines began.[1] is date is in good agreement with the begin- ig of cooling in the upper layers of the mantle ntioned by *Lubimova* [1958] (see above), ough we must not overestimate the signifi- nce of such an accordance.

Since the author aims to present only a gen- al account of his theories in this paper, he does t touch on many essential details of the devel- ment for deep processes both in geosynclines d on platforms. It is more useful to treat ese details separately.

Let us consider the phenomenon of periodicity tectogenesis, which is closely connected with e development of geosynclines and platforms. was mentioned before, periodicity is determined by general oscillations of the earth's crust, which have a larger amplitude in geosynclines than on platforms. It is observed that general oscillations propagate in time from geosynclines to the neighboring platforms: both general subsidence at the beginning of a cycle and general elevation at the end of it begin somewhat later on the platforms than in the geosyncline [*Beloussov*, 1948; 1954*a*].

In this tectonic periodicity we are likely to see a phenomenon comparable to the effect of a lid on a kettle of boiling water. Radioactive heating, and resultant melting, leads to an increase in the volume of the material of the mantle. It begins in geosynclines where the activity of deep faults contributes to melting and the melting becomes extensive. With the rise of temperature and the increase in volume the material spreads toward the neighboring platforms. Then the process of melting and differentiation is activized, and the vertical movement of the material increases. This movement carries a great part of the heat to the surface zones of the mantle, leading to a fall in temperature at the depth and to the corresponding decrease in the volume, earlier and more intensive in geosynclines than on platforms. Then heat begins to accumulate again at depth, and the cycle is repeated.

A possibility of interpreting the origin of periodicity of tectogenesis is found in the succession of magmatism in geosynclines. The subsidence accompanying the beginning of the next tectonic cycle follows the magmatic eruptions at the end of the preceding cycle, i.e., the stage of 'final magmatism,' including granite intrusions, fracture intrusions, and the last phase of surface extrusions, while the general elevation of the second half of the cycle develops after the magmatic phenomena fade away.

Our interpretation of causes of periodicity of tectogenesis makes it possible to establish a relation between general oscillations and wave-like oscillatory movements and, in particular, to explain the increase of contrast of the latter in the epoch of general elevation.

The rough synchronism of tectonic cycles may be explained as follows. Heating occurs simultaneously and all over the mantle, which, on the whole, is of uniform composition, and cooling spreads quickly along the entire mantle after

---

[1] Academician A. A. Polkanov's report at the ssion of the Department of Geological-Geo- aphical Sciences of the Academy of Sciences of e USSR, February 23, 1960.

the deep heated material ascends to the surface in many places. However, it is understandable that this synchronism is not extremely precise.

The expansion of the material of the mantle not only leads to the elevation to the surface and to the intensification of the circulation of this material at the depth; it may also lead to the fracturing of the upper part of the mantle and crust, i.e., to the formation of new deep faults. The end of the tectonic cycle, with its general elevation, is the most favorable time, then, for a renewal of the network of deep faults. In fact, in the period between the Caledonian and Hercynian cycles new deep faults were formed in central Kazakhstan, and between Hercynian and Alpine cycles western Europe was cut across by a system of deep faults.

This theory of the origin of periodicity of tectogenesis enables us to explain why the extension of platforms and the reduction of geocynclines occurs by 'shocks' between tectonic cycles. The intensification of vertical circulation of the material of the mantle at the end of a cycle to the stage of 'final magmatism' leads to a very considerable cooling of the upper layers of the mantle and makes it most probable that at just this epoch cooling reaches the critical value when geosynclinal differentiation in the upper layers ceases.

The fact that platforms being formed in some places then spread with every cycle, covering new areas, shows that the process of cooling in the mantle spreads, from the places where it began, over a larger area.

Large tectonic cycles are complicated by local cycles, determining the complicated periodicity of the process of general oscillations of the earth's crust. The heating of the material of the mantle and the increase in its volume are interrupted by numerous small movements of the material, carrying some of the heat to the upper zones until at last the general accumulation of the heat will not lead to such a considerable displacement of the material which will make the whole 'lid of the kettle of boiling water' subside.

Melting in the Deep Layers of the Mantle and the 'Basaltic' Stage of the Development of the Earth

All the phenomena we have discussed so far refer to the stage of the earth's development that may be called the 'granite' stage. It is ch acterized by the formation of granite contin tal crust.

The actual process of the formation of granite layer is not considered in this arti for this subject is more relevant to a discuss of the details of geosyncline development. shall note only that this process must be c sidered in the light of the idea of granitizat of sedimentary and metamorphic rocks and peated remelting of granites formed earlier a result of the activity of 'through magmatic so tions' rich in silicates, alkalies, and volatile co ponents. These solutions ascend from the man and their movement is closely connected w the above-mentioned differentiation in the up part of the mantle.

The granite stage is the first big stage in development of the earth that can be studied geological methods. Any other, earlier sta lie beyond the possibilities of geology.

The composition of the upper layers of mantle during the granite stage certain changed, since light components were melt out of them. Under geosynclines, by means melting out of eclogite, there was produced certain volume of acid rocks and the compo ents that cause granitization of the crust. Wh differentiation is still going on under platform intermediate and alkaline rocks are melted o of the mantle. These rocks are known to occ mainly in the platforms.

If we accept the ideas of *Kennedy and A* *derson* [1938] on two types of basalt, thole and olivine, differentiation of the first ty giving a calc-alkaline range of rocks charact istic of geosynclines, and differentiation of th second giving a range of alkaline rocks, then may assume that as a result of geosynclin differentiation the material of the upper lay of the mantle changes from the composition tholeite basalt to the composition of olivi basalt.

The next stage of the development of th earth may be called 'basaltic.' It is expressed mass elevation of basalt to the surface and th destruction of the granite crust. On the surfa it is expressed in a whole complex of phenome already mentioned briefly above. We shall em phasize their connection with the elevation basalt to the surface.

First is the phenomenon of postplatform

ization displayed most typically, as has been tioned, in the Tien Shan. Platform or para-ynclinal conditions, in some places already lished in the middle Paleozoic, and in others the beginning of the Mesozoic, were re-ed in the Neocene by extremely energetic ical movements of the earth's crust, leading he sharp relief that we now observe in this on. The location of zones of elevation and sidence was evidently determined by deep ts of very old origin, already in existence at geosynclinal stage. In activization these es were used again, which explains the sur-l of the ancient tectonic plan of the dis-ution of elevations and depressions.

s direct evidence for activization from this it of view, deep seismic soundings in the thern Tien Shan have revealed the presence 'basaltic' but not granitic 'roots,' as had merly been believed to exist, under the acti-ed elevations [*Gamburtsev and Veitsman*, 7; *Gamburtsev, Veitsman, and Tulina*, 1955; *sminskaya*, 1958]. The earth's crust under se elevations appears to be thickened as the ult of an increase in the thickness of the alt layer. Thus we may say that postplat-m activization is connected with irregular ting-out of the mantle's deep layer of basalt ich adheres to the earth's crust from below.

n addition to the Tien Shan, postplatform ivization embraces the Altai Range the west- and eastern Sayan Mountains, and the ikal region. Southward from here is the huge ion of central Asia, the whole of which is vated, especially within the limits of the etan plateau and its immediate surround-s. Very little is known about the deep struc-e of this territory, but undoubtedly the th's crust is exceedingly thick here. We can ume that the thickness of the earth's crust over central Asia is connected with its filling with the basalt melted out of the interior. here are no direct data, but the fact that the en Shan are closely connected with this gion of wide uplift of the earth's crust makes ch an assumption quite probable.

Within the limits of the region of postplat-rm activization are developed large furrows the type of the Baikal graben system. Nu-rous extrusions of basaltic lavas in these abens are well known. But to understand the ture of these furrows better we must turn our attention to a quite different region, to the east African system of grabens. These grabens throughout their entire extent, from the Dead Sea in the north to the mouth of the Zambesi River in the south, are found in the zone where it is impossible not to see the signs of activization, though displayed in a form somewhat different from that of central Asia. As has been shown by *Cloos* [1939], these grabens were located on two vast domelike young (mainly Tertiary) elevations, the area of which goes far beyond the usual platform subgeoanticlines.

Recent geophysical study of the Red Sea grabens led *Girdler* [1958] to the conclusion that along the axis of this enormous graben extends a much narrower graben (about 60 km wide), the bottom of which is composed of basalts evidently elevated from below and penetrating into the earth's crust as a great dike, partly replacing the 'granite' crust. The other grabens of the east African system did not reach such a development as those of the Red Sea; the amplitude of their subsidence is less; there are no grounds to assume that granite crust was replaced by basalts, but basalt takes an active part in the volcanic extrusions developed in these grabens. We do not intend to give the impression that we explain the formation of all grabens by the same mechanisms; we are discussing the largest fault deeps of the 'planetary' scale. Numerous small grabens are formed as a result of fracturing and block subsidences of the crests of elevations, as H. Cloos and others [*Cloos*, 1939; *Beloussov*, 1954*a*] have described. However, we believe that this mechanism of wedging of fractures of extension on the crests of elevations cannot be applied to very large grabens. For these we must assume a deeper cause of subsidence of the earth's crust; we are now studying this problem.

To the category of phenomena connected with the ascent of basalts we refer plateau volcanism, known on the Siberian platform, in India, and in the Paraná basin in South America, among other places.

Finally, the formation of seas of the mediterranean type and the oceans is evidently connected with the ascent of basalts which destroys and replaces the granite crust and ensures a wide development of surface basalt volcanism.

The extreme variety of tectonic and magmatic processes connected directly or indirectly

with the ascent of basalts from the depth to the surface, to the earth's crust or to the strata below it, makes precise terminology essential. The 'basalt' stage connected with the increase of the role of basalt in surface zones of the earth includes the following phenomena:

(*a*) *Tectonic activization,* in which we include the postplatform activization in the form of great intensification of wavelike oscillatory movements (of the type of the Tien Shan, the Altai, eastern Africa, etc.), formations of grabens and basins of Baikal and Transbaikal type, and the formation of the high plateau of the Tibetan and the Pamirs type.

(*b*) *Mass extrusions of plateau basalts* on the continents, accompanied by the intrusion of diabase sills and dikes.

(*c*) *Basaltization* (or basification) of the earth's crust, which is displayed in the formation of separate grabens of the Red Sea type but even more widely in oceanization.

(*d*) *Oceanization,* displayed in the formation of mediterranean seas and oceans on the basis of the destruction of the granitic crust of the earth and its replacement by basaltic crust.

Studying the history of all the phenomena mentioned here we shall see that 'basalt flood' began in different places at different times. But it seems not to have become prominent generally before the end of the Paleozoic, when the oceans began to form, plateau basalts were first extruded on the platforms, and deeps of the Transbaikal type were formed in Transbaikal and Mongolia. This process was undoubtedly intensified during the Mesozoic, Paleocene, and especially Neocene times, when an outbreak of postplatform activization occurred, mediterranean seas and grabens formed, and the oceans increased and deepened considerably. Thus the 'basalt' stage began much later than the 'granite,' but since in many places the 'granite' stage still continues, the two stages overlap each other to a considerable degree.

To avoid misunderstanding we must emphasize that we speak not of all basalt extrusions but of those plateau-basalt extrusions that are characterized by a specific chemical composition of great homogeneity and by huge volumes. We do not refer here to basic extrusions and intrusions belonging to the normal cycle of the development of geosynclines characterized by a small volume and a frequent alternation with the lavas of intermediate and acid compositi[on]. Such basalts are connected, we may assu[me], with the smelting of the material from the u[p]per melting layer during the 'granite' stage.

So how can we explain the mass mobilizat[ion] of basalt in the earth's interior, and what [is] the detailed mechanism of the connection [of] surface and deep processes during this geolo[gic] stage of our planet?

On the basis of her computations *Lubimo[va]* [1958] concludes that in connection with t[he] heating of deep layers of the mantle and t[he] cooling of its upper layers the melting lay[er] gradually shifts inside. It is hardly necessa[ry], however, to think of a continuous downwa[rd] shifting of the layer subjected to melting. W[e] may imagine an independent appearance of t[he] new melting layer at a greater depth in co[n]nection with a continuously increasing heati[ng] of the greater depths which, as it was me[n]tioned, possess a considerable degree of therm[al] autonomy. The formation of this second de[ep] melted layer at a greater depth goes on in para[l]lel with cooling in the upper layers of the man[]tle and with the slackening activity of t[he] upper layer of melting. As a result, the bas[alt] stage commences after geosynclinal conditio[ns] have been widely, but not necessarily whol[ly] replaced by platform conditions: 'the approa[ch] of basalt' may begin while geosynclinal cond[i]tions still prevail on the surface.

We assume that this deep layer of melti[ng] is a source of basalt in all the examples cite[d]. We may only guess the depth of this layer. I[ts] upper limit is extremely indefinite, owing [to] the evolution of the layer about which we sh[all] speak later, but it can hardly be assumed [to] be less than 400 km deep. To determine t[he] lower limit we may use maximum depths of t[he] sources of eathquakes (720 km) or the botto[m] of the so-called Golitsin layer (or the C laye[r]) where the gradient of the increase of seism[ic] wave velocities changes markedly with the dept[h] (900 km). We will assume that our deep mel[t]ing layer covers the whole Golitsin layer (fro[m] 400 to 900 km). We must not think that t[he] whole of it is subjected to melting, howeve[r]. We must rather assume that the melting proc[]ess, having begun in the upper parts of t[he] layer, in the course of time penetrates sti[ll] deeper, that at any given moment it is co[n]centrated in various small melting foci and b[e]

ans of gradual displacement of the latter the ire layer may be subjected to the melting ocess.

An increase of volume and an extension of e upper layers of the mantle must be the re-t of the heating and melting of the material this deep layer. Simultaneously there must ur an extremely strong fracturing of the per part of the mantle and crust and the mation of a new series of faults, deeper than se formed earlier. Along these faults the erheated basalts ascend from the depths. is ascent is caused by a decrease of density e to the transition of eclogite into basalt and an enhancement of volatile components in e basalt.

The question may arise why in a deep melt- layer no such differentiation occurs as was served in the melting of the upper layer and the similar selective melting of light com-nents. Why does extremely homogeneous salt ascend from a deep melting layer almost thout lighter products of melting?

We may assume that mobilization of the ma-rial located at such great depth under high essure implies a considerable rise of tempera-re, and therefore the material is greatly erheated. When the faults arise this material mediately melts as a whole. In the upper yer of melting the process may go on much ore gradually than in the deep layer.

Deep basalts begin their upward movement columns much larger than those formed by e material of the upper layer, inasmuch as ey must overcome the greater resistance of e layers above. These large columns gradually ove to the surface. But in their upper part ey may split into smaller columns and welts, king advantage of the heterogeneities of the ructure of the upper parts of the mantle and umerous faults. The picture is further compli-ted by the fact that deep basalts carrying eat quantities of heat may cause melting of e surrounding regions and an additional mo-lization of their material, which joins the deep salts in their tendency to move to the surface.

In the upper layers of the mantle and in the ust, where deep material moves to the surface ong the separate routes determined by faults, intensive vertical circulation arises, since the cent of overheated material saturated with ses is compensated by the subsidence of a colder and therefore denser material which had previously played a part in the constitution of the mantle and the crust.

The elevation of deep basalts has various results, depending on the penetrability of the earth's crust and on the interaction of basalts with it. If the earth's crust fractures easily, plateau-basalt extrusions are observed with further subsidence of the earth's crust above the emptying local sources of basalt, as, for instance, in the Tunguska basin on the Siberian platform [*Offman*, 1959]. In other places the flow of basalts from below leads to a thickening of the crust and to its elevation in the form of ridges as in the Tien Shan, or in the form of vast plateaus as in the Tibetan or adjacent regions. In still other places overheated basalt interacts with the earth's crust, destroying and replacing its granite layer. The chemistry of such a replacement is not clear, but the fact that it occurs cannot be questioned. *Tikhomirov* [1958] assumes that metasomatism takes place mainly here. We may think of the melting of the granite layer and of its solution. Examples of such a process on a small scale have been cited by *Gorai* [1951], *Reynolds* [1941], and *Turner and Verhoogen* [1951].

Whatever the mechanism of the replacement of granite crust by basalt may be, the question arises about the change in composition of the mantle as a result of the 'absorption' of the granite layer. Like many other questions raised in this paper it needs special consideration, but here we would like to make some general remarks.

Under the influence of the high temperature of deep basalts the continental crust of the earth must be melting. Melting of the crust to the surface will be expressed in the development of volcanism with the prevailing of andesite lavas corresponding to the average composition of the continental crust. This is precisely the picture we now observe along the periphery of the Pacific, where under the influence of overheated basalts ascending from the depth an intensified process of melting of the continental crust is going on. Among the products of volcanism water is prominent; the water content of the granites reaches 7 per cent. This water together with water emanating directly from the ascending basalts fills up the simultaneously formed oceanic deep. At present geo-

chemists agree on ascribing a deep origin to oceanic water [*Ronov,* 1959; *Rubey,* 1951]. According to *Rubey* [1951] it emanated during the crystallization of the granite layer of the earth's crust, though it is likely that large volumes of water may emanate simply from the melting of the earth's crust.

Other gaslike products of andesite volcanism and carbonic acid gas move into the atmosphere and influence its composition. Lavas and solid volcanic products are subjected to subaerial erosion, are destroyed, and finally are redeposited on the bottom of the ocean as sediments, where they partially dissolve and influence the salt composition of oceanic waters.

We may assume that not the entire volume of the granite layer is absorbed by the material of the mantle. What is absorbed is involved in the vertical circulation of the material in the mantle and moves far inside it. Overheated deep basalt with the gases it contains evidently has lower density than the rocks of continental crust, because it is extruded to the surface of the rocks. As a kind of compensation for the surfacing of basalts, the adjacent blocks of the earth's crust together with the blocks of the upper layers of the mantle are carried away by the descending flows, and in the process of the final melting and solution of the granite layer are involved very large volumes of the material of the mantle, evidently much larger than the volume of the granite layer. Thus the influence of this process on the average composition of the mantle may lie within the limits of chemical differences between tholeite and olivine or oceanic basalts.

The emanation of water and of volatile components in the melting of the continental crust increases the average density of the column of solid material remaining after cooling at the place of melting of the crust and beneath it; this leads to a subsidence of the surface of the solid body of the earth and to the formation of sea or oceanic basins. The Mohorovicic discontinuity now requires a new level, determined by the depth of the transition of basalt into eclogite, corresponding to the new conditions of temperature and pressure.

As a result of all these transformations, isostatic adjustments are made: instead of thick granite-basalt continental crust, thin water-basalt oceanic crust is formed, and the surface of eclogite substrata correspondingly rises. Th water layer takes part in the establishing isostatic equilibrium together with the soli layers of the crust and the mantle.

It may seem contradictory that to one an the same process, the elevation of basalts, a ascribed both the elevation of the earth's cru in its activization and the subsidence in i oceanization. But deep overheated basalt caus an elevation of the crust until it overcomes t crust's resistance. If the basalt penetrates to t surface or replaces the granite layer after t emanation of volatile components and cooling, increases the weight of the crust, and as a r sult the surface of solid earth subsides. Fro this point of view it is quite natural that ea collapse (formation of grabens, of sea basin is preceded by an elevation, unless the ascen ing basalt flow immediately penetrates t earth's crust.

The stage of replacement of the earth's cru by basalt is observed in the Red Sea, where the middle part of the graben the continent crust is evidently being replaced by basalt. Th other grabens of the east African system th are still in the earlier stages of development d not show such a phenomenon. We may assum that the process is in the stage of the intrusio of basic rocks into the earth's crust from belo with a slight increase in the weight of the crus

We see examples of the replacement of grani continental crust by basalt in the Mediterra ean, the Caribbean, and the Black seas, in t Sea of Japan, the southern part of the Caspia Sea, and the Gulf of Mexico. In the last two w observe an intermediate state, in which t continental crust has already become thinn (20 to 25 km) but has not been completely r placed by oceanic basalt. Seismic observatio show that either powerful strata of weak condensed sediment rocks (the Gulf of Mexic the south Caspian) are retained above t basalt layer [*Gagelyants, Galperin, Kosmi skaya and Krakshina,* 1958; *Officer, Ewing, E wards, and Johnson,* 1957], or directly und the Mohorovicic discontinuity abnormally lo speeds of seismic waves (7.4 km/sec in the Ca ibbean Sea) are observed, which may be unde stood as the result of penetration of bas emanated from the depth in the upper part eclogite.

At the final stage in this process are t

ans—huge regions of basification of the th's crust. The oceans show especially well it the ascent of deep basalts is connected with strong fracturing of the earth's crust and doubtedly also of the mantle. It is apparent ng the periphery of the northern Atlantic, ecially in Scotland and in Greenland. Scotland known to be crossed by numerous mainly ridional long open fractures, the time of formation of which (Tertiary) coincided with the ne of subsidence of the northern part of the lantic Ocean. Basalts characteristic of the gmatic Thule province covering the whole rthern Atlantic extruded along the fractures. Greenland fractures that are the routes for e extrusion of basalts cut the shore flexure, rmed by Cretaceous and Eocene rocks [*Wager d Deer*, 1938]. According to seismic data a ck layer of basalts (up to 3 km) covers the ttom of the whole northern Atlantic [*Ewing d Ewing*, 1959].

It is likely that the strong regional fracturing Scandinavia and the very sharp fracturing western Europe, displayed from the beginng of the Mesozoic when the main part of the lantic was forming, have some connection with at event.

Along the periphery of the Pacific strong acturing is observed both on the Chinese platrm, where it originated during the Cretaceous riod, when considerable increase of the area d deepening of the Pacific occurred [*Belousv*, 1956], and also in California with its peliar network of faults. The bottom of the acific is broken by an enormous number of ults. In the east they are mainly latitudinal; the center and in the west, mainly northstern and partly northwestern. The ranges basalt volcanic islands and submarine ridges rrespond to these diagonal faults.

The east African grabens mentioned above beng to the obvious indications of fracturing in e zone of the Indian Ocean.

It is quite evident that it is not the formaon of the oceans that causes the fracturing of e earth's crust and the mantle, but, vice versa, e places of maximum fracturing of the surface nes of the earth determine the formations of e oceans, since fracturing provides the routes r the elevation of deep basalts. Fracturing rects the process of general expansion of the rth, of the extension of its mantle and the crust under the influence of radioactive heating.

The evidence of intensified fracturing in the vicinity of oceans reveals the means of the further development of the oceanization process.

In the light of these theories the origin and the place of island arcs in the structure of the earth are of interest. Another article [*Beloussov and Ruditch*, 1960] deals in more detail with this subject and also with the problem of the asymmetry of the Pacific.

Study of their structure and history enables us to distinguish two types of island arcs. Those of the first type are arclike curved folded zones, similar to folded arcs on the continents, such as the Himalayas, the Carpathians, and the Verkhoyansk Range. The arclike form of the folded zones is connected with their history. The simplest succession of events may be stated as follows. In the preceding tectonic cycle (the Hercynian, for Alpine folded arcs) a geosyncline broke down into a number of ovals connected by narrow channels, that being quite characteristic of geosynclines. At the end of the cycle, as a result of the process of inversion, a central uplift originated within the oval. The uplift was surrounded on all sides by arclike foredeeps, which appeared in the next geotectonic cycle (Alpine) as intrageosynclines. During that cycle, as a result of a new inversion from these intrageosynclines, folded ridges of naturally arclike form ascended; the central uplift of the preceding cycle somewhat descended forming what is usually called inner massif in the young geosyncline.

There is no doubt that such is the origin of the folded arc bordering the western part of the Mediterranean Sea, now situated on the subsided inner massif of an Alpine geosyncline. Paleogeographical data lead us to believe that the same inner massif was situated in the Caribbean Sea inside the arc of the Antilles [*Butterlin*, 1956].

The results of the researches of van Bemmelin and other geologists leave no doubt that Indonesian arcs are of the same origin and are young folded uplifts, bordering the inner massifs submerged under ocean waters [*van Bemmelen*, 1949]. A review of geological history leads to the conclusion that Japan also belongs in this same category of island arcs.

The most characteristic feature of arcs of this type is that geosynclinal zones of the crust

weakened by numerous deep faults were utilized in their formation. They are folded ridges formed in the Alpine intrageosynclines, and they have the form of island arcs because median massifs situated inside them subsided deeply in the process of the basification of the crust and oceanization.

A deep ocean trench always accompanies an island arc of this type, beginning to develop at the place of the foredeep of the geosyncline. Later, since it appears to be within the sphere of the oceanization processes, it subsides so quickly that it has no time to be compensated by sufficient sedimentation.

Island arcs of the second type differ greatly from the first. The islands composing them are either the volcanoes of Tertiary or Quaternary time or the blocks of gently dislocated Cretaceous and Tertiary sediments. To this type of island arcs belong the Aleutian, the Kurile, and the Ryukyu Islands and the Bonin-Mariana groups. They had no geosynclinal prehistory, and in their formation they are most likely connected with the origin of new deep faults in the earth's crust.

Arcs of the second type are as a rule younger than those of the first type, as can be seen, for example, in the crossing of the arc of Japan by the Kurile and Bonin-Mariana arcs.

It would be appropriate here to return to the arcs of the first type to mention an element of similarity in the development of the two types. This similarity lies in an intensive Tertiary and Quaternary andesite and basalt volcanism exceeding in its activity the volcanism of regular geosynclinal zones on the continents. We may believe that the formation of deep faults contributed to the intensification of volcanism. However, if new faults originated where there already were arcs of the first type, young geosynclines may have served as weak places so that the earlier faults were reopened.

As has been mentioned, the formation of oceans began with the beginning of the Mesozoic. From that time they increased in area and deepened. Various parts of the world oceans are obviously in different stages of development. The northern Atlantic is very young. It subsided quite recently in the Neocene. The depths are not yet great, and the crust, though it has no granite layer, is still rather thick. In the Norwegian Sea, judging by seismic soundings the upper 3 km of solid crust are compos of recently extruded basalts, under which is layer of 7 km with the intermediate speeds seismic waves (7.5 km/sec), similar to th found under the Caribbean Sea [*Ewing an Ewing*, 1959; *Officer, Ewing, Edwards, a Johnson*, 1957]. Again we assume here a zo of a mixture of ecologite and the basalt ascen ing from the depth. Here as in Scotland a Ireland, subsidence has occurred in the proc of the penetration of the continental eart crust and the mass extrusions of basalts on surface, with their subsequent absorption the blocks of the granite layer.

The south Atlantic and the Indian Oce are more ancient. Here subsidence went on large blocks separated by grabens like th now developed in east Africa, which determin the further direction of the spreading of t ocean. These oceans are deeper than the nor ern Atlantic, and the crust within their lim is of typical oceanic structure.

The Pacific is evidently more ancient on t whole, though it may have deepened mo quickly as the result of especially strong fr turing of the mantle. It is deeper than oth oceans.

With the transition from a shallower to deeper ocean we observe a change in the co position of extruding basalt lavas toward mo basic properties. In fact, in the northern Atla tic olivine basalts alternate with tholeite b salts in approximately equal amounts. In t Indian Ocean olivine basalts have become pr dominant. In the Pacific we find the most ba varieties of basalts.

Therefore it is possible to assume that in t process of oceanization still deeper layers the mantle are mobilized. These layers are co posed of more and more basic material, whic however, in chemical composition is still basa The fact that in the region of the Pacific ve deep layers of the mantle are in motion is se in the depth of the sources of the earthqua reaching 720 km, while focal surfaces inclin under the surrounding continents determi that border along which the most basic de basalt comes into contact with the material u derlying the continent and evidently having l basic composition. The fact that the Pacific surrounded by a volcanic belt points to a stro thermal influence, on the mantle and crust,

ascending overheated basalt where melting ing on actively, as was described above. ntensification of the process of oceanization e Pacific as compared with the other oceans evidently be dated at the end of the ssic period. The peculiarities of the develop- of the Pacific are considered in detail in article by *Beloussov and Ruditch* [1960] dy mentioned. We must emphasize that in most recent geological periods (the Tertiary Quaternary) the process of further oceani- n went on most energetically along the phery of the Pacific whereas in the Atlantic Indian oceans it was concentrated along axes in the zones of median submarine es (see below). Undoubtedly the interac- s between the Pacific and the surrounding inents were different from those between the ntic and Indian oceans and their surround- continents.

he asymmetry of the Pacific displayed in development of island arcs in its western phery and their absence in the east is note- thy. A possible explanation is that at some e of its expansion to the east the oceanic reached the unique geosynclinal zone of Cordilleras and Andes, which was weakened numerous faults, and stopped there. Since, asification and oceanization, the earth's crust crushed and submerged by separate big ks, it is understandable that at a certain e the process of crushing would stop at such ne as a long-existing geosyncline.

ifferent conditions prevailed at the western phery of the Pacific. There was no uniform ctural zone as in the Cordilleras and Andes, the earth's crust was of mosaic structure, alternation of platform and folded regions lifferent ages and orientations.

he process of basification and destruction he earth's crust is undoubtedly directed up- d, and the whole thickness of the earth's st must be penetrated before it is complete. erefore it proceeded more rapidly where the tinental earth's crust was thin than where vas thick. It was further slowed down where crust was still in the process of thickening the result of differentiation.

The complicated line of the border of the an continent and the ocean can be explained accordance with these ideas. It is known that crust of the earth is thinnest on the ancient platforms or on the inner massifs, and thickest under young central uplifts that originated in the Alpine geosynclines. The thickness must be relatively greater under the island arcs both of the first and of the second type, since the formation of these arcs is connected with the differentiation of material in the zone of the deep fault.

Therefore it seems logical that the process of basification penetrated further westward and caused the great expansion of the ocean in the same direction in the zone of the Kolyma inner massif (which caused the deep penetration of the Sea of Okhotsk into the continent), in the region of the northern (the most ancient) part of the Chinese platform (the Yellow Sea), and within the limits of the Indonesian inner massif (the Gulf of Siam). Meanwhile the process of basification and oceanization seemed to avoid the geosynclinal uplift of southern Sakhalin, the southern 'activized' part of the Chinese platform, and the geosynclinal uplifts of Laos and Malacca. For some time the blocks of the continental crust forming the island arcs of both types survived, since the continental crust here was thicker and the process of its thickening continued until recent times.

Seas of the mediterranean type represent a stage in the formation of oceans. We have pointed out a similarity between the west Siberian lowland and the Piedmont lowland (together with the Gulf lowland) in age and position in respect to Hercynian geosynclines. The suggestion was made that the west Siberian lowland is like a 'failed' ocean [*Beloussov*, 1955].

In the location of oceans and mediterranean seas we may see a certain regular geometry. In the light of the theories presented it is determined by irregularities in the process of the fracturing of the expanding earth, by the existence of predominant regions of this fracturing on the surface of the sphere, which is in a state of expansion. It is quite likely that primary heterogeneities of the earth were used in this process as well as the heterogeneities in the structure of the mantle and the crust which remained from the preceding granite stage. Thus for instance it is not accidental that a strip of newly formed seas from the Mediteranean through the Black Sea to the southern part of the Caspian Sea closely coincides with the Alpine geosyncline. It is interesting that on the con-

tinuation of this strip to the east in central and east Asia is a vast region of tectonic activization of the earth's crust, and it is equally interesting that this region opens to the east like a triangle in the direction of the Pacific.

Submarine ridges are very characteristic of the oceans. In the Atlantic and Indian ocean they occupy medial positions; in the Pacific there is no such medial submarine ridge, but in all parts of it are distributed a great number of ridges having mainly northwestern and northeastern trends, as has already been mentioned.

The Middle Atlantic ridge has been most studied. Seismic soundings show a considerable thickening of basalt layer under the ridge. The layer intrudes into underlying substratum in the form of a deep root, up to 30 km thick. Study of the surface of the ridge shows that a graben runs along its crest. [*Ewing and Ewing*, 1959].

The graben certainly indicates the stretching to which the rocks were subjected in the elevation of the ridge. On the other hand the subsidence of the Mohorovicic surface under the ridge indicates that the ridge corresponds to the zone of basalts melted out at depth and also to the zone of the removal of additional heat from below, which led to a deeper location of the border of transition from eclogite to basalt. Thus the connection of the ridge with the deep fault cannot be doubted.

The Middle Atlantic ridge crosses Iceland. A graben is observed in the structure of Iceland on the continuation of this ridge [*van Bemmelen*, 1955]. It is very young (Upper Pliocene), which permits us to speculate that the graben on the submerged parts of the ridge and the whole ridge are young formations.

The Middle Indian ridge near the Chagos Archipelagos has two branches: one trends to the north, and the Deccan plateau basalts are located on its continuation; the other, together with the line of the earthquake epicenters, turns to the northwest and toward the Red Sea.

We believe that these ridges, like the Middle Atlantic ridge, are located on faults along which overheated basalts ascend most actively. Here the influence of the basalts on the earth's crust was greatest, as the structure of the Red Sea testifies, for on the continuation of the ridge the continental crust has been partly destroyed and has become basaltized, and a graben has formed. Its relation to the submarine ridge similar to that of the Iceland graben to Middle Atlantic ridge. Gravimetric studies the region of the Deccan plateau enable us assume that the depression of the continen crust under the extruded plateau basalt up 4000 meters deep was accompanied by a struction of the same crust from below and decrease in its thickness. This is similar to basaltization of the crust that we observed the northern Atlantic. Also similar is the asc of deep overheated basalts in numerous rid on the floor of the Pacific, along the axis which ranges of volcanic islands are locat In good accordance with this idea of the ori of oceanic ridges is the fact that thermal mea urements show the heat flow on the swells to considerably larger than normal—sometimes times as large (from Professor Bullard's repo to the Institute of Physics of the Earth Moscow, in 1959).

There have certainly been many such act faults on the floor of the Atlantic and Indi oceans. They may yet become active. A gre number have remained in an active state in t Pacific until the present, which indicates on more that the Pacific is the region where pecially strong extension and fracturing a now concentrated.

Conclusion

Thus according to our ideas tectogenesis flects the general tendency in the developme of the earth in the direction of its heating radioactive sources of heat. The accumulat heat is partly removed by means of melting a differentiation of the material of the mant Originally melting takes place in the upp layers of the mantle. To this corresponds t first, or granite, stage of tectogenesis, duri which there is observed geosynclinal platfo development of the earth's crust with its wav like oscillatory movements. In this process t crust is filled with acidic (granitic) material.

Later a deeper layer of the mantle is su jected to melting, whence overheated basalt a cends to the surface. In the basalt stage tecto activization is observed, and finally the grani crust is destroyed and oceanization occurs.

Thus elevations and depressions of the earth crust developed in the process of its waveli oscillatory movements, on the one hand, an

formation of sea deeps of the mediterranean ·e (i.e., located on oceanic crust) and oceans, the other hand, present genetically different cesses. They are subjected to different influ-es and must be studied by different methods. e basic difference between them is that move-nts of the first type are compensated by the umulation of sediments and by erosion, ereas those of the second type are not.

All the processes described proceed irregu-ly, both in time and in space.

Irregularity in time is expressed in the fact at melting does not go on over the whole er simultaneously, but occurs only in sepa-e foci and only gradually, in the process of ir migration, does melting come to cover the tire layer. The activity of separate deep faults, influential in the melting process and in the rtical circulation of the material of the antle, is also different at different times. With irregularity of the removal of heat is con-cted a complex periodicity or, it might be tter to say, an alternation of tectogenesis, ich we understand best for the 'granite' stage development.

Irregularity in space is expressed in the fact at different parts of the earth's surface pro-ed from one stage of development to another different times. Regions that are at different ages of development may lie close together the surface of the earth. This increases the mplexity and the variety of the structure of e earth's crust, but it also presents an oppor-nity to review the history of the development the crust by means of a comparative study its different regions.

References

ehrmann, R. B., Die geotektonische Entwick-lung des Apennin-Systems, *Geotektonische Forsch.*, *12*, 1958.

eloussov, V. V., Migration of radio-elements and development of the earth's structure, I and II, *Izvest. Akad. Nauk, SSSR, Ser. Geograf. i Geofiz.*, no. 6, 1942; no. 3, 1943.

eloussov, V. V., Basic regularities of geotectonic process, *Izvest. Akad. Nauk SSSR, Ser. Geol.*, no. 5, 1948.

eloussov, V. V., The problems of inner structure and development of the earth, I and II, *Izvest. Akad. Nauk SSSR, Ser. Geog.* nos. 1 and 2, 1951.

eloussov, V. V., *Fundamental Problems of Geo-tectonics*, Gosgeoltechizdat, Moscow, 1954*a*.

Beloussov, V. V., Recent problems of general geo-tectonics, *Sovet. Geol.*, Collection of papers, no. 41, 1954*b*.

Beloussov, V. V., On geological structure and development of the oceanic deeps, *Izvest. Akad. Nauk, SSSR, Ser. Geol.*, no. 3, 1955.

Beloussov, V. V., Main tectonic peculiarities of central and southern China, *Izvest. Akad. Nauk, SSSR, Ser. Geol.*, no. 8, 1956.

Beloussov, V. V., Types and origin of folding, *Sovet. Geol.*, no. 1, 1958.

Beloussov, V. V., and E. M. Ruditch, Island arcs in the development of the earth's structure, *Sovet. Geol.*, no. 10, 1960.

Bucher, W. H., The pattern of the earth's mobile belts, *J. Geol.*, *32*, 265–290, 1924.

Butterlin, J., *La constitution géologique et la structure des Antilles*, Paris, 1956.

Cloos, H., Hebung-Spaltung-Vulkanismus, *Geol. Rundschau*, *30*, part 4A, 1939.

Ewing, J., and M. Ewing, Seismic-refraction measurements in the Atlantic Ocean basins, in the Mediterranean Sea, on the Mid-Atlantic Ridge and in the Norwegian Sea, *Bull. Geol. Soc. Am.*, *70* (3), 291–318, 1959.

Gagelyants, A. A., E. I. Galperin, I. P. Kosminskaya, and P. M. Krakshina, The structure of the earth's crust of the central part of the Caspian Sea according to the data of deep seismic sounding, *Doklady Akad. Nauk SSSR*, *123*, no. 3, 1958.

Gamburtsev, G. A., and P. S. Veitsman, The peculiarities of the earth's crust structure in the northern Tien Shan according to SDS data and the comparison with the data on geology, seismology and gravimetry, *Bull. sov. po seismolog.*, *Akad. Nauk SSSR*, no. 3, 1957.

Gamburtsev, G. A., P. S. Veitsman, and J. V. Tulina, The earth's crust structure in the region of the northern Tien Shan according to seismic deep sounding data, *Doklady Akad. Nauk SSSR*, *105*, no. 1, 1955.

Girdler, R. W., The relationship of the Red Sea to the east African rift system, *Quart. J. Geol. Soc. London*, *114*, part 1, 1958.

Gorai, M., On the origin of the diversity of igneous rocks, *J. Geol. Soc. Japan*, *57*, no. 672, 1951.

Gutenberg, B., Low-velocity layers in the earth's mantle, *Bull. Geol. Soc. Am.*, *65*, 337–348, 1954.

Hobbs, W. H., Repeating patterns in the relief and in the structure of the land, *Bull. Geol. Soc. Am.*, *22*, no. 2, 123–176, 1911.

Kennedy, W. Q., and E. U. Anderson, Crustal layers and the origin of magmas, *Bull. volcanol.*, [2] *3*, 1938.

Khain, V. E., On block-wave (fold-block) structure of the earth's crust, *Bull. MOIP, otd. geol.*, XXXIII [4], 1958.

Kosminskaya, I. P., The earth's crust structure according to seismic data, *Bull. MOIP, otd. geol.*, XXXIII [4], 1958.

Kropotkin, P. N., Origin of oceans and continents, *Priroda*, no. 4, 1956.

Kropotkin, P. N., E. N. Lustikh, and N. N.

Povalo-Shveikovskaya, Anomalies of gravity on the continents and oceans and their significance for geotectonics, Izd. MGU, 1958.

Kropotkin, P. N., and E. F. Savarensky (editors), Structure of the earth's crust according to seismic data (series of articles), Inoizdat, Moscow, 1959.

Lovering, J. F., The nature of the Mohorovicic discontinuity, *Trans. Am. Geophys. Union, 39,* no. 5, 1958.

Lubimoba, E. A., Thermal history of the earth with consideration of the variable thermal conductivity of its mantle, *Geophys. J. Roy. Astron. Soc., 1,* no. 2, 1958.

Lustikh, E. N., On Talassogenesis hypothesis and the blocks of the earth's crust, *Izvest. Akad. Nauk SSSR, Ser. Geofiz.,* no. 11, 1959.

Magnitsky, V. A., On the question of origin and the ways of development of continents and oceans, *Problems of Cosmogony,* issue 6, 1955.

Magnitsky, V. A., The earth's inner structure, *Priroda,* no. 7, 1956*a*.

Magnitsky, V. A., On the origin of the transitional layer in the earth's mantle at the depth of 400–900 km, *Izvest Akad. Nauk SSSR, Ser. Geofiz.,* no. 6, 1956*b*.

Magnitsky, V. A., and V. A. Kalinin, The earth's mantle properties and the physical origin of the transitional layer, *Izvest. Akad. Nauk SSSR, Ser. Geofiz.,* no. 1, 1959.

Neprotchnov, V. P., The results of seismic researches on the Black Sea in the region of Anapa, *Doklady Ahad. Nauk SSSR, 121,* no. 6, 1958.

Neprotchnov, V. P., Deep structure of the earth's crust under the Black Sea to the southwest from the Crimea according to seismic data, *Doklady Akad. Nauk SSSR, 125,* no. 5, 1959.

Officer, C. B., J. I. Ewing, R. S. Edwards, and H. R. Johnson, Geophysical investigations in the Eastern Caribbean Venezuelen Basin, Antilles island arc and Puerto Rico trench, *Bull. Geol. Soc. Am., 69,* no. 3, 1957.

Offman, P. E., Tectonics and volcanic tubes of the central part of the Siberian platform, *Tectonica SSSR, IV,* Akad. Nauk SSSR, 1959.

Peive, A. V., General characteristics, classification and location in space of deep faults, 1–2, *Izvest. Akad. Nauk SSSR, Ser. Geol.,* no. 1, 3, 1956.

Reynolds, D. L., A gabbro-granodiorite contact in the Slieve Gullion Area and its bearing on Tertiary petrogenesis, *Quart. J. Geol., Soc. London, 97,* part 1, 1941.

Richey, J. E., *Scotland: the Tertiary Volcanic Districts, British Regional Geology,* Edinbur[gh], 1948.

Ronov, A. B., On the succession of geochem[ical] history of atmosphere and hydrosphere, *G[eo]chemistry,* no. 5, 1959.

Rubey, W. W., Geologic history of sea water, *B[ull.] Geol. Soc. Am., 62,* no. 9, 1951.

Rukhin, L. B., *Principles of General Paleoge[og]raphy,* chapter IX, Leningrad, 1959.

Schmidt, O. Y., *Four Lectures on the Eart[h] Origin,* Izd. 3, Akad. Nauk SSSR, 1957.

Shatsky, N. S., On deep dislocations cover[ing] platforms and folded regions (the Volga reg[ion] and the Caucasus), *Izvest. Akad. Nauk SSS[R] Ser. Geol.,* no. 5, 1948.

Shatsky, N. S., On the origin of the Patchel[ma] depression. Comparative tectonics of ancie[nt] platforms, article 5, *Bull. MOIP, otd. ge[ol.]* XXX [5], 1955.

Shirokova, E. I., Some data on character [of] changes of speeds in the upper layers of t[he] earth's mantle, *Izvest. Akad. Nauk SSSR, S[er.] Geofiz.,* no. 8, 1959.

Shoenmann, Y. M., Platforms, folded belts a[nd] the development of the earth's crust, Tr. VNII[1] geology, vip. 49, Magadan, 1959.

Sonder, R. A., Die Lineamenttektonik und i[hre] Probleme, *Ecl. Geol. Helv., 31,* no. 1, 1938.

Tikhomirov, V. V., On the question of develo[p]ment of the earth's crust and the nature [of] granites, *Izvest. Akad. Nauk SSSR, Ser. Ge[of.]* no. 8, 1958.

Turner, F. J., and J. Verhoogen, *Igneous an[d] Metamorphic petrology,* New York, 1951.

Urey, H. G., *The Planets, Their Origin and De[velopment,* New Haven, 1952.

van Bemmelen, R. W., *The Geology of Indones[ia] Ia.* The Hague, 1949.

van Bemmelen, R. W., Notes sur la géologie et [le] volcanisme d'islande, *Bull. soc. belge géol., 6[4]* part 1, 1955.

Vinogradov, A. P., Meteorites and the earth['s] crust, *Izvest. Akad. Nauk SSSR, Ser. Geol.,* n[o.] 10, 1959*a*.

Vinogradov, A. P., Chemical evolution of th[e] earth, Tchtenia im. V. I. Vernadskogo, 1 *Izves[t.] Akad. Nauk SSSR,* 1955*b*.

Wager, L. R., and W. A. Deer, A dike swarm an[d] crustal flexure in east Greenland, *Geol. Mag[.] 75,* 39–46, 1938.

Wilson, J. T., Geophysics and development o[f] continents, *Priroda* no. 8, 1959.

(Manuscript received August 4, 1960.)

Crustal Reflection of Plane *SH* Waves

NORMAN A. HASKELL

Terrestrial Sciences Laboratory
Geophysics Research Directorate
Air Force Research Division
Bedford, Massachusetts

Abstract. An equation has been derived for the amplitude of the free surface displacement due to plane *SH* waves incident at any angle at the base of a layered crust. Numerical computations have been carried through for the case of a single-layered model of the continental crust. At any given angle of incidence the surface amplitude goes through a series of minima and maxima at periods which, in the single layered case, are harmonically related. At nearly grazing angles of incidence the surface amplitude is relatively small except at periods in the neighborhood of the cutoff periods of the second- and higher-order Love-wave modes.

The results throw some doubt on the 'whispering gallery' effect as an explanation of the mode of propagation of long-period (20 to 30 sec) S waves at S_n velocity.

Applied to the case of an alluvial layer over a hard-rock basement, the theory appears to give an adequate explanation of the abnormally large amplitudes that occur on unconsolidated formations in the epicentral region of earthquakes.

Introduction. The relations between the amtudes of incident and reflected plane body ves of longitudinal and transverse type and displacement of the free surface of a homoeous medium are given in many standard xts. As applied to the reflection of seismic ves at the surface of the earth these relations approximately valid only for wavelengths at are very long compared with the total ickness of the crustal layers. For the periods mmonly observed in seismic body waves the ickness of the crustal layers is far from a gligible fraction of a wavelength, and we may pect that for an incident wave of a given type e surface amplitudes and the partition of rected energy between P and S waves will be rongly dependent on the period as well as on e angle of incidence. Explicit expressions for ese quantities may be readily derived in terms the Thomson matrices [*Thomson*, 1950; *Hasll*, 1953] for a crust composed of any number horizontal, homogeneous layers. However, in e case of incident P and SV waves, numerical mputations, covering all angles of incidence d a sufficiently wide range of periods to be of terest, would be too lengthy to be practicable cept by high-speed machine methods, even for e simplest case of a single-layered crust. The se of incident SH waves is far simpler, since ere is no coupling between different wave types, and for a single-layered crust the computational effort involved is trivial. Nevertheless, this simple case may serve as a guide in the choice of a computational net for more complex cases and is, in addition, of some general interest in its own right. It is therefore taken as the subject of the present paper.

Surface amplitude of SH waves. Following the notation used in a previous paper [*Haskell*, 1953], hereafter referred to as I, we number the crustal layers in sequence from the free surface downward and use subscripts to denote the value of a given quantity in the corresponding layer. Let

v' = displacement amplitude of downward traveling SH waves.
v'' = displacement amplitude of upward traveling SH waves.
v_0 = displacement amplitude at the free surface.
ρ = density.
μ = shear modulus.
$\beta = (\mu/\rho)^{1/2}$ = transverse wave velocity.
d = layer thickness.
p = radian frequency.
c = horizontal phase velocity (= 'apparent' velocity).
$k = p/c$.
$r_\beta = [(c/\beta)^2 - 1]^{1/2}$.
$Q = kdr_\beta$.

The phase velocity, c, is related to the angles of incidence, i_m, in the various layers by Snell's law.

$$c = \beta_1 \csc i_1 = \beta_2 \csc i_2 = \cdots = \beta_n \csc i_n \tag{1}$$

Setting the transverse shear stress at the free surface, $(Y_z)_0$, equal to zero in equation 9.8 of I,[1] we have

$$\begin{aligned} v_n' + v_n'' &= A_{11} v_0 \\ v_n'' - v_n' &= A_{21} v_0 / \mu_n r_{\beta n} \end{aligned} \tag{2}$$

where the A's are elements of the 2×2 matrix formed by taking the product, $A = a_{n-1} a_{n-2} \ldots a_2 a_1$, of the matrices a_m, defined for each layer by

$$a_m = \begin{bmatrix} \cos Q_m & i\mu_m^{-1} r_{\beta m}^{-1} \sin Q_m \\ i\mu_m r_{\beta m} \sin Q_m & \cos Q_m \end{bmatrix} \tag{3}$$

Taking the amplitude of the incident wave in the nth layer, v_n'', as given, reflected wave amplitude, v_n', and the surface amplitude, v_0, are given by equations 2 as

$$v_n'/v_n'' = \frac{\mu_n r_{\beta n} A_{11} - A_{21}}{\mu_n r_{\beta n} A_{11} + A_{21}} \tag{4}$$

$$v_0/v_n'' = \frac{2\mu_n r_{\beta n}}{\mu_n r_{\beta n} A_{11} + A_{21}} \tag{5}$$

The numerator and denominator on the right side of equation 4 are conjugate complex quantities. Hence the amplitudes of the incident and reflected waves are equal in absolute value and differ only in phase, as required by energy conservation.

We now specialize to the case of a single-layered crust by setting

$$A_{11} = \cos Q_1$$

$$A_{21} = i\mu_1 r_{\beta 1} \sin Q_1$$

$$n = 2$$

Equations 4 and 5 become

$$v_2'/v_2'' = \frac{\cos Q_1 - ib \sin Q_1}{\cos Q_1 + ib \sin Q_1} \tag{6}$$

$$v_0/v_2'' = \frac{2}{\cos Q_1 + ib \sin Q_1} \tag{7}$$

[1] The quantity A_{12} in the second of these equations is a misprint which should have been written as A_{21}. The negative sign in equation 9.10 of I is also a misprint; the sign should be positive.

where $b(c) = \mu_1 r_{\beta 1} / \mu_2 r_{\beta 2}$

Let c_1 be the value of the phase velocity which $b = 1$. This is given by

$$c_1^2 = \frac{\rho_2^2 \beta_2^4 - \rho_1^2 \beta_1^4}{\rho_2^2 \beta_2^2 - \rho_1^2 \beta_1^2}$$

The behavior of the absolute value of v_0 as function of frequency is different, depend upon whether c is greater than or less than If $c > c_1$, $b < 1$, and the maxima of $|v_0/v_2''|$ occur at frequencies given by $\cos Q_1 = 0$. T value of $|v_0/v_2''|$ at these maxima is $2/b$. T minima of $|v_0/v_2''|$ occur at frequencies given $\sin Q_1 = 0$, and its value at these minima is If $c < c_1$, $b > 1$, and the maxima of $|v_0/v_2''|$ occur at $\sin Q_1 = 0$, with $|v_0/v_2''|_{\max} = 2$. T minima are at $\cos Q_1 = 0$, with $|v_0/v_2''|_{\min} = 2$

For numerical illustration we consider single-layered crust based on the 'standa African crust' of *Press* [1960]. For the densi of the layer we use the mean density of the tw layered crustal model of Press, and for the she wave velocity we use the average velocity of shear wave propagating vertically through t two layers. The layer thickness is taken as t sum of the thicknesses of the two layers. T parameters are then:

$$\rho_1 = 2.869 \text{ g/cm}^3.$$

$$\beta_1 = 3.635 \text{ km/sec}.$$

$$d_1 = 37 \text{ km}.$$

$$\rho_2 = 3.370 \text{ g/cm}^3.$$

$$\beta_2 = 4.600 \text{ km/sec}.$$

In Figure 1 the quantity $|v_0/2v_2''|$ is shown as function of angle of incidence at the base of th crust, i_2, and the period, $T = 2\pi/ck$, in the for of a contour plot. Since in the absence of crust $v_0/v_2'' = 2$ for all angles and periods, thes contours show the factor by which the presenc of the crust increases or decreases the surfac displacement. The loci of the maxima an minima are given by $\sin 2Q_1 = 0$, which equivalent to

$$T_m = 4d_1 r_{\beta 1}/mc \qquad m = 1, 2, 3, \quad \text{etc.} \tag{10}$$

The values shown in Figure 1 extend to $m = 6$ For shorter periods the spacing of the contour becomes too small to be conveniently plotted o the scale used here.

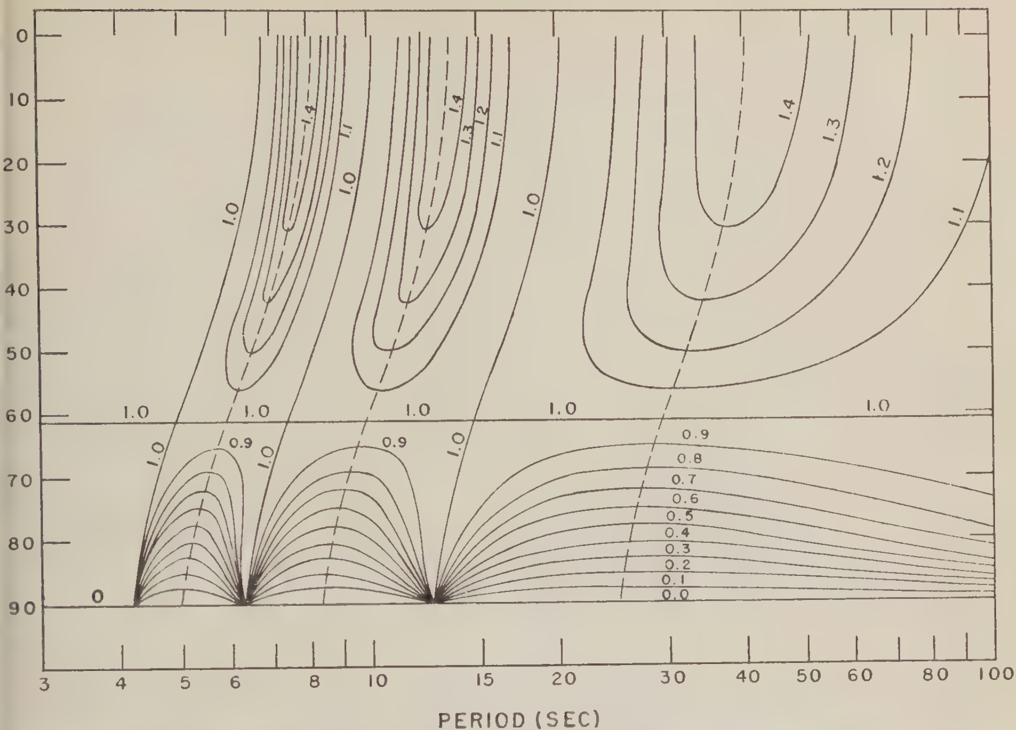

Fig. 1. Surface displacement as a function of period and angle of incidence. Quantity plotted is $|v_o/2v_2''|$.

Along the axis of 90° (grazing) incidence the [illegible]ue of $|v_o/2v_2''|$ is zero for waves of all periods [illegible]ept for those at the singular points where the [illegible]ntours are shown as converging. These points, [illegible]ich are given by equation 10 with $c = \beta_2$ and [illegible]en values of m, are the cutoff periods of the [illegible]ve wave normal modes. In view of the quali[illegible]ive similarity between the dispersion curves [illegible] surface waves of Rayleigh and Love types it [illegible]ems likely that curves showing the effect of [illegible]e crust on the surface displacements caused by [illegible]cident *P* and *SV* waves will exhibit a pattern [illegible]milar to that of Figure 1, but with a some[illegible]hat more complex distribution of minima and [illegible]axima. Pending computations of these more [illegible]mplex cases, it may be of some interest to at[illegible]mpt a few general conclusions on the basis of [illegible]e present simpler case.

'Whispering gallery' propagation. *Press and [illegible]wing* [1955] have suggested that the long-[illegible]eriod *P* and *S* waves that propagate to large [illegible]stances at velocities near those of P_n and S_n [illegible]ay be propagated by repeated reflections at [illegible]early grazing incidence at the base of the crust. Following Rayleigh's discussion of an analagous acoustic problem, they have called this 'whispering gallery' propagation. Figure 1 shows that with such a mode of propagation the surface amplitude of the *SH* component of these waves should be relatively small except at periods in the neighborhood of the cutoff periods of the second and higher Love wave modes. These periods should depend on the thickness and elastic parameters of the crust in the neighborhood of the observing station. For the continental crustal model used here the longest of these periods is 12.48 sec. A similar conclusion may be expected to hold for the *SV* component at periods in the neighborhood of the cutoff periods of the second and higher Rayleigh wave modes. For this crustal model the cutoff period of the second Rayleigh mode has been computed by equation 8.2 of I to be 17.64 sec (compressional wave velocities for the model are taken to be $\alpha_1 = 6.285$, $\alpha_2 = 7.960$ km/sec).

Press and Ewing do not indicate any particular period as characteristic of the S_n group, but state that the periods are generally in the range from

20 to 30 sec. *Caloi* [1953] has also discussed these waves, giving them the designations P_A and S_A and attributing them to channel propagation guided by the Gutenberg velocity minimum in the upper mantle. Caloi gives periods in the range 10 to 30 sec for S_A. The absence of well-defined dominant periods throws some doubt on the whispering gallery effect as an entirely adequate picture of the propagation of these waves, since at periods moderately removed from the cutoff values it seems open to the same objection that may be raised to the channel wave picture, namely, that amplitudes below the crust would have to be very large to produce the observed surface amplitudes. Probably a wholly satisfactory theoretical explanation of these waves will not be possible until normal mode theory has been extended to the point where the effect of the curvature of the earth as well as the variation of velocity within the mantle can be taken into consideration. This has recently been accomplished for very-long-period *SH* waves by *Satô, Landisman, and Ewing* [1960]. Although most of their computations were carried out for longer periods than those of interest here, they noted that a reasonable extrapolation of the group velocity curves for the second and higher modes would pass close to the value of 4.4 km/sec at a period of 20 sec, which would be consistent with observations of S_n.

Amplification by low velocity overburden. At normal incidence ($c = \infty$) the maxima of the quantity $|v_o/2v_2''|$ plotted in Figure 1, occur at periods given by

$$T_m = 4d_1/m\beta_1, \quad m = 1, 3, 5, \quad \text{etc.} \tag{11}$$

At the maxima

$$|v_0/2v_2''| = \rho_2\beta_2/\rho_1\beta_1 \tag{12}$$

For the case considered in the numerical example these maxima are not very large, having the value 1.486. However, applying the theory o[n a] smaller scale and going to an extreme case, [we] might let layer 1 represent an alluvial dep[osit] and regard layer 2 as a granitic or metamor[phic] basement. Average shear wave velocity thro[ugh] the top 100 meters or so of unconsolidated [al]luvium might be around 0.25 km/sec [see, [for] example, the section described in *Dobrin, L[aw]rence, and Sengbush*, 1954]. The density mi[ght] be about 1.7 g/cm³. If the basement had $\rho_2 =$ 2.7, $\beta_2 = 3.5$ km/sec, the maximum surf[ace] amplification factor due to the layer of alluvi[um] would be 22.2. If the layer were 100 meters thi[ck] this maximum would occur at periods of 1[.6,] 0.533, 0.32, 0.229, . . . sec. These periods [are] within the spectral range of the strong moti[on] observed in the epicentral region of earthqua[kes.] The connection with the well-known vuln[er]ability to earthquake damage of structures bu[ilt] on unconsolidated formations seems obvious.

References

Caloi, P., Onde longitudinali e transversali guid[ate] dall' astenosfera, *Atti accad. nazl. Lincei, S[er.] VIII*, 15, 352, 1953.

Dobrin, M. B., P. L. Lawrence, and R. L. Sen[g]bush, Surface and near-surface waves in t[he] Delaware Basin, *Geophysics, 19*, 695–715, 1954.

Haskell, N. A., The dispersion of surface waves [on] multilayered media, *Bull. Seism. Soc. Am.*, [43,] 17–34, 1953.

Press, F., Crustal structure in the California-N[e]vada region, *J. Geophys. Research, 65*, 1039–10[..,] 1960.

Press, F., and M. Ewing, Waves with P_n and [S_n] velocity at great distances, *Proc. Nat'l. Ac[ad.] Sci., 41*, 24–26, 1955.

Satô, Y., M. Landisman, and M. Ewing, Lo[ve] waves in a heterogeneous, spherical earth, [...] Theoretical phase and group velocities, *J. Ge[o]phys. Research, 65*, 2399–2404, 1960.

Thomson, W. T., Transmission of elastic wav[es] through a stratified solid medium, *J. Appl. Phy[s.], 21*, 89–93, 1950.

(Manuscript received September 10, 1960.)

Deformation of an Earth Model by Surface Pressures

L. B. SLICHTER AND MICHELE CAPUTO

Institute of Geophysics, University of California
Los Angeles, California

Abstract. The surface displacements of a spherical earth model consisting of a homogeneous elastic shell enclosing a fluid core are considered, when the surface stress consists of a uniform pressure over equal antipodal circular caps and is zero elsewhere. On the earth, local loads are generally associated with geological structures, ice loads, or the ocean tides. In the present theory, the gravitational effects arising from the deformations are not included—such effects are small when the radius of the loaded area is small.

Values of the surface displacements are listed for four values of the radius of the pressure cap, and for values of the elastic constants which correspond to a simplified representation of *Bullen's* [1947] model. In the shell the elastic constants λ_2 and μ_2 are $14/11 \times 10^{12}$ and 10^{12}, respectively, corresponding to a Poisson's ratio of 0.28. The value of the outer radius of the shell, r_2, is 6.371×10^8 cm; the inner radius, r_1, is $0.545 r_2$. Within the core, $\mu_1 = 0$, and $\lambda_1 \mu_2^{-1} = 8$. The computed results are easily modified for other values of λ_1 and μ_2, provided the value of Poisson's ratio in the shell remains unchanged.

The geophysical implications of the results are discussed.

quations of equilibrium. Elastic problems the sphere and shell have been ussed by *Lamé* [1852], *Lord Kelvin* [1890], *nansi* [1897], *Hoskins* [1920], *Fichera* [1949], many subsequent authors, often with the ect of elucidating questions relating to the avior of the earth under seismic or tidal itations. However, solutions in numerical n for an appropriate earth model with a d core, subject to surface stresses, do not ear to be available. When the applied stresses independent of the longitude ϕ, and the stic parameters λ and μ are constant, the components of displacement u_r, $u_\theta (u_\phi = 0)$ isfy the equilibrium conditions

$$+ 2) \frac{\partial \Delta}{\partial r} - (r^2 \sin\theta)^{-1} \frac{\partial}{\partial \theta}(2r\omega_\phi \sin\theta) = 0, \qquad \gamma \equiv \frac{\lambda}{\mu} \tag{1}$$

$$+ 2)r^{-1} \frac{\partial \Delta}{\partial \theta} + r^{-1} \frac{\partial}{\partial r}(2r\omega_\phi) = 0$$

ere, under the postulated axial symmetry, e dilatation Δ is

$$= r^{-2} \frac{\partial}{\partial r}(r^2 u_r) + (r \sin\theta)^{-1} \frac{\partial}{\partial \theta}(u_\theta \sin\theta) \tag{2}$$

and the curl of the displacement vector has the components

$$2r\omega_\phi = \frac{\partial}{\partial r}(r u_\theta) - \frac{\partial u_r}{\partial \theta} \qquad \omega_\theta = \omega_r = 0 \tag{3}$$

As usual, we shall seek the following type of solutions:

$$u_r = R_1(r, n) P_n(\cos\theta) \qquad u_\theta = R_2(r, n) \frac{\partial P_n(\cos\theta)}{\partial \theta} \tag{4}$$

where P_n is the Legendre polynomial of degree $n(n > 0)$. With these substitutions, equation 1 becomes

$$\begin{aligned} r^2 \ddot{R}_1 + 2r\dot{R}_1 - [(\gamma + 2)^{-1} n(n+1) + 2]R_1 \\ - n(n+1)(\gamma+2)^{-1}[(\gamma+1)r\dot{R}_2 \\ - (\gamma+3)R_2] = 0 \\ r^2 \ddot{R}_2 + 2r\dot{R}_2 - (\gamma+2)n(n+1)R_2 \\ + (\gamma+1)r\dot{R}_1 + 2(\gamma+2)R_1 = 0 \end{aligned} \tag{5}$$

Equations 5 are a special case (for frequency $p = 0$) of an example considered by *Slichter*

[1954] for which the solutions were found to be

$$R_1(r, n) = A_{1,n}r^{n+1} + A_{2,n}r^{-n} + A_{3,n}r^{n-1} + A_{4,n}r^{-n-2} \quad (6)$$

$$R_2(r, n) = B_{1,n}r^{n+1} + B_{2,n}r^{-n} + B_{3,n}r^{n-1} + B_{4,n}r^{-n-2}$$

Equation 5 requires that the constants $A_{i,n}$, $B_{i,n}$ be related as follows:

$$\left.\begin{aligned} B_{1,n} &= \{(n+3)\gamma + n + 5\} \cdot \{(n\gamma + n - 2)(n+1)\}^{-1} A_{1,n} \\ &\equiv K_1(\lambda, \mu) A_{1,n} \\ B_{2,n} &= \{(2-n)\gamma + 4 - n\} \cdot \{[(1+n)\gamma + 3 + n]n\}^{-1} A_{2,n} \\ &\equiv K_2(\lambda, \mu) A_{2,n} \\ B_{3,n} &= n^{-1} A_{3,n} \\ B_{4,n} &= -(n+1)^{-1} A_{4,n} \end{aligned}\right\} \quad (7)$$

The system (5) may also be written in the compact form

$$L\{L\{R_i\}\} = 0, \qquad i = 1, 2 \quad (8)$$

where

$$L\{R_i\} \equiv \left\{\frac{d^2}{dr^2} + \frac{4}{r}\frac{d}{dr} + [2 - (n+1)n]r^{-2}\right\}\{R_i\} \quad (9)$$

This form, in agreement with (6), shows that the constants of material occur in the solutions R_1, R_2 only in the coefficients A_i, B_i. Furthermore, on eliminating Δ and ω_ϕ in the set (5), it is seen that the dilatation and curl of the displacement each satisfies the second-order equation

$$r\frac{d^2 r\begin{pmatrix}\Delta\\ \omega_\phi\end{pmatrix}}{dr^2} - n(n+1)\begin{pmatrix}\Delta\\ \omega_\phi\end{pmatrix} = 0 \quad (10)$$

whose solution is

$$\Delta = [Er^n + Fr^{-n-1}]P_n(\cos\theta)$$
$$\omega_\phi = [Gr^n + Hr^{-n-1}]\frac{\partial P_n(\cos\theta)}{\partial\theta} \quad (11)$$

Boundary conditions. As boundary conditions we require that the displacements and the stresses

$$P_{rr} = \lambda\,\Delta + 2\mu\frac{\partial u_r}{\partial r},$$
$$P_{r\theta} = \mu\left(\frac{\partial u_\theta}{\partial r} - \frac{u_\theta}{r} + \frac{1}{r}\frac{\partial u_r}{\partial\theta}\right) \quad (\text{}$$
$$P_{r\phi} = 0$$

be finite, independent of ϕ, and continuc through the surface of the core of radius and that on the surface of the sphere of rad r_2 the stress equals the applied stress. On th surface $r = r_1$, the shear stresses vanish and th pressure is constant.

The prescribed normal pressure $P(\theta) = -$ on the outer surface is a step function of val P_0 for $0 < \theta < \omega$, $\pi - \omega < \theta < \pi$, and ze elsewhere. This function is represented by t following well-known series:

$$P(\theta, r_2) = P_0[(1 - \cos\omega) + \sum_{n=1}^{\infty}\{P_{2n-1}(\cos\omega) - P_{2n+1}(\cos\omega)\}P_{2n}(\cos\theta)] \quad (13$$

Because of the symmetry of the applied pressur only the even functions, $P_{2n}(\cos\theta)$ occur.

$$P(\theta, r_1) = \text{constant} \quad (13$$
$$P_{r\theta}(\theta, r_2) = 0 \quad (13$$
$$P_{r\theta}(\theta, r_1) = 0 \quad (13$$

On the core boundary the displacements type $u_r(\theta, r_1) = R_1(r_1)P_n(\cos\theta)$, $n > 0$, lead no net change in volume of the core, and th the pressure change at $r = r_1$ contributed b these terms is zero. In the core the pressure independent of θ and is given by

$$P = -\lambda_1\,\Delta = -\lambda_1\left\{\frac{\partial u_r}{\partial r} + \frac{2}{r}u_r\right\}$$

where, in accordance with equation 1, $\partial\Delta/\partial r =$ The required solution of the equation whi leads to a finite pressure at $r = 0$ is

$$u_r = C_{1,0}r, \qquad r < r_1 \quad (1$$
$$P = -3\lambda C_{1,0} \quad (14$$

In the mantle, the corresponding solution is

$$u_r = A_{1,0}r + A_{4,0}r^{-2}, \qquad r_1 \le r \le r_2 \quad (1$$

The boundary conditions

$$\left.\begin{aligned} &\Delta + 2\mu_2 \frac{\partial u_r}{\partial r} \\ &= -P_0(1 - \cos\omega), \qquad r = r_2 \\ &\Delta + 2\mu_2 \frac{\partial u_r}{\partial r} = \lambda_1 \Delta, \qquad r = r_1 \\ &[u_r]_2 = [u_r]_1 , \qquad r = r_1 \end{aligned}\right\} \quad (16)$$

ermine the coefficients $A_{1,0}$, $A_{4,0}$, $C_{1,0}$, and d to the following expression for the constant m $\bar{u}_r$ in the surface displacement

$$\begin{aligned} r_2) &= -r_2\mu_2^{-1}P_0(1 - \cos\omega) \\ &\cdot[3\gamma_1 + 4 + \alpha^3\{2 + 3(\gamma_2 - \gamma_1)\}] \\ &\cdot[(3\gamma_2 + 2)(3\gamma_1 + 4) \\ &- 4\alpha^3\{3(\gamma_2 + 2) - (3\gamma_1 + 4)\}]^{-1} \end{aligned} \quad (17)$$

ere

$$\equiv \lambda_2\mu_2^{-1}, \qquad \gamma_1 \equiv \lambda_1\mu_2^{-1}, \qquad \alpha \equiv r_1r_2^{-1}$$

$$\begin{aligned} n, \omega) &\equiv -\mu_2^{-1}r_2P_0 \\ &\cdot\{P_{n-1}(\cos\omega) - P_{n+1}(\cos\omega)\} \end{aligned}$$

$n > 0$, n even; $S(n, \omega) = 0$ for n odd. Then accordance with equation 6, equation 12, l the four boundary conditions, equations –13d, the coefficients $A_{i,n}$ are determined, in neral (i.e. for n either odd or even), by the ir conditions

$$\left.\begin{aligned} &r_2^{n+1}A_{1,n} + H_2r_2^{-n}A_{2,n} \\ &\quad + H_3r_2^{n-1}A_{3,n} \\ &\quad + H_4r_2^{-n-2}A_{4,n} = S(n, \omega) \\ &K_1 - 1)r_2^{n+1}A_{1,n} \\ &\quad - (1 + (n+1)K_2)r_2^{-n}A_{2,n} \\ &\quad - \frac{2}{n} r_2^{n-1}A_{3,n} + \frac{2}{n+1}A_{4,n} = 0 \\ &r_1^{n+1}A_{1,n} + H_2r_1^{-n}A_{2,n} \\ &+ H_3r_1^{n-1}A_{3,n} + H_4r_1^{-n-2}A_{4,n} = 0 \\ &\bar{K}_1 - 1)r_1^{n+1}A_{1,n} \\ &\quad - (1 + (n+1)\bar{K}_2)r_1^{-n}A_{2,n} \\ &\quad - \frac{2}{n} r_1^{n-1}A_{3,n} \\ &\quad + \frac{2}{n+1} r_1^{-n-2}A_{4,n} = 0 \end{aligned}\right\} \quad (18)$$

Here (see equation 7) a change in sign has been introduced, so

$$\left.\begin{aligned} \bar{K}_i &= -K_i(\lambda_2\mu_2), \\ &\qquad \left(\text{i.e. } -u_\theta = R_2\frac{\partial P_n}{\partial\theta}\right) \\ H_1 &= (\gamma_2 + 2)(n+1) \\ &\qquad + \gamma_2\{2 + n(n+1)\bar{K}_1\} \\ H_2 &= -n(\gamma_2 + 2) \\ &\qquad + \gamma_2\{2 + n(n+1)\bar{K}_2\} \\ H_3 &= 2(n-1) \\ H_4 &= -2(n+2) \end{aligned}\right\} \quad (19)$$

With values of $A_{i,2n}$ determined from (18), the displacements $u_r(r_2, \theta)$ and $u_\theta(r_2, \theta)$ on the outer surface of the sphere are, in accordance with (6),

$$\left.\begin{aligned} &u_r(r_2, \theta) \\ &\quad = \bar{u}_r + \sum_{n=1}^{\infty} P_{2n}(\cos\theta)[R_1(r_2, 2n)] \\ &\qquad\qquad -u_\theta(r_2, \theta) \\ &\quad = \sum_{n=1}^{\infty} \frac{\partial P_{2n}}{\partial\theta}(\cos\theta)[R_2(r_2, 2n)] \end{aligned}\right\} \quad (20)$$

These displacements depend upon the compressibility of the core only through the constant term $\bar{u}_r$. Values of the displacement components computed for four values of the diameter of the pressure cap are presented in the following section.

Computation of displacement.[1] The surface displacements u_r and u_θ were computed with the IBM 709 computer of the Western Data Processing Center, for the model specified in the Abstract. The coefficients $A_{i,n}$ in equation 18 have the following values:

$$A_{1,n} = r_1^{-n-1}\, D^{-1}C_{22} ,$$

$$A_{2,n} = -r_1^{n}\, D^{-1}C_{21}$$

$$\begin{aligned} A_{3,n} = r_1^{-n+1}\, &D^{-1}n[(n\bar{K}_1 - 1) \\ &\cdot(\alpha^{-2n-3} - 1)C_{22} + [(n+1)\bar{K}_2 + 1] \\ &\cdot(\alpha^{-2} - 1)C_{21}]\{2(n-1)(\alpha^{-2n-1} - 1)\}^{-1} \end{aligned} \quad (21)$$

[1] Michele Caputo is the sole author of the remainder of this paper.

TABLE 1. Displacements in Millimeters for Pressure 10^6 dyne/cm². (1 bar). ω = half cone angle of pressure cap at earth's center, d = diameter of cap, θ = polar angle from axis of symmetry.

	$\omega = 4°$		$\omega = 8°$		$\omega = 16°$		$\omega = 25°$	
θ	$-u_r$	u_θ	$-u_r$	u_θ	$-u_r$	u_θ	$-u_r$	u_θ
0°	354	0	751	0	1640	0	2681	0
	342	−10	743	−6	1638	3	2678	11
	327	−17	732	−11	1633	4	2674	22
	298	−29	722	−16	1625	7	2666	33
	230	−35	701	−22	1613	9	2655	44
5°	168	−28	671	−29	1598	10	2642	55
	139	−20	639	−35	1580	12	2625	65
	122	−15	588	−44	1558	13	2605	76
	107	−11	503	−48	1531	14	2583	86
	97	−8	421	−39	1501	15	2557	96
10°	89	−6	374	−27	1465	15	2528	106
	82	−4	342	−19	1425	15	2496	115
	76	−2	313	−12	1381	14	2460	124
	71	−1	290	−6	1326	12	2421	132
	67	0	272	−1	1266	11	2378	140
15°	63	1	254	4	1191	6	2333	148
	59	2	239	7	1080	5	2283	155
	56	3	226	11	971	18	2229	162
	53	4	213	14	898	35	2172	168
	50	4	202	16	839	47	2109	172
20°	48	5	192	19	785	59	2041	177
	45	5	181	21	739	69	1970	180
	43	6	172	23	696	78	1887	182
	41	6	163	25	657	87	1800	185
	39	7	154	27	621	94	1697	183
25°	37	7	146	28	585	101	1558	186
	35	8	138	30	553	108	1419	201
	33	8	131	31	522	113	1318	221
	31	8	123	32	491	119	1231	236
	29	9	116	33	463	124	1148	250
30°	27	9	109	34	435	128	1075	263
	26	9	103	35	409	132	1005	274
	24	9	96	36	383	136	938	285
	23	9	90	37	357	139	876	294
	21	10	84	38	333	142	815	303
35°	19	10	78	38	310	145	757	311
	18	10	72	39	286	147	702	317
	16	10	66	40	264	150	647	323
	15	10	61	40	242	151	595	329
	14	10	55	41	221	153	544	333
40°	12	10	50	41	200	155	495	337
	11	10	45	41	180	150	447	340
	10	10	40	41	160	157	400	343
	9	11	35	42	141	157	355	345
	7	11	30	42	122	158	311	347

	$\omega = 4°$		$\omega = 8°$		$\omega = 16°$		$\omega = 25°$	
θ	$-u_r$	u_θ	$-u_r$	u_θ	$-u_r$	u_θ	$-u_r$	u_θ
45°	6	11	25	42	104	158	267	[illegible]
	5	11	21	42	86	158	226	[illegible]
	4	11	16	42	68	158	185	[illegible]
	3	11	12	41	52	158	145	[illegible]
	2	10	8	41	35	157	107	[illegible]
50°	1	10	4	41	19	156	69	[illegible]
	0	10	−1	41	3	155	33	[illegible]
	−1	10	−4	41	−12	154	−3	[illegible]
	−2	10	−8	40	−26	153	−38	[illegible]
	−3	10	−12	40	−41	151	−71	[illegible]
55°	−4	10	−15	39	−55	149	−104	[illegible]
	−5	10	−19	39	−68	147	−135	[illegible]
	−6	10	−22	38	−81	145	−166	[illegible]
	−6	9	−25	37	−94	143	−196	[illegible]
	−7	9	−28	37	−106	140	−224	[illegible]
60°	−8	9	−31	36	−118	137	−252	[illegible]
	−9	9	−34	35	−129	135	−279	[illegible]
	−9	9	−37	35	−140	132	−304	[illegible]
	−10	9	−40	34	−151	128	−329	[illegible]
	−11	8	−42	33	−161	125	−353	[illegible]
65°	−11	8	−45	32	−170	121	−376	[illegible]
	−12	8	−47	31	−180	118	−398	[illegible]
	−12	8	−49	30	−189	114	−419	[illegible]
	−13	7	−52	29	−197	110	−440	[illegible]
	−14	7	−54	28	−205	106	−459	[illegible]
70°	−14	7	−56	27	−213	102	−477	[illegible]
	−15	6	−57	26	−220	97	−495	[illegible]
	−15	6	−59	24	−227	93	−511	[illegible]
	−15	6	−61	23	−234	88	−527	[illegible]
	−16	6	−62	22	−240	84	−542	[illegible]
75°	−16	5	−64	21	−246	79	−555	[illegible]
	−16	5	−65	19	−251	74	−568	[illegible]
	−17	5	−67	18	−256	69	−580	[illegible]
	−17	4	−68	17	−261	64	−591	[illegible]
	−17	4	−69	16	−265	59	−602	[illegible]
80°	−18	4	−70	14	−269	54	−611	[illegible]
	−18	3	−71	13	−273	49	−619	[illegible]
	−18	3	−72	11	−276	44	−627	9
	−18	3	−72	10	−279	38	−633	8
	−18	2	−73	9	−281	33	−639	[illegible]
85°	−19	2	−73	7	−283	27	−644	[illegible]
	−19	1	−74	6	−285	22	−648	[illegible]
	−19	1	−74	4	−286	17	−651	[illegible]
	−19	1	−74	3	−287	11	−653	[illegible]
	−19	0	−75	1	−288	0	−655	[illegible]
90°	−19	0	−75	0	−288	0	−655	

$$= r_1^{n+2} D^{-1}(n+1)[(n\bar{K}_1 - 1)$$
$$(1-\alpha^2)C_{22} + [(n+1)\bar{K}_2 + 1]$$
$$(1-\alpha^{2n-1})C_{21}]\{2(n+2)(1-\alpha^{2n+1})\}^{-1}$$
$$(C_{11}C_{22} - C_{12}C_{21})S^{-1}(n, \omega), \quad \alpha = r_1 r_2^{-1}$$
$$= [(\gamma_2 + 2)(n+1)$$
$$2\gamma_2 + \gamma_2 n(n+1)\bar{K}_1]\alpha^{-n-1}$$
$$(n\bar{K}_1 - 1)[n(\alpha^{-2n} - \alpha^3)$$
$$(n+1)(\alpha - \alpha^3)]\{\alpha^{-n+1} - \alpha^{n+2}\}^{-1}$$
$$= [-n(\gamma_2 + 2)$$
$$2\gamma_2 + \gamma_2 n(n+1)\bar{K}_2]\alpha^n$$
$$[(n+1)\bar{K}_2 + 1][n(\alpha^{-n+1} - \alpha^{-n-1})$$
$$(n+1)(\alpha^{-n+1} - \alpha^n)]\{\alpha^{-2n-1} - 1\}^{-1} \qquad (22)$$
$$= (\gamma_2 + 2)(n+1) + 2\gamma_2$$
$$\gamma_2 n(n+1)\bar{K}_1 - (n\bar{K}_1 - 1)[n+1$$
$$2n+1)(\alpha^{-2n-3} - 1)\{\alpha^{-2n-1} - 1\}^{-1}]$$
$$= -(\gamma_2 + 2)n$$
$$2\gamma_2 + \gamma_2 n(n+1)\bar{K}_2$$
$$[(n+1)\bar{K}_2 + 1][n+1$$
$$(2n+1)(\alpha^{-2n-2} - 1)\{\alpha^{-2n-1} - 1\}^{-1}]$$

, as noted, only the even coefficients, of $A_{i,2n}$, will enter.

ıe series in equation 20 were truncated after Legendre polynomial of order 140. The rence between the true step function and pproximation so obtained is less than $0.03A$ ere A is the amplitude of the step), except in the interval of width $\pm 1°$ around $\vartheta = \omega$, re the step function decreases from A to zero. he tabulated values of u_r correspond to the e $\gamma_1 = 8$. For other values $\gamma_1 = \gamma_1'$ (with γ_2 l $= 14/11$), we add to each tabulated value $_r$ the constant

$$= P_0 r_2 \mu_2^{-1}(\gamma_1' - 8)(0.0137) \cdot (1 + 0.9932\gamma_1')^{-1}(1 - \cos\omega) \qquad (23)$$

value u_θ remains unchanged.

eophysical implications of present results. The artifice of using a second pressure cap the antipode appears to imply unrealistic l distributions. In reality, however, the ant second cap introduces only minor rmations in the vicinity of the first, when se caps are of moderate size. At the equator, for example, each cap contributes equally to the radial displacement, which is small relative to that at the poles. Specifically, the ratios $-\frac{1}{2}\, u_r(90°)/u_r(0°)$ are 0.027, 0.050, 0.088, and 0.122, respectively, for the four cap sizes. (2) The magnitude of the maximum vertical elastic displacement caused by a uniform ice cap of thickness H cm (producing a pressure $\rho g H$) is readily estimated for the several cap sizes considered. For a cap 900 km in diameter the elastic displacement is 0.03 H; for a cap 1800 km in diameter it is about 0.065 H. For caps of large diameter the gravitational effects reduce the displacements significantly. Therefore, for $\omega = 16°$ and $\omega = 25°$, Tables 1 and 2 indicate only the upper limits for the true displacements. (3) In the observation of earth tides, gravity variations are now being measured with a least scale value of 1/10 microgal. At this level of sensitivity, fluctuations in atmospheric pressure introduce several direct and indirect types of influence upon the gravimeter readings. One such disturbance arises from the local yielding of the earth caused by a passing barometric high or low. It is well known that the double amplitude of the semidiurnal earth tide is about 30 to 35 cm. The amplitude of the earth deformation produced by a change of 1 per cent in barometric pressure on an area 900 km in diameter is, according to Table 1, 0.354 cm. Thus, on such an area, a 1 per cent change in barometer produces about 1 per cent of the yielding associated with the major lunar tide;

TABLE 2. Displacements for Additional Values of θ near Edge of Pressure Disk

$\omega = 4°$			$\omega = 8°$		
θ	$-u_r$	u_θ	θ	$-u_r$	u_θ
1.5°	334	−13	5.5	655	−32
2.5	317	−23	6.5	618	−39
3.5	268	−33	7.5	550	−47
4.5	195	−32	8.5	458	−45
5.5	150	−23	9.5	394	−32
6.5	131	−17	10.5	358	−23
$\omega = 16°$			**$\omega = 25°$**		
θ	$-u_r$	u_θ	θ	$-u_r$	u_θ
13.5	1296	12	22.5	1844	184
14.5	1233	9	23.5	1752	184
15.5	1139	4	24.5	1631	183
16.5	1021	10	25.5	1485	192
17.5	930	27	26.5	1365	211
18.5	868	41	27.5	1274	229

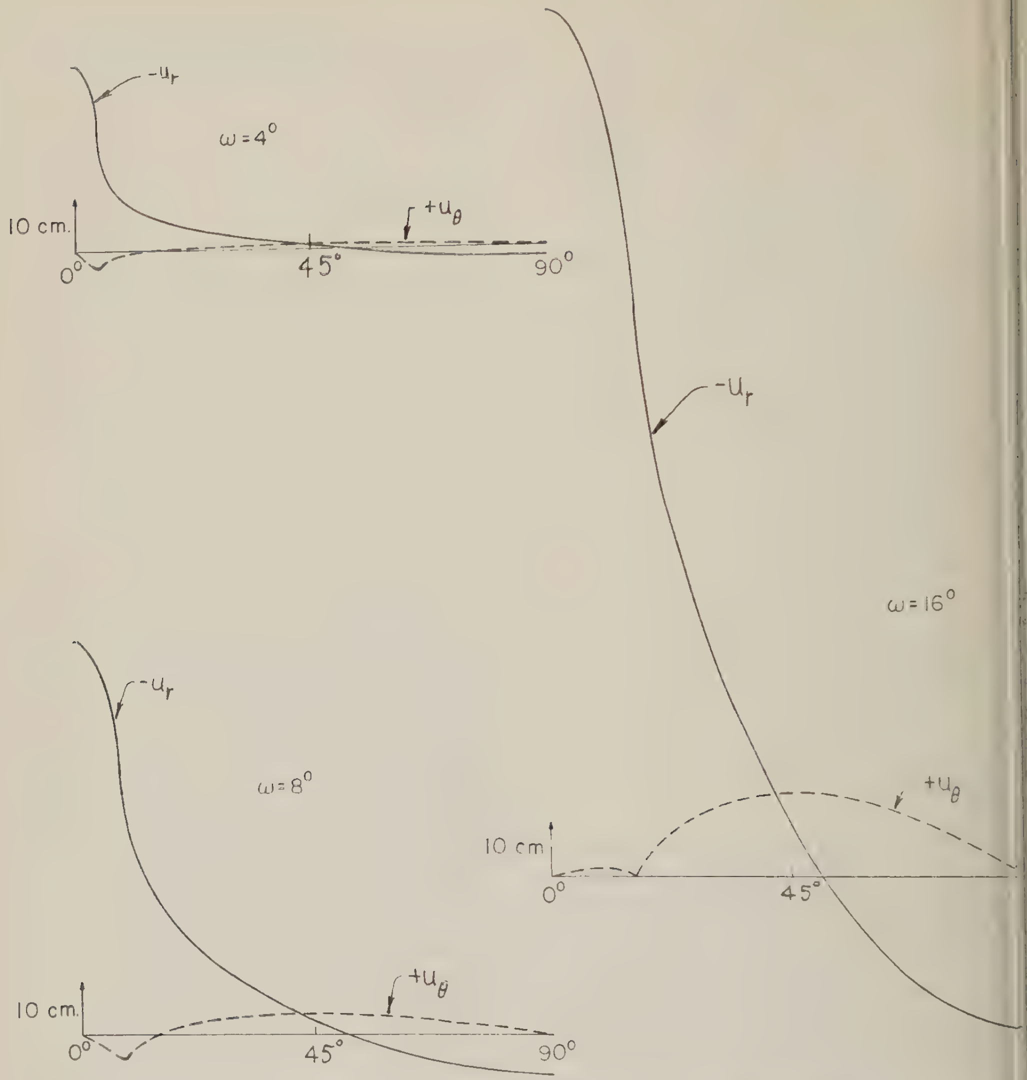

Fig. 1. Radial and tangential displacements on the surface of the earth for $\omega = 4°, 8°, 16°$ for a pressure of 10^6 dyne/cm² (1 bar).

similarly, a 1 per cent change over an area 1800 km in diameter produces a deflection of magnitude 2 per cent that is commonly associated with the major solid earth tide.

References

Almansi, E., Sulla deformazione della sfera elastica, *Rend. Acc. Naz. Lincei*, 6, serie 5, fasc. 7, 61–64, 1897.

Bullen, K. E., *An Introduction to the Theory of Seismology*, Cambridge Univ. Press, 1947.

Fichera, G., Sul calcolo delle deformazioni, dotate di simmetria assiale, di uno strato sferico elastico, *Rend. Acc. Naz. Lincei*, 6, serie 8, fasc. 5, 582–589, 1949.

Hoskins, L. M., The strain of a gravitating sp of variable density and elasticity, *Trans. Math. Soc.*, 1–43, 1920.

Kelvin, Lord, Dynamical problems regarding tic spheroidal shells and spheroids of inc pressible liquid. *Math. and Phys. Papers*, C bridge Univ. Press, vol. 3, 351–386, 1890.

Lamé, G., Leçons sur la theorie mathématiqu l'elasticité des corps solides, Paris, 1852.

Slichter, L. B., Seismic interpretation theory an elastic earth, *Proc. Roy. Soc. London, A*, 43–63, 1954.

Thomson, W., and P. G. Tait, *A Treatise Natural Philosophy*, Oxford Press, 834–838, I

(Manuscript received June 30, 1960; revis September 14, 1960.)

NAL OF GEOPHYSICAL RESEARCH VOLUME 65, NO. 12 DECEMBER 1960

Energy Loss Associated with Impact of Steel Spheres on Rocks

MICHEL AUBERGER AND JOHN S. RINEHART

Mining Research Laboratory, Department of Mining Engineering
Colorado School of Mines, Golden, Colorado

Abstract. The coefficient of restitution for impact between steel spheres and plexiglas, and between steel spheres and nine different rocks has been measured: granite, sandstone, limestone, and six marbles. The energy loss associated with the impact has been studied as a function of the sphere diameter, particularly for three diameters: 1/8 in, 1/32 in, and 1/64 in. Such a study permits a correlation with attenuation of shear wave as a function of frequency in the frequency range of 30 to 240 kc/sec. Attenuation has been found to be strongly dependent on the main constituents of the rocks, their grain size, and the nature and size of their intergranular particles. Attenuation increases with the number of grain boundaries per unit volume and is lowered when the intergranular cement is made up of grains a few microns thick. Shear attenuation is several times larger than longitudinal attenuation in most of the rocks tested.

INTRODUCTION

mong the several kinds of energy sources l in seismological or geophysical experiments he field, heavy balls or weights dropped to ground are frequently employed.

eismologists and geophysicists are mainly cerned with the elastic properties of rocks, generation of elastic waves, and the measnent of longitudinal velocities in rocks. In direction numerous Japanese seismologists e studied the impact of spheres on rocks. *ahara* [1954] dropped steel balls on rocks to estigate the mechanism of generation of elasvaves. In the Soviet Union, *Ozerskaya* [1955] *Kalinina* [1958] tried to correlate the coeffit of restitution with the velocity of propaon of elastic waves in rocks.

is of some importance, however, to point that the coefficient of restitution depends only on the elastic constants of the material ed but also on its attenuation properties and not only longitudinal waves but also shear surface waves are involved in impact.

he purpose of the present work is to sumize the different factors on which the coeffit of restitution depends and to show how, a simple and convenient method, it is sible to get information on the physical perties of a material under high rates of ling.

THE COEFFICIENT OF RESTITUTION

he concept of coefficient of restitution arises onjunction with the collision of two bodies in an impact characterized by a short duration of contact and high transient stresses. The coefficient of restitution is the ratio of the relative normal velocity component after impact to that before collision.

In the general case of two bodies of different shapes and of different initial velocities, the coefficient of restitution depends on the shape of the bodies, their masses, their initial relative normal velocities, their elastic moduli, their radii of curvature at the contact point, and their attenuation properties [*Goldsmith*, 1952].

Mathematically, three particular cases have been of interest: the case of two spheres, extensively treated theoretically and experimentally during the last century and the beginning of the present century; the case of two longitudinal bars, studied by *Saint-Venant* [1867]; and the case of a sphere impinging normally upon the free surface of a semi-infinite solid.

In this last case (which is the only one studied here), the coefficient of restitution can be defined as the ratio of the velocity of the sphere after impact to that before collision. During the impact the sphere loses some kinetic energy ΔE_o, the initial kinetic energy E_o being $\frac{1}{2} mv_0^2$, where m is the mass of the sphere, and v_0, its initial velocity.

If we assume a maximum stress below the elastic limit and no fractures, the energy loss ΔE_o will be made up of two principal parts: the vibrational energy of colliding bodies and the work of plastic deformation.

The energy balance is: E_o, initial kinetic en-

ergy, equals the bulk of energy of motion of the rebouncing sphere plus ΔE_e, with ΔE_e equal to $(1 - e^2)\, E_e$.

The energy loss due to the impulse communicated to the atmosphere by the sudden reversal of the motion of the sphere is negligible for low initial velocities of impact [*Banerji*, 1916, 1918].

Hertz [1896] and *Love* [1934] treated mathematically the contact of two perfectly elastic bodies, but they did not take into account the dissipation of energy. In Hertz's theory three main assumptions are made:

1. The elastic state of the two bodies near the point of impact during the whole duration of impact is very nearly the same as the state of equilibrium which would be produced by the total pressure existing at any instant between the bodies, if the pressure acted for a long time. The deformation is regarded as static.

2. The duration of impact is large compared with the time taken by elastic waves to traverse the impinging bodies. The bodies move practically as rigid bodies except in the immediate neighborhood of the region of contact and no vibrational energy is generated.

3. The stresses set up do not transcend the limits of perfectly elastic recovery; there is no work of plastic deformation.

Hertz gave formulas for the duration of impact, the radius of the surface of contact, and the maximum pressure at the center of impact. Many experimenters [*Tillett*, 1954; *Broberg*, 1956] have verified the validity of Hertz's law for duration of impact on real materials. The radius of the surface of contact is proportional to the radius of the ball dropped. The maximum pressure at the center of impact is independent of the radius of the ball. In all our experiments the stress level will be the same.

The first part of the energy loss, the vibrational energy of colliding bodies, has been studied by many authors. *Lord Rayleigh* [1906] showed that in the case of two impinging spheres the proportion of translational energy transformed into energy of vibration is negligibly small over a considerable range of initial velocities. *Raman* [1920] studied the case of a sphere impinging on a plate and showed how the proportion of energy of impact transformed into energy of elastic wave-motion may be approximately calculated; he gave a semiempirical formula for the variation of the coefficient of restitution with the thickness of the plate. Z [1941] developed a theory which provide much better fit to the data published by Ram He applied this theory to the elastic normal pact of spheres with plates so large that impact is over before the return of waves flected from the boundaries, and he gave a mula for the coefficient of restitution as a fu tion of the parameters of the impact. *Ti* [1954] confirmed Zener's theory experiment for the variation of the coefficient of rest tion with the velocity of impact and with thickness of the specimen. *Hunter* [1957] ca lated the absorption of vibrational energy in form of elastic waves generated by a trans localized force acting normally to the free face of a semi-infinite solid. The result is ap to the Hertzian collision of a small body the plane surface of a massive specimen. H concluded that, for impact velocities small co pared with the propagation velocity of ela waves in the specimen, a negligible propor of the original kinetic energy of the small b (less than 1 per cent) is transferred to specimen by the collision. This proportion independent of the radius of the small sph Thus we shall consider the energy loss due to vibrational energy as being negligible within accuracy of our experiments.

Very little theoretical work has been done the more important part of the energy loss— work of plastic deformation. More than 99 cent of the original kinetic energy of the sph is temporarily stored in the large plate as ela strain energy. The partition of energy betw shear and dilatation is given approximately *Tillett* [1954]. For a Poisson's ratio of 0.4 per cent of the energy stored is dilatational 84 per cent is shear. For Poisson's ratio of 30 per cent is dilatational and 70 per cent shear. This energy loss exists even at very stresses for any real material and is due to anelasticity of the material, depending on rate of loading.

In our experimental investigations of physical properties of plexiglas and rocks, varied only the diameter of the steel b The maximum stress is constant, accor to Hertz, and the duration of impact is p portional to the radius of the sphere; co quently, the rate of loading increases when radius decreases.

Experimental Work

ıe coefficient of restitution of a ball bounc- n a plate was obtained by measurement of neight to which the ball rebounded when ped from a known height: $e^2 = h_1/h_0$ if h_1 e height to which the ball rebounds when ped from a height h_0. The motion of the made to shine by a spotlight, was recorded graphically with a Polaroid camera.

r plexiglas the ball was dropped from an omagnet suspended at a height of 20 cm, the coefficient of restitution was measured for the first bounce so that the measure- s were done for a constant striking velocity 0 cm/sec. For rocks, the ball was dropped and, several successive bounces being re- d. An average value for the coefficient of ution corresponding to impact velocities be- n 200 cm/sec and 100 cm/sec was com- l. In this range of impact velocity the co- ent of restitution did not vary significantly. e maximum stress calculated approximately Hertz's formula ranged from 1 to 5 kg/cm², independent of the size of the balls.

ecision ball bearings of chrome steel in nine ent sizes were used: 1/2 in, 7/16 in, 9/32 in, in, 1/8 in, 1/16 in, 1/32 in, 1/64 in, and mm. The small balls were cleaned with ne. The maximum sphericity tolerance was 004 inch (1/8 in = 3176 μ, 1/32 in = , 1/64 in = 397 μ).

ıe thicknesses of the plates ranged from 2.2 o 14 cm. Except for the limestone, which 2.2 cm thick, the material could be consid- to be infinitely thick for the balls less than nch in diameter. For limestone the value of coefficient of restitution is extrapolated to cm/sec on the curve that shows coefficient stitution e as a function of striking velocity. the rock surfaces were carefully polished, the experiments were done at room tem- ture.

Description of the Results

lts for Plexiglas

gure 1 shows variation of e^2 with the strik- velocity in the range 1.5 to 2.5 m/sec for different sizes of balls. If we assume a ght line from 300 cm/sec to 0, the variation is about 2 per cent, which corresponds well the variation found by *Tillett* [1954].

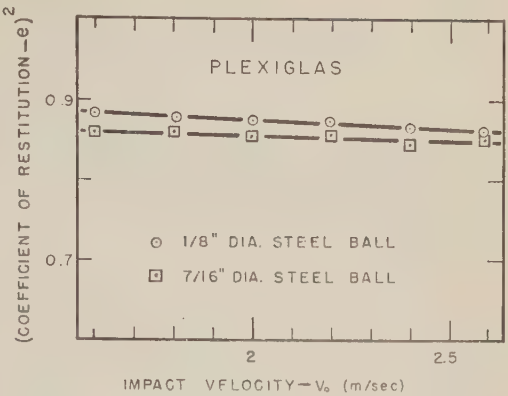

Fig. 1. Variation of the square of the coefficient of restitution with the impact velocity for steel balls striking plexiglas. Two sizes of balls.

Figure 2 shows the fractional energy loss as a function of the inverse of the diameter of the ball for six different sizes of ball. For a 1/2-inch ball, the elastic wave set up in the plate comes back to the ball during the impact and there is also a flexural effect; therefore this value cannot be compared with the other values. The fractional energy loss increases very rapidly as the diameter of the ball decreases.

Results for Rocks

Nine different rocks, including six types of marble, have been tested. The behavior of the several rocks, shown in Figures 3, 4, 5, 6, and 7, is very different, because of the great variety of

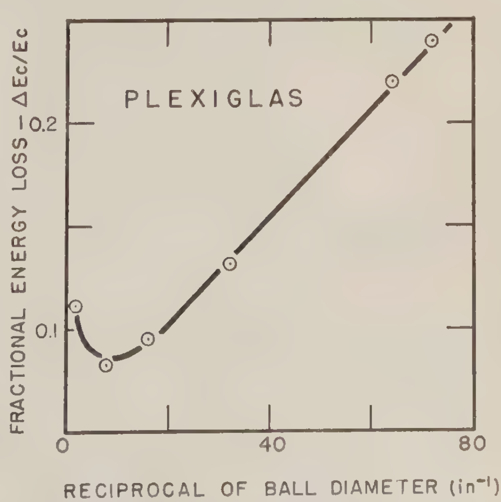

Fig. 2. Fractional energy loss in plexiglas versus reciprocal of ball diameter.

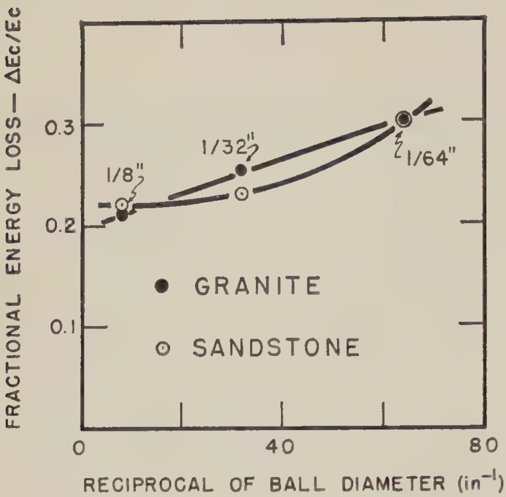

Fig. 3. Fractional energy loss in granite and standstone versus reciprocal of ball diameter.

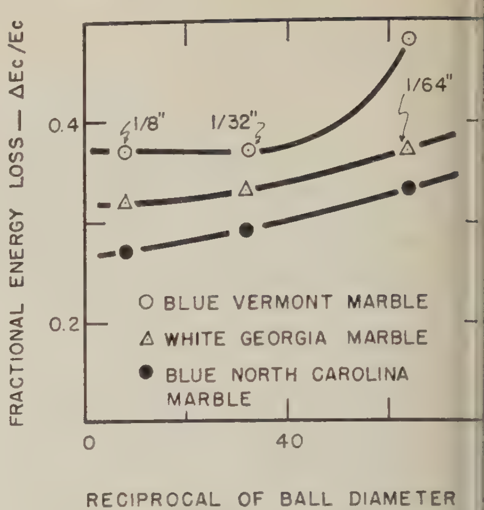

Fig. 5. Fractional energy loss in Nor Carolina marble, blue Vermont, and wh Georgia marbles versus reciprocal of ball ameter.

the rocks, especially in composition, in grain size, and in the nature of the intergranular cement. Only three rocks show a decrease of fractional energy loss with the inverse of the size of the ball, while six show an increase.

For all the rocks, the coefficient of restitution given is an average value, a value probably a little lower than the true value, the difference between the two being about ±5 per cent. The measured value probably is substantially the average of the respective coefficients of the different constituents of the rock.

In red sandstone, the 7/16-inch diameter tested on a specimen 14 cm thick gives the value for e as the 1/8-inch ball. In limestone results for the 1/8-inch and 1/32-inch ball well grouped, but the results for the 1/64 balls are scattered. In blue Vermont marble 1/16-inch ball gives the same value for e a 1/8-inch ball, indicating a constancy of the efficient of restitution for all the balls ran between 1/8 inch and 1/32 inch. In white C

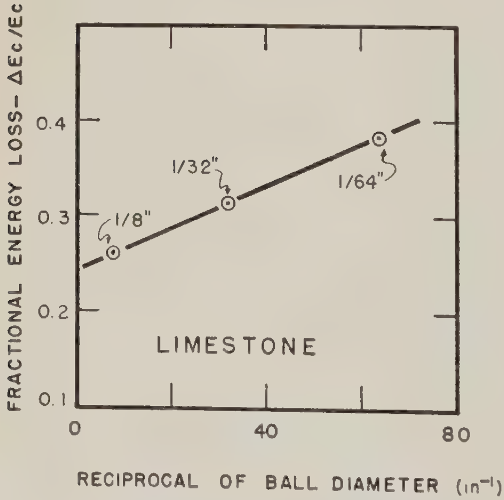

Fig. 4. Fractional energy loss in limestone versus reciprocal of ball diameter.

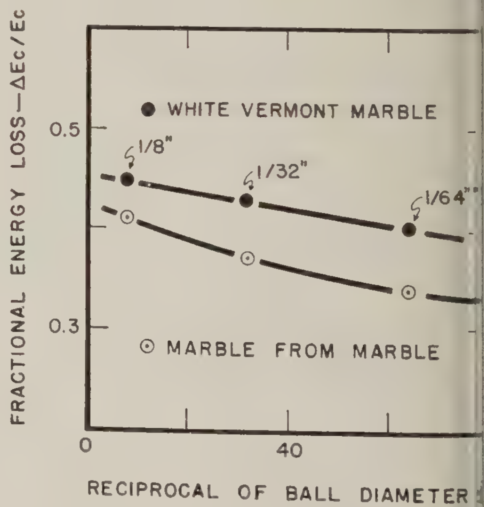

Fig. 6. Fractional energy loss in white C orado marble and Vermont marbles ver reciprocal of ball diameter.

TABLE 1. Petrographic Analysis of the Rocks

Rock	Composition: Mineral	Composition: Volume Percentage	Average Grain Size, μ	Remarks
ce granite, Estes k, Colo.	Quartz	20–25		
	Microcline	45–50		
	Plagioclase	10–15		
	Biotite	8–10		
	Muscovite	1	612	
	Zircon	Trace		
	Magnetite	0.5–1		
	Apatite	0.5–1		
sandstone, ation unknown	Quartz	95.6		The cementing material holding the grains together is silica and to some extent the iron oxide stain. There is very little cement between individual grains and any cement present constitutes what can be called a thin intergranular film. Rock is porous.
	Orthoclase	1.6	155	
	Plagioclase	2.3		
	Iron oxide stain, hematite, and limonite	0.5	...	
	Kaolinite			
	Illite			
as bituminous silty estone, Silverdale, ns.	Calcite	85	19	The silt and the clay contain the following elements: sodium, potassium, calcium, magnesium, iron, titanium, and traces of barium and strontium. Rock is very compact.
	Silt			
	Illite			
	Bituminous or asphaltic material	15	...	
Creek Marble, rble, Colo.	Calcite		527	Only a trace of impurities.
Vermont marble, een Mountain, Vt.	Calcite	98.8	234	
	Quartz and feldspar	1.1	...	
	Muscovite	0.1	...	
e Vermont marble, een Mountain, Vt.	Calcite	98.2	190	
	Quartz and feldspar	1.2	60	
	Muscovite	0.6	...	
e Georgia marble, te, Georgia	Calcite	97.9	1,093	
	Quartz and feldspar	0.9	...	
	Muscovite	0.1	...	
	Actinolite	0.9	...	
	Zircon (detrital)	0.1	...	
North Carolina rble, Marble, N. C.	Calcite	96.6	278	
	Pyrite, hematite, and a trace of chalcopyrite	3.4	8	
Georgia marble, te, Ga.	Calcite	93.8	850	
	Quartz and feldspar	2.5	...	
	Phlogopite	3.4	122 (width) 917 (length)	
	Epidote	0.3	...	
	Zircon (detrital)	0.1	...	

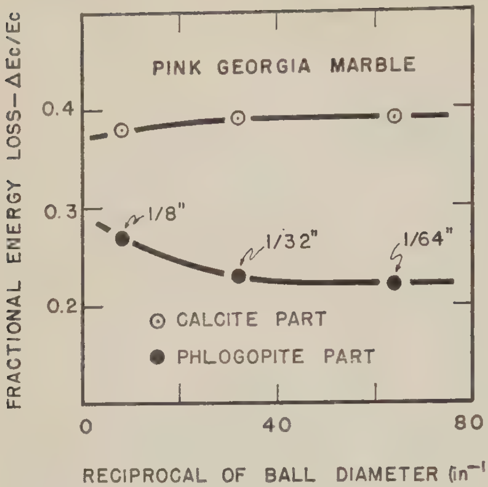

Fig. 7. Fractional energy loss in pink Georgia marble versus reciprocal of ball diameter.

gia marble the results are very scattered. The pink marble from Georgia shows two different coefficients of restitution for its two distinct parts. In the part containing mainly phlogopite the energy loss decreases with the inverse of the size of the ball, whereas in the part containing mainly calcite and no phlogopite the coefficient of restitution remains constant.

The polished surface of each rock was inspected with a stereoscopic microscope after the impact. The white marbles from Vermont and Marble, Colorado, and the granite, to a lesser extent, showed small cracks at the impact areas, the minerals probably being fractured at the surface by shear forces. The energy dissipated in these fractures, probably proportional to the

TABLE 2. Size Distribution of Red Sandstone Grains

Size Range, μ	Numerical Percentage	Cumulative Numerical Percentage
0–50	2.1	2.1
50–100	5.2	7.3
100–150	8.3	15.6
150–200	27.1	42.7
200–250	28.1	70.8
250–300	15.6	86.4
300–350	6.3	92.7
350–400	3.1	95.8
400–450	3.1	98.9
450–500	1.0	99.9

area of contact or to the square of the radiu[s of] the ball, is expected to be negligible for [the] smaller sizes, 1/32 inch and 1/64 inch.

The identification, modal analysis, and average grain size for all rocks are given [in] Table 1. The size distribution of grains in [the] red sandstone is given in Table 2.

In addition, the longitudinal velocities g[iven] in Table 3 have been measured with the p[ulse] technique described by *Hughes, Pondrom,* [and] *Mims* [1949]. The use of barium titanate cer[am]ics for transducers with a 70 volt square p[ulse] gives a stress of approximately the same inte[nsity] as that of the ball impacts. The resonance fre[]quency of the transducers was 500 kc/s.

TABLE 3. Longitudinal Wave Velocity in the Rocks

Rock	Measured Longitudinal Velocity, m
Biotite granite (Colo.)	4200
Red sandstone	4300
Bituminous silty limestone	5300
Marble (Marble, Colo.)	4300
Blue marble (Vermont)	4100
White marble (Vermont)	3500
White marble (Georgia)	3800
Blue marble (North Carolina)	5600
Pink marble (Georgia)	5000

Discussion of the Results

Plexiglas

The fractional energy loss is mainly du[e to] attenuation of the shear wave, since 84 per [cent] of the energy stored is shear energy. As has [been] shown by Tillett, the fractional energy lo[ss is] the logarithmic decrement at an 'equivalent [fre]quency' equal to the reciprocal of twice the [time] of contact. The time of contact T_H is given [by] Hertz's formula:

$$T_H = 2.94R/v_0^{1/5}[5/4\pi\rho_1(1/E_1' + 1/E_2' \ldots$$

where R is the radius of the ball; v_0 is the [im]pact velocity; ρ_1 is the density of the steel; $E_1' = E_1/(1 - \gamma_1^2)$; and $E_2' = E_2/(1 - \gamma_2^2)$ (γ_1, E_1 and γ_2, E_2 are Poisson's ratio and You[ng's] modulus of the materials of the ball and p[late], respectively).

For a 1/8-inch ball in plexiglas, T_H is equ[al to] 34.3 μ sec so that the 'equivalent frequen[cy']

sponding to a 1/8-inch ball, a 1/32-inch and a 1/64-inch ball are 15, 60, and 120 respectively.

e increase of attenuation with observed ency corresponds well with the increase ved by *Rinehart* [1941] in the same fre-cy range, although Rinehart measured only ongitudinal decrement. The linearity of the ase would mean that plexiglas in this fre-cy range behaves more as a Voigt solid than Maxwell solid.

s

otite granite and sandstone. The fractional gy losses in granite and sandstone are nearly same for the 1/8-inch ball, being 0.21 for ite and 0.22 for the sandstone (Fig. 3). Both s are similar in that they contain substantial unts of quartz, which could explain the arity of the results for the 1/8-inch ball. fractional energy loss for the smaller 1/32- ball is greater in granite than in sandstone, ably because there is less than 1 per cent of ent in sandstone. Quartz has a logarithmic ement that is constant with frequency. The e 0.3 obtained for the 1/32-inch ball strik-sandstone is probably fallaciously high be-e the spaces between the grains are com-ble in size to the size of the ball.

ttenuation increases rapidly with frequency iprocal of ball diameter), the frequency e being 30 to 240 kc/s. The increase is more d in granite than in sandstone. These values near decrement, 0.21 for granite and 0.22 for lstone, are much higher than the comparable es, 0.03 and 0.025, respectively, for the itudinal decrement [*Birch*, 1942].

imestone. In limestone the increase of frac-al energy loss is very rapid (Fig. 4). For the llest balls the calcite grains probably become e important statistically, and the fractional gy loss in the limestone therefore approaches fractional energy loss in the other marbles.

hite marbles from Colorado and Vermont. decrease of the fractional energy loss evi-t in Figure 6 is probably due to the micro-tures, which are more effective than was viously expected. The lower loss for the ble from Marble, Colorado, can be explained he absence of appreciable alien constituents a larger average grain size. The fractional rgy loss is higher in fine-grained than in coarse-grained rocks, the number of grain bound-aries per unit volume being greater.

White Vermont and blue Vermont marbles. White Vermont and blue Vermont marbles have approximately the same characteristics. The differences in the values and behavior of the energy loss (Figs. 5 and 6) are probably due to the fractures created in the white marble by impact of the ball. The value 0.48 for the blue marble is due to bad polishing of the rock and has no special significance.

Blue Vermont and white Georgia marbles. The effect of the grain size on energy loss (Fig. 5) is particularly clear for the 1/8-inch ball in the two marbles, blue Vermont and white Geor-gia. For both of them, the difference between the values for the 1/8-inch and 1/32-inch balls is rather small, an indication that quartz and feld-spar probably play an important role in making the grain structure more rigid. The grains move as a whole under the larger balls, and the grain boundary losses are less important for the larger balls than for smaller balls.

Blue North Carolina and blue Vermont mar-bles. In the blue North Carolina and blue Vermont marbles the effect of the cement on energy loss (Fig. 5) is more evident. Both rocks have the same grain size but entirely different structures. The grain of the cement is much larger in blue Vermont marble than in blue North Carolina marble. The fractional energy loss is higher in blue Vermont marble.

Blue North Carolina marble and limestone. The two quite different rocks, marble and lime-stone, are similar in that they both contain very small metallic grains, chiefly pyrite, in the ce-menting material. These metallic inclusions con-siderably reduce the boundary losses and lower the fractional energy loss. (Figs. 4 and 5).

Pink Georgia marble. The coefficient of resti-tution in the phlogopite part of pink Georgia marble decreases with increasing frequency (Fig. 7), probably because of fracturing. But for the smallest size of ball, the fractional energy loss is very small compared with the loss of the other part, which contains more calcite and behaves as the other marbles.

Blue Vermont marble and sandstone. These two dissimilar rocks, blue Vermont marble and sandstone, have a grain size of the same order of magnitude, but sandstone, which contains quartz, is much less attenuating than marble,

which is made up of calcite (Figs. 3 and 5).

Longitudinal velocity and coefficient of restitution.

The granite and sandstone used in these experiments have very nearly the same velocities (Table 3); also, the longitudinal velocities in limestone and blue North Carolina marble are nearly the same. These last two rocks have a higher velocity, probably because they contain fewer intercrystalline vacant spaces, but no sharp dependence of coefficient of restitution on velocity can be found.

Conclusion

From this experimental study, several conclusions can be drawn:

Attenuation in rocks of the same average grain size will be less if the geologic materials contain quartz and feldspars than if they contain calcite.

The grain size plays an important role in attenuation because the frictional losses increase with the number of grain boundaries per unit volume.

A cement made up of tiny particles causes a decrease of the frictional losses. The same effect arises from the presence of quartz or feldspar cement instead of calcite cement.

Shear attenuation is several times larger than longitudinal attenuation in most of the rocks.

It is to be noted that these results are applicable to the range of frequencies, 30 to 240 kc/s. The results may not necessarily be entirely applicable to the range of frequencies involved in seismic exploration and in earthquake seismology. For example, porosity and degree of water saturation of pore spaces may have much greater effect than mineralogical composition in determining attenuation in rocks *in situ* in the seismic exploration range. In the earthquake seismology range, experience certainly does not indicate that shear wave attenuation is an order of magnitude greater than longitudinal wave attenuation.

Acknowledgment. We acknowledge with sincere thanks the help of Mr. William Bertram in setting up the experimental arrangement and of Mr. Kent Perry for petrographic analyses of the rocks.

This work was supported in part by the Lawrence Radiation Laboratory through a con[...] with the Colorado School of Mines Research F[...]dation, Inc.

References

Banerji, Sudhansukumar, On aerial waves ge[...]ated by impact, Part 1, *Phil. Mag., 32,* 96–[...] 1916. Part 2, *Phil. Mag., 35,* 97–111, 1918.

Birch, Francis, Internal friction in vibrating so[...] Handbook of Physical Constants, *Geol. Soc.* [...] *Spec. Paper 36,* 87–92, 1942.

Broberg, K. B., Shock waves in elastic and ela[...] plastic media, Kgl. Fortifikations-förvaltnin[...] Befästningsbyran Forsknings- och Försöks[...]tionen, Rapport nr 109:12, Stockholm, 195[...]

Goldsmith, Werner, The coefficient of restitut[...] *Bull. Mech. Div., Am. Soc. Eng. Ed., 2,* 1[...] 1952.

Hertz, Heinrich, On the contact of elastic so[...] *Miscellaneous Papers.* Macmillan and Co., [...] 146–162, 1896.

Hughes, D. S., W. L. Pondrom, and R. L. M[...] Transmission of elastic pulses in metal r[...] *Phys. Rev., 75,* 1552–1556, 1949.

Hunter, S. C., Energy absorbed by elastic wa[...] during impact, *J. Mech. and Phys. Solids, 5,* [...] 171, 1957.

Kalinina, R. V., The relationship between [...] velocity of propagation of elastic waves and [...] relative elastic characteristic of rocks, *Prik[...] Geofiz., 19,* 216–229, 1958.

Kasahara, Keichi, Experimental studies on [...] mechanism of generation of elastic waves[...] *Bull. Earthquake Research Inst. Tokyo Un[...] 32,* 67–77, 1954.

Love, A. E. H., *Mathematical Theory of Elastic[...]* 4th ed., Cambridge Univ. Press, 198–200, 1[...]

Ozerskaya, M. L., Opyt laboratornogo izmeren[...] uprugikh svoysto gornykh porod (The result[...] laboratory determinations of the elastic prop[...]ties of rocks), *Priklad. Geofiz., 12,* 93–106, 1[...]

Raman, C. V., On some applications of Hertz's t[...]ory of impact, *Phys. Rev., 15,* 277–284, 1920.

Rayleigh, Lord, On the production of vibrati[...] by forces of relatively long duration, with [...]plication to the theory of collisions, *Phil. M[...] 11,* 283–291, 1906.

Rinehart, John S., Temperature dependence [...] Young's modulus and internal friction of lu[...] and karolith, *J. Appl. Phys., 12,* 811–816, 1[...]

De Saint-Venant, B., *J. de Math.* (Liouville), [...] 2, *12,* 257 and 376, 1867.

Tillett, J. P. A., A study of the impact of sph[...] on plates, *Proc. Phys. Soc. London, B, 67,* 6[...] 688, 1954.

Zener, Clarence, The intrinsic inelasticity of la[...] plates, *Phys. Rev., 59,* 669–673, 1941.

(Manuscript received July 5, 1960; revised September 24, 1960.)

Further Study of the Mechanism of Circum-Pacific Earthquakes from Rayleigh Waves[1]

KEIITI AKI

Seismological Laboratory
California Institute of Technology
Pasadena, California

Abstract. The source functions of three earthquakes in the western Pacific are obtained from Rayleigh waves recorded at many IGY stations over the world. The method of interpreting the source function, which was proposed in a previous paper, is applied to these source functions. It is found that the pattern of the force at the source is quadrant for all three earthquakes, in accordance with the model adopted in the fault plane studies. One of the two nodal lines is found to be nearly parallel to the trend of the seismic zone for each of these earthquakes, and if we take this nodal line as the actual fault, the slip directions are right hand for all of them. The result from the recent Chilean shocks also supports the hypothesis that right-hand strike-slip prevails along the circum-Pacific earthquake belt.

.troduction. In a previous paper [*Aki*, ..b], we applied a method of phase equali-.on [*Aki*, 1960*a*] to long-period Rayleigh .es from many circum-Pacific earthquakes .rded at Pasadena to obtain their source .tions. We showed that these source func-. can be interpreted in terms of the direc-. of the force at the source, and we obtained .stematic distribution of the force direction .ughout the circum-Pacific seismic belt.

. interpreting the source function, we .pted the following assumptions:

. Since equalization removes the phase delay . to the dispersive medium and yields the .ce function, the theory of Rayleigh wave .ration in the homogeneous half-space can .ised to interpret the source function.

. The force exerted at the source is a step .ction in time.

. The source is not a singlet, but a couple or .uble couple.

. The earthquake focus is shallow.

. The effect of the finiteness of the fault at . source is neglected.

. the present paper, we shall apply our .hod of interpretation to the source functions .ined from the records of many IGY stations . a few earthquakes. If our method is valid, .should get the pattern of force at the source .ach earthquake, which is consistent with the .mptions, especially the third one.

Data from the IGY stations. Three earthquakes of the western Pacific are studied. The copies of the IGY station records were kindly supplied by the Lamont Geological Observatory of Columbia University. The seismographs are vertical component, Columbia University type; they have a pendulum period of 15 sec and a galvanometer period of 80 sec. The damping is such that $\epsilon = 3\omega$ and $\epsilon_g = \omega_g$. The Pasadena records of these shocks were discussed in the previous paper; the seismograph was of the Press-Ewing type with pendulum period of 30 sec and galvanometer period of 90 sec, both critically damped.

Table 1 gives the names and locations of sta-

TABLE 1. List of Stations

Station	Latitude deg.	min.	sec.	Longitude deg.	min.	sec.
Suva, Fiji	18	08	56 S	178	26	E
Lwiro, B. Congo	2	15	S	28	48	E
Rio de Janeiro	22	53	42 S	43	13	24 W
Honolulu	21	18	13 N	157	49	44 W
Resolute Bay	74	41	N	94	54	00 W
Uppsala	59	51	29 N	17	37	37 E
Perth, Australia	31	57	S	115	50	E
Hong Kong	22	18	13 N	114	10	19 E
Tsukuba, Japan	36	12	7 N	140	06	6 E
Palisades	41	00	N	73	54	W
Pasadena	34	08	54 N	118	10	18 W

[1] Contribution No. 992, Division of Geological .nces, California Institute of Technology.

TABLE 2. List of Earthquakes

Year	Date	Origin Time GCT h. m. s.	Epicenter Latitude deg.	Epicenter Longitude deg.	M	Region
1959	July 18	19:54:45	$15\frac{1}{2}$ N	$120\frac{1}{2}$ E	$6\frac{1}{2}$	Luzon
1958	June 25	09:36:30	3 S	$144\frac{1}{2}$ E	$6\frac{1}{4}$	New Guin
1959	June 27	19:04:27	33 S	179 W	$6\frac{3}{4}$	Kermadec

tions, and Table 2 gives the epicenter and the origin times of the shocks as given by the U. S. Coast and Geodetic Survey. The great-circle paths between the stations and the epicenters are shown in Figure 1.

Method. We obtained the source functions from the vertical motions of Rayleigh waves in the period range from 40 to 150 sec. To obtain the source function, we cross-correlate the actual record with the corresponding impulse response seismogram which was computed from available phase velocity curves of Rayleigh waves. The impulse response seismogram was computed according to the program written by *Aki and Nordquist* [in press] on the Bendix G-15D electronic computer at the Seismological Laboratory, Pasadena. Three different phase velocity curves are used to cover the whole surface of the earth. For the Pacific Ocean, we use the curve for the model 8099 obtained by *Dorman, Ewing, and Oliver* [1960]; for the oceans other than the Pacific, we used a curve which may correspond to a slightly modified model 80 and for the continents we use the one which based on Lehmann's shear velocity data computed by Dorman, Ewing, and Oliver the long-period branch, combined with *Pre* [1960] revised curve for the short-per branch.

The time required for the computation of impulse response seismogram is about 1 h and that for the cross-correlation is also ab 1 hour for each source function.

Our method of interpreting the source fu tion is qualitative; we first classify a giv source function according to its shape [*A* 1960*b*] as one of the following eight types.

$+E$: even function with the positive ma mum.

$+E+O$: intermediate shape between $+E$ a $+O$.

$+O$: odd function with the positive ma mum preceding the negative ma mum.

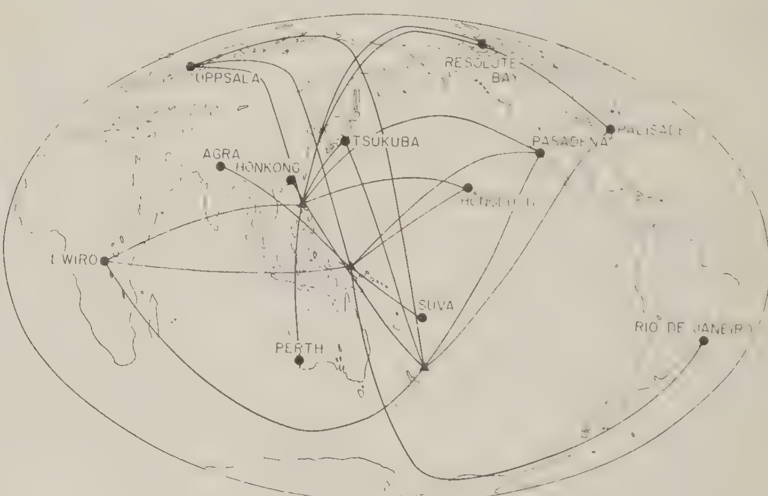

Fig. 1. Map of the stations, epicenters, and the great-circle paths between them.

$E+O$: intermediate shape between $-E$ and $+O$.

$-E$: even function with the negative maximum.

$-E-O$: intermediate shape between $-E$ and $-O$.

$-O$: odd function with the negative maximum preceding the positive maximum.

$+E-O$: intermediate shape between $+E$ and $-O$.

xt, if the source functions were derived from tical motions of Rayleigh waves, we interpret types $+E$ and $+E+O$ as being due to a izontal force directed away from the station, types $+O$ and $-E+O$ to a vertical down- d force, the types $-E$ and $-E-O$ to a izontal force toward the station, and the es $-O$ and $+E-O$ to a vertical upward e.

This simple classification of the source func- n seems to conform to the accuracy of the se velocity data presently available and also the fluctuation of source function due to se disturbances. If we had more accurate and ailed phase velocity data and if we could nehow eliminate noise, it would be practical determine the force direction accurately by a

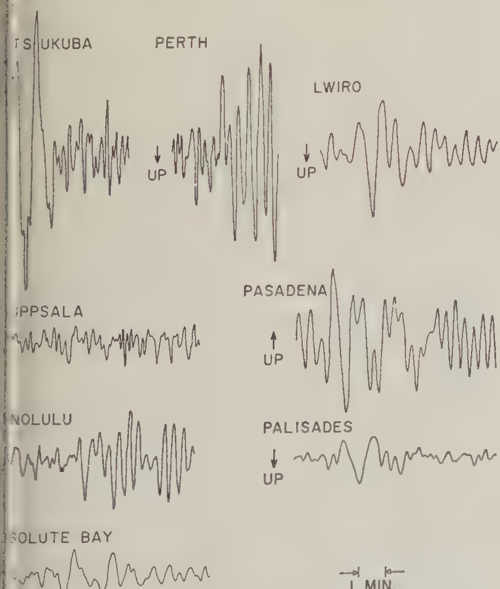

Fig. 2. Original seismograms of Rayleigh waves from the Luzon earthquake of July 18, 1959.

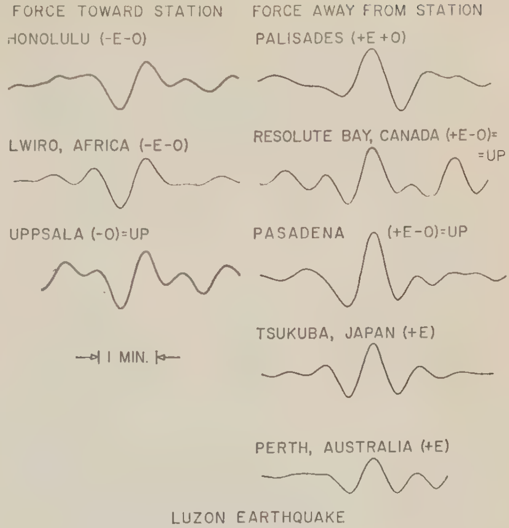

Fig. 3. Source functions of the Luzon earthquake.

quantitative estimation of the phase angle of the source function by Fourier analysis.

Luzon earthquake of July 18, 1959. Figure 2 shows the seismograms of vertical motions of Rayleigh waves from the Luzon earthquake recorded at Resolute Bay, Palisades, Tsukuba, Perth, Honolulu, Lwiro, Uppsala, and Pasadena. The source functions obtained from these records are shown in Figure 3. The waves shorter than the period of 40 sec, which prevail in some of the original seismograms, are cut off in the process of obtaining source functions. Each of the source functions is identified, according to its shape, as one of the eight types defined in the preceding section and shown in Figure 3. The

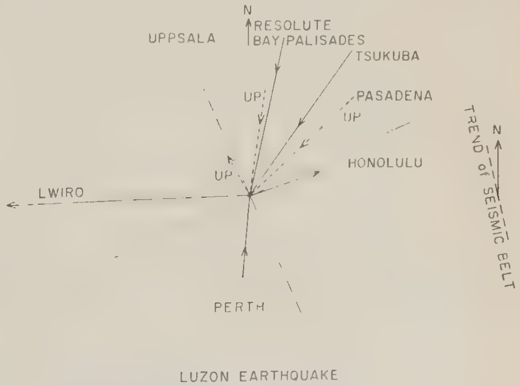

Fig. 4. The pattern of the force at the source of the Luzon earthquake.

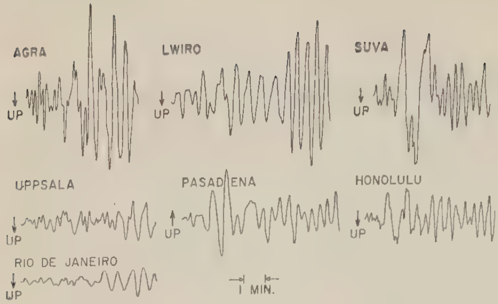

Fig. 5. Original seismograms of Rayleigh waves from the New Guinea earthquake of June 25, 1958.

Palisades, Tsukuba, and Perth source functions show that the force at the source was directed away from these stations. On the other hand, the Honolulu and Lwiro source functions are interpreted as being due to a force toward the stations.

The Pasadena source function was interpreted in the previous paper as being due to a vertical upward force. Since this shape is on the border line between the types $+E$ and $+E-O$, we were not sure whether the force was upward or away from the station. But it is clear that this shape cannot be attributed to a force toward the station or to a downward force.

Resolute Bay and Palisades are in almost the same direction from the epicenter. The difference in the shape of source functions for these stations seems to be due to the noise disturbance on the Resolute Bay record. Despite the noisy character of the Resolute Bay source function, this has a positive maximum as at Palisades,

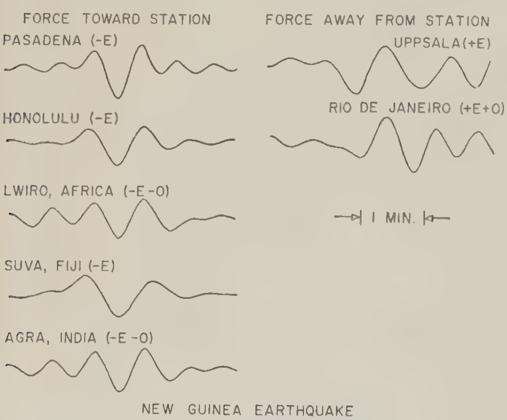

Fig. 6. Source functions of the New Guinea earthquake.

and we can be sure that the sense of force at the source in the horizontal direction is away from, rather than toward, Resolute Bay.

As is shown in Figure 2, the Uppsala record is more complicated than that of Resolute Bay, and the source function is also disturbed. The source function is interpreted as being due to an upward force, but it is closer in shape to the Honolulu and Lwiro source functions than the rest.

The force pattern at the source of this earthquake is shown in Figure 4, in which the arrows show the great-circle direction to the stations and the sense of the force is indicated by the arrowhead. Dotted arrows are used for those source functions that are interpreted as being due to vertical forces and yet suggest preferred sense in the horizontal direction. The length of the arrow is taken proportional to the maximum double amplitude of the source function, which we reduced to the epicenter by taking into account the geometrical spread and assuming a Q-type dissipation with a Q of 150 [*Ewing and Press*, 1954]. The difference in magnification between the Pasadena seismograph and the others is also taken into account. As is shown in Figure 4, not only the sense of the force but also the amplitude shows a quadrant distribution; the two mutually perpendicular nodal lines are indicated on the figure. If we take the nodal line that is nearly parallel to the trend of the seismic zone at this place as the actual fault, this pattern of force represents a right-hand strike-slip earthquake.

New Guinea earthquake of June 25, 1958. Figure 5 shows the seismograms of vertical motions of Rayleigh waves from the New Guinea earthquake recorded at Uppsala, Rio de Janeiro, Honolulu, Lwiro, Suva, Agra, and Pasadena. The source functions obtained from these records are shown in Figure 6.

Pasadena and Honolulu are in almost the same direction from the epicenter, and the source functions obtained from them have very similar shapes despite the difference in epicentral distance. This proves that the phase velocity data used are very accurate. The Pasadena, Honolulu, Lwiro, Suva, and Agra source functions are interpreted as being due to forces directed toward the station. On the other hand, the Uppsala and Rio de Janeiro source functions may be attributed to forces directed away

ı the station, although their shapes are not clearly identifiable, possibly because of e disturbances.

he pattern of force at the source of this hquake is shown in Figure 7 in the same as in Figure 4. Again, the sense of the force vs a quadrant pattern with nodal lines in-ted by thin lines. If we take the nodal line is nearly parallel to the trend of the seismic e at this place as the actual fault, this pat-ı of force again represents a right-hand strike- earthquake.

ermadec earthquake of June 27, 1959. Fig- 8 shows the seismograms of vertical motions Rayleigh waves from the Kermadec earth-ke recorded at Lwiro, Palisades, Hong Kong, kuba, Uppsala, and Pasadena. The source

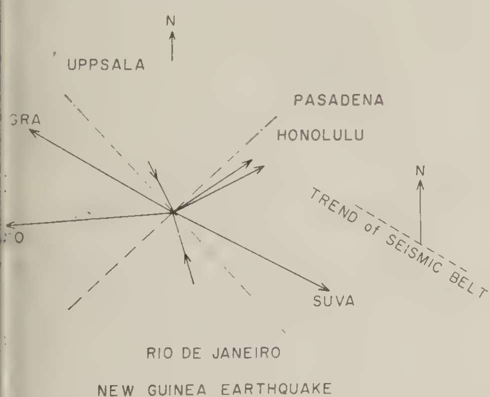

Fig. 7. The pattern of the force at the source of the New Guinea earthquake.

ıctions obtained from these records are shown Figure 9. The Lwiro and Pasadena source ıctions are clearly identifiable as being due a force away from the stations. It is also ar that the Hong Kong source function has a ape corresponding to a force toward the tion.

The Tsukuba source function is interpreted as ing due to a downward force. The shape sug-sts that the sense of the force at the source in e horizontal direction was toward, rather than ay from, Tsukuba.

The Uppsala record is again complicated, and e resulting source function, is very disturbed. e identified this shape as the type correspond-g to a downward force. It is interesting to note at the source functions for the Uppsala rec-ds of the Kermadec and the New Guinea

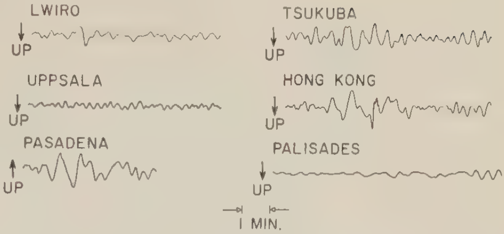

Fig. 8. Original seismograms of Rayleigh waves from the Kermadec earthquake of June 27, 1959.

earthquakes have similar shapes if the sign of one of them is reversed. Since the source function for the New Guinea earthquake was identified a little more clearly as being due to a force away from the station, we may infer that the sense of force at the source of the Kermadec earthquake in the horizontal direction was toward rather than away from Uppsala.

The Palisades source function is also identified as being due to a downward force. In this case, the preferred sense of the force in the horizontal direction was away from the station rather than toward it.

The pattern of the force at the source of this earthquake is shown in Figure 10 in the same way as in Figure 4. Again, the sense of the force shows a quadrant pattern with nodal lines indicated by thin lines. If we take the nodal line that is more nearly parallel to the trend of the seismic zone at this place as the actual fault, this pattern of the force again represents a right-hand strike-slip earthquake.

Discussion. In interpreting the source function, we assumed that the earthquake source is not a singlet but a couple or a double couple.

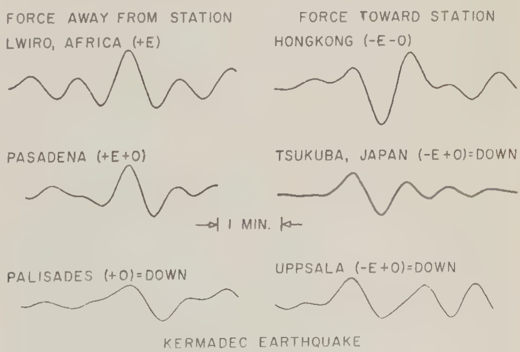

Fig. 9. Source functions of the Kermadec earthquake.

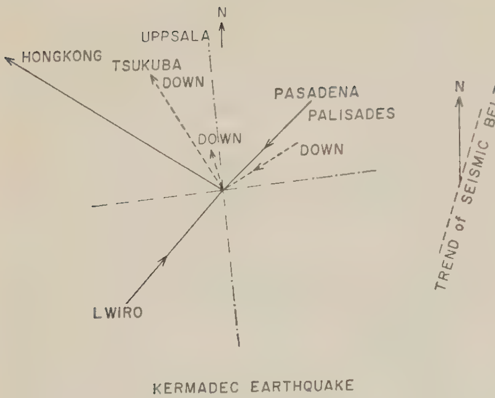

Fig. 10. The pattern of the force at the source of the Kermadec earthquake.

Therefore, if the source is purely strike-slip, the shape of source functions should correspond to a horizontal force, and at the same time the sense of the force deduced from the source functions should have a quadrant pattern. We obtained the quadrant pattern of the force at the sources of three earthquakes, and the majority of the source functions were found to have shapes corresponding to a horizontal force.

It is expected from the result of the previous paper [*Aki*, 1960*b*] that the direction of strike-slip is mostly right hand throughout the circum-Pacific seismic belt, if the fault strike is parallel to the seismic belt. We found that one of the nodal lines is nearly parallel to the seismic belt for all three earthquakes studied, and that if we take this nodal line as the actual fault, all their slip directions are right hand. From these results, we may conclude the following:

1. The phase velocity curves of Rayleigh waves presently available from the records of any station are accurate enough for use in the deduction of the source mechanism of any earthquake (at least for periods longer than 40 sec). The use of waves of shorter than 40 sec period requires more detailed knowledge about the crustal structure than we have at present.

2. The earthquake source is a couple or a double couple even in this long-period range.

3. Our result favors the hypothesis on the circum-Pacific tectonics proposed by *Benioff* [1957] and *St. Amand* [1957], who state that right-hand strike-slips having the fault strike parallel to the trend of the seismic belt prevails throughout the circum-Pacific seismic belt.

4. The present result requires no modificat[ion] of our method of interpreting the source fu[nc]tion which was originally obtained from the an[al]ysis of the Pasadena records of many Pac[ific] earthquakes under the assumptions given in [the] introduction to this paper.

As is shown in the description of individ[ual] earthquakes, some source functions are int[er]preted as being due to vertical forces. T[…]

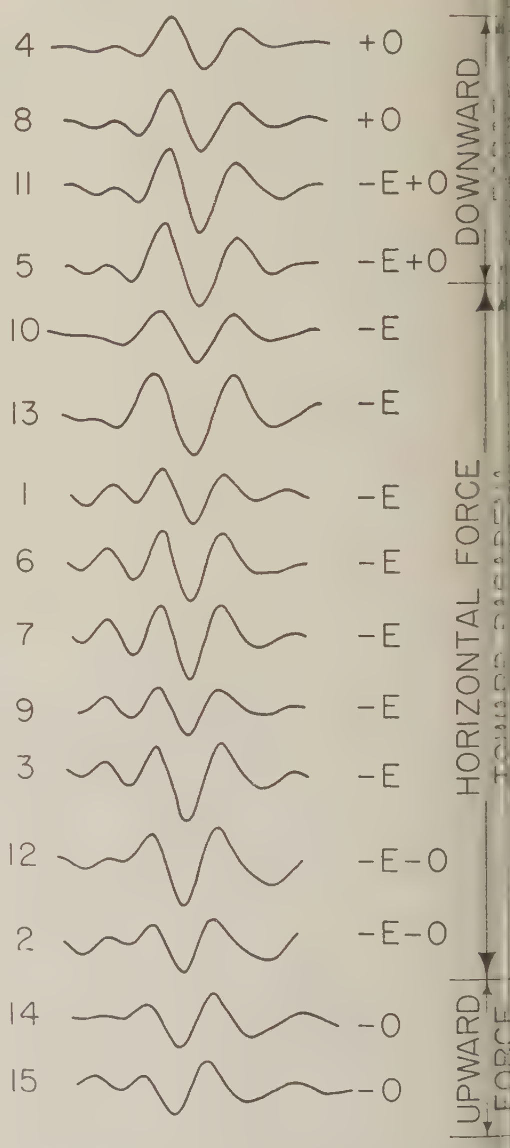

Fig. 11. Source functions of the Chilean aftershocks obtained from vertical displacement of Rayleigh waves. The numbers correspond to those in Table 3.

tical force might be an actual one, because a small amount of dip-slip component exists these shocks, its contribution will be the atest on the auxiliary nodal line of the ke-slip component, and since a vertical force more effective in radiating Rayleigh waves n a horizontal force, a source function cor- ponding to a vertical force may be promi- ntly observed near the auxiliary nodal line, n if the dip-slip component is relatively all. We notice in Figures 4 and 10 that the tical forces usually appear near nodal lines. is, however, puzzling that they appear near h of the nodal lines. Some of them must have n misinterpreted, perhaps owing to the effect noise disturbances. The writer feels that the ct of noise disturbances would be consider- y reduced by the use of seismographs with a ak response around 60 sec instead of the peak ponse of 10 to 15 sec for the present stand- l seismograph of the IGY stations.

A note on the Chilean shocks of May-June, 60. We studied Pasadena records of Rayleigh ves of aftershocks following the series of large cks which occurred on May 21–22, 1960, in thern Chile. The epicenters and origin times en by the U. S. Coast and Geodetic Survey the shocks studied are listed in Table 3. The cks are numbered according to the time of urrence. Unfortunately, shocks of magnitude

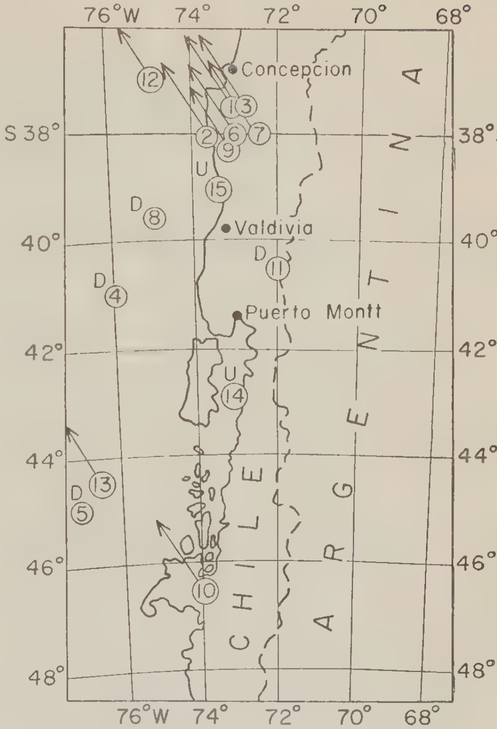

Fig. 12. The distribution of the direction of force at the source (U, upward force on the side of Pasadena; D, downward force on the side of Pasadena).

greater than 6¾ are not included in the present study because the recording instrument is too sensitive for them. We used a vertical seismograph with a pendulum period of 80 sec and a galvanometer period of 90 sec.

The source functions for these shocks obtained from vertical displacement of Rayleigh waves are shown in Figure 11. The numbers in the figure correspond to those in Table 3. It is remarkable that not a single source function whose type is $+E+O$, $+E$, or $+E-O$ is present in the figure. This means that there were no shocks that may be attributed to a source of horizontal force directed away from Pasadena. Nine shocks are interpreted as being due to horizontal force directed toward Pasadena, 4 shocks to downward force, and 2 shocks to upward force on the side of Pasadena. Figure 12 shows the force direction of each shock at its epicenter. The arrow in the figure indicates the great-circle direction to Pasadena and the arrowhead indicates the sense of the force in that direction.

TABLE 3. List of Chilean Aftershocks

Date 1960	Origin Time GCT h. m. s.	φ, deg.	λ, deg.	Remarks
May 22	03 46 22	37½ S	73 W	
May 22	06 01 36	38 S	73½ W	
May 22	08 10 53	37½ S	73 W	
May 27	03 17 21	41 S	76 W	
May 27	23 06 55	45 S	77 W	
May 28	11 05 40	38 S	73 W	
May 29	07 39 29	38 S	72½ W	$M = 6\frac{1}{2}$
May 31	02 40 00	39½ S	75 W	$M = 6$
June 1	05 02 56	38 S	73 W	
June 2	05 58 03	46½ S	74 W	$M = 6\frac{3}{4}$
June 7	05 22 34	40½ S	72 W	
June 12	00 02 55	37 S	75 W	
June 13	05 47 05	44½ S	76½ W	
June 14	02 54 13	43 S	73 W	
July 5	05 45 26	39 S	73½ W	

The result that the horizontal forces were directed toward rather than away from Pasadena is consistent with our previous result on the circum-Pacific earthquakes [*Aki*, 1960*b*], and may be explained by right-hand strike-slip motion along the fault parallel to the seismic belt.

It is interesting to notice in Figure 12 that the shocks interpreted as being due to horizontal forces are located near both ends of the aftershock area, while those due to vertical forces are mostly in between. This seems to suggest that, in the aftershock process, right-hand strike-slip proceeded near both ends of the disturbed area while dip-slip motion of less determined direction occurred within the disturbed area. It is dangerous to conclude from only a single station record, however, that a shock is due to dip-slip, because, as is discussed in the preceding section, a strike-slip source with a small dip-slip component can give in a certain direction the source function for a vertical force.

Acknowledgment. I wish to thank Drs. Frank Press and Hugo Benioff for their helpful advice and discussions in the course of the present study. Thanks are also due the seismologists at the IGY stations who furnished the data on which a part of this study is based.

This work was partially supported by grants from the IGY Interdisciplinary Research Program, and the Air Force Technical Applications Cen under contract AF49(638)-910 as part of the A vanced Research Projects Agency project VEL

References

Aki, K., Study of earthquake mechanism by method of phase equalization applied to Ra leigh and Love waves, *J. Geophys. Research,* 729–740, 1960*a*.

Aki, K., Interpretation of source functions circum-Pacific earthquakes obtained from lon period Rayleigh waves, *J. Geophys. Resear* *65,* 2405–2417, 1960*b*.

Aki, K., and J. M. Nordquist, Automatic com tation of impulse response seismograms of R leigh waves for mixed paths, *Bull. Seism. S* *Am.*, in press.

Benioff, H., Circum-Pacific tectonics, *Publs. D* *minion Obs., 20,* 395–402, 1957.

Dorman, J., M. Ewing, and J. Oliver, Study shear velocity distribution in the upper man by mantle Rayleigh waves, *Bull. Seism. S* *Am., 50,* 87–115, 1960.

Ewing, M., and F. Press, An investigation of ma tle Rayleigh waves, *Bull. Seism. Soc. Am.,* 127–147, 1954.

Press, F., Crustal structure in the Californ Nevada region, *J. Geophys. Research, 65,* 103 1051, 1960.

St. Amand, P., Circum-Pacific orogeny, *Pub* *Dominion Obs., 20,* 403–412, 1957.

(Manuscript received September 20, 1960.)

1000-Million-Year-Old Minerals from the Eastern United States and Canada

G. R. TILTON, G. W. WETHERILL, G. L. DAVIS, AND M. N. BASS

Geophysical Laboratory and Department of Terrestrial Magnetism, Carnegie Institution of Washington, Washington, D. C.

Abstract. Minerals with ages of about 1000 m y have been found in Ontario, along the Appalachians from New York to North Carolina, and also beneath the sedimentary covering in Michigan, Ohio, and West Virginia. Measurements have been made on muscovite, biotite, microcline, uraninite, and zircon. This occurrence is interpreted as indicating the extent of igneous intrusion and metamorphism accompanying a major orogeny about 1000 million years ago.

troduction. The age of a number of urani- s from southern Ontario and Quebec was es- shed at about 1000 m y by some of the est geochronological determinations. *Ells- h* [1932] showed that uraninites and euxe- s from nine localities had Pb/(U + Th) between 950 and 1050 m y (corrected for ern values of the decay constants). The grouping of the ages indicated that a sig- ant geological event occurred then. *Nier* 9] and *Nier, Thompson, and Murphey* 1] published complete isotopic lead ages four samples from the same area showing agreement with the earlier chemical meas- nents. These pioneering studies depended arily on the availability of uranium-rich rals, such as uraninite, in order to obtain milligram amounts of lead required for the surements. Techniques developed during the decade have extended the application of nethods of age determination to include min- obtainable from granites, pegmatites, and sses. This paper presents additional 1000- on-year ages measured for biotite, musco- and zircon samples from rocks of the east- United States.

ge determinations. The analytical data for determinations appear in Tables 1 and 2. procedure for zircon samples was that given *ilton, Davis, Wetherill, and Aldrich* [1957]. uncertainty of the isotopic ratios is 1 per ; the uranium, thorium, and lead concentra- , about 2 per cent. Pb^{204} is not reported in e 1 because the amount found in the analy- was about that which could be expected from the usual blank determinations. All samples had measured ratios of Pb^{206} to Pb^{204} between 1000 and 1500. The procedures for the determination of rubidium, strontium, potassium, and argon were similar to those described by *Aldrich, Davis, Tilton, and Wetherill* [1956] and by *Wetherill, Tilton, Davis, and Aldrich* [1956]. The analytical error of the concentrations of these elements is between 1 and 2 per cent.

The decay constants used for the calculation of ages are:

U^{238}	$1.54 \times 10^{-10}\ yr^{-1}$
U^{235}	$9.72 \times 10^{-10}\ yr^{-1}$
Th^{232}	$4.99 \times 10^{-11}\ yr^{-1}$
Rb^{87}	$1.39 \times 10^{-11}\ yr^{-1}$
$K^{40}(\lambda_\beta)$	$4.72 \times 10^{-10}\ yr^{-1}$
$K^{40}(\lambda_e)$	$0.585 \times 10^{-10}\ yr^{-1}$

A newer value for the decay constant for Rb^{87} has recently been given by *Flynn and Glendenin* [1959] as $1.47 \times 10^{-11}\ yr^{-1}$. If this value were used the ages given in this paper would be lowered by 5.5 per cent. The value 137.8 is used for the atomic ratio, U^{238}/U^{235}. Other isotopic compositions used are: $Rb^{87} = 0.283$ g/g Rb; $K^{40} = 1.22 \times 10^{-4}$ g/g K; and K^{39}/K^{41}, 13.5 (atoms).

The locations and petrographic descriptions of the samples in Tables 1 and 2 are given in the appendix.

Table 3 lists the lead ages for the minerals that are about 1000 million years old. Only those minerals for which complete, nearly concordant, isotopic uranium-lead ages are available are included. The age values from the Besner Mine

TABLE 1. Analytical Data for Zircon Samples

Map No.	Location and Source Rock	Concentration, parts per million			Atomic Abundance			
		U	Th	Pb^{206}	Pb^{204}	Pb^{206}	Pb^{207}	Pb
8	Bear Mtn., N. Y., Storm King granite	2210	361	303	0	100	7.37	4.6
8	Bear Mtn., N. Y., Canada Hill gneiss	353	46.1	58.2	0	100	7.80	3.7
10	Conshohocken, Pa., Baltimore gneiss	990	320	143	0	100	7.60	9.7
12	Shenandoah National Park, Va., gneiss	451	146	69.7	0	100	7.72	10.6
13	Blowing Rock, N. C., gneiss	475	140	67.2	0	100	7.37	9.4

appear to be lower than the rest; however, a Pb^{207}–Pb^{206} age of 940 m y has been reported for another specimen of uraninite from the mine [*Cumming, Wilson, Farquhar, and Russell,* 1955]. The same report also summarizes the earlier nonisotopic age measurements and lists minerals giving Pb^{207}–Pb^{206} ages of 1000 m y, but for which complete isotopic ages are not available.

Table 4 lists ages of micas whose rubidium-strontium ages are about 1000 m y. Their potassium-argon ages are uniformly about 10 per cent less than the corresponding rubidium values. The rubidium ages are generally less than the uranium-lead ages, even for coexisting minerals. These discordances most likely are due either to effects of diffusion or to differences in the stability of minerals under conditions of metamorphism; however, the uncertainty in the decay constants for rubidium and potassium may account for the 10 per cent differences betwe these ages.

The rubidium-strontium age values for biot from the Baltimore gneiss of the Philadelph area, shown in Table 5, are definitely under 10 m y, but the potassium-argon ages, in each ca greater than the rubidium age, are almost 10 m y for two samples. The Baltimore gneiss ne Baltimore shows this same pattern [*Tilto Wetherill, Davis, and Hopson,* 1958]. The cau of this pattern has not been determined. It ma be that the high argon ages are caused by i corporation of radiogenic argon at the time metamorphism. If this is so, the agreement the 1000 m y biotite argon ages from Deva with other 'Grenville' ages must be regarded coincidental.

The locations from which the rock sampl were collected are indicated in Figure 1. Al shown is an inferred western boundary in Oh

TABLE 2. Analytical Data for Biotite

Map No.	Location and Source Rock	Concentration, parts per million				Radiogenic Sr^{87} / Total Sr
		K^{40}	Radiogenic A^{40}	Rb^{87}	Radiogenic Sr^{87}	
1	Wavy Lake, Ont., granite	8.60	0.650	68.7	1.029	0.31
8	Bear Mtn., N. Y., Storm King granite	9.60	0.598	351	4.56	0.95
8	Bear Mtn., N. Y., Canada Hill gneiss	9.18	0.518	144	1.78	0.65
9	Hibernia, N. J., gneiss 1	9.59	0.551	344	4.35	0.88
9	Hibernia, N. J., gneiss 2	8.95	0.388	267	3.14	0.73
10	Conshohocken, Pa., Baltimore gneiss	9.32	0.349	121	0.639	0.36
10	Devault, Pa., Baltimore gneiss *A*	8.42	0.564	107	0.938	0.17
10	Devault, Pa., Baltimore gneiss *B*	8.75	0.685	111	0.754	0.35
12	Shenandoah National Park, Va., gneiss	8.90	0.516	202	2.47	0.65
14	Pardee Point, Tenn., Cranberry gneiss	8.06	0.451	262	3.27	0.76

the 900 to 1000 m y mica ages. This has been [illegible]mated by *Bass* [1960], taking into account [illegible]rographic evidence obtained from examina[illegible]n of well drillings.

[illegible]iscussion. Rocks containing minerals hav[illegible] ages in the range from 900 to 1100 m y have been found along the Appalachian orogenic belt from New York to North Carolina. Most of these occur in the sedimentary part of the belt where Paleozoic metamorphism was not intense. Others are from the Piedmont province to the east where metamorphism was more severe.

TABLE 3. Isotopic Lead Ages of Minerals

[illegible]p	Location and Source	Mineral*	Age, million years Pb^{206}/U^{238}	Pb^{207}/U^{235}	Pb^{207}/Pb^{206}	Pb^{208}/Th^{232}	Reference
[illegible]	Henvey Twp., Ont., Besner Mine	U	750	780	830	800	*Nier*, 1939
[illegible]	Conger Twp., Parry Sound, Ont.	U	1000	1015	1035	960	*Nier, Thompson, and Murphey*, 1941
[illegible]	Conger Twp., Parry Sound, Ont.	U	995	995	995	895	*Wasserburg and Hayden*, 1955
4	Tory Hill, Ont., granite	Z	1040	1060	1090	390	*Tilton, Patterson, Brown, Inghram, Hayden, Hess, and Larsen, Jr.*, 1955.
4	Tory Hill, Ont., syenite	Z	940	960	1015	—	*Tilton, Davis, Wetherill, and Aldrich*, 1957
5	Wilberforce, Ont., Fission Mine	U	1060	1055	1040	1000	*Nier*, 1939
5	Wilberforce, Ont., Fission Mine	U	1150	1110	1030	1130	*Collins, Farquhar, and Russell*, 1954
5	Wilberforce, Ont., Fission Mine	U	1040	1060	1090	1010	*Aldrich, Wetherill, Davis, and Tilton*, 1958
5	Wilberforce, Ont., Cardiff Uranium Mine	U	1000	1010	1030	870	*Wasserburg and Hayden*, 1955
5	Wilberforce, Ont., Cardiff Uranium Mine	U	1020	1020	1020	995	*Aldrich, Wetherill, Davis, and Tilton*, 1958
5	Wilberforce, Ont., Cardiff Uranium Mine	Z	900	930	1000	990	*Tilton, Davis, Wetherill, and Aldrich*, 1957
6	Pied des Monts, Que.	C	865	885	925	—	*Nier*, 1939
6	Pied des Monts, Que.	C	950	970	1000	—	*Cumming, Wilson, Farquhar, and Russell*, 1955
7	Natural Bridge, N. Y., contact	Z	1025	1065	1140	—	*Tilton, Davis, Wetherill, and Aldrich*, 1957
8	Bear Mtn., N. Y., Storm King granite	Z	960	990	1060	850	This report
8	Bear Mtn., N. Y., Canada Hill gneiss	Z	1140	1150	1170	1030	This report
[illegible]	Conshohocken, Pa., Baltimore gneiss	Z	1010	1050	1120	950	This report
1	Baltimore, Md., Baltimore gneiss	Z	1040	1070	1120	940	*Tilton, Wetherill, Davis, and Hopson*, 1958
1	Baltimore, Md., Baltimore gneiss	Z	960	1020	1120	1100	*Tilton, Wetherill, Davis, and Hopson*, 1958
2	Shenandoah National Park, Va., gneiss	Z	1070	1100	1150	1110	This report
3	Blowing Rock, N. C., gneiss	Z	990	1010	1060	1000	This report

* U, uraninite; Z, zircon; C, cleveite.

TABLE 4. Ages of Micas

Map No.	Location and Source	Mica*	Age, million years	
			Rb-Sr	K-A
1	Wavy Lake, Ont., granite	B	1070	990
5	Wilberforce, Ont., Fission Mine	B	1000†	920†
5	Wilberforce, Ont., Cardiff Uranium Mine	B	1030†	960†
8	Bear Mtn., N. Y, Storm King granite	B	930	840
8	Bear Mtn., N. Y., Canada Hill gneiss	B	880	780
9	Hibernia, N. J., gneiss 1	B	900	790
9	Hibernia, N. J., gneiss 2	B	840	630
12	Shenandoah National Park, Va., gneiss	B	880	800
14	Pardee Point, Tenn., Cranberry gneiss	B	890‡	800‡
14	Pardee Point, Tenn., Cranberry gneiss	B	890	770
15	Parkersburg, W. Va., gneiss	B	870§	
16	Fayette Co., Ohio, basic amphibolite	B	940	
16	Fayette Co., Ohio, granite	M	980	
16	Fayette Co., Ohio, basic amphibolite	B	930	
17	Delaware Co., Ohio, gneiss	B	950	
17	Delaware Co., Ohio, gneiss	M	950	
18	Huron Co., Ohio, gneiss	B	920	
19	Sandusky Co., Ohio, gneiss	B	940	
20	Wood Co., Ohio, gneiss	B	950	
21	Washtenaw Co., Mich., gneiss	B	970	
21	Washtenaw Co., Mich.	B	890	
22	St. Claire Co., Mich., gneiss	B	950	

* B, biotite; M, muscovite.
† *Aldrich, Wetherill, Davis, and Tilton*, 1958.
‡ *Long, Kulp, and Eckelmann*, 1959.
§ Analytical data for samples 15–22 are given in *Bass*, 1960.

Here the mica ages are substantially lower, 380 to 630 m y, as shown by the rubidium-strontium ages in Table 5. Still lower ages have been reported for the Baltimore gneiss near Baltimore by *Tilton, Wetherill, Davis, and Hopson* [1958], who found rubidium-strontium ages of 300 m y and a potassium-argon age of 340 m y for biotite. They gave reasons for believing that the gneiss has been a crystalline rock for the past 1000 or 1150 million years. Although zircon might be detrital and reflect the age of the source rock, microcline of nonclastic character gave a rubidium age of about 1100 m y. These arguments probably apply to the gneiss at Philadelphia as well.

TABLE 5. Ages of Biotite from the Baltimore Gneiss near Philadelphia

Sample	Age, million years	
	Rb-Sr	K-A
Conshohocken	380	550
Devault, gneiss *A*	630	900
Devault, gneiss *B*	485	1010

The indications of the presence of old rocks in a young mountain belt near the margin of the continent may influence the interpretation of theories of continental growth by accretion resulting from orogenic processes. Between New York and Maryland the continent has not grown by more than about 250 kilometers in the last 1000 million years, the distance to the edge of the continental shelf. In California, *Wasserburg, Wetherill, and Wright* [1959] have reported ages of 1700 m y from Death Valley, about 325 kilometers from the western continental margin. *Silver, McKinney, Deutsch, and Bolinger* [1960] report an age of 1200 m y for zircon from a pegmatite in the San Gabriel Mountains near Los Angeles, within 80 kilometers of the margin. Only limited accretions to the continent can have occurred in any of these localities since Precambrian time. In North Carolina the easternmost Precambrian rock

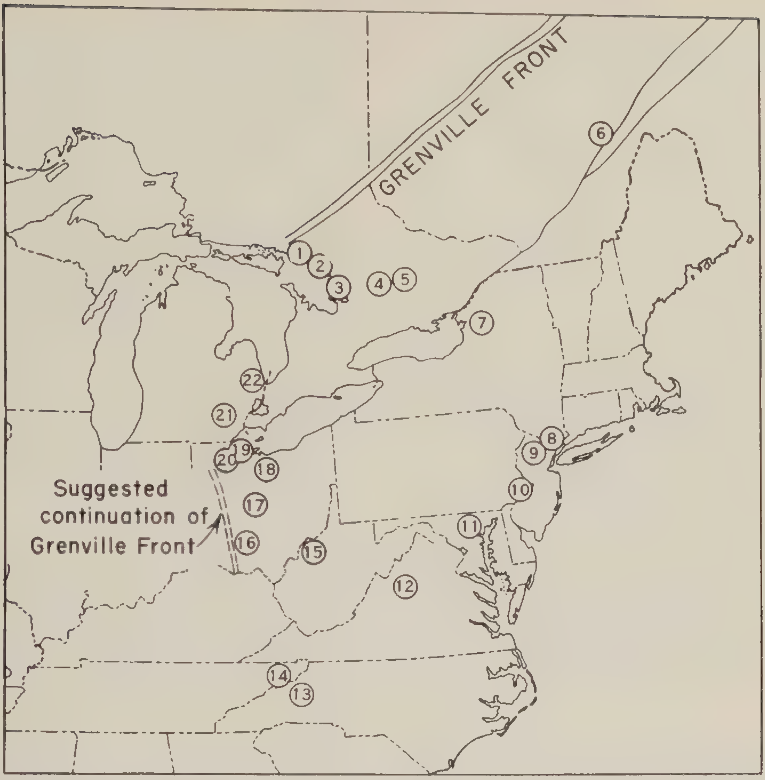

Fig. 1. Location of 1000-million-year-old minerals in the eastern United States and Canada. The sample numbers correspond to those in the tables.

Blowing Rock gneiss) is some 500 kilometers om the edge of the continental shelf. In this ırt of the southeastern United States considerable additions to the continent since the Preımbrian cannot be excluded.

It is apparent from Figure 1 that metaıorphism and mineral crystallization occurred)0 to 1150 million years ago in a considerable ortion of the eastern United States and Canada. ı Ontario where the 1000-million-year-old rocks re well exposed, they appear to belong to an rogenic belt. In the United States mica, feldpar, and zircon ages exhibit an impressive uniormity with the exception of effects that can e ascribed to later Appalachian metamorphism. 'his whole region is believed, therefore, to be a art of an orogenic belt that is roughly parlleled by the more recent Appalachian belt.

Appendix

1. Wavy Lake granite. Collected by H. W. 'airbairn from the shore of Wavy Lake, Onario. A granitic rock containing (usually) unzoned plagioclase, somewhat sericitized, some fresh but mostly chloritized biotite, the quartz and feldspars showing effect of granulation and strain.

8. Storm King granite. Palisades Interstate Park, Bear Mountain, N. Y. Collected beside abandoned road leading off circle on Perkins Drive, ¼ mile from circle. This is a hornblende granite of magmatic origin [*Lowe,* 1950], possibly slightly modified, rich in zircon but, where collected, containing no biotite in the massive rock. Biotite was obtained from a small pegmatite cutting the granite at this location. The typical zircon concentrated from the granite has a dark brown outer zone over a light brown, fractured, semiopaque core of lower refractive index. The stubby crystals ranged from rounded to euhedral in form with 'curved' terminal faces. Cracks radiating from the cores suggest a change in composition between the nucleus and the last part of the mineral to crystallize.

8. Canada Hill granite gneiss. Collected in Palisades Interstate Park, Bear Mountain, N. Y.,

¼ mile up Perkins Drive from gateway. A medium-gray, medium-grained biotite granite with the biotite oriented in layers, containing little or no potassium feldspar. The accessory minerals noted were epidote, sphene, garnet, and zircon. The rock sampled is from the Canada Hill granite phase described by *Lowe* [1950]. The separated zircon sample consisted of light reddish-brown, unzoned, subhedral mineral grains free from inclusions.

9. Gneiss 1, Hibernia, N. J. Collected from a road-cut on state highway 513, 2.3 miles north of Rockaway. The rock is darker than gneiss 2, with unchloritized but bent biotite appearing to be later than the potassium feldspar. The plagioclase appears less crushed than in gneiss 2. Metamorphism of the rock is indicated by the presence of 'wohm' lamellae in the quartz.

9. Gneiss 2, Hibernia, N. J. Collected from a road-cut on state highway 513, 0.1 mile north of the Hibernia fire house. This gneiss might almost be called a granite. Metamorphism has resulted in subhedral feldspar grains, recrystallized quartz, and partial chloritization of the biotite.

10. Baltimore gneiss, Conshohocken, Pa. This sample was collected from a road-cut on River Road, 4.5 miles southeast of Spring Mill, near Conshohocken. It is a metamorphosed rock in which greenish biotite replaces hornblende. The zircon is honey-colored, occurring in rounded to stubby rounded euhedral crystals, 90 per cent or more having fractured cores and a clear outer zone. Some have no cores; few have inclusions.

10. Baltimore gneiss, Devault, Pa. Collected from the Difrancesco Bros. quarry, ½ mile north of Devault. Two samples were taken, differing in dark mineral content. The darker rock, *A*, appears to be a silicified metamorphic rock with biotite replacing hornblende. The quartz is crushed and there is no potassium feldspar. Plagioclase is not twinned and biotite is rutillated and not chloritized. Sample *B* is lighter in shade and differs from *A* in that there is less quartz, less staining of the quartz, and the plagioclase is much less altered.

12. Hypersthene granodiorite gneiss, Shenandoah National Park, Va. Collected from dumped material from the north end of Mary's Rock Tunnel on the Skyline Drive, south of Thornton Gap. Typically, this rock has been described by *Watson and Cline* [1916]. This weakly foliated rock is composed of plagioclase, hornblende-mantled pyroxene, quartz, rare biotite, and accessory garnet, apatite, and zircon. The mantling of the hypersthene, the presence of magnetite and pyrite, and of zoisite in the plagioclase, as well as the crushed appearance of the plagioclase can be taken as evidence of post-crystallization metamorphism. The rare biotite appears fresh and undistorted.

13. Blowing Rock gneiss. Collected from a road-cut 1 mile north of Blowing Rock, N. C., at the junction of U. S. 221 and U. S. 321. A cataclastic granite gneiss containing biotite, with later sericite, and carbonate along fractures. The accessory minerals are sphene and zircon.

14. Pardee Point gneiss. Pardee Point overlooks the Doe River gorge, 18 miles south-southeast of Elizabethton, Tenn. The gneiss was collected 100 feet west of the third tunnel from Hampton along the road bed of the abandoned ET & WNC railroad. The rock contains fresh microcline, slightly strained. The biotite flakes are scarce, bent, corroded, and chloritized in layers.

Acknowledgments. Assistance in the selection and collection of many of the rock samples was given by P. W. Gast, Columbia University; A. C. Waters, the Johns Hopkins University; Bruce Bryant and J. C. Reed, Jr., United States Geological Survey; and Stuart Maher, Tennessee Department of Conservation.

REFERENCES

Aldrich, L. T., G. L. Davis, G. R. Tilton, and G. W. Wetherill, Radioactive ages of minerals from the Brown Derby Mine and the Quartz Creek granite near Gunnison, Colorado, *J. Geophys. Research, 61*, 215–232, 1956.

Aldrich, L. T., G. W. Wetherill, G. L. Davis, and G. R. Tilton, Radioactive ages of micas from granitic rocks by Rb-Sr and K-A methods, *Trans. Am. Geophys. Union, 39*, 1124–1134, 1958.

Bass, M. N., The Grenville boundary in Ohio, *J. Geol.*, 1960, in press.

Collins, C. B., R. M. Farquhar, and R. D. Russell, Isotopic composition of radiogenic leads and the measurement of geologic time, *Bull. Geol. Soc. Am., 65*, 1–22, 1954.

Cumming, G. L., J. T. Wilson, R. M. Farquhar, and R. D. Russell, Some dates and divisions of the Canadian Shield, *Proc. Geol. Assoc. Can., 7*, 27–79, 1955.

Ellsworth, H. V., Rare-element minerals of Canada, *Can. Dept. Mines, Econ. Geol. Ser. No. 11*, 272 pp., 1932.

Flynn, K. F., and L. E. Glendenin, Half-life and

beta spectrum of Rb^{87}, *Phys. Rev., 116,* 744–748, 1959.

ng, L. E., J. L. Kulp, and F. D. Eckelmann, Chronology of major metamorphic events in the southeastern United States, *Am. J. Sci., 257,* 585–603, 1959.

we, K. E., Storm King granite at Bear Mountain, New York, *Bull. Geol. Soc. Am., 61,* 137–190, 1950.

er, A. O., The isotopic constitution of radiogenic leads and the measurement of geological time, II, *Phys. Rev., 55,* 154–163, 1939.

ier, A. O., R. W. Thompson, and B. F. Murphey, The isotopic constitution of lead and the measurement of geological time, III, *Phys. Rev., 60,* 112–116, 1941.

ver, L. T., C. R. McKinney, Sarah Deutsch, and Jane Bolinger, Precambrian age determinations in some crystalline rocks of the San Gabriel Mountains of Southern California (Abstract), *J. Geophys. Research, 65,* 2522–2523, 1960.

lton, G. R., G. L. Davis, G. W. Wetherill, and L. T. Aldrich, Isotopic ages of zircon from granites and pegmatites, *Trans. Am. Geophys. Union, 38,* 360–371, 1957.

ilton, G. R., Claire Patterson, Harrison Brown, Mark Inghram, Richard Hayden, David Hess, and Esper Larsen, Jr., Isotopic composition and distribution of lead, uranium, and thorium in a Precambrian granite, *Bull. Geol. Soc. Am., 66,* 1131–1148, 1955.

Tilton, G. R., G. W. Wetherill, G. L. Davis, and C. A. Hopson, Ages of minerals from the Baltimore gneiss near Baltimore, Maryland, *Bull. Geol. Soc. Am., 69,* 1469–1474, 1958.

Wasserburg, G. J., and R. J. Hayden, A^{40}–K^{40} dating, *Geochim. et Cosmochim. Acta, 7,* 51–60, 1955.

Wasserburg, G. J., G. W. Wetherill, and L. A. Wright, Ages in the Precambrian terrane of Death Valley, California, *J. Geol., 67,* 702–708, 1959.

Watson, T. L., and J. H. Cline, Hypersthene syenite and related rocks of the Blue Ridge region, Virginia, *Bull. Geol. Soc. Am., 27,* 193–234, 1916.

Wetherill, G. W., G. R. Tilton, G. L. Davis, and L. T. Aldrich, New determinations of the age of the Bob Ingersoll pegmatite, Keystone, S. Dakota, *Geochim. et Cosmochim. Acta, 9,* 292–297, 1956.

(Manuscript received September 8, 1960.)

Iodine Content of Meteorites and Their I^{129}–Xe^{129} Ages

GORDON G. GOLES, AND EDWARD ANDERS

Enrico Fermi Institute for Nuclear Studies and Department of Chemistry
University of Chicago
Chicago, Illinois

Abstract. Iodine and tellurium abundances in chondritic meteorites were determined by neutron activation analysis. For bronzite and hypersthene chondrites (6 analyses) iodine abundances from 37 to 104 ppb were found; for enstatite and carbonaceous chondrites (9 analyses), the range is from 127 to 560 ppb. The tellurium abundances range from 0.42 to 0.73 ppm and 1.23 to 3.4 ppm respectively. I^{129} – Xe^{129} decay intervals, measured from the cessation of nucleosynthesis, were calculated for the meteorites Richardton $\left(119^{+9}_{-6}\text{ m.y.}\right)$ and Indarch $\left(97^{+17}_{-10}\text{ m.y.}\right)$, using the continuous nucleosynthesis model. The significance of these results is discussed.

Introduction. The recent discovery of excess Xe^{129} from the decay of 1.64×10^7 year[1] I^{129} in several chondritic meteorites [*Reynolds*, 1960*a*, *b*, has created a need for accurate estimates of iodine in meteorites, in order that one may calculate I – Xe decay intervals. In addition, meteoritic abundances of iodine may serve to delineate the 'cosmic' abundance curve [*Suess and Urey*, 1956] in the poorly defined region near mass 130. Iodine contents are best obtained by modern techniques such as neutron activation, which are more reliable than the classical methods used by *von Fellenberg* [1927]. This paper comprises a preliminary report on the results of neutron activation analyses for iodine in a number of chondritic meteorites, and includes some data on Te and U-Th contents, which were also determined by our procedure.

Experimental procedure. Meteorite samples used in this work were, in most cases, freshly broken fragments, 0.5 to 2 grams in weight. They were irradiated for 30 minutes, along with flux monitors, in the 'rabbit' facility of the Argonne CP-5 reactor at fluxes of one or two times 10^{13} neutrons cm^{-2} sec^{-1}. The irradiated sample was fused in the presence of I^- carrier with a NaOH—Na_2O_2 mix in a zirconium crucible, after which the fusion cake was leached with water and acidified with HF. H_2O_2 was destroyed and IO_3^- reduced to I^-, which was then put through four cycles of oxidation to I_2, extraction with CCl_4, and reduction, before precipitating as AgI. Decontamination was generally satisfactory (less than 10 cpm assignable to other than iodine activities, compared to 150 to 10,000 cpm from I^{128}), although some $Br^{80m,82,83}$ activities were observed in several of the early runs. Chemical yields for the samples ranged from 34 per cent to 71 per cent.

The iodine activities in the samples arise in three different ways:

$$I^{127}(n, \gamma)I^{128}$$

$$[U^{235,238}, Th^{232}](n, f)I^{131-135}$$

and

$$Te^{130}(n, \gamma)\, Te^{131} \xrightarrow{\beta^-} I^{131}.$$

Accordingly, while the principal aim of this investigation is the determination of I^{127} abundances, information on Te and on combined U – Th abundances has also been obtained. Beta-counting in a proportional counter was used to determine I^{128} and the total decay curve of fission-product iodine; in addition, I^{133} (fission product) and I^{131} (essentially all from Te activation) were counted by β-γ coincidence spectrometry.

Among the meteorite samples analyzed in the course of this work were those generously supplied by Dr. S. K. Roy of the Chicago Natural History Museum (Richardton, Indarch, and Mighei), and Dr. E. P. Henderson of the U. S. National Museum (Murray). We obtained meteorites by exchange from Prof. E. W. Heinrich

[1] The 16.4 m.y. half-life of I^{129} used in this paper is the average of two literature values as suggested by *Kohman* [1960].

of the University of Michigan (Beardsley; our sample was picked up within a day after infall), Dr. K. R. Dawson of the Geological Survey of Canada (Abee; this enstatite chondrite fell June 10, 1952, near Abee, Alberta), and Dr. A. W. Crompton of the South African Museum, Cape Town (St. Marks enstatite chondrite).

Results. Table 1 presents the data on I and Te. Terrestrial isotopic composition has been assumed for the meteoritic tellurium. The errors quoted are at the 95 per cent confidence limit and are derived from counting statistics and an estimate of the remaining experimental errors. The first group of samples are hypersthene and bronzite chondrites (samples 1–6). The second (samples 7–12) and third (samples 13–15) groups are enstatite and carbonaceous chondrites.

The Te abundances of bronzite chondrites agree with those of *Schindewolf* [1960]; the U − Th levels are not yet known absolutely, but their ratios agree with those of *Reed, Kigoshi, and Turkevich* [1960]. These facts encourage us to believe that exchange of carrier and radioiodine is rapid and complete, and that no gross errors are involved in our work.

Although the data are not sufficiently extensive to permit rigorous conclusions to be drawn about the nature of the variances exhibited, two important trends seem to be present. First, the variation in iodine content among different samples of the same meteorite is frequently much greater than experimental error. This effect is not likely to have been caused b[y] contamination of the samples before irradiation since the Te and I abundances display a hig[h] degree of correlation. We suspect that there is real and substantial variation of the iodine con[-]tent of different samples of the same meteorite and infer that both I and Te probably reside i[n] a minor phase of inhomogeneous distribution.

The second trend to be noted is that both [I] and Te seem to be more abundant in enstatit[e] and carbonaceous chondrites than in bronzit[e] and hypersthene chondrites. Even greater vari[-]ations of elemental abundances among thes[e] classes of chondrites were found for Tl, Pb, an[d] Bi by *Reed, Kigoshi, and Turkevich* [1960]. These points will be discussed in a future paper whe[n] additional data are available.

Discussion. From our iodine abundances an[d] data on Xe^{129} reported by *Reynolds* [1960*a*, *b*, *c*] and by *Wasserburg and Hayden* [1955], I − X[e] decay intervals for Richardton, Indarch, Mur[-]ray, and Beardsley were calculated (Table 2) for the case of a constant rate of nucleosynthesis during the history of the galaxy prior to the isolation of the solar system. *Wasserburg, Fowler, and Hoyle* [1960], in their discussion of the continuous nucleosynthesis model, have given the relation:

$$\ln (I^{127}/Xe^{129}) = \Delta t/\tau + \ln (T/\tau) + \ln (K_{127}/K_{129}) \qquad (1)$$

TABLE 1. Neutron Activation Analyses for Iodine in Chondrites

Sample	Sample Weight, g	I, ppb	Te, ppm
1. Beardsley II	1.293	71 ± 10	—
2. Beardsley III	0.816	104 ± 12	—
3. Richardton I	0.486	57 ± 10	0.73 ± 0.08
4. Richardton II	0.512	37 ± 8	0.44 ± 0.07
5. Plainview III	1.58	40 ± 6	0.49 ± 0.09
6. Plainview IV	1.49	78 ± 9	0.42 ± 0.02
7. Indarch I	1.014	283 ± 15	1.82 ± 0.35
8. Indarch III	0.632	455 ± 35	3.4 ± 0.4
9. Abee I	1.132	204 ± 17	2.25 ± 0.18
10. Abee II	1.327	219 ± 20	2.14 ± 0.25
11. St. Marks I	1.767	127 ± 10	1.31 ± 0.14
12. St. Marks II	1.320	138 ± 20	1.55 ± 0.21
13. Murray II	1.690	234 ± 17	1.23 ± 0.18
14. Mighei I*	1.016	557 ± 50	2.63 ± 0.31
15. Mighei II*	0.905	374 ± 29	1.88 ± 0.15

* Mighei samples were powdered material.

TABLE 2. Iodine-Xenon Decay Intervals

eteorite	Excess Xe^{129}, 10^{-9}cc STP/g*	I^{127}, ppb	Δt, m. y.
chardton	0.13 ± 0.01	47 ± 14	119^{+9}_{-6}
darch	2.5 ± 1.0	370 ± 120	97^{+17}_{-10}
urray	1.09 ± 0.11	230 ± 70†	106^{+9}_{-6}
ardsley	≤ 0.013	88 ± 24	≥ 190

* Data on the first three meteorites are from eynolds [1960*a*, *b*, *c*], using the Xe^{136} normalization.
† Relative error assumed to be ±30 per cent, agreement with other entries.

here Δt is the interval between the isolation of e solar system and the retention of Xe^{129} by e meteorite (the 'I — Xe decay interval'), τ is e mean lifetime of I^{129}, T is the interval during hich nucleosynthesis took place, and the K's re the rates of production of I^{127} and I^{129}. In iese calculations, we have assumed $T = 10^{10}$ ears and $K_{127}/K_{129} = 1$.[3] The iodine content of ichardton is about a factor of 20 less than that reviously assumed by Reynolds, so that the ecay interval is considerably shorter than his riginal estimate. The apparent difference in the alues for Richardton and Indarch clearly is not atistically significant. It will be of great interest see whether further work will disclose real ge differences between these meteorites, in view f their marked differences in texture, minerlogy, and iodine content.

The data for the remaining two meteorites re considerably more ambiguous. If Reynolds' ormalization to Xe^{136} is used, the Murray value s close to those for Richardton and Indarch, but vith the *Kuroda* [1960*a*, *b*] normalization to Xe^{130}, the excess Xe^{129} content falls to $(-0.02 \pm 0.11) \times 10^{-9}$ cc STP/g, corresponding to a lower imit for the decay interval of ≥ 150 m.y. This discrepancy will be discussed in a separate paper [*Goles and Anders*, 1961].

For Beardsley, *Wasserburg and Hayden* [1955] have given an upper limit to the excess Xe^{129} content. With the new iodine value, this corresponds to a lower limit of ≥ 190 m.y. for the decay interval. It is now known, however, that the trace metal content of the Wasserburg and Hayden sample of Beardsley had been severely altered by exposure to ground water [*Gast*, 1960; *Anders and Stevens*, 1960]. Although an argument may be proposed why Beardsley should not contain any excess Xe^{129}, a remeasurement of our unweathered Beardsley sample would be very desirable.

The question of the contemporaneity of events in the history of the meteorites is an extremely important one, since it bears directly upon the time scale of meteoritic synthesis and thus upon the nature of the early solar system. Application of the $Pb^{207} - Pb^{206}$ dating method has shown that the separations of iron and silicate phases were contemporaneous to within perhaps ±100 m.y., the approximate limit of error of the method [*Patterson*, 1956; *Marshall and Hess*, 1958; *Hess and Marshall*, 1960]. In principle, dating methods based on extinct radioactivity could be used to establish the contemporaneity of meteoritic phase separations with inherently greater resolution. For a gas-solid phase separation, such as the I — Xe system, however, a dispersion in apparent decay intervals could occur even if the eras of intense heating were of identical length in each case. Bodies of 150-km radius, once molten at their centers, would require about 100 million years to cool to temperatures low enough to retain Xe in their interiors [*Goles, Fish, and Anders*, 1960], and even for an object as small as 100-km in radius, the cooling time is about 40 million years. If at least some of the meteorites had originated in bodies within this size range, as is strongly suggested by the low K-Ar ages of the crystalline chondrites and the shergottites [*Goles, Fish, and Anders*, 1960], a dispersion of I — Xe decay intervals would be observable, due solely to differing thermal histories. Present data suggest that such a dispersion of the ages actually exists [*Wasserburg and Hayden*, 1955, *Reynolds and Lipson*, 1957, *Reynolds*, 1960*c*; *Zahringer and Gentner*, 1960], but either the iodine contents, or the xenon measurements of most of these meteorites are in doubt, so that it would be premature to

[3] Until some of the required parameters become irmly established, it is expedient to use the mathenatically simple scheme of *Wasserburg, Fowler, and Hoyle* [1960], rather than more complex models uch as those of *Kohman* [1960] or *Fowler and Hoyle* [1960]. Use of these alternative models vould change the absolute values of the I — Xe lecay intervals, but not their relative values. Our choices of T and K_{127}/K_{129} are not likely to be n error by factors greater than 2 and 1.5, respectively.

attempt to draw definitive conclusions. It is interesting to note that the correlation predicted by *Goles, Fish, and Anders* [1960] between 'well-refrigerated meteorites' and high Xe contents, has been largely borne out for *primordial* xenon: the friable chondrites Richardton and Kapoeta and a number of carbonaceous chondrites contain large amounts of noble gases. Conversely, the hard, compact chondrite Beardsley and the howardite Nuevo Laredo have very low Xe contents, as would be expected from their proposed locations in the parent bodies [*Fish, Goles, and Anders,* 1960]. The trends are less regular in regard to Xe^{129}, but this way be due, at least in part, to disagreement about the xenon measurements, and to selective diffusion losses [*Goles and Anders,* 1961]. The enstatite chondrites are an apparent exception [*Reynolds, 1960c*] in that they are hard and dense, yet contain radiogenic Xe^{129}, but their incomplete segregation of metal and silicate [*Smith,* 1950] and certain trends in their chemical composition [*Fish, Goles, and Anders,* 1960, and unpublished work] suggest their origin in small bodies with low central temperatures, which would cool rapidly.

These questions of the contemporaneity of meteorites and of the nature and extent of systematic differences between true and apparent I — Xe ages are of such great interest that we hope that their resolution, which depends upon analyses of the iodine and xenon in a large number of selected meteorites, will not be long delayed.

Acknowledgments. The authors are indebted to Professor John H. Reynolds for many helpful discussions of his experimental work and advance information concerning it. The assistance and advice of members of the staff of Argonne National Laboratory, particularly Drs. E. Steinberg and A. Stehney, Mr. R. Meschke and Miss B. A. Lore, is gratefully acknowledged. One of us (GGG) received fellowship support from the Monsanto Chemical Company during part of the time spent on this project. This work was supported in part by the U. S. Atomic Energy Commission.

References

Anders, E., and C. M. Stevens, Search for extinct lead 205 in meteorites, *J. Geophys. Research, 65,* 3043–3047, 1960.

Fish, R. A., G. G. Goles, and E. Anders, The record in the meteorites, III, On the development of meteorites in asteroidal bodies, *Astrophys. J., 132,* 243, 1960.

Fowler, W. A., and F. Hoyle, Nuclear cosmochr ology, *Annals of Physics, 10,* 280, 1960.

Gast, P. W., Strontium and rubidium in sto meteorites, *Proc. Highland Park Conf. on Nucle Geology,* in press, 1960.

Goles, G. G., and E. Anders, On the chronology the early solar system, *J. Geophys. Res.,* press, 1961.

Goles, G. G., R. A. Fish, and E. Anders, The reco in the meteorites, I, The former environme of stone meteorites as deduced from K^{40}–A ages, *Geochim. et Cosmochim. Acta, 19,* 177, 196

Hess, D. C., and R. R. Marshall, The isoto composition and concentrations of lead in so chondritic stone meteorites, *Geochim. et Cosm chim. Acta,* in press, 1960.

Kohman, T. P., Chronology of nucleosynthes and extinct natural radioactivity, *J. Chem. Ed* in press, 1960.

Kuroda, P. K., Nuclear fission in the early histo of the earth, *Nature, 187,* 36, 1960*a*.

Kuroda, P. K., On the 'extinct' transuraniu elements, in press, 1960*b*.

Marshall, R. R., and D. C. Hess, Lead from so stone meteorites, *J. Chem. Phys., 28,* 1258, 195

Patterson, C., Age of meteorites and the eart *Geochim. et Cosmochim. Acta, 10,* 230, 195

Reed, G. W., K. Kigoshi, and A. Turkevic Concentrations of some heavy elements meteorites by activation analysis, *Geochim. Cosmochim. Acta,* in press, 1960.

Reynolds, J. H., Determination of the age of th elements, *Phys. Rev. Letters, 4,* 8, 1960*a*.

Reynolds, J. H., Isotopic composition of primordi xenon, *Phys. Rev. Letters, 4,* 351, 1960*b*.

Reynolds, J. H., Xenon in stone meteorites, *Pro Highland Park Conf. on Nuclear Geology,* i press, 1960*c*.

Reynolds, J. H., and J. I. Lipson, Rare gases fro the Nuevo Laredo stone meteorite, *Geochim et Cosmochim. Acta, 12,* 330, 1957.

Schindewolf, U., Selenium and tellurium conte of stony meteorites by neutron activatio *Geochim. et Cosmochim. Acta, 19,* 134, 1960

Smith, W. C., Stony meteorites, *The Advanceme of Science, Section C, 26,* 1, 1950,

Suess, H. E., and H. C. Urey, Abundances of th elements, *Rev. Mod. Phys., 28,* 53, 1956.

von Fellenberg, T., Untersuchungen über da Vorkommen von Jod in der Natur, 11, Zu Geochemie des Jods, 2., *Biochem. Zeitschr., 187* 1, 1927.

Wasserburg, G. J., W. A. Fowler, and F. Hoyle The duration of nucleosynthesis, in press, 1960

Wasserburg, G., and R. Hayden, Time interva between nucleogenesis and the formation o meteorites, *Nature, 176,* 130, 1955.

Zahringer, J., and W. Gentner, Uredelgase in einiger steinmeteoriten, *Zeit. fur Naturforsch., 15a,* 600, 1960.

(Manuscript received September 20, 1960; revised October 4, 1960.)

On Correlation between Variables of Constant Sum

F. CHAYES

Geophysical Laboratory, Carnegie Institution of Washington
Washington, D. C.

Abstract. Composition data are subject to the condition that the sum of the parent variables in any item is constant. This imposes a linear restraint which suppresses positive and increases negative covariance. Neither the resulting 'spurious' correlation itself nor the difficulty it creates with regard to the interpretation of composition data has been adequately described, and no general remedy has yet been suggested. This note describes some of the more important effects of a constant item-sum on correlation. It also proposes a test against the alternative of 'spurious' correlation arising from interaction between variables of equal variance, and a modification that may prove applicable to arrays characterized by inhomogeneous variance.

Introduction. In many areas of scientific ıquiry the initial observations are percentages, · their conversion to percentages is a pre-·quisite to meaningful comparison of sample ems with each other. In either event, the umerical data available for interpretation are ıbject to the bothersome restriction that the ım of all the variables in any item (including ıose of no present interest) is a constant. The fect of a constant item-sum on covariance may e both drastic and devious. It can nearly lways be ignored with safety if an hypothesis ın be tested by means of interrelations be-ween variables whose contribution to the total ariance of the array is small. It may also be educed or, for practical purposes, eliminated, y relating the restricted variables to an 'outside' ariable, e.g., time, position, etc., instead of) each other. Often, however, this latter strata-em merely serves to camouflage and complicate ıther than eliminate the difficulty.

Neither alternative will usually be available o the petrologist, in whose work observations ubject to this restriction are of central im-ortance. Ordinarily he is concerned with inter-elations between variables whose contribution o the total variance of the array is large, and nly rarely is he able to press into service an outside' variable to reduce or mask the bias rising from the constant item-sum. Petrology hus provides excellent examples of the un-voidable use and frequent misuse of data of his sort. Indeed, these are so common that pecific documentation of the illustrative material used below is neither necessary nor entirely fair.

On the necessity of negative correlation in a closed table. Letting X_{ij} represent the amount of i in the jth item in a sample of size N, $\bar{x}_i$ the sample average for i, and $x_{ij} = (X_{ij} - \bar{x}_i)$, we define as 'closed' any table containing measurements such that

$$\sum_{i=1}^{M} X_{ij} = \sum_{i=1}^{M} \bar{x}_i = K \qquad (1a)$$

for all j. The most important consequence of (1a) is simply that

$$x_{1j} + x_{2j} + x_{3j} + \cdots + x_{mj} = 0 \qquad (1b)$$

Squaring (1b), summing the squares and cross-products over $1 \leq j \leq N$, and dividing through by $(N - 1)$, we have that

$$\sum_{i=1}^{M} V_i + 2 \sum_{i=1}^{M-1} \sum_{k=i+1}^{M} p_{ik} = 0 \qquad (2)$$

where V_i is the variance of i and p_{ik} is the covariance of i and k.

Substracting x_{ij} from both sides of (1b) and repeating the squaring, summing, and division, we also have

$$\sum_{i=2}^{M} V_i + 2 \sum_{i=2}^{M-1} \sum_{k=i+1}^{M} p_{ik} = V_1 \qquad (3)$$

Next, substracting (3) from (2)

$$V_1 + \sum_{k=2}^{M} p_{1k} = 0 \qquad (4)$$

Since the numbering of variables in (1b) is arbitrary, we have thus shown that

$$V_i + \sum_{\substack{k=1\\k\neq i}}^{M} p_{ik} = 0 \quad \text{for} \quad 1 \leq i \leq M \tag{5}$$

i.e., every row of the covariance matrix sums to zero.

V_i being by definition positive, at least one of the $(M - 1)$ covariances attached to each variable must be negative. Now if $p_{ij} < 0$ and the others are positive, we have from (5) that

$$|p_{ij}| \geq V_i \tag{6}$$

But $|p_{ij}| \leq s_i s_j$, where s_i and s_j are standard deviations, so that

$$s_i s_j \geq V_i$$

and, dividing through by s_i,

$$s_j \geq s_i \tag{7}$$

Thus p_{ij} may be the only negative covariance of X_i if and only if $s_j \geq s_i$; otherwise (5) will require more than one negative covariance. From (7), further, if p_{ij} is in fact the only negative covariance of X_i it cannot perform the same function for X_j, which must accordingly have at least two negative covariances. The smallest number of negative covariances which will satisfy (5) for all i is $(M - 1)$. If, for instance, the $(M - 1)$ covariances attached to the variable of maximum variance are negative it is possible, at least in principle, for all other covariances to be nonnegative.

Since the sign of the covariance fixes the sign of the correlation coefficient, it follows that in any closed table containing M variables,

(*a*) Of the $(M - 1)$ correlations involving each variable, at least one must be negative. For the variable of maximum variance at least two must be negative.

(*b*) Of the $\binom{M}{2}$ total correlations that can be formed from the table, at least $(M - 1)$ must be negative. There is no a priori algebraic requirement that any of the remainder be positive, and it is quite unlikely that they will all be so unless one of the variances is very much larger than the others.

Dividing (5) by s_i gives

$$s_i + \sum_{\substack{k=1\\k\neq i}}^{M} r_{ik} s_k = 0 \tag{8}$$

from which, since $/r_{ik}s_k/ \leq s_k$, it is evident that if s_i is greater than the sum of any j of the other standard deviations, at least $(j + 1)$ of the covariances of variable i must be negative. In particular, if $j = (M - 2)$, all the covariances of variable i will be negative. If we are told, for instance, that standard deviations of 0.5, 1.4, 1.5, 3.0, are associated, respectively, with variables X_1, X_2, X_3, X_4 in a 4-variable system, we know at once that all covariances involving X_4 must be negative.

It is easy to show, however, that positive correlation must exist somewhere in the array if some one of the variances, say V_1, is enough larger than the others. If

$$V_1 \geq \sum_{2}^{M} V_i$$

we have, because of (8), that all the covariances of X_1 are negative, and from (3) that one or more of the covariances relating variables X_2, X_3, $X_4 \cdots X_M$ must be positive.

Although

$$V_1 > \sum_{2}^{M} V_i$$

is evidently a sufficient condition for the emergence of positive correlation among variables $2 \leq i \leq M$, I do not believe it can be shown to be necessary except if $M = 3$, for which see below.

Correlation in a closed table with three variables. If $M = 2$ the whole notion of correlation is, of course, trivial, for if $X + Y = \bar{x} + \bar{y} = K$, it is obvious that $V_x = V_y$ and $r_{xy} = -1$. When $M = 3$ the situation is far more complex, as much petrographic experience attests. It is nevertheless true that although each of the three correlation coefficients is now in principle free to vary from -1 to $+1$, any assumed or observed set of variances completely fixes all three coefficients. (Whether we regard the variances as dependent on the covariances, or vice versa, is to some extent, a matter of taste. In a descriptive science it is always desirable to classify objects before discussing their relations with each other. From this point of view variance appears a more fundamental property than covariance, and

ughout this note, accordingly, it is taken dependent.) We first prove this assertion. sing (5) to obtain

$$V_i + p_{ij} + p_{ik} = 0 \qquad (11)$$

readily find, by rotating subscripts in (11) solving the resulting set of simultaneous tions, that

$$p_{ij} = \tfrac{1}{2}[V_k - (V_i + V_j)] \qquad (12)$$

which

$$r_{ij} = \frac{1}{2}\left[\frac{V_k - (V_i + V_j)}{s_i s_j}\right] \qquad (13)$$

hat if $M = 3$, r_{ij} is a single valued function V_i, V_j and V_k.

e note that $r_{ij} > 0$ if and only if $V_k > + V_j)$. Positive correlation need not occur ll, but if it does appear it is confined to the tion between the variables of least and rmediate variance. Correlation between the able of maximum variance and each of the rs must be negative. If $V_k = V_i + V_j$, ables i and j will appear to be unrelated, in sense that $r_{ij} = 0$. If no variance is greater the sum of the other two, all three cortions will be negative.

Ve do not ordinarily suppose that the choice nineral or oxide ranges, upon which most ographic classifications are based, determines ther the variables concerned vary directly inversely, or how strongly they do either. (13) shows that something very like this st happen if $M = 3$. Whether, in the sialic tion of a series of granites, for instance, rtz and alkali-feldspar tend to vary directly depend on how variable plagioclase is. ess the variance of plagioclase is larger than sum of the variances of quartz and alkalispar, there is no possibility of positive relation between the latter, and unless it is siderably larger than this sum the correlation fail of significance. Now in rocks called nite' the permissible range—and hence to a e extent the variance—of plagioclase content depend on taxonomy and nomenclature. deciding that classification is not worth rying about, petrologists have in effect ided that this question is not worth answering. Equation 5 is also useful in setting limits to permissible variation in a three variable classification. Dividing its expansion for $M = 3$ (equation 11 above) by s_i gives

$$s_i + s_j r_{ij} + s_k r_{ik} = 0 \qquad (14)$$

and since $r \geq -1$ it follows immediately that

$$s_i \leq s_j + s_k\,,$$

and

$$s_i \geq |s_j - s_k| \qquad (15)$$

The force of (15) will perhaps be made a little clearer by the reminder that in the absence of (1) there is no a priori relation between s_i, s_j, and s_k. In any array subject to (1), however, it will always be true that, if $M = 3$, the sum of any two of the standard deviations will equal or exceed the third.

Correlation in a closed table with four variables. We have just noted that if $M = 3$ the correlations are completely fixed by any legitimate choice of variances, so that hypotheses about covariance are no more than disguised hypotheses about variance. The interrelation between variance and covariance is both more complex and less specific if $M = 4$. Writing (1) in the form

$$x_i + x_j = -x_k - x_l$$

squaring, summing, and dividing by $(N - 1)$, as before, we obtain

$$V_i + V_j + 2p_{ij} = V_k + V_l + 2p_{kl} \qquad (16)$$

Bearing in mind that $V_i = s_i^2$ and $|p_{ij}| \leq s_i s_j$, we find, after some rearrangement, that

$$\frac{1}{2s_i s_j}[(s_k - s_l)^2 - (s_i^2 + s_j^2)] \leq r_{ij}$$

$$\leq \frac{1}{2s_i s_j}[(s_k + s_l)^2 - (s_i^2 + s_j^2)] \qquad (17)$$

an inequality which is the 4-variable analogue of (13). It is obviously much less restrictive; if, for instance, the variances are taken as equal, we have from (13) that $r_{ij} = -0.5$ exactly, but from (17) only that $-1 \leq r_{ij} \leq +1$.

Since the latter range is precisely that characteristic of open data, it is tempting to assume that if $M \geq 4$ the 'spurious' correlation characteristic of the closed form becomes small enough to ignore. Unfortunately, this is not so.

Despite our inability to fix the exact value of any correlation from a knowledge of the variances, it is clear from (5) that *at least 3 of the coefficients in any set of 6 must be negative.*

For $M = 4$, eq. 5 becomes

$$V_i + p_{ij} + p_{ik} + p_{il} = 0 \qquad (18)$$

so that

$$s_i + s_j r_{ij} + s_k r_{ik} + s_l r_{il} = 0 \qquad (19)$$

Since $r \geq -1$ it follows that

$$\text{and} \quad \left.\begin{array}{l} s_i \leq s_j + s_k + s_l \\ |s_i - s_j| \leq s_k + s_l \end{array}\right\} \qquad (20)$$

The largest standard deviation must not be greater than the sum of the other three, and the sum of any two must not be less than the difference between the other two. Extension of these results to the multivariate case is immediate. The largest standard deviation will never be larger than the sum of the other $(M - 1)$, and the difference between the largest and the smallest will never be larger than the sum of the other $(M - 2)$.

By forming a new variable, $X_{(k+l)} = X_k + X_l$, we may examine more closely the relation between r_{ij} and r_{kl}. For we then have, from (13), that

$$r_{ij} = \frac{1}{2}\left[\frac{V_{(k+l)} - (V_i + V_j)}{s_i s_j}\right] \qquad (21)$$

which will be positive if and only if $V_{(k+l)} > V_i + V_j$. Expanding the left side of this inequality by the usual rule for the variance of a sum, and rearranging terms, we find that

$$r_{ij} > 0 \quad \text{if and only if}$$

$$r_{kl} > \frac{1}{2s_k s_l}[(V_i + V_j) - (V_k + V_l)] \qquad (22)$$

In the example used earlier, $s_1 = 0.5$, $s_2 = 1.4$, $s_3 = 1.5$, $s_4 = 3.0$, and it was shown that, because of (8), r_{14}, r_{24}, and r_{34} must all be negative. By means of (22) we may now show that r_{12}, r_{13} and r_{23} must all be positive. Thus the signs of all six correlations are fixed by (1) and the sample variances. More generally, we may note from inspection of (22) that:

(*a*) If $(V_k + V_l) - (V_i + V_j) > 2s_k s_l$, r_{ij} will be positive.

(*b*) If $(V_k + V_l) = (V_i + V_j)$, r_{ij} will be positive if and only if k_{kl} is positive.

(*c*) If $(V_i + V_j) - (V_k + V_l) > 2s_k s_l$, r_{ij} will be negative.

As a special case of (*b*), if the variances a[illegible] equal the number of positive correlations mu[illegible] be either two or zero, and $r_{ij} = r_{kl}$.

Whether or not the variances are equal, [illegible] hypothesis that implies some specific relati[illegible] between any two of the variables implies so[illegible] specific, though not necessarily identical, relati[illegible] between the other two; this is evident from (1[illegible] so that if r_{kl} is known there is no need to compu[illegible] r_{ij}. It may be difficult to decide objective[illegible] which of these correlations is to be tested f[illegible] significance, but clearly it will be specious [illegible] test both.

Finally, if any two covariances having [illegible] common variable are known, the remaining fo[illegible] covariances may be expressed as additive fun[illegible] tions of these two and the variances; the thi[illegible] covariance of the variable may be gotten b[illegible] difference, from (5), and the three from whic[illegible] it is lacking by successive application of (16[illegible]

Thus, if we are working with assigne[illegible] variances—such as are often implied by petr[illegible] graphic classifications—and the hypothesis [illegible] question implies specific values for ρ_{ij} and ρ_{kl} it also implies equally specific expectations f[illegible] r_{il}, r_{jk}, r_{jl}, and r_{kl}. In a 4-variable closed tab[illegible] there will never be more than two potential[illegible] independent correlations.

These essentially nonstatistical controls ov[illegible] covariance greatly complicate the statistic[illegible] testing and interpretation of correlation [illegible] closed arrays. It is fair to add—in fact it is on[illegible] of the principal objectives of this note to poi[illegible] out—that the difficulty is not eliminated b[illegible] rejecting statistics in favor of convention[illegible] interpretive procedures, whether of the 'geneti[illegible] or 'common sense' variety. By thinking sole[illegible] in terms of geochemical associations, gradu[illegible] transitions, petrographic affinities, liquid descen[illegible] lines, etc., we may manage to remain comfortab[illegible] unaware of the problem; we do not, howeve[illegible] solve it.

Inferences about open variables from observatio[illegible] on closed variables. Enough has been said t[illegible] indicate that the problem is puzzling and seriou[illegible] Unless the number of variables is much larg[illegible] than is common in petrography, or the quantit[illegible]

$$(V_k + V_l) \ll \sum_{1}^{M} V_i$$

the effect of the closed form of statement on r_k[illegible] cannot be ignored. What can be done about it[illegible]

n the assumption that the *parent* variables n fact subject to no such restraint, and that percentage form of statement is merely an voidable condition of observation, *Sarmanov Vistelius* [1958] have recently pointed out its effect can be removed if some one of parent variables may be presumed constant. trick is simply to divide each closed vari- representing an open variable of nonzero ance by the closed variable representing open variable of zero variance.

sing α for closed and x for open variables, lefine

$$\alpha_j = \frac{x_j}{\sum_1^n x_i}$$

if, by hypothesis or assumption, $V_1 > 0$, $= 0$, $V_3 > 0$ for instance, we form new iables

$$\beta_1 = \frac{\alpha_1}{\alpha_2} = \frac{x_1}{x_2}; \qquad \beta_3 = \frac{\alpha_3}{\alpha_2} = \frac{x_3}{x_2}$$

ince x_2 is constant, the correlation of β_1 h β_3 will be exactly that which would be ulated between x_1 and x_3 in the same sample, he open variables could be measured directly. authors refer to this as the 'concretionary eme.'

armanov and Vistelius also show, in the ne paper, that if two open variables—say, x_2 l x_4—are independent of each other and of remaining variables, the correlation co- cient between the ratios

$$\beta_1 = \frac{\alpha_1}{\alpha_2}; \qquad \beta_3 = \frac{\alpha_3}{\alpha_4}$$

l be of the same sign as that between x_1 and but smaller; this arrangement they call the etasomatic scheme.'

Their results can also be obtained as approxi- tions from the *Pearson* [1896–1897] general mula for ratio correlation [*Reed*, 1921; see also *ayes*, 1949, p. 241, (2)]. For the 'concretionary' eme the Pearson general formula gives

$$r_{\beta_1\beta_3} = \frac{r_{13}C_1C_3 + C_2^2}{(C_1^2 + C_2^2)^{1/2}(C_3^2 + C_2^2)^{1/2}} = r_{13} \quad (23)$$

ce $C_2 = 0$ (C is the coefficient of variation). r the 'metasomatic' scheme Pearson's general rmula reduces to

$$r_{\beta_1\beta_3} = \frac{r_{13}C_1C_3}{(C_1^2 + C_2^2)^{1/2}(C_3^2 + C_4^2)^{1/2}} \leq r_{13} \quad (24)$$

since in this arrangement $C_2 > 0$, $C_4 > 0$. Note that the sign of the ratio correlation will be the same as that of r_{13}, as required. Pearson's derivation is an approximation in the sense that it assumes normally distributed 'open' variables with C small enough so that 3d and higher powers of it may be ignored. Sarmanov and Vistelius now show that the solution for the 'concretionary' scheme requires neither assumption, and that the same holds for the 'metasomatic' scheme if no numerical estimate of the ratio correlation is required.)

In the Sarmanov-Vistelius approach, as in Pearson's original discussion of index correlation, interest centers on hypothetical parent variables *not* subject to (1). From hypothesis or prior knowledge we are able to make reasonable assumptions about certain of the open parent variables; these assumptions enable us to make valid inferences about relations between other open variables, from data that can be obtained only in closed form.

In many petrographic problems, however, we have no way of deducing the necessary a priori relations between the open variables. In still others, including some of the commonest and most important, we have no particular reason to suppose the open variables exist. Equation (1) and the 'spurious' correlation to which it gives rise are always encountered in percentage data, whether or not we are able to regard the percentage form of statement as a mere condition of observation. For the analysis of closed data without assumption about the nature or even the existence of underlying open variables, we obviously require a technique quite different from that proposed by Sarmanov and Vistelius.

On the value of ρ indicative of unrelatedness in a closed array. For the open variables of ordinary experience we use $\rho = 0$ as a criterion of independence, concluding that if the quantity $|r_{12} - 0|$ is not sufficiently large the sample offers no reason for supposing $\rho_{12} \neq 0$. This convention is useful not only because of the intuitively appealing relation it establishes between regression and correlation, but also because in samples drawn from a normal population the distribution of r about $\rho = 0$ is known, so that a simple significance test is possible.

The whole arrangement presumes that the

variables might be statistically independent, however, and we have already seen that the variables of a closed array cannot be independent. Indeed, if the number of variables is reasonably small—about that normally encountered in petrology—the signs and sometimes even the relative sizes of many of the correlations can be established from an examination of the variances alone, with no reference to, and possibly also with little bearing on, the causal nexus often inferred from these associations. The problem of deciding when a particular correlation is strong enough to warrant the inference of nonrandom association remains. We require some working definition of 'unrelatedness' in a closed array, and, based on this definition, a numerical value of ρ to replace the zero of the conventional null hypothesis.

From (2) we note that in any closed array

$$\sum_{i=1}^{M-1} \sum_{j=i+1}^{M} p_{ij} = -\frac{1}{2} \sum_{1}^{M} V_i \qquad (25)$$

If as an entry to the problem, we suppose the variances equal, the right side of (25) is simply $-M\sigma^2/2$. Dividing this by the number of items on the left side of the equation, we obtain for the average, or expected value, of the covariance

$$E(p_{ij}) = -\frac{M\sigma^2}{2\binom{M}{2}} = \frac{\sigma^2}{1 - M} \qquad (26)$$

and, dividing through by $\sigma_i \sigma_j$,

$$\rho = (1 - M)^{-1} \qquad (27)$$

Thus, if the only relation between a set of variables of equal variance is the restraint imposed by (1)—so that they are, from the petrographic point of view, unrelated—the expected value of the sample correlation coefficient is $(1 - M)^{-1}$. If our objective is to detect departures from randomness in the association of any two of the variables, we should test r not against $\rho = 0$, as in the conventional null hypothesis, but against $\rho = (1 - M)^{-1}$, by means of the Fisher z transformation[1].

In practice, of course, the sample varian[ces] will nearly always be unequal. The very fa[ct] that the variance of an accessory or min[or] constituent must be small while that of a maj[or] one may be large practically assures varian[ce] inhomogeneity in any sample of reasonab[le] size. The use of $(1 - M)^{-1}$ as a criterion [of] unrelatedness provides more protection th[an] the null hypothesis against errors of the fir[st] kind in the testing of negative correlation[s] and against those of the second kind in testi[ng] positive ones. But if the variances are marked[ly] inhomogeneous, the protection it affords w[ill] certainly vary from comparison to compariso[n].

Expanding (5) for V_1 and V_2 and subtracti[ng] the second expansion from the first, we hav[e], after eliminating $p_{12}(=p_{21})$ and rearrangi[ng] terms, that

$$\sum_{3}^{M} (p_{2j} - p_{1j}) = V_1 - V_2 \qquad (2\ldots)$$

so that

$$E(p_{2j} - p_{1j}) = \frac{V_1 - V_2}{M - 2} \quad \text{for} \quad j \geq 3 \qquad (2\ldots)$$

and if $V_1 \geq V_2$ the expected covariance $p_{\ldots}$ will necessarily be a smaller negative number tha[n] the expected covariance p_{1j}. (It is obvious fro[m] (5) that the expected covariance $E(p_{jk}) \leq$ [0] for any $j \neq k$.) Since $\sigma_1 > \sigma_2$ this also follow[s] for the correlation coefficients formed fro[m] these covariances unless $p_{2j}/p_{1j} < \sigma_2/\sigma_{\ldots}$ Except in this latter circumstance, then, it [is] to be expected that in the absence of nonrando[m] associations between the variables of a close[d] array the larger negative correlations will b[e] found among the variables of larger varianc[e].

In view of this it is reasonable to inquire ho[w] much sense it makes to test every correlatio[n] in an array against $(1 - M)^{-1}$. The answe[r], I believe, is that the procedure is quite soun[d] if the ratio of maximum to minimum varianc[e] is small, and little superior to the null hypothes[is] if this ratio is large. Correlation analysis of [...]

---

[1] Although the emphasis throughout this paper is on correlation, it is obvious that equation 5 also imposes severe restrictions on regression coefficients. Dividing (5) by V_i we have at once that $\sum b_{ki} = -1$, so that $E(b_{ki}) = (1 - M)^{-1}$, just as for ρ, though in the case of b no assumption about variance homogeneity is required. In the tradition[al] 'variation diagram' of petrology the other six maj[or] oxides are plotted against SiO_2, and the small neg[a]tive slope of many of these indicated regression[s] is well known. The possibility that they are to b[e] regarded as estimates of $(1 - M)^{-1}$ in the null cas[e] is well worth exploring; I hope to discuss it late[r] in another place.

ıer extensive collection of modal analyses arly all those published by Y. Suzuki and self, together with considerable unpublished terial of my own) indicates that in granitic ks the range of variances is large enough so t routine use of $(1 - M)^{-1}$ as a criterion of elatedness would often be inefficient and entially misleading.

. summary of these computations is given Table 1, in which the quantity M' denotes variance rank of the least variable member the group whose average correlation is shown the column headed $r(\bar{z})$. Numbering the iances in an array in order of decreasing , the $r(\bar{z})$ entry in the row headed $M' = 4$, instance, is the r corresponding to

$$= \tfrac{1}{6}(z_{12} + z_{13} + z_{14} + z_{23} + z_{24} + z_{34})$$

l so forth. Comparison of the columns headed and $(1 - M')^{-1}$ indicates that in this ticular body of data the quantity $(1 - M')^{-1}$ rather good estimator of average correlation ween variables of variance rank $\leq M'$, $M' > 2$. How general this relation may be author is not yet able to say. To propose use in a routine significance test would tainly be premature; it nevertheless seems ong enough to warrant further careful study.

Numerical experimentation. Although (27) is entially algebraic rather than statistical, it is h a curious result that some test of it seems irable. Fortunately, it is not difficult to struct a suitable test in any high-speed culator of reasonable capacity. The procedure o generate in the machine an $M \times N$ array of correlated positive variates of mean μ and iance σ^2, divide each entry in the jth row by

$$\sum_{i=1}^{M} X_{ij}$$

$1 \leq j \leq N$, calculate the covariance matrix the resulting $M \times N$ closed array, compute average Fisher z for the $(M)(M - 1)/2$ co-riances, and transform $\bar{z}$ to $r(\bar{z})$. (On a machine the capacity of the IBM 704 this requires nsiderably less than 30 seconds if $M \leq 6$ and ≤ 400.)

between each pair of columns of the original en array is zero. The expected mean of each umn of the closed array is $1/M$. Ignoring a s which decreases rapidly with increase in M, d is in any event the same for each column of any particular array, the expected variance per column of the closed array is $\sigma^2\mu^{-2}M^{-3}(M - 1)$. If (27) is correct, $r(\bar{z})$ calculated from an array generated in this fashion should be such as might be expected from a parent having $\rho = (1 - M)^{-1}$. The results of a test of this kind, made with two runs of $N = 400$ at each value of M, are shown in Table 2. Further testing of (27) would appear to be superfluous.

A similar test of the quantity $(1 - M')^{-1}$, which we may refer to as the 'variance rank correlation,' is more difficult because if either the means or the variances of the open variables differ, the relation between open and closed variances becomes rather complicated. The effect illustrated in Table 1 can hardly be as general as that just discussed; indeed, it is a rather reasonable guess that it will not hold unless the range of (closed) means and variances is quite considerable. A useful test thus requires the generation of an open array whose transformation will yield a closed array with variables characterized by means and variances at least roughly comparable with those encountered in practice.

TABLE 1. Average 'Effective Variance' or 'Variance Rank' Correlation for 543 Modal Analyses[1] For definition of M', see text.

M'	$\bar{z}(M')$	$r(\bar{z})$	$(1 - M')^{-1}$	Number of Groups	Number of Analyses
2	−0.9175	−0.7247	−1.0000	33	543
3	−0.5113	−0.4710	−0.5000	33	543
4	−0.3461	−0.3329	−0.3333	33	543
5	−0.2494	−0.2444	−0.2500	32	526
6	−0.1929	−0.1905	−0.2000	27	476
7	−0.1710	−0.1694	−0.1667	2	41

[1] Data of Suzuki and Chayes.

TABLE 2. Test of Equation 27

M	$\rho = (1 - M)^{-1}$	$r(\bar{z})$
3	−.5000	−.5005
4	−.3333	−.3336
5	−.2500	−.2506
6	−.2000	−.2005

It is nearly self-evident that

$$E\left(\frac{X_{ij}}{T_j}\right) = \frac{\mu_i}{\tau} \tag{30}$$

where

$$\tau = \sum_{i=1}^{M} \mu_i, \quad \rho_{ik} = 0, \quad T_j = \sum_{i=1}^{M} X_{ij},$$

and Greek letters refer to population parameters of the open variables.

Using a theorem of *Fieller* [1939] for the variance of a ratio, and the well-known formula for the part-whole correlation [see *Snedecor*, 1956, p. 189], it may be shown that

$$\operatorname{Var}\left(\frac{X_i}{T}\right) = \left(\frac{\mu_i}{\tau}\right)^2 \left[\frac{\sigma_i^{\,2}}{\mu_i^{\,2}} + \frac{\sigma_t^{\,2}}{\tau^2} - 2\,\frac{\sigma_i^{\,2}}{\mu_i \tau}\right] \tag{31}$$

where, in addition to the previous conditions, we also require that

$$\sigma_t^{\,2} = \sum_{i=1}^{M} \sigma_i^{\,2}$$

which will of course be true if $\rho_{ik} = 0$ for all i and k, $i \neq k$.

TABLE 3. Bellingham Granite Data ($N = 15$) Compared with Statistics Computed from a Numerical Model ($N = 400$) Generated from Uncorrelated Open Variables

A. Means and Standard Deviations

Mineral	Averages: Observed	Averages: Computed	Standard Deviations: Observed	Standard Deviations: Computed
Quartz	29.4	29.5	4.42	4.63
K-feldspar	34.2	33.9	5.98	5.89
Plagioclase	29.9	30.1	4.54	4.38
Biotite	4.5	4.5	2.49	2.45
Muscovite	2.1	2.0	1.01	1.04

B. Average Correlations

M'	$\bar{r}(M')$ Observed	$\bar{r}(M')$ Computed	$(1 - M')^{-1}$
2	−.65	−.57	
3	−.47	−.46	−.50
4	−.34	−.31	−.33
5	−.22	−.21	−.25

The right side of (30) is the expected mean the ith closed variable, and the right side of (3 is its expected variance. Although the relati between open and closed variances is very from simple—it will be noted from (31), instance, that the closed variance cannot zero even if the corresponding open variab is a constant—it is possible, by repeated app cation of (31), to design open arrays which, transformation, yield closed variables cha acterized by realistic means and variances. example is shown in Table 3; the 'real data' calculated from unpublished modes of 15 spe mens of the Bellingham, Minn., granite. T means and variances of the 'numerical mod generated from uncorrelated open variabl agree fairly well with those of the actual measu ments, and the agreement could be improv by further trial and error applications of (3 The average values of $\bar{r}(M')$ obviously show t same general trend in real modes and numeri model. It is clear that in this array a significan test based on $\rho = 0$ is completely unwarrant a test based on $\rho = (1 - M)^{-1}$ is considerab more realistic, and one based on $\rho = (1 - M'$ even more so. How often, or under what c cumstances, $(1 - M')^{-1}$ is preferable $(1 - M)^{-1}$ as a criterion of unrelatedness I not yet know. The treatment of this aspect the problem is still scarely more than prelimina

Some petrological considerations. Althou petrologists generally prefer some form graphical evaluation to formal statistical analy of their data, the underlying assumptions of t two procedures are essentially identical. 'lack of relation' the petrologist usually mea just about what is implied by a sample corre tion which fails of significance against t alternative that $\rho = 0$. In refraining from formal test he sacrifices efficiency, accepts t risk of failing to detect minor subjective diff ences between observers, and devotes to drafti the time he might otherwise spend in calculati But his preference for graphical procedur however wasteful is not essentially unsou provided only that the assumptions underly correlation analysis are in fact valid in t context of his work.

It is the chief burden of this note that th assumptions are decidedly *invalid* in studies relations between the major constituents o closed array. Such studies are of course a ma stay of chemical and theoretical petrolo

means of one type or another of variation gram we incessantly ask what relations hold ween the variables, without bothering to uire whether they are related by more than circumstance that they have certain means l variances and exist in the same body at same time. With a little ingenuity it is ally possible to devise some projection in ich the points will be close enough to a simple ugh curve that a new magmatic or metaso- tic 'trend' can be announced, or an old one firmed.

Between major constituents the great majority such correlations are negative, and with ard to 'genetic' interpretations of these, moral of the preceding discussion is painfully vious. In small samples—even in samples isiderably larger than those we often use— egative correlation must be very strong indeed be significant; the proper criterion of un- atedness is much more likely to be in the inity of -0.5 than of the zero which is licitly assumed in the null hypothesis and itly assumed in graphical procedures. This y be annoying but is not, after all, particularly wildering; and the remedy is as obvious as the ficulty. Either we must confine our attention exceedingly strong negative correlations or must materially enlarge our samples.

The interpretation of small positive sample rrelations, or indeed of those which fall be- een zero and the appropriate negative criterion 'unrelatedness,' on the other hand, seems first-class puzzle. A sample correlation of zero, instance, may indicate a highly significant parture from random association in the di- ction of what we ordinarily regard as positive rrelation. Yet the correlated variance of ichever variable is taken as dependent will negligible, information about either variable ll permit no reliable inference about the other, d in a scatter diagram the data points will stribute themselves in the fashion we have me to regard as indicative of randomness or nrelation. In short, the usual elegant rela- on between the geometrical and analytical pects of product-moment correlation vanishes mpletely. So, too, does the possibility of making sense of the data by the customary empathic appreciation of variation diagrams.

An example of this conflict between inter- pretations of 'open' and 'closed' correlations occurs in the data for Bellingham. Since plagio- clase and quartz have, respectively, the variance ranks 2 and 3, our argument suggests that in the absence of nonrandom effects the correlation coefficient for the pair should be in the neighbor- hood of -0.5, and, as shown in Table 3, the average correlation of the three most variable constituents is very close to this. The observed correlation between quartz and plagioclase, however, is $+.0086$. A sample value of $r = +.0086$ as between a pair of open variables would certainly be taken to indicate the absence of nonrandom factors governing the association. Given the information that the variables are members of a 5-variable closed array, and have variance ranks 2 and 3, we should have to announce an exactly opposite conclusion.

Acknowledgments. I am indebted to J. M. Cameron for much helpful discussion, particularly of the relation between closed and open variances, and to Mrs. R. W. Varner, who supervised all and did some of the programming. The calculations leading to Tables 1–3 were run at the National Bureau of Standards.

References

Chayes, F., A petrographic criterion for the possible replacement origin of rocks, *Am. J. Sci., 246,* 413–425, 1948.

Chayes, F., Ratio correlation in petrography, *J. Geol., 57,* 239–254, 1949.

Fieller, E. C. The distribution of the index in a normal bivariate population, *Biometrika, 24,* 428–440, 1932.

Pearson, K., On a form of spurious correlation, etc., *Proc. Roy. Soc.* (London), *60,* 489–502, 1896–1897.

Reed, L. J., On the correlation between any two functions, etc., *Wash. Acad. Sci. J., 11,* 449–455, 1921.

Sarmanov, O. V., and A. B. Vistelius, On the correlation of percentage values, *Doklady Akad. Nauk SSSR, 126,* 22–25, 1958. (In Russian.)

Snedecor, G. W., *Statistical Methods,* 5th ed., Iowa State College Press, 1956.

(Manuscript received September 27, 1960.)

Geomagnetic and Solar Data

J. VIRGINIA LINCOLN

Central Radio Propagation Laboratory
National Bureau of Standards
Boulder, Colorado

INTERNATIONAL DATA ON MAGNETIC DISTURBANCES

This report continues the series which has ap-ared regularly in this *Journal* since vol-ne *54* (3), 295, 1949. Please refer to that first port for an explanation of the data given, and *59* (3), 423, 1954 for the definition of *Ap*.

Note: Additional and final 'Geomagnetic and lar Data' appears in due course in the following international publications: *Quarterly Bulletin on Solar Activity*, International Astronomical Union, c/o Eidgen. Steinwarte, Zurich, Switzerland; *IAGA Bulletins, Geomagnetic Indices K and C*, by J. Bartels, A. Romaña, and J. Veldkamp, International Union of Geodesy and Geophysics, Association of Geomagnetism and Aeronomy, c/o V. Laursen, Meteorologisk Institut, Charlottenlund, Denmark.

PRINCIPAL MAGNETIC STORMS

(Advance knowledge of the character of the records at some observatories as regards disturbances)

Observatory (Observer-in-Charge) (1)	Greenwich date (2)	Storm-time: GMT of begin. (3)	Storm-time: GMT of ending[1] (4)	Sudden commencement: Type[2] (5)	Sudden commencement: Amplitudes[3] D (6)	Amplitudes[3] H (7)	Amplitudes[3] Z (8)	C-figure, degree of activity[4] (9)	Maximal activity on K-scale 0 to 9: Gr. day (10)	Gr. 3-hr. period (11)	K-index (12)	Ranges: D (13)	H (14)	Z (15)
	1960	*h m*	*d h*		′	γ	γ					′	γ	γ
ollege	Mar. 31	04 30	2 14	.....	....	....	....	s	1	5	9	516	3030	1940
J. Beers)	Apr. 2	23 12	3 11	s.c.*	−18	*+258*	−21	s	3	2	8	266	1960	770
	Apr. 10	1 27	10 18	s.c.*	−7	+69	+6	ms	10	4	6	105	1030	2980
	Apr. 23	21 ..	25 22	.....	....	....	....	ms	24	3,5,7	6	162	1260	910
									25	3,4				
	Apr. 27	20 00	29 20	s.c.*	−14	−174	−9	ms	28	5,6,7	7	399	1700	1180
									29	4				
	Apr. 30	01 32	1 15	s.c.*	+40	+555	+43	s	30	6	9	563	3540	3540
	May 5	18 54	7 08	.....	....	....	....	ms	6	7	7	177	1750	620
	May 7	08 46	8 00	s.c.*	−7	−101	−9	ms	7	5	6	118	720	530
	May 8	04 21	9 07	s.c.*	−42	+491	+44	s	8	6	8	416	2250	1260
	Jun. 4	21 15	05 18	.....	....	....	....	ms	5	3	7	184	1360	970
	Jun. 27	01 47	27 13	s.c.*	−31	+315	−63	ms	27	2,3,4	6	178	1440	940
	Jun. 29	19 38	30 06	s.c.*	+35	+70	+53	ms	30	2	6	189	825	920
tka	Apr. 2	23 13	3 11	s.c.	+4	−56	−12	ms	3	2,3,4	7	90	950	600
M. L. Cleven)	Apr. 13	05 00	13 09	.....	....	....	....	ms	13	3	7	60	660	540
	Apr. 16	12 00	17 11	.....	....	....	....	ms	16	5	7	90	650	690
	Apr. 24	01 00	25 17	.....	....	....	....	ms	24	1,3,5	7	105	950	530
									25	1	7			
	Apr. 27	20 00	29 14	s.c.*	+27	−67	−42	s	28	3,5	8	130	1440	730
	Apr. 30	01 32	1 14	s.c.*	−12	+235	+40	s	30	5,6	9	460	3650	1800
	May 6	06 00	9 13	.....	....	....	....	s	8	5,6	9	175	2050	920
	May 11	04 34	12 15	s.c.*	+9	+85	+21	ms	11	2,3	7	70	720	490
	May 28	20 19	30 16	s.c.*	+21	+63	−32	ms	29	1	7	95	800	560
	Jun. 4	02 30	6 14	.....	....	....	....	s	5	4	8	160	1480	670
	Jun. 25	12 30	28 13	.....	....	....	....	s	27	1	9	136	1880	765
	Jun. 29	19 39	30 06	s.c.*	+17	+44	−26	s	30	2	8	100	920	520

[1]Approximate time of ending of storm construed as the time of cessation of reasonably marked disturbance movements in the aces; more specifically, when the *K*-index measure diminished to 2 or less for a reasonable period.

[2]s.c. = sudden commencement; s.c.* = small initial impulse followed by main impulse (the amplitude in this case is that of the in impulse only, neglecting the initial brief pulse); ... = gradual commencement.

[3]Signs of amplitudes of *D* and *Z* taken algebraically: *D* reckoned positive if towards the East and *Z* reckoned positive if verti-lly downwards.

[4]Storm described by three degrees of activity: *m* for moderate (when *K*-index as great as 5); *ms* for moderately severe (when = 6 or 7); *s* for severe (when *K* = 8 or 9).

PRINCIPAL MAGNETIC STORMS—Continued

Observatory (Observer-in-Charge) (1)	Greenwich date (2)	Storm-time: GMT of begin. (3)	Storm-time: GMT of ending[1] (4)	Sudden commencement: Type[2] (5)	Sudden commencement: Amplitudes[3] D (6)	H (7)	Z (8)	C-figure, degree of activity[4] (9)	Maximal activity on K-scale 0 to 9: Gr. day (10)	Gr. 3-hr period (11)	K-index (12)	Ranges: D (13)	H (14)
	1960	*h m*	*d h*		′	γ	γ					′	γ
Witteveen (D. V. Sabben)	Apr. 2	23 13	3 19	s.c.*	−4	+36	0	ms	3	1,2,3	6	40	160
	Apr. 5	12 59	5 21	s.c.*	−4	+56	0	ms	5	6	6	30	145
	Apr. 10	01 27	12 10	s.c.*	−2	+18	0	ms	10	8	6	35	155
	Apr. 16	12 00	17 05	.....	....	....	....	ms	17	1	6	30	90
	Apr. 23	21 00	25 24	.....	....	....	....	ms	24	1,8			
									25	1	6	55	270
	Apr. 27	20 01	1 17	s.c.	−3	+95	0	s	30	6	9	105	960
	May 6	16 50	9 18	s.c.*	+1	−12	0	ms	6	7	7	45	380
									8	4,5,6			
	May 11	04 35	11 13	s.c.*	−12	+38	−1	ms	11	2,3	6	20	190
	May 16	13 50	16 24	s.c.*	−3	+85	+3	ms	16	6	7	30	255
	May 23	14 00	24 08	.....	....	....	....	ms	23	5	6	20	240
	May 28	20 19	29 24	s.c.	−6	+133	0	ms	29	1	7	45	210
	Jun. 4	02 50	5 21	s.c.	−5	+47	0	ms	4	2	6	25	215
	Jun. 25	11 00	26 06	.....	....	....	....	m	25	6,8			
									26	2	5	20	165
	Jun. 27	01 45	28 21	s.c.	−5	+36	0	ms	27	6,7	6	30	220
	Jun. 29	19 39	1 21	s.c.*	−6	+95	0	ms	29	8			
									30	1,6,7	6	35	270
Fredericksburg (R.E.Gebhardt)	Apr. 2	23 14	5 09	s.c.*	−2	+60	−7	ms	3	1,2,3	6	36	223
	Apr. 10	01 27	13 12	s.c.*	+1	+20	−3	m	10	8	5	33	119
									11	8	5		
									12	1,2	5		
									13	1,2,3	5		
	Apr. 16	12 ..	18 12	.....	....	....	....	m	17	1	5	32	107
									18	1			
	Apr. 23	21 ..	26 11	.....	....	....	....	ms	24	1,2,8	6	40	209
									25	1			
	Apr. 27	20 00	2 12	s.c.*	+1	+105	−10	s	30	5,6	9	97	791
	May 5	20 ..	8 01	.....	....	....	....	ms	6	8	7	33	216
	May 8	04 22	9 12	s.c.*	+7	+107	−19	ms	8	4	7	45	313
	May 11	04 34	12 22	s.c.*	+2	+64	−10	ms	11	2	6	22	149
	May 16	13 51	17 14	s.c.*	+6	+23	−2	ms	16	7,8	6	23	214
	May 23	12 ..	25 05	.....	....	....	....	ms	23	7	6	25	190
	May 28	20 19	30 17	s.c.*	−1	+131	−13	ms	29	1	7	38	212
	Jun. 3	18 ..		.....	....	....	....	ms	4	2,3,8	6	33	216
	Jun. 4	02 50	6 18	s.c.	−1	+90	−12						
	Jun. 25	12 ..	26 11	.....	....	....	....	m	26	1	5	24	97
	Jun. 27	01 44	29 09	s.c.	−1	+84	−11	ms	27	2	6	37	172
	Jun. 29	19 38		s.c.*	−2	+85	−10	ms	30	1,7	6	25	235
Tucson (R. L. Viets)	Apr. 2	23 14	5 18	s.c.	−2	+44	+3	ms	3	2,3	6	18	135
									5	2			
	Apr. 10	01 27	13 09	.....	....	....	....	ms	13	3	6	21	133
	Apr. 23	21 ..	25 18	.....	....	....	....	ms	24	1	7	21	218
	Apr. 27	20 00	29 17	s.c.	1	+36	+1	ms	27	8	6	26	169
									28	3			
									29	3			
	Apr. 30	01 32	1 10	s.c.	2	+50	+4	s	30	6	9	51	629
	May 5	20 00	7 24	.....	....	....	....	ms	6	8	6	19	199
									7	2			
	May 8	04 22	9 17	s.c.*	−6	+72	+7	ms	8	2,4,6,7,8	6	16	150
	May 11	04 34	11 13	s.c.*	3	45	3	ms	11	2,3	6	21	112
	May 16	13 27	17 14	.....	....	....	....	ms	16	6,7,8	6	21	153
	May 28	20 19	30 17	s.c.	3	73	3	ms	29	1	6	20	152
	Jun. 4	02 50	5 13	s.c.	−2	+78	+1	ms	4	1,2	6	21	151
									5	3			
	Jun. 27	01 45	28 13	s.c.	−2	+73	+6	ms	27	2	7	19	158
	Jun. 29	19 39	2 16	s.c.	−1	+51	+3	ms	29	8	6	19	185
									30	1,7			
San Juan (M. Vazquez)	Apr. 27	20 00	29 09	s.c.	+1	+34	−8	ms	27	8	6	14	180
	Apr. 30	01 32	1 10	s.c.	−1	+40	−14	s	30	6	9	26	382
	May 6	17 ..	7 24	.....	....	....	....	ms	6	8	6	18	162
									7	1			
	May 8	04 22	9 12	s.c.	+1	+52	−20	ms	8	2,4,6,8	6	12	165
	May 11	04 35	11 10	s.c.	....	+29	−10	m	11	2,3	5	5	67
	May 16	13 51	17 03	.....	....	....	....	ms	16	7	6	11	58
	May 28	20 19	29 24	s.c.	−1	+49	−15	ms	29	1	6	7	122

PRINCIPAL MAGNETIC STORMS—Continued

Observatory (Observer-in-Charge)	Green-wich date	Storm-time		Sudden commencement				C-figure, degree of ac-tivity[4]	Maximal activity on K-scale 0 to 9			Ranges		
		GMT of begin.	GMT of ending[1]	Type[2]	Amplitudes[3]				Gr. day	Gr. 3-hr. period	K-index	D	H	Z
					D	H	Z							
(1)	(2)	(3)	(4)	(5)	(6)	(7)	(8)	(9)	(10)	(11)	(12)	(13)	(14)	(15)
	1960	h m	d h		′	γ	γ					′	γ	γ
onolulu	Apr. 2	23 13	3 15	s.c.	−1	+25	+15	ms	3	2,3	6	5	185	35
. .E.Haraden)	Apr. 27	20 01	29 15	s.c.	+2	+35	+15	ms	28	3	6	4	115	35
	Apr. 30	12 13	1 09	s.c.	−1	+112	+73	s	30	5	8	15	300	105
	May 8	04 22	9 15	s.c.*	−1	+30	+26	ms	8	4,8	6	4	110	40
	May 11	04 35	12 18	s.c.	−1	+22	+15	m	11	2,3,4	5	5	70	30
	May 16	11 ..	17 18	.....	....	....	....	ms	16	7,8	6	6	60	35
	May 28	20 19	30 15	s.c.	+1	+45	+16	ms	29	1	6	4	95	45
	Jun. 4	02 50	5 12	s.c.*	−3	+36	+10	ms	4	1,2	6	4	170	25
									5	1				
. K.	Jun. 27	01 46	28 21	s.c.	−2	+39	+20	ms	27	2	6	5	160	25
McCaffrey)	Jun. 29	19 39	1 18	s.c.	+2	+30	+12	ms	30	1	6	5	180	30
uancayo	Apr. 2	23 12	5 21	.....	....	....	....	m	3	1	5	8	262	52
.. Giesecke)									5	7				
	Apr. 7	15 11	8 03	s.c.*	+3	+122	+7	ms	7	7	6	5	366	19
	Apr. 23	22 00	25 18	.....	....	....	....	ms	24	2	6	5	393	19
	Apr. 27	20 01	29 08	s.c.*	−1	+114	+12	m	27	7	5	9	402	65
	Apr. 30	01 32	1 20	s.c.	−1	+60	+10	s	30	6	9	22	1038	153
	May 6	00 40	7 24	.....	....	....	....	ms	6	6,7	6	6	460	56
									7	5				
	May 8	04 22	9 17	s.c.	0	+84	+14	ms	8	6	7	9	348	44
	May 16	12 30	17 18	.....	....	....	....	ms	16	7	6	9	373	44
	May 23	14 00	24 07	.....	....	....	....	m	23	5,7	5	6	285	27
	May 28	20 19	29 22	s.c.	−1	+106	+13	ms	29	5	6	5	242	27
	Jun. 4	02 50	5 13	s.c.	−1	+68	+14	m	4	4,5	5	6	256	33
	Jun. 25	12 00	25 23	.....	....	....	....	m	25	6	5	3	219	28
	Jun. 27	01 46	28 13	s.c.	−1	+64	+11	m	27	6,7	5	8	335	49
	Jun. 30	12 00	30 22	.....	....	....	....	m	30	6,7	5	7	199	42
ort Moresby	Apr. 2	23 12	3 15	s.c.	+1	+30	+19	ms	3	2,3	7	8	212	81
J. A. Brooks)	Apr. 27	20 01	28 21	s.c.*	+1*	+17	+17	m	28	1,3,5	6	5	222	100
	Apr. 30	12 14	1 10	s.c.*	−5*	+97	+65	s	30	5,6,7	8	9	395	246
	May 8	04 21	9 11	s.c.	+2	+55	+30	ms	8	4	7	11	208	139
	May 16	11 20	17 14	.....	....	....	....	m	16	7,8	6	4	141	75
	May 28	20 19	29 18	s.c.	+1	+26	+29	m	29	1	6	5	100	73
	Jun. 4	02 50	5 13	s.c.	−1	+55	+43	m	4	2,3	6	5	239	101
	Jun. 27	01 45	28 14	s.c.	−1	+50	+36	m	27	1,2	6	6	188	87
pia	Apr. 2	23 13	6 03	s.c.	0	+28	−10	ms	3	1,2,3	6	7	140	39
J. G. Keys)	Apr. 10	01 27	13 10	.....	....	....	....	m	13	2	5	3	123	28
	Apr. 16	13 04	18 12	.....	....	....	....	m	18	1	5	4	91	24
	Apr. 23	23 17	27 00	.....	....	....	....	ms	24	1	6	6	212	50
	Apr. 27	20 00	29 13	s.c.	0	+32	−7	ms	27	8				
									28	3	6	7	229	47
	Apr. 30	01 32	30 12	s.c.	0	+25	−11	ms	30	4	6	5	116	38
	Apr. 30	12 14	2 13	s.c.	0	+71	−32	s	30	6	8	14	408	67
	May 5	20 32	8 01	.....	....	....	....	ms	6	8	6	5	112	29
	May 8	04 21	9 14	s.c.	0	+34	−18	ms	8	4	6	6	155	34
	May 11	04 35	12 15	s.c.	0	+18	−9	m	11	2,3,4	5	5	103	26
	May 16	11 20	17 15	.....	....	....	....	ms	16	7,8	6	6	125	32
	May 28	20 19	30 15	s.c.	0	+36	−10	m	29	1	5	4	101	29
	Jun. 4	02 49	6 13	s.c.	−1	+33	−7	ms	4	2,3	6	5	185	42
	Jun. 27	01 46	29 12	s.c.	−0	+31	−11	ms	27	2	6	6	172	51
	Jun. 29	19 39	1 15	s.c.	0	+26	−9	ms	29	8	6	5	180	48
Hermanus	Mar. 31	10 ..	2 13	.....	....	....	....	s	31	6	8	81	380	480
(A.M. van Wijk)									1	6,7	8			
	Apr. 2	23 13	3 20	s.c.	+2	+20	+16	m	3	1,2,3	5	19	105	68
	Apr. 5	00 ..	5 21	.....	....	....	....	m	5	3	5	21	83	70
			Sharp impulses at 0842 and 1300.											
	Apr. 7	15 11	8 14	s.c.	+1	+4	+3	m	7	6,7	5	17	93	114
	Apr. 10	01 27	11 06	s.c.	+1	+9	+9	ms	10	8	6	14	97	84
	Apr. 11	21 ..	12 15	.....	....	....	....	m	12	1,2,3	5	14	84	60
	Apr. 12	21 ..	13 12	bays	....	....	....	m	13	2	5	11	69	36
	Apr. 15	04 ..	15 08	bay	....	....	....	m	15	2	5	15	14	26
	Apr. 16	11 ..	18 12	.....	....	....	....	m	16	6	5	20	108	101
									17	1	5			
									18	1	5			
	Apr. 23	19 ..	26 02	.....	....	....	....	ms	24	2,8	6	25	135	122
	Apr. 26	22 ..	27 01	bay	....	....	....	m	26	8	5	7	46	47

PRINCIPAL MAGNETIC STORMS—Concluded

Observatory (Observer-in-Charge) (1)	Greenwich date (2)	Storm-time: GMT of begin. (2)	Storm-time: GMT of ending[1] (4)	Sudden commencement: Type[2] (5)	Sudden commencement: Amplitudes[3] D (6)	Amplitudes[3] H (7)	Amplitudes[3] Z (8)	C-figure, degree of activity[4] (9)	Maximal activity on K-scale 0 to 9: Gr. day (10)	Gr. 3-hr. period (11)	K-index (12)	Ranges: D (13)	Ranges: H (14)	Ranges: Z (1[illegible]
	1960	h m	d h		′	γ	γ					′	γ	γ
Hermanus —Continued	Apr. 27	20 00	30 07	s.c.	+1	+23	+12	ms	27	8	6	34	205	1[illegible]
(A. M. van Wijk)									28	1,7	6			
	Sharp impulse at 0132 on Apr. 30													
	Apr. 30	12 14	1 23	s.c.	+5	+66	+53	s	30	6	9	67	414	5[illegible]
	May 6	16 ..	8 01	.....	....	....	....	m	6	6,7,8	5	27	129	1[illegible]
									7	1,4,5,6	5			
	May 8	04 22	9 14	s.c.*	+9*	+39	+36	ms	8	5,6,8	6	29	249	1[illegible]
	Large reverse impulse in D													
	May 11	04 37	11 17	s.c.*	+5*	+16	+18	m	11	2,3	5	14	77	[illegible]
	May 16	13 51	17 17	s.c.	+2	+21	+16	m	16	5,6,7,8	5	18	63	1[illegible]
	May 24	05 ..	24 10	bay	....	....	....	m	24	3	5	15	29	[illegible]
	May 28	20 20	30 05	s.c.	+2	+32	+25	m	29	1,3,7,8	5	18	118	10[illegible]
	Jun. 1	02 ..	1 16	bays	....	....	....	m	1	2	5	15	104	[illegible]
	Jun. 4	02 ..	5 13	.....	....	....	....	ms	4	3	6	25	112	8[illegible]
	Jun. 25	12 ..	26 11	.....	....	....	....	m	26	1,2	5	17	71	[illegible]
	Jun. 26	19 ..	27 11	.....	....	....	....	m	27	1,2	5	20	101	[illegible]
	Jun. 27	16 ..	28 15	.....	....	....	....	m	27	8	5	12	112	8[illegible]
									28	3,4	5			
	Jun. 29	19 39	1 05	s.c.	2	23	19	m	29	8	5	18	82	7[illegible]
									30	1,7,8	5			
Gnangara (P. M. McGregor)	Apr. 2	23 12	3 13	s.c.*	−6	....	−30*	ms	3	1	7	26	120	12[illegible]
	Apr. 23	21 10	26 01	.....	....	....	....	ms	24	5	6	26	166	12[illegible]
									25	1,5				
	Apr. 27	20 00	29 20	s.c.*	+7*	+25	+34*	ms	28	5	7	47	175	2[illegible]
	Apr. 30	01 31		s.c.*	+4*	−12	−16*	s	30	6	9	82	508	5[illegible]
	May 5	20 ..	7 21	.....	....	....	....	m	6	7,8	5	21	97	1[illegible]
									7	6	5			
	May 8	04 21	9 13	s.c.	−5	−36	−19	ms	8	4,6	6	35	145	(21[illegible]
	May 28	20 19	30 16	s.c.*	+7*	+10	+31*	m	29	1	5	16	107	8[illegible]
	No record 2300 10th–1200 11th May													
	Jun. 4	02 47	5 14	s.c.*	−5	+31*	−18*	m	4	2,3	5	14	129	10[illegible]
									5	4	5			
	Jun. 27	01 46	28 14	s.c.*	−5*	+19	....	m	27	1	5	14	106	...
									28	4	5			
	No Z record for 27th June													
Toolangi (C. A. van der Waal)	Apr. 2	23 13	3 10	s.c.*	+7*	+9	0	ms	3	2	6	30	160	10[illegible]
	Apr. 27	20 01	29 12	s.c.*	+5*	+18	+2	ms	28	3,5	6	35	225	13[illegible]
	Apr. 30	01 32	.. ..	s.c.*	−4*	+51*	−1*	m	30	1,2,4	5	25	150	7[illegible]
	Apr. 30	12 14	1 10	s.c.*	−12	+125	−6	s	30	6	9	55	665	>28[illegible]
	May 5	23 ..	7 24	.....	....	....	....	ms	6	7	6	27	152	8[illegible]
	May 8	04 20	9 18	s.c.*	+6	−28	....	ms	8	6	7	39	180	10[illegible]
	Jun. 4	02 ..	5 16	.....	....	....	....	m	4	2,3,4	5	26	160	9[illegible]
									5	4				
	Jun. 27	01 46	29 11	s.c.	−5	+43	+7	ms	28	4	6	32	175	6[illegible]
Amberley (A. L. Cullington)	Apr. 3	23 12	5 10	.....	....	....	....	ms	3	1,2	6	23	174	12[illegible]
	Apr. 11	23 00	13 10	.....	....	....	....	m	12	3	5	20	89	4[illegible]
	Apr. 27	20 02	29 16	s.c.*	+3	+14	−11	ms	28	3	6	39	191	17[illegible]
	Apr. 30	01 33	.. ..	s.c.*	−4	+35	+18	ms	30	4	6	24	141	7[illegible]
	Apr. 30	12 15	1 10	s.c.*	+1	+134	−10	s	30	5,6	8	55	588	53[illegible]
	May 5	19 03	con-tinues	s.c.	−1	+4	+3	m	6	5	5	27	74	3[illegible]
	May 6	19 18	8 01	s.c.*	−2	+23	+8	m	6	7,8	5	18	145	8[illegible]
	May 8	04 24	9 15	s.c.	−3	+50	+10	ms	8	5,6	6	34	203	22[illegible]
	May 11	04 35	11 13	s.c.*	+4	+77	−15	ms	11	2,3	6	21	149	6[illegible]
	May 23	14 ..	24 13	.....	....	....	....	m	24	3	5	15	142	5[illegible]
	May 28	20 21	30 17	s.c.*	−1	+16	+4	m	29	1	5	16	128	4[illegible]
	Jun. 4	02 06	4 12	.....	....	....	....	m	4	2,3	5	23	141	10[illegible]
	Jun. 27	01 48	27 11	s.c.	+1	+51	−4	ms	27	2	6	23	157	8[illegible]
	Jun. 27	16 37	28 13	.....	....	....	....	m	28	4	5	26	122	3[illegible]
	Jun. 29	19 40	30 06	s.c.	−4	+16	+13	m	30	2	5	17	152	7[illegible]

SELECTED GEOMAGNETIC AND SOLAR DATA

Kp, Ci, Cp, Ap, K_{Fr}, *Rz*, and Selected Days

August 1960†

Day[1]	Three-hour Range Indices Kp[2] 1	2	3	4	5	6	7	8	Sum	Prel.[3] Ci	Cp[4]	Ap[5]	3-hr. Range Indices K_{Fr}[6] Values	Sum	Prov.[7] Rz
1	3−	3o	3o	3o	4o	2−	2−	3−	22−	0.7	0.8	14	3333 3223	22	63
2	3−	4+	3o	3−	2+	3o	3+	4o	25+	0.9	1.0	18	3533 2133	23	53
3 q	3−	1+	2−	2o	2o	2o	1+	2−	15−	0.4	0.3	7	2122 2212	14	31
4 Q	2+	2+	2o	3o	1+	1−	1o	1−	13+	0.4	0.3	7	3324 1121	17	32
5 Q	1−	1o	1o	1−	1o	1−	1−	0+	6o	0.1	0.1	3	1221 1110	09	25
6 q	1−	1−	2+	2+	1+	2o	2+	2+	14o	0.4	0.3	7	1143 2133	18	24
7 q	3o	2o	2−	2−	2−	3−	1+	0o	14o	0.5	0.4	7	4222 3221	18	57
8	1−	2−	4−	3−	3+	4−	3+	4o	23o	1.0	0.9	16	1242 3334	22	57
9	4−	5o	5−	4o	3−	2+	2+	2o	27−	1.1	1.1	22	4544 3222	26	76
10	3−	2o	4−	3o	3o	3+	3−	2o	22+	0.8	0.8	14	2233 2322	19	94
11	2+	5o	3+	4+	4o	4−	4−	2+	29−	1.2	1.1	23	3544 3342	28	156
12	3+	4+	5o	5−	4−	3o	2o	2+	28+	1.1	1.1	24	3454 3233	27	207
13 q	2−	2+	2−	2+	3−	2−	2o	2−	16o	0.5	0.4	8	2312 2222	16	235
14	2o	2+	2−	2−	2o	4+	4o	3+	21+	1.0	0.8	14	3323 2443	24	236
15	3+	3−	2+	2o	1+	2−	1+	1o	16−	0.5	0.4	8	4422 1121	17	252
16 D	2−	1−	1−	2−	6+	7o	6+	6o	30+	1.4	1.6	52	1012 6645	25	244
17 D	8−	8−	7o	5+	4+	7−	6+	6−	51−	1.8	1.9	106	6655 3444	37	232
18	4−	3o	4−	5−	3−	2−	2−	1+	22+	1.0	0.9	16	4345 2122	23	225
19	2o	1o	2o	3+	3−	4+	4+	5+	25o	1.2	1.1	21	3123 3344	23	217
20	2+	5−	6o	3o	3o	3−	3+	3+	28+	1.3	1.2	26	2453 3233	25	202
21 D	4o	4o	5−	5o	3o	4−	4o	4−	32o	1.2	1.2	28	4444 4333	29	177
22	5−	3−	2−	2+	2−	2+	3+	2+	21o	0.8	0.8	14	5311 1333	20	168
23 q	2+	2+	2o	2−	1o	2+	2+	1o	15o	0.4	0.4	7	3321 1122	15	130
24 Q	2−	1o	2o	3o	1−	1+	1+	1−	12−	0.2	0.3	6	2123 0122	13	113
25 Q	1−	0+	1−	0+	1o	1+	1+	1−	6+	0.1	0.1	3	1100 0111	05	131
26 Q	0o	0+	1o	1o	1−	1o	1+	2o	7+	0.1	0.1	4	0111 1113	09	140
27	3+	3−	2o	2+	2o	4−	5−	3+	24o	1.1	0.9	16	3311 2453	22	109
28	3−	4+	4o	1o	3−	3o	1−	1o	19+	0.8	0.8	14	4541 2211	20	98
29 D	5o	7−	5o	3+	4+	4+	4−	5o	37+	1.5	1.5	45	5643 3345	33	97
30 D	6−	7o	7o	5o	4o	4+	3o	2o	38o	1.4	1.7	58	5764 3332	33	96
31	3+	4o	4+	3o	3−	2−	2−	3−	23+	0.8	0.9	16	3444 3002	20	84
									Means:	0.83	0.81	20			131.0
									No. of days:	31	31	31			31

† In the Nov. issue, this table was incorrectly dated Jan. 1960. The date should have been July 1960.

Notes:

1 Five quiet days (Q), ten quiet days (Q or q), five disturbed days (D) selected by Committee on Characterization of Magnetic Disturbances, J. Veldkamp, Kon. Nederlandsch Meteorologisch Instituut, DeBilt, Holland.

2 Geomagnetic planetary three-hour-range indices Kp prepared by Committee on Characterization of Magnetic Disturbances, J. Bartels, Chairman, University, Göttingen, Germany.

3 Preliminary magnetic character-figures, Ci, prepared by J. Veldkamp.

4 Magnetic character-figures, Cp, prepared by J. Bartels.

5 Average amplitudes Ap (unit 2γ), prepared by J. Bartels.

6 Fredericksburg three-hour-range indices K ($K9 = 500\gamma$); scale-values of variometers in γ/mm: $D = 2.7$; $H = 2.5$, $Z = 3.1$) prepared by Robert E. Gebhardt, Observer-in-Charge, Fredericksburg Magnetic Observatory, Corbin, Virginia.

7 Provisional sunspot-numbers (dependent on observations at Zurich Observatory and its stations at Locarno and Arosa) prepared by M. Waldmeier, Swiss Federal Observatory, Zurich, Switzerland.

Letters to the Editor

Solar Flare Cosmic-Ray Increase of May 4, 1960

R. B. Brode and R. R. Brown

Department of Physics
University of California
Berkeley, California

and

W. R. Steiger

Department of Physics
University of Hawaii
Honolulu, Hawaii

It is the purpose of this letter to present observations of cosmic-ray intensity obtained with neutron monitors during the period 1000 to 1200 UT of May 4, 1960. This particular period is of interest in that at 1020 UT a solar flare of importance 2 in a region near the west limb of the sun accelerated particles to cosmic-ray energies and was the source of a brief increase in cosmic-ray intensity both at the earth and in interplanetary space.

The neutron monitors were located at Berkeley, California, and Makapuu Point, Hawaii, fo which the cutoff rigidities are 4.4 and 11.3 B respectively [*Quenby and Webber*, 1959]. Th monitors were arranged in a 'folded' geometr one section located above the other. Typic counting rates of the monitors under undi turbed conditions are 400 and 300 counts pe minute, respectively.

Following the flare of importance 2 at 10

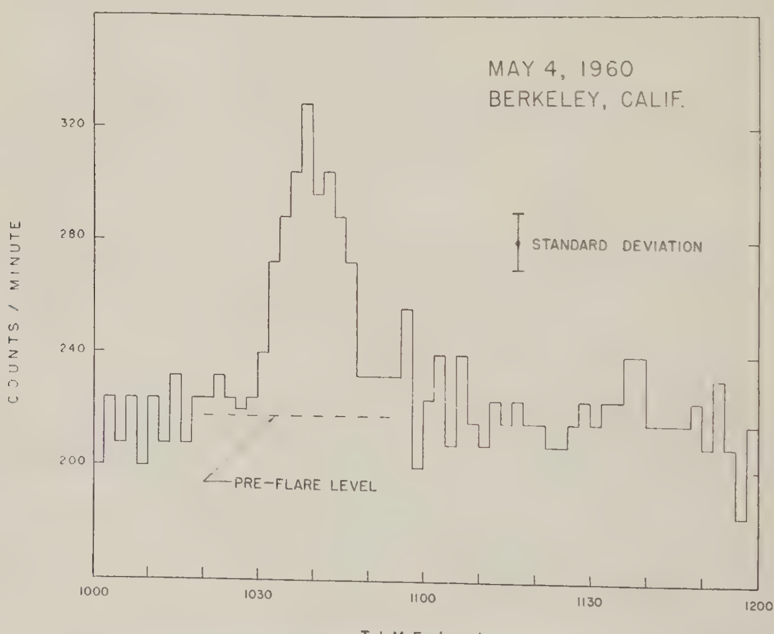

Fig. 1. Counting rate of the Berkeley neutron monitor during May 4 flare event.

T on May 4, 1960, the counting rate of the Berkeley monitor showed an increase of approximately 50 per cent. The counting rate of one section of the monitor is shown in Figure 1; the data from the other section were not recorded due to an optical failure in the recording system. From this record it is seen that the intensity was increasing beyond the preflare level between 1030 and 1032 UT, reached its maximum value between 1038 and 1040 UT, and then had returned to the preflare level by 1100 UT. During the same interval of time the Makapuu Point monitor showed no intensity variations other than those which would be attributed to statistical fluctuations in the counting rate.

It is interesting to compare the intensity variations observed with the Berkeley monitor during the May event with those associated with the great event of February 23, 1956 [*Brode and Goodwin*, 1956], especially since both flares occurred near the west limb of the sun. In both cases the times for rise of the flare radiation to maximum intensity were about the same, although the decay times of the flare radiation were quite different. During the February 1956 event, the radiation had disappeared about 3 to 4 hours after the flare while in the recent event the increase was quite brief, lasting altogether 30 to 40 minutes. The difference in storage times for these two events appears to be related to differences in electromagnetic conditions in interplanetary space; the February 1956 event occurred very close to the middle of a large 27-day decrease while the May 1960 event occurred late in the recovery phase of a moderate Forbush decrease. This suggests that the degree of disorder of the interplanetary field is closely related to the level of solar activity.

Acknowledgments. We are indebted to Mr. Wayne B. Hughes and Mr. Roy Nojima for assistance in maintaining the neutron monitors.

References

Quenby, J. J., and W. R. Webber, *Phil. Mag.*, *4*, 90, 1959.

Brode, R. B., and A. Goodwin, *Phys. Rev.*, *103*, 377, 1956.

(Received September 21, 1960.)

Preliminary Report on Crustal Magnetotelluric Measurements

T. Cantwell and T. R. Madden

Department of Geology and Geophysics
Massachusetts Institute of Technology,
Cambridge, Massachusetts

Some preliminary work on the determination of the earth's electric conductivity structure through simultaneous measurements of the natural electric and magnetic fields is reported in this letter. *Cagniard* [1953] coined the name 'magnetotelluric' for studies of this type. The present work was confined to frequencies of .005 to 1 cps, having skin depths distributed through the crust.

Magnetotelluric studies have been underway in the M.I.T. Geophysics Laboratory for several years. *Nevés* [1957] studied two-dimensional effects, and more recently the measurements described here were made [*Cantwell*, 1960]. Further field investigations are under way at this time, and will be incorporated in a more complete paper in the near future.

The idea of using geomagnetic and geoelectric measurements in combination to elucidate the electric conductivity structure of the earth is one that a number of investigators have studied. *Cagniard* [1953, 1956] has perhaps put the theory in its most satisfactory form. Useful field results have not been numerous in the literature, and field magnetotellurics is still in the developmental stage. This letter reports on some field measurements made in the latter part of 1959 and incorporates an analysis of the data based on two-layer master curves by *Cagniard* [1953].

To treat the magnetotelluric fields and their interaction with the earth, we assume them to consist of plane waves. The validity of the assumption depends on having these fields uniform over wide areas, and evidence for this uniformity has been summarized by *Cagniard* [1956] and reported by others.

The magnetotelluric method allows each measurement to be independent of other measurements. The impedance normal to the earth is defined as the ratio of the tangential electric field intensity to the tangential magnetic field intensity, and it is these tangential fields that are measured. For a plane wave incident on a uniform earth the ratio of tangential E to tangential H is given by

$$E_x/H_y = (\rho\mu\omega)^{1/2}e^{i\pi/4}$$

where ρ is the resistivity in ohm-meters, μ is the permeability in henrys/meter, ω is the radial frequency, E_x is the electric field in the x-direction (say north), and H_y is the magnetic field in the y-direction (say east). Determining this ratio for a uniform earth gives an interpretation of the conductivity, since μ is generally constant.

In the two-layer case the formula is modified so that the phase angle and the apparent resistivity vary as a function of the frequency. Master curves for this two-layer case were presented by *Cagniard* [1953].

Our field measurements were largely confined to Massachusetts, with the majority of the data

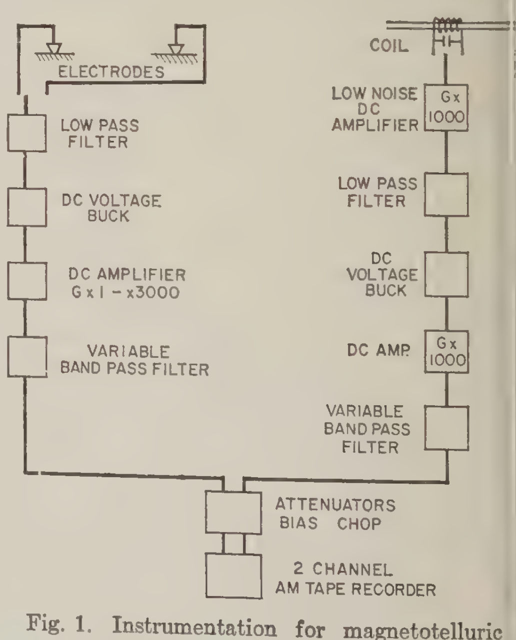

Fig. 1. Instrumentation for magnetotelluric field measurements.

obtained at Littleton, Mass. The field instrumentation is shown schematically in Figure 1.

The electrode spacing was at least a kilometer, giving easily detectable electric fluctuations. The magnetic pick-up coil consisted of 00,000 turns of wire on a 5-foot, Permalloy bar, 1 inch in diameter. This produced 0.25 mv/γ/sec and the over-all sensitivity was .003 γ/sec in an octave band. In practice, this sensitivity was sometimes difficult to achieve owing to mechanical motion of the coil.

The instrumentation system was chosen to allow small signals to be extracted from a larger background of extraneous signals. The band-pass filters allowed examination of narrow frequency bands. Typical bands studied were .005 to .02 cps, .02 to .06 cps, .06 to .2 cps, and .6 to 1 cps. The system as tested in the laboratory had a dynamic range of 60db in the frequency bands of interest.

The magnetic tapes produced in the field were played back in the laboratory onto dual-channel paper-tape records. These records were then digitized for computer use.

The analysis of the records was done by performing power spectral estimates using standard statistical techniques [*Robinson,* 1954; *Blackman and Tukey,* 1958]. The most important advantage of these methods, which are based on the auto- and cross-correlations of the data, is that an estimate of the coherency between the electric and magnetic signals is obtained. It is possible for the signal received from the magnetic transducer to be not due to magnetic fluctuations, and it is also possible for the electric signals to be not due to current flow in the earth. Such spurious signals may be considered to be noise, and they would lower the coherency between the electric and magnetic signals. Noise tests performed in the field indicated that the magnetic system is the most likely to produce false signals. Most of this noise is due to mechanical instability of the coil mounts and can be reduced by proper supports. Robinson states that an expression for the coherency is

TABLE 1. Sample Coherency Analyses

Record No.	Frequency, cps	Δf, cps	Coherency Amplitude	Coherency Phase, deg
27–4	.010	.0025	0.89	−2
(.005–.02)	.012	.0025	0.82	−3
cps	.015	.0025	0.63	−70
	.017	.0025	0.76	−36
	.020	.0025	0.84	−31
27–5	.020	.005	0.91	−18
(.02–.06)	.025	.005	0.87	−19
cps	.030	.005	0.81	−26
	.035	.005	0.86	−36
	.040	.005	0.91	−42
	.045	.005	0.87	−38

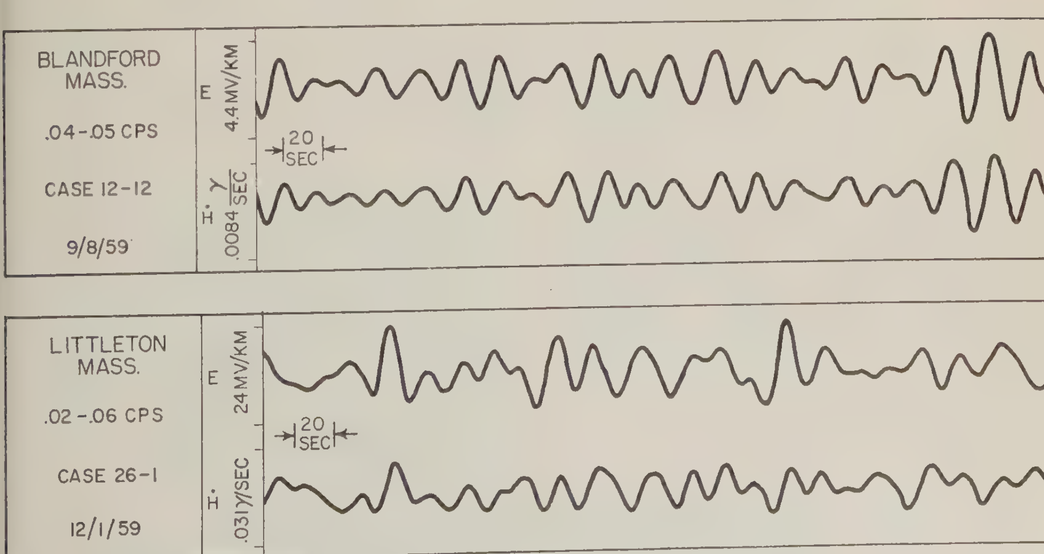

Fig. 2. Electric-magnetic records.

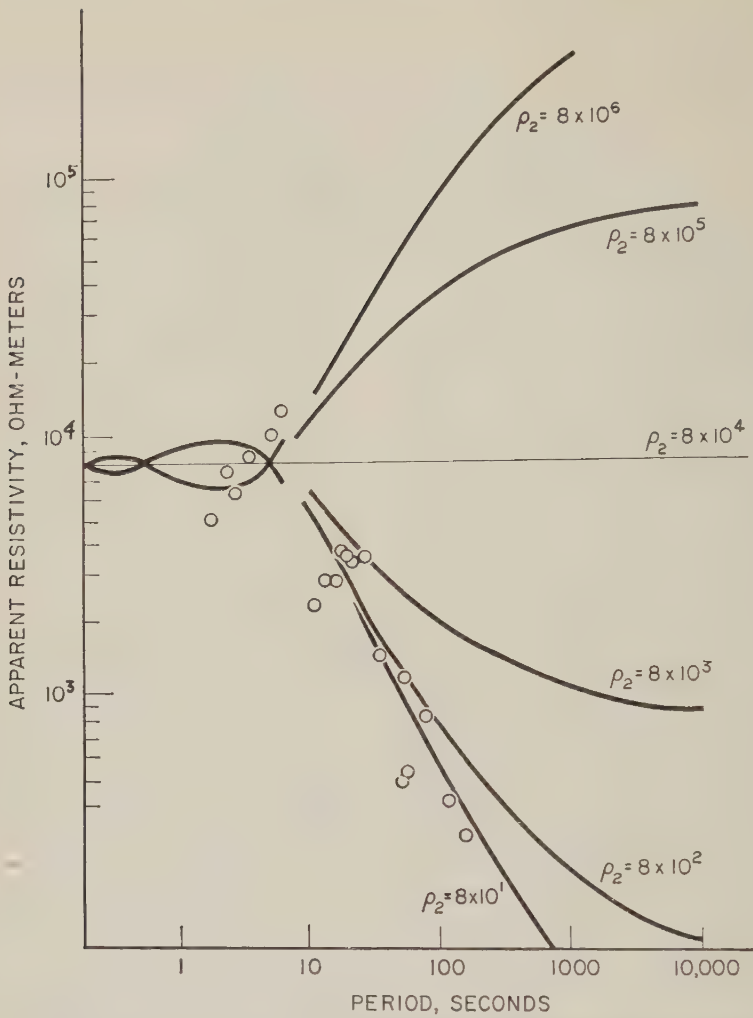

Fig. 3. Apparent resistivity versus (period)$^{1/2}$. Magnetotelluric data from Littleton and Cagniard two-layer curves.

$$\mathrm{coh}_{xy}(\omega) = \Phi_{xy}(\omega)/\sqrt{\Phi_{xx}(\omega)\Phi_{yy}(\omega)}$$

where $\Phi_{xy}(\omega)$ is the power spectrum of the x-y cross-correlation and $\Phi_{xx}{}^{(\omega)}$ and $\Phi_{yy}{}^{(\omega)}$ are the power spectra of the autocorrelations. Perfectly coherent signals would produce a $\mathrm{coh}_{xy} = 1.0$. The magnetotelluric records often gave coherency values of 0.8 or better in the passband. Highly coherent magnetotelluric records have the following characteristics:

1. Different records at the same location give consistent estimates of the resistivity.

2. The apparent resistivities calculated are smoothly varying as a function of frequency.

Typical records are shown in Figure 2. Sample coherency analyses are shown in Table 1. The calculations were performed on the IBM 704 at the M.I.T. Computation Center.

Nine records having good coherency were used in obtaining the plot shown in Figure 3. This plot can be interpreted as is done in *Cagniard* [1953] if a two-layer model is assumed. The first step in such an interpretation is the assumption of a resistivity for the upper layer. The magnetotelluric data did not extend to high enough frequencies to determine the near-surface resistivities, but resistivity measurements made by *Slichter* [1934] and *Hauck*

[1960] indicate that a value of 8000 ohm-meters is not unreasonable [*Hauck*, 1960].

If this value is used for the resistivity of the upper layer, the two-layer interpretation yields a value of 70 km for the upper-layer thickness. The resistivity of the lower layer is estimated to be less than 80 ohm-meters.

The two-layer interpretation fits the data reasonably well, but it is not suggested that the earth's conductivity structure is as simple as this. The fit of the data does indicate that a rapid change of resistivity with depth must occur at around 70 km. The lower limits of resistivity cannot be determined until data involving lower frequencies are analyzed.

The interpretation is also subject to error because of the inaccuracies of the data and the complications of an inhomogeneous earth. Some preliminary calculations on the effect of horizontal variations of conductivity show that the ocean would not have much effect on the readings recorded. Superficial conductivity variations under the electric line can produce large errors, however. It is doubtful in this case that the apparent resistivity values can be assigned a standard deviation of less than a factor of 2. It is hoped that further work will improve the techniques.

Several interesting questions have arisen as to the validity of the interpretation. The assigning of the upper layer resistivity to be 8000 ohm-meters does not have much effect on the interpretation of the location of the apparent discontinuity in resistivity, but it does lead to implications concerning the electrical environment in the crust. If this low figure can be demonstrated to be valid, it would seem to imply that some porosity still remains in the deeper crustal rocks.

The sharp break in resistivity to a still lower value at a depth of 70 km may be explained on the basis of temperature effects. Using various temperature models given recently by *MacDonald* [1959] and laboratory data on mineral conductivities [*Hughes*, 1953], one can predict resistivity profiles not unlike the two-layer model. The near-surface conductivity must involve other conductivity mechanisms, however, which we believe to be attributable to a small residual porosity.

More data and better analysis of the data are necessary before attempting geologic interpretations of these magnetotelluric results, but the technique appears to hold some promise. Magnetotelluric investigation of the earth's electrical conductivity structure over a larger continental area is now in progress.

Acknowledgments. We wish to acknowledge the support of the National Science Foundation through grant G-6602. The statistical calculations were done at the M.I.T. Computation Center. We also wish to acknowledge the help of Mr. Neil Dulaney and Mr. Charles Racer in collecting and analyzing the data.

References

Blackman, R. B., and J. W. Tukey, *The Measurement of Power Spectra*, Dover Publications, New York, 190 pp., 1958.

Cagniard, L., Basic theory of the magnetotelluric method, *Geophysics, 8*, 605–635, 1953.

Cagniard, L., Electricite tellurique, *Handbuch der Physik, 47*, 407–469, 1956.

Cantwell, T., Detection and analysis of low frequency magnetotelluric signals, Ph.D. thesis, Geology and Geophysics, M.I.T., 170 pp., 1960.

Hauck, A. M., Deep structure resistivity measurements in Massachusetts, M.S. Thesis, Geology and Geophysics, M.I.T., 57 pp., 1960.

Hughes, H., The electrical conductivity of the earth's interior, Ph.D. Thesis, University of Cambridge, 1953.

MacDonald, G. J. F., Calculations on the thermal heating of the earth, *J. Geophys. Research, 64*, 1967–2000, 1959.

Nevés, A. S., The magnetotelluric method in two-dimensional structures, Ph.D. Thesis, Geology and Geophysics, M.I.T., 122 pp., 1957.

Robinson, E. A., Predictive decomposition of time series with applications to seismic exploration, Ph.D. Thesis, Geology and Geophysics, M.I.T., 255 pp., 1954.

Slichter, L. B., An engineering problem in geophysics, *Tech Engineering News*, M.I.T. Cambridge, Mass., 8–9, 1934.

(Received August 30, 1960.)

Correlation between Solar Activity and Sudden Movements in Geomagnetic Disturbances

Hachiro Takahashi[1]

Faculty of Liberal Arts, Iwate University
Morioka, Japan

The time variation in sudden movements in geomagnetic disturbances has been investigated by many workers. Their studies, however, are mainly restricted to comparatively short-term variations in relation to occurrence frequency and local time dependency. Studies concerned with long-term variations in magnitude and speed of sudden movements are more numerous.

Correlating geomagnetic disturbance with solar activity yields interesting statistical results in relation to long-term variation, as indicated in Figures 1–3.

Geomagnetic (and solar) data[2] used in this study were obtained at the Kakioka Magnetic Observatory (geomagnetic latitude 26.°0N, longitude 154.°0W) in the period 1924–1958. Solar data were the final relative sunspot numbers in the same period for the whole disk of the sun, based on observations made at the Zürich observatory.

In this letter, discussion is limited to sudden movements of horizontal intensity (H) in geomagnetic disturbances. The sudden movements adopted here include 536 sudden commencements (SC, SC*) and 250 sudden impulses (SI) in the above-mentioned period without any distinction among them, as *Newton* [1948] and others did, and negative values (H : southward) are excluded. The total number of disturbances used are 786.

Figure 1 (a), (b), and (c) shows the correlations between $\bar{R}$ and $\overline{\Delta t}$, $\overline{\Delta H}$, and $\overline{\Delta H/\Delta t}$, respectively, where $\bar{R}$ is the annual mean of relative sunspot numbers (R), $\overline{\Delta t}$ is the annual mean of the duration (Δt) of sudden change in H, $\overline{\Delta H}$ is the annual mean of the amplitude (ΔH), and $\overline{\Delta H/\Delta t}$ is the annual mean of the ratio of ΔH to Δt. These have the interesting characteristic that $\overline{\Delta H}$ and $\overline{\Delta H/\Delta t}$ increase with increasing $\bar{R}$, while $\overline{\Delta t}$ shows the opposite tendency. If the single correlation coefficients between $\bar{R}$ and $\overline{\Delta t}$, $\bar{R}$ and $\overline{\Delta H}$, $\bar{R}$ and $\overline{\Delta H/\Delta t}$, and $\overline{\Delta t}$ and $\overline{\Delta H}$ are denoted by γ_{12}, γ_{13}, γ_{14}, and γ_{23} respectively, and the partial correlation coefficient between $\overline{\Delta H}$ and $\overline{\Delta t}$ if $\bar{R}$ is eliminated is denoted by $\gamma_{32.1}$, the numerical values can be obtained by a simple calculation as $\gamma_{12} = -0.728$, $\gamma_{13} = 0.727$, $\gamma_{14} = 0.850$, $\gamma_{23} = -0.682$, and $\gamma_{32.1} = -0.325$. By testing significance it is found that all these correlations except the last are significant. Thus it is clear that $\overline{\Delta t}$ has significant correlation with $\bar{R}$ irrespective of $\overline{\Delta H}$, and $\overline{\Delta H/\Delta t}$ has the best correlation with $\bar{R}$.

Figure 2 is a different representation of these correlations. Note that $\overline{\Delta t}$ is plotted in inverse scale. Overlooking small irregularities in the figure, it will be seen that there exists a pronounced correlation, apparently associated with one solar cycle. $\overline{\Delta t}$ is clearly inversely correlated with sunspot-numbers, while $\overline{\Delta H}$ and $\overline{\Delta H/\Delta t}$ are clearly positively correlated with sunspot numbers. Each of them ($\overline{\Delta H/\Delta t}$, $\overline{\Delta H}$, $\overline{\Delta t}$) has a marked variation with solar cycles. $\overline{\Delta H/\Delta t}$ means an average speed (gradient) of sudden rise of horizontal components at sudden commencements or sudden impulses in geomagnetic disturbances. The fact that these quantities have rather good correlation with solar activity suggests an interesting application to the theory of magnetic storms and auroras.

Figure 3 shows how the frequency distributions of $\Delta H/\Delta t$, ΔH, and Δt (not an annual mean) depend upon $\bar{R}$. For convenience, $\bar{R}$ is divided into the following three intervals: (1) $\bar{R} \geq 150$, (2) $65 \leq \bar{R} \leq 80$, (3) $\bar{R} \leq 15$; and in the figure the values of $\Delta H/\Delta t$, ΔH, and Δt are plotted against the values of $\Delta H/\Delta t$, ΔH, and Δt, which belong to the years corresponding to each interval of $\bar{R}$. The numbers of events correspond-

---

[1] Present address: Cosmic-Ray Laboratory, the Institute of Physical and Chemical Research, 3569, Itabashi-6, Itabashi-ku, Tokyo, Japan.

[2] Data in the period 1924–1951 are due to *Yokouchi* [1953].

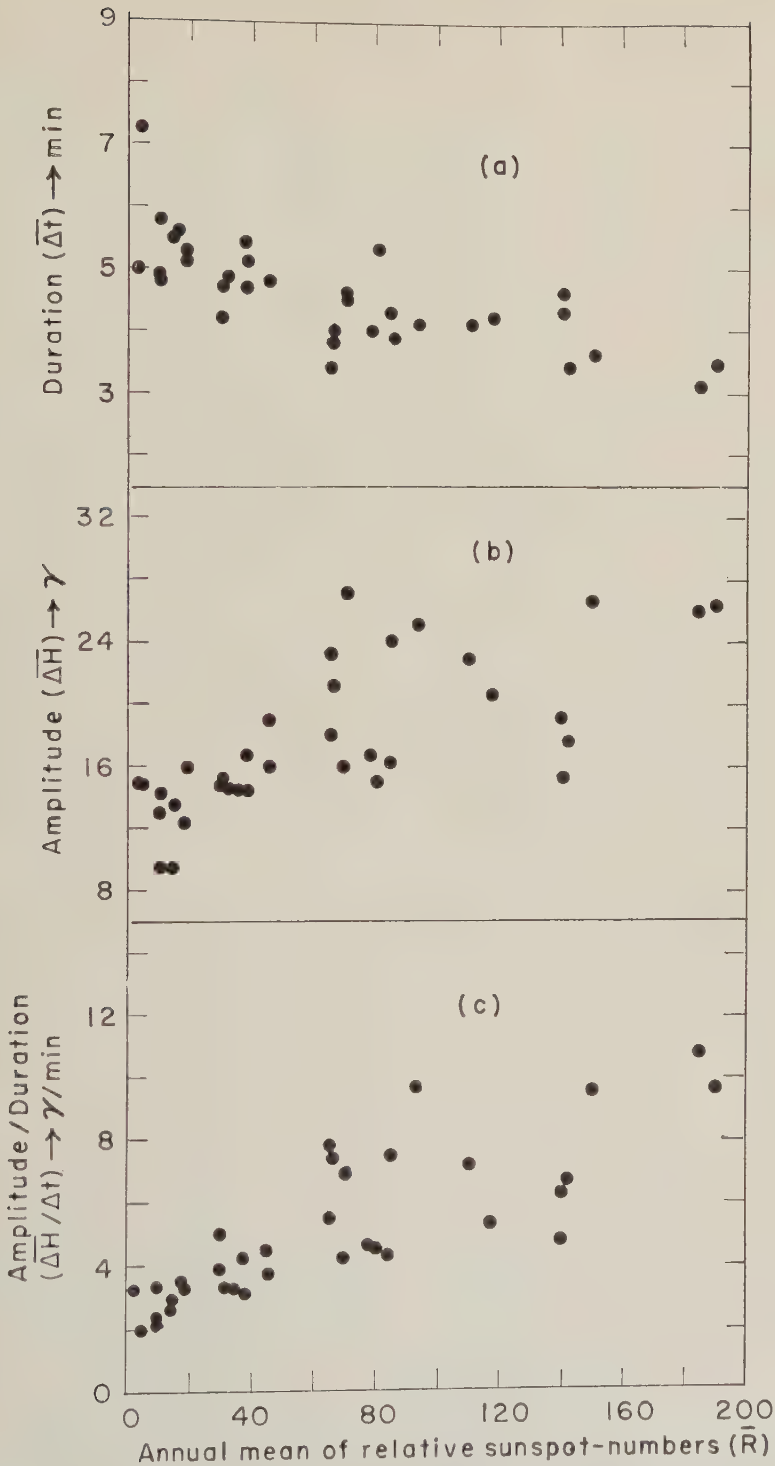

Fig. 1. Correlations between relative sunspot numbers ($\bar{R}$) and sudden movements of horizontal intensity in geomagnetic disturbances. (a) $\bar{R}$ and $\overline{\Delta t}$, (b) $\bar{R}$ and $\overline{\Delta H}$, (c) $\bar{R}$ and $\overline{\Delta H/\Delta t}$.

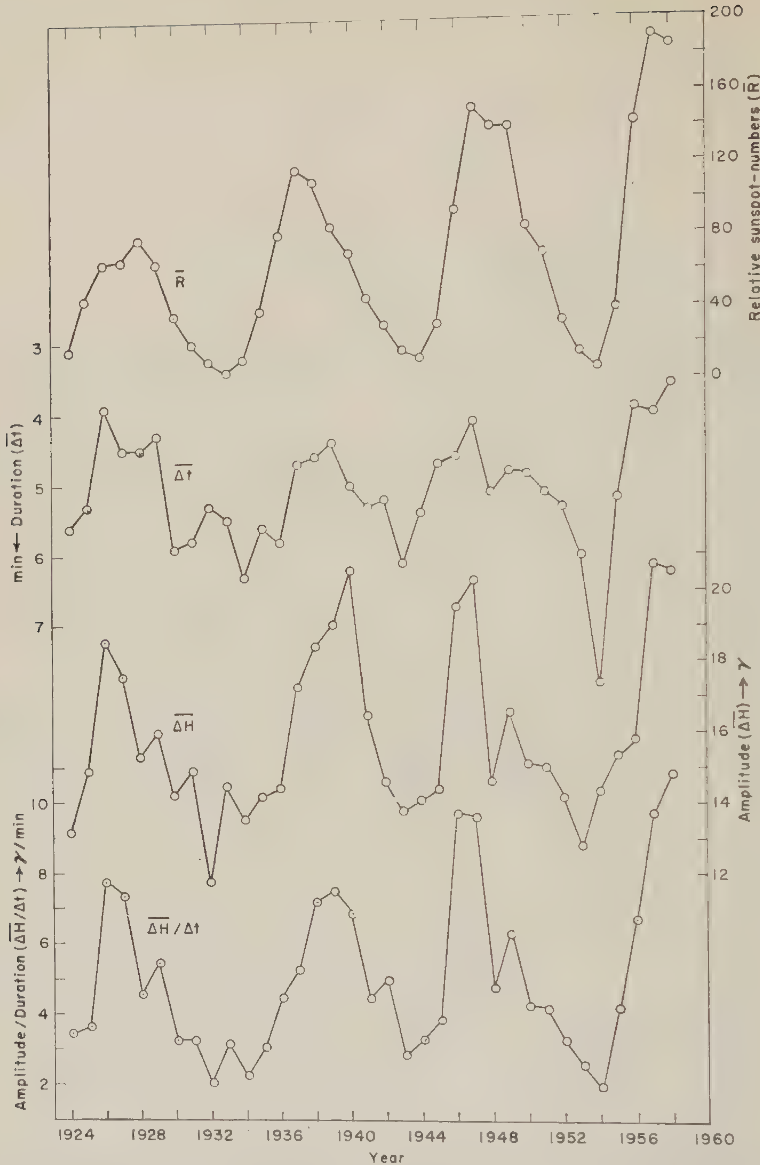

Fig. 2. Variations of duration $(\overline{\Delta t})$, amplitude $(\overline{\Delta H})$, and ratio of ΔH to $\Delta t(\overline{\Delta H/\Delta t})$ with solar cycles.

ing to the intervals (1), (2) and (3) are 112, 148, and 62, respectively. This frequency-distribution diagram shows their contribution to the tendency indicated in Figures 1 and 2 and the degree of scattering around the averaged values. Furthermore, it is clear that the lowest row of diagrams have a different distribution from the middle and the upper rows. The lowest diagrams were obtained during the calm period of the sun's activity and the upper during the active period. Figures 1 and 2 seem to show the combined effect of these two phenomena.

Acknowledgment. I am much indebted to Prof. Y. Kato of the Tohoku University, and Dr. Y. Miyazaki and the members of Cosmic-Ray Laboratory, The Institute of Physical and Chemical Research, for their interest and help in this study.

References

Newton, H. W., *Mon. Not. R. Astr. Soc., Geophys. Sup. 5*, 159, 1948.

Yokouchi, Y., *Mem. Kakioka Magnetic Observatory, 6* (2), 204, 1953.

(Received August 8, 1960; revised September 23, 1960.)

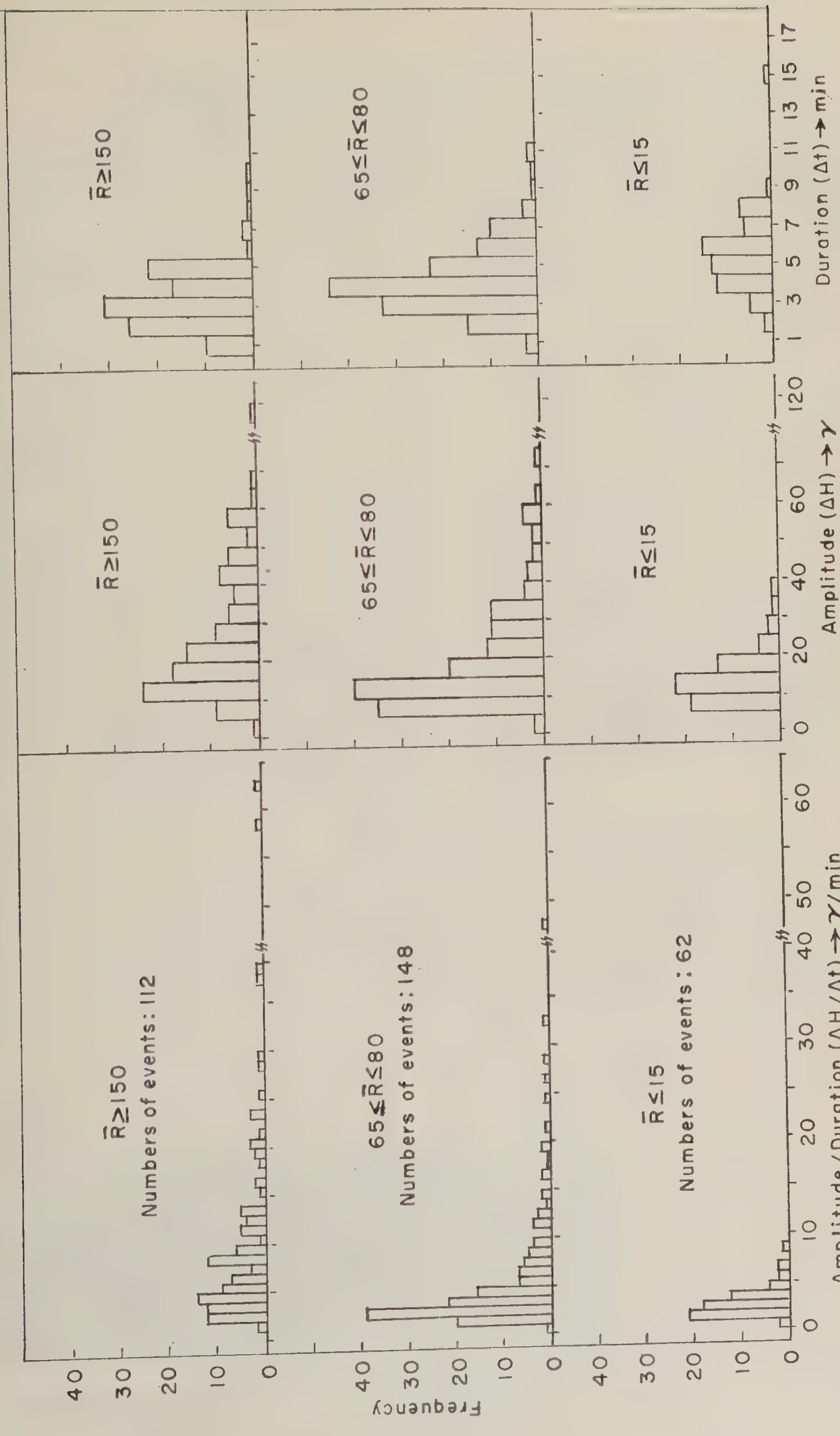

Fig. 3. Dependency of frequency distribution of $\Delta H/\Delta t$, ΔH, and Δt upon relative sunspot numbers ($\bar{R}$).

Sudden Amplitude Variations of Sputnik III Signals

H. Whitney, H. Strick, J. Aarons, and J. Mott

Air Force Cambridge Research Laboratories
Bedford, Massachusetts

For a period of almost one and one-half years, amplitude recordings of the 20 Mc/s signals from Sputnik III (1958 Delta II) were made at the Sagamore Hill Radio Observatory in Massachusetts. A vertical whip antenna was used for most of the measurments but, during some time periods, additional data for both the signal and its 40 Mc harmonic were obtained from Yagi antennas pointing north.

An interesting feature of the recordings was the presence of dropouts; i.e., sudden decreases of the signal either to noise level or close to noise level. This phenomenon is illustrated in Figure 1, a recording taken on July 26, 1959, in which the signal is seen to decrease to noise level at 2309 30″ and to return to normal signal level at 2310. The position of the satellite is noted above the chart. Two different types of events responsible for these dropouts are postulated in this letter.

Several studies were made in an attempt to find the reason for the dropout of energy. First, auroral backscatter records were analyzed in an attempt to find some correlation with the dropout effect. A frequency of 19 Mc was used and backscatter equipment was located 8 miles distant from the site of the observatory. It was found that neither individual auroral reflections nor periods of auroral reflection matched the dropout effect in time.

The next hypothesis investigated was that the effects were due to the fact that the transmitter in the satellite was not operating. If this were the case, several stations would observe the signal decrease simultaneously. Therefore, a list of the times at which dropouts occurred were compared with the Ohio State University observations (Professor John Kraus). Although several of the dropout periods observed at Sagamore Hill correspond exactly with the Ohio State observations, there were some which showed no correspondence. A similar discrepancy was found when the Sagamore Hill records taken at different frequencies were compared. For a period of time, 40 Mc records were taken simultaneously with the 20 Mc data. During one pass of the satellite the signal decreased suddenly on the 20 Mc record but not on the 40 Mc one. This is illustrated in Figure 2, in which dropout starts at 1158 15″.

Thus, a comparison of our own records at different frequencies, as well as a comparison of our records with those of Ohio State University, indicates many instances of correspondence as well as some discrepancy. This fact shows that there are probably two distinct events responsi-

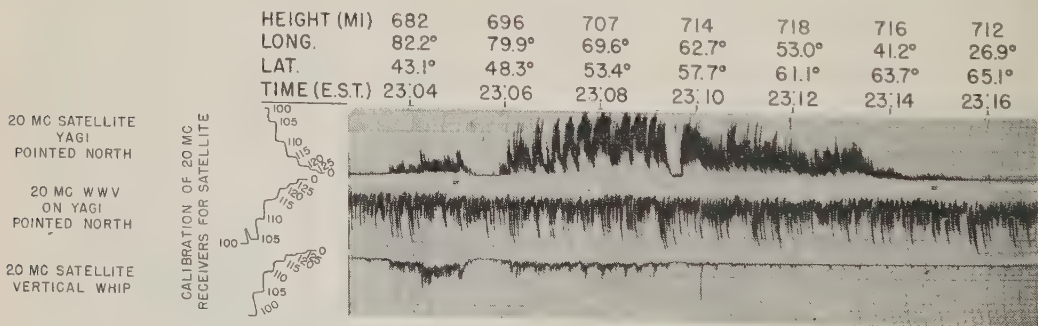

Fig. 1. Signal amplitude record of 20 Mc signals from 1958 δ2 (Sputnik III) revolution 6169, July 26, 1959.

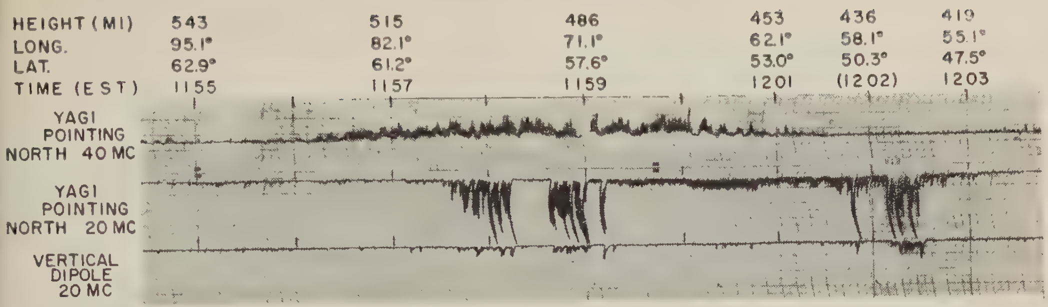

Fig. 2. Revolution 7135 of Sputnik III 1958 $\delta 2$; decreased signal on 20 Mc is not evident on 40 Mc signal.

ble for the phenomenon. One event is wide in geographical extent and the other is a localized effect which is frequency dependent.

The same problem has been studied in a larger work in progress, reported upon in ERD Technical Report 60–174. In that study, a group of six European radio observatories and this laboratory collaborated on an analysis of 1958 Delta II passes. The hypothesis advanced in that report and as a result of the recordings on which this letter is based is that the 'dropout' phenomenon in 1958 Delta II was due mainly to changing transmitter characteristics resulting in reduced power output. The cause of the changing characteristics (pulse-width modulation and reduced transmitter power) was that the satellite had entered a region of high-electron flux. In the instances in which dropout was observed at some locations or frequencies and not at others, the reduced signal was due to the intervening medium rather than to the transmitter itself.

Thus, there are two distinct reasons for the sudden decrease of amplitude of 1958 Delta II signals. One of these is the change in transmitter characteristics and the other is a localized absorbing or scattering region in the ionosphere. The two causes are best differentiated by taking simultaneous observations at several geographical positions.

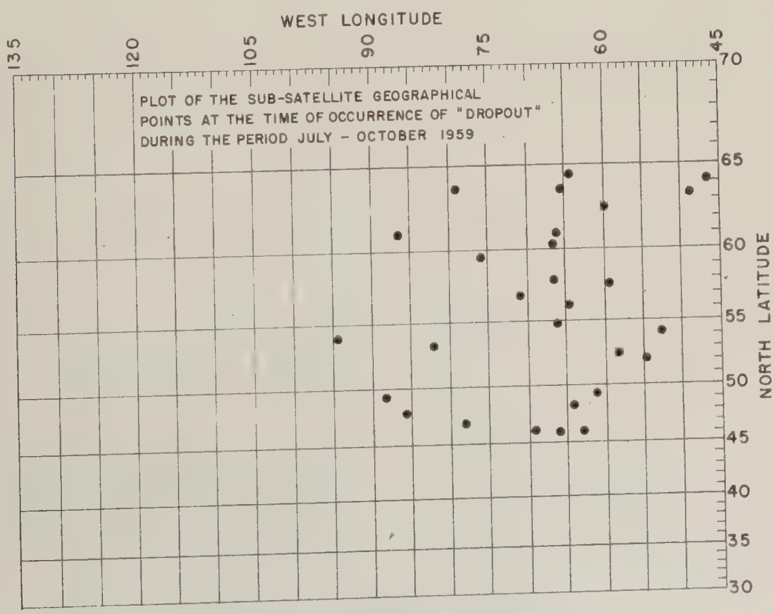

Fig. 3.

In order to determine whether or not the dropout effect depended upon the geographical position of the satellite, all dropouts which were clear, i.e., which showed a sharp drop and an equally sharp return to normal signal, were plotted as shown in Figure 3. The geographical distribution of the satellite position at the times at which dropouts occurred showed a concentration above 45°N latitude. Therefore, for this site, the region of high-electron flux responsible for the dropouts was concentrated north of the site.

Reference

ERD-TR-60-174, Atmospheric phenomena noted in simultaneous observations of 1958 Delta II (Sputnik III), Electronics Research Directorate, AFCRL, Bedford, Massachusetts.

(Received September 25, 1960.)

Direct Recording of Small Geomagnetic Fluctuations

R. R. Unterberger

California Research Corporation
La Habra, California

The earth's magnetic field is usually measured by magnetometers of permanent station type such as those used by the U. S. Coast and Geodetic Survey observatories for the normal and rapid-run magnetograms. Surveys of the magnetic field can be carried out on the ground with portable Askania magnetometers. Flux gate magnetometers are used for aerial surveys. None of these instruments is absolute, and they must therefore be calibrated. Their sensitivity is about 1 γ.

Recently, proton precession magnetometers [*Packard and Varian*, 1954; *Waters and Francis*, 1958] have been developed. These have the merit of being absolute instruments; i.e., their calibration depends on the value of known physical constants. On the other hand, they are not continuous measuring devices, but require polarizing, after which they average the magnetic field over a second or two of relaxation time. *Skripov* [1958] more recently reported a continuous nuclear magnetic resonance generator which 'follows the changes in H practically instantaneously.' He used water flowing through a magnetizing coil of 400 gauss and then to a receiving coil 150 cm away. His present system is limited to an accuracy of ½ γ at best because of the inhomogeneity of magnetic field produced at the receiving coil by the strong magnetizing field, even though six compensating coils were used. It is more difficult to measure accurately the low frequencies associated with nuclear resonance magnetometers than to measure the higher frequencies associated with electron resonance.

Other types of magnetometers investigated included those based on the bending of a beam of electrons [*Marton, Leder, Coleman, and Schubert*, 1959], the Hall effect [*Richmond*, 1959], and the Zeeman splitting of absorption lines of alkali-metal atoms [*Skillman and Bender*, 1958], or of metastable helium atoms [*Franken and Colegrove*, 1958; *DeBolt*, 1960; *Colegrove and Franken*, 1960]. Advantages of the last two types of devices over most of the others are (1) the increased sensitivity available ($\approx 10^{-3}\ \gamma$), (2) continuous recording of the earth's magnetic field, and (3) the absolute nature of the magnetic resonance instruments. The sensitivity of these instruments far surpasses their absolute accuracy only because of our lack of knowledge of the absolute values of some physical constants. However, this is not critical so long as the physical constants are really constant.

We have constructed several instruments of the alkali vapor type, similar to the one pioneered by *Skillman and Bender* [1958] but with additions, improvements, and modifications. The instruments utilize the magnetic transition between weak-field Zeeman levels of the hyperfine structure of the Rb^{87} atom in the ground state to measure the earth's magnetic field. The heart of the system is a 500-ml pyrex bulb containing Rb^{87} at low ($\approx 10^{-7}$ mm of Hg) vapor pressure and a buffer gas. Because of the small number of Rb atoms present to exhibit magnetic resonance and the small difference in population of the closely spaced Zeeman energy levels, a trick known as optical pumping [*Kastler*, 1950][1] must be used to disturb the Boltzmann distribution of the energy levels of the Rb atoms in the ground state to the advantage of the detection of the resonance signal. A 7947 A light beam is right circularly polarized to 'pump' the Rb atoms to an emissive state. This light beam also serves to detect the rubidium Zeeman resonance.

---

[1] This pumping is similar to microwave pumping as used in masers. The difference here is that optical photons are used rather than microwave photons. The result, however—that of rearranging the atomic population distribution in the Zeeman magnetic sublevels to give a thermodynamic nonequilibrium state—is the same.

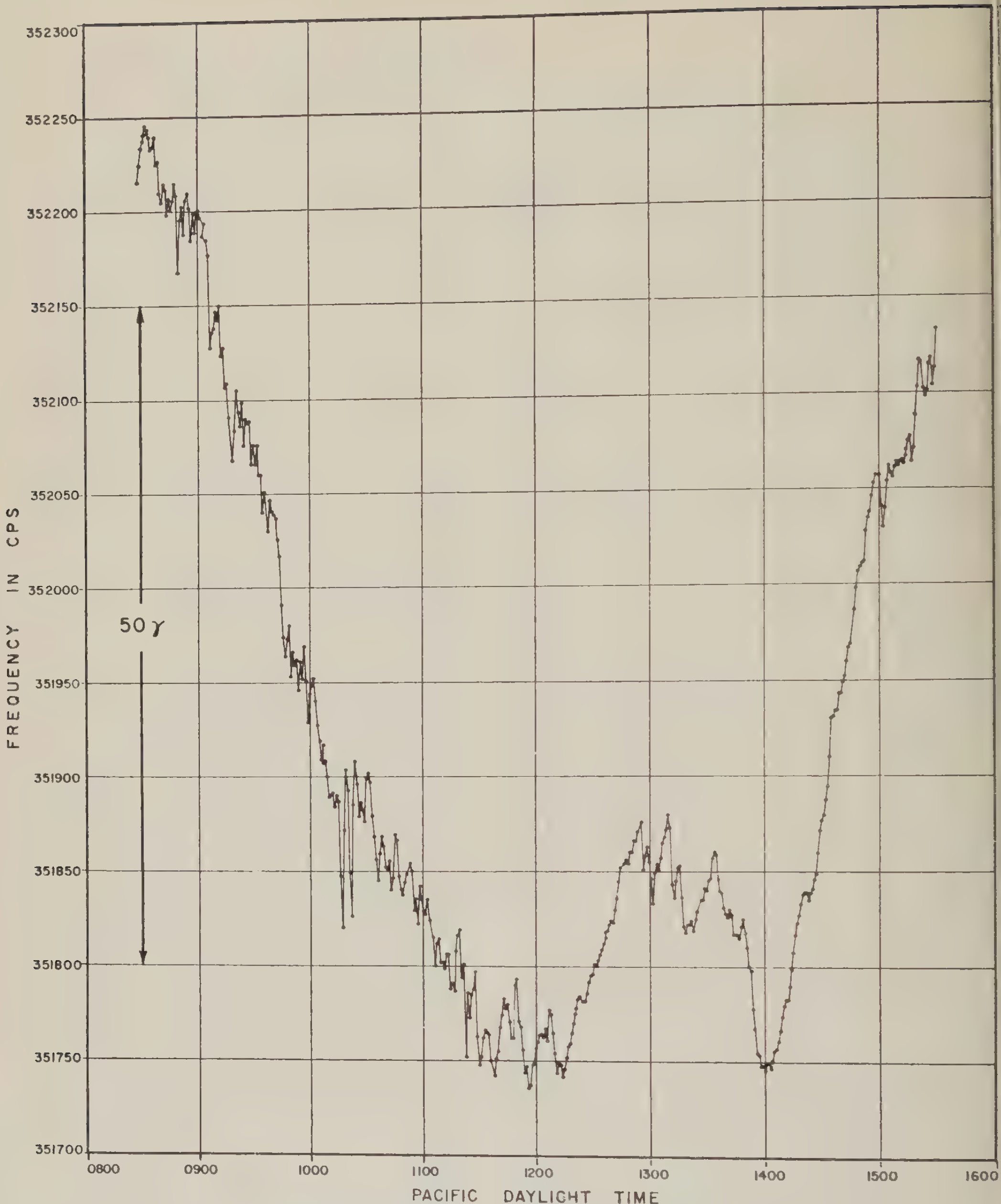

Fig. 1. Record of K-6 magnetic storm, September 21, 1959, La Habra, Calif. $A = 37.7$ cps $\approx 1\gamma$.

A solar battery detects a small change in the light transmission characteristics of the rubidium vapor in the glass bulb at the resonant frequency for the $F = 2,\ m_F = 2 \rightarrow F = 2,\ m_F = 1$ rubidium atom transition. In weak magnetic fields, such as the ½-gauss earth's field, the electron and nuclear spin couple together to give a total angular momentum vector **F**. The projection of this vector on the direction of the external magnetic field (Z direction) is m_F. Changes in this quantum number are induced by the radio frequency oscillator, resulting in more photon absorption by the rubidium vapor. A small magnetic field modulation at low fre-

quency is applied collinear with the direction of the earth's magnetic field. This magnetic modulation varies the photon absorption and, hence, modulates the light beam. This permits narrowband amplification at the modulation frequency. A phase detector employing a reference signal from the low-frequency modulation source is used in conjunction with the resonance signal itself ($d\chi''/dt$, the derivative of the absorption signal). The output of the phase detector sends a signal to the servomechanism which keeps the radio frequency oscillator tuned to the rubidium atom resonance. As the earth's field changes, the rubidium resonance frequency changes. The oscillator frequency follows the resonance frequency automatically. Thus, the earth's magnetic field H in gauss measured at any time is related to the frequency in cycles per second of resonance of the rubidium atoms by the *Breit-Rabi* [1931] formula, which, for 6+ pumping, can be shown to reduce to

$$\nu = 699632\, H - 216\, H^2$$

Thus to first order the frequency of resonance is approximately 7 cps per γ of earth's magnetic field.[1] With an electronic counter, we can measure the resonance frequency to 0.1 cps; a maximum sensitivity of 0.01 γ is obtained. With this

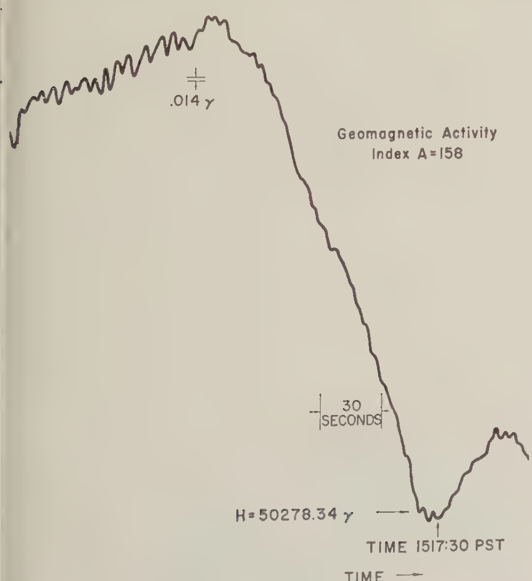

Fig. 2. Part of magnetic storm recording, April 1, 1960, La Habra, Calif.

[1] Cf. nuclear magnetic resonance: 1/25 cps per γ.

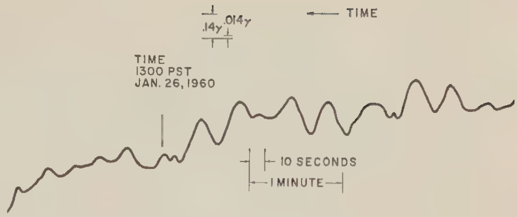

Fig. 3. Geomagnetic micropulsations recorded at La Habra, Calif.

sensitivity, the normal spatial change in the earth's magnetic field over a 4-foot distance in a north-south direction is easily noticeable.

Figure 1 shows a magnetic storm (time variation) recorded at La Habra, California, on September 21, 1959, at a reduced instrument sensitivity of 0.1 γ. The original recording took data every 2 seconds, the field being averaged over 1 second. Figure 1 shows values of the earth's magnetic field only every minute. It is interesting to note that the large increase in magnetic field of 12 γ recorded from 1018 to 1020 PDT at La Habra was also recorded at the same time by the Tucson Magnetic Observatory located about 450 miles distant. Figures 2 and 3 show portions of subsequent records taken with increased instrument sensitivity of 0.01 γ and an expanded time scale. Note that the micropulsations of Figure 3 on this very quiet day have a peak-to-peak amplitude of less than 0.25 γ. These would not be directly visible on other magnetic recording instruments, such as the rapid-run observatory magnetograms (which have a sensitivity of about 2 γ/mm), or on a proton precession magnetometer.

The sensitivity of the rubidium vapor magnetometer described above is well beyond (10 to 50 times) that of any presently commercially available magnetometer. Instruments of this type promise to open a new area of research investigation into small-amplitude magnetic phenomena previously unknown. Increased sensitivity beyond that reported here is to be expected by reducing line widths, increasing the available signal-to-noise ratio, or both. Linewidth reductions are to be expected from further research on spin exchange.

References

Breit, G., and I. Rabi, Measurement of nuclear spin, *Phys. Rev.*, *38*, 2082–2083, 1931.

Colegrove, F. D., and P. A. Franken, Optical

pumping of helium in the $^3S_1$ metastable state, *Phys. Rev.*, *119*, 680–690, 1960.

DeBolt, H. E., Magnetometer system for orientation in space, *Electronics 3* (15), 55–58, 1960.

Franken, P. A., and F. D. Colegrove, Alignment of metastable helium atoms by unpolarized resonance radiation, *Phys. Rev. Letters*, *1*, 316–318, 1958.

Hurwitz, L., and J. H. Nelson, Proton vector magnetometer, *J. Geophys. Research*, *65*, 1759–1765, 1960.

Kastler, A., Quelques suggestions concernant la production optique et la detection optique d'une inegalite de population des niveaux de quantification spatiale des atomes, *J. Phys. Radium*, *11*, 225–263, 1950.

Marton, L., L. B. Leder, J. W. Coleman, and D. C. Schubert, Electron beam magnetometer, *J. Research NBS*, *63C*, 69–75, 1959.

Packard, M., and R. Varian, Free nuclear induction in the earth's magnetic field, *Phys. Rev.*, *93*, 941, 1954.

Richmond, I. J., Solid state devices, *Research Applied in Industry*, *12*, 374–380, 1959.

Skillman, T. L., and P. L. Bender, Measurement of the earth's magnetic field with a rubidium vapor magnetometer, *J. Geophys. Research*, *63*, 513–515, 1958.

Skripov, F. I., A nuclear magnetic resonance generator in the earth's magnetic field, translated from the Physics Section of *Akad. Nauk SSSR* in *Soviet Phys. Doklady*, *3*, 806–808, 1958.

Waters, G. S., and P. D. Francis, A nuclear magnetometer, *J. Sci. Instr.*, *35*, 88–93, 1958.

(Received August 4, 1960; revised September 23, 1960.)

Discussion of Paper by D. M. Hershfield and M. A. Kohler, 'An Empirical Appraisal of the Gumbel Extreme-Value Procedure'

D. L. BRAKENSIEK

Agricultural Research Service
U. S. Department of Agriculture
Beltsville, Maryland

As was pointed out by *Hershfield and Kohler* [1960], the user of forecast information must be prepared to face up to the problem of uncertainty. Their Figure 5 provides a means for incorporating the uncertainty factor into hydraulic structure design computations.

In this discussion the writer will present what may be a simple development of a relation similar to that exhibited in Figure 5. However, what follows in no way adds to the completeness and excellence of the study by Hershfield and Kohler.

Thomas [1948] and *Gumbel and von Schelling* [1950] presented the distribution $P(n, m, N, x)$ of the number of exceedances, x, over the mth largest among n observations in N future trials as

$$P(n, m, N, x) = \frac{\binom{n}{m} m \binom{N}{x}}{(N+n)\binom{N+n-1}{m+x-1}} \tag{1}$$

If we are interested in the dependence of $P(n, m, N, x)$ on x only, (1) is simply written $P(x)$. The conditions for m and x, and for the probability $P(x)$ are

$$1 \leq m \leq n$$

$$0 \leq x \leq N$$

$$\sum_{x+0}^{N} P(x) = 1$$

The probability $P(x)$ thus depends on the parameters n, m, and N and is also distribution free.

Following from (1), the requirement that the largest ($m = 1$) among n past events will not be equaled or exceeded ($x = 0$) in N future events gives the following probability

$$P(x = 0) = \frac{n}{N+n} \tag{2}$$

Thus the probability for at least one event to equal or exceed the largest among n past observations is

$$[1 - P(x = 0)] = \frac{N}{N+n} \tag{3}$$

The left-hand side of (3) is now defined as the risk of a failure, R. N is defined as the desired lifetime of a structure, and n is defined as the design return period. Explicit in the last definition is a past record of n events. Of course as n becomes large it is more frequently the case that the record must be extended by distributional procedures. For an application, equation 3 would be written as

$$n = N[(1/R) - 1]$$

Thus, for a given lifetime of a structure, N, and a risk R that we are willing to take of having a failure during the structure's lifetime, a design return period can be calculated. The utility of (3) may come from its being a very simple expression to use.

Equation 3 can also be written to correspond to the authors Figure 5 as

$$T = T_d[(1/R) - 1] \tag{4}$$

where R is the risk of a failure. It should be noted that this equation starts to depart from the authors Figure 5 as the risk R approaches 50 per cent.

Using *Gumbel's* [1955] notation, equation 4 would be written as

$$T_w = N_w[(1/W_w) - 1]$$

and as W_w becomes small it approaches

$$T_w \sim (N_w/W_w)$$

This last equation corresponds to *Gumbel's* [1955] equation 10.

REFERENCES

Gumbel, E. J., and H. von Schelling, The distribution of the number of exceedances, *Ann. Math. Statist.*, *21*, 247–262, 1950.

Gumbel, E. J., The calculated risk in flood control, *Appl. Sci. Research*, *A*, *5*, 273–280, 1955.

Hershfield, D. M., and M. A. Kohler, An empirical appraisal of the Gumbel extreme-value procedure, *J. Geophys. Research*, *65*, 1737–1746, 1960.

Thomas, H. A., Jr., Frequency of minor floods, *J. Boston Soc. Civil Engrs.*, *35*, 425–442, 1948

(Received October 7, 1960.)

Note on 'Gravity Anomalies over a Buried Step'

A. M. BANCROFT

Dominion Observatory, Ottawa, Canada

An unknown correspondent in Moscow has brought to my attention the fact that the formulas I derived in a recent note [*Bancroft*, 1960] had been previously published [*Lustikh*, 1944].

Readers who compare the two papers will appreciate the extent of my embarrassment, and the sincerity of my regrets.

REFERENCES

Bancroft, A. M., Gravity anomalies over a buried step, *J. Geophys. Research*, *65*, 1630–1631, 1960.

Lustikh, E. N., On the use of gravitational survey data of reconnoitring nature, *Doklady Akad. Nauk SSSR*, *43*(6), 242–243, 1944.

(Received October 19, 1960)

Discussion of Paper by D. M. Hershfield and M. A. Kohler, 'An Empirical Appraisal of the Gumbel Extreme-Value Procedure'

M. A. Benson

U. S. Geological Survey
Washington 25, D. C.

Hershfield and Kohler [1960] say, 'It is axiomatic in statistics that the reliability of estimates based on a limited sample improves as the sample size is increased.' As a corollary, it may be expected that if there is an underlying distribution, conformance to the distribution should be improved as the sample size is increased. The results of this study, as analyzed by the writer, indicate a poorer fit with a larger sample, leading to some doubt as to the goodness of fit.

The writer has applied the χ^2 test of goodness of fit to the figures shown in Tables 2 and 3. The conformance of the data to the Gumbel distribution is evaluated by this test, where the number of occurrences in the intervals between the listed recurrence periods are used. In Table 2, based on comparisons with results from 15-year computed curves, the computed χ^2 values give no reason to suspect that the Gumbel distribution is not a good fit. On the other hand, they do not prove that there is a good fit. In Table 3, the computed χ^2 values show highly significant departures (at the 1 per cent level) for results from 10-year records and significant departures (at the 5 per cent level) for 15-, 20-, and 25-year records. Table 2 was based on 1920 items of data whereas Table 3 was based on 3200 items. The results might be interpreted as demonstrating that 1920 items were insufficient to reveal the significant departure of the data from the Gumbel distribution but that 3200 items were sufficient to show it.

When geographic randomness has not been demonstrated, it is risky to combine data over a wide area and draw general conclusions. Thus even though a good fit is demonstrated as the average result for stations distributed nationwide, is this justification for using the Gumbel distribution (or any other) in a local area? For example, consider a region like New England, in which it has been found in (unpublished) studies made by the writer that most frequency distributions, for both peak discharges and daily rainfall, are concave upward on Gumbel (and log-probability) plots. Use of the Gumbel distribution in that region leads to computed curves that are consistently to the right of the data at the top and bottom ends and to the left in the middle range.

The paper does not demonstrate, of course, that the Gumbel distribution is the best fitting distribution. Other theoretical distributions may give as good or better fits. A study of annual minimum discharges by *Matalas* [1958] showed that the Gumbel and the Pearson type III distributions fitted this type of data equally well. In general, hydrologic data are not necessarily limited to fitting by only one type of distribution. The question of whether the Gumbel distribution provides a statistically good fit for maximum annual hourly precipitation is still uncertain. Moreover, the possibility remains that the use of a predetermined theoretical distribution may lead to error under conditions such as are cited above.

References

Hershfield, D. M., and M. A. Kohler, An empirical appraisal of the Gumbel extreme-value procedure, *J. Geophys. Research, 65*, 1737–1746, 1960.

Matalas, N. C., Statistical analysis of droughts, Thesis for Ph.D. degree, Harvard Univ., Div. of Eng. and Appl. Physics, May 1958.

(Received August 5, 1960.)

Discussion of Paper by D. M. Hershfield and M. A. Kohler, 'An Empirical Appraisal of the Gumbel Extreme-Value Procedure'

IRVING I. GRINGORTEN

Air Force Cambridge Research Laboratories
Bedford, Massachusetts

In Tables 1, 2, and 3 *Hershfield and Kohler* [1960] show a comparison of the estimated number of events that have a return period of 2, 5, 10, ... years with the corresponding computed number of events based upon the Gumbel method of curve fitting to extreme-value data. They point to a bias in the results of Table 1 using the dependent data and to an apparent lack of bias in Tables 2 and 3 when they test their results on independent data. Ordinarily one expects that an equation of estimate will perform better upon the data sample from which it is derived than it would upon an independent sample. But the authors apparently suggest that the reverse is true.

My purpose in writing is to point out that Lieblein, in the authors' fifth reference, has shown that Gumbel's equation of estimate introduces more bias than the more simplified equation of estimate:

$$\hat{x} = \bar{x} + s_x(y - 0.5772)/1.28255$$

Where $\bar{x}$, s_x are, respectively, the sample mean and standard deviation, the figure 0.5772 is Euler's constant, and the figure 1.28255 is $\pi/\sqrt{6}$. This estimate is not dependent upon the number of years of sampling, as is Gumbel's estimate.

To show how the simpler equation changes the authors' results, I have prepared a table in which the authors' figures (Table 1) of the computed numbers of events of 60-minute rainfall, in a 20-year record at 128 stations, for a total of 2560 events, are compared with the number of events that should be expected when Gumbel's equation is used. Symbolically, this correction is made by using the above equation (instead of Gumbel's equation) to determine y from each observed x, together with the equation to find the corresponding return period n from

TABLE 1. Comparison of Computed and Expected Number of 20-Year Events for 128 Stations

Return Period years	Gumbel Method	Should Expect
2	1237	1280
5	421	417
10	185	177
25	64	56
50	23	25
100	4	10
200	1	5
500	0	2
1000	0	1

$$1 - 1/n = \exp\{-\exp(y)\}$$

and with the equation to find the expected number N_e out of the total N:

$$N_e = N/n$$

Actually, the correction was made by using extreme probability paper.

From the evidence of the data presented the bias in the dependent data is nearly gone. On the other hand, I found a large bias in the authors' figures for the independent trials.

REFERENCE

Hershfield, D. M., and M. A. Kohler, An empirical appraisal of the Gumbel extreme-value procedure, *J. Geophys. Research*, *65*, 1737–1746, 1960.

(Received September 12, 1960.)

Discussion of Paper by E. C. Childs, 'The Nonsteady State of the Water Table in Drained Land'

J. N. LUTHIN

Department of Irrigation, University of California
Davis, California

Childs [1960] clearly illustrated a weakness the assumption of a constant specific yield r the drainage of soils. When the water table is ose to the soil surface the specific yield becomes meaningless term because the water table can op a considerable distance with very little lease of water from the soil above it. The ssumption becomes reasonable however when oplied to water-table fluctuations in sands and avels at some depth below the soil surface— aterials for which the concept of specific yield as originally developed.

Childs also indicated that the problem of the lling water table is a more difficult one involving e nonlinear diffusion equation. It is the purpose f this note to briefly elaborate on some phases f this difficulty and to present evidence in lustration of the problems involved.

Basically the difficulty lies in the assumption f an unvarying moisture profile as the water ble falls.

In a dynamic situation the moisture content bove the water table is constantly changing, nd the negative pressure head is *not* equal to he vertical distance above the water table. The greatest discrepancies will occur with a apidly moving water table in the zone of greatest oisture-content change. For tile drainage of oils the discrepancy will be greatest immediately ver and adjacent to the tile line and least at he midpoint between tile lines. If the tile pacing is wide and the water-table drop is low, the equilibrium values given by the moisture haracteristic can be applied with reasonable ccuracy. However, in the vertical drainage of a olumn of soil, the equilibrium curve bears little elation to the actual soil-moisture curve. The rainage of a soil column has been studied xperimentally by *Luthin and Miller* [1953] nd their data are used to illustrate the point. o quote from their article,

'When water is percolated through a homogeneous column of soil before drainage starts, the hydraulic head varies linearly with the distance above the bottom of the column. If the water table is defined as the locus of points at atmospheric pressure, it is diffused throughout the column when the ponded water film is negligibly thin. As soon as the ponded water disappears from the soil surface and drainage commences, the hydraulic head drops rapidly and negative pressures are recorded throughout the column with the exception of the bottom of the column where the pressure is slightly above atmospheric. The water table is now at the bottom of the soil column, yet drainage of

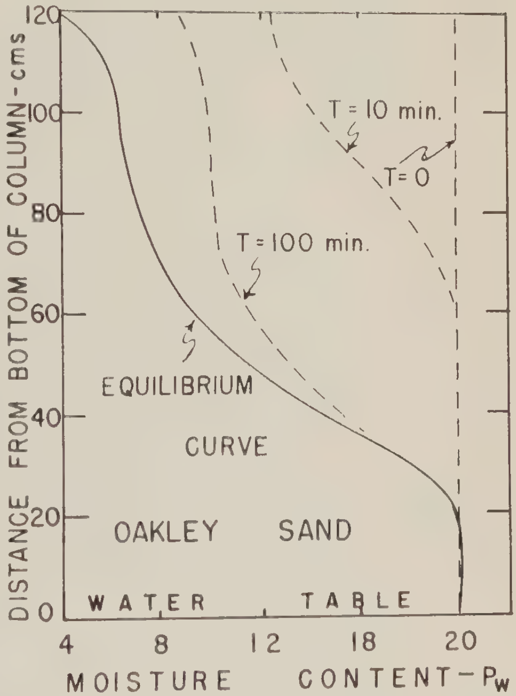

Fig. 1. Distribution of moisture (per cent by weight) in a column of Oakley sand at various times after the start of drainage.

the soil column has just started. The soil is "saturated" to the surface.'

In Figure 1 the data of Luthin and Miller are replotted to show the moisture distribution at various times after the start of drainage of the Oakley sand. Note the difference between the actual moisture contents and the equilibrium moisture contents. The actual moisture contents were not measured during drainage but were obtained from the measured relationship between soil moisture negative pressure head and moisture content. In a dynamic situation this relationship is not valid, as was pointed out by Dr. Don Nielsen of our staff in private conversation. An additional unknown (but not compensating) error results from this assumption.

References

Childs, E. C., The nonsteady state of the water table in drained land, *J. Geophys. Research*, *65*, 780–782, 1960.

Luthin, J. N., and R. D. Miller, Pressure distribution in soil columns draining into the atmosphere, *Soil Sci. Soc. Am. Proc.*, *17*, 329–333, 1953.

(Received September 17, 1960.)

Spectrum Analysis of T-Phases from the Agadir Earthquake, February 29, 1960, 23h 40m 12s GCT, 30°N, 9°W (USCGS)[1]

JOHN NORTHROP, MAURICE BLAIK, AND IVAN TOLSTOY

Columbia University, Hudson Laboratories
Dobbs Ferry, N. Y.

T-phases[2] from the Agadir earthquake of ebruary 29, 1960 (23h40m12s GCT at 30°N, W, according to USCGS), were recorded from veral SOFAR-type bottomed geophones. The cordings were then examined with spectrum alysis equipment of a few cps resolution. racings of this *T*-phase arrival at three of the ceiver stations are shown in Figure 1.

There is a considerable amount of dispersion the signal, as can be seen from the figure. For e travel path at 6500 km, the general 'Christmas tree' shape of the signal is typical and had been noted on previous records. However, this was the first time that this type of arrival could definitely be correlated with the *T*-phase from a known earthquake [*Northrop and Berman*, 1959]. It is now apparent that the early branches of the 'tree' correspond to the velocity maximum and the 'peak' to the 'rider' wave of *Pekeris* [1948] (commonly referred to as *D* in shot work). The 'stem' shows the beginning of the Airy phase [as pointed out by *Ewing, Mueller, Landisman, and Satô*, 1959]. The trailing edge varies considerably from station to station and is probably due to reverberation, local excitation, and the arrival of later modes, including the Rayleigh mode.

The signals at other stations showed similar patterns for epicentral distances ranging from 5300 to 6500 km. The velocities computed for *T*

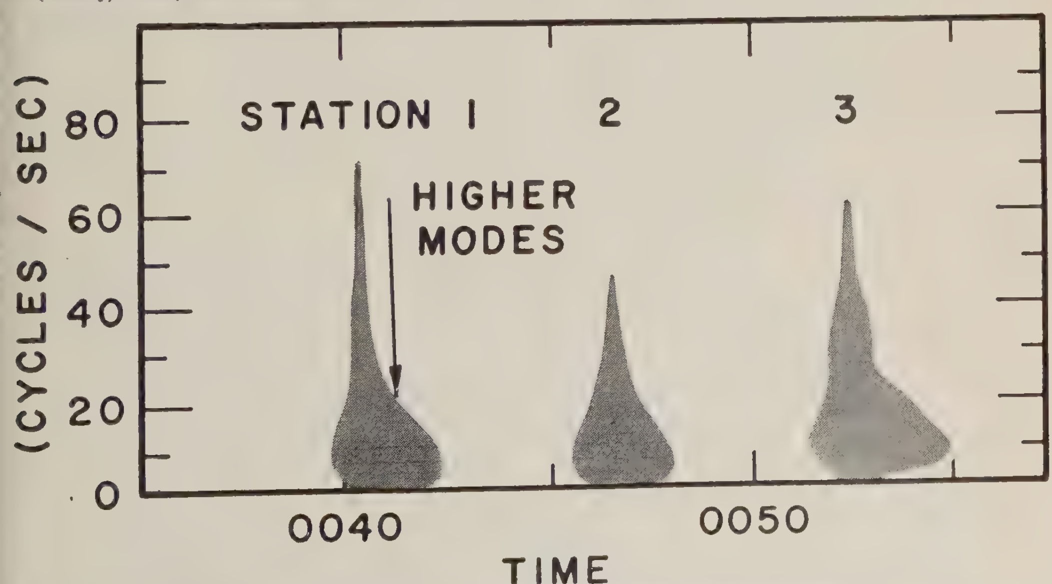

Fig. 1. Transient spectrum analyses of T-phases from the Agadir earthquake. The range to the epicenter is 5300 km from Station 1, 5850 km from Station 2, and 6500 km from Station 3. The time is GCT, March 1, 1960.

[1] Hudson Laboratories Contribution No. 83.

[2] The *T*-phase can be considered a train of waves period between about 1/2 and 1/100 sec propaated across ocean basins from earthquakes having picenters in the basin or very near its margin, and ceived on seismographs on islands or near the ast [*Ewing, Press, and Worzel*, 1952].

are 1.49 ± .005 km/sec for all the paths.[3] These velocities are comparable to those computed by *Ewing, Press, and Worzel* [1952] and *Burke-Gaffney* [1954] but are lower than those reported by *Leet, Linehan, and Berger* [1951].

From frequency analysis of these T-phases, it is clear that there is good reason for the velocity of T to be disputed. Not only does the phase last for a long time, about 5 minutes here, but it also consists of a train of waves corresponding to different modes, and as often as not a correction has to be made for a land travel path. The frequency content is mostly above 1 cps, except for the Airy phase, so T is generally not recorded by land-based seismographs. *Tolstoy and Ewing* [1950] concluded that the mid-Atlantic ridge and Azores plateau stop or greatly reduce the amount of energy in T-phases in the Atlantic and thus account for the fact that T-phases from transatlantic quakes are rarely observed. Indeed, the T-phase reported here is the first such recorded to our knowledge.

From a detailed study of the spectrum of T-phases, it may be possible to determine some of the parameters of the travel path, i.e., sediment thickness and velocity, holes in the mid-Atlantic ridge that have passed T-phase energy, and refraction of rays toward the lower-velocity northern water paths. As pointed out by *Milne* [1959], frequency analysis of T-phases may pro vide a way to distinguish atomic blasts fron earthquakes. In the present paper, it is apparen that the later modes form a characteristic of th signal. A T-phase signature like this woul probably not be excited by surface bomb ex plosions.

[3] These velocities were computed by assuming a P velocity of 5.5 km/sec for the 60-mile land travel path between the epicenter and the continental slope. The mechanism for transformation of elastic waves from P to T at the continental slope was discussed by *Shurbet and Ewing* [1957].

Acknowledgment. This work was supported b the Office of Naval Research.

REFERENCES

Burke-Gaffney, T. N., The T-phase from the Ne Zealand region, *J. and Proc. Royal Soc. Ne South Wales, 88*, 50–54, 1954.

Ewing, M. S. Mueller, M. Landisman, and Y. Sat Transient analysis of earthquake and explosiv arrivals, *Geofis. pura e appl., 44*, 83–118, 195

Ewing, M., F. Press, and J. L. Worzel, Furthe study of the T phase, *Bull. Seism. Soc. Am., 4* 37–51, 1952.

Leet, D., D. Linehan, and P. R. Berger, Investiga tion of the T phase, *Bull. Seism. Soc. Am., 41* 123–141, 1951.

Milne, A. R., Comparison of spectra of an earth quake T phase with similar signals from nuclea explosions, *Bull. Seism. Soc. Am., 49*, 317–329 1959.

Northrop, J., and A. Berman, Correlation of som SOFAR arrivals in the western North Atlanti (Abstract), *J. Acoust, Soc. Am., 31*, 838, 1959

Pekeris, C. L., Propagation of sound in the ocean *Geol. Soc. Am. Mem. 27*, 1948.

Shurbet, D. H., and M. Ewing, T phases at Bermud and transformation of elastic waves, *Bull. Seism Soc. Am., 47*, 251–262, 1957.

Tolstoy, I. and M. Ewing, The T phase of shallow focus earthquakes, *Bull. Seism. Soc. Am., 40*, 25–51, 1950.

(Received August 27, 1960.)

Journal of

GEOPHYSICAL RESEARCH

Tables of Contents

VOLUME 65, NO. 1, JANUARY 1960

VOLUME 65, NO. 2, FEBRUARY 1960

VOLUME 65, NO. 3, MARCH 1960

VOLUME 65, NO. 4, APRIL 1960

VOLUME 65, NO. 5, MAY 1960

VOLUME 65, NO. 6, JUNE 1960

VOLUME 65, NO. 7, JULY 1960

VOLUME 65, NO. 8, AUGUST 1960

VOLUME 65, NO. 9, SEPTEMBER 1960

Letters to the Editor:

VOLUME 65, NO. 10, OCTOBER 1960

VOLUME 65, NO. 11, NOVEMBER 1960

Letters to the Editor:

VOLUME 65, NO. 12, DECEMBER 1960

Index of Names

Journal of Geophysical Research, Volume 65

January–December 1960

Note. (*a*) *indicates abstract;* (*l*) *indicates letter to the editor;* (*c*) *indicates corrigendum*

J. Geophys. Research, 65 (1), 1–384; (2), 385–798; (3), 799–1082; (4), 1083–1330; (5), 1331–1644; (6), 1645–1864; (7), 1865–2212; (8), 2213–2562; (9), 2563–3024; (10), 3025–3514; (11), 3515–3858; (12), 3859–4248.

J. Geophys. Research, 65 (1), 1-384; (2), 385-798; (3), 799-1082; (4), 1083-1330; (5), 1331-1644; (6), 1645-1864; (7), 1865-2212; (8), 2213-2562; (9), 2563-3024; (10), 3025-3514; (11), 3515-3858; (12), 3859-4248.